THE TELECONNECTIONS BETWEEN ENSO AND THE CLIMATE VARIABILITY OF ANTARCTICA

by

RICHENDA ELOUISE HOUSEAGO

A thesis submitted to the Faculty of Science
of The University of Birmingham
for the degree of
DOCTOR OF PHILOSOPHY

School of Geography and
Environmental Sciences
Faculty of Science
The University of Birmingham
August 1998

Abstract

The overall goal of this study is to identify the teleconnection mechanisms that underlie ENSO-Antarctic climate links. Initially time series plots and cross correlation analysis of Antarctic surface and upper air climate data are used to search for high latitude atmospheric signals during Pacific Ocean warm (ENSO) and cold (La Niña) events. Consistent increases (decreases) in pressure were found during warm (cold) events, with a variable response in temperature. Upper air data demonstrate consistent changes in windspeed, cloud cover geopotential height, wind speeds and direction, temperature and relative humidity during ENSO events. Spatial anomaly plots, Hovmöller, harmonic and cluster analyses are used to identify ENSO related climate anomaly wavetrains, teleconnections and propagation mechanisms that link Southern Hemisphere low and high latitudes. Although inter-warm and cold event variability is a characteristic, strong meridional anomaly contrasts, equatorward and poleward anomaly propagation, and distinct jetstream behaviour were apparent in all events studied. In warm (cold) events subtropical jet strength increases (decreases) and polar jet strength decreases (increases) resulting in a decrease (increase) in poleward moving cyclonicity. The jetstreams are considered to play a major role in ENSO related climate anomaly propagations.

To Roger

Acknowledgements

I would like to thank my supervisor Dr. Glenn McGregor for all of his help, advice, encouragement and useful discussions throughout the last three years.

I am also grateful to Dr. John King and Steve Harangozo from British Antarctic Survey for providing me with data and helpful comments on my work.

Thanks are also due to Geoff Wootton from Information Services for helping me to retrieve data from tapes and in making disk space available on the ISDUX. Thanks also to Dr. Xiaoming Cai for setting up GrADS on his UNIX machine for me.

My fellow postgraduates, on the 12th floor Muirhead Tower, particularly Ant Veal (who has also taught me about real ale!), Dan Cornford, Ian D. Phillips and David Hannah are acknowledged for many useful discussions as well as a warm and friendly atmosphere. I would also like to thank the lecturers and support staff, particularly Jim Hales and John Kings, who have helped to make my time here at Birmingham enjoyable.

I would like to thank all of those friends who have provided diversions from my PhD, especially Sue Jowett (for teaching me about cricket), Sam Hoad (a fellow soap viewer and wine brewer), Roger Ward (for always knowing when to turn up at the bar for a free drink), Emma Cochrane, Julian Pittard, Cathy Barnett (for being a good housemate), Ian T. Phillips (for chats whilst making tea), Jon Oldfield (for very random conversations), Joanna Ball and Sarah Abrahams.

I would like to say thank you to my parents for the love and support they've shown me over the years.

Last, and by no means least, special thanks go to Roger, my fiancé, for all of his support and encouragement during my PhD.

Table of Contents

List of Figures

List of Tables

List of Abbreviations

AA ..... Australian Bureau of Meteorology Analyses

CAC..... Climate Analysis Center

EN..... El Niño

ENSO... El Niño-Southern Oscillation

ITCZ .... Intertropical Convergence Zone

PNA ..... Pacific-North American

PSA..... Pacific-South American

SAO ..... Semi-annual Oscillation

SO..... Southern Oscillation

SOI..... Southern Oscillation Index

SOO ..... Southern Oceanic Oscillation

SPCZ.... South Pacific Convergence Zone

SST ..... Sea Surface Temperature

CHAPTER 1

INTRODUCTION

1.1 Introduction

On a global scale the ENSO (El Niño-Southern Oscillation) phenomenon is the largest single source of interannual climate variability. It is of considerable economic importance to countries across the Pacific, with El Niño (warm) events being responsible for droughts in Australia (Chiew et al., 1988) and Indonesia and excess rainfall in South America (Rutllant and Fuenzalida, 1991; Pisciottano et al., 1994) and south-eastern USA (Yin, 1994). Warm events have also been found to be responsible for reduced precipitation in the Indian monsoon (Webster and Yang, 1992) and the South African summer (van Heerden et al., 1988; Lindesay, 1988; Nicholson and Kim, 1997). To date a large amount of research has been undertaken on these zonal teleconnections between ENSO and highly variable aspects of the global climate, but little work has been carried out on meridional teleconnections, which are also thought to be a function of ENSO. The ideal study area for identifying these longitudinal teleconnections is Antarctica, which due to its size, asymmetry, topography and position plays a major role in the climate of the Southern Hemisphere. In this study particular attention is given to the Antarctic Peninsula, which, as well as being the most northerly region of the continent, is to the south of the eastern Pacific, one of the ENSO 'centres of action', and so is thought to be ideal for studying these longitudinal interactions. Despite ENSO-Antarctic links having been established, previous studies are limited in the number of variables they consider and the length of the record used. The purpose of this research is therefore to determine the exact nature of the ENSO-Antarctic teleconnections and attempt to identify the mechanisms responsible for the propagation of climate signals between the low and high latitudes of the Southern Hemisphere.

1.2 Research Aims and Objectives

In order to establish the nature of ENSO-Antarctic climate teleconnections five objectives will be set and addressed in this study. These are:

1. *To explore further the effect of ENSO on the climate variability of Antarctica, with special reference to the Antarctic Peninsula.*
2. *To assess whether there is a propagation of anomalies between the low and high latitudes along an ENSO sensitive meridian .*
3. *To identify the possible movement of sea level pressure anomalies in the Southern Hemisphere on a spatial scale, during both ENSO and non-ENSO events.*
4. *To uncover any spatial signals in the phases of the first harmonics of 500 height, temperature and mixing ratio anomalies, and from the height anomalies identify teleconnections in the Southern Hemisphere.*
5. *To consider the role of the jetstreams in the propagation of the ENSO signal between the tropics and high latitudes of the Southern Hemisphere.*

These objectives will be used to uncover the nature of the response of the Antarctic climate to ENSO, with the ultimate aim being the identification of the mechanisms that drive the signal propagation.

1.3 Thesis structure

This thesis reports the research in a structured manner following the objectives outlined in Section 1.2, as summarised in Figure 1.1. The investigation is divided up into seven chapters. This chapter is followed by a review of the literature on the nature of ENSO, its mechanisms and global impacts (Chapter 2). The literature review is used to identify the research gaps which this study will address. Study methodology and data analysis are described in Chapter 3. Specifically, the study area, the nature of the data required to fulfil the study objectives and the processing techniques will be described as well as detailing the methodology associated with each of the study objectives outlined in Section 1.2. Chapter 4 focuses on the impacts of ENSO on the climate variability of Antarctica. Initially station and upper air data are used to identify the relationships between the Southern Oscillation Index (SOI) and a range of climate

time series. Cross correlation analysis is applied to identify concurrent and lead and lag associations between the Antarctic climate and the SOI. In order to identify the spatial patterns in the ENSO signal across the Antarctic continent, pressure and temperature cross correlations are compared for a number of stations across the Antarctic continent. Chapter 5 is concerned with the analysis of spatial patterns of climate anomalies associated with ENSO for the entire Southern Hemisphere. This chapter provides the basis for identifying the mechanisms by which ENSO signals reach the Antarctic (Chapter 5). Initially Hovmöller diagrams are used to study the movement of anomalies along the 230° longitude line, a meridian considered to be ENSO sensitive. Following this the spatial patterns of climate anomalies are considered at a larger spatial scale. In order to capture the spatial and temporal response of climate anomalies to ENSO at the hemispheric scale and also identify teleconnection patterns, harmonic analysis is applied to grid point climate anomaly data. The results of this analysis are presented in Chapter 5. Following this zonally averaged Hovmöller plots are used to identify the overall pattern in the height anomalies and uncover the nature of subtropical and polar jetstream behaviour during ENSO and non-ENSO events and thus assess their candidacy as an ENSO-Antarctic climate anomaly propagation mechanism. Research findings are brought together in the discussion chapter (Chapter 6). This chapter considers the nature of the response of the climate to ENSO at the Antarctic continental and Southern Hemisphere scales as a means for identifying the processes linking ENSO and Antarctic climate variability. Chapter 7 summarises the major research findings of this study in the context of the five objectives, identified in Section 1.2. It also presents a schematic model describing the major low to high latitude teleconnections in the study area as well as the mechanisms underlying the teleconnections. Suggestions for further research are also presented in this final chapter.

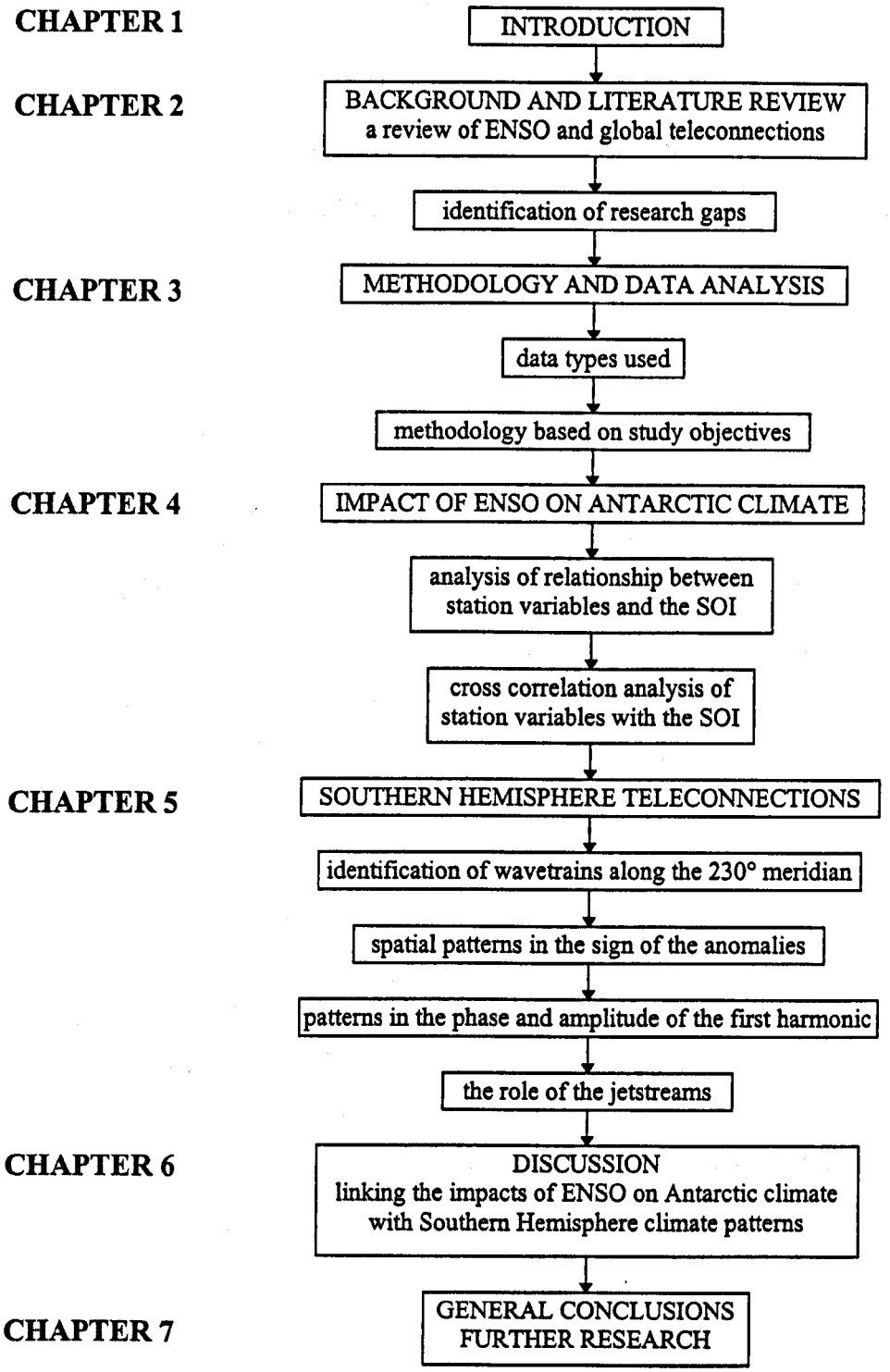

Figure 1.1 Flow diagram outlining the thesis structure.

CHAPTER 2

BACKGROUND AND LITERATURE REVIEW

2.1 Introduction

This chapter sets the scene for the thesis, it gives a relevant review of the literature on the ocean-atmosphere phenomenon ENSO (El Niño-Southern Oscillation), its development, variability, measurement and teleconnections, both within the tropics and with the high latitudes of the Southern Hemisphere. This study specifically addresses the atmospheric part of the ENSO phenomenon as temperature changes in the ocean are smaller and less rapid than in the atmosphere (Henderson-Sellers and Robinson, 1986) and so not suited to the timescales involved in this study. This chapter also identifies the research gaps, allowing the research aims, identified in Chapter 1 to be clarified.

2.2 The global climate system

The global climate system is extremely complex. Its behaviour is governed by the interactions between five different components: the atmosphere, the hydrosphere (oceans), the biosphere (vegetative cover and oceanic flora and fauna), the lithosphere (earth's surface, including hydrology and volcanism) and the cryosphere (polar ice fields and sea-ice, continental snow cover) (Figure 2.1). Each of these components is coupled with the others. The atmosphere and hydrosphere are coupled through the exchange of energy, momentum and matter on a variety of spatial and temporal scales. The vegetative cover of the biosphere affects the surface roughness, albedo, evaporation, precipitation and moisture capacity of the soil. The lakes, rivers and ground water of the lithosphere are essential parts of the hydrological cycle and are connected to the atmosphere via evaporation and precipitation. Changes in snow cover affect the surface albedo and variations in sea-ice affect the exchanges between the oceans and atmosphere (Daley, 1991).

The atmosphere is the most variable component of the climate system in both space and time. The function of the atmosphere system is to store and redistribute the heat received from the sun (Daley, 1991). Within the atmosphere system the ENSO phenomenon is the largest single source of interannual climatic variability on a global scale (Trenberth, 1991; Diaz and Markgraf, 1992). The effect of ENSO on the global climate variability is discussed in greater detail below (Section 2.9).

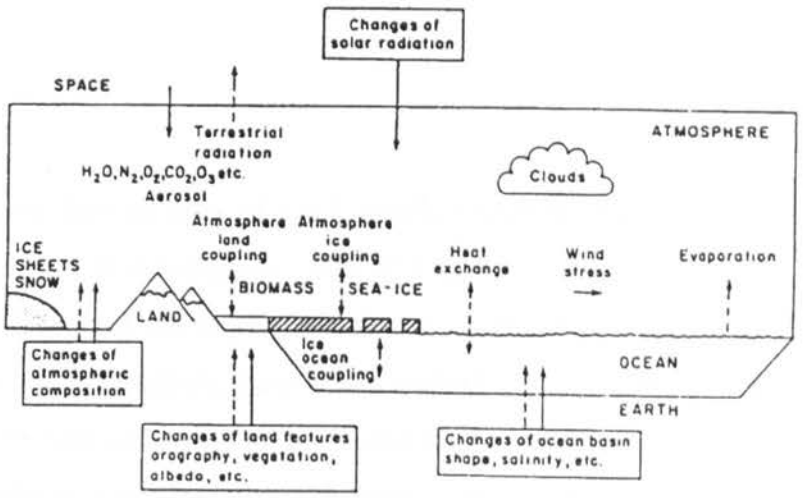

Figure 2.1 Schematic illustration of the components of the climate system. Full arrows are examples of external processes and dashed arrows are examples of internal processes (source: GARP, 1975).

2.3 The general characteristics of the Southern Hemisphere climate

2.3.1 Pressure

The distribution of land and sea affects the symmetry of the pressure patterns across both of the hemispheres and as a result the Southern Hemisphere has a more zonal symmetrical pattern of pressure than the Northern Hemisphere. In the equatorial regions the sea level pressure is generally low rising poleward in the tropics to a peak in the subtropics, where each ocean has an anticyclonic centre. Due to the greater amount of sea compared to land these high pressure areas form an almost continuous zonal belt. South of the subtropical high the pressure drops steeply to the circumpolar trough, which is between 60 and 70°S. In the Southern Hemisphere the greatest number of cyclogenesis events take place in the 60-70°S band, which is on the northern part of the circumpolar trough, which is thought to be due to

the strong baroclinicity at this latitude (Turner et al., 1998). To the south of the circumpolar trough sea level pressure increases (van Loon, 1972a).

In the Southern Hemisphere there is a semi-annual variation in sea level pressure in the middle and high latitudes (van Loon, 1972a, 1972b). This variation has been termed the semi-annual oscillation (SAO) and is linked to a twice yearly oscillation in the position and intensity of the circumpolar trough (Meehl, 1987). This feature is described in more detail in Section 2.8.

2.3.2 Airflow

Around the equator lies an area of slack winds which is associated with an area of low pressure, the intertropical convergence zone (ITCZ) where the trade winds from the Northern and Southern Hemispheres converge. This area is on the edge of one of the three major wind belts of the Southern Hemisphere, the tropical and subtropical easterlies, the other wind zones are the midlatitude and subpolar westerlies and the polar easterlies (van Loon, 1972b). The Southern Hemisphere westerlies are associated with weather disturbances, and are more intense than the Northern Hemisphere westerlies with respect to both zonal and meridional circulation (van Loon, 1972b). Within the westerlies there are two jetstreams, which are well defined bands of strong winds. The subtropical jetstream has a circumpolar path between 20 and 35°S, whilst the polar jetstream has a path between 35 and 65°S. The polar easterlies are highly variable winds south of the circumpolar trough.

2.4 Impact of Antarctica on Southern Hemisphere Climate

Antarctica is the fifth largest continent with an area, including the ice shelves and surrounding islands of approximately 14,120,000 km^2 (Astapenko, 1964; Taljaard, 1972). Antarctica is normally divided into two parts, West and East Antarctica. West Antarctica faces the Pacific and southwest Atlantic and includes the Antarctic Peninsula, which stretches through 10° of latitude, with a backbone of mountains that act as a barrier to low level circulation (Taljaard, 1972). East Antarctica is a massive ice dome rising to over 4km, and thus is completely different to West Antarctica. Due to its size, asymmetry, topography as well as its position, Antarctica has a large climatic effect on the circulation patterns of the whole of the Southern

Hemisphere and combined with the effects of the Andes dominates the orography of the Southern Hemisphere (Sturman, 1976; James, 1988). The effect of Antarctica on the Southern Hemisphere climate may be direct, in forcing a midlatitude long-wave pattern with a New Zealand split jet, or indirect, in that this long wave pattern will steer and distort baroclinic disturbances (James, 1988).

The Antarctic Circumpolar Current, which is the only current to flow around the globe without encountering any continuous land barrier (Pickard and Emery, 1990), plays a vital role in the global circulation (Whitworth, 1988), with alterations in the sea surface temperature and sea-ice distribution in this region contributing to adjustments in the hemispheric circulation (Taljaard, 1972), through the alteration of planetary waves (van Loon and Jenne, 1972). As described later, in Section 2.11, variations in the climate in the Antarctic region may lead to changes in the mid-Pacific, thus Antarctic climate may play an active as well as a passive role in an interactive Antarctic-ENSO system.

2.5 ENSO (El Niño-Southern Oscillation)

2.5.1 El Niño and La Niña

El Niño, meaning 'the Christ child', in Spanish, is a term that was first used by South American fishermen to describe the weak Pacific Ocean current that flows south off the coasts of Ecuador and Peru every year at about Christmas time, displacing the cold Peru current and upwelling cold water (Streten, 1975), hence the current bringing warm water to these regions was named after the time of year when it occurs (Ramage and Hori, 1981; Cane, 1983; Bigg, 1990). This phrase was then adopted to describe the occasional unusually large warmings that occur every few years with a radical change in ocean circulation (Trenberth, 1991). Initially the term referred to the warmings down the coast, but is now associated with the warming across the whole of the tropical Pacific basin, as far as the dateline (Philander and Rasmusson, 1985; Trenberth, 1991). To cover the many uses of this phrase Glantz (1996) has proposed the dictionary definition of El Niño:

> El Niño \ 'el nē' nyō *noun* [Spanish] \ 1: The Christ Child 2: the name given by Peruvian sailors to a seasonal, warm southward-moving current along the Peruvian coast <la corriente del Niño> 3: name given to the occasional return of unusually warm water in

the normally cold water [upwelling] region along the Peruvian coast, disrupting local fish and bird populations 4: name given to a Pacific basin-wide increase in both sea surface temperatures in the central and/or eastern equatorial Pacific Ocean and in sea level atmospheric pressure in the western Pacific (Southern Oscillation) 5: used interchangeably with ENSO (El Niño-Southern Oscillation) which describes the basin-wide changes in air-sea interaction in the equatorial Pacific region 6: ENSO warm event *synonym* warm event *antonym* La Niña \ [Spanish] \ the young girl; cold event; ENSO cold event; non-El Niño year; anti-El Niño or anti-ENSO (pejorative); El Viejo \ 'el vyă hō \ noun [Spanish] \ the old man.

The warm surface waters in the eastern Pacific are the most important oceanic factor in this phenomenon, as sea surface temperature is the only oceanic parameter to have any significant effect on the atmosphere (Philander, 1990). The eastern Pacific warming has an opposite phase in its oscillation that has been termed La Niña, meaning 'the girl' in Spanish. The term anti-El Niño has also been used in the past for this phenomenon, but La Niña, introduced by Philander (1985), is now the preferred term.

The El Niño is of considerable economic importance to countries across the Pacific. In Australia drier than normal conditions occurring during El Niño events (Chiew et al., 1998) have consequences for agriculture, native vegetation and wildlife (Nicholls and Kariko, 1993). El Niño events also promote drier than normal conditions in the Indonesian region leading to environmental disasters such as the 1997 forest fires and resultant thick smogs over the region. In Hawaii there are frequent droughts in the winter and spring following El Niño events (Chu, 1995) with resultant economic consequences. In Peru and Ecuador it has a serious adverse effect on the anchoveta fishery. During El Niño the break in the upwelling of cool nutrient-rich water leads to a reduction in phytoplankton and zooplankton (Trenberth, 1997a), which is the main food source of anchovy and krill, leading to a worldwide shortage (Streten, 1975; Ramage and Hori, 1981; Priddle et al., 1988).

2.5.2 The Southern Oscillation

The term Southern Oscillation was first used by Walker (1928), to describe the climatic 'seesaw' occurring on average every four years, between the western and eastern Pacific, although it has been known to operate at periods of between two and ten years (Trenberth, 1976; Trenberth, 1984b). Early this century Lockyer and Lockyer (1902a) found that the pressure of Cordoba, South America, was the inverse of the pressure of Bombay, India, with

this seesaw having a periodicity of approximately 3.5 years. They showed that this oscillation extended from Australia to the southern states of the USA (Lockyer and Lockyer, 1902b). According to Walker and Bliss (1932) '*when pressure is high in the Pacific Ocean, it tends to be low in the Indian Ocean from Africa to Australia; these conditions are associated with low temperatures in both areas, and rainfall varies in the opposite direction to pressure*'. Walker found that the Southern Oscillation was associated with drought in India, and cool, wet winters in the southeastern United States (Kiladis and Diaz, 1989). The Southern Oscillation is the single most prominent signal in year-to-year global climate variability with a coherent pattern of pressure, temperature and rainfall fluctuations (Rasmusson and Wallace, 1983; Philander and Rasmusson, 1985; Philander, 1990). It is associated with major shifts in the Intertropical Convergence Zone (ITCZ) and the South Pacific Convergence Zone (SPCZ), over the Pacific Ocean (Trenberth, 1984b). The SPCZ is the focal point for ENSO events, and is shifted northeast of its average position during El Niño events, and southwest during La Niña events (Vincent, 1994). The 'centres of action' of the Southern Oscillation are located over Indonesia and the tropical South Pacific Ocean and are linked by a zonal east-west circulation along the equator with rising motion in the western Pacific and sinking motion in the east (Trenberth, 1976; Trenberth, 1991). Higher than average pressures over one centre tend to coincide with lower than average pressures over the other (Trenberth and Paolino, 1981). Bjerknes (1969) named this circulation system the Walker circulation as it is an important part of Walker's Southern Oscillation.

2.5.3 ENSO

ENSO events are classified according to the sign of the temperature anomalies in the eastern Pacific. During 'cold' events there is a cold tongue of water along the equator, with a reduction in temperature and resultant higher atmospheric pressures in the eastern Pacific. During 'warm' events, there are warmer than 'normal' temperatures, associated with the general warmth of the eastern tropical Pacific Ocean, resulting from El Niño. Such warm temperatures result in the warming of the lower atmosphere and hence low pressure. The terms 'cold' and 'warm' events were first used by Horel and Wallace (1981) and Rasmusson and Carpenter (1982) to classify events based on the response of sea level pressure and surface air temperature in the tropical eastern Pacific. During the colder conditions high

pressure forms due to a reduction in temperature in the eastern Pacific, whilst low pressure forms in the western Pacific, where the temperature tends to be higher, thus leading to a strengthened pressure gradient and strong easterly trades. At higher levels during cold conditions the corresponding flow is westerly, leading to the enhancement of a circulation cell known as the Walker circulation (Figure 2.2). The cold stage of the cycle is characterised by the large scale upwelling of cold water off the western coast of South America. The alteration of the trade winds induced by these differences in sea surface temperature drives a strong westward surface flow of the ocean, which is known as the South Equatorial Current (Bigg, 1990). To balance this strong surface flow of water a stronger undercurrent flows east at a depth of about 100m, which is responsible for the continued upwelling of the cold water off the South American coast. These mechanisms form part of a large positive feedback loop, in which conditions are amplified over a period of time.

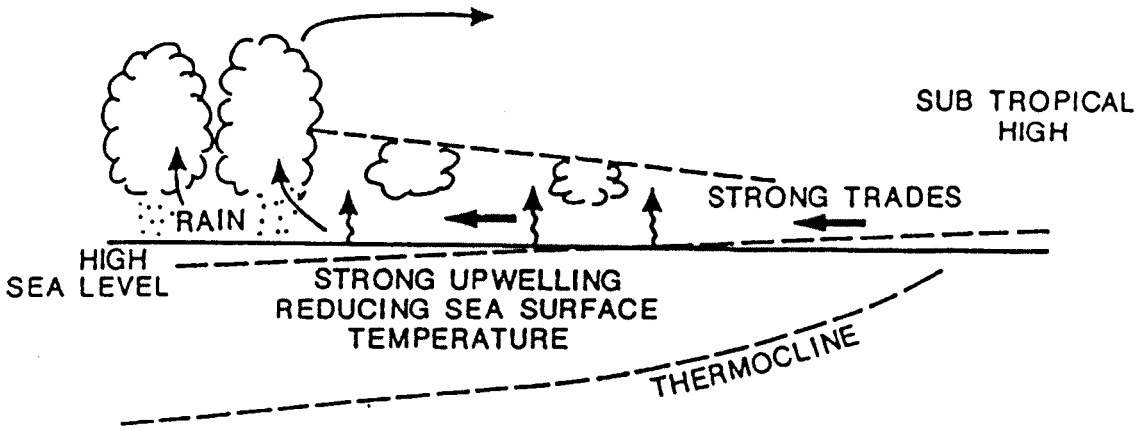

Figure 2.2 The Walker circulation: a schematic cross-section of the atmospheric and oceanic features in the normal phase of the Southern Oscillation (source: Bigg, 1990).

Every few years the cold circulation, which tends to be the most frequently occurring system, is interrupted and found to reverse giving rise to the extreme warm state. In the first stage of the warm event, which starts at around the end of the calendar year in the tropical Pacific Ocean, the southeast Pacific anticyclone weakens (Philander and Rasmusson, 1985) and the trade winds slacken (Cane, 1983). The alteration in the trade winds generates oceanic Kelvin waves that propagate eastward reaching the South American coast in a few months. The Kelvin waves are associated with the deepening of the thermocline, which is the stratified layer that separates the warm surface waters from the cold water at depth, which results in surface warming in the eastern Pacific as the cold water is prevented from being upwelled

(Trenberth, 1996). The reduction in the strength of the trade winds reduces the surface wind stress, altering the ocean slope, with a drop in sea level in the western Pacific and a rise by tens of cm in the east, and so the warm water in the western Pacific spreads eastwards, reducing, and then reversing the flow of the strong undercurrent, preventing the upwelling of cold water in the east. The thermocline slopes downward toward the west so that the surface mixed layer is over 150m deep in the west, but disappears in the east (Philander and Rasmusson, 1985) (Figure 2.3). At this time circulation anomalies occur in the upper-tropical

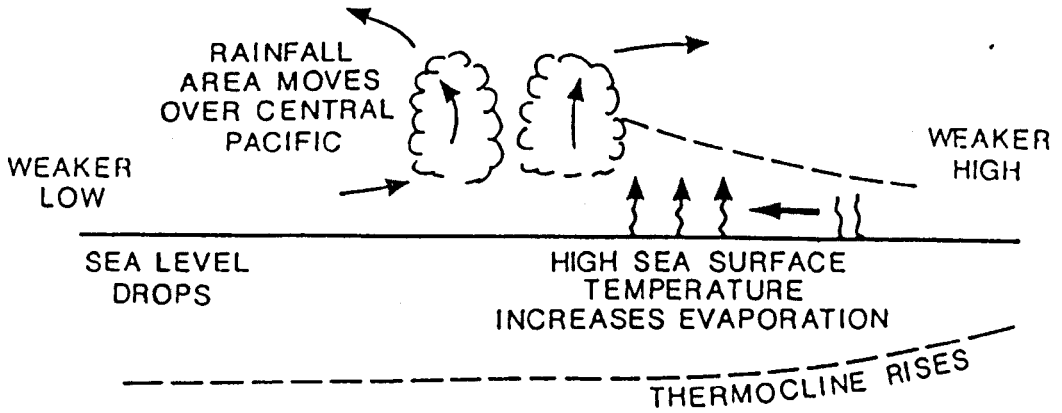

Figure 2.3 El Niño circulation: a schematic cross-section of the atmospheric and oceanic features in the warm phase of the Southern Oscillation (source: Bigg, 1990).

troposphere, with an eastward displacement of the upward branch of the Walker circulation, generating anticyclonic upper-troposphere vorticity in the central equatorial Pacific, which is associated with the development of an anomalous anticyclonic circulation cell south of the equator occurring at about the time of the second phase (Philander, 1983). The second stage starts towards the middle of the following year, about six months after the appearance of unusual conditions in the east, and involves an eastward displacement of the convective zone, that is normally over the western Pacific, an increase in sea level pressure at Darwin, a collapse in the central Pacific equatorial easterlies and an increase in central equatorial rainfall anomalies (Ramage and Hori, 1981; Philander, 1983; Philander and Rasmusson, 1985). Philander and Rasmusson (1985) found that the anomaly pattern, occurring during this second stage, reflects an eastward extension of the upper-troposphere monsoon high, normally located over the western Pacific at this time, resulting in the suppression of convection in the monsoons over southern Asia, often leading to decreased precipitation in the Indian monsoon (Meehl, 1987; Kripalani and Kulkarni, 1997). These conditions reach a maximum near the

end of the year, and by early in the new year, west of the dateline, normal conditions are restored, with the anomalies gradually decreasing during the rest of the year (Philander and Rasmusson, 1985). An ENSO event usually evolves through both these stages, the first stage mainly involving the eastern Pacific, with the second stage also involving the central and western Pacific (Philander, 1983). The difference between ENSO events is normally based on the relative strengths and occurrence of these two stages, for example the extreme 1982 event bypassed the first stage (Rasmusson and Wallace, 1983; Philander and Rasmusson, 1985). The ENSO conditions decay in a similar manner to which they developed, primarily low sea surface temperatures and intense tradewinds first appear in the southeastern tropical Pacific Ocean and then propagate westward until normal conditions are restored approximately 12 to 18 months after initiation over the entire tropical Pacific Ocean (Philander, 1983). It has been shown that ENSO appears to exhibit quasi-biennial characteristics (Allan et al., 1996), that is it appears to change from one phase to the other over a two year period, thus year +1 of a warm event has the characteristics of year 0 of a cold event, for example in the 1960's, 1963 was a warm event, 1964 a cold event, 1965 a warm event and 1966 a cold event.

The link between the two circulation systems, El Niño (EN) and the Southern Oscillation (SO), was first identified by Bjerknes (1966, 1969), who found that the interannual fluctuations in sea surface temperatures across the eastern equatorial Pacific are clearly linked to the related changes in the Walker circulation and the large scale equatorial Pacific precipitation regime. However, this link is not necessarily on a direct basis as changes in sea surface temperatures have occurred without a swing in the Southern Oscillation (Deser and Wallace, 1987). For example, there was warming in 1979 without a major swing in the Southern Oscillation, and in 1986 tropical Pacific sea surface temperatures rose long before there was an alteration in the Southern Oscillation (Trenberth and Shea, 1987).

There is continuous debate as to whether the ocean affects the atmosphere, i.e. the variations in the atmosphere are caused by changes in sea surface temperature, or whether the atmosphere affects the ocean, i.e. the sea surface temperatures are caused by atmospheric variability, during these events (Philander, 1985). The reason for the reversal of the ocean-atmosphere system is not known. However, it has been hypothesised that a warm event could be triggered by an irregularity in the seasonal cycle, as seasonal movements determine where

atmospheric instabilities are initiated, which in turn could be initiated by factors outside the Pacific Ocean (Philander and Rasmusson, 1985). The ENSO system is thought to be most vulnerable to outside influences during spring, when the ocean atmosphere link is the least robust (Webster and Yang, 1992). Thus the spring conditions determine whether an event will take place. It is thought that the duration of the cold stage may be determined by the time that is required to recharge the heat to the system, as during the warm stage heat is distributed from the water in the low latitudes to both the atmosphere and to higher latitudes. Alternatively the ocean-atmosphere system may occur as a natural oscillator, acting independently of extratropical influences (Trenberth, 1991).

2.6 ENSO Indices

In order to identify the pattern and influence of ENSO through the use of statistics, and to compare the timing and intensity of events, it is necessary to have some form of index to represent it. ENSO indices have been developed in an attempt to quantitatively describe the ocean-atmosphere interaction, or climate state, through the use of a single number.

There are several different indices used to measure the magnitude of the Southern Oscillation. The first indices developed for the Southern Oscillation were calculated by Walker in the early 1930's, for the boreal summer and the boreal winter (Allan et al., 1996, p14). The indices, derived by Walker, are for three month averages and are based on the sign and size of the anomaly (Troup, 1965). The fields of sea surface temperatures, rainfall and pressure in the 'core ENSO regions', the western and eastern Pacific, are strongly coupled, with their fluctuations occurring simultaneously to within a month (Wright, 1984), although the correlation between these variables is greatest from July through to November (Wright et al., 1988), thus they are all ideal as indices for the Southern Oscillation (Rasmusson and Carpenter, 1982).

Sea surface temperatures are used for some of the most commonly used indices. The most widely used of the Pacific sea surface temperature indices, devised in the early 1980's by Rasmusson at the Climate Analysis Centre (CAC) (Allan et al., 1996), are for the Niño 1, 2, 3 and 4 regions (Figure 2.4). The monthly sea surface temperature anomalies in each Niño

region are averaged for the area to produce each of the indices. Originally much attention was focused on the Niño 3 region, a key diagnostic region, but recently it has become apparent that the key region for ENSO related coupled ocean-atmosphere interactions is farther west (Wang, 1995; Trenberth, 1997b), consequently a new region has been proposed, termed Niño 3.5. This straddles the Niño 3 and Niño 4 regions, from 120° to 180°W, 5°N to 10°S. The Climate Prediction Center has also proposed a new sea surface temperature index. This differs slightly from the (CAC) Niño 3.5 region, and covers the region 120° to 170°W, 5°N to 5°S, and has been named Niño 3.4 (Trenberth, 1997b). The Niño 3 and 3.4 indices are now the most commonly used sea surface temperature indices.

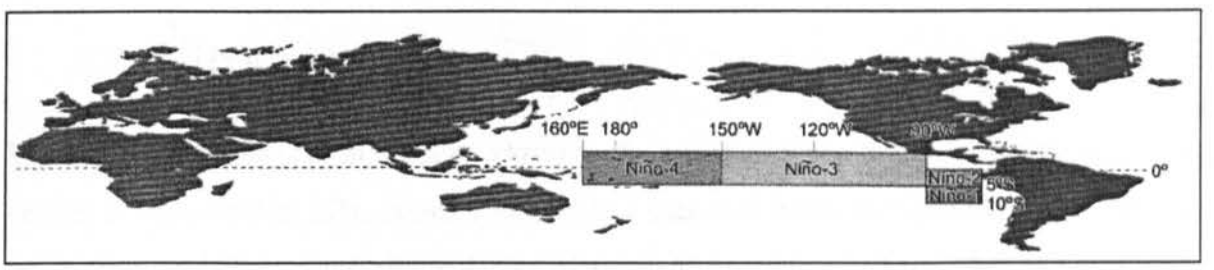

Figure 2.4 The locations of the Niño 1,2, 3 and 4 regions across the equatorial Pacific Ocean (source: Allan et al., 1996)

Sea surface temperature indices have an advantage over pressure indices in that sea level pressure indices have a large month-to-month variability, so are only useful if smoothed over time or averaged over seasons, however, sea temperature indices are subject to inhomogeneities due to changes in the method of measurement (Wright, 1989), although satellites are now used to overcome this.

Rainfall indices have also been calculated (Wright, 1984), and like the SST indices are useful as they do not require smoothing. Wright calculated a rainfall index using a combination of 6 stations in the sector 160°E to 150°W close to the equator. The rainfall means for the period 1948-67 were obtained for each month for each individual station using the formula:

$$R = \frac{1}{N}\sum_{n=1}^{N} D_n^{1/3} \qquad (2.1)$$

Where R is the monthly mean transformed rainfall, D_n is the rainfall for an individual month in tens of millimetres, and where N is the available number of years. To calculate the index

from this equation the cube root of the actual monthly value is expressed as a percentage of the corresponding mean, calculated from equation 2.2:

$$SOI = \frac{\sqrt[3]{v}}{R} \times \frac{100}{1} \tag{2.2}$$

Where v is the actual monthly value and R is taken from equation 2.1 above.

Sea level pressure is the most widely used variable for indices (Wright, 1989). Wright (1975) used pressure from eight stations, Cape Town, Bombay, Djakarta, Darwin, Adelaide, Apia, Honolulu and Santiago, to create a seasonal index using the formula:

$$SOI = \sum_{j=1}^{8} \left[P(jys) - M(js) \right] W(js) \tag{2.3}$$

Where j denotes the station number, $P(jys)$ is the seasonal mean pressure for station j, year y, season s, expressed in hPa, minus 1000, M is a seasonal mean correctional factor dependent on station, and W is a weighting factor, dependent on station. The index is calculated by combining the results from each of the stations. Wright et al. (1985) used the annual means of monthly pressure anomalies at Darwin to create an index. The majority of pressure indices use a combination of the pressure at Darwin and Tahiti because these are near the 'centres of action' or ENSO core regions. The mostly widely used being the Tahiti-Darwin Southern Oscillation Index (SOI) (Ropelewski and Jones, 1987; Wright, 1989; Allan et al., 1991). Tahiti and Darwin are used in the calculation as there is an out of phase relationship between stations in the South Pacific (Tahiti) and Darwin (Trenberth, 1976; Trenberth and Shea, 1987) (Figure 2.5).

The Tahiti-Darwin index, by using locations at opposite sides of the Pacific, distinguishes between the warm conditions, (El Niños), which result in a low value of the SOI, hence are termed 'minimums', and cold conditions (La Niñas), which result in a high value of the SOI, and are conversely termed 'maximums'. The Tahiti-Darwin Southern Oscillation Index has been computed in a variety of ways by different investigators. All of these methods yield the same qualitative description of the state of the Southern Oscillation (Ropelewski and Jones, 1987). Two of these methods are almost identical (McBride and Nicholls, 1983; Kawamura et al., 1998) the Climate Analysis Center's (CAC) operational index, used in this study, and

the 'Troup' index (Ropelewski and Jones, 1987). A third index was defined by Trenberth (1984b). However, this index has a greater signal-to-noise ratio than the other two. In the Trenberth index, the monthly means are separately normalised by the mean of the 12 month standard deviations (Ropelewski and Jones, 1987). It is calculated using the following formula:

$$SOI = \left[T_n - D_n \right] \tag{2.4}$$

Where T is sea level pressure at Tahiti, and D is sea level pressure at Darwin and n denotes normalisation by the overall standard deviation of each series. With all of these indices the annual cycle of pressure at both stations has to be removed (Trenberth, 1984b). In the case of the CAC index, the trend is removed by calculating monthly anomalies for Darwin and Tahiti and then normalising these to produce standardised values with the result that Tahiti minus standard Darwin produces a standardised sea level pressure difference (Ropelewski and Jones, 1987). For the 'Troup' index, anomalies of monthly Tahiti-Darwin pressure differences are standardised by the standard deviation of the Tahiti minus Darwin series.

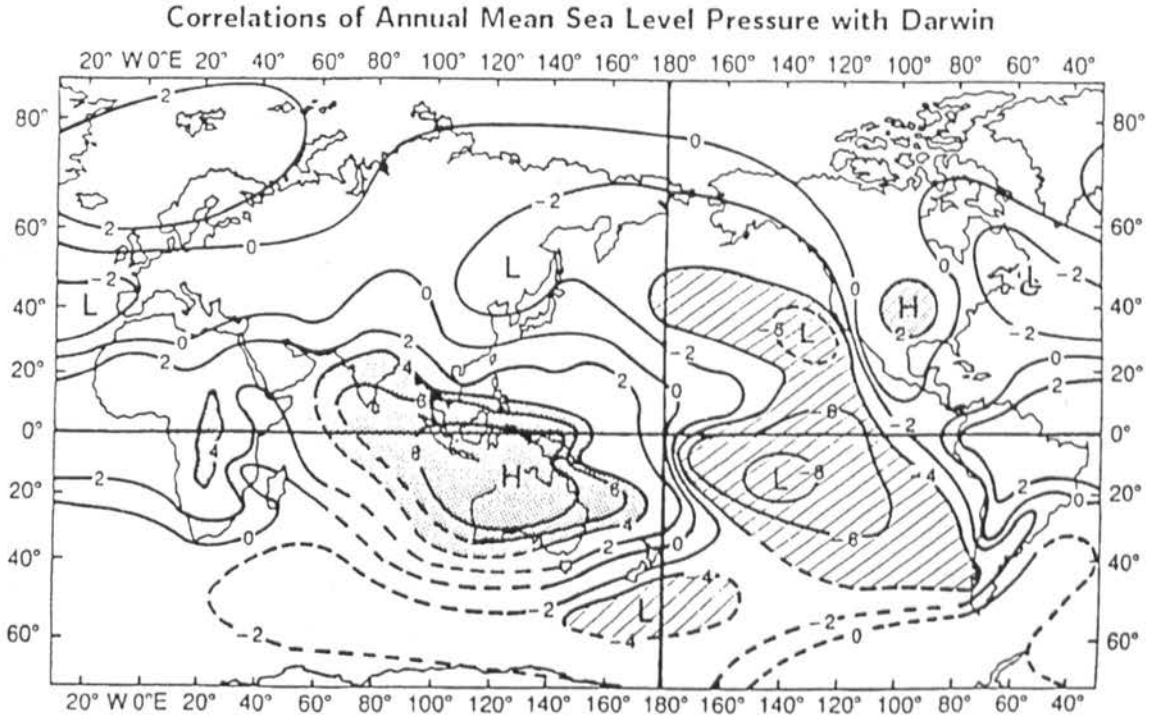

Figure 2.5 Composite of the correlations (x 10) of annual mean sea level pressures with Darwin (source: Trenberth and Shea, 1987)

More recently Kuhnel (1998) has developed a multifactor Southern Oscillation Index based on the Troup index described above. This has been applied to the analysis of annual hailstorm frequencies in Sydney and is calculated as follows:

$$SOI_{multifactor} = SOI_{Oct-jun} + SOI_{Nov-Feb} - \left| \frac{1}{8} \sum_{i=Jun}^{Jan} SOI_i \right| \tag{2.5}$$

where $SOI_{Oct\text{-}Jun}$ and $SOI_{Nov\text{-}Feb}$ are the spring minus winter and the spring minus autumn SOI gradients respectively. The gradients are the differences between the start and end month SOI values. The third factor in the equation is a stabilising term to account for the tendency of hailstorms to occur during years where the second half of the year has a near zero SOI signal. This index was created as the SOI gradients were found to be more accurate indicators of hailstorm frequencies than the original SOI.

Due to the varying manner in which the various SOI indices are calculated different indices give slightly different results for the timing and magnitudes of the event peaks as well as for the evolution and decline of events (Wright, 1989). It has also led to the classification of events varying from author to author (Klaßen et al., 1994).

2.7 Variations in ENSO

There is good evidence from cores of coral in the Pacific, glacial ice in the Andes (Trenberth, 1997a), alerce trees from southern Chile (Lara and Villalba, 1993) and flood evidence from Peru dating back to 500 BC (Quinn et al., 1987) that this phenomena has occurred for millennia. From studying the long records, compiled by Quinn et al. (1987), Enfield and Cid (1991) have found that warm events have a return interval of about 3.2 years whilst strong warm events appear to have a return interval of 8.8 years.

There has been a great deal of variability of the ENSO cycle over time. Around the turn of the century the intensity of ENSO was relatively large (Gu and Philander, 1995) as manifest by the extreme event of 1891 (Ramage and Hori, 1981). From about 1915 ENSO events were relatively small but have increased in intensity since about 1960 (Wang and Ropelewski, 1995), coinciding with the more recent extreme events of 1982/83 and 1997. It is believed that the nature of the onset of El Niño has also changed since the late 1970's (Wang, 1995;

Zhang et al., 1998), with the 1982, 1986 and 1991 events having central Pacific warming that was not preceded by South American warming. A further change since the late 1970's has been in the oscillatory nature of ENSO. The earlier, pre-1970, epoch had a distinctive two year rhythm in cold and warm events. However this was lacking in the later epoch (Mitchell and Wallace, 1996).

ENSO variability often manifests itself in the form of inter-event contrasts of the Pacific windfield. A number of speculations have been made regarding the cause of the initial changes in the Pacific windfield, including the development of twin cyclones in the western central Pacific (Keen, 1982), cold surges from the Indian monsoon (Hacket and Hastenrath, 1986) and the persistent development of the intraseasonal oscillation (Lau and Chan, 1986). There are two types of climate variability occurring in the Pacific, which may both be inter-linked, however, they have been considered separately to date, the first involves a shift in the climate base state, whilst the second appears to be more oscillatory in nature (Latif and Barnett, 1996). Recently, Wang (1995) has suggested that changes in the onset of the ENSO events have occurred due to the alteration in the precursor to the changes in the trade winds. Prior to the late 1970's, the precursor to the onset was characterised by an anomalous cyclone over east Australia, which brought anomalous westerlies into the western equatorial Pacific, resulting in basin wide warming. The trades in the south eastern Pacific relaxed resulting in a South American coastal warming, which led the central Pacific warming by about three seasons. However, following the late 1970's the anomalous cyclone was found to occur over the Philippine Sea establishing anomalous westerlies in the western equatorial Pacific north of the equator. The trades were then enhanced in the south eastern Pacific so the warming off Peru occurred after the central Pacific warming (Wang, 1995). Wang believes that the atmospheric anomalies occurring as a precursor to the onset phase of ENSO (Section 2.8) are controlled by the background sea surface temperatures (SST's). The tropical Pacific between 20°S and 20°N experienced an abrupt warming in the late 1970's, concurrent with a cooling in the extratropical North Pacific and South Pacific and a deepening of the Aleutian Low. Zhang et al. (1998) found that in the early 1970's a subsurface warm anomaly formed in the midlatitudes of the North Pacific Ocean from warm surface water subducted into the thermocline. The warm subsurface anomaly moved equatorward and westward around the subtropical gyre penetrating through the subtropics into the tropics, thus affecting the tropical

thermocline and driving the formation of a warm surface water anomaly. This teleconnection of extratropical thermal anomalies to the tropics is believed to operate on interdecadal time scale, via a subsurface ocean 'bridge' between the tropics and extratropics (Zhang et al., 1998). The timescale involved in the movement of anomalies is decadal with the subsurface warm anomalies in the midlatitudes in the late 1960's and early 1970's responsible for the upper ocean warming in the tropical Pacific in the 1980's (Zhang et al., 1998). The transition between stages in this perfectly periodic decadal oscillation is believed to be very abrupt (Gu and Philander, 1997).

It has also been found that since the late 1970's there has been an alteration in the balance between cold and warm events. Prior to this, when the base state was relatively cool, cold events occurred most frequently, with shifts to warm events occurring every three or four years, however, this trend now appears to have reversed with the warm base state, resulting in warm events occurring more frequently and lasting for longer than cold events (Wang and Ropelewski, 1995), for example the prolonged 1991 warm event.

It is thought that there is a possible modulation in ENSO by the greenhouse effect (Allan et al., 1991), however, there are a number of different views on the degree of change. Wang and Ropelewski (1995) have found that the frequency and amplitude of ENSO variability appears to be related to the climate base state. When the climatic mean state for sea surface temperature is relatively warm, warm events tend to occur more frequently with a greater amplitude, than occur with a relatively cold base state (Wang and Ropelewski, 1995). This warming of the base state, which is thought likely to occur with global warming, will lead to a pattern similar to that described by Wang (1995) as occurring following the late 1970's, with a potential for more frequent and intense warm events. Meehl et al. (1993) have suggested that with climate change there will be little change in the patterns of anomalously wet and dry conditions in the tropics, however, the resulting anomalies from warm events would be larger. Meehl et al. (1993) also suggest that there may be a change in ENSO teleconnections, with an increased zonalization of anomalies. There is a suggestion that stronger trades, which have been suggested from observations and model data, resulting from a strengthening of the southeastern Pacific High and the equatorial trough in the eastern/central Pacific (Inoue and Bigg, 1995), will cool the eastern and central Pacific whilst the western Pacific might slightly

warm, with unstable ocean-atmosphere interactions amplifying this tendency (Latif et al., 1997). However, it has also been suggested that with global warming the size of the sea surface temperature anomalies during warm and cold events may not be significantly different from today (Tett, 1995).

2.8 The Evolution of ENSO events

The simplest explanation behind the evolution of ENSO events is that the ocean, with its great source of moisture and heat capacity, drives the whole system. In this theory the ocean-atmosphere system acts as a 'delayed oscillator' (Schopf and Suarez, 1988; Trenberth, 1996), with the previous ENSO event sowing the seeds for the following one (Graham and White, 1988). In the 'delayed oscillator' theory, the mechanisms necessary in the ENSO cycle are contained within the tropical Pacific (Zebiak and Cane, 1987). Off equatorial Rossby modes in the ocean along with reflections off the western boundary of the tropical Pacific provide a delayed feedback necessary to produce quasiperiodicity (Schopf and Suarez, 1988). In this delayed oscillator mechanism the prevailing easterly wind anomalies over the western Pacific, during cold events, force upwelling Kelvin waves, which propagate eastward causing cooling in the eastern Pacific, where the thermocline is shallow (Figure 2.6). These Kelvin waves are forced at speeds sufficient to cross the equatorial Pacific in two to three months, approximately 250 cm s^{-1} (Graham and White, 1988). The easterly winds in the western Pacific result in downwelling westward propagating Rossby waves, which have the strongest signals off the equator. The Rossby waves, which will move much slower than the Kelvin waves cross the equatorial Pacific in about nine months (Graham and White, 1988), then are reflected at the western boundary into downwelling Kelvin waves, which propagate eastward. Once these Kelvin waves have propagated far enough into the eastern Pacific they are able to affect the sea surface temperature. If the signal is strong enough, a sea surface temperature anomaly develops serving as a possible El Niño seed (Latif et al., 1993). At a certain point in time the thermocline in the east stops deepening, with an associated change in sea surface temperature, the warm event starts to decay and the cold event starts to develop (Chao and Philander, 1993). Modifications of this 'delayed oscillator' mechanism have also been used to describe the evolution of events. Latif et al. (1993) revealed that the ENSO cycle involves standing sea surface temperature anomalies and slow eastward propagation in the upper ocean

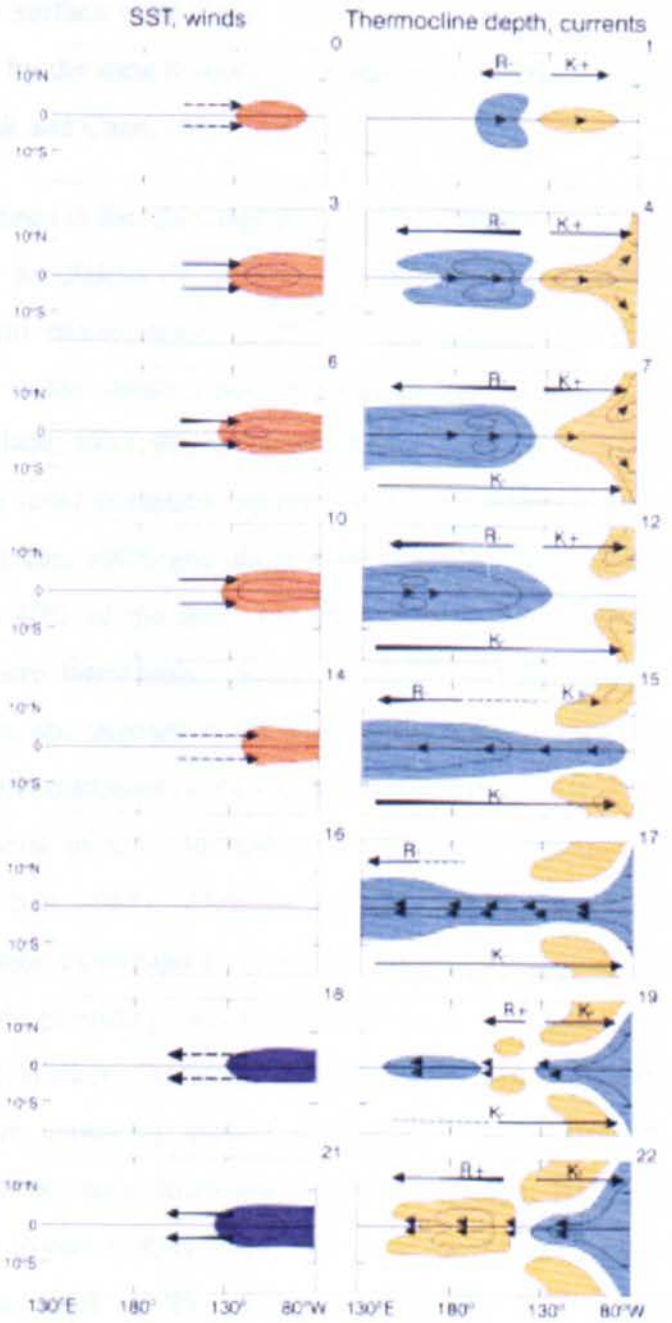

Figure 2.6 Schematic 'delayed oscillator' behaviour of a coupled ocean-atmosphere model over the Pacific basin in response to the introduction of a westerly wind anomaly across the Central Equatorial Pacific. In the left hand panels, arrows indicate anomalies (thickness indicating relative strength) and shadings indicating sea surface temperature anomalies (positive red, negative blue). In the right hand panels thin dashed and solid arrows are ocean current anomalies and thicker arrows labelled K+ and K-, R+ and R- indicate the longitudinal progress of positive and negative Kelvin and Rossby waves respectively (thickness of arrows indicates relative strength). Orange shaded anomalies are positive (deeper than average) and green shaded regions are negative (shallower than average) thermocline depth anomalies. Numbers outside each of the individual panels indicate the elapsed time in months since the anomaly forcing was applied to the model simulation (source: Allen et al., 1996)

heat content and the surface wind field. It has been suggested that the time scale between events is determined by the time it takes for warm water in the tropics to recharge the system (Wyrtki, 1985; Zebiak and Cane, 1987; Trenberth, 1991).

An alternative hypothesis is that the amplification of atmospheric variability such as the 40-50 day (Madden-Julian) oscillation (Trenberth, 1991) by air sea interaction may be responsible for the occurrence and enhancement of ENSO (Lau and Chan, 1985, 1988). Whereas the Southern Oscillation is the single most prominent signal in year-to-year climate variability (Rasmusson and Wallace, 1983; Philander and Rasmusson, 1985; Philander, 1990), the 40-50 day oscillation is the most dominant component of the intraseasonal variability of tropical convection (Lau and Chan, 1985) and oscillations occurring at 10-50 days have been found to contribute more than 40% of the daily variance in 500 hPa height over the mid- and high latitudes of the Southern Hemisphere (Kidson, 1991). The 40-50 day dipole oscillations, in anomalous convection, are oriented in the east-west direction, between the equatorial central Pacific and the maritime continent of Borneo and Indonesia. Thus, due to the proximity of the two systems, alterations in this oscillation are likely to lead to changes in the Walker circulation (Lau and Chan, 1985). When the dipole centre of the 40-50 day oscillation is over the Indian Ocean, major extratropical anomalies are found over the Asian sector, with the associated convection extending south-eastward over northern Australia towards New Zealand, affecting the Walker circulation and the South Pacific Convergence Zone (SPCZ). In contrast, when the centre is shifted eastward to the equatorial central Pacific the extratropical anomalies are most pronounced over the eastern North Pacific (Lau and Chan, 1985). Anyamba and Weare (1995) found that an enhancement of the 40-50 day oscillation occurred prior to the onset of the 1976, 1982/83 and 1986 warm events. However, enhancement of the oscillation also occurred during 1981, which was a non-ENSO year.

There are several theories behind the evolution of ENSO events involving the extra-equatorial regions. One theory behind the evolution is thought to be the Indian monsoon (Philander, 1983; Barnett et al., 1991; Trenberth, 1991). Trenberth (1984a) discovered that the La Niña event during the Global Weather Experiment (1978-79) occurred at the same time as anomalous monsoon circulation, with the monsoon intensity being below normal and the summer monsoon being almost two weeks late in arriving. Webster and Yang (1992) have

found that during the springtime the rapidly growing monsoon dominates the Walker circulation, however, during the winter the Walker circulation dominates the weaker monsoon circulation. It may be possible for the monsoon to modulate the ENSO cycle in the Northern Hemisphere spring when the ocean-atmosphere system is least robust (Trenberth, 1991) and so especially sensitive to outside influences, and thus affected through an anomalous trade wind regime (Webster and Yang, 1992; Nigam, 1994) (Figure 2.7). Normand (1953) found

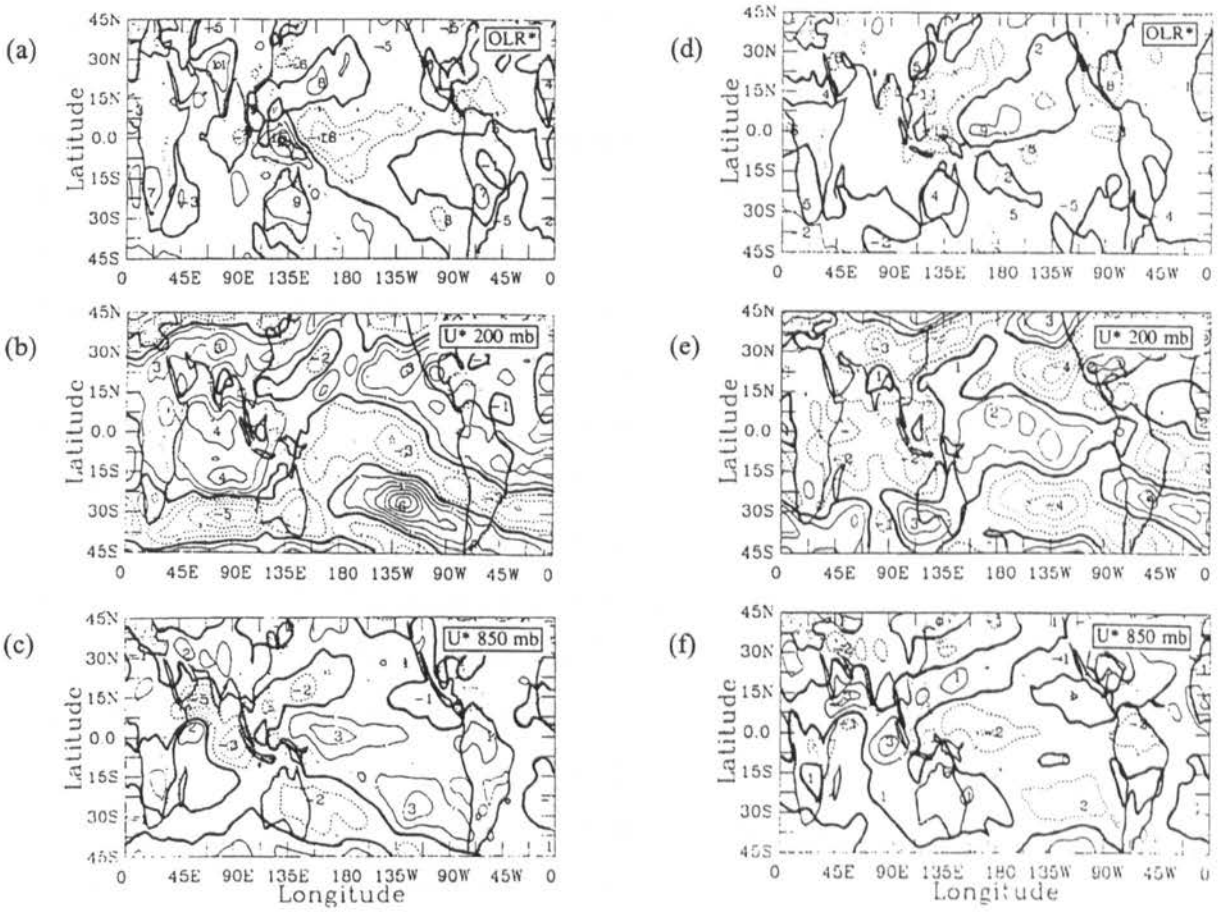

Figure 2.7 Composites of the anomalous out going longwave radiation (OLR) field and the anomalous 200 mb and 850 mb zonal wind fields for (a-c) the 'weak' monsoon years (1979, 1982, 1983, 1987) and (d-f) the 'strong' monsoon years (1984, 1985, 1986). Contour intervals are for 5 Wm^{-2} for OLR* and 1 ms^{-1} for the wind fields. The zero contours are bold (source: Webster and Yang, 1992).*

that there was a more significant correlation between the Indian monsoonal rainfall and the Southern Oscillation for the following winter, +0.8, than for the previous winter, -0.2, leading him to believe that the '*Indian monsoon...stands out as an active, not a passive feature in world weather*' (Normand, 1953, p469). Eurasian snow cover appears to be linked to

monsoonal rainfall in the following year, as excessive Eurasian snow cover is associated with a weak monsoon characterised by higher sea level pressures over India, a weaker Somali jet, weaker lower tropospheric westerlies and weaker upper tropospheric easterlies (Barnett et al., 1991; Klaßen et al., 1994; Vernekar et al., 1995). Eurasian snow cover thus appears to be a precursor to monsoon rainfall, which in turn is thought to be a precursor to the Southern Oscillation.

A second theory is that the semi-annual oscillation (SAO) plays an important role in the evolution of the Southern Oscillation. The semi-annual oscillation was identified by van Loon (1972a) as a half yearly wave in the pressure of the Southern Hemisphere. The semi-annual oscillation is a twice yearly oscillation in the position and intensity of the Southern Hemisphere circumpolar trough, which has been found to weaken and move equatorward in June and December, whilst contracting and intensifying in the austral spring and autumn (Meehl, 1987). There are two main aspects of the semi-annual oscillation, the 'coreless winter' over Antarctica and the annual cycle of sea surface temperatures and oceanic heat storage near 50°S. Thus the semi-annual oscillation could be linked to the Southern Oscillation or to the strength of the Indian monsoon (Meehl, 1991). Previous studies have shown a connection between the phase of the semi-annual oscillation in May-June-July and the beginning of an ENSO event. A more intense and expanded trough, at this time of year, in the midlatitudes of the South Pacific and Indian Oceans, as part of the seasonal cycle of the semi-annual oscillation, would weaken the subtropical high, which would reduce the trade winds (Kiladis and van Loon, 1988) leading to a warming of sea surface temperatures in the equatorial Pacific, whilst in the Indian Ocean, a weakening of the Mascarene high would be associated with a weaker Indian monsoon (Meehl, 1991). This association between the semi-annual oscillation and both the Southern Oscillation and the Indian monsoon could explain the linkages between these two events, as found by Nigam (1994). Van Loon and Shea (1985, 1987) have shown that the period of May-June-July is very important in the development of warm events, when the trough is strongest. Trenberth and Shea (1987) regard this mechanism as a central component in the evolution of the Southern Oscillation.

An alternative, and probably less dominant factor, thought to initiate ENSO events is the effect of the Indonesian sea surface temperatures, which have been found to be closely related

to ENSO (Nicholls, 1984). This region would be affected by anomalies in equatorial diabatic heating, resulting in an increase in the sea surface temperature, which would lead to a decrease in the atmospheric pressure of the region. This would consequently alter the strength and direction of the prevailing wind in the region, altering the strength of the trades, thus altering the mixing in the upper ocean and affecting the thermocline (Nicholls, 1984). However, the differential heating observed in the Indonesian region, as well as the atmospheric and oceanic anomalies in the south-western Pacific may actually occur as a result of the Indian monsoons, and so may be responsible for the propagation of the monsoon signal into the western Pacific, thus initiating the ENSO conditions along the equator. Kiladis and van Loon (1988) identified this propagating mechanism occurring between the Indian and Pacific sectors from year -1 to year 0 of both cold and warm events, which they found occurs as an eastward movement of below normal surface pressure from the Australasian region into the central Pacific for warm events, with a westward movement of above normal pressure from the central North Pacific into eastern Asia occurring at the same time.

2.9 ENSO Teleconnections

The impacts of ENSO, which are experienced in both marine and terrestrial environments, are thought to be extended to latitudes outside the equatorial belt by the rotation of the Earth, which is thought to cause a large quasi-stationary wave pattern which gives rise to substantial anomalies in the extratropical circulation (Rasmusson and Wallace, 1983), these anomalies then affect various aspects of the global climate through a series of 'teleconnections' (Trenberth, 1976). The term 'teleconnection', as popularised by Bjerknes (1969), is used whenever there is a shortage of physical explanations regarding a relationship within a very large data set, with possible time lags (Ramage, 1983). The term was first used in relation to tropical-extratropical links. Teleconnections are identified through the search for large correlation coefficients within large data sets, with the hope identifying spatially interdependent 'centres of action' (Trenberth and Paolino, 1981), through which it may be possible to identify a physical explanation for the relationship. Teleconnections have been used extensively in the study of ENSO related impacts, as the actual mechanisms behind the transfer of the ENSO signal globally are not yet known in any great detail.

(a)

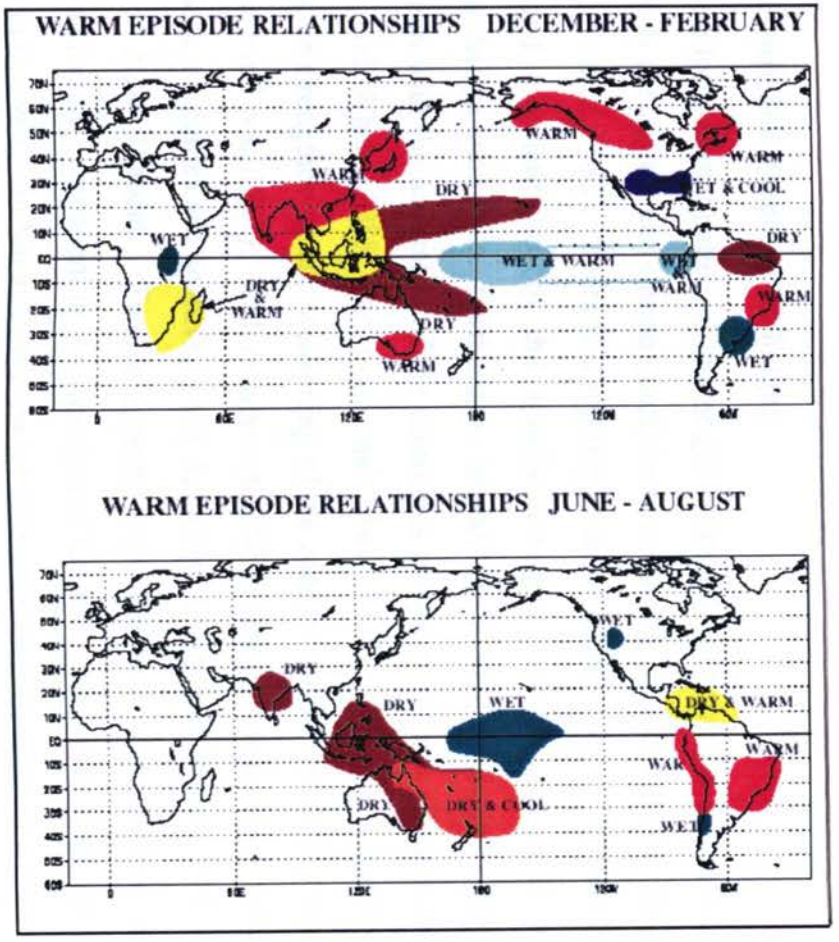

(b)

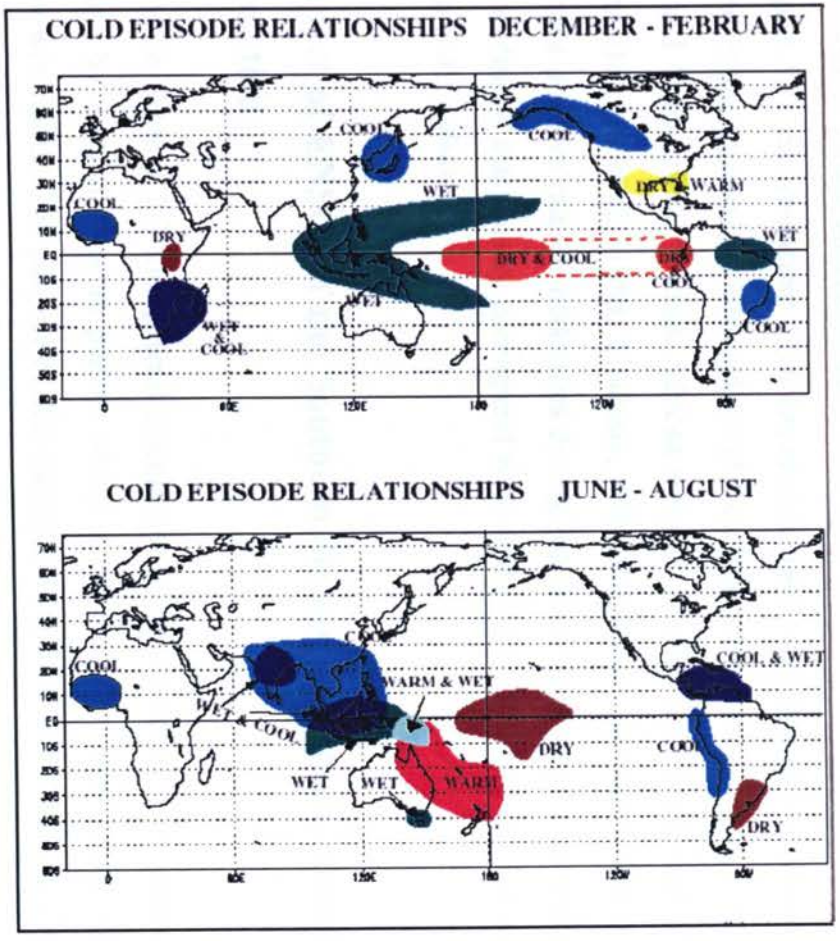

Figure 2.8 Major ENSO teleconnections during warm and cold events (source: Climate Prediction Center, NOAA http://nic.fb4.noaa.gov:80/products/analysis_monitoring/impacts/).

A large number of global teleconnections have been found to date, affecting all parts of the world (Figure 2.8). South-eastern USA has an increase in moisture in warm event years (Yin, 1994). The Indian monsoon (Normand, 1953) has less precipitation in the warm event years (Webster and Yang, 1992). South African summer rainfall is reduced markedly in warm events (van Heerden et al., 1988; Lindesay, 1988; Nicholson and Kim, 1997). Chile and Uruguay have positive rainfall anomalies during the developing stage of a warm event, and have dry conditions that closely correspond with cold events (Rutllant and Fuenzalida, 1991; Pisciottano et al., 1994).

2.10 Impact of ENSO on the Southern Hemisphere high latitude general circulation

As outlined in Section 2.3 the general circulation of the Southern Hemisphere climate is characterised by a zonal pressure pattern which is influenced by two strong jetstreams and three major wind belts. The purpose of this section is to review how these circulation features are affected by ENSO with particular focus on the Antarctic region.

2.10.1 Pressure and geopotential height

There is a uniform spatial pattern in the negative pressure correlations across Antarctica with the SOI, with the largest correlation coefficients occurring 12 months after the event peaks (Smith and Stearns, 1993). There is a significant out-of-phase positive relationship, between the high and low latitudes, of the zonally averaged monthly sea level pressure and geopotential height anomalies. Furthermore midlatitude anomalies display a negative out-of-phase relation with the anomalies of the subtropics and polar regions (Rogers and van Loon, 1982; Mo and White, 1985; van Loon and Shea, 1987). This is a barotropic pattern suggesting the strengthening and weakening of the zonal winds in alternating latitudinal belts (Rogers and van Loon, 1982). With reference to ENSO timing, a year before warm events sea level pressure anomalies are positive in the Antarctic, negative at around 50°S, and positive northeast of New Zealand. Twelve months later the anomalous pattern changes sign indicating a biennial component in the variation of the anomalies when linked to the SOI (van Loon and Shea, 1987). In the austral summer in the developing stage of a warm event there

are stable zonally symmetric anomalies in Southern Hemisphere circulation with increased height in low latitudes and decreased height in middle latitudes. However, in the austral winter preceding a warm event there is a more variable wave-train pattern of negative pressure anomalies extending poleward and eastward over the Pacific Ocean, associated with the developing stage of the event (Karoly, 1989). As sea level pressure and geopotential height anomalies in the Southern Hemisphere appear ahead of any in the Northern Hemisphere, it can be said that Australasian tropical-subtropical South Pacific region appears to either play an important role in the forcing of the Southern Oscillation (van Loon and Shea, 1987) or is extremely sensitive to minor climatic perturbations.

In the austral summer the pressure in east Antarctica is positively correlated with the pressure of the tropical Indian Ocean (van Loon and Madden, 1981). In Section 2.8 the effect of the monsoon on the evolution of ENSO events, and the links between the monsoon and the Walker circulation were outlined, and consequently it can be said that the correlations between east Antarctica and the tropical Indian Ocean are also correlations with the Southern Oscillation. During warm event summers there is an inverse relationship between the subtropical and tropical parts of the Pacific Ocean and the Pacific sector of the Subantarctic low-pressure belt, where pressure tends to be comparatively high. Furthermore, compared to cold events, stronger easterlies tend to occur in the Atlantic and Indian Oceans to the south of the Subantarctic trough in association with weaker polar easterlies in the Pacific Ocean during warm events (van Loon and Madden, 1981).

2.10.2 Temperature

There are significant regional contrasts in the nature of temperature anomalies across Antarctica with ENSO. Smith and Stearns (1993) have shown that the largest temperature correlations with the SOI appear to occur at Amundsen-Scott (the geographical South Pole) at a lag of 10 months, i.e. with the SOI leading, with the next five largest correlation coefficients occurring with lead times of 9 to 12 months (Smith and Stearns, 1993). Prior to the warm event peak the Ross and Amery Ice shelves had negative temperature anomalies, whilst the centre of the continent, from the Antarctic Peninsula to Dumont d'Urville had positive temperature anomalies, with the sign of these anomalies changing after the peak (Smith and Stearns, 1993). The lead time in some of these ENSO temperature correlations indicate that

the ENSO signal may be much more complex than first thought. There is either a weak temperature anomaly signal appearing over the Antarctic prior to the establishment of the circulation anomalies in the Pacific, or the climate of Antarctica is responsible for initiating or intensifying the events in the mid-Pacific. This observation agrees with that made by van Loon and Shea (1987) regarding the occurrence of Southern Hemisphere high latitude anomalies prior to the onset of ENSO.

One quarter to one third of the temperature anomalies in Antarctica in summer and winter are related to alterations in the 500 hPa hemispheric flow, although in the solstice seasons less of the variance is explained by this. When the 500 hPa westerlies are strong (weak) mainland Antarctic stations are colder (warmer) than normal whilst Peninsula temperatures are anomalously warm (cold) (Rogers, 1983). It has been thought that the geographical differences in temperature over Antarctica result in katabatic wind flows, which affect the 500 hPa hemispheric flow maintaining the New Zealand blocking high and the associated cut off low which consequently affect the western branch of the Southern Oscillation (van Loon and Shea, 1987; Smith and Stearns, 1993). The inverse of this mechanism is described in more detail in Section 2.11 in which it is shown how the New Zealand blocking high effects Antarctic sea-ice and katabatic surges. Instead of being an effect of ENSO on Antarctic climate this may actually be a mechanism by which Antarctica affects ENSO.

2.10.3 Synoptic scale activity

Synoptic scale activity concerns atmospheric airflow disturbances occurring over an area 1500-3000km in diameter over periods of 4-7 days (Barry and Chorley, 1987). This activity is linked to the larger planetary scale (longwave) behaviour in that the longwaves determine the latitudes of the cyclones.

In the developing stages of warm events there are more frequent major winter storms in Chile which are associated with blocking highs occurring around the Bellinghausen Sea. In this situation the blocking ridge is amplified and stays for longer than usual owing to a resonance effect with a wavetrain of geopotential height anomalies emerging from the central equatorial Pacific (Rutllant and Fuenzalida, 1991). Streten (1975) found a 20% increase in the cyclonic activity in the autumn, winter and spring of 1972 over the ocean to the west of Chile

accompanied by an eastward trend in the movement of the South Pacific cloud band. To the southeast of the South American continent the frequent cyclonic circulation leads to a dipole type sea level pressure anomaly structure, which changes sign from the year before to the year of the warm event. During warm events, when there is excessive rainfall in South America, waves develop in the southern circumpolar vortex, giving rise to the deformation or breakdown of the subtropical anticyclone and to an increase in the spatial variability of pressure (20 to 30°S) (Minetti and Sierra, 1989). These waves were not present during cold events. During cold events there is a tendency for cyclonic anomalies in the Bellinghausen Sea area, and anticyclonic anomalies in the southwest Atlantic. This anomaly is dipolar and of opposite sign to that for warm events (Rutllant and Fuenzalida, 1991). The alteration in the position and frequency of cyclonic events around Antarctica is thought to be responsible for the pressure and precipitation anomalies over the continent and its coastal margins as well as affecting the development and extent of polynyas. A polynya is an area of combined open water and thin ice surrounded by sea and/or land ice which alters the nature of the ocean-atmosphere heat and fresh water exchange (Gordon, 1988).

Antarctic precipitation variability has also been linked to ENSO events. In the South Pacific sector of Antarctica, for the period 1980-1990, there was a strong correlation between precipitation variability and ENSO. However, the region became anti-correlated following this period due to a strong east Antarctic ridging pattern which coincided with the start of the extended 1991 warm event (Cullather et al., 1996). The position of the Amundsen Sea low, itself a product of the large scale circulation, the South Pacific storm track and mass transport associated with Antarctic katabatic flows is thought to act as a catalyst in the ENSO precipitation variability (Cullather et al., 1996).

2.11 Impact of ENSO on Antarctic Sea-ice

Antarctic sea-ice extent plays a major role in the climate of the high southern latitudes (Simmonds and Jacka, 1995), so it is necessary to consider its interaction with the Southern Oscillation to gain a full picture of the large scale circulation. The sea-ice conditions around Antarctica are a product of the interaction between the large scale atmospheric circulation of the region and the ocean circulation characteristics, both of which are believed to be

modulated by ENSO (Carleton, 1988). Anomalous anticyclonic circulation and northerly flow components in the Weddell Sea area, typical in the spring exactly one year before a warm event, are consistent with the observations of reduced open water and greater ice-water concentrations occurring due to the convergence of pack-ice (Carleton, 1988). Twelve months later in the spring preceding a warm event peak, the amount of open water is related to a more cyclonic circulation, with southerly flow components in the Weddell Sea region, leading to divergence of the pack. Carleton (1988) indicates that there seems to have been a westward shift in the centre of the anticyclonic anomaly for warm events since about 1950, although the accuracy of the data prior to this period is questionable. The regions of ice growth around Antarctica are located to the west of the cyclonic centres, with the most rapid growth associated with the most intense centres (Cavalieri and Parkinson, 1981). Antarctic ice growth results from the advection of colder polar air and/or transport of the ice by the wind (Cavalieri and Parkinson, 1981).

Enhanced katabatic flows have been proposed as a likely candidate for explaining the northward sea-ice expansion. The sequence of events leading to katabatic wind surges has been outlined by Bromwich et al. (1993) (see Figure 2.9). Initially there is the development of a midtropospheric ridge over Wilkes Land (1), which results in the enhancement of the split jet and reinforcement of the New Zealand blocking high (2). Following this more frequent and/or intensified synoptic scale cyclones are steered towards the Amundsen Sea (3) where they become stationary inducing a pressure field with isobars parallel to the Transantarctic mountains (4), resulting in strengthened katabatic winds across the Ross Ice Shelf (5), leading to the expansion of the persistent polynya, just east of Ross Island. The implications of this sequence of events for the atmosphere circulation and climate have been discussed by King (1994). Specifically the sea-ice conditions will act in a positive feedback loop with the atmospheric circulation system. Due to the large albedo of ice compared to that of the open ocean, the surface radiation balance and thus climate is altered. Sea-ice concentrations may therefore amplify the magnitude of the climatic anomalies in Antarctica associated with ENSO. An alteration in the high latitude atmospheric circulation patterns resulting from ENSO interactions will effect the sea-ice distribution around the continent. However, the mechanisms behind this atmosphere to sea-ice association may actually be occurring in

reverse, where the association is an atmospheric response to ENSO induced variations in sea-ice distribution.

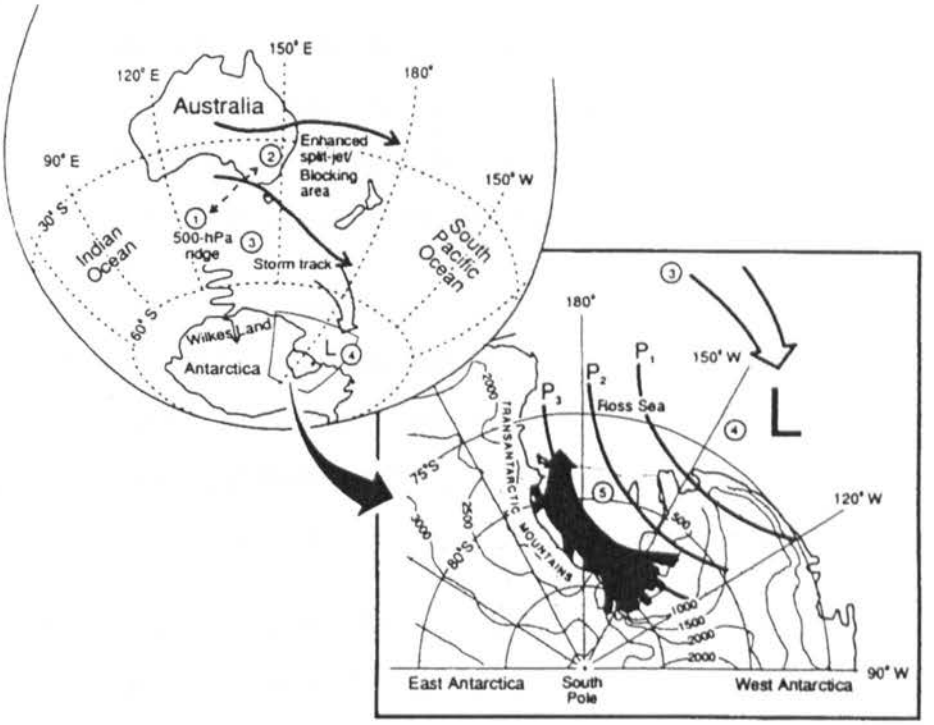

Figure 2.9 Schematic illustration showing the sequence of events associated with the evolution of katabatic winds. P_{1-3} are isolines showing the approximate orientation of isobars near the Ross Ice Shelf, the numbers are referenced in the text (source: Bromwich et al., 1993)

The climatic effects of ENSO in Antarctica may actually be amplified by the alteration in the oceanographic circulation around the continent, which subsequently affects the sea-ice conditions and hence the continental albedo (Streten and Pike, 1980).

The southward displacement of the sea-ice boundaries following the 1982 warm event has been related to strong northerly airflows associated with anomalously low pressure over the Bellinghausen and Amundsen Seas and unusually high pressure over the eastern Weddell Sea and the South Atlantic Ocean, during the winter following the warm event. This southward directed airflow, resulted in the displacement of the frontal zones around Antarctica, as well as the wind forced flow of surface waters (Priddle et al., 1988).

As well as associations with the wind field, sea-ice behaviour has been linked to sea surface temperature and SOI variation. Simmonds and Jacka (1995) identify four key sectors where

sea-ice has links with the SOI, these are the southwest Indian Ocean, the southwest and southeast Pacific Oceans and a sector to the west of the Ross Sea. Although in winter sea-ice in the southwest Indian and southwestern Pacific Oceans is highly correlated with the SOI values for the previous twelve months, there is little relationship between Atlantic sea-ice and the SOI. For the Australasian region the sea-ice appears to lead the SOI (Simmonds and Jacka, 1995). Overall there is a positive correlation between the sea-ice extent in the months from April to July and the SOI during the previous twelve months.

The sea surface temperature of the equatorial Pacific is inversely related to the sea-ice in the Ross and Weddell Seas, with a quasi-contemporary and a quasi-1.5 year lag respectively (Xie et al., 1994). This strong meridional oceanic oscillation exists between both sides of the South Pacific, the central equatorial Pacific and the Ross Sea, and is called the Southern Oceanic Oscillation (SOO) (Xie et al., 1994).

The sea-ice extent in the South Pacific is thought to vary due to changes in the lower tropospheric meridional circulation brought about by adjustments to the semi-annual oscillation (SAO) (Harangozo, 1995). This is because the semi-annual oscillation of the southern circumpolar trough controls the mean windfield and divergence / convergence characteristics of sea-ice (Hanna, 1996). Although the SAO may play a role in the evolution of the Southern Oscillation (Section 2.8) it is also thought that ENSO may control the SAO (Hanna, 1996).

2.12 Teleconnection Mechanisms

One of the most challenging issues relating to ENSO-Antarctic climate links is the identification of a teleconnection mechanism. A number of theories have been proposed concerning how the ENSO signal may be transferred from equatorial areas to higher latitudes (Figure 2.10). The first is that the ENSO signal may be transferred through the alteration of the midlatitude trade winds, which in turn have impacts on the Intertropical Convergence Zone (ITCZ) and the South Pacific Convergence Zone (SPCZ) (Trenberth, 1991). This was also found by Aceituno (1988) who discovered that during warm events relatively high pressure occurs in the tropical South Atlantic, which is consistent with the displacement north of the equatorial low pressure trough which in turn affects the trade wind flow; during cold

events the opposite occurs. This mechanism was found by Aceituno (1988) to be an important factor in the interannual climate variability of the entire South American continent. It has therefore been suggested as one possible mechanism by which ENSO affects extratropical latitudes.

Secondly, ENSO-Antarctic climate teleconnections may reflect a Rossby wave-train that propagates along a great circular path into higher latitudes from the equatorial region (Horel and Wallace, 1981), as the heating of the tropical troposphere during ENSO events will excite these large scale planetary waves (Philander, 1983), which in turn will effect the climate of the whole hemisphere. This theory links with the work of White and Peterson (1996) who have found that the sea surface temperature anomalies in the western subtropical South Pacific spread south and eastward into the Southern Ocean. From here the anomalies propagate eastward, mainly due to the Antarctic Circumpolar Current, giving rise to an oceanic feature known as the Antarctic Circumpolar Wave. In association with this wave sea level pressure, wind stress, sea surface temperature and sea-ice extent anomalies propagate eastward with the circumpolar flow with a period of 4-5 years, taking 8-10 years to encircle the pole (White and Peterson, 1996). Due to Ekman layer flow, from the prevailing easterly winds, the anomalies spread northward into the subtropics, branching off into the southern Peru current, the southern Benguela current in the eastern South Atlantic and into the South Indian Ocean (White and Peterson, 1996). This 4-5 year periodicity ties in with the ENSO periodicity (Section 2.5.2) which is approximately 4 years (Trenberth, 1976; Trenberth, 1984b).

A few studies have been carried out to look at the propagation of mean sea level pressure anomalies from the tropics to the mid- and high latitudes of both hemispheres. Krishnamurti et al. (1986) found that both zonal and meridional propagation occurred on 2 to 6 year as well as decadal timescales between the south and north poles. Barnett (1985) suggested that sea level pressure anomalies were propagated from the Indian to Pacific regions. Barnett (1988) looked at the propagation between the tropics and midlatitudes finding that the propagation occurred in an anticlockwise trajectory. These studies have begun to look at the propagation of the ENSO signal, however this is an area still in need of further examination.

An alternative explanation relates to the sea surface temperature and Walker Circulation interactions. During warm events anomalous sea surface temperatures in the tropical Pacific

may lead to a weakening of the Walker Circulation, which is thought to cause an intensification of the neighbouring Hadley circulation (Trenberth, 1976; Philander, 1990; Oort and Yienger, 1996) which would transport increased momentum poleward to intensify the midlatitude westerlies (Bjerknes, 1966; Kidson, 1975) thus affecting the locations of surface cyclones and upper-level waves in the high southern latitudes (Rogers, 1983).

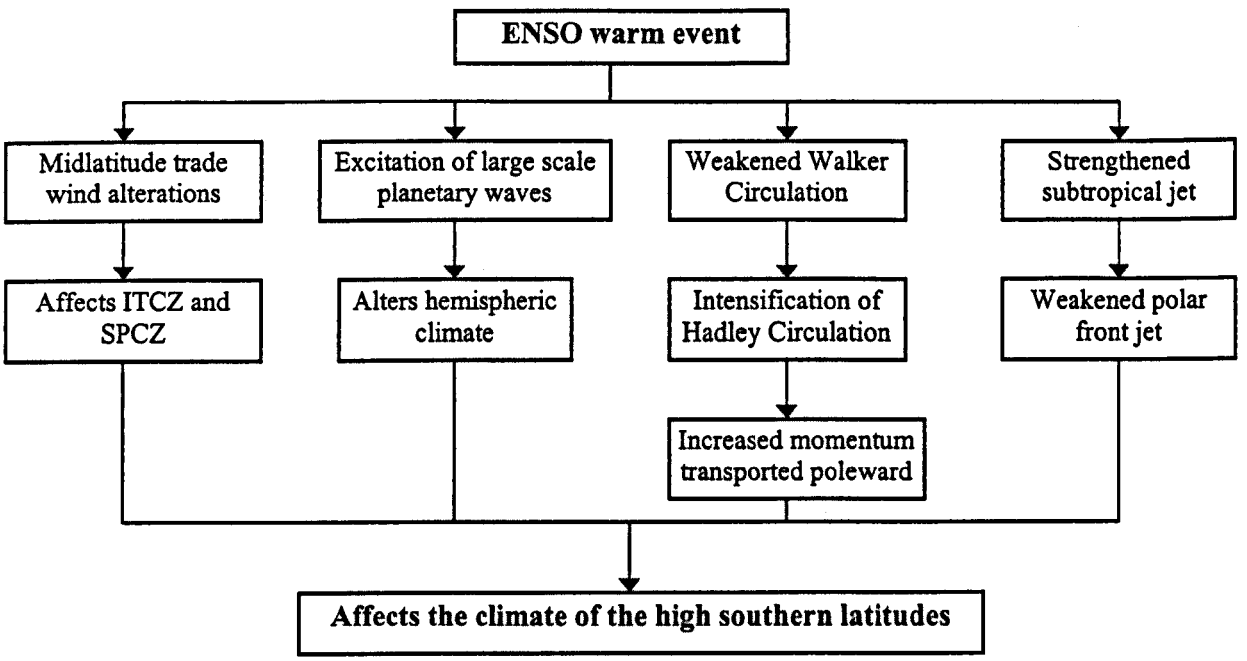

Figure 2.10 Diagram illustrating the mechanisms by which the ENSO signal reaches the high latitudes of the Southern Hemisphere.

The role of Southern Hemisphere jets as a propagation mechanism has also received some attention. Pisciottano et al. (1994) have suggested that it is the position of the subtropical jet stream that plays a key role in determining the Southern Hemisphere extratropical teleconnections, as this would explain the majority of the rainfall anomaly patterns that they found for southeastern South America. Chen et al. (1996) suggested that variations in the split jet effect the poleward propagation of the ENSO signal via the SPCZ. During a warm phase the SPCZ and the subtropical jet are strong, whilst the polar front jet is weak. Conversely, during a cold event the southwardly displaced SPCZ and subtropical jet are weak whilst the polar front jet is strong (Chen et al., 1996). As the position of the split jet influences the tracks of cyclones and anticyclones in the Antarctic region (Sinclair, 1996), during a cold event there is an increase in poleward cyclonic activity, with two possible sources: the storm track from south of Australia (Streten and Troup, 1973) and storms of

subtropical origin leaving the southwardly displaced SPCZ (Vincent, 1985). During the Global Weather Experiment (1978-79), which was a weak La Niña event, there was an exceptionally deep circumpolar trough, an increase in westerlies between 45-70°S, a southward shift in the main westerly jet and a considerably enhanced and southward displaced polar jet, during the summer, confirming the supposition of Chen et al. (1996), although there was a weaker subtropical jet in winter (Trenberth, 1984a). However, the actual mechanism responsible for the teleconnections between the tropical Pacific and the high latitudes of the Southern Hemisphere may be a combination of some or all of these factors, as the atmosphere is a complex interacting system.

2.13 Research gaps and approach

The literature review has revealed, through the limited number of studies conducted to date, the effects of ENSO on the climate variability of Antarctica. These studies consider the anomalies associated with circulation (Trenberth, 1980; van Loon and Madden, 1981; Carleton, 1988), pressure and temperature (van Loon and Madden, 1981; Smith and Stearns, 1993), synoptic activity (Streten, 1975; Bromwich et al., 1993), geopotential height (Mo and White, 1985; Karoly, 1989), moisture convergence (Cullather et al., 1996), sea surface temperature (van Loon and Shea, 1987) and sea-ice (Bromwich et al., 1993; Simmonds and Jacka, 1995; Gloersen, 1995). Although these studies have detected an ENSO signal, they are limited in the number of variables they consider as well as the length of record used. The majority of these studies combine the events in composites. However, as described earlier, ENSO events are very variable in their evolution and structure, so their impacts will reflect these variations. Therefore, as well as studying composites, it is imperative that the individual events are studied in order to gain an appreciation of the range of possible teleconnection mechanisms that may exist.

There are a number of unresolved issues regarding ENSO and the high southern latitudes, the most important of which is identifying the propagation mechanism by which the signal reaches Antarctica. As outlined above, a number of suggestions have been put forward regarding teleconnection mechanisms (Section 2.12). The purpose of this research, therefore, is to undertake in-depth analyses of a number of ENSO events in order to identify the exact

nature of ENSO-Antarctic climate teleconnection mechanisms and the related atmospheric processes. In doing so, this research will attempt to answer the question whether a single mechanism is, or a combination of mechanisms are, responsible for the propagation of climate signals between the Southern Hemisphere low and high latitudes.

CHAPTER 3

METHODOLOGY AND DATA ANALYSIS

3.1 Introduction

The methodology of this study is based on the five main objectives, identified in Chapter 1. These are:

1. *To explore further the effect of ENSO on the climate variability of Antarctica, with special reference to the Antarctic Peninsula.*
2. *To assess whether there is a propagation of anomalies between the low and high latitudes through an ENSO sensitive meridian.*
3. *To identify the possible movement of sea level pressure anomalies in the Southern Hemisphere on a spatial scale, during both ENSO and non-ENSO events.*
4. *To uncover the spatial signals in the phases of the first harmonics of 500 hPa height, temperature and mixing ratio anomalies, and from the height anomalies identify teleconnections in the Southern Hemisphere.*
5 *To consider the role of the jetstreams in the propagation of the ENSO signal between the tropics and high latitudes of the Southern Hemisphere.*

The aim of this study is to use these objectives to discover the nature of the response of the Antarctic climate to ENSO, with the ultimate aim being to identify mechanisms behind this signal propagation. Figure 3.1 shows the structure of this chapter with respect to the methodology used to fulfil these objectives.

3.2 Data

3.2.1 Station Data

In order to search for ENSO signals in the surface climate of Antarctica, data was required that covers a variety of ENSO events. Thus, in choosing stations to use it was necessary to

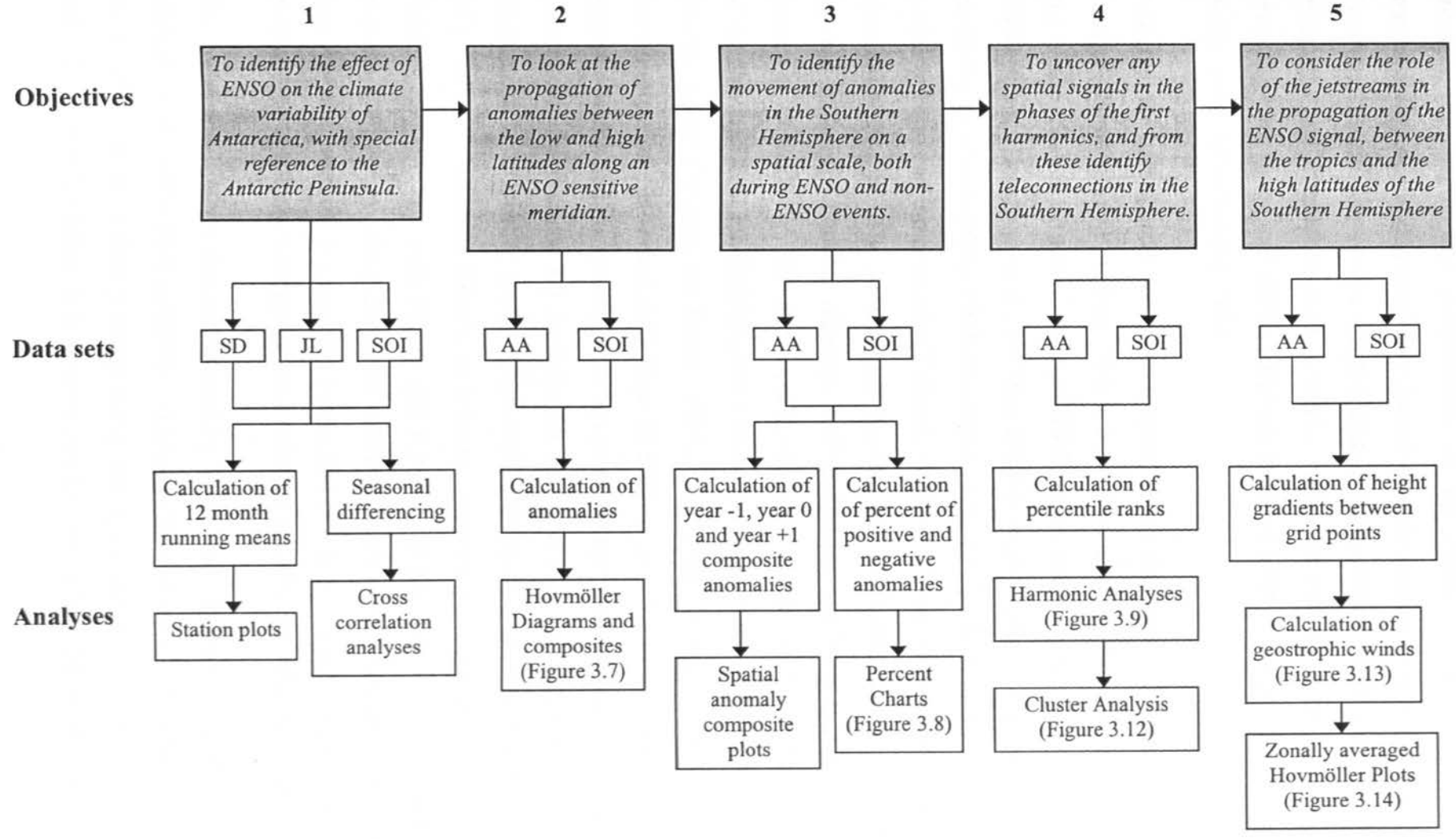

Fig 3.1 Objectives and methodology used in this study. Where SD is station data, JL is the Jones and Limbert data set, SOI is the Southern Oscillation Index and AA are the Australian Bureau of Meteorology Analyses.

consider the length, and completeness of the record. Due to the remoteness and inaccessibility of the continent only limited climate records exist, only about thirty staffed Antarctic climate and weather stations exist, the majority of which are located on the coast (Braganza and Simmonds, pers. comm.). Most of the Antarctic stations have records extending back to the mid-1950's, although there are a few extending back to the 1940's, and in the case of Islas Orcadas, 1903.

Although the hemispheric scale is considered in this study particular attention is given to the Antarctic Peninsula (AP) region. This is because it occurs to the south of the eastern Pacific, one of the 'centres of action' during ENSO events, and has been shown to demonstrate an ENSO signal (Houseago et al., 1997) in addition to possessing a high degree of interannual variability of climate (King, 1994; McGregor et al., 1997). Also, as the Peninsula is the most northerly region of the continent (Taljaard, 1972) it is likely to be affected by lower latitude circulation systems. The AP analyses focus on two bases administered by British Antarctic Survey; Halley and Faraday, although in 1995 Faraday was 'sold' to the Ukraine. Halley is located at 75 °S 26 °W, 30m above sea level (Table 3.1) about 10 km from the seaward edge of the moving Brunt Ice Shelf (Figure 3.2), and is the most southerly of the British Antarctic Survey stations (Wattam and Turner, 1995). Halley has been periodically relocated over the recording period. However, sites have all been located within approximately 10 km of the present position and the resulting data has been homogenised (Harangozo and Colwell, 1995). Continuous observations are available for Halley at 3 hourly intervals from January 1957 (Harangozo and Colwell, 1995). Continuous observations are available for Faraday (Table 3.1), formerly Argentine Islands, at 3 hourly intervals from January 1956 (Harangozo and Colwell, 1995). For both Halley and Faraday, monthly station data comprising station pressure, temperature, cloud cover and windspeed were used in this analysis. Halley upper air data was also used for two pressure levels, 850 hPa and 500 hPa height, comprising relative humidity, temperature, windspeed, wind direction and 850-500 hPa thickness.

The Jones and Limbert data set, as used by Smith and Stearns (1993), was also used in this analysis, to provide a more extensive coverage of the continent. This data set consists of data for monthly mean surface pressure (hPa) and temperature (°C) for 29 manned Antarctic stations. Antarctic climate data is notorious for having bad data points (Smith and Stearns,

1993), however, Jones and Limbert reviewed the accuracy of their temperature and pressure data set and removed the erroneous values prior to release (Jones and Limbert, 1987). Seven stations were chosen for this study, based on the length and completeness of their record, and their distribution around the continent. These stations are Amundsen-Scott, Casey, Mawson, McMurdo, Mirnyy, SANAE and Vostok (Table 3.1).

Station	Location	Height above sea level
Halley	75°S 26°W	30m
Faraday	65°S 64°W	11m
Amundsen-Scott	90°S 180°W	2835m
Casey	66°S 111°E	12m
Mawson	68°S 62°E	8m
McMurdo	78°S 167°E	24m
Mirnyy	67°S 93°E	40m
SANAE	70°S 2°W	30m
Vostok	79°S 106°E	3486m

Table 3.1 Location and elevation of Antarctic stations used in this analysis.

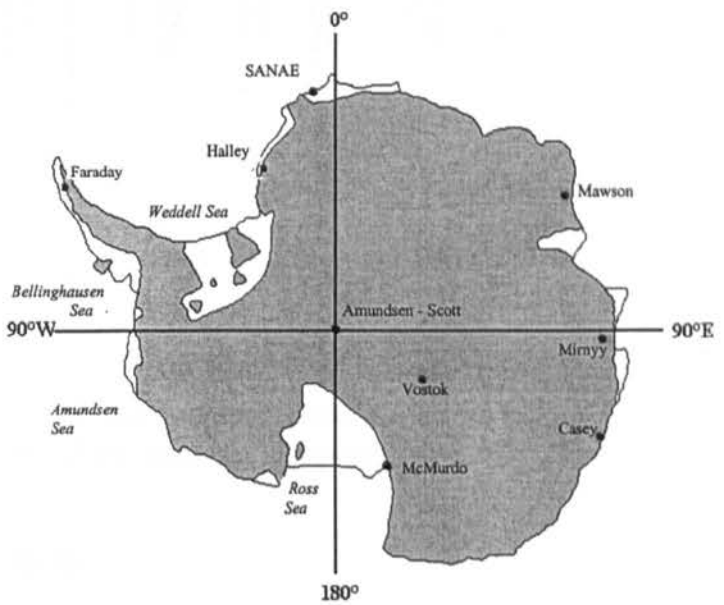

Figure 3.2 Map of Antarctica showing the location of the stations used in this study

It was not seen as necessary to consider upper air data for a variety of stations around the continent, in the analysis of the Antarctic climate, as this is incorporated in the later part of the study when analysis data is used for the entire Southern Hemisphere.

3.2.2 Southern Oscillation Index

The Southern Oscillation Index (SOI) used here is the Climate Analysis Centre (CAC) version, described in detail in Section 2.6, obtained from the Climate Prediction Center (at http://nic.fb4.noaa.gov/data/cddb/cddb/soi). This SOI data set consists of monthly values covering the period from 1951 to 1995 (Figure 3.3). SOI values are negative (positive) during a warm El Niño (cold La Niña) phase of the ENSO cycle.

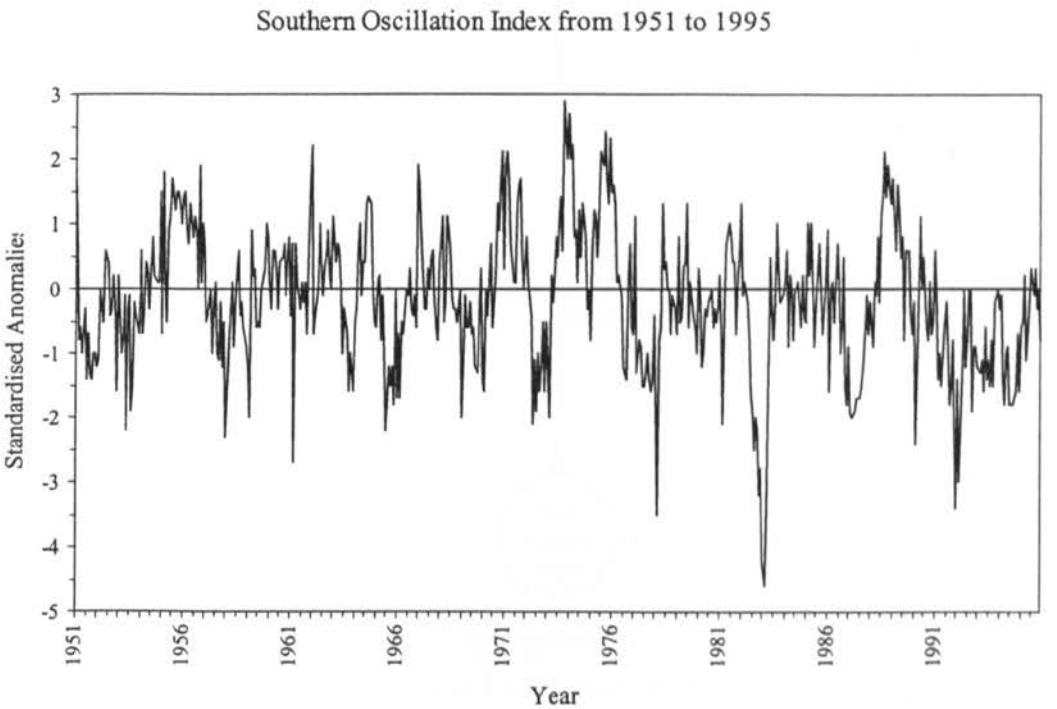

Figure 3.3 Time series of the Southern Oscillation index from 1951 to 1995, Tahiti minus Darwin normalised sea level pressures, in standardised units.

3.2.3 Hemispheric Data

Due to the sparse nature of the Southern Hemisphere observational network, hemispheric analysis data is useful for studying the variability of hemispheric climate. These analyses use observations by ships and aircraft as well as satellite data (both subjective and vertical temperature profile radiometer data) and manual intervention, to help fill in the data sparse regions such as the oceans (Trenberth, 1979). There are a variety of hemispheric analysis data sets available that include the South African, the U.S. National Meteorological Center and the Australian Bureau of Meteorology Analyses (AA). The South African hemispheric analyses

were not used in this study as they were found by Trenberth (1979) to have systematic errors over Antarctica, especially in the Australasian sector whilst the U.S. National Meteorological Center (NMC) hemispheric analyses were found to have errors in geopotential height of several hundred metres in and around Antarctica (Trenberth, 1979). However, the AA were found by Trenberth (1979) to be the best set available for the Southern Hemisphere.

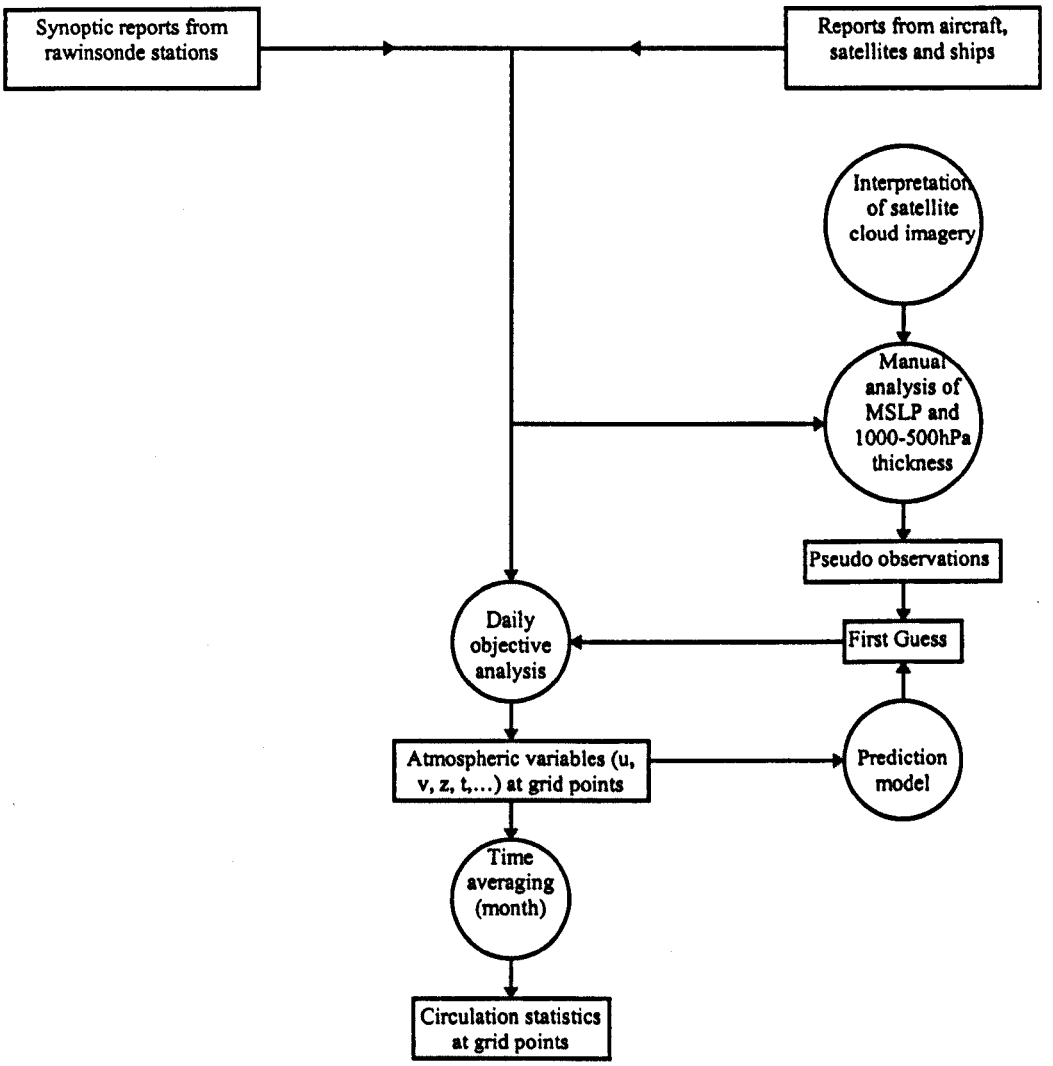

Figure 3.4 Flow diagram illustrating the processing scheme used for compiling the Australian analyses (source: Karoly and Oort, 1987).

The AA daily analyses are a product of a four dimensional assimilation of the meteorological observations that are used to initialise global forecast models. The data base used in the analyses consist of ship and surface observations, radiosonde and rawinsonde data, drifting ocean buoy data and lower level cloud data, when available, and supplemented from 1976 and 1979 respectively with vertical temperature profile radiometer (VTPR) data and second

generation sounding data from Tiros N/NOAA A-G series satellites (Le Marshall et al., 1985). The analysis scheme for this data set is given in Figure 3.4. Assessments of the utility of these analyses for large scale climatological studies (Trenberth, 1979; Swanson and Trenberth, 1981a, 1981b; Le Marshall et al., 1985; Karoly and Oort, 1987) have shown that monthly mean fields are more reliable than daily fields, as deficiencies in low latitude temperature and height fields, especially below the 850 hPa level, are a problem when daily data is used. Table 3.2 gives the mean differences between the daily AA for geopotential height and reported observations from '*Monthly Climatic Data of the World*' (Swanson and Trenberth, 1981a), illustrating the errors involved when daily data is used.

The AA 700 and 500 hPa height, temperature and 500 hPa mixing ratio (the ratio of the mass of water vapour to the mass of dry air with which the vapour is associated) data were obtained through the British Antarctic Survey and were used in this study, to look at the movement of the ENSO signals across the whole of the Southern Hemisphere. The study utilises the daily values and monthly means of the AA daily analyses obtained for 1100 and 2300 U.T.C., configured on a five degree grid, for the entire Southern Hemisphere for the period January 1973 to June 1994.

	Level (hPa)				
Station	850	700	500	300	200
Rapa Island (28°S 144°W)	-0.5 ± 1.2	1.8 ± 1.5	-0.3 ± 2.3	-8.2 ± 4.2	-14.8 ± 5.6
Gough Island (40°S 10°W)	0.3 ± 1.6	4.2 ± 1.9	-0.5 ± 2.8	0.1 ± 4.7	4.3 ± 5.4
Easter Island (27°S 109°W)	8.6 ± 2.7	22.1 ± 3.9	20.1 ± 6.3	22.9 ± 10.6	39.5 ± 13.8
Rio Gallegos (52°S 69°W)	-13.8 ± 5.7	-12.7 ± 6.7	-8.0 ± 11.6	-17.1± 15.4	-24.7 ± 18.4

Table 3.2 Differences between the Australian analyses heights and reported observations for selected stations with 95% confidence intervals (gpm) (source: Swanson and Trenberth, 1981a).

One of the main problems encountered in this study with the use of AA data was missing files. However, as the files were daily files the missing data was on a temporal rather than a spatial scale, thus there was no problem with missing values in 'centres of action'. Due to the

presence of missing files (Table 3.3) it was necessary to replace the missing values prior to

year	total number of files possible	number of files present	number of files missing
1973	730	623	107
1974	730	728	2
1975	730	716	14
1976	732	730	2
1977	730	722	8
1978	730	724	6
1979	730	693	37
1980	732	726	6
1981	730	709	21
1982	730	728	2
1983	730	730	0
1984	732	732	0
1985	730	730	0
1986	730	724	6
1987	730	730	0
1988	732	732	0
1989	730	730	0
1990	730	715	15
1991	730	726	4
1992	732	732	0
1993	730	727	3
1994	366	366	0

Table 3.3 The number of missing data files within the analysis data for each year.

analysis. As the files were missing on a temporal scale, rather than a spatial scale, linear interpolation was used to replace the missing days. For this the following equation was used:

$$x_0 = \frac{(x_1 + x_{-1})}{2} \tag{3.1}$$

where x_0 is the missing value, x_{-1} is the value preceding the missing value and x_1 is the value following the missing value. This interpolation technique is the most appropriate for the time series as it only involves the preceding and following values, thus not masking any signals within the data series. A maximum limit beyond which missing data would not be replaced was determined as 5 days as this was the scale used to calculate anomalies described in detail below.

3.2.4 Data processing

The station climate data used in the study has been left largely intact, with limited data processing. The data was plotted in order to identify whether there were any inconsistencies within the data. This was found not to be the case. To look for trends within the station data for both the Halley and Faraday stations and the stations selected from the Jones and Limbert data set, twelve month running means were calculated. To allow for comparison twelve month running means were also calculated for the Southern Oscillation Index. The timing of the running mean was taken as the midpoint between the values used i.e. the running mean for June 1986 was the mean of the values from January to December 1986. This manipulation of the data removed any bias from inaccuracies within the data records. As well as twelve month running means seasonal differencing was applied to the data set to remove the annual cycle prior to cross correlation analysis (Section 3.3). Seasonal differencing uses the difference between the series values and those 12 months earlier.

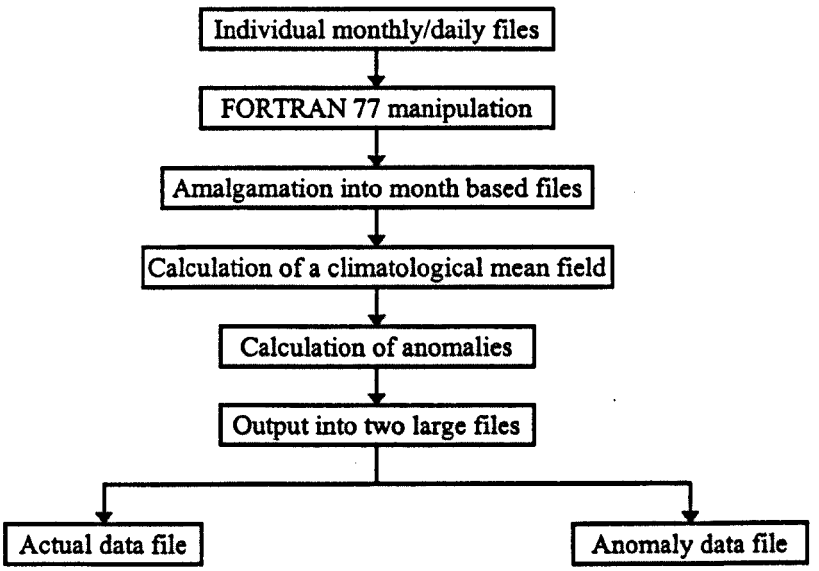

Figure 3.5 Diagram illustrating the steps involved in processing the hemispheric analysis data.

The Southern Hemisphere gridded analyses consist of individual monthly and daily files. Prior to using the data, it was therefore necessary to manipulate these files using FORTRAN 77 programs in order to produce one large data set; these FORTRAN programs are given in Appendix 1. Initially the monthly data was amalgamated into twelve month based files to make them more manageable (Figure 3.5). Individual monthly mean fields were constructed

from these twelve files for 500 hPa and 700 hPa height and 700 hPa temperature for the 22 year period. A 22 year monthly climatological mean field was also prepared and used to calculate monthly anomaly fields. Anomalies were calculated for each 5° grid point, using the following equation:

$$a = x - \bar{x} \tag{3.2}$$

where x is the actual value, $\bar{x}$ is the monthly mean and a is the anomaly value. It was necessary to calculate the anomalies, as this process removes the large annual cycle in the climatic data which would mask the ENSO signals (Smith and Stearns, 1993). Following the calculation of anomalies the monthly anomaly and actual data were written out to two separate files.

As gridded daily data for the entire Southern Hemisphere is logistically difficult to manipulate 5 day averages were calculated. This filtering of the data, using 5 day means, eliminated the short and meso-scale waves, leaving the long and very long waves (Neale and Trenberth, 1978) which are of interest in this study. Following anomaly calculation the 5 day anomalies were subject to the same data processing protocols as the monthly data (Figure 3.5).

Composite or mean warm and cold event data files were also calculated, using both the monthly and 5 day data, for the purposes of inter-event comparison and assessing event uniqueness. These composites were created based on the timing of the warm and cold events peaks (Table 3.4). The warm composite comprised the years 1976, 1982, 1986 and 1991 warm events, whilst the cold composite comprised the years 1975, 1978 and 1988. Composites were constructed for a 36 month period; from 12 months prior to the event peak, to 24 months after. It was decided to use an asymmetric period as this would allow the ENSO signal both prior to and following the event to appear, as well as the return to 'normal' conditions following the event. It was also seen as necessary to increase the time following the event peak to allow the prolonged 1991 warm event to be compared to the other warm events. The events analysed are those as identified by Carleton (1988), Trenberth (1991) and Wang (1995), however, the classification of events tends to vary from author to author (Klaßen et al., 1994). Event peaks were determined by locating the Southern Oscillation Index (SOI) maximum (cold) or minimum (warm). It can be seen in Table 3.4, that the peak

of the 1982/3 event is late in the year, a product of its anomalously late initiation and differing nature compared to the other events (Rasmusson and Wallace, 1983). As the data set only extends back to early 1973, the 1972-73 warm event was not included in the analysis.

Year	Event type	Identified by	Event Peak
1975	Cold	FM, KD, HR	September 1975
1976	Warm	FM, LS, KD	September 1976
1978	Cold	FM, LS	November 1978
1982	Warm	FM, LS, KD, HR	February 1983
1986	Warm	FM, KD	December 1986
1988	Cold	FM, KD, HR	September 1988
1991	Warm	FM	January 1992

Table 3.4 The ENSO events and peaks used in this study. These ENSO events have been identified by Fraedrich and Müller (1992) (FM), van Loon and Shea (1985) (LS), Kiladis and Diaz (1989) (KD) and Halpert and Ropelewski (1992) (HR) (adapted from: Klaßen et al., 1994).

3.3 The effects of ENSO in Antarctica

There are two approaches taken in searching for the effects of ENSO in Antarctica, a qualitative approach, the time series plots, and a quantitative approach, the cross correlation analyses (Figure 3.1 column 1). Twelve month running means for each of the variables for each station were plotted against the twelve month running means of the SOI, using Excel, to identify the associations between the data sets, as these allow the base states of the data sets to be compared by removing the seasonal cycle.

A cross correlation approach was adopted in the search for ENSO-Antarctic climate links. This involved using a seasonally differenced time series for each of the variables for each station (Table 3.1). The cross correlation analysis with the SOI, carried out in SPSS, used Pearson's product moment to identify associations between the data sets. This cross correlation methodology is similar to that used by Smith and Stearns (1993) who used the same data set. However, in this study seasonal differencing of the data set is carried out rather than using a twelve month running mean. It is hoped that this methodology may reveal more of the interactions. This study also considers cross correlation plots rather than just using the most significant correlations, thus allowing the patterns involved in the interactions to be seen more clearly. Cross correlations were constructed for the station data leading the SOI by 15 months to the station data lagging the SOI by 15 months. This 31 month time step was used

to gain the best indication of the two year ENSO cycle and to identify the biennial tendency in the response of the Antarctic climate to ENSO.

3.4 The propagation of anomalies between low and high latitudes

Pressure, temperature and mixing ratio anomaly fields were analysed using a form of Hovmöller diagram. Hovmöller (1949) first used these diagrams to identify the movement of troughs and ridges over time, however, they have also been used to study the deviation in zonally averaged height and wind components (Trenberth, 1979), changes in eddy momentum fluxes (Chen et al., 1996) and the movement of sea surface temperatures anomalies (Li, 1997) over time. Hovmöller analyses are very useful in identifying movements of anomalies over time over a selected latitudinal or longitudinal band. Traditionally, Hovmöller diagrams plot longitude and time while holding latitude constant (Hovmöller, 1949). However, in this analysis, longitude is held constant while time and latitude vary. This approach is taken because it is the propagation of anomalies from low to high latitudes over time that is of interest; the second study objective (Figure 3.1 column 2). The Southern Hemisphere meridian chosen for the construction of these Hovmöller diagrams was 230° (130°W). This meridian was chosen as it crosses a major centre of action 'upstream' of the Antarctic Peninsula, with strong correlations existing between this region and the Antarctic Peninsula climate (Figure 3.6). It is also a region of great climatic variability with maximum correlation with the Southern Oscillation Index (Jones and Simmonds, 1994; Houseago et al., 1997, 1998). The Hovmöller charts were constructed for each of the warm and cold events shown in Table 3.4 using UNIMAP (Figure 3.7), a UNIX plotting package. Bilinear interpolation was used to interpolate between the 5° grid squares. As monthly anomaly data was used in the Hovmöller analyses, only the planetary scale patterns were revealed as shorter wave trains cannot be captured by this temporal scale (Trenberth, 1978).

Hovmöller diagrams were constructed for a 36 month period, as described in Section 3.2 for four warm (El Niño) and three cold (La Niña) events (Table 3.4).

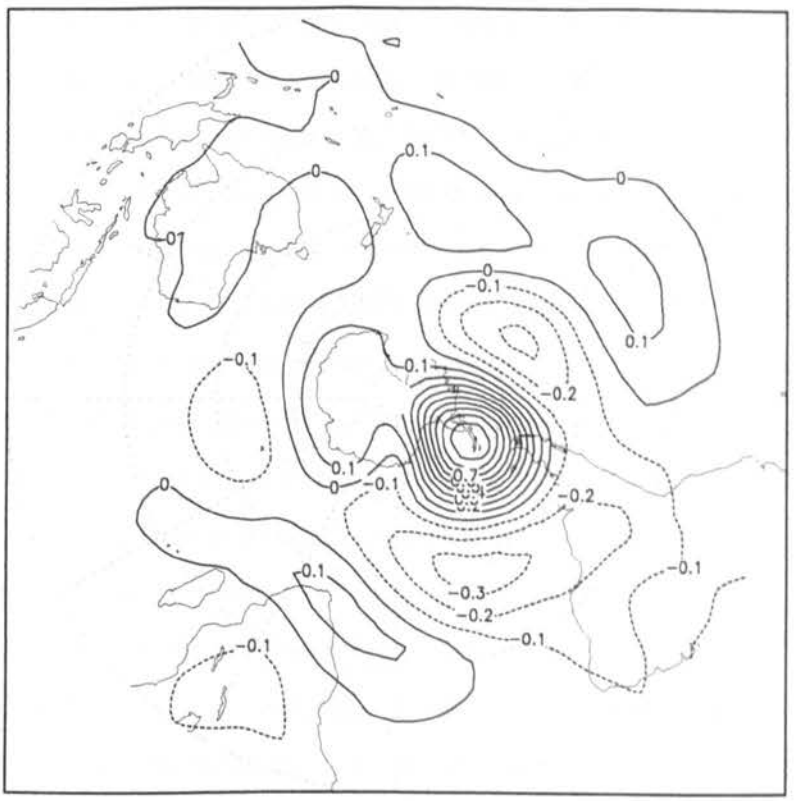

Figure 3.6 The correlation between 500 hPa height anomalies at Faraday, on the Antarctic Peninsula, and the entire Southern Hemisphere

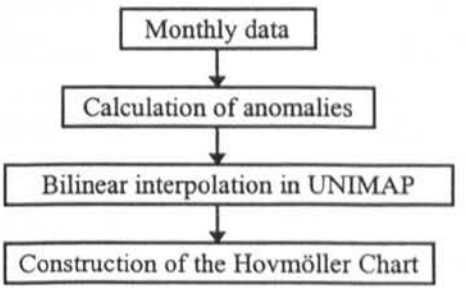

Figure 3.7 Flow diagram illustrating the procedure involved in constructing the Hovmöller diagrams.

3.5 Spatial Dynamics of Anomalies

To corroborate the underlying patterns found from the Hovmöller charts, annual spatial anomaly composite charts were constructed for year-1, year 0 and year +1 for 500 hPa and 700 hPa height and 700 hPa temperature (Figure 3.1 column 3). The anomalies were calculated using the long term mean fields, as for the Hovmöller diagrams. Based on the timing of the event peaks, identified in Table 3.4, annual mean composite charts were constructed, using UNIMAP, for year -1, year 0 and year +1 for both warm and cold events. In order to extend this analysis and to identify the underlying spatial trends in the movement of anomalies in both ENSO and non-ENSO events, spatial percentage anomaly charts for sea level pressure, from the 5 day data were constructed. The percentage anomaly charts show the percentage of 5 day periods over a 3 month period for which either positive or negative anomalies existed (Figure 3.1 column 3) regardless of anomaly magnitude. Such percentage plots are considered superior to mean plots as they are not biased by large values as is the case for mean charts. These percentage anomaly charts are similar to those constructed for 300 hPa height anomalies for the entire Southern Hemisphere on a monthly basis by the Climate Prediction Center (CPC) / National Center for Environment Protection (NCEP) (http://nic.fb4.noaa.gov/products/analysis_monitoring/bulletin/posnegsh.gif). Percentage

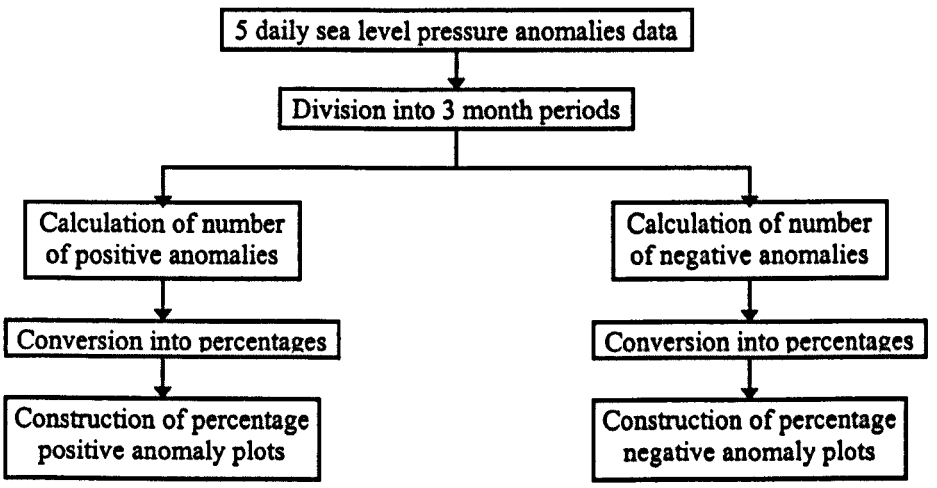

Figure 3.8 Flow diagram illustrating the procedure involved in constructing the spatial percentage anomaly plots

anomaly charts were produced for both warm and cold events, as well as the time between events, with the aim of identifying the spatial movement of anomalies. The percentages of positive and negative anomalies were calculated using FORTRAN 77 on a three month running mean basis for the entire period (Appendix 1). Spatial percentage anomaly plots were then constructed, using UNIMAP with bilinear interpolation to interpolate between the grid points (Figure 3.8). Three month running mean charts, as opposed to seasonal charts, which only provide snapshots in time were constructed to allow the progression of anomalies to be clearly tracked over time.

3.6 Harmonic analysis

In order to gain a full insight into the effects of ENSO on the higher latitudes of the Southern Hemisphere and how ENSO signals may be propagated over space and time the combined temporal and spatial behaviour of climate anomalies (500 hPa height, temperature and mixing ratio) should be considered (Figure 3.1 column 4). Harmonic analysis, which is a technique used to describe periodic phenomena (Oliver, 1981) can meet such analysis demands. It has proved a useful tool in identifying the ENSO impact on rainfall in Africa (Nicholson and Kim, 1997), precipitation and temperature in North American (Ropelewski and Halpert, 1987a), and temperature over North America, Japan and Western Europe (Halpert and Ropelewski, 1992). The first harmonic is used in identifying the ENSO signal, as it describes the greatest variability within the data and as the ENSO phenomenon is the largest single source of interannual climatic variability on a global scale (Trenberth, 1991; Diaz and Markgraf, 1992) it seems appropriate. In harmonic analysis the phase and amplitude of the first harmonic describes the overall periodic behaviour of a time series in the form of a harmonic curve. Where the anomalies are the most positive there tends to be a peak in the curve, with a trough where the anomalies are most negative.

Many climatic series show periodic behaviour from a daily time scale to an annual time scale and beyond. Harmonic analysis represents these variations within time series as the adding together of a series of sine and cosine functions (Wilks, 1995). The first harmonic represents a single cosine function fitting the entire time series as a single wave. Adding more harmonics will improve the fit. The biennial nature of the ENSO phenomenon and its interactions suit the analysis of the first harmonic as in this analysis the peak and the trough

are fitted to the data half the time series apart with the two year period used matching the biennial nature of ENSO. The phase and amplitude of the harmonic represents the time within each of the ENSO sequences when the anomalies had the strongest apparent positive response (Ropelewski and Halpert, 1987a), with the amplitude indicating the total magnitude of height variation over the 2 year period (Nicholson and Kim, 1997). By plotting the harmonics as vectors on a map, it is possible to identify the major trends as well as geographic regions of similar response. The phase and amplitude of the harmonic are plotted in the form of a harmonic dial (Figure 3.9). The length of the arrow is determined by the amplitude, C_1, and the direction is determined by the phase, ϕ, of the first harmonic. As in Halpert and Ropelewski (1992), the vector points toward the positive part of the cycle; however, it must be remembered that the practical importance may be on the negative side of the vector, which will be one year out of phase with the indicated direction (Ropelewski and Halpert, 1987a).

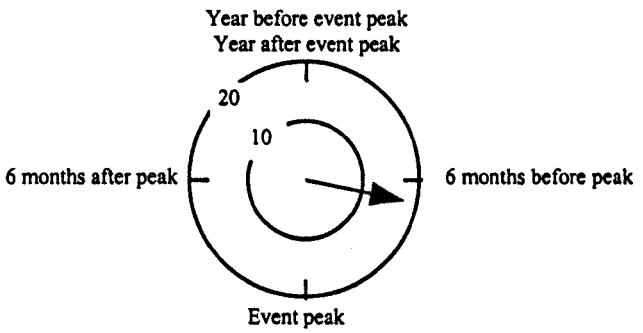

Figure 3.9 A harmonic dial with the arrow indicating the phase of the strongest apparent positive response, and the length of the arrow indicative of the amplitude of the harmonic curve.

The harmonic analysis is based on the fitting of a harmonic curve to the series with amplitude, C_1, and phase, ϕ, produced by the formulae below. This curve is also represented as the sum of an unshifted cosine and unshifted sine curve with amplitudes A_1 and B_1. As the data values are equally spaced in time, with no missing values, equations 3.3 and 3.4 can be used to calculate the least squares parameters, A_1 and B_1 (Wilks, 1995), as the properties of the sine and cosine functions allow these values to be obtained more easily using these formulae. The theory behind the method is as follows:

$$A_1 = \frac{2}{n}\sum_{t=1}^{n} y_t \cos\left(\frac{2\pi t}{n}\right) \tag{3.3}$$

$$B_1 = \frac{2}{n}\sum_{t=1}^{n} y_t \sin\left(\frac{2\pi t}{n}\right) \tag{3.4}$$

Where t is the record number, n is the number of values, and y_t are the ranked values. The least squares parameters, A_1 and B_1, are then used in equations 3.5 and 3.6 to calculate the amplitude, C_1, and the phase, ϕ, of the first harmonic.

$$C_1 = \left[A_1^2 + B_1^2\right]^{1/2} \tag{3.5}$$

$$\phi = \begin{cases} \tan^{-1}\left(B_1/A_1\right) & A_1 > 0 \\ \tan^{-1}\left(B_1/A_1\right) \pm \pi & A_1 < 0 \\ \pi/2 & A_1 = 0 \end{cases} \tag{3.6}$$

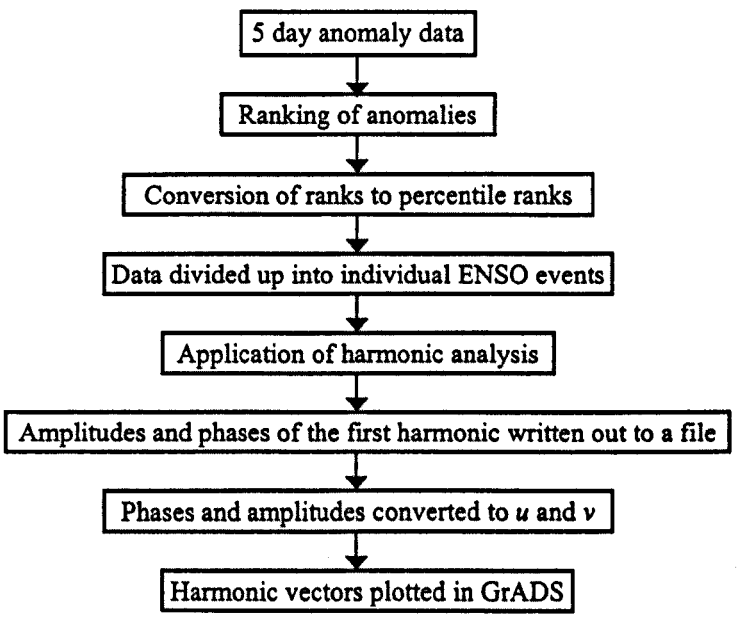

Figure 3.10 Flow diagram illustrating the procedure involved in the harmonic analysis

The various steps involved in performing harmonic analysis are shown in Figure 3.10. Due to the computational demands associated with undertaking the harmonic analysis of a large spatial and temporal data set a number of FORTRAN 77 programs were written for each of the harmonic analysis steps (Appendix 1) which follows the methodology of Ropelewski and Halpert (1987a, 1987b) and Halpert and Ropelewski (1992). The first step involved ranking

the climate anomalies for each grid point, each 5 day value was ranked from 1 for the most negative anomaly upwards, as described by Ropelewski and Halpert (1987a) and Halpert and Ropelewski (1992). This was performed to remove any bias from the large anomalies. These ranks were then transformed into percentile ranks, allowing greater inter-comparison between grid points. Percentile ranking of the anomalies has the advantage that it provides a systematic way of dealing with the disparities between different grid points and is immune to the biases that arise because of extreme values within a data set (Ropelewski and Halpert, 1987a). Following this, the data was divided up according to the four warm and three cold events identified in Table 3.4. Warm and cold composites were also constructed based around the event peaks, as described above in Section 3.4 for the Hovmöller diagrams, for the purpose of comparison and assessing event uniqueness. The time span used in this section differs from that used for the Hovmöller diagrams as one of the most important features of ENSO events is their biennial tendency which will only be picked up in harmonic analysis if a two year period is used. The period used in the analysis was one year before to one year after the event peak, where the peaks were determined by locating the Southern Oscillation Index (SOI) maximum (cold) or minimum (warm) as described in Section 3.4.

The harmonic analysis was performed on each of the 2 year percentile ranked series of 500 hPa height, temperature and mixing ratio data using a series of FORTRAN 77 programs based on the algorithms presented in Wilks (1995). To make sure there were no errors within the programs, which may have affected the vector phases and amplitudes, a selection of grid point harmonics were calculated manually and compared to the FORTRAN output.

To illustrate the application of equations 3.3-3.6 to the data, the steps involved in calculating the first harmonic for the 5 day 500 hPa height data for 15°S 155°W for the 1975 cold event are described below. Table 3.5 shows the calculations necessary to obtain least squares estimates for the parameters, A_1 and B_1, of the harmonic for this example. The percentile ranks are in the column labelled y_t. In this study this procedure was carried out in the to calculate the amplitude, C_1, and phase, ϕ, in the same way using FORTRAN 77 programs for each grid point for each event.

Equations 3.3 to 3.6 are applied to the results from Table 3.5 in order to determine the least squares parameters, A_1 and B_1, and therefore the amplitude, C_1, and phase, ϕ, of the first harmonic. Where:

$$A_1 = (2/146) \times -275.2753 = -3.77 \quad \text{(3.3 above)}$$

$$B_1 = (2/146) \times 1329.2388 = 18.21 \quad \text{(3.4 above)}$$

$$C_1 = [-3.77^2 + 18.21^2]^{1/2} = 18.59 \quad \text{(3.5 above)}$$

$$\phi = \tan^{-1}(18.21/-3.77) + \pi = 1.78 \quad \text{(3.6 above)}$$

t	y_t	$\cos(2\pi t/n)$	$\sin(2\pi t/n)$	$y_t \cos(2\pi t/n)$	$y_t \sin(2\pi t/n)$
1	71.81	0.9990741	0.0430222	71.753464	3.0898551
2	52.12	0.9962982	0.0859648	51.927087	4.4804876
3	33.20	0.9916773	0.1287482	32.926533	4.2748091
4	80.62	0.9852201	0.1712931	79.434576	13.810719
5	22.50	0.9769385	0.2135209	21.985896	4.8052653
6	12.19	0.9668478	0.2553533	11.793904	3.1148772
7	89.23	0.9549668	0.2967128	85.218168	26.4777
140	1.50	0.9668478	-0.255353	1.4505871	-0.383113
141	20.28	0.9769385	-0.213521	19.81917	-4.331701
142	43.37	0.9852201	-0.171293	42.737859	-7.430521
143	25.96	0.9916773	-0.128748	25.746091	-3.342579
144	23.67	0.9962982	-0.085965	23.591405	-2.035564
145	37.37	0.9990741	-0.043022	37.343084	-1.608068
146	14.28	1	9.282E-08	14.285714	1.326E-06
Total:	6276.32	2.156E-06	0	-275.2753	1329.2388

Table 3.5 Mechanics of using equations 3.3 and 3.4 to estimate parameters of the first harmonic

Therefore for grid point 15°S 155°W the amplitude (C_1) and phase (ϕ) of the first harmonic are 18.59 gpm and 1.78 radians (6.8 months) respectively indicating that at this grid point the most positive 500 hPa height anomalies occur 5.2 months prior to the 1975 cold event peak with an amplitude of 18.6 gpm. These values can then be plotted against the ranked data to give the curve shown in Figure 3.11, where the equation of the curve is:

$$y = \bar{y} + C_1 \cos\left(\frac{2\pi t}{n} - \phi\right) \tag{3.7}$$

where $\bar{y}$ is the mean of y_t. The values calculated above can then be used to draw the curve of the first harmonic for the grid point 15°S 155°W, using the values calculated above to give the equation for the curve in Figure 3.11:

$$y = 42.99 + 18.59\cos\left(\frac{2\pi t}{146} - 1.78\right) \tag{3.7 above}$$

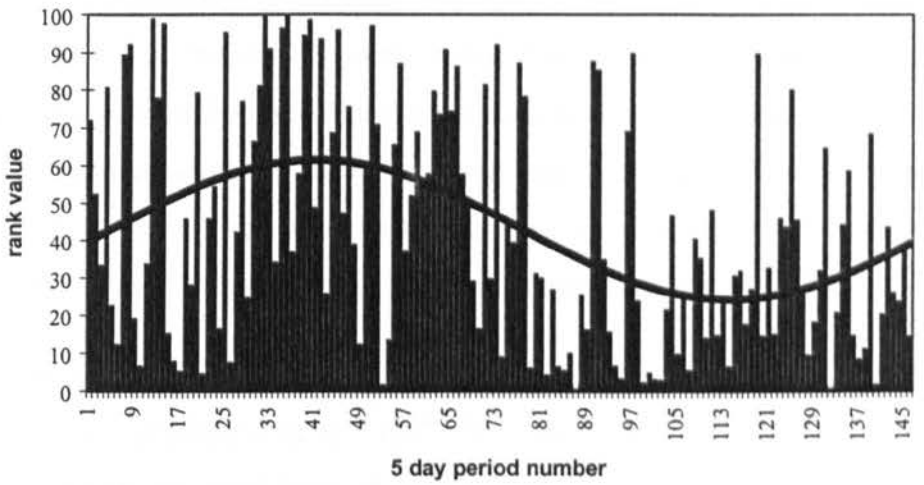

Figure 3.11 First harmonic of 500 hPa height for grid point 15°S 155°W for the 1975 cold event. The bars represent the ranked anomalies whilst the line represents the phase and amplitude generated by harmonic analysis of this data.

The UNIX plotting package GrADS was used to plot the phase and amplitude of the first harmonics in the form of two vectors, u and v such that:

$$u = C_1 \sin(\phi - \pi) \tag{3.8}$$

$$v = C_1 \cos(\phi - \pi) \tag{3.9}$$

where the amplitude and phase for each grid point are C_1 and ϕ respectively. The u and v components were calculated for each grid point for each event and then written to individual event files in binary form to make them compatible with GrADS format requirements. The harmonic vectors were then plotted onto base maps for the entire Southern Hemisphere.

3.6.1 Cluster analysis

In order to gain an understanding of the nature of possible teleconnections and the spatial extent of similar climate anomaly amplitude and phases cluster analysis was applied to the results of the harmonic analysis to produce a grouping of the harmonics to identify regions of similar response. From these regions it was hoped that some idea of the teleconnections operating within the individual ENSO events could be gained. Coherence testing has been used in previous studies as a method for grouping together the harmonics (Ropelewski and Halpert, 1987a), in which the ratio of the harmonic vector average for the sectors, which are selected by looking for coherent ENSO signals, to the average scalar magnitude of the regional vectors are assessed (Nicholson and Kim, 1997). In this study the use of 1368 vectors and analysis of individual events rather than a single composite means that this coherence technique is far from ideal, making a statistical grouping technique necessary. The most useful method of grouping the phases and amplitudes generated from the harmonics analysis in a data set of this size was cluster analysis. This clustering was applied to both the phases and amplitudes in order to group areas with similar climate anomalies.

Cluster analysis is used to describe a set of techniques to group regions (or days) into discrete, homogenous groups (Kalkstein et al., 1987; Kovach, 1995). Clustering is the most well-developed and commonly used form of analysis used to combine data (Arabie and Hubert, 1996). There are a number of different clustering methodologies, but they all have the same common aim of maximising within-group similarity whilst minimising the between group similarity (Balling, 1984). The variety of clustering techniques can be divided into two main groups, non-hierarchical and hierarchical. Non-hierarchical methods divide the values into groups without showing the relationships between the groups, whilst hierarchical methods arrange the clusters so that the relationships between the groups are apparent (Kovach, 1995). Hierarchical methods are divided up into agglomerative and divisive methods. Agglomerative clustering techniques start with the individual values amalgamating the most similar pairs until all are in a single, hierarchical group (van Tongeren, 1995; Gordon, 1996). These are the most frequently used methods. Divisive clustering starts with all the clusters in one group, dividing the existing classes into smaller homogeneous offspring classes based on their

similarity to each other (Kovach, 1995; Gordon, 1996), however, this technique is now largely neglected (van Tongeren, 1995).

Cluster analysis was carried out on the 500 hPa height harmonic analysis phases, ϕ and amplitudes, C_1, using the statistics package SPSS, for the 4 warm, 3 cold and two composite events, to place them into homogenous groups (Kalkstein et al., 1990) and thus identify regions of coherent response (Figure 3.12). To give equal weighting to the amplitudes and

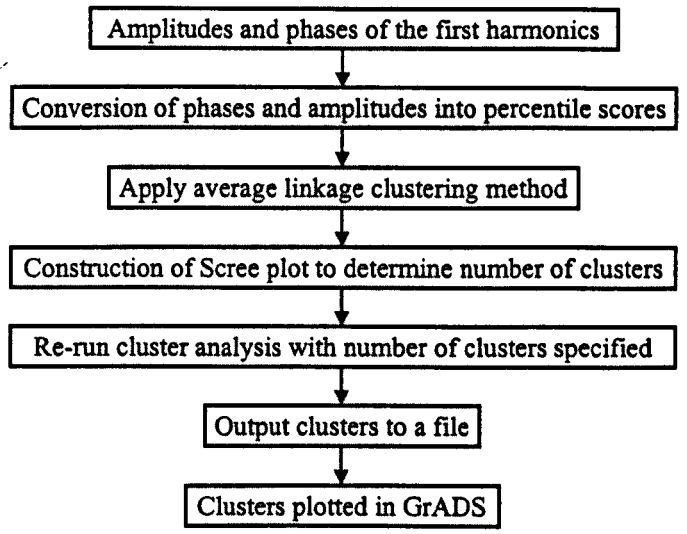

Figure 3.12 Flow diagram illustrating the procedure involved in the cluster analysis.

phases, it was necessary to convert both sets of values into percentile scores, thus both variables were then graded from 0 to 100. As a variety of clustering algorithms exist (average linkage, Wards etc.) the output from a range of cluster analyses was reviewed and based on a comparison of results it was decided that the 'average linkage' clustering method gave the best results. The 'average linkage' method was used as it is a hierarchical and agglomerative clustering procedure, producing clusters possessing small within group variances and large between group variances (Kalkstein et al., 1987, 1990). In this method the distances between groups are represented as an average distance (Kovach, 1995) with the groups being combined until one group remains. The number of clusters used for each event was determined through the use of scree plots (Cattell, 1966), which indicate where unlike clusters are being forced together and, therefore, can be used to determine the number of clusters (Yarnal, 1993). The

scree plots were studied for a break in slope to determine where the unlike clusters were being forced together, and thus the number of clusters was determined for each event. The cluster analysis was then run again for each event for the designated number of clusters thus assigning a cluster number to each grid point. The clusters were then written out in binary using FORTRAN programs and the clusters plotted in GrADS for each event for the entire Southern Hemisphere.

3.7 The role of jetstreams

In order to identify the mechanisms behind the ENSO teleconnections with the high latitudes of the Southern Hemisphere the role of the jetstreams was considered. Following the Hovmöller and harmonic analyses it had become clear that there were significant patterns in the anomalies in the regions of the jetstreams. As it has been suggested that the jetstreams are an important factor in the propagation of the ENSO signal with the subtropical jet being strong (weak) and the polar front jet being weak (strong) in warm (cold) events (Chen et al., 1996) it was decided to consider the role of the jetstreams in more detail. The role of the jetstreams in ENSO-Antarctic climate teleconnections has been considered by Chen et al. (1996) for the period 1986 to 1989, the transition from a warm to a cold event, however, the aim of this study is to extend this to look at variations over the 1973 to 1994 period, with four warm events and three cold events, to assess the importance of jetstreams across a number of events.

3.7.1 Calculation of geostrophic wind

In order to look at the role of the jetstreams it was necessary to use wind data for 500 hPa for the Southern Hemisphere. Due to difficulties involved in obtaining AA wind data for the entire Southern Hemisphere the required wind fields were calculated using the geostrophic wind equation (3.10) from the 500 hPa height data (Figure 3.13). It was decided to calculate the wind data from the 500 hPa height data rather than the sea level pressure data as this data would be independent of any orographic effects.

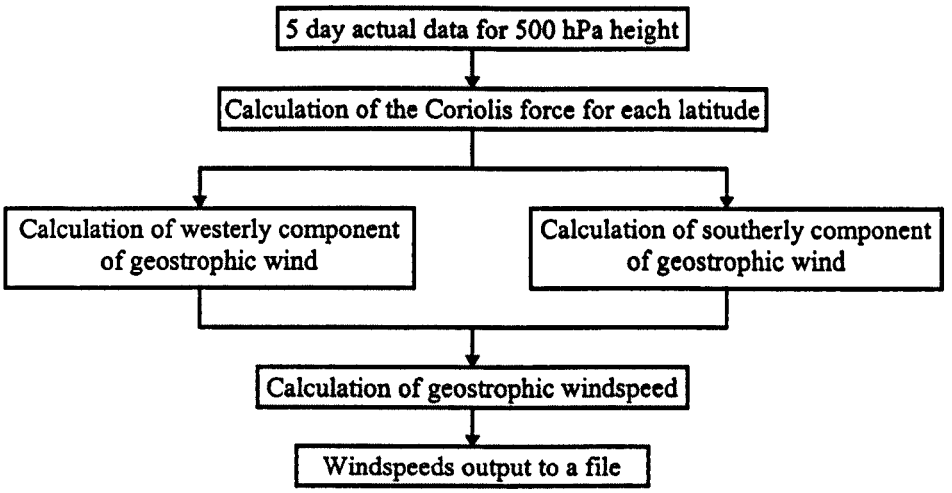

Figure 3.13 Flow diagram illustrating the procedure involved in the calculation of the geostrophic wind

$$V_g = \frac{g}{f} \text{ grad } z \quad \text{(Forecasters' Reference Book, 1993)} \qquad (3.10)$$

where g is the gravitational force, grad z is the height gradient along a constant pressure surface (in m m^{-1}), and f is the coriolis force calculated in equation 3.11 below. The height gradient grad z was calculated as the change in geopotential height between two grid points

latitude (°)	0	15	30	45	50	55	60	75	85	90
distance (km)	558	539	483	394	358	319	278	143	48	0

Table 3.6 Distance corresponding to 5 degrees of longitude at given latitudes (adapted from: Forecasters' Reference Book, 1993)

divided by the distance between the two grid points. The distance between grid points varies with latitude due to the curvature of the earth (Table 3.6). The coriolis force f is given by:

$$f = 2\Omega \sin \theta \qquad (3.11)$$

where Ω, the rate of rotation, is taken as 7.29×10^{-5} s^{-1} and θ is latitude. This method was also been used by Carleton (1988) to determine sea-ice circulation interactions in the Weddell Sea in relation to the Southern Oscillation. The geostrophic wind had to be calculated for both the westerly (V_{west}) and southerly (V_{south}) directions, as the data is gridded, and the overall geostrophic windspeed (V_{speed}) was calculated using equation (3.12):

$$V_{speed} = \sqrt{V_{west}^2 + V_{south}^2} \quad (3.12)$$

These calculations were carried out using FORTRAN programs for each 5° grid point for every 5 day period and the results written out to a file (Appendix 1).

3.7.2 Zonally averaged Hovmöller Plots

In order to look at the relative changes in the strength of the jetstreams over time Hovmöller charts were used to display the geostrophic windspeed data (Figure 3.1 column 5). The methodology of Chen et al. (1996) was followed, which used zonally and temporally averaged data in the form of Hovmöller charts. Zonal and temporal averaging was used in order to see the most obvious trends within the series minimising the effects of the small scale spatial and temporal variability of the geopotential height and jetstreams. The temporal averaging would also serve to remove the seasonal cycle from the series. The simplest way to zonally average the data was to use 60° longitude sectors as this would give six zonal segments, one of which would incorporate the area around 130°W (230° longitude), used in the Hovmöller diagrams (Section 3.4), where the maximum variability and correlation with the SOI appears to occur (Jones and Simmonds, 1994; Houseago et al., 1997, 1998); this area would be the 120 to 180°W (180 to 240°) sector. Since the ENSO cycle is found to have close association with the annual cycle (van Loon and Shea, 1985, 1987), and the phases of ENSO belong to strong or weak annual cycles (Meehl, 1987) - although it appears that this association was less with the 1982-83 warm event (Wang, 1992) - the methodology of Chen et al. (1996) was followed and the 12 month running means for the period 1973 to 1993 used (Figure 3.14). For consistency twelve month running means were also calculated for the SOI. Zonally averaged Hovmöller diagrams were constructed for the 500 hPa heights, height anomalies and geostrophic windspeeds in an attempt to find comparable results, with line graphs of the SOI constructed, at the same scale, to compare the series.

To add to the findings from these Hovmöller plots the percentage of positive and negative anomalies in geostrophic windspeeds over time, in the regions of the jetstreams, were calculated through the use of a FORTRAN program. These were constructed to determine the

relative importance in the extent and persistence of both the subtropical and polar jets during warm and cold events. These results were plotted in Excel.

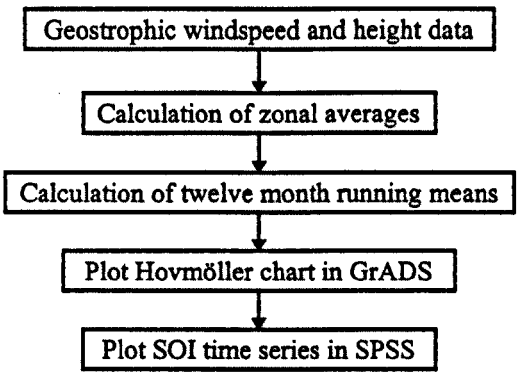

Figure 3.14 Flow diagram illustrating the procedure involved in the construction of the zonally averaged Hovmöller diagrams.

3.8 Summary

Subjective visual as well as objective cross correlation analyses of time series plots of the SOI and a range of climate parameters were used in this study to identify the ENSO signals in Antarctic climate. Following the identification of the ENSO signals in Antarctica the study area was extended to incorporate the entire Southern Hemisphere. Initially, Hovmöller diagrams were constructed, for the 230° meridian, for 500 hPa height, 700 hPa height and 700 hPa temperature anomalies, to identify wavetrains of anomalies between the Southern Hemisphere low and high latitudes. Composite spatial anomaly plots for year -1, year 0 and year +1 for 500 hPa height, 700 hPa height and 700 hPa temperature as well as percentage sea level pressure anomaly plots were constructed to put the findings of the Hovmöller analysis into a spatial context. Harmonic analysis of 500 hPa height, temperature and mixing ratio anomalies was carried out to incorporate the spatial and temporal aspects of the Southern Hemisphere ENSO signals to identify the movement of anomalies across the hemisphere. Cluster analysis was applied to the results of the harmonic analysis to identify regions of similar response and hence identify teleconnections. Finally zonally averaged Hovmöller diagrams were constructed for 500 hPa height and geostrophic windspeed to identify the role

of the jetstreams in the propagation of the ENSO signal between the Southern Hemisphere low and high latitudes.

CHAPTER 4

IDENTIFICATION OF THE ENSO SIGNAL IN ANTARCTICA

4.1 Introduction

From a review of the limited number of studies conducted to date it is clear that ENSO is linked to the variability of high latitude Southern Hemisphere climates in a variety of ways. Previous studies highlight the anomalous circulation (Trenberth, 1980; van Loon and Madden, 1981; Carleton, 1988), sea surface temperature (van Loon and Shea, 1987), pressure and temperature (van Loon and Madden, 1981; Smith and Stearns, 1993), synoptic activity (Streten, 1975; Bromwich et al., 1993), geopotential height (Mo and White, 1985; Karoly, 1989), moisture convergence (Cullather et al., 1996) and sea ice conditions (Bromwich et al., 1993; Simmonds and Jacka, 1995; Gloersen, 1995) in the Antarctic associated with warm events. Previous studies have detected an ENSO signal in high latitudes although they are limited in record length as well as the range of climate variables they use. There is no single study that considers a full range of climate variables, combining both the surface and the upper air. This chapter is concerned with identifying the impact of ENSO on the climate variability of Antarctica, using a variety of variables over the time period 1957 to 1994. The time period used here is longer than that used with the Australian Analyses later in the study, as the Australian Analyses have only been extended back to 1973, whilst the majority of observations in Antarctica commenced during the International Geophysical Year, 1957/8. In order to identify the ENSO signals two approaches are taken. Initially a purely descriptive approach is taken using twelve month running means to study individual events. This is carried out for the two British Antarctic Survey bases, Halley and Faraday, with Halley upper air soundings, for 500 and 850 hPa levels, also used. These two stations are used primarily as they are to the south of the eastern Pacific, which is one of the 'centres of action' during ENSO events. Following this an assessment of the nature of the impacts of ENSO on station

pressure and temperature at various locations around the continent is undertaken using cross correlation analysis. The stations and their data selection criteria are described in detail in Section 3.2.1. The lead (anomalies in Antarctica precede anomalies in the tropical Pacific) and lag (anomalies in Antarctica occur after anomalies in the tropical Pacific) relationships between the Antarctic climate and ENSO can be identified through the use of cross correlation analysis. From the cross correlation analysis the most significant correlations with the SOI can be identified for each station and the spatial patterns can be found. Previous studies have looked at the spatial distribution of anomalies in warm and cold event composites, however, this study aims to look at the spatial patterns in the most significant correlations with the SOI.

4.2 Signals at Halley

Table 4.1 shows the monthly and annual means for each of the variables for Halley station, located at 75 °S 26°W 30m above sea level on the seaward edge of the Brunt Ice Shelf (Wattam and Turner, 1995). The station climate means in Table 4.1 allow the ENSO induced climate anomalies to be put into context.

	Jan	Feb	Mar	Apr	May	Jun	Jul	Aug	Sep	Oct	Nov	Dec	Mean
Pressure (hPa)	992.8	990.8	987.6	988.6	991.1	991.8	989.2	987.9	985.9	984.4	986.5	991.6	989.0
Temperature (°C)	-4.57	-9.84	-16.23	-20.85	-24.82	-26.42	-28.63	-28.40	-26.27	-19.55	-11.58	-5.16	-18.50
Cloud (oktas)	5.98	5.87	5.72	5.51	4.85	4.59	4.67	5.03	5.38	5.79	5.92	5.92	5.44
Windspeed (m)	10.45	11.33	13.41	13.79	13.18	13.72	13.51	14.56	14.38	14.59	13.08	10.78	13.06
850 hPa height (gpm)	1215	1187	1147	1142	1146	1145	1116	1112	1099	1107	1143	1203	1147
850 hPa RH (%)	67.83	69.93	65.64	67.12	63.66	62.95	61.33	60.31	60.71	60.50	64.14	65.24	64.10
850 hPa temp (°C)	-9.36	-11.56	-13.72	-15.77	-18.02	-19.35	-20.72	-20.68	-19.43	-16.95	-13.75	-10.07	-15.86
850 hPa windspeed (ms^{-1})	12.70	12.19	14.77	14.91	15.53	17.42	17.54	16.26	16.01	16.56	14.35	12.67	15.07
850 hPa southerly (ms^{-1})	-1.22	-0.65	-0.67	-1.43	-1.55	-1.66	-1.43	-0.55	-1.51	-2.03	-1.97	-1.29	-1.33
850 hPa westerly (ms^{-1})	-1.81	-1.53	-2.12	-2.20	-2.92	-4.02	-3.81	-2.48	-2.17	-2.59	-3.06	-2.17	-2.58
500 hPa height (gpm)	5153	5100	5026	4999	4978	4956	4912	4910	4916	4953	5021	5128	5003
500 hPa RH (%)	51.15	51.50	50.44	51.86	50.13	49.82	48.88	48.65	48.44	47.17	47.94	49.14	49.58
500 hPa temp (°C)	-31.02	-32.32	-34.25	-36.11	-37.75	-39.21	-40.07	-39.99	-38.81	-37.13	-34.75	-32.33	-36.17
500 hPa windspeed (ms^{-1})	8.95	9.44	10.92	12.52	12.01	13.06	13.47	12.93	12.17	12.13	9.35	8.81	11.33
500 hPa southerly (ms^{-1})	-0.37	1.02	2.21	1.70	1.26	1.87	2.93	4.35	3.51	3.30	0.18	-0.33	1.81
500 hPa westerly (ms^{-1})	1.49	3.09	2.82	3.72	2.86	0.58	2.50	3.39	3.99	3.35	0.48	0.61	2.41
850-500 hPa thickness (gpm)	3938	3913	3879	3857	3832	3811	3796	3798	3817	3846	3878	3925	3857

Table 4.1 Monthly and annual means for Halley for the period 1957 to 1994.

4.2.1 Twelve month running means

Figures 4.1a-d show the twelve month running means (Section 3.3) of station pressure, temperature, cloud cover and windspeed with the SOI. There appears to be an inverse relationship between pressure at Halley and the SOI (Figure 4.1a) such that during warm

(cold) events the pressure at Halley is higher (lower) than 'normal'. This relationship is especially clear for the 1982/3 and 1991 warm events, when the twelve month running means are 1.71 hPa and 2.49 hPa above the mean respectively. Inverse relationships are also clear for the 1975 and 1978 cold events, when the running means are 2.53 hPa and 4.00 hPa below the mean respectively. However, this inverse relationship is not consistent for all events, for example the 1964 cold event does not coincide with a reduction in sea level pressure, but an increase of 4.59 hPa above the mean, while the 1969 warm event coincides with a reduction, of 1.17 hPa below the mean, in sea level pressure.

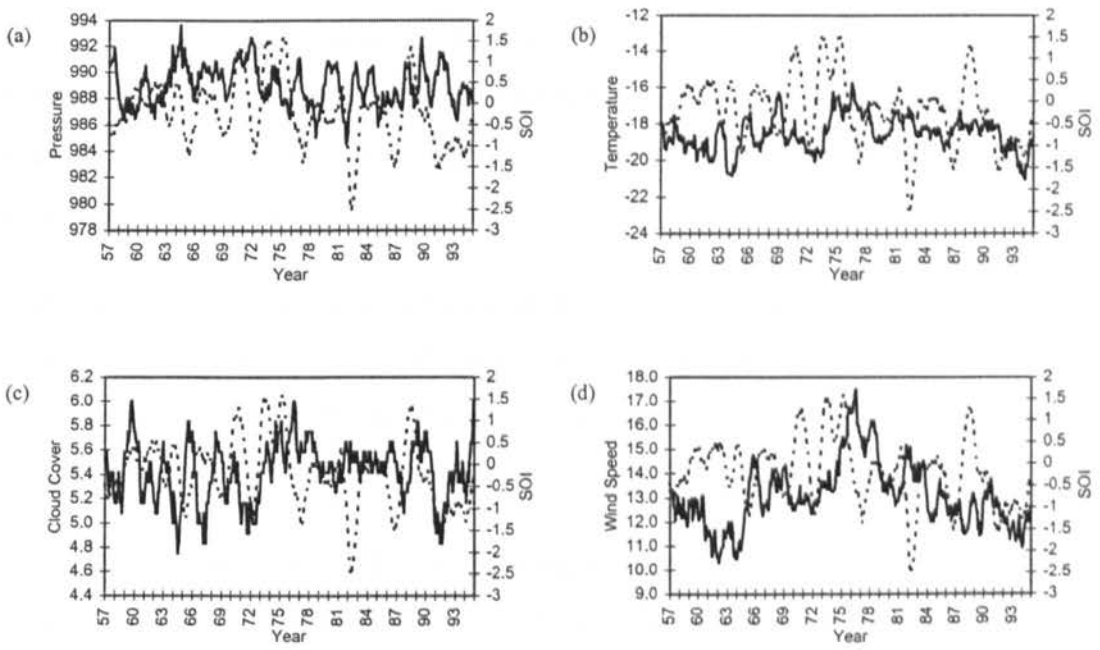

Figure 4.1 Twelve month running means for Halley (a) pressure, (b) temperature, (c) cloud cover and (d) windspeed with the SOI (dashed line).

The relationship between Halley temperature and the SOI twelve month running means (Figure 4.1b) is not as clear as for Halley pressure and the SOI. There appears to be an inverse relationship between the SOI and temperature. However, this relationship is clearest towards the beginning of the period, becoming less obvious from the mid-1970's onwards. The clearest indicators of this inverse relationship are the elevated temperatures during the 1963 warm event, when the twelve month running mean is 0.62°C above the mean, and the lower temperatures during the 1964 cold event, when the running mean is 2.33°C below the mean.

Figure 4.1c shows the inverse relationship between Halley cloud cover and the SOI. As for Halley temperature, the relationship seems to break down from the mid-1970's onwards, reversing to become a positive relationship from the late 1980's. The inverse relationship towards the start of the time series is especially clear in the case of the 1964 cold event, with the twelve month running mean at 0.67 oktas below the mean. This reduction in cloudiness coincides with the reduced temperatures identified above during the same event most likely indicative of an increase in radiative heat loss. Also associated with this inverse relationship is the increase in cloud during the 1965 and 1976 warm events, when the running means were 0.41 and 0.58 oktas greater than the mean, respectively. Towards the end of the cycle, the SOI cloud cover relationship appears to have become positive, there is increased cloudiness during the 1988 cold event, when the running mean was 0.41 oktas greater than the mean, and reduced cloud during the 1991 warm event, when the twelve month running mean was 0.59 oktas below the mean.

There also appears to be an inverse relationship between Halley windspeed and the SOI (Figure 4.1d). It is most marked towards the beginning of the period, however, it appears to breakdown around 1970 before resuming prior to the 1976 warm event, although towards the end of the period the relationship once again loses its clarity.

The analysis of twelve month running means has revealed that there is a great deal of inter-ENSO event variability between the SOI and the response of pressure, temperature, cloud cover and windspeed. There also appears to be a change in the response of temperature, cloud cover and windspeed to the SOI over the time series. A limitation in use of twelve month running means, in smoothing the time series, is that it can result in the shifting of the peaks forward in time and the troughs back in time (Davis, 1986). By using cross correlation analysis, it is possible to extend the findings from the twelve month running means to identify the variations in the timing of the response. The overall relationship between the variables and the SOI will be looked at in greater detail through the use of cross correlation analysis.

4.2.2 Cross correlation analysis

Correlograms are used to identify lead and lag correlations within a time series. They are used in this study to identify whether a signal in the Antarctic time series is occurring ahead

of the SOI (a lead) or occurring following the SOI (a lag). A sign convention will be used to identify the leads and lags in the following sections: where t represents the concurrent relationship, 't-' will be used to indicate a lead relationship (i.e. climate anomalies in Antarctica occur ahead of those in the tropical Pacific) and 't+' will be used to indicate a lag relationship (i.e. climate anomalies in Antarctica occur after those in the tropical Pacific). The level of significance in the correlograms is measured as 2 standard errors. Correlograms for Halley temperature and pressure with the SOI (Figures 4.2a-b) show that overall, there is an inverse relationship between both of these variables and the SOI agreeing with the findings above (Section 4.2.1). For Halley pressure (Figure 4.2a) the most significant correlation with the SOI occurs at t+4 months (Table 4.2). Although Smith and Stearns (1993) uncovered a positive lag of 12 months (t+12) between SOI and pressure, Figure 4.2a does display a less significant peak at t+11-12 months. These differences may be attributed to the fact that the methodology and time period used in this study differs from that used by Smith and Stearns (1993). Smith and Stearns (1993) calculated monthly anomalies for each station by subtracting long term means from monthly mean values. From these monthly anomalies twelve month running means were calculated, which were then used in the cross correlation analysis. However, this study only used seasonal differencing (Section 3.3) of the original data to remove the annual cycle prior to cross correlation. Smith and Stearns (1993) also limited their period of analysis to the period from March 1957 to March 1984, whilst this study used an extended period April 1957 to December 1993.

t +/-	-9	-8	-1	+3	+4	+11	+12	+14	+15
correlation	.129	.134	-.111	-.136	-.164	.150	.103	.110	.146

Table 4.2 Correlation coefficients greater than 2 standard errors for Halley pressure.

The correlation between Halley temperature and the SOI (Figure 4.2b) has the most significant correlation at t-12 months (Table 4.3). This disagrees with the negative correlation at t-3 months calculated by Smith and Stearns (1993). Also apparent in the pressure and temperature charts is the biennial tendency (van Loon and Shea, 1987) of the correlation between these variables and the SOI, i.e. there are significant inverse correlations 12 months either side of the most significant correlation.

t +/-	-12	+0	+2
correlation	.139	-.108	-.122

Table 4.3 Correlation coefficients greater than 2 standard errors for Halley temperature.

There is no significant correlation between the cloud cover at Halley and the SOI. However, this is probably due to the reversal in the relationship between cloud cover and the SOI towards the end of the time series (Figure 4.2c) identified from the twelve month running mean charts. There is an inverse relationship between windspeed and the SOI for t-9 and t-5 to t-4 months, however, there are no concurrent or significant correlations with the SOI after t-4 months. The most significant, negative, windspeed correlation (Figure 4.2d) occurs at t-5 months to the SOI (Table 4.4).

t +/-	-9	-5	-4
correlation	-.118	-.135	-.113

Table 4.4 Correlation coefficients greater than 2 standard errors for Halley windspeed.

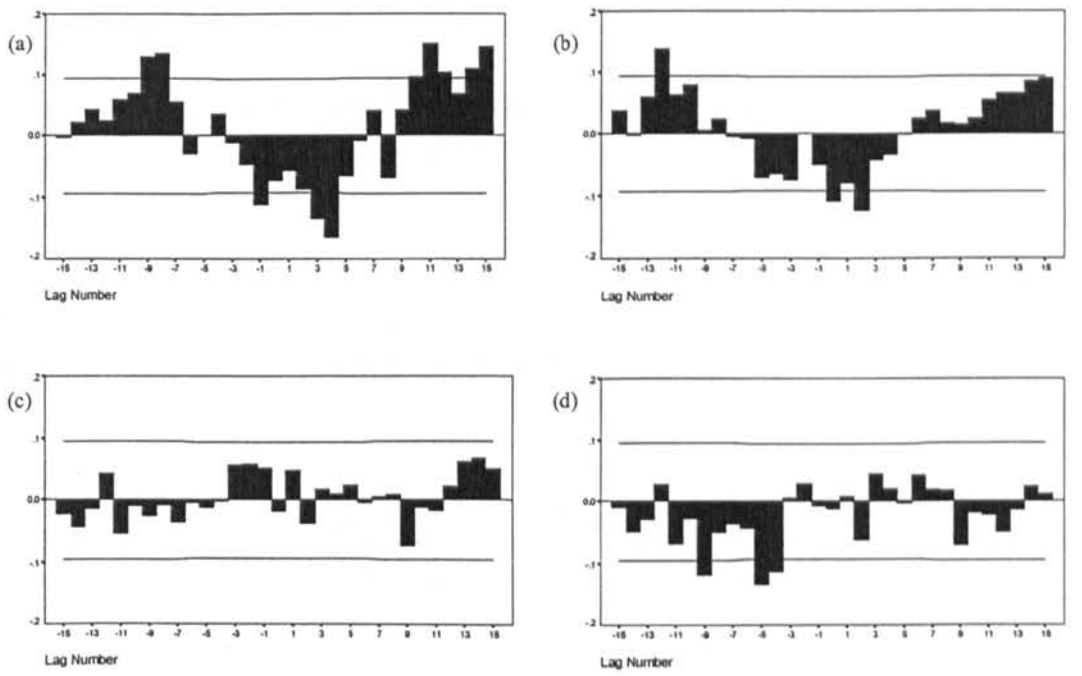

Figure 4.2 Correlograms for Halley (a) pressure, (b) temperature, (c) cloud cover and (d) windspeed with the SOI. The horizontal lines are two standard error limits.

Summarising briefly, for Halley during warm (cold) events there is a tendency to higher (lower) surface pressure and temperatures, whilst prior to warm (cold) events, there is a tendency for windspeeds to increase (decrease).

Figures 4.3a-f show the relationship between climate variables at the 850 hPa level with the SOI. There is an inverse relationship between 850 hPa height and the SOI (Figure 4.3a), with the most significant correlation occurring at t+11 months (Table 4.5). The relationship between height and SOI increases from t-6 months.

t +/-	-6	-1	+0	+4	+10	+11	+12	+14	+15
correlation	-.118	-.104	-.104	-.122	.102	.167	.138	.102	.123

Table 4.5 Correlation coefficients greater than 2 standard errors for Halley 850 hPa height.

The 850 hPa relative humidity is also inversely correlated with the SOI (Figure 4.3b), with the most significant correlation occurring at lag t+0 months (Table 4.6). As in Halley surface temperature the positive correlation at t-12 months is indicative of the biennial nature

t +/-	-12	-3	+0	+2
correlation	.137	-.115	-.138	-.102

Table 4.6 Correlation coefficients greater than 2 standard errors for Halley 850 hPa relative humidity.

of the response to ENSO. There is also an inverse relationship between 850 hPa temperature and the SOI (Figure 4.3c) although this relationship is not as clear as for the other variables.

t +/-	-6	+2	+8
correlation	-.117	-.120	-.100

Table 4.7 Correlation coefficients greater than 2 standard errors for Halley 850 hPa temperature.

t +/-	-2	+9	+10	+12	+13
correlation	.123	-.162	-.113	-.131	-.117

Table 4.8 Correlation coefficients greater than 2 standard errors for Halley 850 hPa windspeed.

The most significant correlation is at t+2 months (Table 4.7). For windspeed, decreases (increases) tend to occur leading up to a warm (cold) event SOI peak, followed by increases (decreases) after the peak. (Figure 4.3d). The most significant correlation between the SOI and 850 hPa windspeed occurs at t+9 months (Table 4.8). There is also a significant correlation at t-2 months indicative of a strong biennial tendency in the response of windspeed.

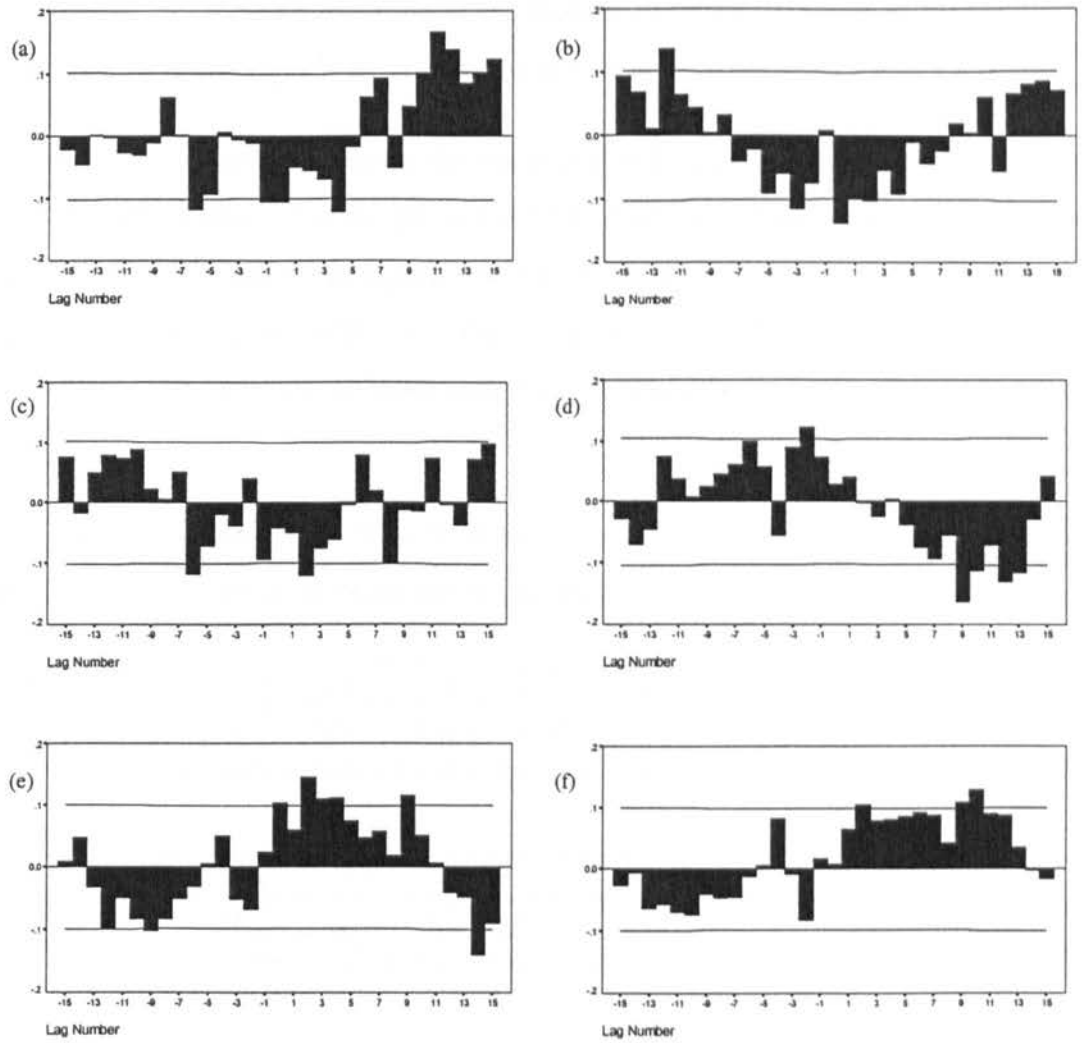

Figure 4.3 Correlograms for Halley 850 hPa (a) height, (b) relative humidity, (c) temperature, (d) windspeed, and (e) southerly and (f) westerly wind components with the SOI. The horizontal lines are two standard error limits.

t +/-	-9	+0	+2	+3	+4	+9	+14
correlation	-.102	.104	.145	.111	.112	.115	-.139

Table 4.9 Correlation coefficients greater than 2 standard errors for Halley 850 hPa southerly wind components.

t +/-	+2	+9	+10
correlation	.104	.108	.128

Table 4.10 Correlation coefficients greater than 2 standard errors for Halley 850 hPa westerly wind components.

The southerly (Figure 4.3e) and westerly (Figure 4.3f) wind components, unlike the variables discussed above, have a positive relationship with the SOI. The southerly wind component

has the most significant correlation at t+2 months (Table 4.9), however for the westerly wind component the most significant correlation occurs at t+10 months (Table 4.10).

To summarise the above findings, for warm (cold) events at 850 hPa at Halley there tends to be an increase (decrease) in height and relative humidity, higher (lower) temperatures, and a predominance of weaker (stronger), north-easterly (south-westerly) winds. The trend of the wind components agrees with the composite analyses of van Loon and Madden (1981) such that during warm events weak polar easterlies are found to the south of the subantarctic trough in the Pacific Ocean.

The cross correlation trends for 500 hPa (Table 4.11-4.17) (Figure 4.4a-f) are similar to the 850 hPa level for all variables, except temperature.

t +/-	-8	+4	+8	+11	+15
correlation	.121	-.121	-.104	.144	.117

Table 4.11 Correlation coefficients greater than 2 standard errors for Halley 500 hPa height.

t +/-	-6	-5	-4	+1	+2
correlation	-.148	-.158	-.162	-.123	-.123

Table 4.12 Correlation coefficients greater than 2 standard errors for Halley 500 hPa relative humidity.

The cross correlations between 500 hPa temperature and SOI do not show a clear trend (Figure 4.4c), however, there are positive correlations t+12 months. There is, however, a significant positive correlation at t-10 months (Table 4.13).

t +/-	-10
correlation	.128

Table 4.13 Correlation coefficients greater than 2 standard errors for Halley 500 hPa temperature.

t +/-	-13	-7	-6	-5	-3	-1	+8
correlation	-.148	.103	.105	.119	.111	.102	-.106

Table 4.14 Correlation coefficients greater than 2 standard errors for Halley 500 hPa windspeed.

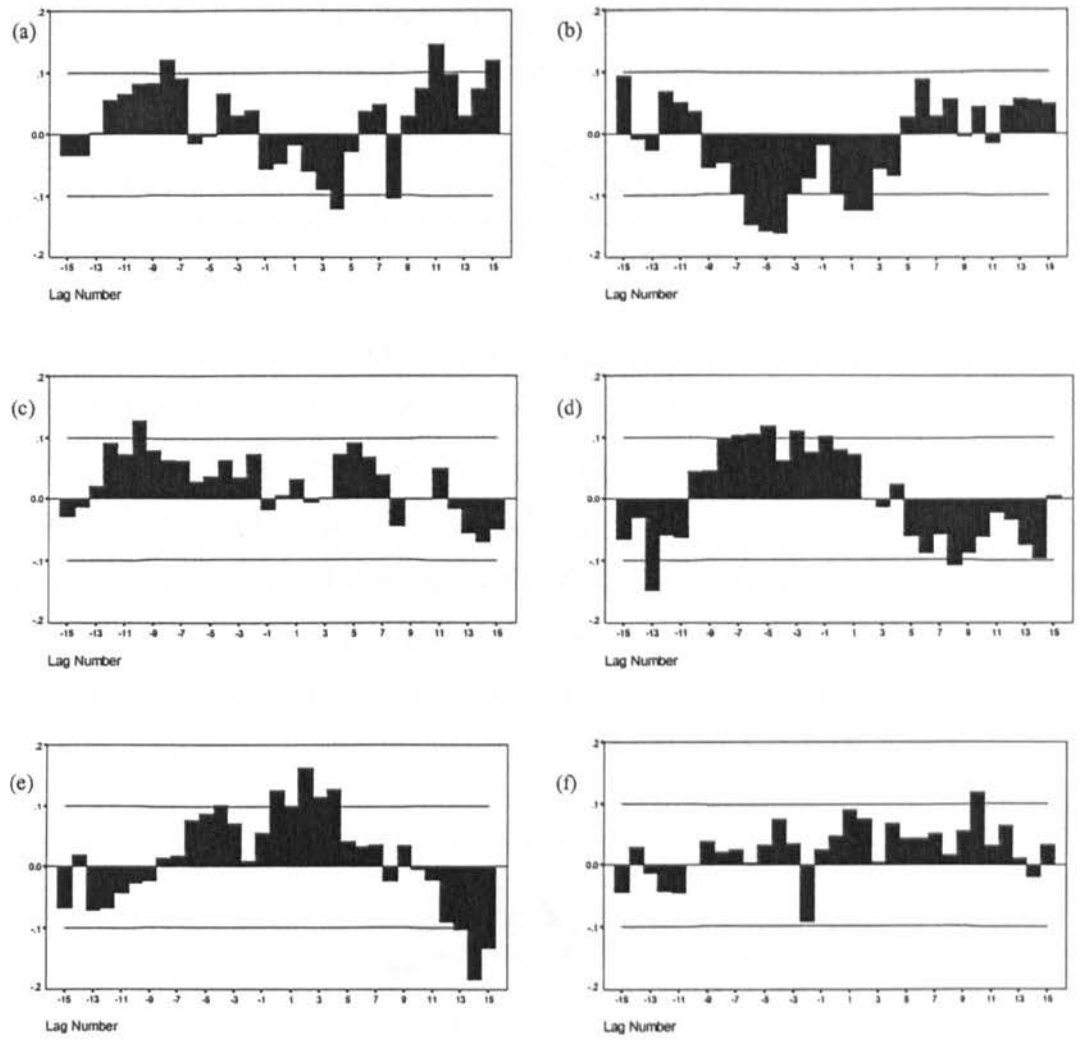

Figure 4.4 Correlograms for Halley 500 hPa (a) height, (b) relative humidity, (c) temperature, (d) windspeed, and (e) southerly and (f) westerly wind components with the SOI. The horizontal lines are two standard error limits.

t +/-	-4	+0	+1	+2	+3	+4	+13	+14	+15
correlation	.100	.125	.100	.163	.115	.126	-.102	-.183	-.132

Table 4.15 Correlation coefficients greater than 2 standard errors for Halley 500 hPa southerly wind components.

t +/-	+10
correlation	.117

Table 4.16 Correlation coefficients greater than 2 standard errors for Halley 500 hPa westerly wind components.

Summarising for the 500 hPa level, during warm (cold) events there are increases (decreases) in heights and relative humidity, with weaker (stronger) northerly (southerly) winds.

t +/-	-11	-10	-7	-2	+8
correlation	.103	.126	.148	.116	-.117

Table 4.17 Correlation coefficients greater than 2 standard errors for Halley 850-500 thickness.

The 850-500 hPa thickness, which is the difference in gpm between the 850 hPa height and the 500 hPa height, is also considered in this study as it gives an insight into the air mass type, by identifying whether the overlying air is warm or cold. There is a positive correlation between the 850-500 hPa thickness and the SOI (Figure 4.5) with the most significant correlation occurring at t-7 months (Table 4.17). Thus, about 7 months prior to warm (cold) events there is a reduction (increase) in the 850 to 500 hPa thickness at this station, indicative of a cooler (warmer) air mass associated with decreased (increased) surface pressure and geopotential height.

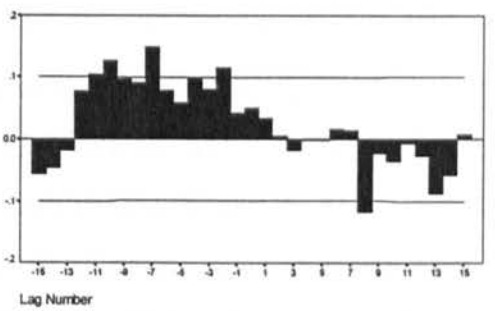

Figure 4.5 Correlogram for Halley 850 hPa to 500 hPa thickness with the SOI. The horizontal lines are two standard error limits.

4.3 Signals at Faraday

Faraday is located at 65°S 64°W, 11m above sea level, on the Argentine Islands (Wattam and Turner, 1995). Table 4.18 shows the monthly and annual means of pressure, temperature, cloud cover and windspeed for this station.

	Jan	Feb	Mar	Apr	May	Jun	Jul	Aug	Sep	Oct	Nov	Dec	Mean
Pressure (hPa)	990.7	988.8	988.3	989.1	992.1	992.5	993.0	990.4	987.8	986.7	985.7	990.3	989.6
Temperature (°C)	0.69	0.56	-0.64	-2.65	-4.79	-7.09	-9.70	-9.98	-7.54	-5.15	-2.17	-0.22	-4.10
Cloud (oktas)	6.78	6.73	6.80	6.68	6.33	6.03	6.05	6.30	6.80	6.90	6.88	6.78	6.59
Windspeed (m)	5.23	6.53	7.95	8.15	7.80	8.20	8.23	8.73	10.18	9.43	8.13	5.88	7.87

Table 4.18 Monthly and annual means for Faraday for the period 1957 to 1994.

4.3.1 Twelve month running means

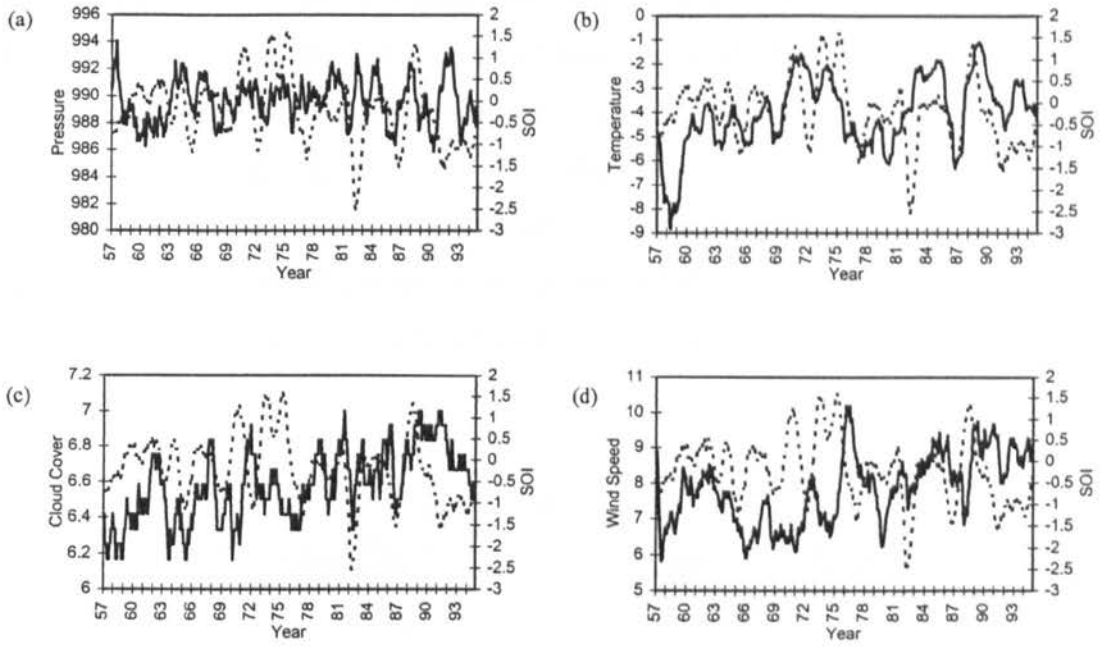

Figure 4.6 Twelve month running means for Faraday (a) pressure, (b) temperature, (c) cloud cover and (d) windspeed with the SOI (dashed line).

Figures 4.6a-d show the twelve month running means of station pressure, temperature, cloud cover and windspeed at Faraday with the SOI. As for Halley there appears to be an inverse relationship between the pressure at Faraday and the SOI. This is clearest during the 1982 and 1991 warm events, when the twelve month running means were 3.47 hPa and 3.92 hPa above the mean respectively (Figure 4.6a). However, this relationship is not apparent for the entire time series, for example, for the 1965 warm event there was a reduction in pressure at Faraday, the running mean was 0.84 hPa below the mean, and for the 1964 cold event, when the running mean was 2.72 hPa above the mean.

The relationship between Faraday temperature and the SOI is clearly a positive relationship (Figure 4.6b), with the temperature trend closely mirroring changes in the SOI. The 1988 cold event saw elevated temperatures at Faraday, when the twelve month running mean was 2.94°C above the mean, and during the 1986 warm event there were cooler temperatures at this station, the running mean was 2.19°C below the mean. The 1982 event, however, does not appear to follow the trend with the temperature regime remaining fairly constant during this event, with the running mean remaining within 1°C of the mean.

There is a fairly complex relationship between Faraday cloud cover and the SOI. Overall, there appears to be a positive relationship between the two (Figure 4.6c). The 1978 cold event appears to coincide with increased cloud amount, the twelve month running mean was 0.25 oktas greater than the mean, whilst the 1983 warm event seems to coincide with a reduction in cloud cover, the running mean was 0.24 oktas below than the mean. However, there also appears to be an underlying trend in the 12 month running means of cloud cover, with a gradual increase in cloud amount over the period 1957 to 1994. This trend was tested using linear regression, however, it was found to have an R^2 value of 0.4438, and is not significant (Figure 4.7a).

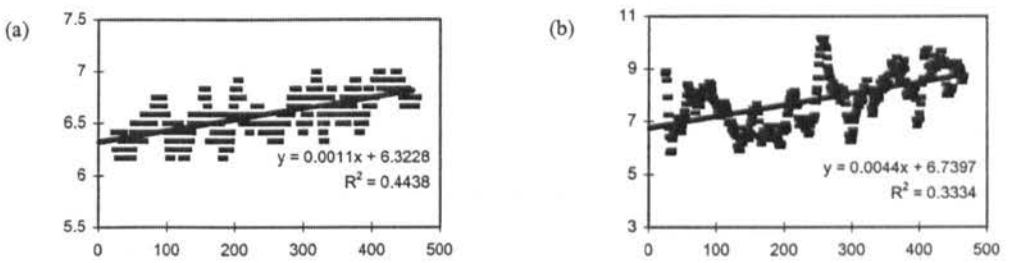

Figure 4.7 Linear regression plots of Faraday (a) cloud cover and (b) windspeed to test the significance of the trend in the twelve month running means.

Faraday windspeed also appears to show a positive relationship with the SOI (Figure 4.6d) especially at the beginning and end of the record. As was found for Halley, the early 1970's was a period of uncertainty in SOI-Faraday windspeed relationships. During the 1988 cold event there was an increase in windspeed, when the twelve month running mean was 1.84 ms^{-1} above the mean; throughout the 1991 warm event there was a decrease in windspeed. As for cloud cover there appears to be an increase in the underlying trend of windspeed over the period 1957 to 1994. This trend is not, however, statistically significant ($R^2 = 0.3334$) (Figure 4.7b).

For Faraday consideration of the general behaviour of the SOI and climate variable time series suggests an inverse relationship between the SOI and pressure where as SOI and cloud cover, temperature and windspeed relationships are positive. Therefore, during warm (cold) events at Faraday, there is an increase (decrease) in pressure, indicative of a decrease (increase) in cyclonicity and a decrease (increase) in temperature, cloud cover and windspeed.

4.3.2 Cross correlation analysis

Cross correlation analysis confirms the overall concurrent inverse relationship between Faraday pressure and the SOI discussed in the previous section. However the strength of the SOI-pressure lead and lag associations exceeds that for the concurrent situation (Figure 4.8a). The most significant SOI-pressure correlation occurs at t-9 months, with other significant correlations occurring between t-11 and t-8 months (Table 4.19). This indicates that the strongest SOI-pressure relationships at Faraday are occurring well in advance of the SOI. Significant lag correlations occur at t+1 and t+3 months (Figure 4.8a). Smith and Stearns (1993) found the most significant, negative, correlation at t-1 month disagreeing with the findings from this study, however their finding is close to the significant lag of t-1 month found in this study.

For temperature strong positive correlations with the SOI occur (Figure 4.8b) centred around t+2 months (Table 4.20). Smith and Stearns (1993) found that the strongest positive correlation occurred at t+5 months. Although this finding disagrees with the most significant correlation at t+2 months found in this study the correlation at t+5 months was found to be significant; the results of the two studies therefore only vary with regards to the timing of the most significant correlation.

t +/-	-11	-10	-9	-8	+1	+3
correlation	.133	.131	.167	.133	-.101	-.124

Table 4.19 Correlation coefficients greater than 2 standard errors for Faraday pressure.

t +/-	-15	-14	-13	-12	-11	-10	-3	-2	-1
correlation	-.127	-.107	-.114	-.114	-.115	-.122	.132	.105	.117

t +/- (contd.)	+0	+1	+2	+3	+4	+5	+6	+7
correlation (contd.)	.179	.208	.214	.196	.185	.192	.183	.126

Table 4.20 Correlation coefficients greater than 2 standard errors for Faraday temperature.

Overall there is a positive lag correlation between cloud cover and the SOI (Figure 4.8c). Conversely negative correlations dominate the lead relationships between the SOI and cloud (Table 4.21). These are especially strong 9 to 10 months before a SOI peak.

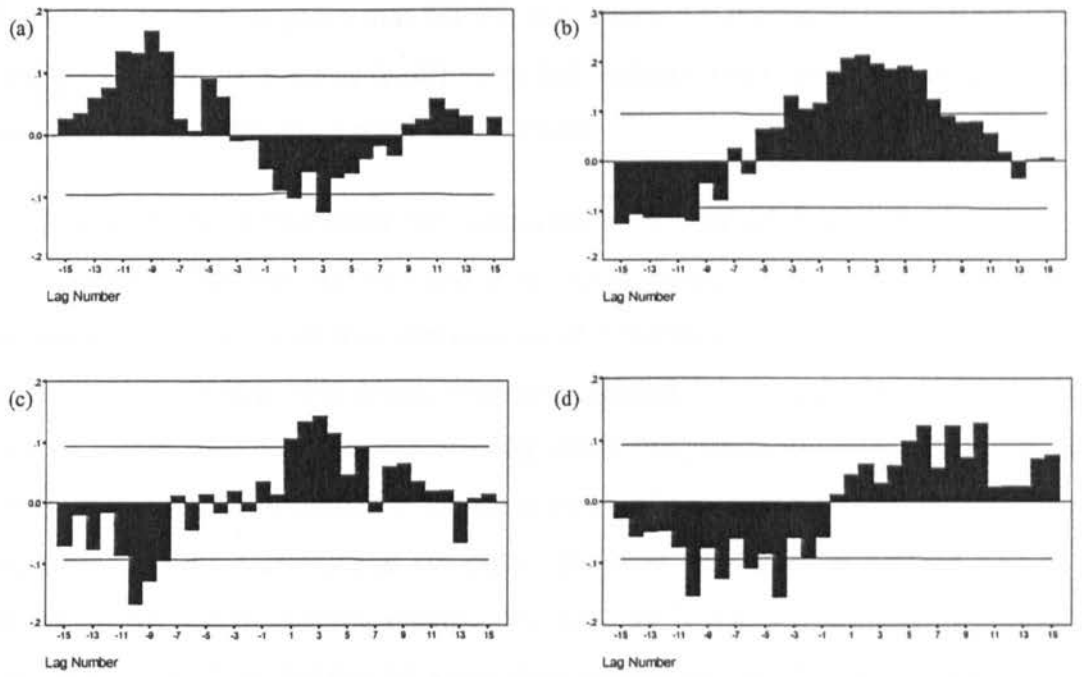

Figure 4.8 Correlograms for Faraday (a) pressure, (b) temperature, (c) cloud cover and (d) windspeed with the SOI. The horizontal lines are two standard error lines.

t +/-	-10	-9	+1	+2	+3	+4
correlation	-.166	-.129	.106	.133	.144	.114

Table 4.21 Correlation coefficients greater than 2 standard errors for Faraday cloud cover.

The SOI-windspeed lead and lag associations are of great interest as the positive and negative correlations are almost symmetrical for up to 15 months demonstrating persistent lead and lag SOI-windspeed associations (Figure 4.8d). The most significant correlation between windspeed and the SOI occurs at t-4 months, however, the significant lag correlations are almost completely mirrored by the significant lead components (Table 4.22). The cross correlation analysis suggests that preceding a warm event peak the windspeeds are generally high whereas following the peak the windspeeds are reduced in strength. The symmetry of the correlations indicates the rapidity of the switch in the wind regime.

t +/-	-10	-8	-6	-4	+5	+6	+8	+10
correlation	-.153	-.125	-.108	-.156	.099	.124	.124	.129

Table 4.22 Correlation coefficients greater than 2 standard errors for Faraday windspeed.

Given the above it appears that for Faraday there are increased (decreased) pressures and windspeeds prior to a warm (cold) event but reduced (increased) windspeeds, temperatures and cloud cover following a warm (cold) event.

In an attempt to demonstrate the importance of methodology, correlograms have been constructed for Faraday pressure and temperature based on the methodology used by Smith and Stearns (1993). Instead of using seasonal differencing prior to applying cross correlation analysis, as is used in this study, monthly anomalies were calculated, from twelve month running means. For the purposes of comparison the period to which the Smith and Stearns (1993) methodology is applied is the same as used in this study; 1957 to 1994. As is seen in Figures 4.9a-b the correlograms are much smoother than those in Figures 4.8a-b, due to the use of twelve month running means. Figure 4.9a is the correlogram for Faraday pressure against the SOI. This plot has the same inverse relationship, between pressure and the SOI, as found in Figure 4.8a above. The most significant correlation occurs at t+4 months (Table 4.23), differing from the most significant correlation at t-9 months found above. However, it agrees with the significant correlation at t+3 months identified in Table 4.23. This correlogram also demonstrates the importance of the time period used as the most significant correlation obtained here differs from that of t-1 month found by Smith and Stearns (1993) using the period March 1957 to March 1984.

t +/-	-12	-11	-10	-9	-8	-7	+0	+1	+2
correlation	.096	.116	.129	.132	.123	.104	-.107	-.132	-.150

t +/- (contd.)	+3	+4	+5	+6	+7	+8	+9	+10
correlation (contd.)	-.164	-.167	-.166	-.160	-.150	-.140	-.128	-.119

t +/- (contd.)	+11	+12	+13	+14	+15
correlation (contd.)	-.111	-.108	-.109	-.112	-.116

Table 4.23 Correlation coefficients greater than 2 standard errors for Faraday pressure using the methodology of Smith and Stearns (1993).

The correlogram for Faraday temperature (Figure 4.9b) shows a positive relationship between temperature and the SOI, as in the correlogram produced above (Figure 4.8b). Using this methodology the most significant correlation occurs at t+3 months (Table 4.24) which is similar to t+2 months found in Table 4.20. The t+5 months found by Smith and Stearns (1993) in their study is the product of a different period of analysis.

t +/-	-6	-5	-4	-3	-2	-1	+0	+1	+2
correlation	.121	.154	.185	.214	.241	.264	.284	.298	.307

t +/- (contd.)	+3	+4	+5	+6	+7	+8	+9	+10
correlation (contd.)	.310	.307	.298	.284	.264	.240	.213	.184

t +/- (contd.)	+11	+12
correlation (contd.)	.153	.120

Table 4.24 Correlation coefficients greater than 2 standard errors for Faraday temperature using the methodology of Smith and Stearns (1993).

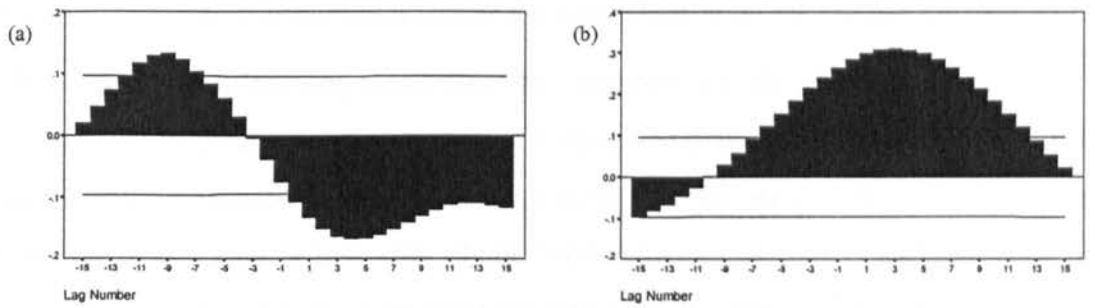

Figure 4.9 Correlograms for Faraday (a) pressure and (b) temperature with the SOI using the methodology of Smith and Sterns (1993). The horizontal lines are two standard error lines.

In summary it can be said that the lags obtained using the methodology of Smith and Stearns (1993) for Faraday temperature and pressure do not differ greatly from those calculated in this study, with the overall trend remaining the same. The most significant difference in results between the two studies seems to be due to differences in the time period used for the analysis, i.e. different ENSO events appear to have differing influences on the Antarctic climate.

4.4 Signals over the rest of the continent

In order to compare the results obtained from Halley and Faraday with those across the Antarctic continent seven stations have been chosen from the Jones and Limbert data set (Section 3.2.1) based on the length and completeness of their records and their distribution

around the continent. The SOI-pressure and temperature relationships are considered for each of the seven stations in this section.

4.4.1 Amundsen-Scott

Amundsen-Scott is located at 90°S 180°W at the geographical South Pole, 2835m above sea level. Table 4.25 shows the monthly and annual means for pressure and temperature for this station.

	Jan	Feb	Mar	Apr	May	Jun	Jul	Aug	Sep	Oct	Nov	Dec	Mean
Pressure (hPa)	690.3	686.1	681.4	680.8	680.6	680.9	676.9	676.1	674.9	676.4	682.1	688.9	681.3
Temperature (°C)	-28.38	-40.49	-53.97	-57.31	-57.86	-58.38	-59.69	-59.96	-59.05	-51.37	-38.42	-27.56	-49.42

Table 4.25 Monthly and annual means for Amundsen-Scott for the period 1957 to 1993.

The twelve month running mean plots for Amundsen-Scott, appear to show little concurrent relationship of pressure and temperature with the SOI (Figure 4.10). The early ENSO events within this time period appear to show an inverse relationship with pressure and temperature, however, this signal is lost after about 1963. Cross correlation analysis, however, reveals significant inverse relationships between pressure and the SOI at t+2 to t+4 months (Table 4.26). These switch to positive relationships from t+11 to t+15 of which lags t+11, t+14 and t+15 are significant (Figure 4.11a). Although the timing of the most significant correlation disagrees with the positive correlation at t+12 months found by Smith and Stearns (1993) significant correlations in this study coincide with this. Significant, positive correlations also

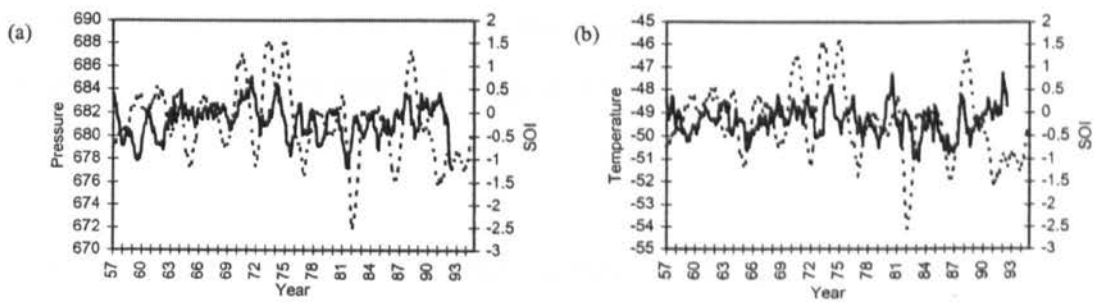

Figure 4.10 Twelve month running means for Amundsen-Scott (a) pressure and (b) temperature with the SOI (dashed line).

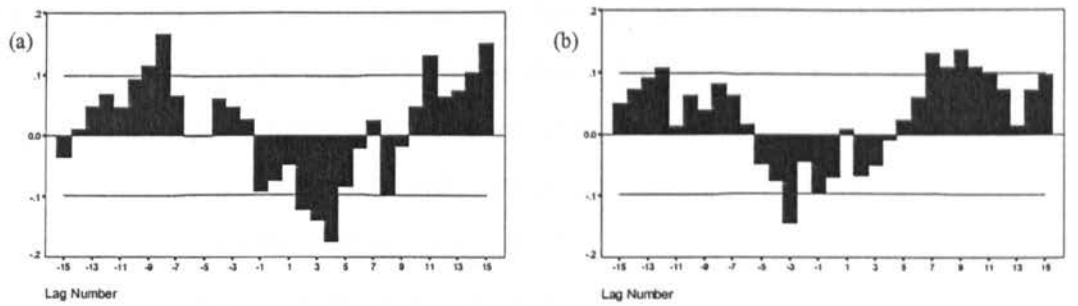

Figure 4.11 Correlograms for Amundsen-Scott (a) pressure and (b) temperature with the SOI. The horizontal lines are two standard error limits.

t +/-	-9	-8	+2	+3	+4	+11	+14	+15
correlation	.114	.166	-.122	-.139	-.174	.130	.102	.150

Table 4.26 Correlation coefficients greater than 2 standard errors for Amundsen-Scott pressure.

t +/-	-12	-3	+7	+8	+9	+10	+11
correlation	.107	-.145	.131	.109	.136	.108	.099

Table 4.27 Correlation coefficients greater than 2 standard errors for Amundsen-Scott temperature.

occur at t-8 and t-9 months. For temperature significant, negative, correlations with the SOI occur (Figure 4.11b) for t-3 and t-12 months (Table 4.27). Significant correlations at t+7 to t+11 months coincide with the positive correlation of t+10 months found by Smith and Stearns (1993) for temperature and the SOI. From a consideration of cross correlation charts for Amundsen-Scott it appears that at the peak of warm (cold) events there tends to be an increase (decrease) in pressure and temperature.

4.4.2 Casey

Casey is located at 66°S 111°E on the coast of east Antarctica, 12m above sea level. Table 4.28 displays the monthly and annual means for pressure and temperature for the period 1957 to 1994.

	Jan	Feb	Mar	Apr	May	Jun	Jul	Aug	Sep	Oct	Nov	Dec	Mean
Pressure (hPa)	988.6	986.2	983.3	984.9	986.7	988.5	983.7	981.4	978.9	979.8	983.8	988.1	984.5
Temperature (°C)	0.03	-2.21	-6.48	-11.28	-13.64	-14.52	-14.80	-15.08	-15.00	-11.21	-5.63	-0.96	-9.32

Table 4.28 Monthly and annual means for Casey for the period 1957 to 1994.

There appears to be very little relationship between the pressure and temperature at Casey and the SOI as shown in the twelve months running means plots (Figure 4.12). However, for the period 1966 to 1986 there appears to be temperature-SOI relationships when warm events tend to coincide with reduced temperatures, for example, the 1969 and 1982 warm events, when the twelve month running means were 0.83 and 3.04°C below the mean, respectively. Cold events tend to coincide with increased temperatures, for example the 1966 cold event, when the running mean was 1.87°C above the mean (Figure 4.12b). A similar signal is not

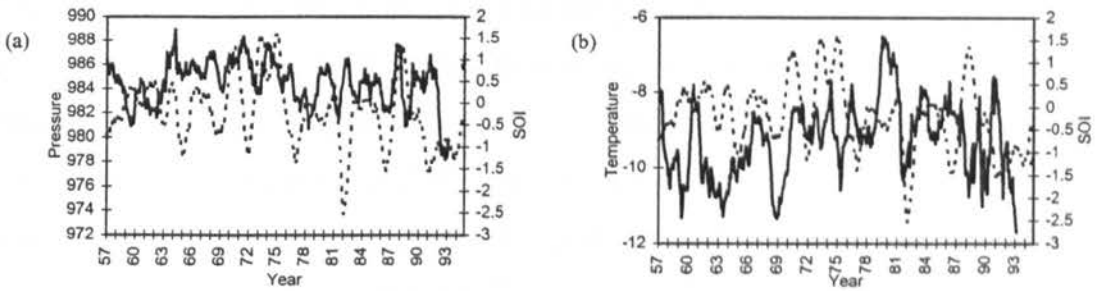

Figure 4.12 Twelve month running means for Casey (a) pressure and (b) temperature with the SOI (dashed line).

apparent between the SOI and station pressure (Figure 4.12a). Apart from the significant cross correlation coefficient for temperature, at t-5 months (Table 4.29), there is an absence of any clear associations between the SOI and pressure and temperature (Figure 4.13a-b). This contrasts with the findings of Smith and Stearns (1993) who found a very significant positive

t +/-	-5
correlation	.132

Table 4.29 Correlation coefficients greater than 2 standard errors for Casey temperature

correlation between the pressure at Casey and the SOI at t+12 months. However, the tendency in the cross correlation chart (Figure 4.13a) mimics that of Smith and Stearns (1993) i.e. a positive coefficient at a t+12 months. They also found significant negative correlations between Casey temperature and the SOI at t-12 months. Consideration of the trends in the correlograms, however, does agree in general terms with the findings of Smith and Stearns (1993) such that at Casey there is a tendency for a reduction (increase) in temperature 5 to 6 months prior to warm (cold) event peaks, but no apparent trend in the pressure at this station.

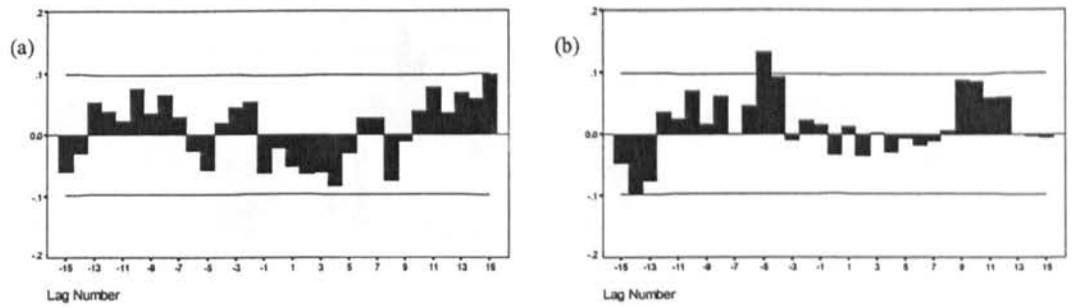

Figure 4.13 Correlograms for Casey (a) pressure and (b) temperature with the SOI. The horizontal lines are two standard error limits.

There appears to be a variation in the SOI-temperature relationship at Casey over the period, as identified in Figure 4.12b. Thus to investigate this variation further correlograms have been constructed for 3 periods; 1957 to 1965, 1966 to 1986 and 1987 to 1994. The correlogram for the period 1957 to 1965 (Figure 4.14a) indicates that over this period there was an inverse correlation between temperature and the SOI, with the most significant correlation occurring at t+10 months (Table 4.30). This period contrasts with the correlogram for the entire period (Figure 4.13b) in which there appeared to be no concurrent relationship between the SOI and Casey temperature. For the period 1966 to 1986 (Figure 4.14b) a positive SOI-temperature relationship exists centred around t-4 to t-5 months (Table 4.31), contrasting with the correlogram for the previous period. This relationship was identified above in the twelve month running mean plots. The correlogram for the final period, 1987 to 1994 displays no significant relationship between the SOI and Casey temperature (Figure 4.14c), however, there is a tendency for an inverse relationship concurrent with the event peaks similar to that found in the initial period, 1957 to 1966.

t +/-	-3	-2	+10
correlation	-.207	-.247	.289

Table 4.30 Correlation coefficients greater than 2 standard errors for Casey temperature for the period 1957 to 1965.

t +/-	-14	-5	-4
correlation	-.136	.236	.165

Table 4.31 Correlation coefficients greater than 2 standard errors for Casey temperature for the period 1966 to 1986.

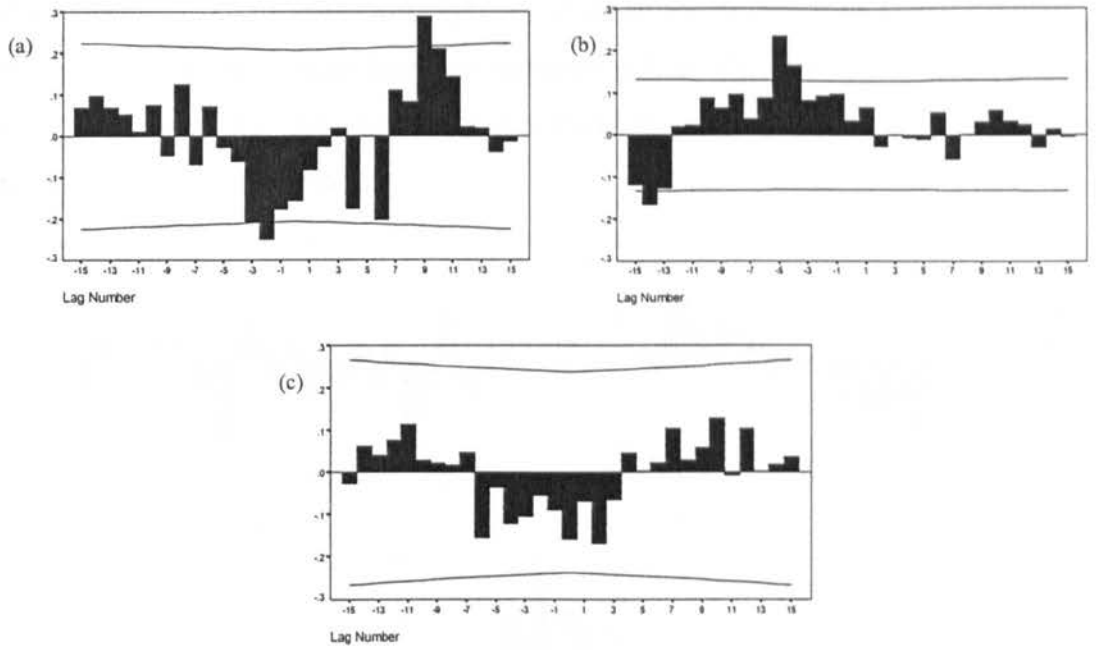

Figure 4.14 Correlograms for Casey temperature with the SOI for the periods (a) 1957 to 1965, (b) 1966 to 1986 and (c) 1987 to 1994. The horizontal lines are two standard error limits.

t +/-	-13	-1	+0	+2	+3	+4	+10	+11	+12
correlation	.137	-.133	-.130	-.141	-.160	-.171	.156	.171	.158

t +/- (contd.)	+13	+14	+15
correlation (contd.)	.198	.198	.249

Table 4.32 Correlation coefficients greater than 2 standard errors for Casey pressure for the period 1966 to 1986.

t +/-	-4	-2	0
correlation	.258	.333	.277

Table 4.33 Correlation coefficients greater than 2 standard errors for Casey pressure for the period 1987 to 1994.

As cross correlation analysis for the period 1957 to 1994 (Figure 4.13a) showed very little relationship between pressure and the SOI, the same analyses were re-run for sub-periods in the above temperature analysis. For the period 1957 to 1965 (Figure 4.15a) no significant SOI-pressure correlations were found. The period 1966 to 1986, however, displayed a strong inverse correlation between pressure and the SOI (Figure 4.14b), with the most significant peak at t+15 months (Table 4.32). This period also exhibits a strong biennial tendency. The

final period, 1987 to 1994, displays a reversal in the correlations (Figure 4.15c). There are strong positive correlations between pressure and the SOI centred around t-2 months (Table 4.33). A year after the peak of events there is a rapid reversal in the relationship, with negative correlations a feature.

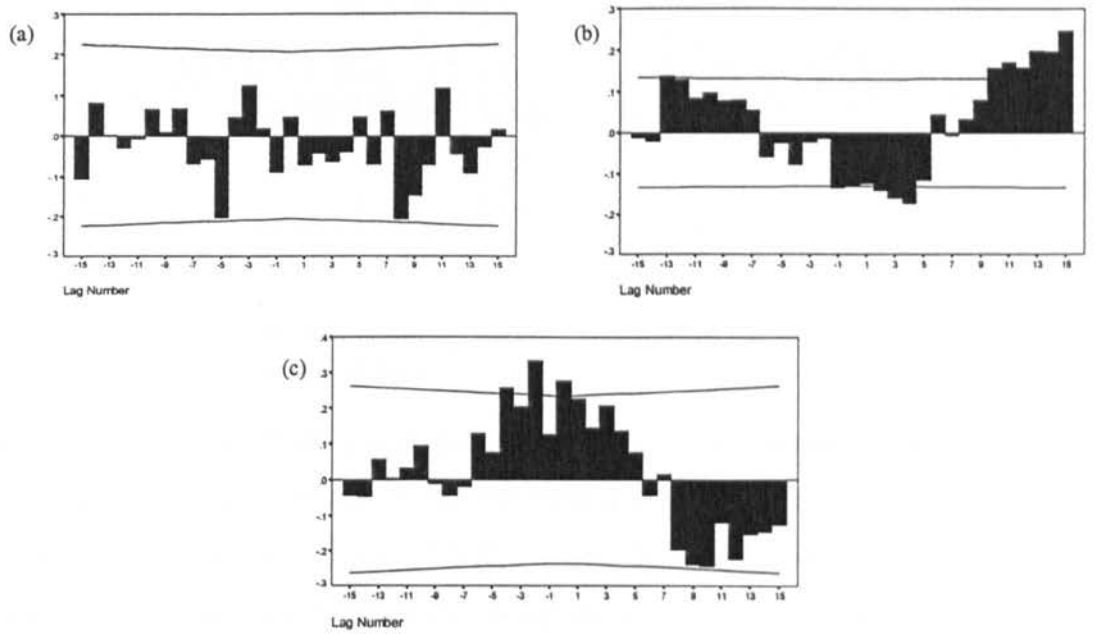

Figure 4.15 Correlograms for Casey pressure with the SOI for the periods (a) 1957 to 1965, (b) 1966 to 1986 and (c) 1987 to 1994. The horizontal lines are two standard error limits.

In summary, the cross correlation analyses for the period 1957-94 reveal little relationship between the SOI and pressure and temperature. However, analyses for 3 sub-periods revealed that reversals in SOI-climate relationships were responsible for the lack of an overall relationship. These results emphasise the importance of the choice of analysis period when searching for climate-SOI relationships as these may not be stable over time. Due to the length of the time period used in this study is not possible to determine whether the SOI climate reversals are part of a longer oscillatory pattern.

4.4.3 Mawson

Mawson is located at 68°S 62°E on the coast of east Antarctica close to the Amery Ice Shelf, 8 m above sea level. Table 4.34 shows the monthly and annual means for pressure and temperature for the period 1957 to 1994.

	Jan	Feb	Mar	Apr	May	Jun	Jul	Aug	Sep	Oct	Nov	Dec	Mean
Pressure (hPa)	990.5	989.8	988.8	990.4	992.2	992.5	988.9	986.6	984.5	984.1	986.5	989.3	988.7
Temperature (°C)	0.11	-4.28	-10.17	-14.48	-16.42	-16.87	-18.21	-18.87	-17.61	-12.99	-5.86	-0.46	-11.40

Table 4.34 Monthly and annual means for Mawson for the period 1957 to 1994.

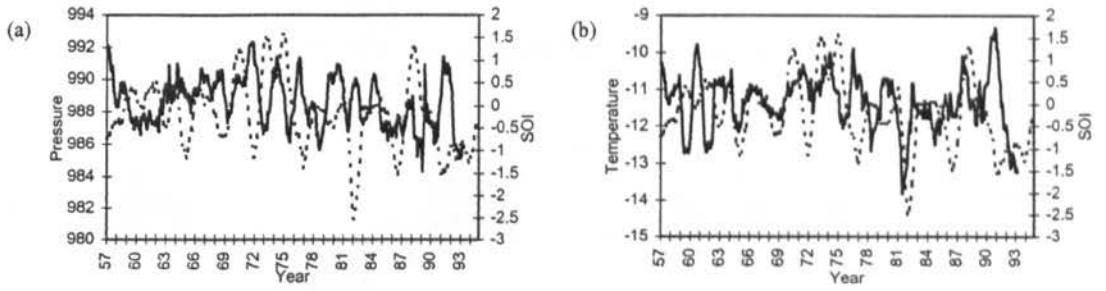

Figure 4.16 Twelve month running means for Mawson (a) pressure and (b) temperature with the SOI (dashed line).

It appears that there is an inverse relationship between the station pressure at Mawson and the SOI, with increased pressure during the 1982 and 1991 warm events, when the twelve month running means were 1.34 and 2.29 hPa above the mean, respectively. These tendencies are matched by reductions in pressure during the 1975 and 1988 cold events, when the twelve month running means were 2.58 and 3.84 hPa below the mean, respectively (Figure 4.16a). The relationship between the temperature at Mawson and the SOI is more complex. From 1957 to 1964 there appears to be an inverse relationship, however, this reverses to a positive relationship that persists until 1985, before returning to an inverse relationship once again (Figure 4.16b). For example, for the 1963 and 1991 warm events, running means were 0.60°C and 2.58°C above the mean. In contrast for the 1982 warm event, the running mean was 2.54°C below the mean.

t +/-	-11	-9	-1	+0	+1	+2	+3	+4	+10
correlation	.103	.104	-.149	-.147	-.118	-.129	-.124	-.165	.098

t +/- (contd.)	+11	+12	+14	+15
correlation (contd.)	.162	.128	.118	.140

Table 4.35 Correlation coefficients greater than 2 standard errors for Mawson pressure.

The cross correlation results for pressure reveal a strong inverse relationship of the SOI and pressure (Figure 4.17a). Significant inverse correlations occur between t-1 month through to t+4 months (Table 4.35). Significant positive correlation peaks occur at t+10-12 and t+14-15

months. For this station Smith and Stearns (1993) found a significant positive correlation of t+12 months between pressure and the SOI, which corresponds to a less significant peak

t +/-	+11	+12
correlation	.107	.109

Table 4.36 Correlation coefficients greater than 2 standard errors for Mawson temperature.

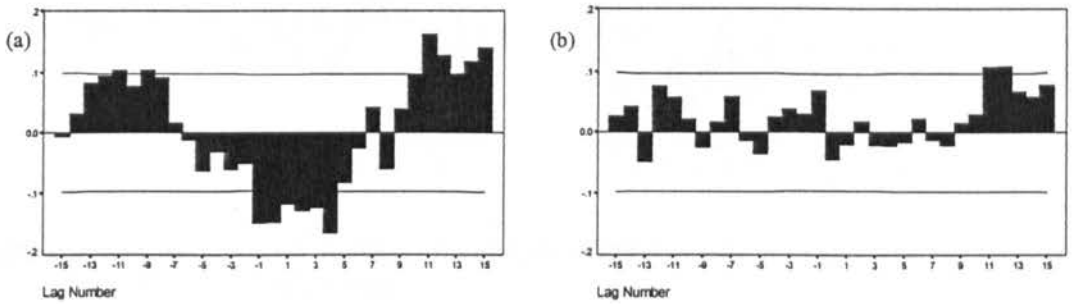

Figure 4.17 Correlograms for Mawson (a) pressure and (b) temperature with the SOI. The horizontal lines are two standard error limits.

found in this study (Figure 4.17a). The temperature correlogram (Figure 4.17b) illustrates a significant positive correlation at t+11-12 months (Table 4.36). This disagrees with the findings of Smith and Stearns (1993) who found significant positive correlations at t-9 months. According to the results presented here generally, at the peak of warm (cold) events the pressure at Mawson tends to be higher (lower) than 'normal' and 12 months after the warm (cold) event peak both temperatures and pressures are lower (higher) than 'normal'.

4.4.4 McMurdo

	Jan	Feb	Mar	Apr	May	Jun	Jul	Aug	Sep	Oct	Nov	Dec	Mean
Pressure (hPa)	992.5	990.9	989.1	990.2	991.2	991.2	988.8	987.9	984.5	981.5	984.0	991.2	988.6
Temperature (°C)	-3.14	-9.25	-17.52	-20.64	-22.81	-23.36	-25.65	-26.65	-24.59	-19.12	-9.63	-3.36	-16.96

Table 4.37 Monthly and annual means for McMurdo for the period 1957 to 1993.

McMurdo is at 78°S 167°E to the east of the Ross Ice Shelf, 24m above sea level. The monthly and annual pressure and temperature means for the period 1957 to 1993 for McMurdo are shown in Table 4.37.

There is a strong inverse relationship between pressure at McMurdo and the SOI until the early 1980's, for example the 1965 warm event, when the twelve month running mean was 3.69 hPa above the mean, coinciding with increased pressure (Figure 4.18a). This pattern

breaks down from the early 1980's, from when there appears to be little relationship between the two. There is an inverse relationship between the temperature at McMurdo and the SOI, especially prior to 1970, however, towards the middle of the time series this relationship

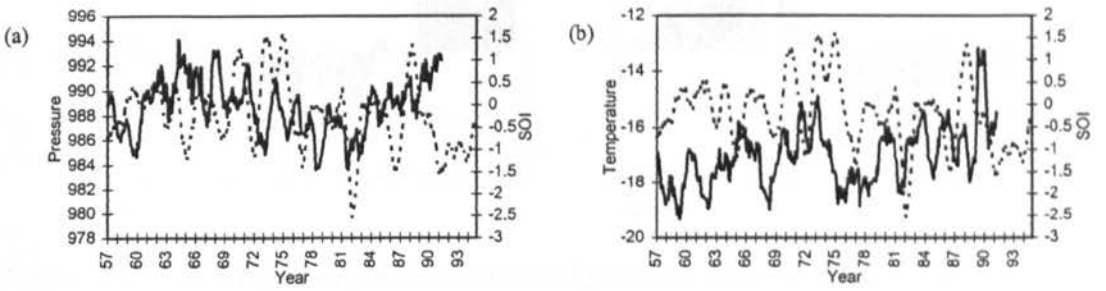

Figure 4.18 Twelve month running means for McMurdo (a) pressure and (b) temperature with the SOI (dashed line).

appears to become positive with increases in temperature corresponding with cold events (Figure 4.18b). Cross correlation analyses for pressure reveal persistent significant or near significant positive correlations (Figure 4.19a) for t+9-15 months (Table 4.38). Significant, negative, correlations at t+3-4 months occur for temperature and the SOI (Table 4.39), however, the most significant correlation is positive at t-9 months (Figure 4.19b). The opposition of these correlations, i.e. their spacing of 12 months and opposite signs, is

t +/-	+9	+10	+11	+12	+14	+15
correlation	.103	.125	.142	.110	.111	.171

Table 4.38 Correlation coefficients greater than 2 standard errors for McMurdo pressure.

indicative of the biennial nature of the teleconnections. Although McMurdo was not used in the analysis of Smith and Stearns (1993) nearby Scott Base was. For this station Smith and Stearns (1993) found there is a significant positive correlation in temperature at t-9 months, agreeing with the findings in this study for McMurdo. The positive pressure

t +/-	-9	-8	-5	+3	+4
correlation	.142	.117	.103	-.134	-.110

Table 4.39 Correlation coefficients greater than 2 standard errors for McMurdo temperature.

correlations at t+9-15 months found here for McMurdo agree in general with the most significant correlation of Smith and Stearns (1993) at t+12 months. Based on the results presented here and those of Smith and Stearns (1993) it appears that with warm (cold) events

there is a tendency for increased (decreased) temperatures at McMurdo following the peak of the event and below (above) 'normal' pressure a year after the warm (cold) event peak.

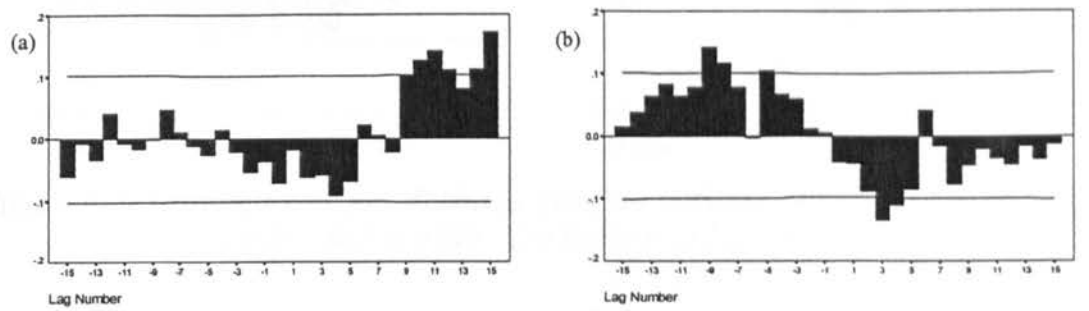

Figure 4.19 Correlograms for McMurdo (a) pressure and (b) temperature with the SOI. The horizontal lines are two standard error limits.

As in the correlograms for Casey, the correlogram for McMurdo pressure shows little relationship between pressure and the SOI prior to t+9 months (Figure 4.19a), thus the period was divided into two periods (1957-81, 1982-93) based on an analysis of the twelve month running mean plot (Figure 4.18a). For the period 1957 to 1981 an inverse SOI-pressure relationship appears to exist (Figure 4.20a). However, unlike Figure 4.19a, this correlogram reveals additional significant negative correlations at t+2 months and a t-5 months (Table 4.40). The period, 1982 to 1993 (Figure 4.20b), reveals a trend similar to that of Figure 4.19a,

t +/-	-5	+2	+10	+11	+14	+15
correlation	-.136	-.123	.126	.162	.180	.217

Table 4.40 Correlation coefficients greater than 2 standard errors for McMurdo pressure for the period 1957 to 1981.

with a significant correlation at t+9 months (Table 4.41) but no significant correlations coinciding with the peak. Based on these findings there appears to be a small difference between the two periods analysed above indicating the differing response of the Antarctic climate to ENSO events. However, unlike Casey, these two periods have many similarities which have been incorporated into the correlogram for the entire period (Figure 4.19a)

t +/-	+9
correlation	.200

Table 4.41 Correlation coefficients greater than 2 standard errors for McMurdo pressure for the period 1982 to 1993.

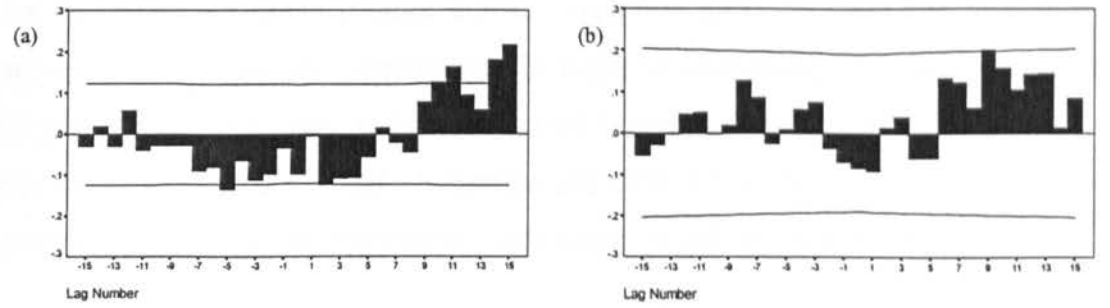

Figure 4.20 Correlograms for McMurdo pressure with the SOI for the periods (a) 1957 to 1981 and (b) 1982 to 1993. The horizontal lines are two standard error limits.

4.4.5 Mirnyy

Mirnyy is located at 67°S 93°E on the coast of east Antarctica approximately midway between Mawson and Casey, 40m above sea level. The monthly and annual means for pressure and temperature for Mirnyy from 1957 to 1994 are shown in Table 4.42.

	Jan	Feb	Mar	Apr	May	Jun	Jul	Aug	Sep	Oct	Nov	Dec	Mean
Pressure (hPa)	990.3	988.3	986.2	987.9	989.1	989.7	986.2	984.1	981.9	981.8	985.5	988.8	986.7
Temperature (°C)	-1.70	-5.21	-10.13	-13.78	-15.54	-15.60	-16.78	-17.10	-17.05	-13.44	-7.41	-2.56	-11.35

Table 4.42 Monthly and annual means for Mirnyy for the period 1957 to 1994.

Based on the information presented in Figure 4.21a there appears to be an inverse relationship between pressure and the SOI at Mirnyy. For example over the period of the 1978 cold event there were decreases in pressure; the twelve month running mean was 3.47 hPa below the mean. For temperature there appears to be a positive relationship with the SOI; there was a peak in temperature preceding the 1988 cold event, when the running mean was 1.08°C above the mean, and a drop in temperature prior to the extreme 1982 event, with the running mean

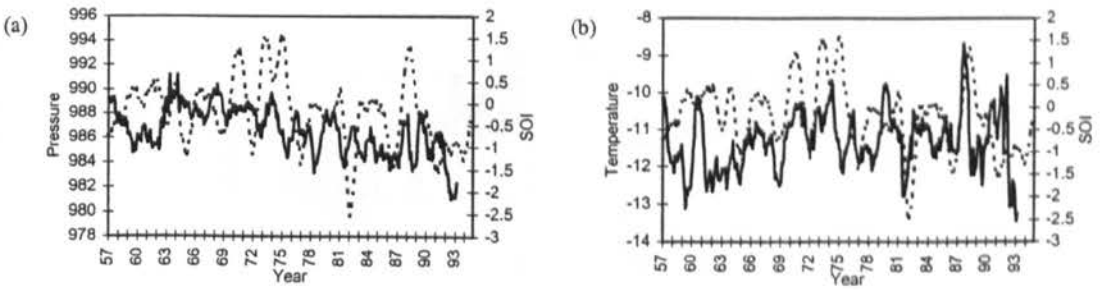

Figure 4.21 Twelve month running means for Mirnyy (a) pressure and (b) temperature with the SOI (dashed line).

1.47°C below the mean (Figure 4.21b). However, prior to 1964 this relationship did not appear to exist. From the correlograms the negative relationship between pressure and the SOI (Figure 4.22a) can be seen with a duration of 5 months (t+1-5) (Table 4.43). Other significant correlations occur at t-8 and t-9 months and t+11, t+14 and t+15 months. These pressure correlations are not in agreement with those found by Smith and Stearns (1993) who

t +/-	-9	-8	+1	+2	+3	+4	+5	+11
correlation	.106	.109	-.102	-.126	-.148	-.137	-.102	.104

t +/- (contd.)	+14	+15
correlation (contd.)	.117	.139

Table 4.43 Correlation coefficients greater than 2 standard errors for Mirnyy pressure.

identified the most significant positive correlation at t-12 months. The cross correlation coefficients show that there is a significant positive correlation between Mirnyy temperature and the SOI (Figure 4.22b) with the most significant correlation occurring at t-5 months (Table 4.44). This agrees with that found by Smith and Stearns (1993).

t +/-	-5
correlation	.118

Table 4.44 Correlation coefficients greater than 2 standard errors for Mirnyy temperature

Given the above it appears that at Mirnyy prior to a warm (cold) event there are increased (decreased) temperatures, and at the peak of the warm (cold) event there is an increase (decrease) in the station pressure.

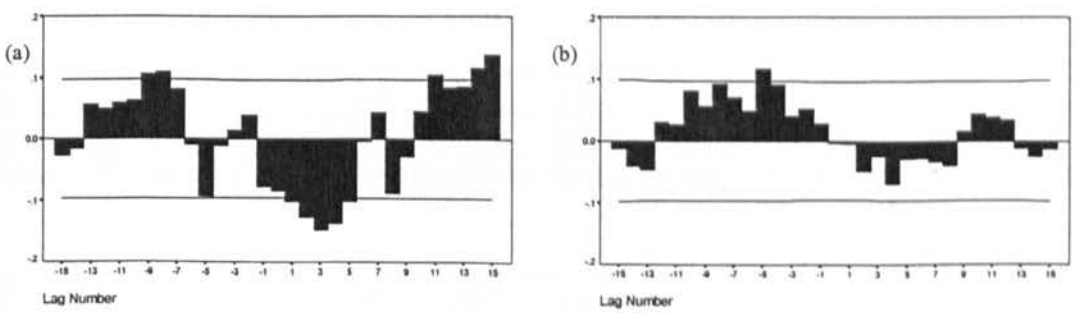

Figure 4.22 Correlograms for Mirnyy (a) pressure and (b) temperature with the SOI. The horizontal lines are two standard error limits.

4.4.6 SANAE

SANAE is situated at 70°S 2°W to the east of the Antarctic Peninsula, 30m above sea level. Table 4.45 shows the monthly and annual pressure and temperature means for SANAE from 1957 to 1992.

	Jan	Feb	Mar	Apr	May	Jun	Jul	Aug	Sep	Oct	Nov	Dec	Mean
Pressure (hPa)	991.8	990.1	986.2	987.2	989.8	990.4	987.7	987.2	985.3	984.4	986.1	991.3	988.2
Temperature (°C)	-4.02	-8.81	-13.51	-19.08	-21.13	-23.23	-26.62	-27.06	-24.70	-18.72	-10.85	-4.96	-16.95

Table 4.45 Monthly and annual means for SANAE for the period 1957 to 1992.

Inverse relationships between SANAE pressure (Figure 4.23a) and temperature (Figure 4.23b) and the SOI occur. Unlike many of the other locations this inverse relationship appears to persist throughout the length of the record for pressure. For temperature there is a breakdown in the signal from the 1980's. Cross correlation analyses reveal clear inverse relationship between pressure and the SOI (Figure 4.24a) for t-1 and t+2-4 months (Table 4.46). Other significant peaks occur at t+14 and t+15 months. Temperature displays significant correlations at t-11-13 months (Table 4.47) but, overall around the event peaks have an

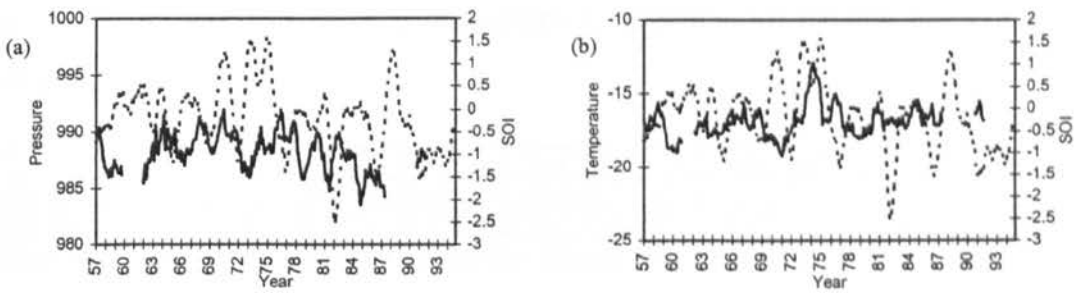

Figure 4.23 Twelve month running means for SANAE (a) pressure and (b) temperature with the SOI (dashed line).

t +/-	-1	+2	+3	+4	+14	+15
correlation	-.107	-.114	-.110	-.141	.110	.146

Table 4.46 Correlation coefficients greater than 2 standard errors for SANAE pressure.

t +/-	-13	-12	-11	+2
correlation	.128	.141	.138	-.105

Table 4.47 Correlation coefficients greater than 2 standard errors for SANAE temperature.

inverse relationship with the SOI (Figure 4.24b). Overall during warm (cold) events there is an increase (decrease) in temperature and pressure at SANAE, but up to 12 months in advance of these warm (cold) events there are pressure decreases (increases).

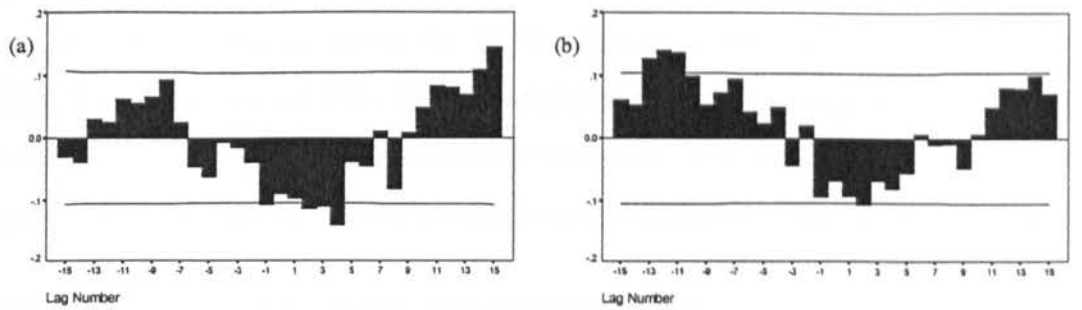

Figure 4.24 Correlograms for SANAE (a) pressure and (b) temperature with the SOI. The horizontal lines are two standard error limits.

4.4.7 Vostok

Vostok is located at 79°S 106°E, 3486m above sea level on the east Antarctic ice dome. Table 4.48 shows the monthly and annual means for pressure and temperature for Vostok from 1958 to 1994. Elevation is responsible in large part for the low temperatures at Vostok (Dalrymple, 1966).

	Jan	Feb	Mar	Apr	May	Jun	Jul	Aug	Sep	Oct	Nov	Dec	Mean
Pressure (hPa)	634.0	629.8	624.7	623.4	623.8	624.1	622.4	619.9	617.6	618.9	625.6	633.4	624.9
Temperature (°C)	-32.08	-44.43	-57.9	-64.69	-65.84	-65.31	-67.01	-68.23	-65.97	-55.85	-43.16	-31.95	-55.24

Table 4.48 Monthly and annual means for Vostok for the period 1958 to 1994.

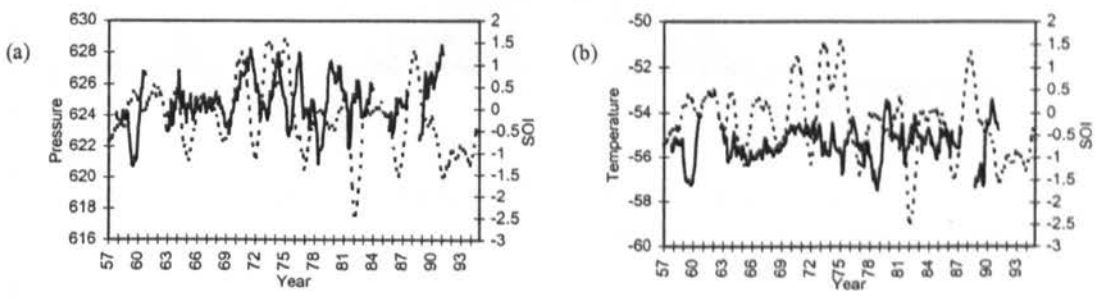

Figure 4.25 Twelve month running means for Vostok (a) pressure and (b) temperature with the SOI (dashed line).

The signal at Vostok is complex as it varies throughout the 1958 to 1994 record. From 1970, the relationship between pressure and the SOI is an inverse one, however, prior to this the

relationship appears to be positive (Figure 4.25a). This inverse relationship is especially clear for the 1982 warm event, when the twelve month running mean was 3.17°C above the mean, and the 1975 cold event, when the running mean was 2.16°C below the mean. The relationship between temperature and the SOI is not clear. However, there does appear to be a clear inverse relationship during the 1978 cold event, when the running mean was 3.96°C below the mean (Figure 4.25b). The correlograms for temperature and pressure (Figure 4.26a-b) indicate the strength of these inverse correlations. For pressure and temperature there are negative relationships for periods around the SOI maximum. Significant correlations between

t +/-	+4	+11	+12	+13	+15
correlation	-.119	.124	.117	.140	.137

Table 4.49 Correlation coefficients greater than 2 standard errors for Vostok pressure.

pressure and the SOI also occur for t+11-13 and t+15 months (Table 4.49). Temperature appears to have a stronger negative association with the SOI compared to pressure especially

t +/-	+0	+2	+3
correlation	-.103	-.116	-.144

Table 4.50 Correlation coefficients greater than 2 standard errors for Vostok temperature.

for the months centred on t+3 (Table 4.50). Based on the cross correlation analysis results, for Vostok there is a tendency for above (below) normal temperatures and pressures to occur during warm (cold) events.

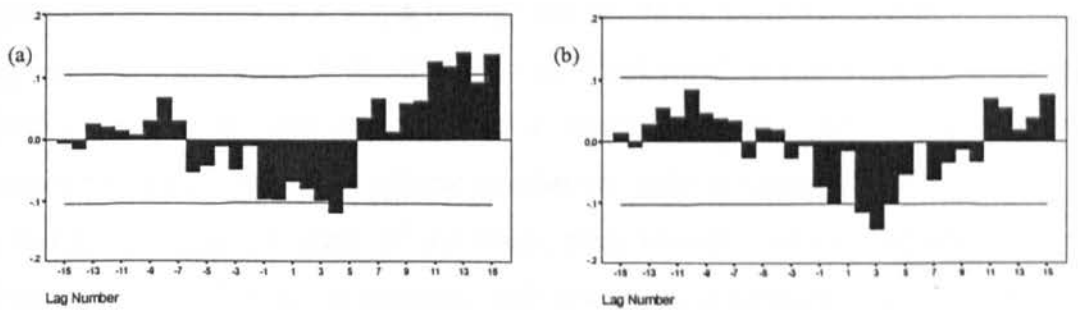

Figure 4.26 Correlograms for Vostok (a) pressure and (b) temperature with the SOI. The horizontal lines are two standard error limits.

4.5 Summary

Analyses of concurrent, lead and lag associations between the SOI and a range of climate variables has revealed that ENSO signals in the climate time series considered are not constant over time or space. The twelve month running means plots clearly display the differing climate response to each ENSO event, however, the cross correlation analyses indicate overall patterns when continuous time series are compared. A comparison of this study's results with the findings of Smith and Stearns (1993) has revealed that methodology plays a major role in determining conclusions concerning the timing of the lead and lag correlations. In this study seasonal differencing was undertaken before cross correlation analysis. However, in the study by Smith and Stearns (1993), averages were calculated and the data was smoothed by taking twelve month running means of the anomalies prior to cross correlation analysis. As smoothing of the data can lead to the displacement of the peak and troughs as well as averaging the responses over time this may account for some of the study result differences. However, the major differences between the timings of the leads and lags for this study and that of Smith and Stearns (1993) appear to be a result of the differences in the time periods used, their study covered the period 1957 to 1984, whilst this used 1957 to 1993/4. This emphasises further the differing response of Antarctic climate to ENSO over time. Figures 4.27 and 4.28 indicate the overall spatial patterns of the most significant pressure and temperature correlations for each of the stations. If the biennial nature of the response to ENSO is taken into account, i.e. negative anomalies are replaced by positive anomalies 12 months later, it can be said that across the continent pressure responses occur at lags of 3 to 4 months (t+3-4). Thus during warm (cold) events there are positive (negative) pressure anomalies with lags of 3 to 4 months (t+3-4). All of the Antarctic stations considered in this study have general similarities in the response of pressure to the SOI during a warm event. At the peak of the event, even though levels of significance vary, all the stations have an increase in pressure, with decreases in pressure in the year prior to and the year after the warm event peak, indicative of a strong biennial tendency in the response of Antarctic station pressure to the SOI. The temperature response is not as clear, although different stations will have differing responses to the same situation, for example the response of temperature at a maritime station such as Faraday to an increase in pressure is very different to that of a continental station such as Vostok. Around the peak of a warm event

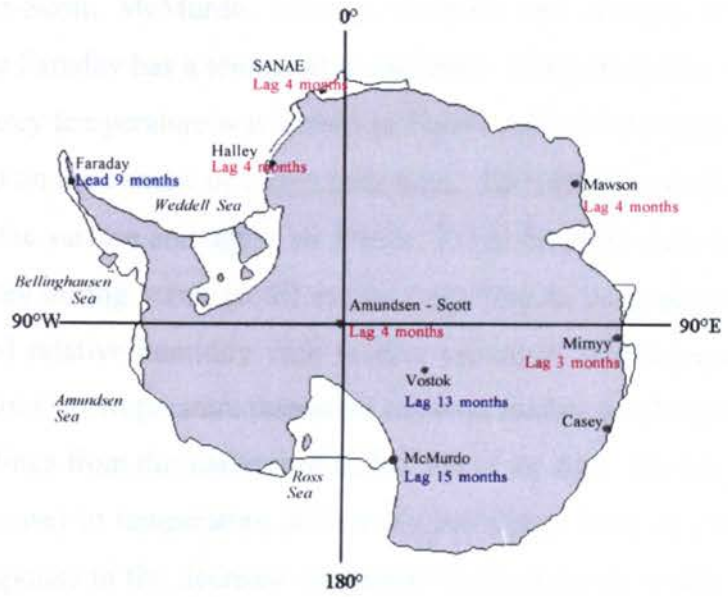

Figure 4.27 Most significant lead and lags of station pressure with the SOI calculated using cross correlation analysis, showing the response of pressure during warm events. Increases in pressure are in red, reductions in pressure are in blue.

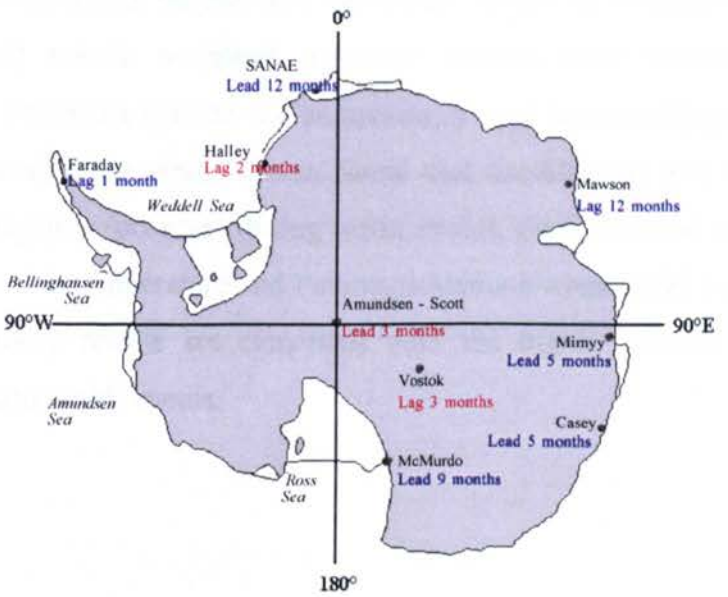

Figure 4.28 Most significant lead and lags of station temperature with the SOI calculated using cross correlation analysis, showing the response of temperature during warm events. Increases in temperature are in red, reductions in temperature are in blue

Halley, Amundsen-Scott, McMurdo, Mirnyy, SANAE and Vostok all have increases in temperature, whilst Faraday has a temperature decrease. Casey shows no difference, although the response of Casey temperature was shown in Figure 4.15 to be produced by a variation in the effect of ENSO on the climate of Casey over time. The results at Halley were shown to be consistent at both the surface and upper air levels. From the cross correlation analysis it was shown that at Halley during warm (cold) events there was an increase (decrease) in 500 and 850 hPa height and relative humidity with weaker (stronger) north-easterly (south-westerly) winds. The variations in temperature responses between Halley and Faraday can be explained in terms of the findings from the analysis of Halley upper air data. During warm (cold) events the reduction (increase) in temperature at Faraday associated with an increase (decrease) in pressure, was a response to the decrease (increase) in cloud cover which caused an increase (decrease) in the radiative heat loss. Whilst until the mid-1970's at Halley during warm (cold) events the increase (decrease) in temperature associated with increased (decreased) pressure can be explained by an increase (decrease) in cloud cover, limiting (increasing) the radiative heat loss. The difference between the station temperature responses can also be explained by the alteration in the strength of the 500 hPa westerlies. When the westerlies are weak (strong) during warm (cold) events, mainland Antarctic stations have increases (decreases) in temperature whilst Peninsula stations are anomalously cold (warm) (Rogers, 1983). This is confirmed in this analysis in which it was found that the 850 and 500 hPa westerly wind components were negative (positive) during warm events, thus mainland stations would have an increase (decrease) in temperature and Peninsula stations would have a decrease (increase) in temperature. These results are consistent with the higher (lower) pressure over the continent during warm (cold) events.

CHAPTER 5

SEARCHING FOR TELECONNECTIONS OVER THE ENTIRE SOUTHERN HEMISPHERE

5.1 Introduction

The previous chapter considered the effects of ENSO on the climate variability of Antarctica without considering the mechanisms by which the signal reaches the high latitudes. This chapter looks at the entire Southern Hemisphere to investigate the propagation of the ENSO signal from the tropics to the high latitudes on a spatial as well as a temporal scale. By considering the entire Southern Hemisphere it will be possible to investigate the movements of anomaly wavetrains both zonally and meridionally between the tropics and the poles.

With regard to this endeavour five types of analysis were undertaken. Initially, Hovmöller charts were used to investigate the movement of height and temperature anomalies, between the tropics and the poles, along a single meridian (Section 5.2). From this it was hoped to identify the time scale at which climate anomalies appear to propagate between Southern Hemisphere low and high latitudes. In Section 5.3.1 composite annual anomaly plots for year -1, year 0 and year +1 of cold and warm events are considered for the spatial movement of height and temperature anomalies. As an extension of this analysis three month percentage anomaly charts for sea level pressure were investigated for patterns in the anomalies at the peaks of warm and cold events (Section 5.3.2). From these analyses the climatic situation at the peak of the events will be identified which will aid the interpretation of the harmonic analysis results presented in the following section. Harmonics analysis was carried out in an attempt to identify the combined temporal and spatial movement of anomalies across the entire Southern Hemisphere. The phase and amplitude of the first harmonic of climate anomalies were derived and mapped in order to identify the timing of the strongest anomalies at each 5×5° grid point covering the Southern Hemisphere (Section 5.4). The phase and amplitude of the first harmonic for all grid points were subjected to cluster analysis in order to

identify the spatial extent of any teleconnections between regions of similar anomaly peak timing. Finally, in Section 5.5, the mechanisms behind the propagation are sought through the use and analysis of zonally averaged Hovmöller plots.

5.2 Hovmöller analysis

This section considers the movement of 500 hPa and 700 hPa height and 700 hPa temperature anomalies during individual warm and cold events along the 230° longitude line, a meridian which crosses a major centre of action associated with ENSO. The purpose of this analysis is to identify any ENSO related anomaly wavetrains moving between the tropics and the poles. Individual event based analyses and composites are compared in the section in order to identify any similarities or differences in the signal propagation within and between groups of warm and cold events (Table 3.4).

5.2.1 Cold Events

Figure 5.1a-c are the Hovmöller plots for 500 hPa and 700 hPa height and 700 hPa temperature anomalies, for the 1975 cold event. To aid interpretation a plot of the SOI is also given. The moderate 1975 cold event was characterised by weak positive height anomalies in the low latitudes, apart from two short periods in the year following the event peak (Figure 5.1). Twelve months before the event peak negative anomalies appear to have propagated from the midlatitudes to the outer subtropics. This feature was extremely clear in the 1978 event to be discussed below. Five to six months prior to the event peak strong positive anomalies developed in subtropical latitudes; these propagated poleward, intensified in the midlatitudes and reached a maximum in subpolar latitudes centred on 70°S soon after the event peak. Strong positive anomalies persisted at these latitudes well into year 0. A feature of interest in year +1 was the development and persistence of strong negative anomalies in the outer subtropics that appear to have a subtropical origin. These inversely mimicked their subpolar latitude counterparts.

A distinct feature of the weak 1978 cold event was the poleward movement to about 55°S of negative height anomalies to the middle of year -1 followed by an intensification and

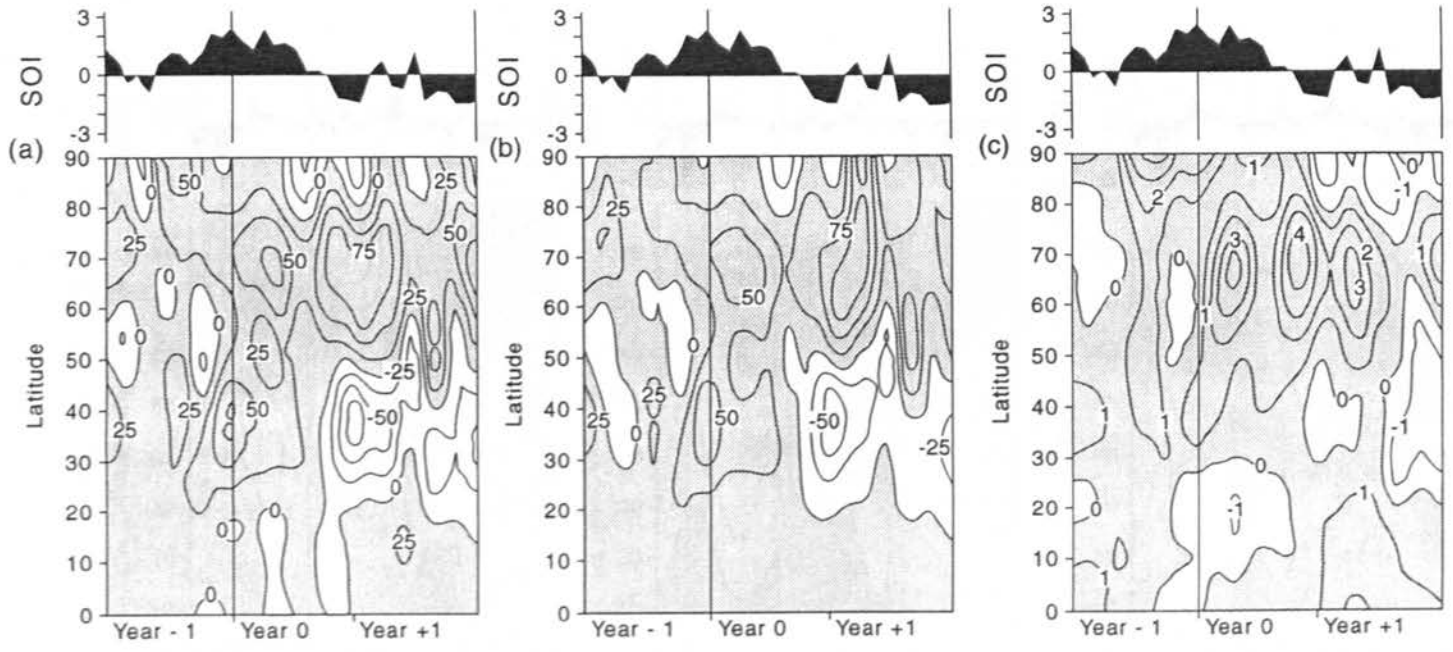

Figure 5.1 Hovmöller diagrams of anomalies in (a) 500 hPa height (in metres), (b) 700 hPa height (in metres) and (c) 700 hPa temperature (in °C) for 230° longitude for the 1975 cold event. Above is the Southern Oscillation Index (in hPa).

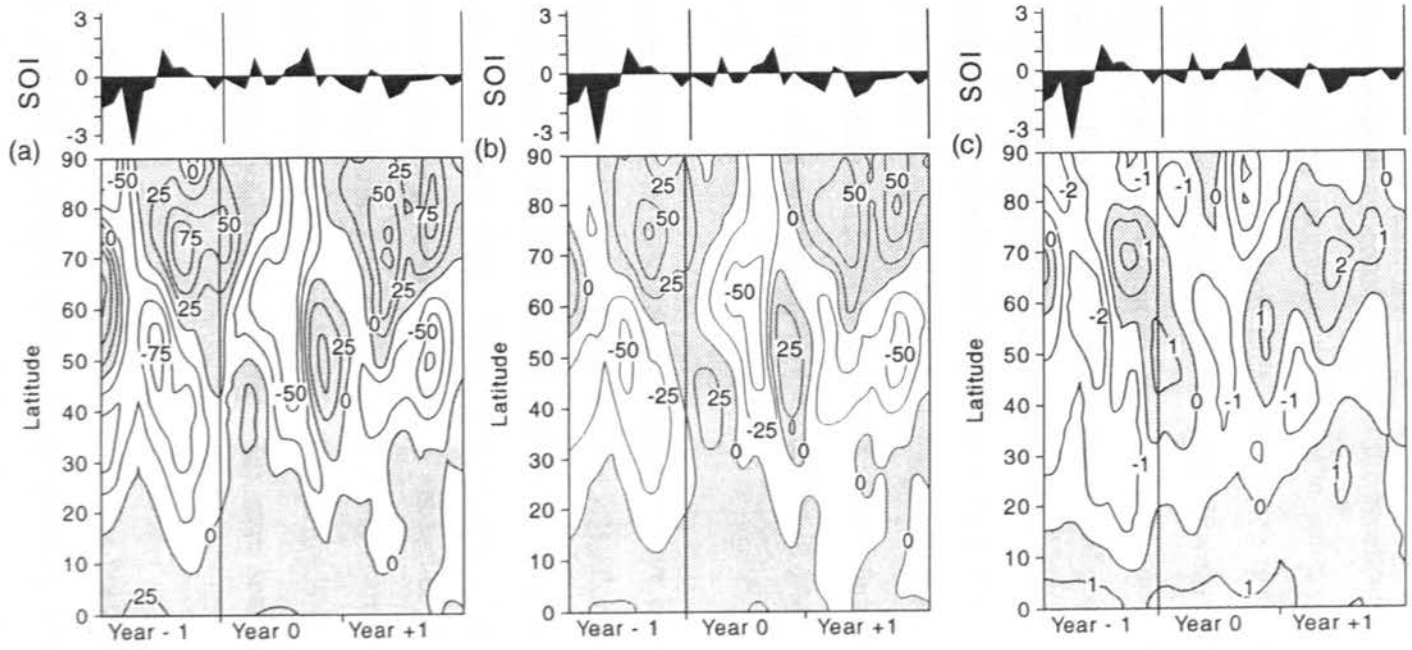

Figure 5.2 Hovmöller diagrams of anomalies in (a) 500 hPa height (in metres), (b) 700 hPa height (in metres) and (c) 700 hPa temperature (in °C) for 230° longitude for the 1978 cold event. Above is the Southern Oscillation Index (in hPa).

equatorward propagation of these to subtropical latitudes prior to the event peak (Figure 5.2). A further feature was the initiation of a clear equatorward propagation of positive height anomalies from high latitudes in year -1. At the same time, subtropical latitudes were experiencing negative pressure departures, consistent with the weakening of the subtropical jet. The high latitude positive height anomalies reached the subtropical latitudes by the middle of year 0 and replaced the negative anomalies that existed here throughout year -1. Similarly the high latitude positive height departures in year -1 were replaced by negative departures in year 0 which at this time extended over a large meridional range to the midlatitudes and subsequently into the subtropics towards the end of year 0. Associated with the northerly migration of high latitude positive height anomalies over the period year -1 to year 0 were also perturbations in the meridional temperature field (Figure 5.2c). As in the 1975 event, there appears to have been a seesaw in the sign of the high latitude height anomalies. Negative anomalies dominated prior to the event. These then switched to positive anomalies with event peak onset, after which negative anomalies in year 0 were followed by positive anomalies in year +1.

For the strong 1988 cold event (Nicholls, 1991) there appears to have been little propagation of anomalies between the tropics and the polar regions (Figure 5.3). For the high latitudes the negative anomalies that dominated in the first half of year -1 switched suddenly to positive anomalies in the latter half of the same year. These were sustained until the event peak (Figure 5.4a) after which there was a reversal to negative anomalies (Figure 5.4b), which persisted throughout year 0 and partly into year +1, to the north between 45°S and 20°S. Such a pattern represents a large meridional contrast in the climate fields (Figure 5.4a-b). The meridional trends in the temperature anomalies (Figure 5.3c) were seen to mimic the height trends.

The cold event composite (Figure 5.5) was characterised by the northward propagation of anomalies from the high latitudes to around 50°S. These positive anomalies in the high latitudes switch suddenly after the event peak to negative anomalies, persisting until the end of year 0 before switching back to positive anomalies. This composite identifies some of the characteristics present within the individual events. However, due to the variable nature of the

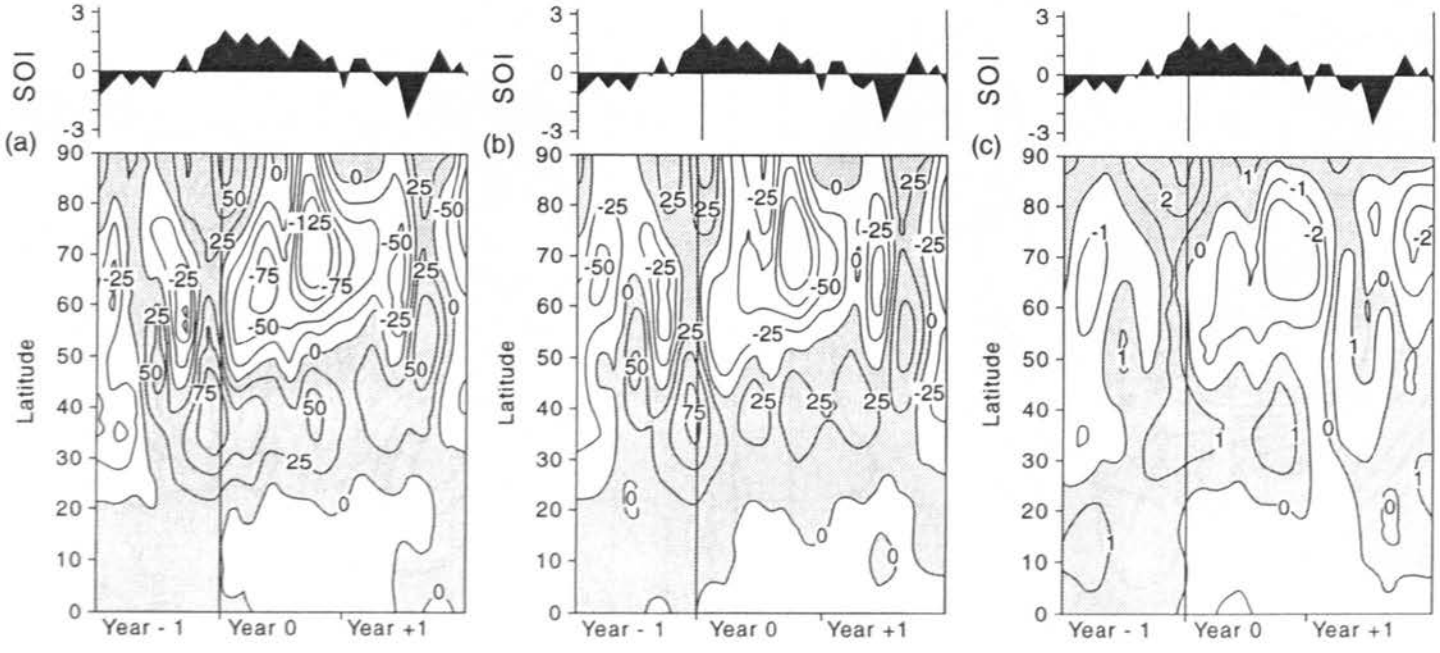

Figure 5.3 Hovmöller diagrams of anomalies in (a) 500 hPa height (in metres), (b) 700 hPa height (in metres) and (c) 700 hPa temperature (in °C) for 230° longitude for the 1988 cold event. Above is the Southern Oscillation Index (in hPa).

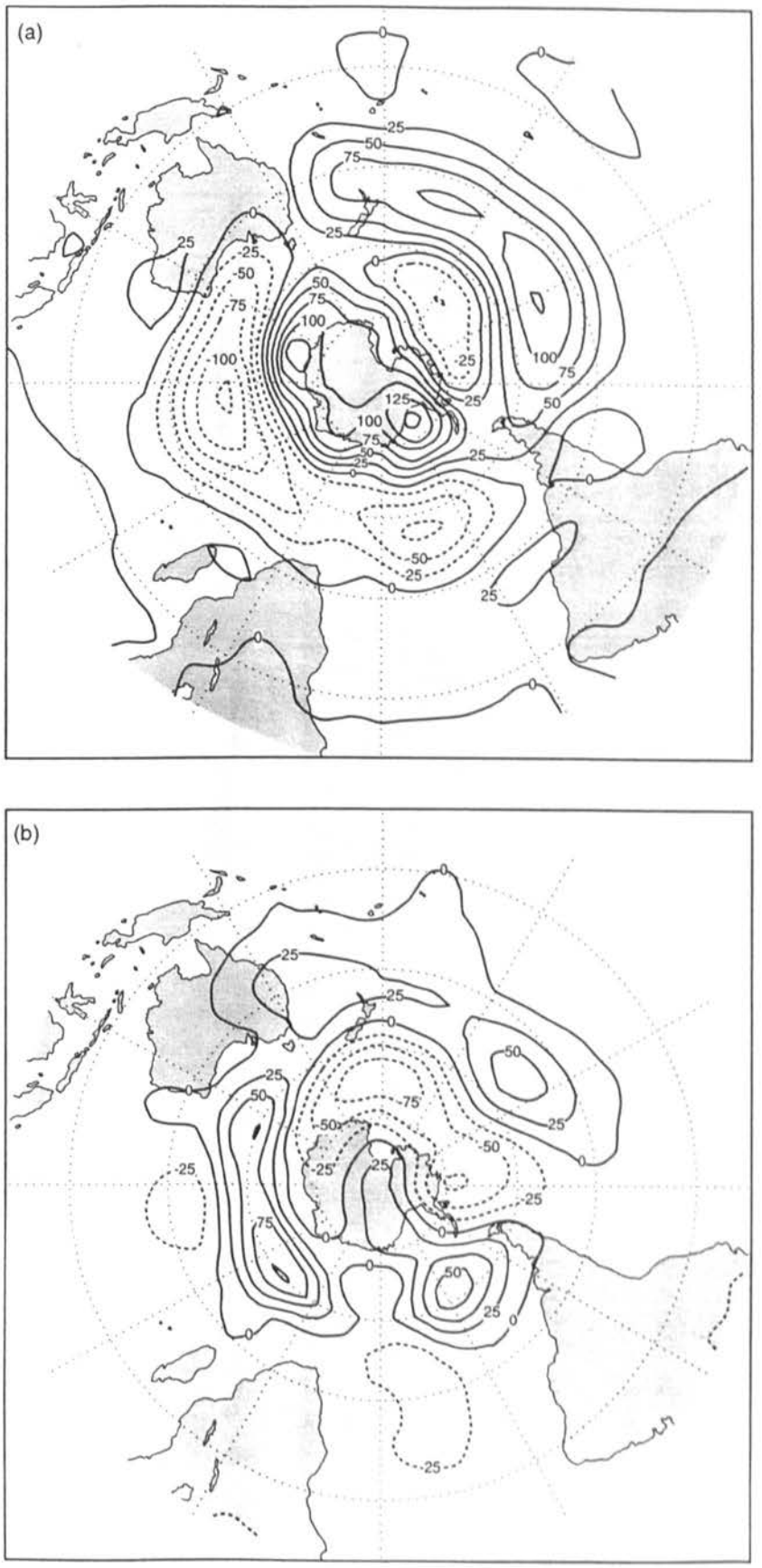

Figure 5.4 Spatial plots of 500 hPa height anomalies (in hPa) for (a) the peak of the 1988 cold event and (b) six months after the peak of the 1988 cold event.

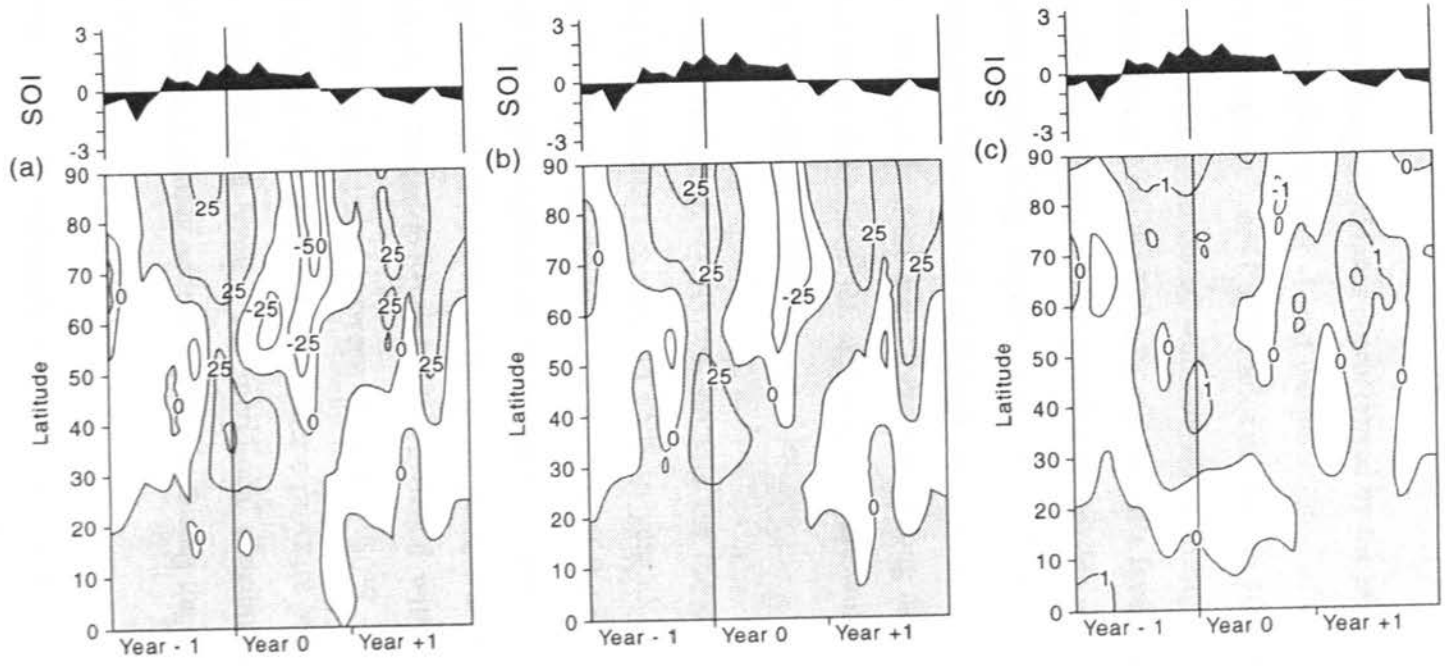

Figure 5.5 Hovmöller diagrams of anomalies in (a) 500 hPa height (in metres), (b) 700 hPa height (in metres) and (c) 700 hPa temperature (in °C) for 230° longitude for the cold events composite. Above is the Southern Oscillation Index (in hPa).

signal propagation within individual events other important trends have been lost, such as the persistence of anomalies centred around 70°S during the 1975 cold event.

5.2.2 Warm Events

The moderate 1976 warm event (Wang, 1995) was characterised by the poleward propagation, from the tropics, of positive anomalies in year -1 and the persistence of these and associated strong temperature anomalies throughout year -1 at latitudes centred on 70°S consistent with a change in the strength of the polar jet. Associated with this was a strong meridional contrast of height and temperature anomalies at both the 500 hPa and 700 hPa levels throughout year 0 (Figure 5.6 a-b). The persistent year 0 high latitude positive anomalies were finally replaced by equatorward and poleward propagating negative anomalies in year +1. These were matched with a switch to negative temperature anomalies over most of the subtropical to middle latitudes in year +1. At the peak of the event there were strong negative anomalies at 35°S, indicating an alteration of the subtropical jet, agreeing with the work of Mo and White (1985) who found a summer ENSO signal in the subtropical jet.

The extreme 1982 warm event (Trenberth, 1991) was notable for the clear propagation of negative anomalies from the high latitudes centred on 75°S in year -1 towards the tropics around 30°S (Figure 5.7), indicating an alteration in the strength of the subtropical jet at the peak of the event, followed by a propagation of these back towards the pole in year 0. Notable also in the periods that span either side of the event peak, was the transition from positive to negative anomalies at latitudes beyond 55°S matched with a transition from negative to positive anomalies for latitudes between 20°S and 50°S. This represents a complete and well-defined reversal of meridional atmospheric pressure patterns from year -1 to year 0 at both 500 hPa and 700 hPa levels. The meridional distribution of temperature anomalies matches well the height anomaly pattern especially during the period immediately prior to and during the event peak.

For the high latitudes, the weak to moderate 1986 warm event (Jordán, 1991) was characterised by a clear seesaw of height anomalies from year -1 through to year +1 and a clear meridional contrast in height anomalies for up to one year following the event peak (Figure 5.8a-b). High latitude negative anomalies prior to the event peak were replaced by

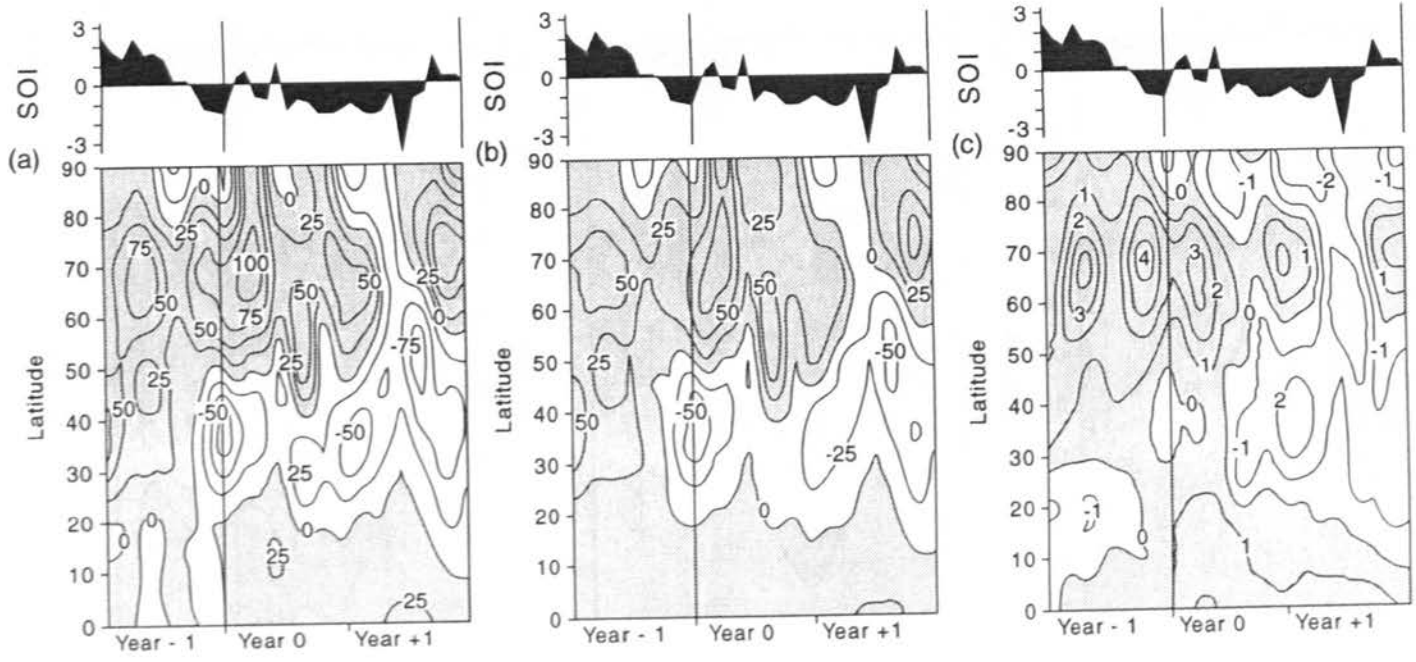

Figure 5.6 Hovmöller diagrams of anomalies in (a) 500 hPa height (in metres), (b) 700 hPa height (in metres) and (c) 700 hPa temperature (in °C) for 230° longitude for the 1976 warm event. Above is the Southern Oscillation Index (in hPa).

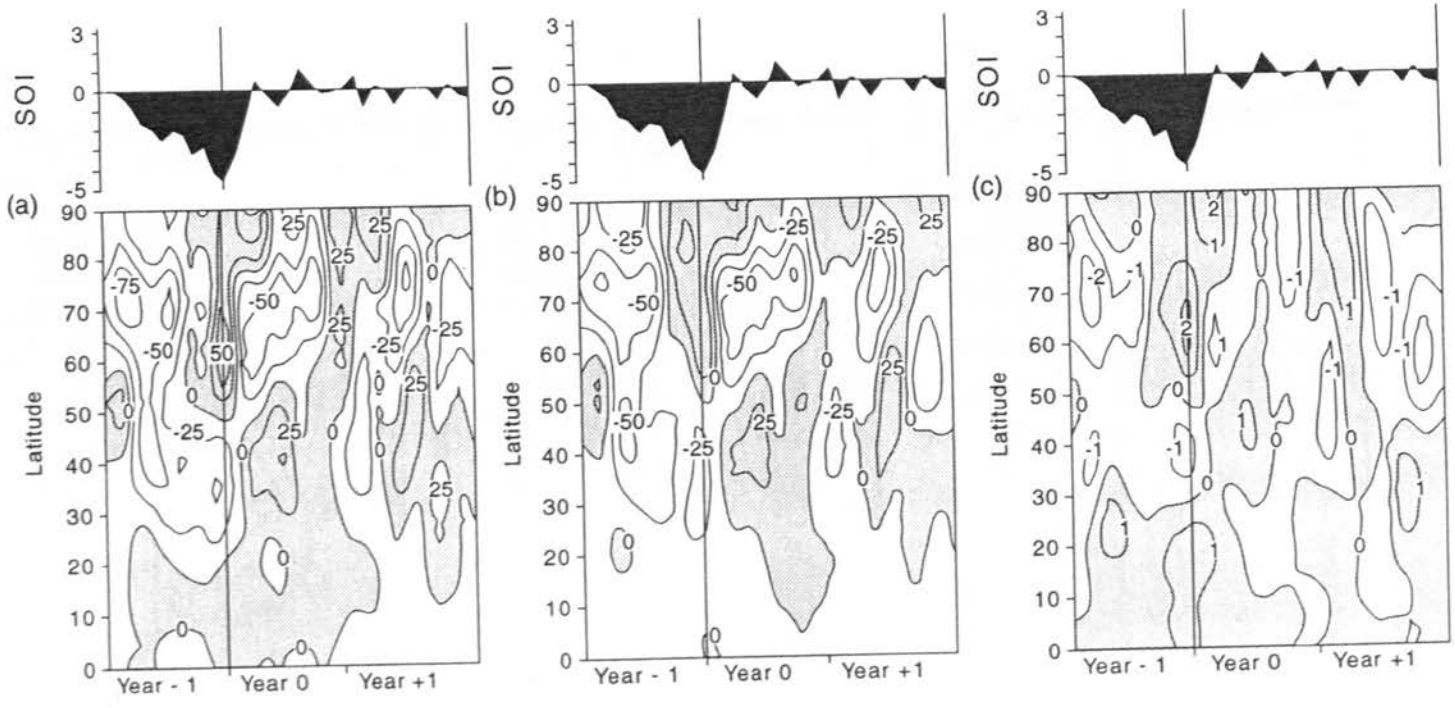

Figure 5.7 Hovmöller diagrams of anomalies in (a) 500 hPa height (in metres), (b) 700 hPa height (in metres) and (c) 700 hPa temperature (in °C) for 230° longitude for the 1982 warm event. Above is the Southern Oscillation Index (in hPa).

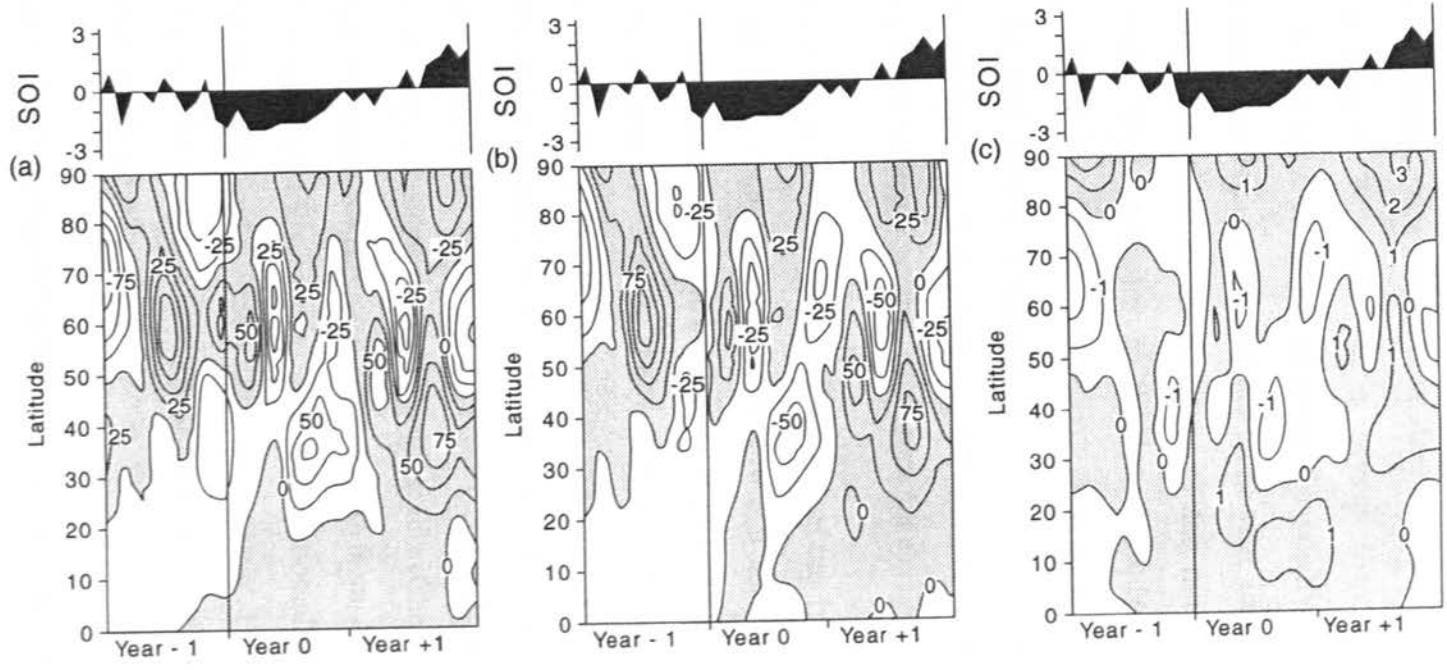

Figure 5.8 Hovmöller diagrams of anomalies in (a) 500 hPa height (in metres), (b) 700 hPa height (in metres) and (c) 700 hPa temperature (in °C) for 230° longitude for the 1986 warm event. Above is the Southern Oscillation Index (in hPa).

positive ones which subsequently appear to have propagated from the pole to the midlatitudes. At the peak of the event there seems to be a short-lived tropical-high latitude link of negative anomalies, which could be indicative of a short lived change in the strength of the subtropical jet. However, this was replaced by a meridional pattern of high latitude positive and subtropical latitude negative anomalies: a pattern consistent for the two previously discussed events. The subtropical negative anomalies persist beyond their high latitude positive counterparts and appear to propagate poleward replacing the positive anomalies previously found here. Reaching a maximum high latitude intensity one year after the warm event peak these then appeared to propagate back in the direction of the midlatitudes where strong positive anomalies existed. These extended to the low latitudes throughout year +1. Temperature anomalies reflect the height anomalies, especially in the high latitudes immediately following the peak (above average temperatures) and also in the subtropical latitudes in the transition between year 0 and year +1 where negative temperature anomalies were matched with strong negative height anomalies (Figure 5.8 c).

The moderate 1991 warm event in many ways resembled that of the 1976 event apart from its long duration. As for the 1976 event, in year -1 there was a slow propagation of strong positive anomalies (up to 100 gpm) from the tropics to the high latitudes where they persisted in a broad latitudinal band centred on 65°S for over one year, well into year 0 (Figure 5.9). From the latter half of year 0 to the early part of year +1 the same positive anomalies appear to have extended northwards to around 45°S. As for other events, the event peak was characterised by meridional height and temperature anomaly contrasts, a result of the change in the relative strengths of both the polar and the subtropical jets (Chen et al., 1996). A year after the event peak negative anomalies migrated equatorward from Antarctica, followed by another pulse in negative anomalies six months later. The anomalies at higher latitudes, especially at the 700 hPa level, followed a seesaw pattern from year -1 to year +1; negative in year -1, positive at the time of the peak and throughout most of year 0, followed by a switch back to negative anomalies from year +1.

The warm event composite was characterised by the poleward migration of positive anomalies from the subtropics, which persisted in the region centred around 70°S into year +1 (Figure 5.10). This composite illustrates the strong meridional contrast between the tropics and the

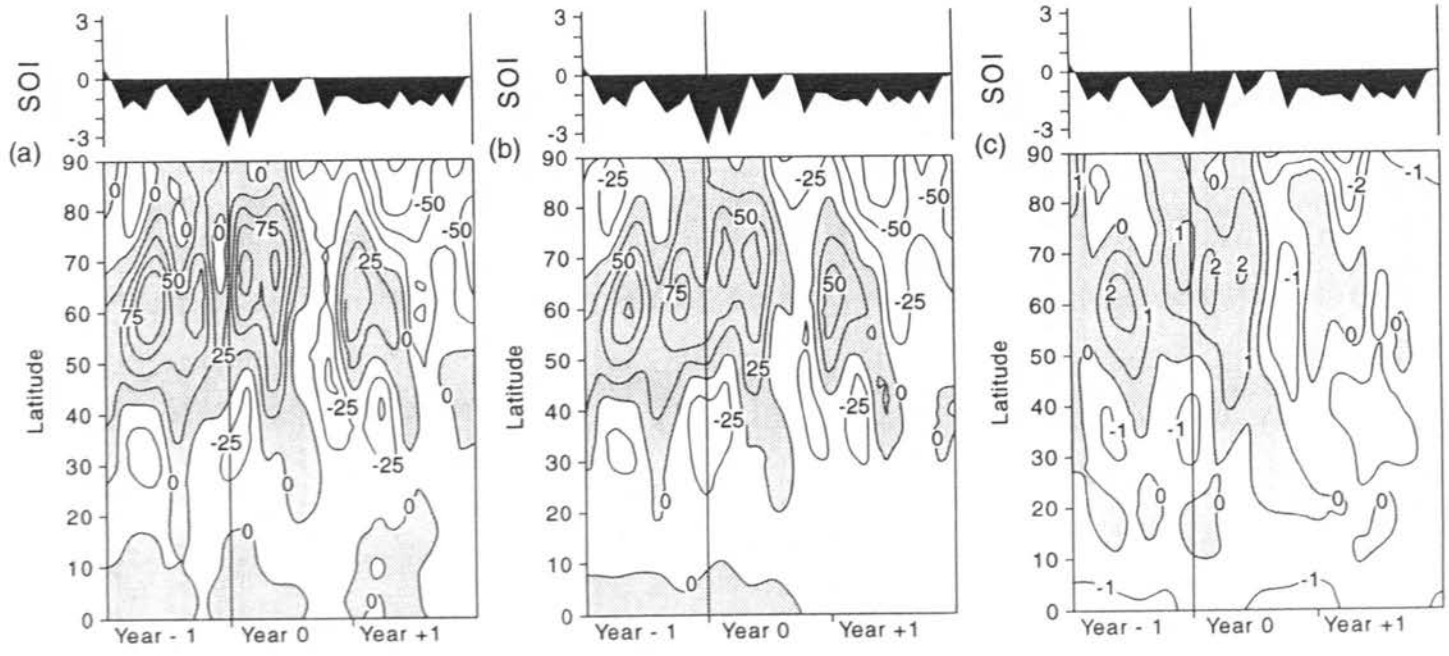

Figure 5.9 Hovmöller diagrams of anomalies in (a) 500 hPa height (in metres), (b) 700 hPa height (in metres) and (c) 700 hPa temperature (in °C) for 230° longitude for the 1991 warm event. Above is the Southern Oscillation Index (in hPa).

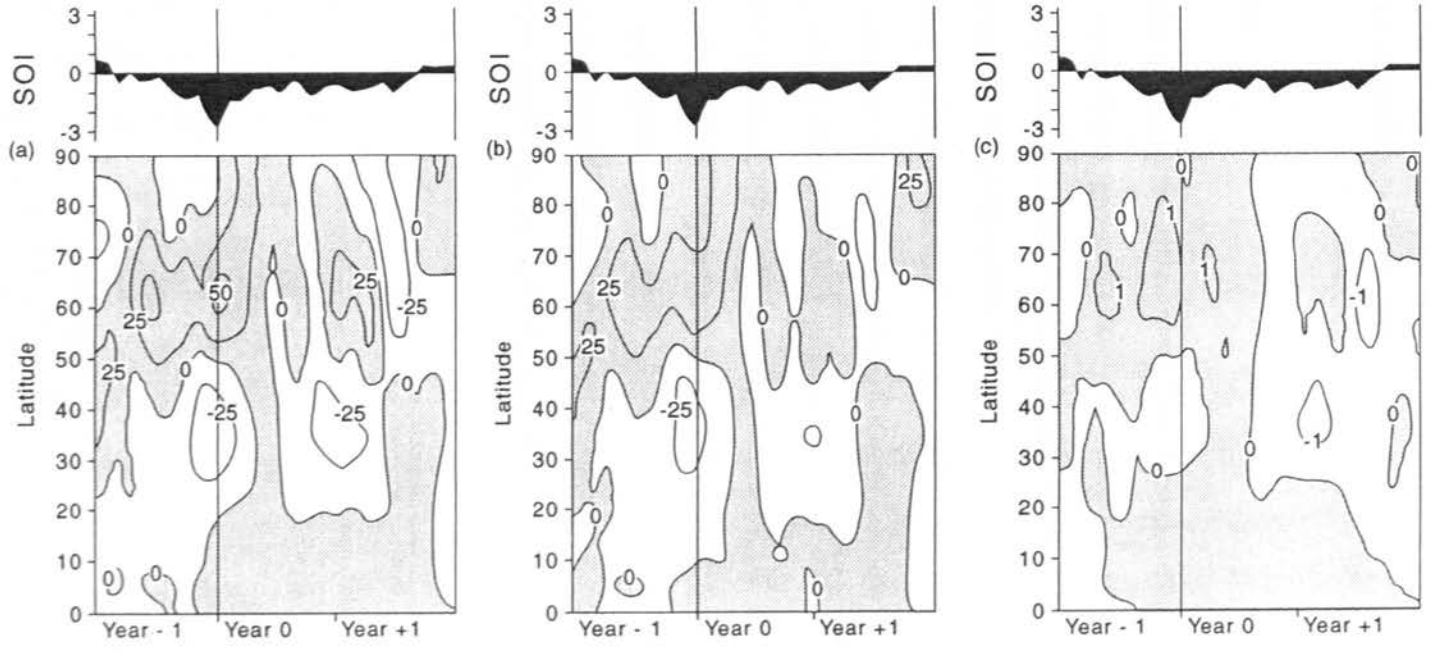

Figure 5.10 Hovmöller diagrams of anomalies in (a) 500 hPa height (in metres), (b) 700 hPa height (in metres) and (c) 700 hPa temperature (in °C) for 230° longitude for the warm events composite. Above is the Southern Oscillation Index (in hPa).

high latitudes, with negative anomalies persisting in the subtropics into year +1. At the start of year +1 there was a northward propagation of negative anomalies from the Antarctic region, coinciding with a southward moving wavetrain of negative anomalies from the outer sub-tropics. Due to the varied nature of the warm events, the warm composite picks up few of the signals identified for the individual warm events.

5.3 Spatial Anomalies

This section primarily looks at annual Southern Hemisphere composites for 500 hPa and 700 hPa height and 700 hPa temperature anomalies for year-1, year 0 and year +1 of cold and warm events. The anomalies were calculated from the long term mean fields for height and temperature. Annual composites were calculated for year -1, year 0 and year +1 of the warm and cold events based on the timing of the event peaks (Table 3.4), where year -1 and year 0 are divided by the event peak, as in the Hovmöller diagrams (Section 5.2). The anomalies associated with individual events are considered in more detail in Section 5.3.2 by comparing percentages of positive and negative sea level pressure anomalies at the peaks of individual events. The percentage of positive and negative anomalies were calculated from the 5 day sea level pressure anomalies and spatial plots were constructed for every three months, on a running basis. Due to space restrictions only the patterns at the peaks are included in this chapter. The complete set of charts can be found in Appendix 2.

5.3.1 Long term means

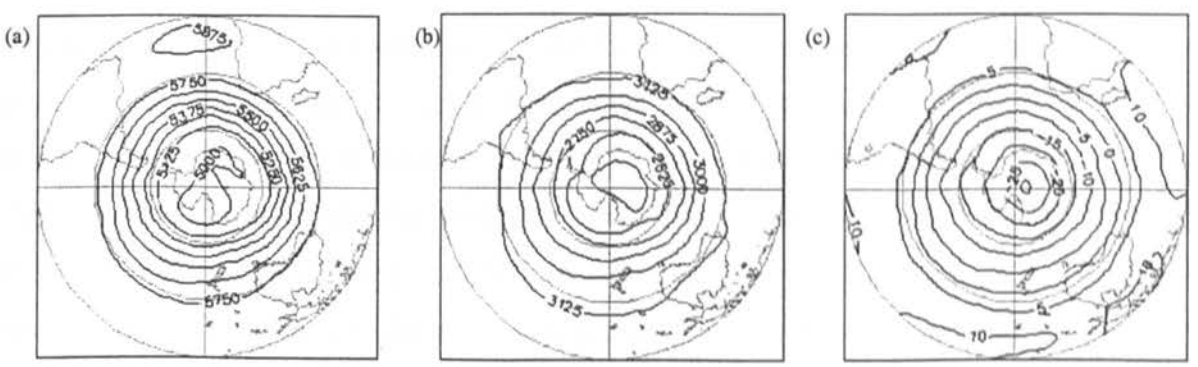

Figure 5.11 Spatial plots of long term means of (a) 500 hPa height, (b) 700 hPa height and (c) 700 hPa temperature for the period 1973 to 1994.

Figure 5.11a-c are the long term means for 500 hPa and 700 hPa height and 700 hPa temperature for the period 1973 to 1994. They form the basis of the comparison for the height and temperature anomaly plots that follow.

5.3.1.1 Annual charts for Cold events

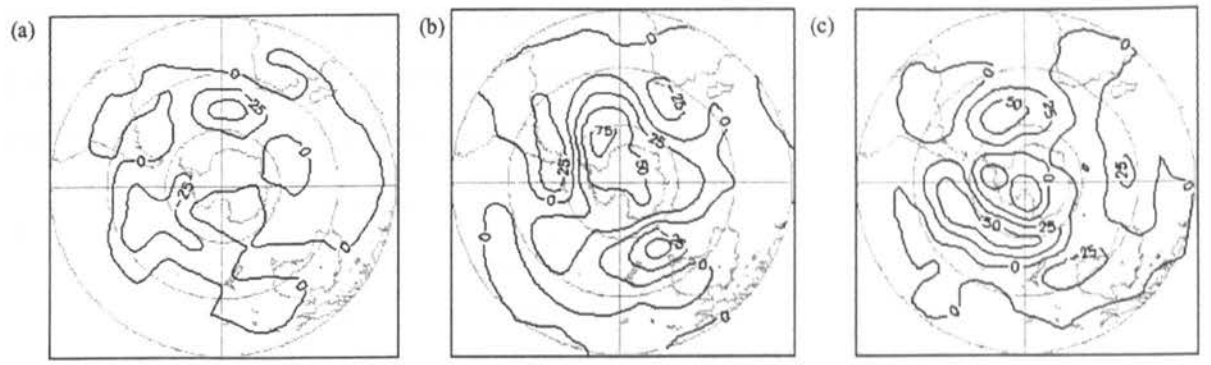

Figure 5.12 Spatial plots of 500 hPa height anomalies for (a) year -1, (b) year 0 and (c) year +1 of composite cold events.

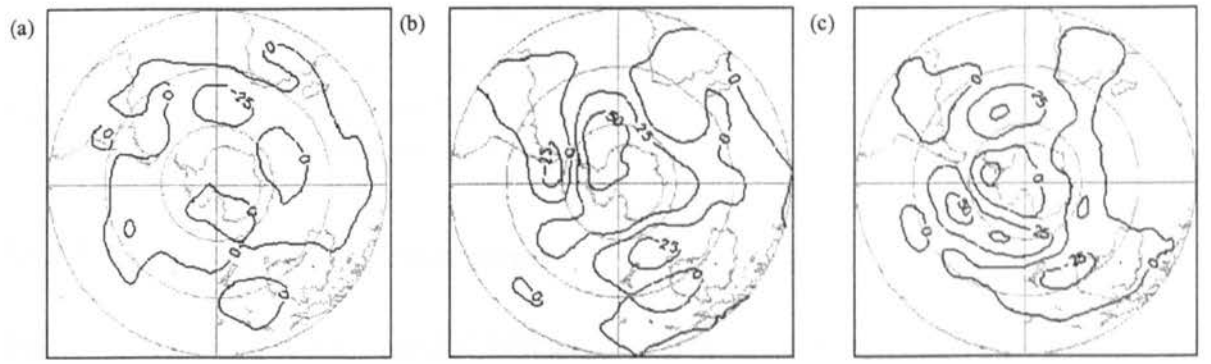

Figure 5.13 Spatial plots of 700 hPa height anomalies for (a) year -1, (b) year 0 and (c) year +1 of composite cold events.

Figures 5.12a-c and 5.13a-c are 500 hPa and 700 hPa cold composite height anomaly plots for year -1, year 0 and year +1. Prior to the cold composite peak there appeared to be few anomaly signals. During both year 0 and year +1 there was a strong meridional contrast in the sign of the anomalies across the Southern Hemisphere, as identified by Mo and White (1985) being most pronounced along the 270° meridian. However, a reversal in the sign of the anomalies occurred between these two periods with strong positive anomalies in the Antarctic region in year 0 replaced by negative anomalies in year +1 and strong negative anomalies in

the midlatitudes in year 0 replaced by extremely strong positive anomalies in year +1, in excess of 50 gpm.

The temperature plots for the Southern Hemisphere (Figure 5.14a-c) also display the meridional contrasts apparent in the height plots, with the strongest contrast occurring during year 0. In both year -1 and year 0 there were positive temperature anomalies in the high latitudes, with negative anomalies in the midlatitudes. As for the height plots (Figures 5.12b-c and 5.13b-c) this pattern reversed in year +1 with negative anomalies at high latitudes and positive anomalies in the midlatitudes.

Figure 5.14 Spatial plots of 700 hPa temperature anomalies for (a) year -1, (b) year 0 and (c) year +1 of composite cold events.

5.3.1.2 Annual charts for Warm events

Figures 5.15a-c and 5.16a-c are 500 hPa and 700 hPa warm composite height anomaly plots for year -1, year 0 and year +1. From these it can be seen that prior to a warm event there were negative height anomalies at around 60°S 160°W, these switched to positive height anomalies during year 0 which were preserved, although they shifted eastward during year +1. The strong positive anomalies during year 0 and were also apparent in the Hovmöller plots, as each of the warm events had strong positive anomalies at this latitude coinciding with, and following the event peak (Section 5.2). The anomalies along the 160° meridian were part of extremely strong set of meridional contrasts in the Pacific region as to the north of this anomalous area there were positive anomalies in year -1, which switched to negative anomalies in year 0, remaining in year +1. In the Antarctic region the positive anomalies which have been found to characterise warm events (Chapter 4) were not present in these composite plots. However, during year +1 there were negative height anomalies across the

Antarctic continent resulting from the biennial nature of the ENSO response. For 500 and 700 hPa height there appears to have been a reversal in the sign of the anomalies between year -1 and year 0, however this contrasts with the reversal in anomaly sign for the cold events in which the strongest reversals occurred between year 0 and year +1.

Figure 5.15 Spatial plots of 500 hPa height anomalies for (a) year -1, (b) year 0 and (c) year +1 of composite warm events.

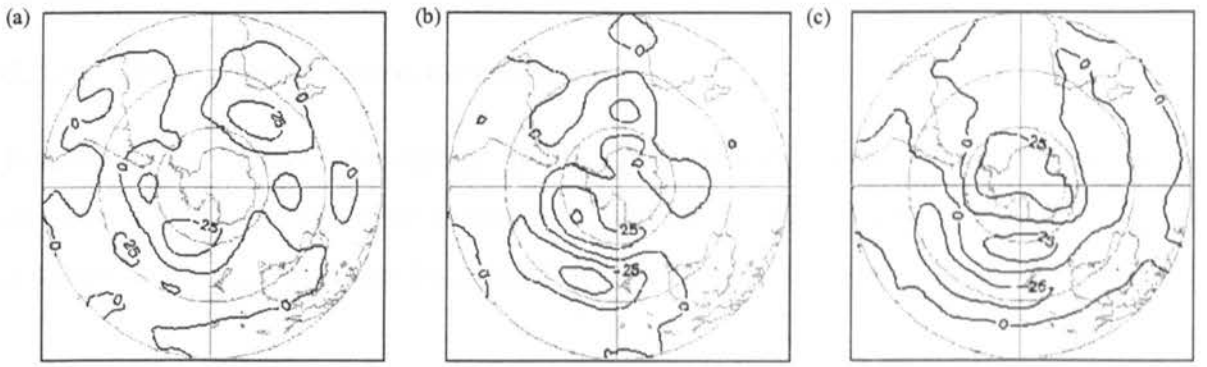

Figure 5.16 Spatial plots of 700 hPa height anomalies for (a) year -1, (b) year 0 and (c) year +1 of composite warm events.

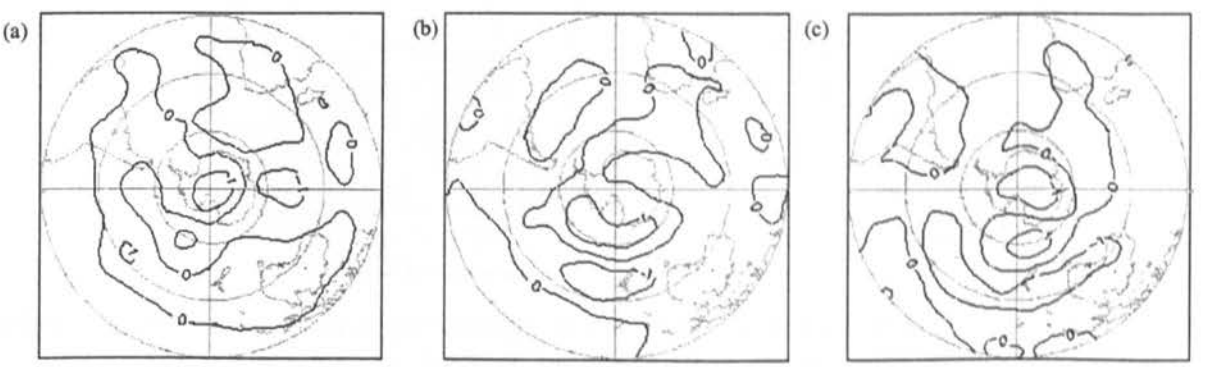

Figure 5.17 Spatial plots of 700 hPa temperature anomalies for (a) year -1, (b) year 0 and (c) year +1 of composite warm events.

The composite temperature anomalies during warm events in the high latitudes follow the same pattern in the sign of the anomalies as the height composites, with similar patterns in the

Pacific region during year 0 and year +1, contrasting with year -1 (Figure 5.17a-c). Along the 160°W meridian during year -1 negative anomalies were present in the subpolar regions, which reversed to positive anomalies in year 0 and year +1, whilst strong negative anomalies developed in the subtropics.

5.3.2 Three month running means

The annual composites show the dominant climate features occurring before, during and after each ENSO event, however, as every ENSO event was different the composites mask many of the features associated with the events. The annual composites also mask the signals occurring at time periods of less than a year. A finer temporal resolution was required to clearly discover the relationships between ENSO and Southern Hemisphere climate variability. The sea level pressure anomalies over Antarctica should be viewed with caution as some of these have been extrapolated down from over 4km to sea level height.

5.3.2.1 Three monthly charts for cold events

Figure 5.18a-b shows the percentage of 5 day periods with positive or negative anomalies in sea level pressure for the three months surrounding the peak of the 1975 cold event (Table 3.4) across the whole of the Southern Hemisphere. At the peak of the event there were

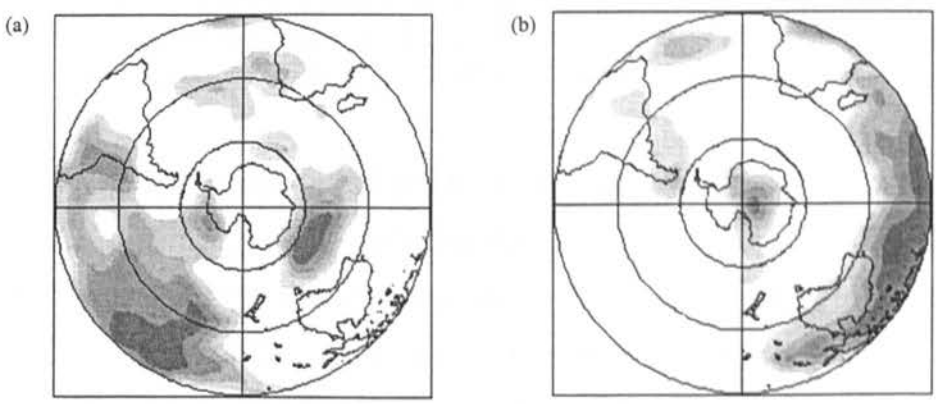

Figure 5.18 Spatial plots of percentage of (a) positive and (b) negative sea level pressure anomalies for the peak of the 1975 cold event. The grey shading indicates anomalies greater than 60%, with the intensity of the grey increasing in 10% bands.

negative pressure anomalies over the centre of the Antarctic continent, which agree with the findings from Chapter 4, and in the region of the Indian Ocean, both of which had persisted

from six months prior to the peak. There were positive anomalies in the Bellinghausen Sea and prior to the event in the Antarctic coastal regions. There were also positive anomalies to the south of Australia and across the mid-Pacific, which developed at least 3 months prior to the peak, persisting until well after the peak. The predominance of positive pressure anomalies in the mid-Pacific can be attributed to the higher pressure resulting from the upwelling of cold water in this region during this moderate cold event. There was a very strong meridional contrast in the sign of the anomalies from east Antarctica northwards along the 90°E meridian, with negative anomalies at the pole, switching to positive anomalies in the midlatitudes and strong negative anomalies over the Indian Ocean. This meridional contrast was strongest at the peak of the cold event, when the percentages of both positive and negative anomalies were the greatest.

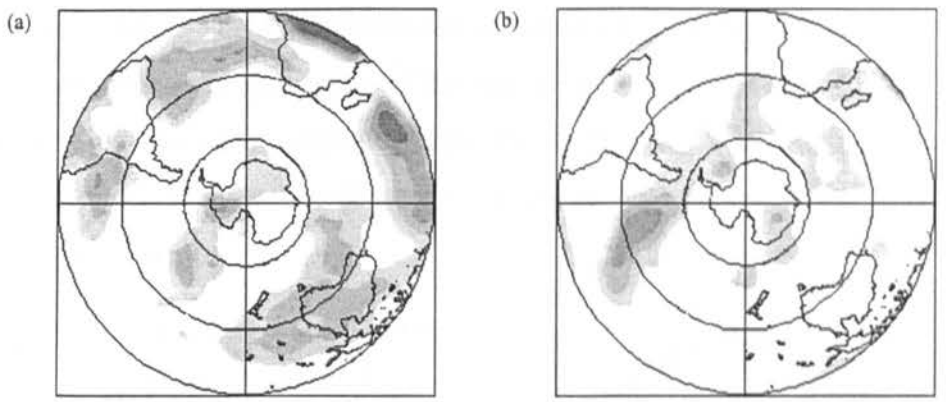

Figure 5.19 Spatial plots of percentage of (a) positive and (b) negative sea level pressure anomalies for the peak of the 1978 cold event. The grey shading indicates anomalies greater than 60%, with the intensity of the grey increasing in 10% bands.

The 1978 cold event was a weak event and so lacked the strong positive pressure anomalies across the Pacific (Figure 5.19a-b) identified in the 1975 event (Figure 5.18a-b). Also missing from this event were the clear negative anomalies over the centre of the Antarctic continent found in Chapter 4, although these were seen to develop 6 months after the peak. At the peak of this event there were short-lived positive anomalies across west Antarctica and the Bellinghausen Sea, spilling over into east Antarctica, with limited negative anomalies occurring over Wilkes Land. However, these built to produce the negative anomalies over the continent 6 months after the peak. As in the 1975 cold event (Figure 5.18a-b) this event had a strong meridional contrast in the sign of the anomalies between the pole and the Indian Ocean

area. However, there were positive anomalies in the polar region, negative anomalies in the midlatitudes and positive anomalies in the Indian Ocean region, which was the reverse of that described above for the 1975 event (Figure 5.18a-b).

At the peak of the strong 1988 cold event there were strong positive anomalies in sea level pressure across the entire Antarctic continent (Figure 5.20a-b), contrasting with the sign of anomalies found in Chapter 4, however, these were short-lived, developing at the event peak and disappearing within 3 months. This contrasts with the 1975 event when there were negative anomalies across the continent (Figure 5.18b), however, for the 1978 event there were positive anomalies across most of the continent (Figure 5.19a). There was a strong meridional contrast in the sign of the anomalies along the 180° meridion, with positive anomalies in the polar region, negative anomalies to the south of New Zealand and positive anomalies in the tropics. One of the most significant features at the peak of this event was the strong contrast between the subtropics of the Pacific and Indian Oceans. The Pacific Ocean had strong positive anomalies, resulting from the cold event whilst the Indian Ocean has strong negative pressure anomalies (Figure 5.20a-b), as were present at the peak of the 1975 cold event (Figure 5.18a-b).

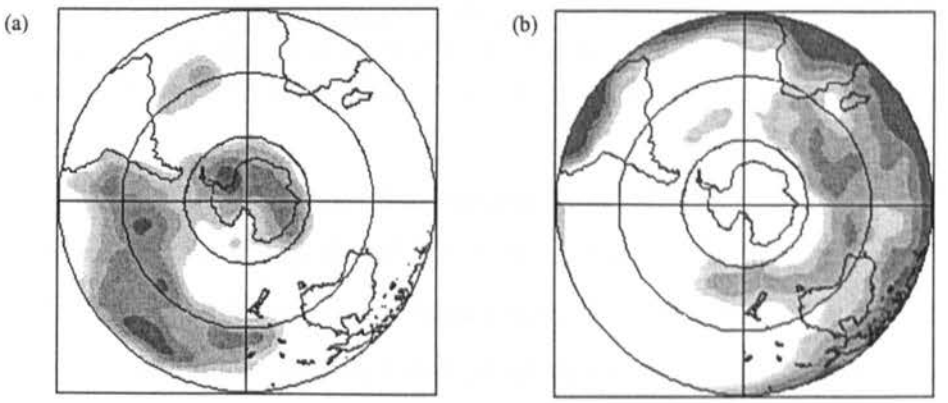

Figure 5.20 Spatial plots of percentage of (a) positive and (b) negative sea level pressure anomalies for the peak of the 1988 cold event. The grey shading indicates anomalies greater than 60%, with the intensity of the grey increasing in 10% bands.

5.3.2.2 Three monthly charts for warm events

The peak of the moderate 1976 event was characterised by negative sea level pressure anomalies in the Weddell Sea region and over east Antarctica near the Amery Ice Shelf

(Figure 5.21b), however, positive anomalies extended inland over Wilkes Land (Figure 5.21a). Positive anomalies present to the southwest and southeast of New Zealand, extending over the Amundsen Sea, at the event peak moved poleward following the peak resulting in positive anomalies over the Antarctic continent which were found in Chapter 4 to be characteristic of warm events. To the north of New Zealand there was a predominance of negative pressure anomalies, strongest 2 months after the peak, indicative of the low pressure associated with the westward branch of the warm event. These plots also illustrate the meridional contrast in the sign of the anomalies, common to the cold events described above, especially in the mid-Pacific region.

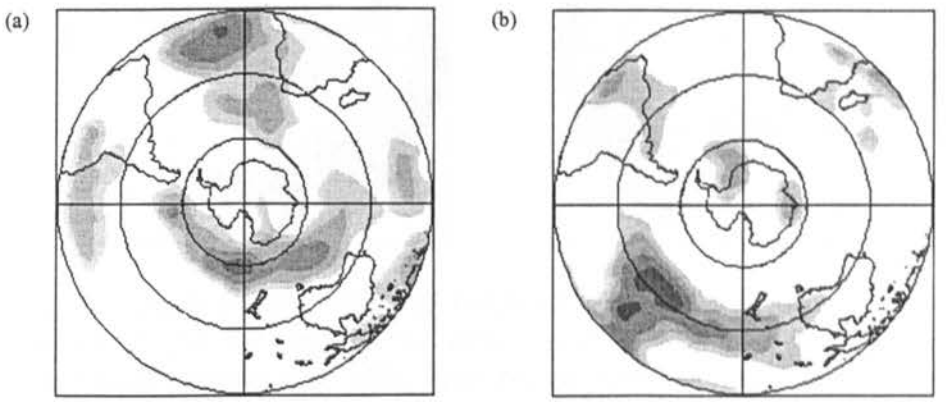

Figure 5.21 Spatial plots of percentage of (a) positive and (b) negative sea level pressure anomalies for the peak of the 1976 warm event. The grey shading indicates anomalies greater than 60%, with the intensity of the grey increasing in 10% bands.

Figure 5.22a-b shows the sea level pressure anomalies associated with the peak of the strong 1982-83 warm event. At the peak of this event there was a predominance of positive anomalies across the Antarctic continent, which were strongest 3 months prior to the event peak, with positive anomalies also in the Bellinghausen and Weddell Seas. The positive anomalies across Antarctica agree with the results from Chapter 4, in which it was found that increases (decreases) in pressure over Antarctica coincide with warm (cold) events. Prior to and following the peak of this event there was a reduction of sea level pressure in the Amundsen Sea area indicative of the development of the Amundsen Sea low, which is thought by Cullather et al. (1996) to be an ENSO response resulting in an increase in storm activity in the Amundsen Sea. This resembles the behaviour of the Aleutian low in the Northern Hemisphere during warm events. The negative anomalies across the Pacific, the

atmospheric response to a warm event, were linked to negative anomalies to the south of New Zealand. These anomalies were part of a strong meridional contrast along the 180° meridian where there were positive anomalies across Antarctica, negative anomalies to the south of New Zealand and positive anomalies to the north of New Zealand. Positive anomalies were present across the whole of the Indian Ocean, the inverse of the anomaly pattern found for both the 1975 (Figure 5.18b) and 1988 (Figure 5.20b) cold events.

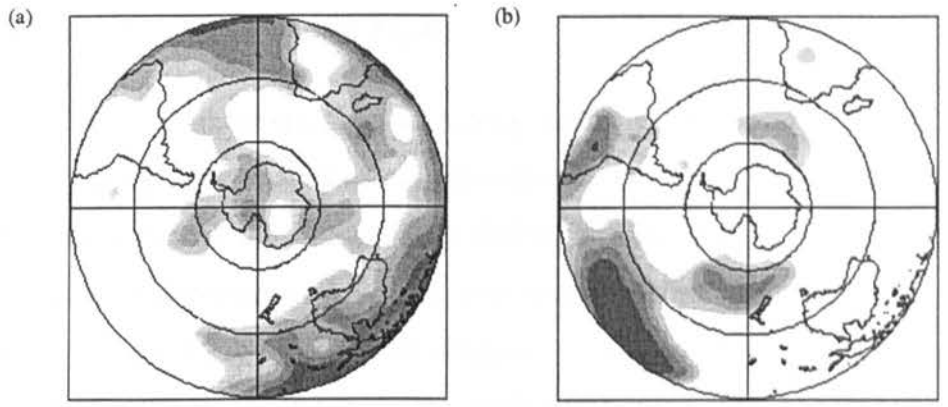

Figure 5.22 Spatial plots of percentage of (a) positive and (b) negative sea level pressure anomalies for the peak of the 1982 warm event. The grey shading indicates anomalies greater than 60%, with the intensity of the grey increasing in 10% bands.

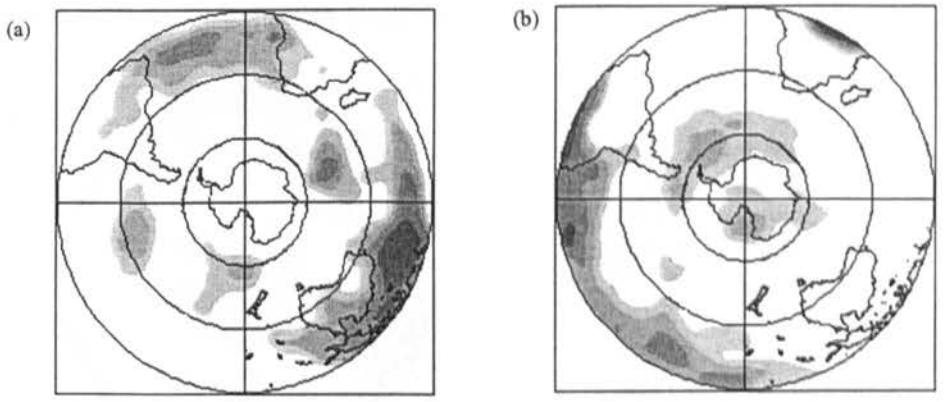

Figure 5.23 Spatial plots of percentage of (a) positive and (b) negative sea level pressure anomalies for the peak of the 1986 warm event. The grey shading indicates anomalies greater than 60%, with the intensity of the grey increasing in 10% bands.

The peak of the weak to moderate 1986 warm event (Figure 5.23b), unlike the 1982 event (Figure 5.22b) and general characteristics identified in Chapter 4, was characterised by negative sea level pressure anomalies across Antarctica, with negative anomalies in the

Weddell and Ross Sea regions (Figure 5.23a-b). These anomalies were strongest a month prior to the warm event peak. As in the 1982 warm event (Figure 5.22a) there were positive anomalies across most of the Indian Ocean, from northern Australia, with warm event induced negative anomalies across the low latitude Pacific. Strong meridional contrasts in the sign of the anomalies occur in two regions for this event, the 180° and 260° meridians. Along these meridians there were negative sea level pressure anomalies in the high latitudes, positive anomalies in the midlatitudes and negative anomalies in the low latitudes, a contrast similar to that of the 1976 warm event (Figure 5.21a-b).

The moderate 1991 warm event (Figure 5.24a), like the 1982 event (Figure 5.22a), was characterised by positive anomalies across the Antarctic continent, extending to around 60°S, with positive anomalies in the Weddell and Bellinghausen Seas. These positive sea level pressure anomalies were strongest 2 months prior to and 2 months after the peak. Once again, as in the 1982 (Figure 5.22a-b) and 1986 (Figure 5.23a-b) warm events there were positive anomalies extending across the Indian Ocean, with warm event induced negative anomalies in the low latitudes of the Pacific (Figure 5.24a-b). The meridional contrast, of positive-negative-positive, between the low, mid- and high latitudes at the peak of this event (Figure 5.24a-b) can be seen particularly well in the Pacific Ocean region, a pattern found for the 1982 warm event but further west (Figure 5.22a-b)

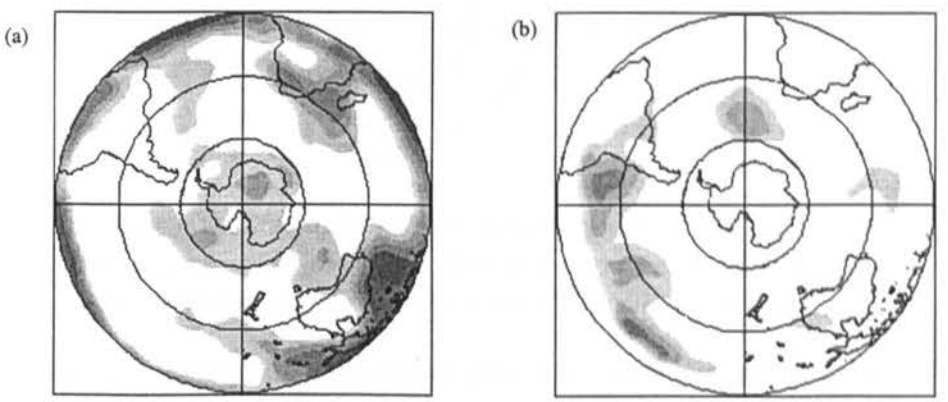

Figure 5.24 Spatial plots of percentage of (a) positive and (b) negative sea level pressure anomalies for the peak of the 1991 warm event. The grey shading indicates anomalies greater than 60%, with the intensity of the grey increasing in 10% bands.

5.4 Harmonic analysis

The Hovmöller diagrams and spatial anomaly plots consider separate aspects of the effects of ENSO on the higher latitudes of the Southern Hemisphere. Therefore to investigate teleconnection patterns and possible mechanisms it is necessary to consider both the temporal and spatial aspects of ENSO-climate interactions. In harmonic analysis the first harmonic is used in identifying the ENSO signal, as it describes the greatest variability within the data. The background and methodology is described in detail in Section 3.6.1. Prior to applying harmonic analysis the data was ranked, and these ranks were converted into percentile ranks, to allow greater comparison between grid points by removing the bias from extreme values and disparities occurring between grid points (Ropelewski and Halpert, 1986). Following this the data was divided up into individual events and harmonic analysis was applied. Unlike the Hovmöller diagrams the period used for each event was one year prior to and one year following the event to allow the harmonic analysis to make use of the biennial nature of the response to ENSO identified in Chapter 4, the Hovmöller diagrams (Section 5.2) and the spatial anomaly plots (Section 5.3).

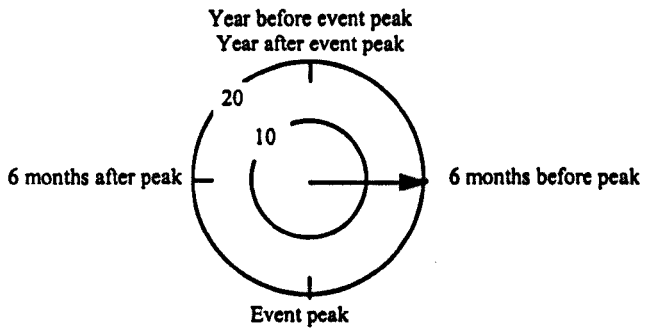

Figure 5.25 A harmonic dial with the arrow direction indicating the timing of the greatest positive anomalies (6 months before the event peak), and the length of the arrow indicative of the magnitude of the anomalies (20 units).

In harmonic analysis each grid point is designated a phase and an amplitude based on the timing and height of the fitted harmonic curve (Section 3.6.1) which are plotted as harmonic dials (Figure 5.25). Dial convention is such that the length and direction of the arrow represents the amplitude and the phase of the first harmonic respectively. As in Halpert and Ropelewski (1992), the vector points toward the positive part of the cycle; however, it must

be remembered that the physical significance may be on the negative side of the vector, which will be one year out of phase with the indicated direction (Ropelewski and Halpert, 1987).

The amplitude and phase of the first harmonic were mapped to aid the identification of the movement of climate anomalies over time. To identify teleconnections between different regions in terms of amplitude and timing cluster analysis was used. The aim of cluster analysis was to achieve a regionalisation of anomalies based on their strength and timing. By identifying regions where both the timing and amplitudes are similar and linking these together, teleconnections can be explored.

5.4.1 Cold Events

The maps of harmonic analysis vectors for 500 hPa height, temperature and mixing ratio for the 1975 cold event show several distinctive patterns (Figure 5.26a-c). Across the eastern Pacific between 10 and 20°S there were strong positive height anomalies 6 months prior to the event peak, March to May 1975, indicative of the increasing strength of the subtropical high during the cold event which can be seen in the sea level pressure plots (Appendix 2). These anomalies then propagated south to the midlatitudes of the central Pacific over a period of about 6 months. The temperature and mixing ratio anomalies in this region were strongest 2 months prior to the peak, preceding the height anomalies. The strong positive anomalies 4 months before the peak in eastern Antarctica, and coincident with positive sea level pressure anomalies (May to July 1975, Appendix 2), appear to have weakened slightly as they propagated northward, in the region of the 60° meridian, to the midlatitudes over 10 months. The strong temperature and mixing ratio anomalies appear, however, to lack this northward propagation. The strong sea level pressure anomalies in east Antarctica 4 months prior to the event peak (May to July 1975, Appendix 2) which agree with the phase of the positive harmonic in this region, were replaced by negative sea level pressure 12 months later (May to July 1976, Appendix 2) in agreement with the negative phase of the harmonic. This behaviour is indicative of the biennial nature of the response to ENSO.

In the Antarctic Peninsula region there were positive height (Figure 5.26a) and sea level pressure anomalies (August to October 1975, Appendix 2) coinciding with the event peak, with positive temperature and mixing ratio anomalies about 3 months after the peak. The

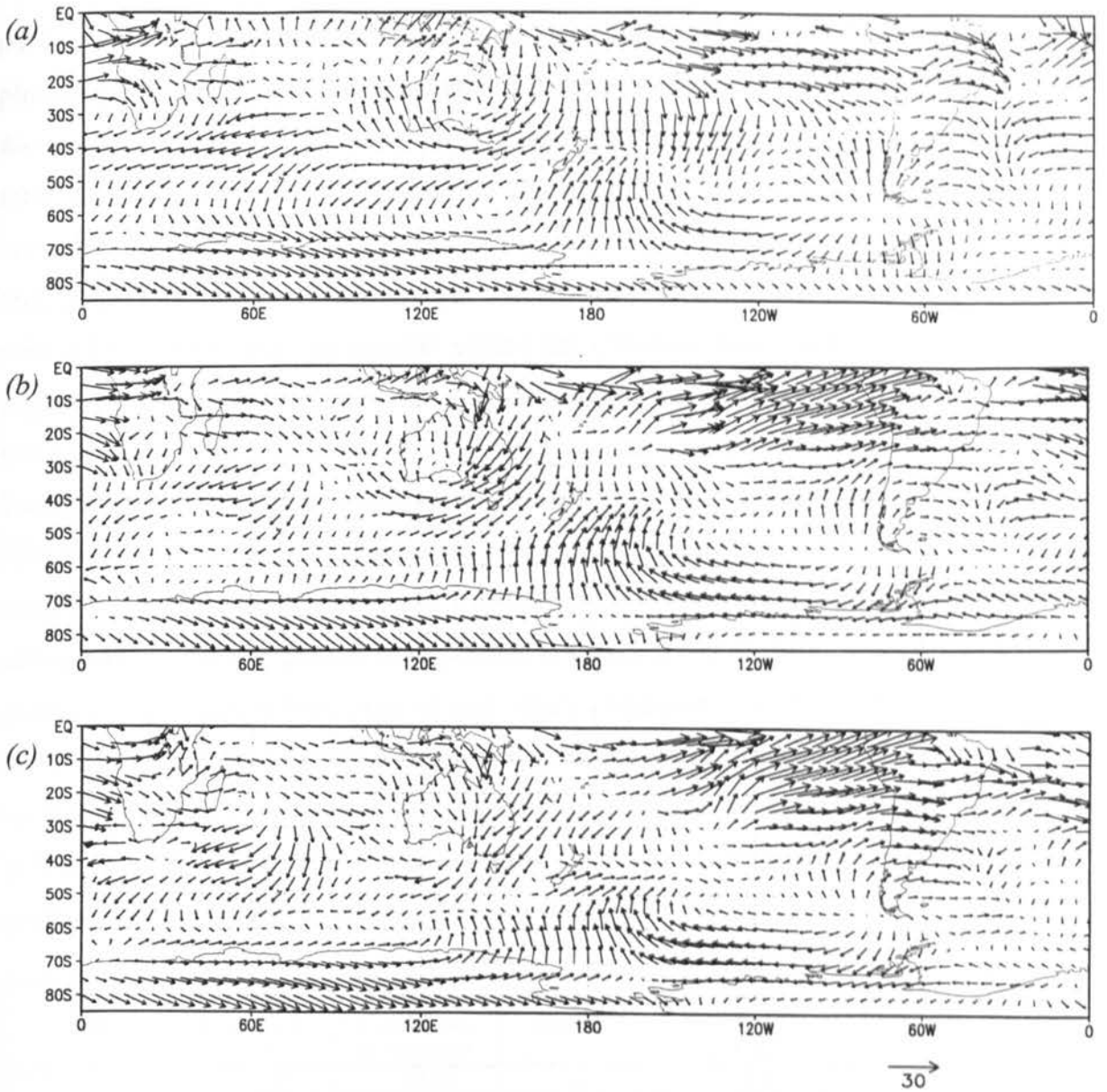

Figure 5.26 Grid point vectors based on the 24 month harmonic fitted to the 500 hPa (a) height, (b) temperature and (c) mixing ratio anomalies for the 1975 cold event.

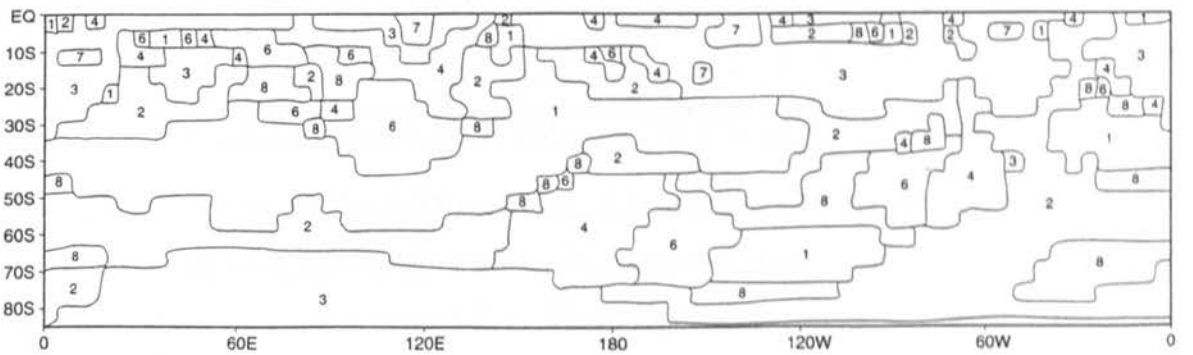

Figure 5.27 Clusters of the grid point vectors based on the 24 month harmonic of 500 hPa height anomalies for the 1975 cold event.

positive anomalies in Antarctica appear to disagree with the findings from the spatial anomaly plots (Figure 5.18a-b) where it was found that there were negative anomalies in the centre of the Antarctic continent. However, due to mapping restrictions, the harmonic plots only reach 80°S, thus the negative anomalies prior to and at the event peak were not visible. In the area around Australia there was a very interesting pattern in the phase of the height, temperature and mixing ratio vectors. It appears that anomalies off the east coast, at around the time of the peak of the event, were propagated around the continent itself, reaching the western side approximately a year after the peak. This propagation was not mirrored in the sign of the sea level pressure anomalies (Appendix 2). Two months after the event peak in the region of Patagonia negative height, temperature, mixing ratio (Figure 5.26a-c), and sea level pressure (October to December 1975, Appendix 2) anomalies, appear to have propagated in an easterly direction into the South Atlantic over a period of 6 months. Five months after the event peak strong negative height, and sea level pressure (January to March 1976, Appendix 2) anomalies in the South Atlantic off the coast of west Africa propagated inland before heading south-east to 40°S (Figure 5.26c). There was also a very strong set of negative height and mixing ratio anomalies, about 7 months after the peak, over the region of the Amazon Basin. These appear to have strengthened as they moved eastward. This movement was mirrored in the sea level pressure anomalies (March to May 1976, Appendix 2).

Cluster Number	Mean Amplitude (gpm)	Amplitude Coefficient of Variation	Mean Phase (months)	Phase Coefficient of Variation	Number of Grid Points
1	9.27	22.54	15.75	14.41	251
2	4.77	34.59	10.38	27.26	340
3	12.53	23.46	6.82	23.75	360
4	7.10	34.79	2.36	58.05	119
5	17.26	16.40	23.16	2.46	9
6	7.38	36.72	22.15	5.64	106
7	24.17	7.82	5.13	37.04	15
8	3.03	36.63	17.67	9.22	97

Table 5.1 Cluster statistics for the 1975 cold event 500 hPa height harmonics.

Cluster analysis results for the 1975 cold event first harmonic reveal possible teleconnections between east Antarctica, the eastern Pacific, the area near Madagascar as well as the area east of northern South America (Figure 5.27). These regions all belong to Cluster 3 and possess strong positive anomalies occurring around 6 months prior to and strong negative anomalies occurring around 6 months following the event peak (Table 5.1). Cluster 4 is characterised by

positive anomalies occurring around 10 months prior to, or negative anomalies 2 months after the peak, although with smaller amplitudes, and greater variability, compared to Cluster 3. It occurs in the region south of New Zealand, in southern South America and north western Australia. Cluster 6 and Cluster 4 are very similar, but vary according to the timing of the anomalies (Table 5.1). If negative anomalies had been clustered Clusters 6 and 4 would both have maximum amplitudes at around the event peak, and would probably be grouped together. However, as only positive anomalies were clustered they are separated. Cluster 1 appears to be the inverse of Cluster 3, occurring at the opposite phase. This cluster tends to be restricted to the midlatitudes. This contrast between the midlatitudes and the high and low latitudes is illustrative of the meridional contrasts present in the Southern Hemisphere as identified above in the Hovmöller diagrams (Section 5.2) and spatial anomaly plots (Section 5.3). Cluster 2 and 8 are the other dominant clusters for this event, however, they consist of harmonics with small amplitudes, and are thus descriptive of transition regions between high amplitude regions. These two clusters tend to occur in the subtropical and subpolar regions, which are the transition zones through which the jetstreams tend to migrate.

As found from the sea level pressure spatial anomaly plots (Figure 5.19a-b) the weak 1978 cold event lacked the strong height anomalies in the eastern Pacific region (Figure 5.28a) characteristic of cold events as for the 1975 cold event (Figure 5.26a). Despite this strong temperature and mixing ratio vector anomalies occurred (Figure 5.28b-c); positive anomalies 11 months after the peak, indicative of negative anomalies 1 month prior to the peak. There was a northward propagation of negative height anomalies from east Antarctica, 8 months after the 1978 event, to 50°S over a 4 month period. These did not extend as far into the midlatitudes as the in the 1975 event, arriving a year after the event peak (Figure 5.28a-c). The Antarctic Peninsula region, unlike the east Antarctic had no strong signals in the harmonics. In the South Indian Ocean region there were very strong positive height, temperature and mixing ratio anomalies occurring about 12 months after the peak. These were mirrored by the response of sea level pressure, in which there were strong positive anomalies a year before and a year after the peak (Appendix 2) possibly indicative of an ENSO-monsoon link, with positive height, temperature and mixing ratio anomalies a year after the cold event peak or negative anomalies at the peak of the event. This event was found by Trenberth (1984a) to occur at the same time as anomalous monsoon circulation, with the

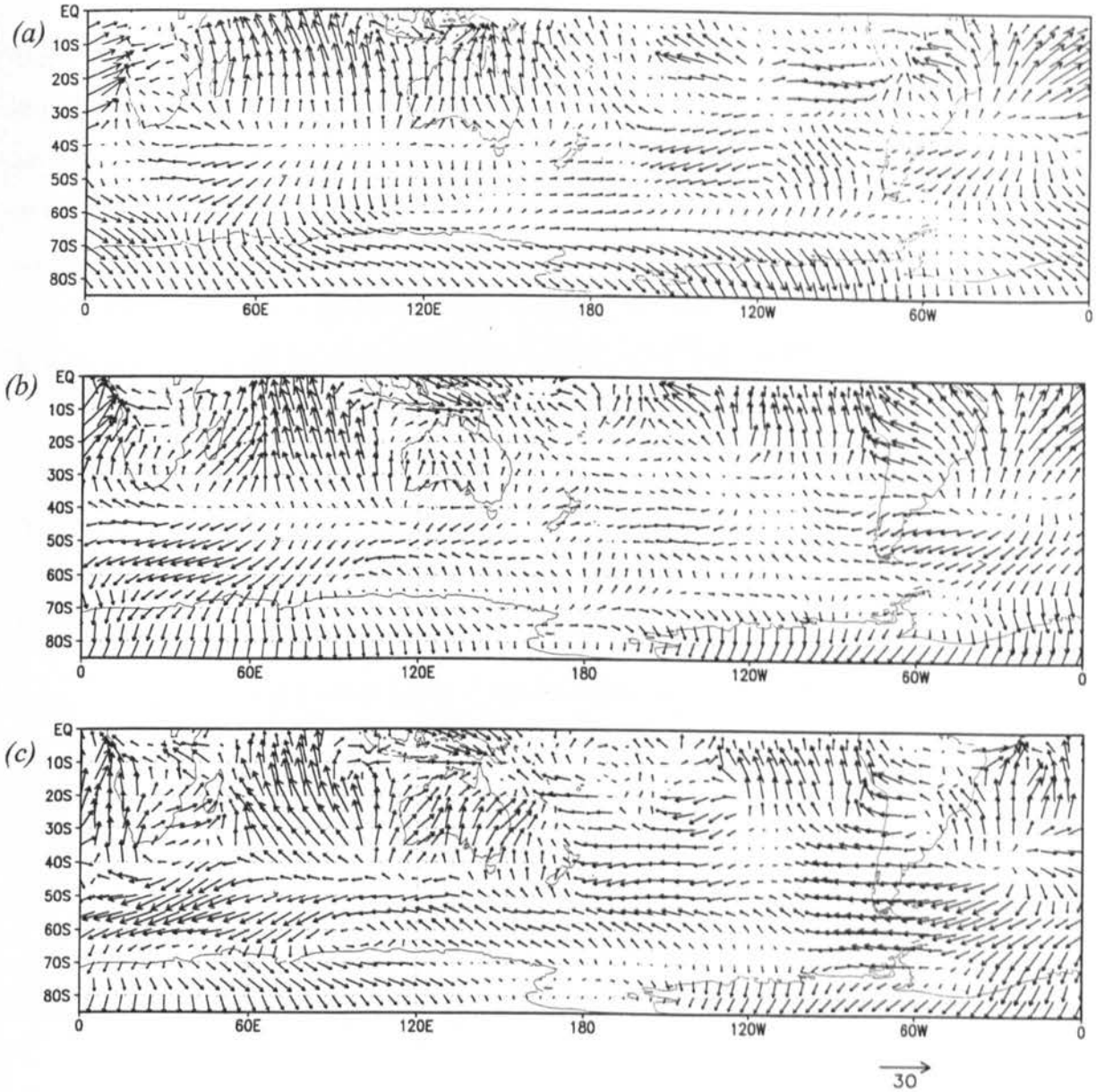

Figure 5.28 Grid point vectors based on the 24 month harmonic fitted to the 500 hPa (a) height, (b) temperature and (c) mixing ratio anomalies for the 1978 cold event.

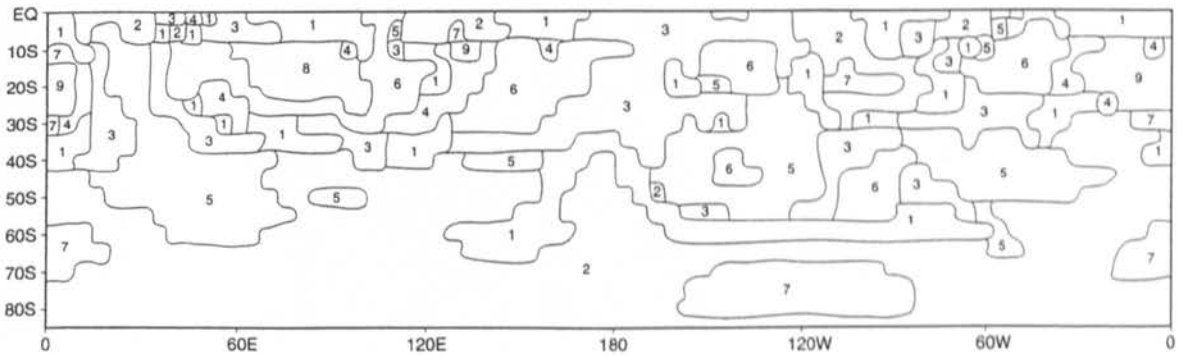

Figure 5.29 Clusters of the grid point vectors based on the 24 month harmonic of 500 hPa height anomalies for the 1978 cold event.

monsoon intensity below normal and onset date late. This anomalous 1978 monsoon would explain the negative mixing ratio anomalies in this region coinciding with the peak of the event. This pattern, which appears in the harmonic analysis, was indicative of the biennial response of ENSO events, as it has been shown that there was an opposition of signals between year -1 and year 0 of both warm and cold events (Kiladis and Diaz, 1989). As in the 1975 cold event there appears to have been a strengthening of the negative height and temperature anomalies over the Amazon Basin, 3 months prior to the peak. From the harmonic vectors it appears that these anomalies propagated eastwards across the Atlantic over a period of 8 months, however, from the sea level pressure anomalies it was clear that the positive anomalies occurring 9 months before the peak (January to March 1978, Appendix 2) were not connected to the negative height anomalies over the Amazon Basin 3 months prior to the peak.

The 1978 cold event clusters were not as well defined as the clusters for some of the other events (Figure 5.29). However, it can be seen from Table 5.2 that the most dominant cluster was Cluster 2. This cluster appears to dominate the subpolar to high latitudes during this event, with the majority of its anomalies occurring at around 3 months prior to the event peak. Teleconnections appear to exist for Cluster 2 between the high and low latitudes, with Cluster 2 also occurring around the low latitude eastern Pacific. Cluster 7 also has low-high latitude teleconnections, occurring between the area to the west of the Antarctic Peninsula and the

Cluster Number	Mean Amplitude (gpm)	Amplitude Coefficient of Variation	Mean Phase (months)	Phase Coefficient of Variation	Number of Grid Points
1	4.19	55.85	2.71	64.58	173
2	6.69	41.26	9.10	23.30	509
3	4.40	45.23	22.08	5.07	175
4	11.96	15.64	1.25	89.60	33
5	6.11	41.24	16.84	10.63	170
6	11.93	21.71	21.85	8.51	120
7	14.40	9.93	8.68	20.05	69
8	20.99	12.86	22.84	1.84	23
9	19.14	14.05	3.63	21.76	25

Table 5.2 Cluster statistics for the 1978 cold event 500 hPa height harmonics.

eastern Pacific, with anomalies occurring on average 3 months prior to the event peak. This event, unlike the 1975 event, appears to be characterised by low latitude anomaly phase

contrasts. For example at latitudes less than 30°S, Clusters 6 and 8 and Clusters 2 and 7 possess opposing phases (Table 5.2). For the 1978 event the transition clusters, characterised by small amplitudes, appear to be Clusters 1 and 3. However, unlike for the 1975 event these transition clusters extend right through the low and midlatitudes, rather than being restricted to areas dominated by the jetstreams. Cluster 5, which dominates the midlatitudes, was the opposing cluster to Cluster 2, thus gives rise to a low, mid-, high latitude pattern of 2, 5, 2. The same meridional contrast was found to occur for the 1975 event as identified in the Hovmöller diagrams (Section 5.2).

The strong 1988 cold event had strong height, temperature and mixing ratio anomalies in the low latitudes occurring about 6 months before the event peak (Figure 5.30a-c). During this event there appears to have been a movement of positive height and mixing ratio anomalies from the mid-Pacific eastwards over the course of three months in contrast to a westward movement of the temperature anomalies. Over eastern Antarctica the positive anomalies were of the same phase as for the 1978 cold event. These anomalies appear to have moved north-eastward over a 10 month period to around 45°S. The anomalies over the Antarctic Peninsula were of the same phase as the anomalies over east Antarctica, with positive anomalies coinciding with the event peak. The response of the height, temperature and mixing ratio anomalies over the Antarctic Peninsula (Figure 5.30a-c) were mirrored in the sea level pressure plots, with positive anomalies dominating this region (August to October 1988, Appendix 2). To the west of the Antarctic Peninsula there was a poleward movement of positive anomalies from 55°S from 4 months before the peak, over the course of 4 months. These anomalies coincide with the region of great climatic variability, the focus of the Hovmöller analyses. To the north of the Peninsula there were clear meridional contrasts in the phases of the anomalies, however this pattern disappears further west where there was little difference between the phases of the mid- and high latitudes. As for the 1975 and 1978 cold events the intensification of height and temperature anomalies over the Amazon Basin was also a feature of the 1988 event. Over southern South America the circular propagation of height and temperature anomalies, resembles that observed over Australia in the 1975 event, although for this event the propagation duration was about 15 rather than 12 months as in the case of 1975. Anomalies at around 50°S 90°E appeared to migrate northward and then south-eastward towards south-eastern Australia over a period of 12 months. As these positive

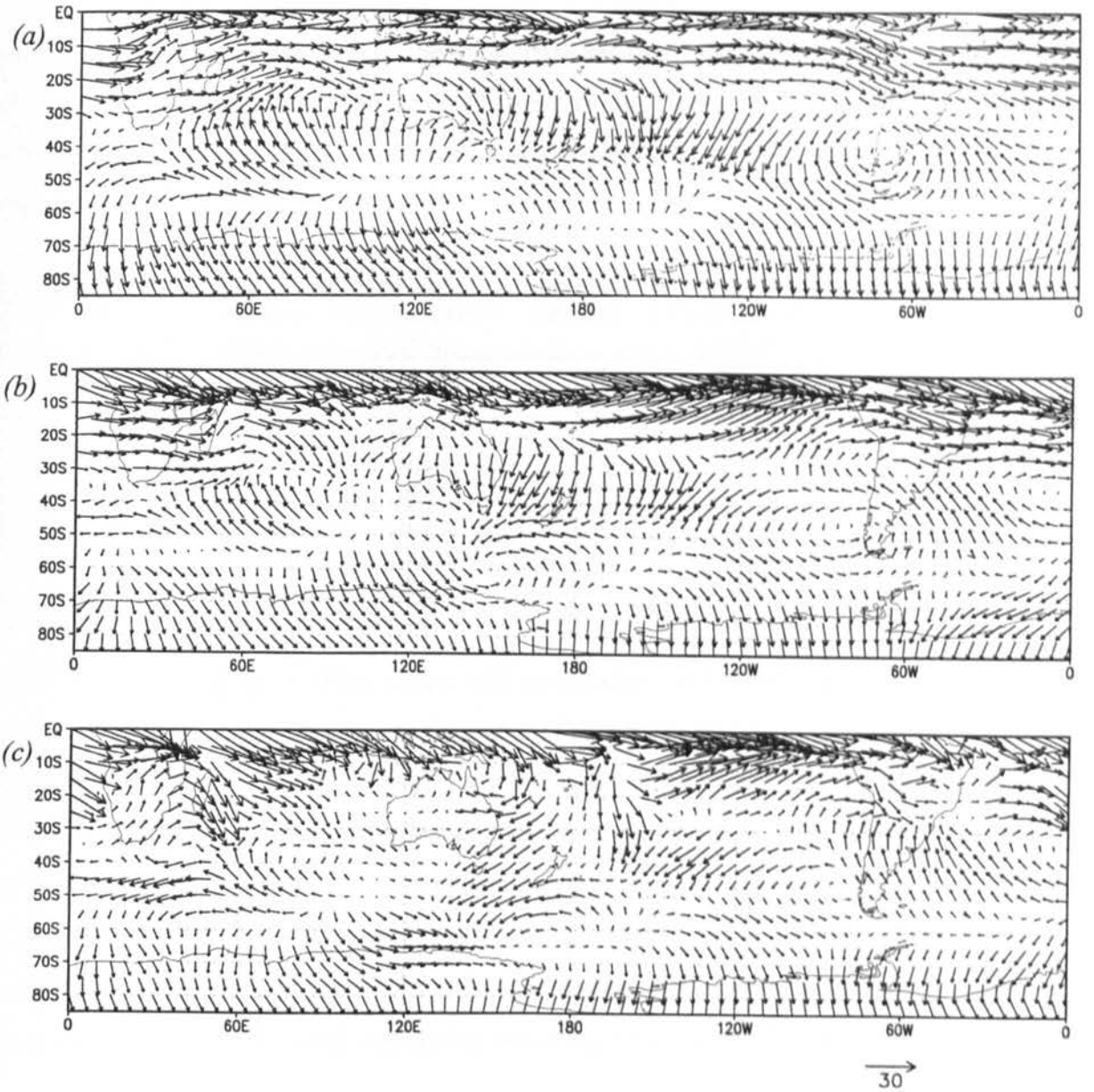

Figure 5.30 Grid point vectors based on the 24 month harmonic fitted to the 500 hPa (a) height, (b) temperature and (c) mixing ratio anomalies for the 1988 cold event.

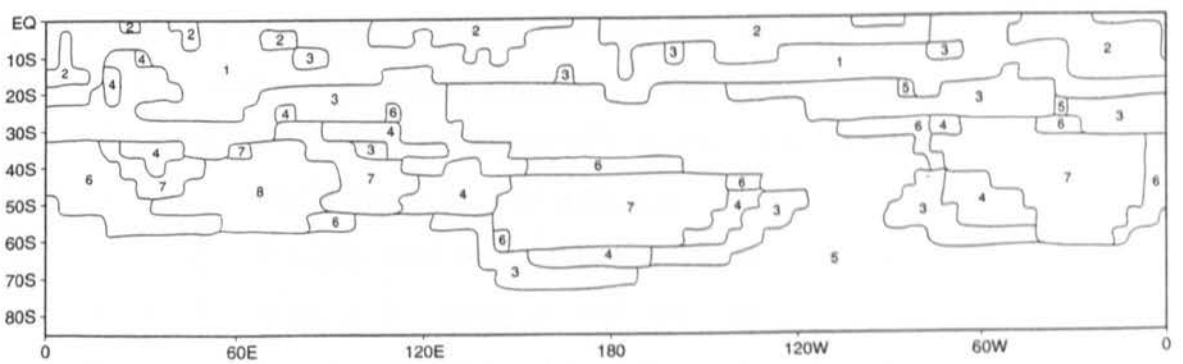

Figure 5.31 Clusters of the grid point vectors based on the 24 month harmonic of 500 hPa height anomalies for the 1988 cold event.

anomalies appear to have crossed the break between the year before and after the peak, these anomalies are likely to be indicative of negative anomalies around the peak of the event, which was confirmed by the sea level pressure plots for the peak of the event (August to October 1988, Appendix 2).

Cluster Number	Mean Amplitude (gpm)	Amplitude Coefficient of Variation	Mean Phase (months)	Phase Coefficient of Variation	Number of Grid Points
1	19.87	14.85	6.00	14.83	191
2	28.72	8.46	6.27	8.77	107
3	8.44	43.48	6.69	33.78	175
4	5.04	44.64	2.34	58.55	62
5	12.94	24.57	11.01	13.26	514
6	5.31	35.59	15.28	10.14	64
7	6.74	41.25	21.00	8.86	144
8	14.50	15.45	20.99	6.05	40

Table 5.3 Cluster statistics for the 1988 cold event 500 hPa height harmonics.

From the cluster analysis of the phases and amplitudes for the 1988 cold event it can be seen that the most extensive cluster was Cluster 5 (Table 5.3). Cluster 5 covers the high latitudes and extends up to 20°S in the eastern Pacific (Figure 5.31). The phase for this cluster was on average 1 month prior to the event peak. The opposing clusters are Clusters 7 and 8. These two clusters occur across the midlatitudes, with a phase of 9 months after the event peak. Clusters 1, 2 and 3 are restricted to the low latitudes. Although these display amplitude contrasts they all have phases of about 6 months prior to the event peak. Clusters 4 and 6 are transition clusters, with small amplitudes, occurring between the clusters of opposing phases.

The cold composite captures some of the individual event anomalies such as the strong height, temperature and mixing ratio anomalies over the low latitude Pacific occurring up to six months before the peak (Figure 5.32a-c). The anomalies over east Antarctica are also a clear feature of the composite. These have a maximum amplitude 3 months before the composite peak and propagate northward over a period of 9 months. Also apparent from the composite was the variation in the timing of the first harmonic over Antarctica. Anomalies over east Antarctica precede anomalies over west Antarctica. In the Antarctic Peninsula region the positive height anomalies, which coincide with the peak of the composite, precede the temperature and mixing ratio anomalies. This contrasts with the patterns in east Antarctica where the anomalies in height, temperature and mixing ratio coincide. There was also a

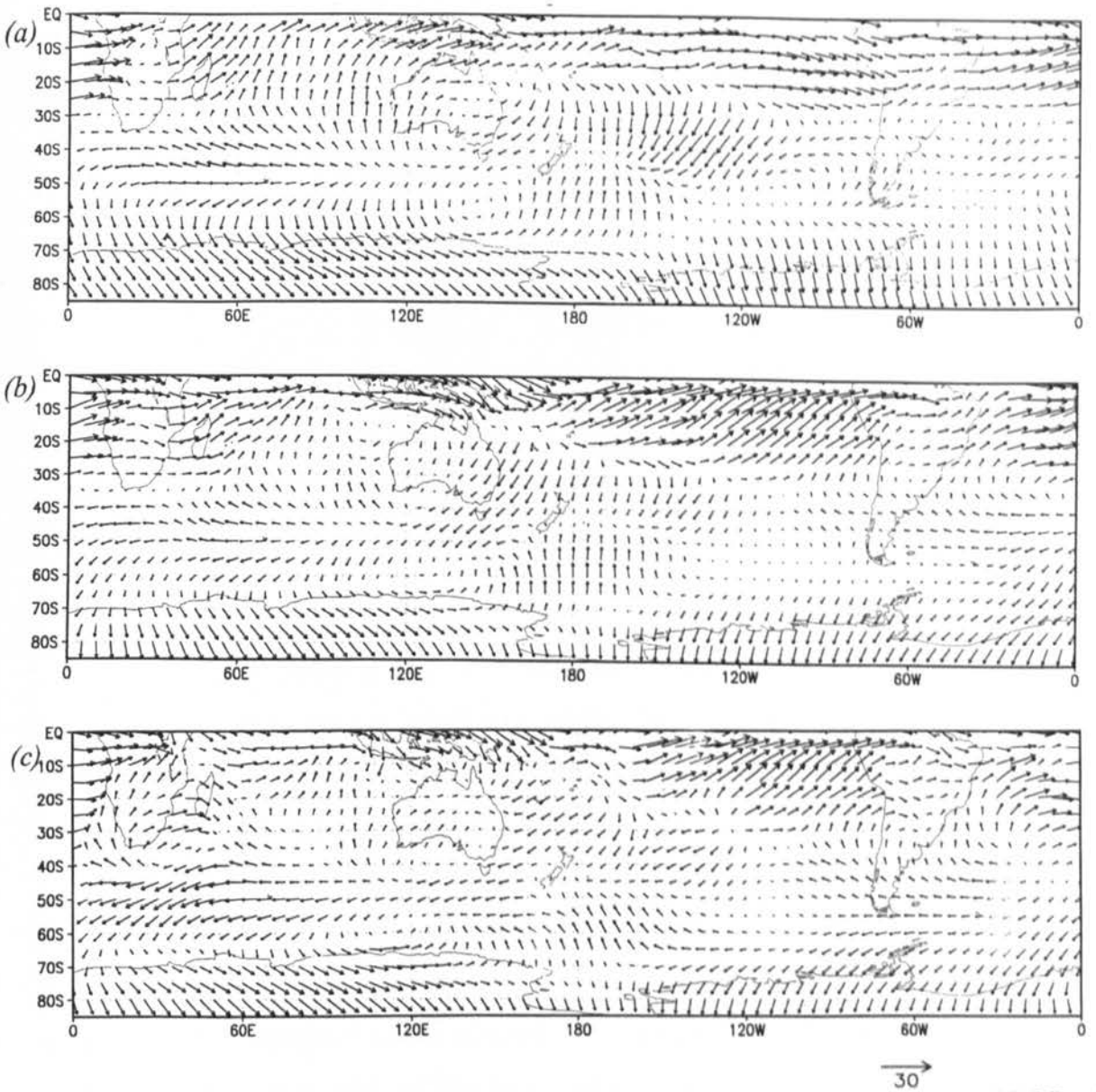

Figure 5.32 Grid point vectors based on the 24 month harmonic fitted to the 500 hPa (a) height, (b) temperature and (c) mixing ratio anomalies for the cold events composite.

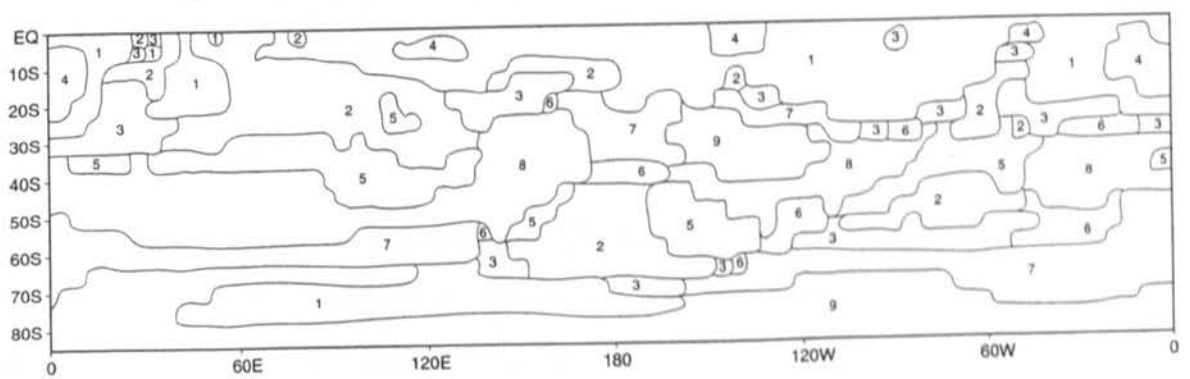

Figure 5.33 Clusters of the grid point vectors based on the 24 month harmonic of 500 hPa height anomalies for the cold events composite.

strengthening in the positive anomalies across the tropical Atlantic in all three variables 6 months prior to the event peak.

Cluster Number	Mean Amplitude (gpm)	Amplitude Coefficient of Variation	Mean Phase (months)	Phase Coefficient of Variation	Number of Grid Points
1	10.50	22.67	6.11	23.73	297
2	5.49	36.07	2.05	62.44	167
3	3.32	41.57	6.42	25.55	89
4	17.89	7.55	5.44	8.82	34
5	4.04	46.78	21.50	7.49	102
6	1.59	42.14	11.73	12.70	37
7	6.07	23.72	11.28	8.42	147
8	4.75	46.53	16.57	9.41	179
9	10.11	10.09	10.31	14.45	245

Table 5.4 Cluster statistics for the cold events composite 500 hPa height harmonics.

That extensive regions of like phases and amplitudes exist for cold events was confirmed by the results of cluster analysis of grid point phase and amplitude anomalies (Figure 5.33, Table 5.4). Cluster 1, which represents maximum amplitudes 6 months prior to the peak dominates the low latitudes. Moreover it shows a clear teleconnection with the high latitudes, in the area of east Antarctica (Figure 5.33). Clusters 7 and 9 also occur in the high latitudes with phases of around 1 to 2 months prior to the peak, differing from each other only in amplitude. Cluster 4 only appears to occur in the low latitudes along with Cluster 1, of which it was a subset, picking up on the large anomalies in this region, especially over the western region of southern Africa. Clusters 5 and 8 dominate the midlatitudes and contrast with the phases evident for both the high and low latitudes. These clusters form part of the low, mid-, high latitude meridional contrast previously identified in the individual cold events. Clusters 3 and 6 are the transition regions, with small amplitudes, and are found bordering the regions with clear amplitude and phase signatures.

5.4.2 Warm Events

The moderate 1976 warm event (Wang, 1995) showed the inverse of some of the features identified for the 1975 cold event described above. Strong positive height, temperature and mixing ratio anomalies occurred across the western Pacific between 10 and 20°S approximately six months after the event peak. These strong anomalies extended westwards into the Indian Ocean and equatorial Africa (Figure 5.34a-c), with the anomalies in the Indian

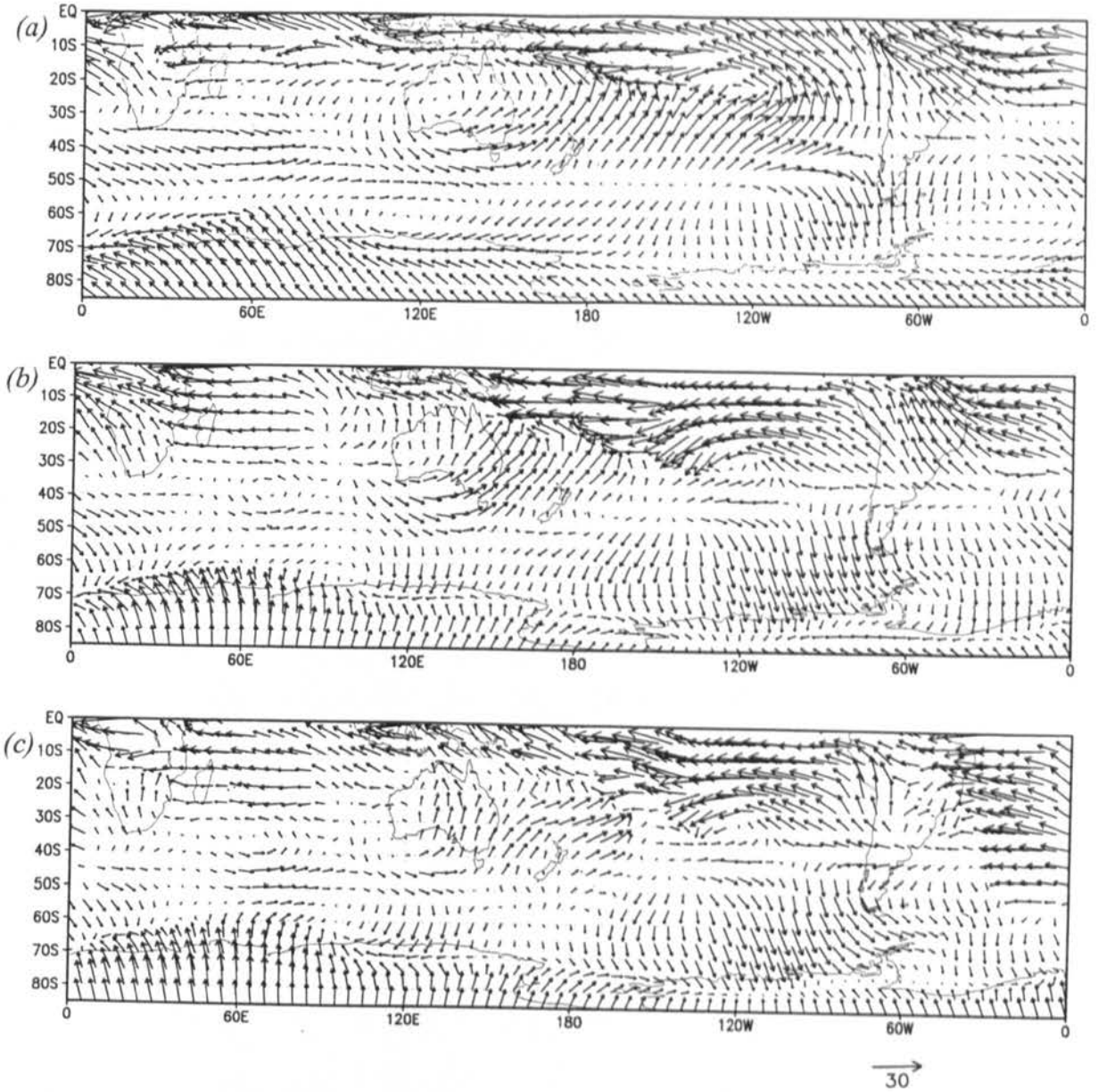

Figure 5.34 Grid point vectors based on the 24 month harmonic fitted to the 500 hPa (a) height, (b) temperature and (c) mixing ratio anomalies for the 1976 warm event.

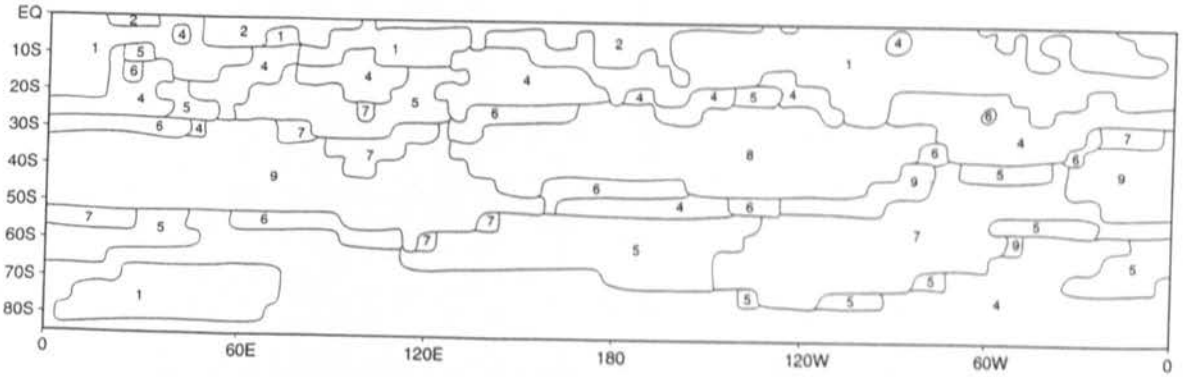

Figure 5.35 Clusters of the grid point vectors based on the 24 month harmonic of 500 hPa height anomalies for the 1976 warm event.

Ocean region mirrored in the sea level pressure plots (February to April 1977, Appendix 2). As in the 1975 event these anomalies also propagated south over a period of six months, although due to the displacement of these anomalies westward, this propagation was nearer to New Zealand. This event also shows the movement of positive anomalies around Australia over the period of a year, however, as the year preceding this event overlapped the year following the 1975 event care must be taken in treating these events in isolation. This event appears to have differed from the 1975 cold event in that the positive Antarctic anomalies, occurring 9 months to a year after the peak, migrated towards the continent rather than away from it, additionally the phase of the east Antarctic positive anomalies was exactly opposite to those of the 1975 event. A further feature of this event was the movement of positive anomalies from around 35°S 120°W southwards and eastwards towards the Antarctic Peninsula over a period of 7 months, reaching the Peninsula around the time of the event peak. The region through which these anomalies propagated is considered to be an area with maximum correlation with the SOI as well as a region of great climatic variability (Houseago et al., 1997; 1998). In the 1975 cold event it appeared that the Amazon Basin region intensified the eastward moving anomalies, however, in this warm event, the same region appeared to be an area of intensifying westward moving height and temperature anomalies. From the Ross Sea area there appears to have been a northward movement of temperature and mixing ratio anomalies from 6 months prior to the peak over a period of 6 months.

Cluster Number	Mean Amplitude (gpm)	Amplitude Coefficient of Variation	Mean Phase (months)	Phase Coefficient of Variation	Number of Grid Points
1	21.17	16.82	19.51	6.46	222
2	32.88	8..45	18.51	3.67	80
3	43.94	-	19.32	-	1
4	8.61	45.76	20.00	7.60	396
5	0.37	10.81	15.13	8.79	155
6	4.00	48.00	2.10	5.62	47
7	5.93	60.20	11.22	8.02	122
8	13.4	27.31	3.16	42.72	122
9	6.82	38.71	7.16	16.76	152

Table 5.5 Cluster statistics for the 1976 warm event 500 hPa height harmonics.

The phase-amplitude regionalisation analysis for the 1976 warm event shows teleconnections between the eastern Pacific, although Cluster 1 also appears to extend around most of the low latitudes, and east Antarctica between 0 and 60°E (Figure 5.35). This region has a strong amplitude, and an average phase of around 7 months after the event peak (Table 5.5),

contrasting with the Cluster 3 anomalies for the 1975 cold event (Table 5.1). Regions 1 to 4 are all the same apart from slightly different amplitudes and occur in both high and low latitudes, indicating a teleconnection between these two areas, approximately 8 months after the event peak. Clusters 8 and 9, dominate the midlatitudes and contrast with Clusters 1 to 4 in terms of anomaly timing (Table 5.5). The Cluster 7 anomalies occur at around the time of the peak, but tend to occupy the transition areas between the low and midlatitudes and the mid- to high latitudes. Clusters 5 and 6 tend to be the transition clusters, with small amplitudes. These are comparable to Clusters 2 and 8 of the 1975 cold event.

The very strong 1982 warm event (Trenberth, 1991), as expected, was characterised by strong positive height, temperature and mixing ratio anomalies across the whole Pacific with the greatest positive amplitude in the sub-equatorial eastern Pacific just after the peak of the event (Figure 5.36a-c). This was six months earlier than the 1976 event anomalies in this region (Figure 5.34a-c). However, as for the 1976 event, these strong anomalies extended across into the Indian Ocean. The low latitude amplitudes appear to be stronger for temperature and mixing ratio than for height. The height anomalies over east Antarctica did not replicate those found for the 1976 warm event, as they occurred at around the time of the peak rather than 9 months after. These height anomalies appear to have propagated eastwards before moving southwards down the 110°E meridian towards the continent over a period of about 2 months, similar to the previous warm event. This movement of anomalies was also apparent in the sea level pressure anomalies surrounding the event peak (August to October 1976, Appendix 2). In the region east of the Antarctic Peninsula the anomalies appear to have migrated north to around 60°S over about 6 months in contrast to the west of the Peninsula where the anomalies propagated southward over a 2 month period. Six months after the event peak a wavetrain of positive height, temperature, mixing ratio (Figure 5.36a-c) and sea level pressure (July to September 1983, Appendix 2) anomalies occurred off north and west New Zealand. One set of anomalies appears to have migrated poleward to about 60°S, whilst a second set appears to have migrated eastwards to about 80°W, both with a duration of about 5 months. As in the previous events the height and temperature anomalies appeared to intensify over the Amazon Basin, however, unlike the 1976 warm event these anomalies appear to have propagated eastward over a period of about 3 months. This region has been found to be particularly sensitive to the Southern Oscillation in a number of previous studies (Hastenrath and Heller,

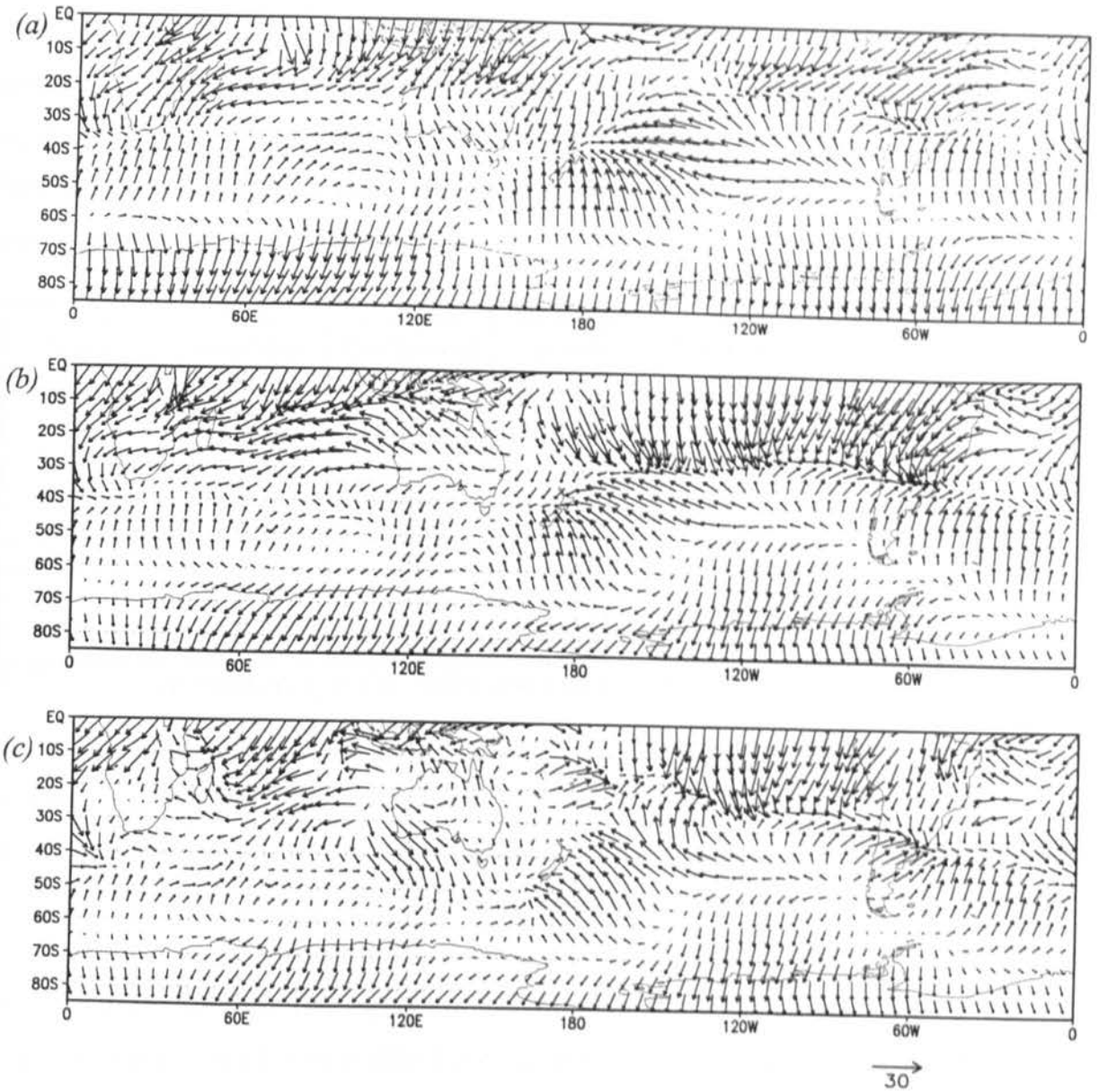

Figure 5.36 Grid point vectors based on the 24 month harmonic fitted to the 500 hPa (a) height, (b) temperature and (c) mixing ratio anomalies for the 1982 warm event.

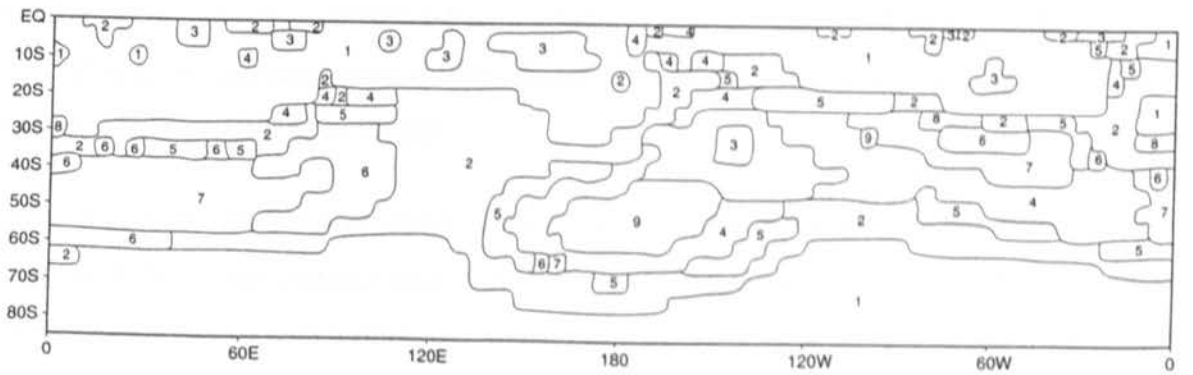

Figure 5.37 Clusters of the grid point vectors based on the 24 month harmonic of 500 hPa height anomalies for the 1982 warm event.

1977; Ropelewski and Halpert, 1987; Aceituno, 1988; Kousky and Kayano, 1994) when a pattern of strong upper-tropospheric westerlies occurs over this region, extending into the equatorial Atlantic during warm events (Kousky and Kayano, 1994). Off the coast of Southern Africa anomalies occurring just after the peak appear to have migrated north-east over a period of about 4 months.

Cluster Number	Mean Amplitude (gpm)	Amplitude Coefficient of Variation	Mean Phase (months)	Phase Coefficient of Variation	Number of Grid Points
1	12.84	17.21	13.96	14.61	629
2	5.70	30.00	12.52	19.41	257
3	19.17	6.05	15.09	13.32	29
4	8.31	21.18	21.40	10.070	124
5	2.84	47.89	18.62	14.34	68
6	4.45	19.10	4.43	37.92	56
7	8.19	24.79	1.32	73.48	93
8	11.41	5.96	8.53	16.99	7
9	14.24	9.48	22.83	4.51	34

Table 5.6 Cluster statistics for the 1982 warm event 500 hPa height harmonics.

The 1982 event clusters show very clear low-high latitude teleconnections as manifest by Cluster 1 (Figure 5.37), which dominates the low latitudes and the high latitudes, accounting for 46% of the grid points (Table 5.6). This cluster has an average phase of around 2 months after the event peak and a high amplitude. Clusters 4, 7 and 9 represent the anti-phase of Cluster 1 and are predominantly found in the midlatitudes highlighting the strong meridional contrast in the Southern Hemisphere as found by Mo and White (1985). Their phases occur either a year before or a year after the event peak, indicating that their negative anomalies would coincide with the event peak. Clusters 2, 5 and 6 are transition clusters with small amplitudes and tend to occur between the mid- and high latitudes and the low and midlatitudes. Cluster 2 is of interest as it straddles a large latitudinal range in the region of 120°E. Due to the low amplitude of this cluster this indicates that across this region there was a reduction in the response to ENSO.

For the moderate 1986 warm event (Jordán, 1991) there were once again strong positive height, temperature and mixing ratio anomalies in the low latitudes extending right around the globe (Figure 5.38a-c) with a timing of about 3 months after the event peak, mid-way between the phases of the 1976 and 1982 events. For this event there appears to have been a movement of negative height anomalies, about 8 months prior the peak, from Indonesia

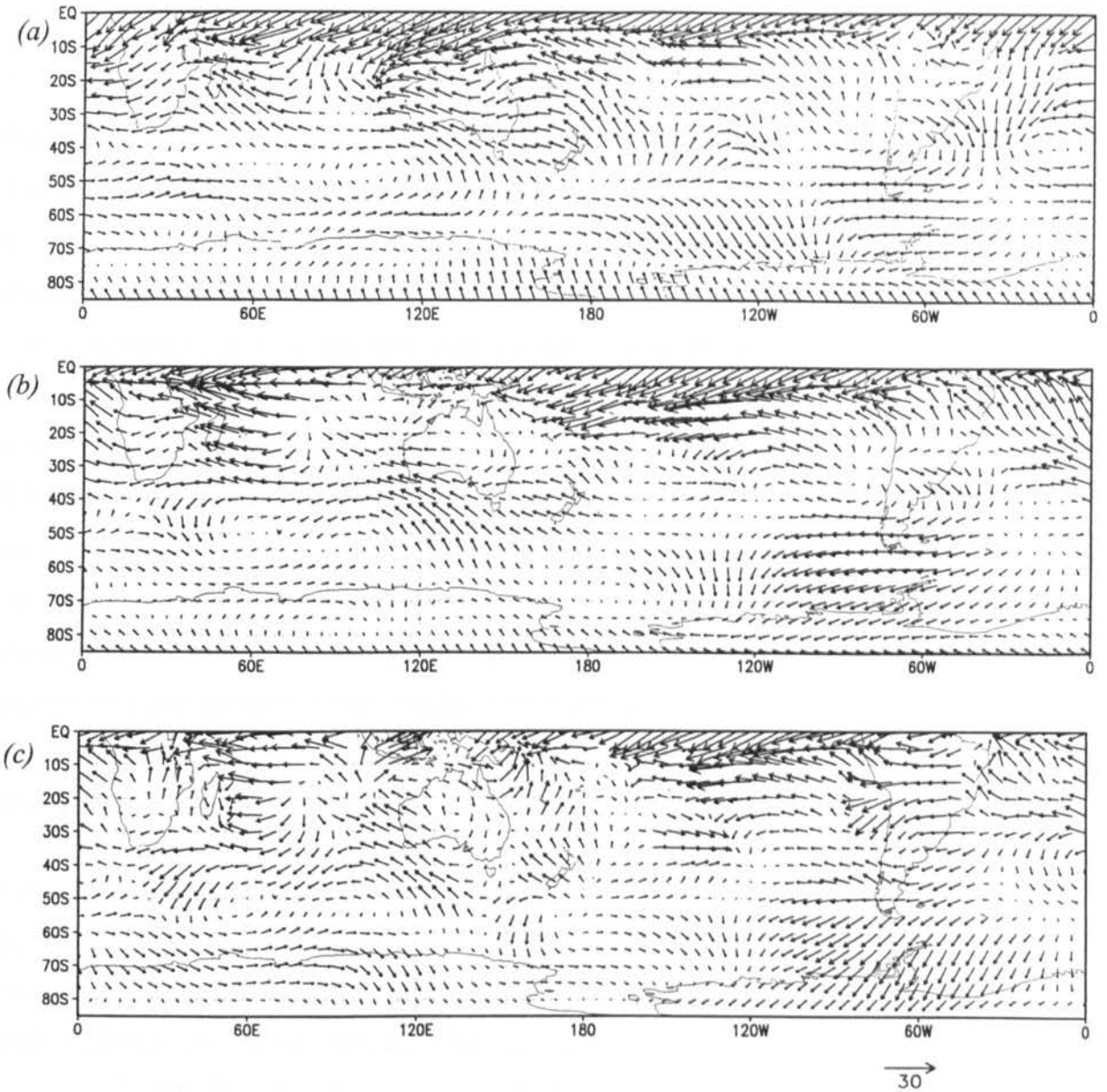

Figure 5.38 Grid point vectors based on the 24 month harmonic fitted to the 500 hPa (a) height, (b) temperature and (c) mixing ratio anomalies for the 1986 warm event.

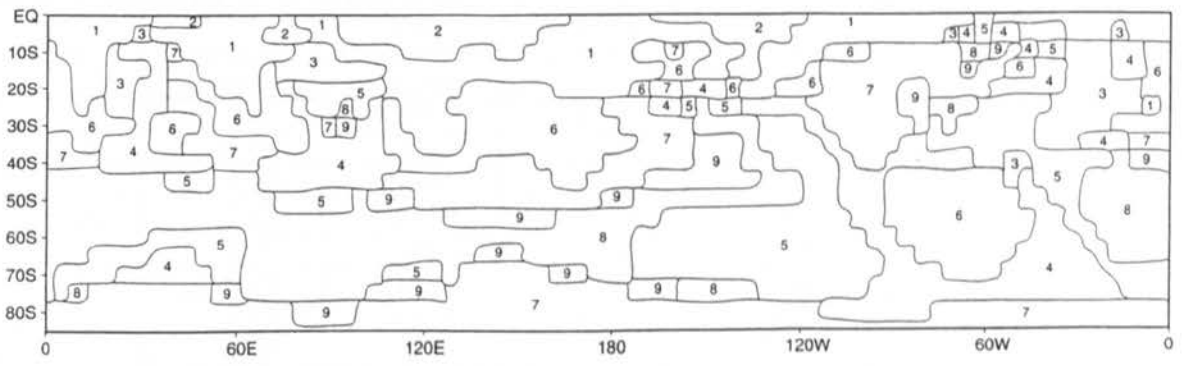

Figure 5.39 Clusters of the grid point vectors based on the 24 month harmonic of 500 hPa height anomalies for the 1986 warm event.

towards the Pacific, as confirmed by sea level pressure plots (March to May 1986, Appendix 2). The positive anomalies over eastern Antarctica have the same phase as those of the 1976 warm event, occurring about 9 months after the peak. However, they were of a much smaller magnitude, than for the previous two warm events. Furthermore there did not appear to have been anomaly propagation either to or from east Antarctica. From the sea level pressure charts it appears that the negative anomalies 3 months before the peak (August to October 1986, Appendix 2) were stronger than the positive anomalies 9 months after (August to October 1987, Appendix 2), thus the negative anomalies were the most important factor in the determination of the phase in east Antarctica. In the region west of the Antarctic Peninsula there appears to have been a movement of anomalies north-eastward from about the time of the peak of the event. During the 1975 and 1976 events there was a 12 month cycle in the movement of anomalies around Australia. This trend was also apparent in 1986, although it occurred to the south west of Australia, rather than over the continental land mass. A similar pattern was also apparent in the height and temperature diagrams (Figures 5.38a-b) over the South American continent. In this event the Amazon Basin does not appear to have played a role in intensifying the anomalies.

For the 1986 warm event the clearest teleconnection pattern seems to occur with Cluster 7, between the low latitude eastern Pacific and Antarctica (Figure 5.39). From the analysis above, this cluster has a negative phase of about 2 months after the event peak, rather than the positive phase 10 months after, identified in Table 5.7. Cluster 6 appears to be of a similar phase to Cluster 7, although it was greater in amplitude. Together they occur across the

Cluster Number	Mean Amplitude (gpm)	Amplitude Coefficient of Variation	Mean Phase (months)	Phase Coefficient of Variation	Number of Grid Points
1	15.85	14.83	17.36	8.35	171
2	23.83	10.45	16.49	3.69	59
3	8.73	16.61	14.15	9.61	55
4	3.87	39.79	16.17	10.69	154
5	5.39	51.02	9.45	13.97	168
6	9.19	16.21	18.41	6.08	158
7	5.85	37.26	21.73	5.29	281
8	4.69	40.08	5.65	21.77	196
9	3.67	62.39	1.44	75.00	55

Table 5.7 Cluster statistics for the 1986 warm event 500 hPa height harmonics.

subtropics and the polar regions. Clusters 1 and 2 dominate the low latitudes, and characterise the regions with the greatest amplitudes, which occur about 5 months after the event peak. The clusters with the opposing phase to Clusters 6 and 7 are Clusters 5 and 8. These have phases of between 3 and 6 months prior to the event peak, however, these clusters occur in a more southerly location than the usual midlatitude contrast of anomalies. Clusters 4 and 9 appear to be the transition clusters with small amplitudes. Clusters 1, 2, 6 and 7 appear to combine to form a low latitude to subtropical set of positive anomalies, as they all have similar phases, however, like the midlatitude clusters, these clusters tend to extend further south than for the other events.

The moderate 1991 warm event was different from the other warm events due to its long duration. The height, temperature and mixing ratio anomalies across the Pacific were not nearly as strong as for the other events (Figure 5.40a-c). This event differed from the 1976 warm event in that the anomalies in east Antarctica occurred about 3 months before the event peak, thus resembling the anomalous 1982 warm event. These anomalies migrated north-east over a period of 8 months. In the Antarctic Peninsula region there were weak positive post-event signatures in the anomalies, confirmed by the sea level pressure plots (February to April 1992, Appendix 2). In this event, as in the 1976 warm event, there was a significant movement of positive anomalies from around 45°S towards the area to the west of the Antarctic Peninsula, over a period of about 12 months, arriving approximately 2 months after the peak. To the east of the Peninsula there was a northward propagation of negative anomalies 1 month after the event peak agreeing with the sea level pressure plots (January to March 1992, Appendix 2). As in the 1986 warm event there was once again a 12 month propagation of positive anomalies in a clockwise direction south of Australia. In this event the intensification of height and temperature anomalies from the Amazon Basin appeared to occur, although the amplitude of this was smaller than in other events. Just off the east coast of Africa there seems to have been a southward propagation of anomalies to around 40°S.

The 1991 warm event clusters, like the 1978 cold event clusters, show very few clear patterns (Figure 5.41). The Antarctic region was dominated by Clusters 6, 7 and 8. The phase for these clusters was from 2 months prior to the event peak to the event peak itself (Table 5.8). Cluster 7, which occurs over east Antarctica, was the cluster containing the anomalies with

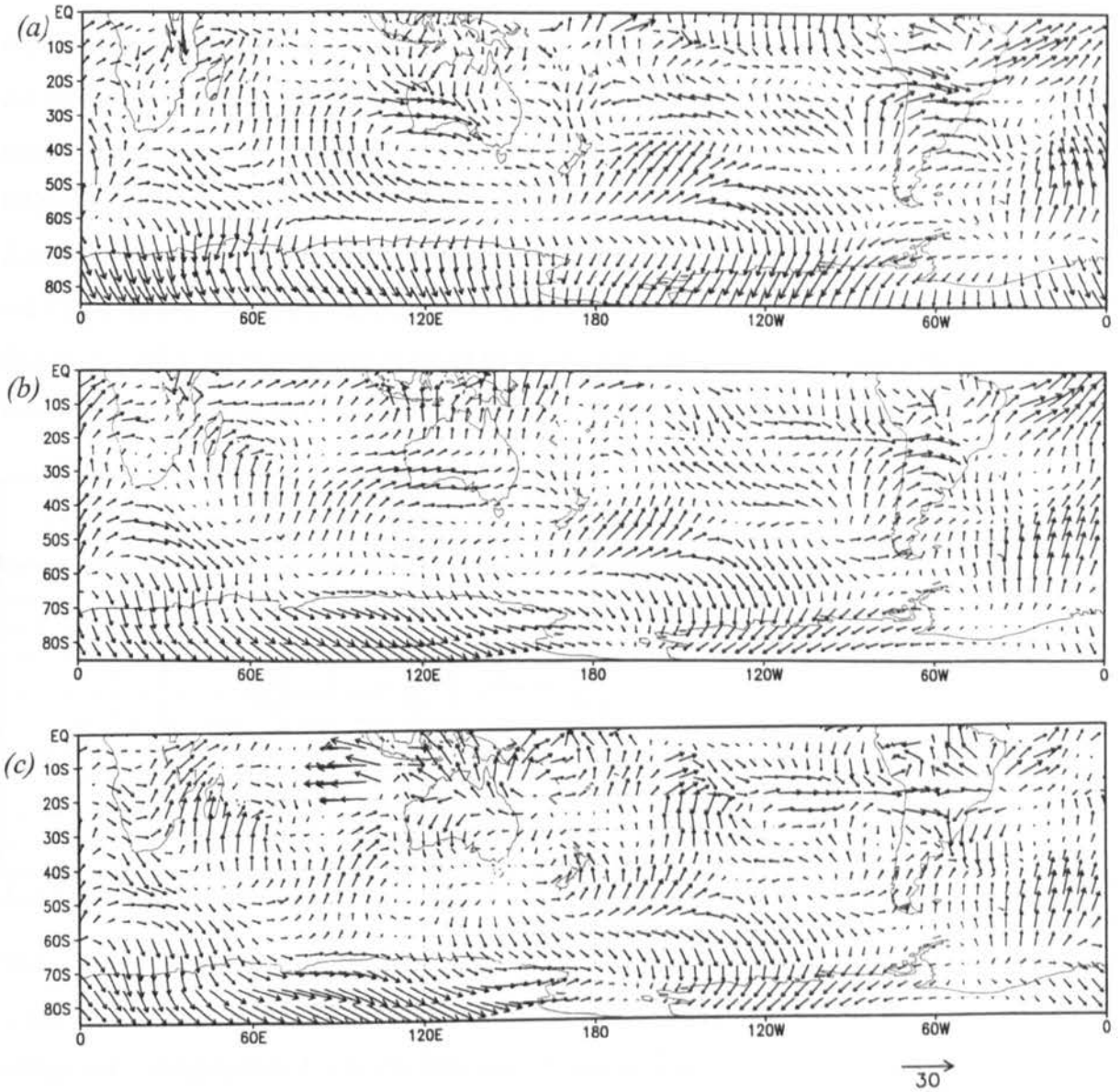

Figure 5.40 Grid point vectors based on the 24 month harmonic fitted to the 500 hPa (a) height, (b) temperature and (c) mixing ratio anomalies for the 1991 warm event.

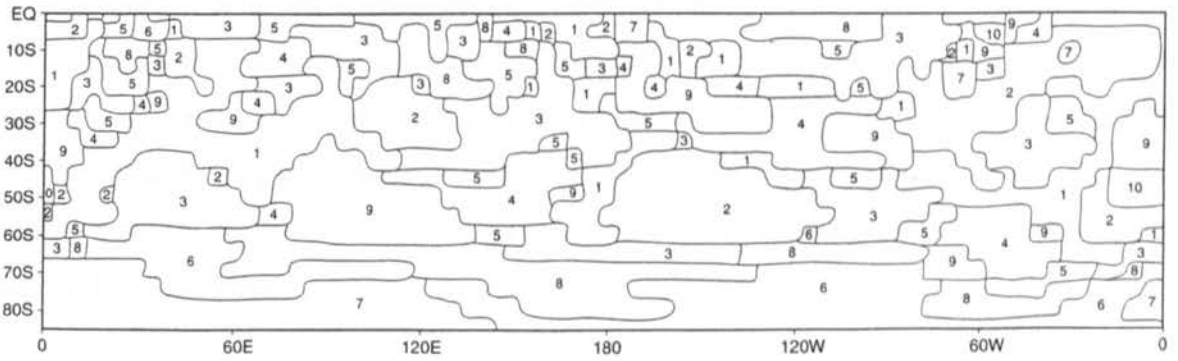

Figure 5.41 Clusters of the grid point vectors based on the 24 month harmonic of 500 hPa height anomalies for the 1991 warm event.

the greatest magnitudes, whilst Cluster 8 has the smallest amplitudes. Cluster 1, 3, 4 and 5 are the transition clusters for this event. Unlike the other events they were not restricted to the areas between the mid- and high latitudes or low to midlatitudes as they also occur in the low latitudes. This was because the 1991 event lacked the strong global low latitude anomalies found for the other events. Clusters 2 and 9 are of the opposite phase to Clusters 6 and 7, and are found across the midlatitudes, as well as across South America and into the Atlantic. Thus this event lacks the meridional contrast in anomalies found for the other events, in which the low and high latitudes are similar and contrast with the midlatitudes.

Cluster Number	Mean Amplitude (gpm)	Amplitude Coefficient of Variation	Mean Phase (months)	Phase Coefficient of Variation	Number of Grid Points
1	5.24	31.49	2.46	63.41	183
2	10.65	19.72	4.46	47.98	171
3	5.26	37.83	8.27	20.56	227
4	3.98	35.68	20.45	9.19	106
5	3.07	49.19	12.93	16.16	88
6	13.57	12.68	11.95	13.47	152
7	19.79	11.42	9.54	14.98	89
8	8.68	17.40	12.64	9.02	139
9	8.06	19.73	20.79	11.74	132
10	14.89	9.27	22.47	7.17	10

Table 5.8 Cluster statistics for the 1991 warm event 500 hPa height harmonics.

The warm composite vectors show some of the features common to warm events (Figure 5.42a-c), however, some of the trends apparent in the individual events were masked by the composite. Despite this the strong low latitude anomalies, occurring about 5 months after the event peak, were a distinct feature. These appear to migrate south-eastwards over a period of about 8 months arriving in the mid-Pacific about a year after the event. The signals over east Antarctica were lost in the composites, however, to the west of the Peninsula, along the 120°W meridian, there were positive height, temperature and mixing ratio anomalies. These appear to propagate south to arrive over the continent at the peak of the events composite. Along the 100°W meridian there was a marked meridional contrast in the sign of the anomalies between the subtropics and high latitudes. This pattern has been found in all of the warm events considered.

For the warm composite it can be seen that the dominant clusters in the high latitudes were Cluster 4 and 5 (Figure 5.43). Clusters 4 and 5 have phases coinciding with the composite peak, however, the amplitude of Cluster 5 was greater (Table 5.9). Clusters 3, 6 and 7 appear

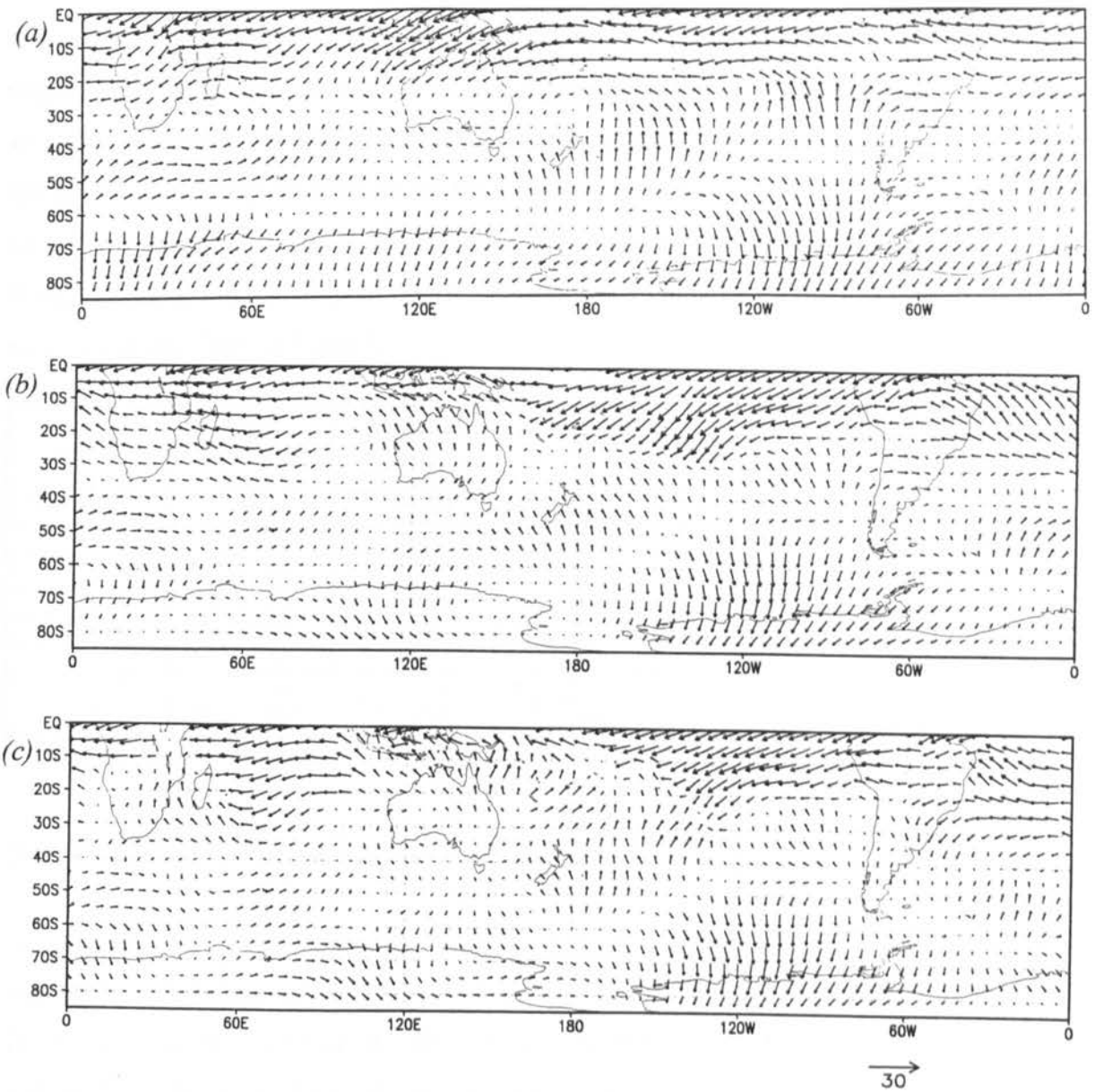

Figure 5.42 Grid point vectors based on the 24 month harmonic fitted to the 500 hPa (a) height, (b) temperature and (c) mixing ratio anomalies for the warm events composite.

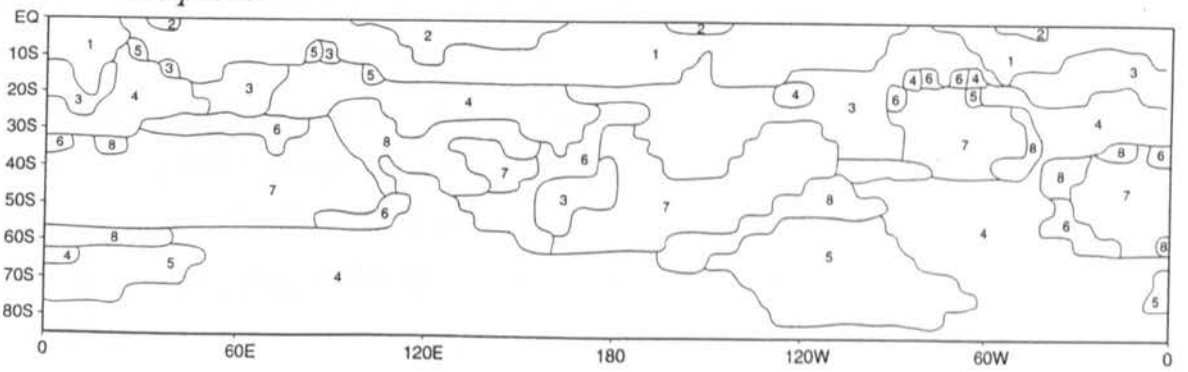

Figure 5.43 Clusters of the grid point vectors based on the 24 month harmonic of 500 hPa height anomalies for the warm events composite.

to be similar with positive phases of approximately 8 to 10 months after composite peak, and negative phases 4 months prior to the event peak. This suggests negative anomalies in the subtropical eastern Pacific at the same time as positive anomalies in the polar regions, indicative of the meridional contrasts found in the individual events. Cluster 1 and 2 pick up on the strong anomalies in the low latitudes, occurring about 5 months after the peak. Cluster 8 was the transition cluster, and occurs between the boundaries of the contrasting clusters, as well as linking Clusters 3 and 5.

Cluster Number	Mean Amplitude (gpm)	Amplitude Coefficient of Variation	Mean Phase (months)	Phase Coefficient of Variation	Number of Grid Points
1	10.83	16.44	17.33	5.37	186
2	16.58	8.38	16.64	4.74	36
3	6.61	19.82	20.04	11.43	145
4	3.84	38.80	14.61	12.18	465
5	7.75	11.09	12.47	11.79	97
6	2.25	41.78	22.15	5.64	60
7	4.04	41.34	20.74	9.06	234
8	2.34	52.14	8.00	23.34	74

Table 5.9 Cluster statistics for the warm events composite 500 hPa height harmonics.

5.5 Zonally averaged Hovmöller Plots

In order to identify the underlying trends in the movement of anomalies across the Southern Hemisphere zonally averaged Hovmöller plots were constructed. These plots yield different information to the longitudinal Hovmöller plots (Section 5.2) as they both zonally and temporally average the data. By averaging 60° longitude they remove orographic effects as well as capture anomalies propagated over a wider area. The temporal averaging, through the use of 12 month running means, will reduce the signals of small anomalies whilst increasing the weighting of strong persistent anomalies. Zonally averaged plots for the Southern Hemisphere were constructed for 6 zonal bands each spanning 60° longitude. However, the only marked ENSO related signals appeared in the 120 to 180°W (180 to 240° longitude) sector; the western Pacific. This band corresponds to the meridian chosen for the construction of the Hovmöller charts in Section 5.2, and crosses one of the 'centres of action' associated with ENSO.

Figure 5.44 shows the zonally averaged, twelve month running mean of 500 hPa height in the 120 to 180°W sector. From this it can be seen that the 5600, 5700 and 5800 gpm contours retreat equatorward during warm events, whilst extending poleward during cold events. However, the 5000 gpm line appears to extend poleward during warm events with the exception of the 1982 event, and retreat equatorward during cold event years, indicative of a greater intensity of synoptic scale systems at higher latitudes. During the 1982, 1986 and 1991 warm events there were increased heights in the high latitudes, indicative of higher than 'normal' pressures in this region. However the signals at high latitudes should be interpreted with caution as the Australian Analyses, at these latitudes, have been found to be less reliable than the mid- and low latitudes.

Figure 5.45 is a zonally averaged Hovmöller diagram of the 500 hPa height anomalies in the 120 to 180°W sector. In the region of the subtropical jetstream (35°S), there is a warm to cold event alternation in the sign of the height anomalies; during warm (cold) events there were negative (positive) anomalies. The negative anomalies were particularly intense during the strong 1982 event, and prolonged during the 1991 event. In the polar front jet latitudes (60°S) the signal is more variable. Positive height anomalies were associated with the 1976, 1986 and 1991 warm events, in contrast to the negative anomalies evident for the 1982 event. Negative anomalies were also associated with the 1978 and 1988 cold events, but not with the 1975 cold event. Over the high latitudes there were positive anomalies during the 1982, 1986 and 1991 warm events, agreeing with the findings presented in Figure 5.44; higher than 'normal' pressure in this region during warm events. However, an inverse signal for cold events does not appear to exist. This contrasts with the zonally averaged windspeed in the same sector (Figure 5.46).

During warm events the wind speeds tend to be greatest around 30°S, the region of the subtropical jet, and during cold events the wind speeds were greatest in the region around the region of 55°S (Figure 5.46). From this it appears that there is a seesaw in the strength of the two jetstreams between warm and cold events as shown clearly in a plot of the twelve month running mean of the percentage of positive geopotential windspeed anomalies between 120°W and 180°W (Figure 5.47). During warm (cold) events there were decreases (increases) in the

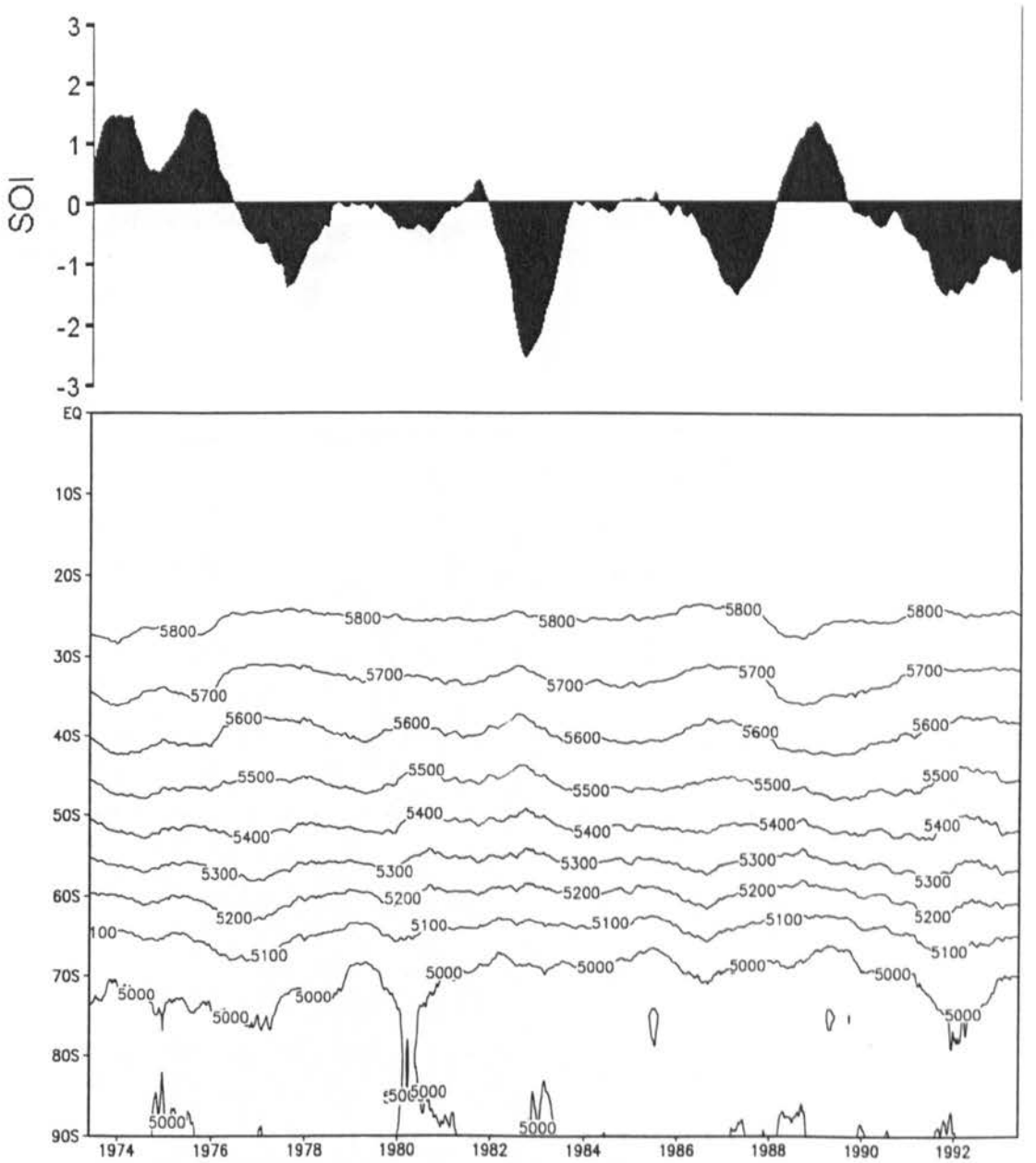

Figure 5.44 Hovmöller diagram of annual running mean 500 hPa height over 120°W to 180°W, in gpm. Above is the annual running mean of the SOI in hPa.

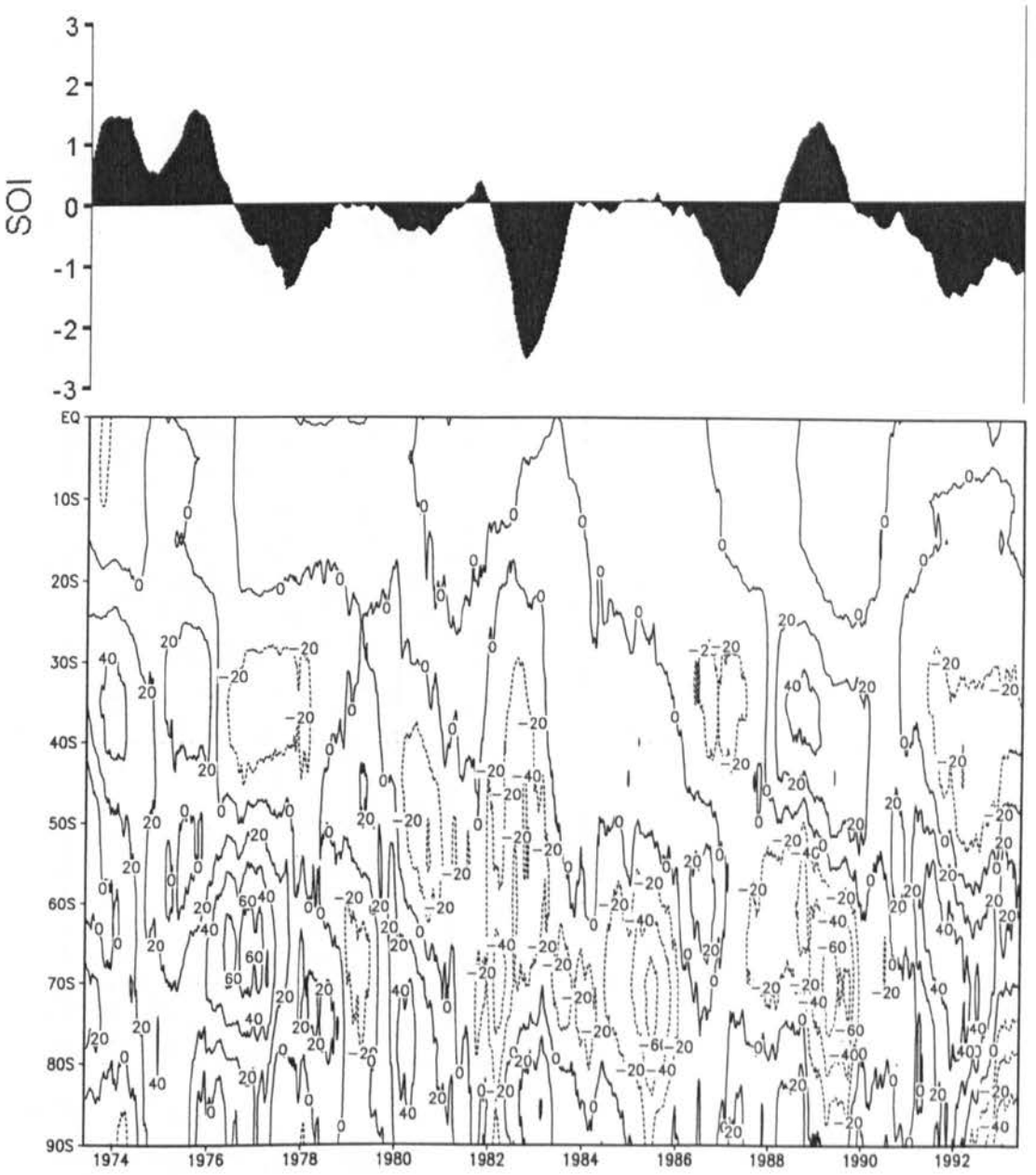

Figure 5.45 Hovmöller diagram of annual running mean 500 hPa height anomalies over 120°W to 180°W, in gpm. Above is the annual running mean of the SOI in hPa.

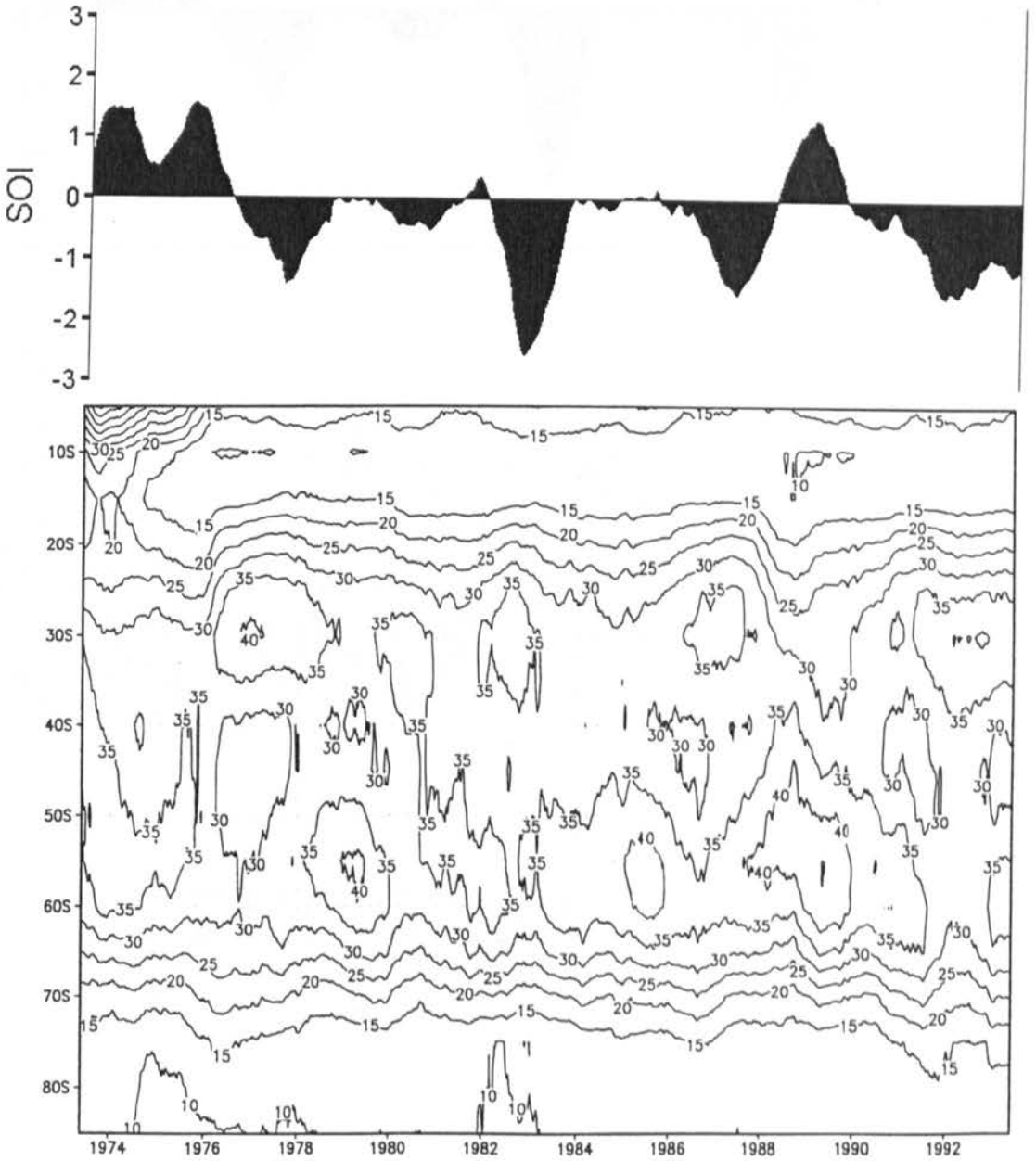

Figure 5.46 Hovmöller diagram of annual running mean 500 hPa zonal geopotential windspeed over 120°W to 180°W, in ms^{-1}. Above is the annual running mean of the SOI in hPa.

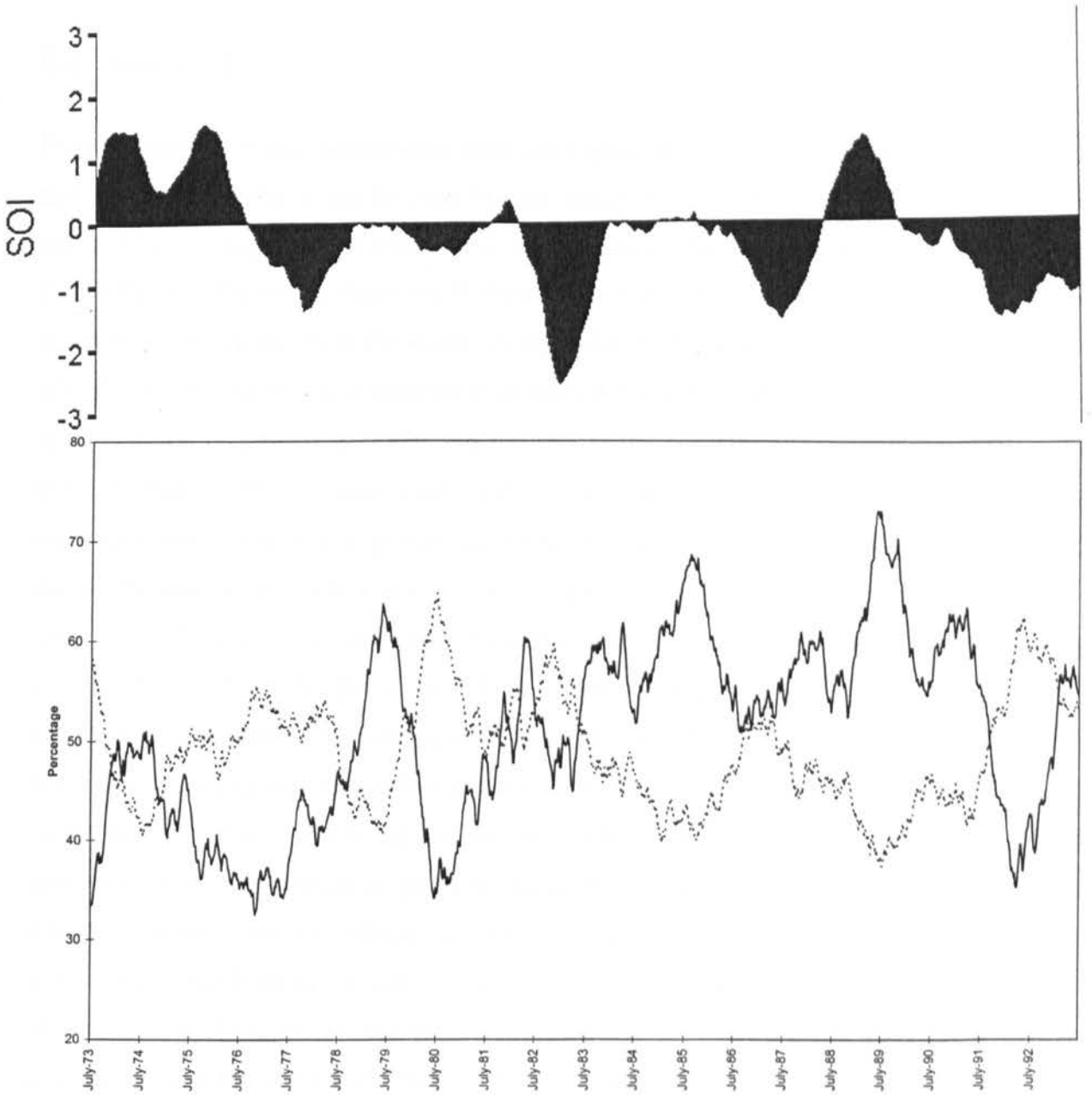

Figure 5.47 Annual running mean of positive anomalies in 500 hPa zonal geopotential windspeed over 120°W to 180°W for 25°S to 35°S (dashed line) and 50°S to 60°S (solid line). Above is the annual running mean of the SOI in hPa.

intensity of the polar jet, whilst for the subtropical jet there were increases (decreases) in intensity during warm (cold) events.

5.6 Summary

From an analysis of the latitude-time behaviour along the 230° meridian for individual events and event composites it can be seen that the response of height and temperature anomalies along the 230° longitude line varies from event to event. Despite this there appear to be some inter-cold and inter-warm event similarities. These include negative (positive) anomalies in the subtropical jet region at the warm (cold) event peak and positive anomalies in the high latitudes at the time of the cold event peak with positive anomalies following the peak. The spatial composite plots of 500 hPa and 700 hPa height and 700 hPa temperature identify the overall trends associated with warm and cold events. However, one disadvantage of the composite analysis is that it groups the events together masking the event differences. To extend the analysis of anomalies on a spatial scale the three month running mean spatial plots were used to identify the inter event similarities and differences by considering each of the events individually. From these it was found that across the Southern Hemisphere there were strong meridional contrasts in the sign of the anomalies. It was also found that the anomalies across Antarctica varied from event to event. However, when the anomalies were considered in a broader context it was found that the results agreed with those found in Chapter 4, and that there were predominantly positive (negative) anomalies at the peak of warm (cold) events. The harmonic analysis, by combining both the spatial and temporal aspects of the anomalies, in the form of harmonic dials, was able to identify the movement of the strongest anomalies over the Southern Hemisphere. This analysis once again found that there were both inter-event similarities and differences. From this analyses it was found that for cold events there tended to be low latitude 500 hPa height, temperature and mixing ratio positive anomalies 6 months before the peak, and positive anomalies over east Antarctica about 3 months prior to the event peak. For the warm events there were positive anomalies in the Pacific 5 months after the peak of the events consistent with negative anomalies 7 months prior to the peak. However, the similarities in the Antarctic region during the cold events did not occur with the warm events. Cluster analysis was carried out on the harmonic analysis results to identify regions with similar phases and amplitudes. This analysis aided in the

identification of meridional contrasts between the low, mid- and high latitudes, as well as possible teleconnections between the tropical Pacific and the high latitudes. The zonally averaged Hovmöller plots were able to describe the most pronounced trends over the time series, clarifying the mechanisms behind the teleconnections. Trends within the height and wind data corresponding to warm and cold events were identified such that during warm (cold) events there were decreases (increases) in height in the subtropics. At higher latitudes there were decreases (increases) in the intensity of the polar jet during warm (cold) events as well as increases (decreases) in intensity of the subtropical jet.

CHAPTER 6

THE TRANSFER OF THE ENSO SIGNAL FROM THE TROPICS TO THE ANTARCTIC

6.1 Introduction

This chapter discusses the results presented in Chapters 4 and 5. Initially it considers the spatial and temporal response of the Antarctic stations to ENSO events, as identified from an analysis of twelve month running mean plots and cross correlation analyses of Antarctic station climate data with the SOI (Section 6.2). The movement of climate anomalies along the 230° meridian is discussed (Section 6.3), and a comparison of events and composites will be made in this section in order to identify the similarities and differences in wavetrain propagation characteristics between events. An attempt at linking the movement of climate anomalies along the 230° meridian to the climate of the entire Southern Hemisphere is made in Section 6.4 by considering the results of the analysis of hemispheric scale climate anomaly spatial patterns. The results of the harmonic and cluster analyses will be discussed and linked to preceding analyses in Section 6.5. Finally the possible mechanisms at work in the transfer of the ENSO signal to the high latitudes, particularly the role of the jetstreams will be discussed in Sections 6.6 and 6.7.

6.2 The response of the Antarctic climate to ENSO

The variability of the response of Antarctic climate to different ENSO events was first identified by Karoly (1989) who found that during the developing stage of an ENSO event the Southern Hemisphere circulation features are stable in low latitudes, but quite variable at middle and high latitudes. However, during an ENSO mature phase in the austral summer, midlatitude features were noted to become stable, whilst high latitude circulation features remained more variable. The variability of the response of the Antarctic climate is governed by the ability of ENSO induced anomalies to propagate to high latitudes, which is affected by

differences in the medium through which the propagation is occurring. Differences arise due to the changing seasons and the location of the forcing relative to the background climatological planetary waves (Trenberth, 1997a).

In previous studies the effect of ENSO on a number of Antarctic climate variables has been considered. However, their findings are restricted to either surface or upper air variables. In addition to looking at station data this study has also considered Halley upper air variables as well as sea level, 850, 700 and 500 hPa analysis data in order to identify ENSO-Antarctic climate interactions at both the surface and upper levels. This study also considers the variation in the relationship of Antarctic pressure and temperature with the SOI over time. In contrast previous studies have not conducted longitudinal studies but have been more concerned with general overviews as obtained through analyses of composites. Therefore, as well as discovering the general relationships between ENSO and the climate of Antarctica this study does not neglect the variations behind these relationships. The analysis of a range of Antarctic climate variables carried out in this study has revealed that ENSO signals, over the time period considered, are neither temporally or spatially uniform.

	Warm event peak	Cold event peak
Pressure	increase	decrease
Temperature	increase	decrease
Cloud Cover	variable	variable
Windspeed	increase prior	decrease prior

Table 6.1 The response of Halley station climate to warm and cold events.

	Warm event peak	Cold event peak
Pressure	increase	decrease
Temperature	decrease	increase
Cloud Cover	decrease	increase
Windspeed	increase prior decrease following	decrease prior increase following

Table 6.2 The response of Faraday station climate to warm and cold events.

From a subjective assessment of twelve month running mean plots of climate variables and the SOI inverse relationships between pressure and the SOI were found to exist at Halley (Table 6.1), Faraday (Table 6.2), Amundsen-Scott, Mawson, Mirnyy, SANAE, McMurdo, until the early 1980's, and Vostok, from 1970. No clear relationship is apparent for Casey. To investigate these associations further cross correlation analysis was used to identify

significant lag and lead relationships as well as the underlying trend between pressure and the SOI at each station. Cross correlation results revealed that all the Antarctic stations considered in this study had increases (decreases) in pressure coinciding with the peak of a warm (cold) event, with decreases (increases) in pressure a year prior to and a year following the warm (cold) event peak (Figure 6.1). This pressure pattern is indicative of a biennial tendency in the response of the Antarctic climate to ENSO (van Loon and Shea, 1987), mirroring the biennial tendency of the ENSO phenomena itself. The timings of the most significant ENSO-Antarctic climate associations were also found to be fairly uniform in nature. If the biennial nature of the response to ENSO is taken into account, i.e. anomalously low pressure is replaced by anomalously high pressure 12 months later, negative pressure anomalies across the continent occur at lags of 3 to 4 months following the SOI peak (Figure 4.27). The exception is Casey where a significant correlation with the SOI was not found when using the entire time period, however, significant correlations were found when the time series was divided into 3 sub-periods (Figure 4.15). These results agree with those of van Loon and Madden (1981), van Loon and Shea (1987) and Karoly (1989) who found positive pressure anomalies across the Antarctic continent at the peak of warm events. In a similar study, based on cross correlation analysis, Smith and Stearns (1993) found the same inverse relationship between pressure and the SOI as in this study, however, the most significant pressure-SOI correlations occurred 12 months after the event peaks. This differs from the results obtained in this study. The reasons for such contrasts are discussed below in Section 6.2.1. In an application of this study's results to an independent ENSO event it was also found that the recent strong 1997 warm event followed the pattern identified above with positive anomalies over the Antarctic continent in the austral summer season, i.e. around the warm event peak (Figure 6.2a). In agreement with the surface results, Halley upper air data also displayed an inverse relationship between both 850 and 500 hPa height and the SOI. Cross correlation analysis also revealed that this relationship had a strong biennial tendency. This inverse relationship also existed for the recent strong 1997 warm event, which saw an increase in 500 hPa height during November 1997, around the time of the peak of the event (Figure 6.2b). The cross correlation also revealed that during warm (cold) events the increase (decrease) in geopotential height, causes increases (decreases) in thickness, which are linked to increases (decreases) in geopotential temperature (Table 6.3). Also associated with the

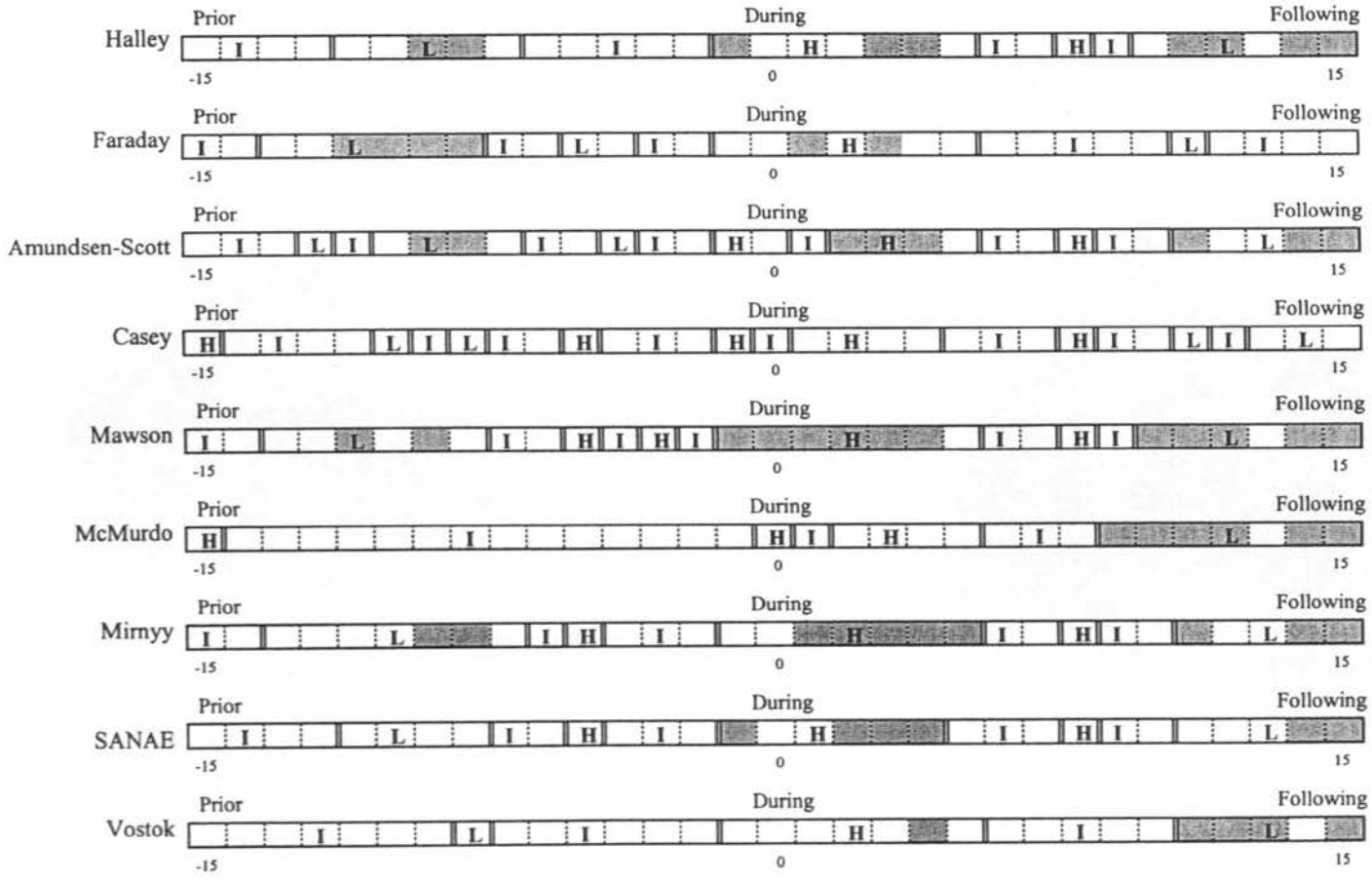

Figure 6.1 Station pressure prior to, during and following a warm event. Where L is low, H is high and I is intermediate pressure, based on correlations greater than one standard error. || is the boundary between the periods with distinct SOI-pressure trends. The shading indicates correlations greater than two standard errors. The divisions are in months, with 0 representing the event peak.

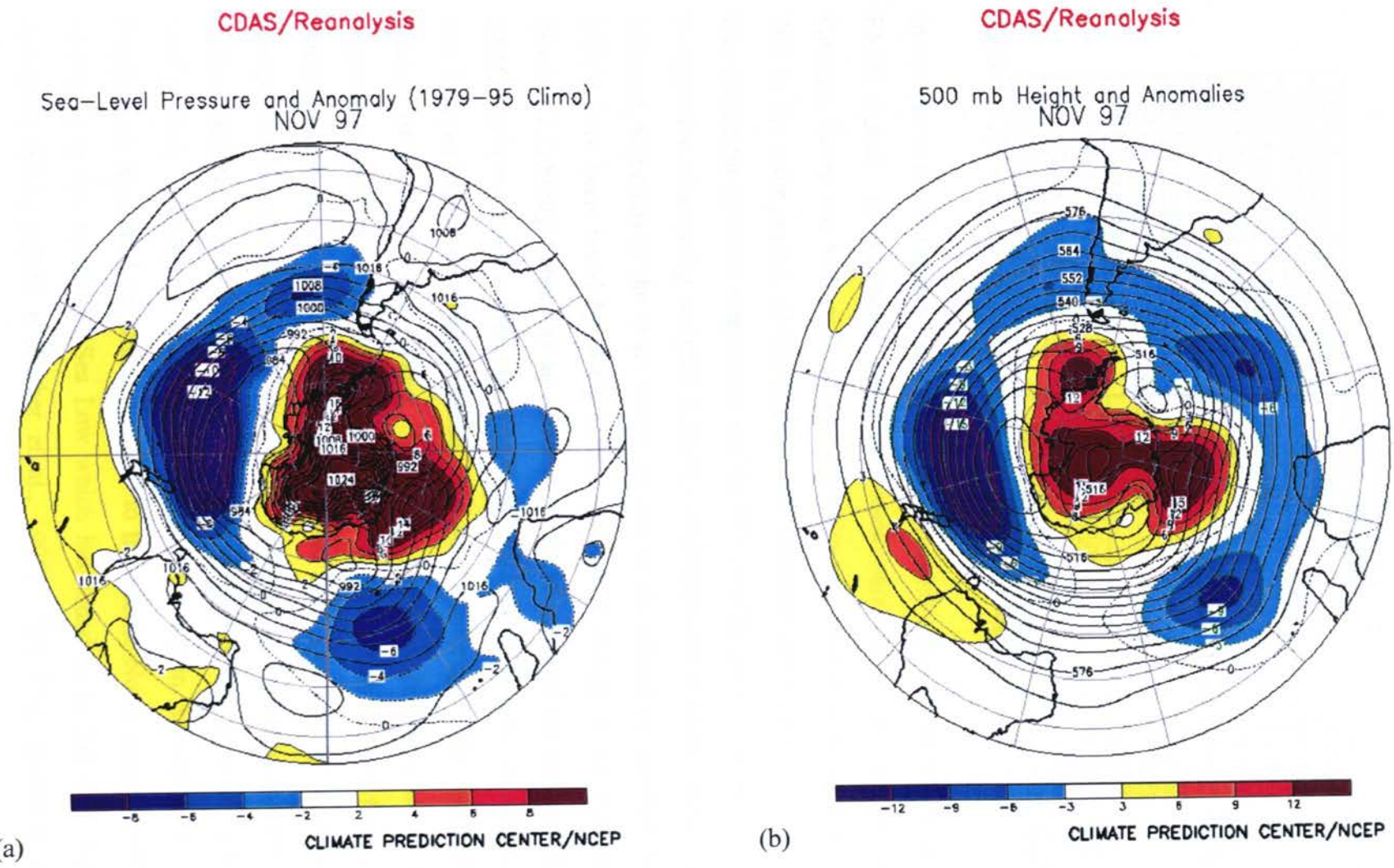

Figure 6.2 Southern Hemisphere (a) sea level pressure and anomalies and (b) 500 hPa height and anomalies for November 1997 (from the Climate Diagnostics Bulletin, Climate Prediction Center, U.S. Department of Commerce)

increases (decreases) in height and pressure during warm (cold) events are decreases (increases) in the upper air windspeeds (Table 6.3).

	Warm event peak	Cold event peak
850 hPa geopotential height	increase	decrease
500 hPa geopotential height	increase	decrease
850 hPa relative humidity	increase	decrease
500 hPa relative humidity	increase	decrease
850 hPa temperature	decrease 1 year prior	increase 1 year prior
500 hPa temperature	increase	decrease
850 hPa windspeed	decrease	increase
500 hPa windspeed	decrease	increase
850 hPa wind direction	north-easterly	south-westerly
500 hPa wind direction	northerly	southerly
850-500 hPa thickness	decrease 7 months prior	increase 7 months prior

Table 6.3 The response of Halley upper air climate to warm and cold events.

In contrast to the situation for pressure, Antarctic temperature fields do not demonstrate clear ENSO signals. At Amundsen-Scott and Vostok there was an inverse relationship whilst at Faraday, Casey and Mirnyy there was a positive relationship between temperature and the SOI for the entire period. At Halley, Mawson, McMurdo and SANAE there was a variation in the relationship between temperature and the SOI over the period. Reversals from an inverse to a positive relationship occurred at Halley, McMurdo and SANAE around the late 1970's, however, variations in the exact timing are due to the subjective approach taken. The late 1970's have been found by Wang (1995) to mark a change in the evolution of El Niño (Section 2.7) brought about by an alteration in the background sea surface temperatures. As ENSO has been shown to affect the variability of Antarctic climate, alterations in ENSO will also have an impact on ENSO-Antarctic climate relationships. The suggested evolutionary changes of El Niño events (Wang, 1995) may, therefore, be linked to the changes in the response of temperature at Halley, McMurdo and SANAE to the SOI from the late 1970's. Another change since the late 1970's has resulted from a reversal in the decadal oscillation. Abrupt warming occurred at this time in the tropical Pacific concurrent with cooling in the extratropical North and South Pacific and a deepening of the Aleutian Low (Zhang et al., 1998) (these mechanisms are described in more detail in Section 2.7). The Northern Hemisphere Aleutian Low which is linked to the Pacific-North American (PNA) pattern is analogous to the Amundsen Sea Low which has found to be linked to the Pacific-South American (PSA) pattern (Cullather et al., 1996). The PSA pattern is an atmospheric

wavetrain linking ENSO with the climate of the entire Southern Hemisphere. Therefore the changes in the decadal oscillation are likely to have a direct impact on the Antarctic climate. From consideration of Figure 6.3 the overall trends identified from the cross correlation analysis can be seen. At the peak of warm events Halley, Amundsen-Scott, McMurdo, Mirnyy, SANAE and Vostok have elevated temperatures, whilst Faraday and Mawson have reduced temperatures, and Casey has no change in temperature (Figure 6.3). As in the analysis of the temperature-SOI correlations carried out by Smith and Stearns (1993) this analysis shows that the response of temperature, to the SOI, across the continent is much more variable than the response of pressure. This is because Antarctic temperatures have been found to be more closely associated with cloud cover than changes in the meridional circulation (King, 1994), although changes in cloud cover reflect changes in the atmospheric circulation. Cloud cover can be used to explain the variation in temperature responses to the SOI at both Faraday and Halley. During warm (cold) events the reduction (increase) in temperature at Faraday associated with an increase (decrease) in pressure, was a response to the decrease (increase) in cloud cover (Table 6.2) which caused an increase (decrease) in the radiative heat loss. Whilst until the mid-1970's at Halley during warm (cold) events the increase (decrease) in temperature associated with increased (decreased) pressure can be explained by an increase (decrease) in cloud cover (Table 6.1), limiting (increasing) radiative heat loss (King et al., 1996), the relationship appears to have broken down from the mid-1970's.

The difference between the station temperature responses can also be explained by the alteration in the strength of the 500 hPa westerlies. When the westerlies are weak (strong) during warm (cold) events, mainland Antarctic stations have increases (decreases) in temperature whilst Peninsula stations are anomalously cold (warm) (Rogers, 1983). This is confirmed in this analysis in which it was found that the 850 and 500 hPa westerly wind components were negative (positive) during warm events, thus mainland stations would have an increase (decrease) in temperature and Peninsula stations would have a decrease (increase) in temperature. The increase in cloud cover with higher pressure during warm events at Halley is likely to be caused by the increase in north-easterly winds aloft which led to an increase in 850 and 500 hPa relative humidity (Table 6.3) as more winds will have their origin over the oceans, thus will contain more water vapour than air masses originating over the

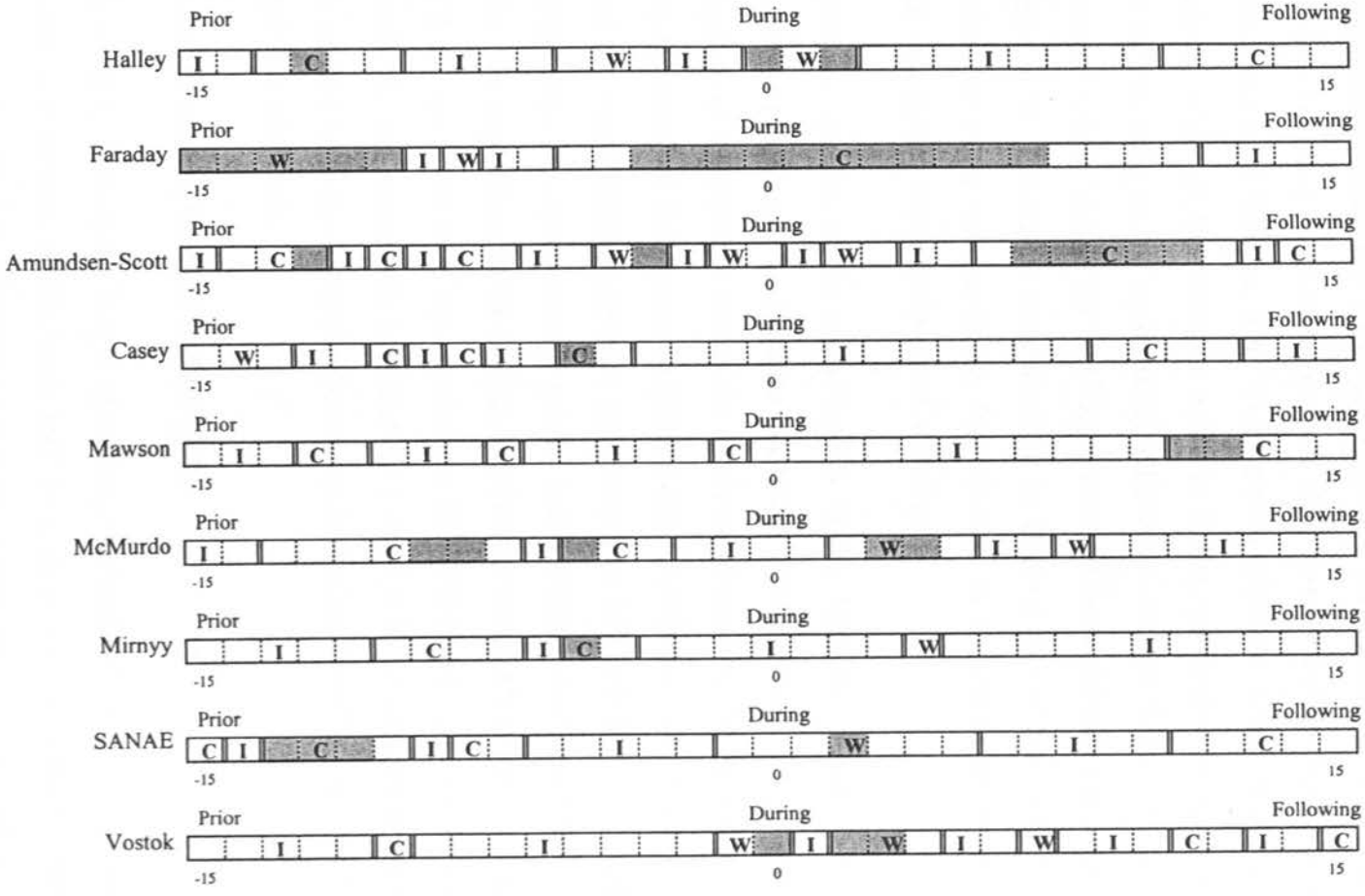

Figure 6.3 Station temperature prior to, during and following a warm event. Where C is cool, W is warm and I is intermediate temperature, based on correlations greater than one standard error. || is the boundary between the periods with distinct SOI-temperature trends. The shading indicates correlations greater than two standard errors. The divisions are in months, with 0 representing the event peak.

land. However, at Faraday the cloud cover is likely to be higher during cyclonic conditions due to its more northerly location and proximity to the circumpolar trough. This study found that during warm (cold) events not only did the westerlies decrease (increase) but that there was an increase in both 500 and 850 hPa north-easterly (south-westerly) winds, which in turn are linked to the increase (decrease) in geopotential height at Halley as with increased (decreased) pressure the upper air winds are predominantly north-easterly (south-westerly) (Table 6.3). With north-easterly winds aloft easterly surface winds are most common, which is the only wind direction from which strong winds are observed at Halley (King, 1994). As easterly winds are the strongest winds at Halley, partly due to topography and partly due to the station being to the south of the subantarctic trough (King, 1994), a reversal of the wind direction would lead to the breakdown of an SOI-windspeed relationship, as was observed in Figure 4.2d. Faraday is more likely to be affected by cyclonic activity and stronger westerly winds due to its more northerly location and so does not experience the breakdown in the SOI-windspeed relationship found at Halley.

From the analysis of the many aspects of the Antarctic climate it has been found that the increases (decreases) in pressure occurring during warm (cold) events result in a varying response of temperature across the continent (Figure 4.27). Analysis of the Halley upper air data has revealed that the warm (cold) event related increases (decreases) in Antarctic pressure lead to corresponding increases (decreases) in 850 and 500 hPa height, relative humidity, temperature and north-easterly winds, and decreases in 850 and 500 hPa windspeed (Table 6.3). An implication of the finding that the relationship between the Antarctic climate and the SOI are not stable over time, is that the ENSO impacts on climate, as summarised in Tables 6.1-3, will not necessarily be found for every ENSO event, as every ENSO event is different the response of the Antarctic climate to individual ENSO events will vary especially at the multi-decadal scale.

6.2.1 The importance of methodology

As noted in Section 4.5 length of study period and differences between this study and that of Smith and Stearns (1993) have lead to contrasting conclusions regarding the relationship between the climate variables of Antarctica and the SOI. Therefore, different results from

studies using different time periods, and event composites will identify different responses of the Antarctic climate to ENSO.

A comparison of the findings of SOI and climate variables from the cross correlation analyses of this study and those of Smith and Stearns (1993) was made in an attempt to understand inter-study contrasts of results. This study and that of Smith and Stearns (1993) used different methodologies and time periods to identify SOI signals across the continent. To assess the importance of methodology in explaining results contrasts the Smith and Stearns (1993) methodology (Section 4.3.2) was used on the same period as used in this study. The Smith and Stearns (1993) methodology produced results for the period 1957-94 that were similar to those found in this study for the same period rather than those of Smith and Stearns (1993) for the period 1957-84. Given this result it appears that the methodology was not the cause of the inconsistent results, but the time period used. In order to test this supposition a secondary type of analysis was carried out to assess the importance of the time period used. For this analysis Casey was chosen as this location demonstrated few statistical relationships between pressure and temperature and the SOI. Based on the fact that the twelve month running means displayed differing SOI-climate relationships across the time series, the time series for Casey was divided subjectively into three periods namely, 1957 to 1965, 1966 to 1986 and 1987 to 1994. Cross correlation analysis revealed that for temperature there was a strong inverse relationship in the first period, a positive relationship in the second period and a less significant inverse relationship in the third period. For pressure there was no significant relationship in the first period, an inverse relationship in the second period and a positive relationship in the third period. Based on these results it appears clear that the lack of a relationship between Casey pressure and temperature and the SOI was not due to there being no relationship, but due to the relationship varying over time. Therefore the time period used for the analysis of ENSO-climate relationships is fundamental as there is a clear variation in the response of the Antarctic climate to ENSO over time. Thus combining events across a time period to identify the impacts of ENSO as well as using composited events, is not ideal for discovering the most significant relationships.

6.3 The movement of anomalies down the 230° longitude line

The systematic analysis of the development of a number of Pacific Ocean warm (El Niño) and cold (La Niña) events presented in Section 5.2 has revealed a considerable amount of inter-cold and warm event variability in the propagation of height and temperature anomaly patterns. Consequently when composites are constructed, clear and unequivocal propagation signals common to all cold and warm events are not revealed (Figures 5.5 and 5.10). This is because the anomaly sign as well as the direction of anomaly movement is rarely consistent from one warm (cold) event to another, especially in the subtropical to subpolar latitudinal range.

Of the cold events analysed in this study, the 1975 event stands apart from those of 1978 and 1988 as this event displayed strong and persistent positive height and temperature anomalies centred on 70°S for up to two years following the event peak (Figure 5.1a-c). This contrasts with 1978 and 1988 when negative height and temperature anomalies were a feature of the months that followed the event peak (Figures 5.2 and 5.3). The anomaly propagation patterns for 1975 also demonstrate differences to those displayed for 1978 and 1988. In 1975, the persistent post event peak positive height and temperature anomalies, centred on 70°S, appear to be a product of the propagation of positive anomalies from both high and subtropical latitudes in year -1. In contrast, for the months in year -1 leading up to the 1978 and 1988 cold event peaks, the propagation of negative anomalies from both high and subtropical latitudes to latitudes centred on 50°S, especially in 1978, dominated. The northward movement of positive anomalies in the spring of year -1 of the 1978 event, which reached the subtropics in the autumn of year 0, is consistent with the end of high latitude blocking from the 1976 warm event, and the weakening of the subtropical jet, a trend also apparent for the 1988 cold event. As for year -1 and year 0 of the 1978 and 1988 events, inter-event consistencies in the year +1 anomaly and propagation patterns are also a feature as in both events positive height and temperature anomalies tend to move polewards. This feature is not seen in year +1 of the 1975 event. The most likely explanation for why 1975 is at odds with 1978 and 1988, especially in year +1 which shows the most dramatic contrasts in the 50°S to 80°S latitudinal range, is because, of the three cold events analysed here, only 1975 is followed immediately by the rapid transition to a warm event. As year 0 of warm events and

the months preceding the warm event peak are generally characterised by positive anomalies at these latitudes (Figure 5.6) this may well explain the anomalous (compared to 1978 and 1988) situation in year 0 and year +1 of the 1975 event as these years are, in fact, year -1 and year 0 respectively of the 1976 warm event.

At latitudes beyond 70°S the situation regarding anomaly patterns for all three cold events appears to be much more uniform compared to the subtropical to subpolar latitudinal range, as over the high latitudes there is a general agreement in the sign of the anomalies for the cold events. For the 1978 and 1988 events there were negative anomalies prior to the peak. For all three events there are positive anomalies at the time of the peak, which switch to negative anomalies and back to positive anomalies following the peak. Although the timing and duration of the high latitude anomalies vary the overall patterns are very similar, as can be seen in the composite (Figure 5.5).

Given the above it is no surprise that due to the moderating effects of the anomalous 1975 event, the cold composite anomaly plot in the subtropical to subpolar range, only reflects the semi-consistent anomaly and propagation features noted for 1978 and 1988 where these are particularly strong (Figure 5.5). Features notable in the composite are the northwards propagation of negative anomalies from the high latitudes to about 50°S in year -1, propagation to the tropics from the high latitudes of negative anomalies at around the time of the peak, and the non-periodic but oscillatory behaviour of anomalies in the Antarctic region throughout the course of year -1 to year +1. Also apparent in the cold composites are the positive anomalies in the subtropical jet region at the peak, which appear in all the cold events. There are no negative anomalies in the region of the polar jet at the time of the composite SOI maximum. These are delayed, occurring about six months after the peak.

The magnitude and propagation characteristics of the height and temperature anomaly patterns for the 1976, 1982, 1986 and 1991 warm events, although demonstrating a considerable deal of inter-event variability, do display some event to event consistencies. All the warm events appear to show a change in the intensity of the subtropical and polar jets at around the peak of the event. This observation agrees with the findings of Mo and White (1985) regarding possible ENSO related latitudinal shifts in the positions of the jets. The change in the intensity of the jets appears clearly in the warm event composites. While a clear warm-cold

antiphase exists for the intensity of the subtropical jet the response of the polar jet varies in its timing between the cold and warm composites. The poleward propagation, from subtropical latitudes, of positive anomalies to 70°S in year -1 and the persistence of these for at least two years is a common feature of the 1976 and 1991 events (Figures 5.6 and 5.9). Such positive height and temperature anomalies are no doubt linked with the warm event related increase in high latitude cyclonic activity associated with the New Zealand blocking high noted by Streten (1975), Karoly (1989) and Bromwich et al. (1993). For the 1972 warm event (not included in this study) Streten (1975) found that warm event related increases in cyclonic frequency are accompanied by a decay in the Southeast Pacific High and an apparent eastward advance of the mid-ocean long wave trough. The slow poleward propagation of positive anomalies noted for the 1976 and 1991 events, which appear clearly in the warm composite with anomalies of over 75 gpm at the 500 hPa level, may be a manifestation of such a feature. Height and temperature anomaly dynamics for the 1982 and 1986 events contrast with those of the 1976 and 1991 events. Prior to the 1982 event a wavetrain of negative anomalies moved equatorwards and then appeared to move poleward just after the event peak (Figure 5.7), whilst prior to the 1986 event positive anomalies tended to move equatorward (Figure 5.8). In the transition period from year 0 to year +1 of the 1976, 1982 and 1986 events a wavetrain of negative anomalies propagated polewards, however, the propagation rate varied between events. For both the 1976 and 1986 events these anomalies fold back equatorwards from the mid- to high latitudes. The poleward movement of negative anomalies in year 0 to year +1 noted here for the 1976, 1982 and 1986 events is the reverse of the situation found following the 1978 and 1988 cold events suggesting that cold events produce a true anti-phase in the region of study as far as height and temperature anomaly patterns are concerned. Although the 1982 event demonstrates some similarities with the other warm events, the period in which the greatest divergence can be found is that of year -1 when a wavetrain of strong negative anomalies moved from high latitudes equatorwards. This feature is not replicated in the composite at all and appears to be unique to the 1982 event. In fact, the year -1 anomaly pattern in the warm composite is the complete reverse of that demonstrated for 1982. It can be seen that for the warm events the anomalies prior to and around the peak tend to be stronger than those following the peak. This could be a result of the rapid change in the ENSO signal in year 0, with the ENSO induced signals being reduced as a consequence.

For the high latitudes the degree of agreement in the sign of the anomalies for the warm events is very limited. Although there is a basic trend with a sign change from negative to positive anomalies before and after the peak, agreeing with the findings of Smith and Stearns (1993) across the Antarctic continent, there is a large inter-event variation in the timing of the sign reversal. Notwithstanding matters of timing, Smith and Stearns (1993) believed that such a reversing anomaly pattern in the high latitudes would strengthen the trough over the Ross and Amery ice shelves and a ridge aloft near Dumont d'Urville containing the New Zealand blocking high. The 1976 and 1986 events show some similarity, both events have positive anomalies in the year prior to the peak which switch to negative anomalies just before the peak, back to positive in the following year, briefly negative and then positive once again. These two warm events contrast well with the trends identified for the cold events, with a reversal in the signs as one would expect. However, the 1982 and 1991 events are different. For both events there are positive anomalies at the time of the peak with negative anomalies prior to it. The 1982 event follows a seesaw pattern alternating between negative anomalies and positive anomalies following the peak but the 1991 event appears to indicate that there were persistent negative anomalies in the high latitudes following the peak. The dissimilarity of the effects of the warm events at high latitudes is indicated by the increased complexity of the warm event composites. The timing of the events is thought to be very important with regard to extratropical response. The sub/extratropical response is thought to be greatest in winter (van Loon and Rogers, 1981) which probably represents some degree of phase locking at this time of year between the tropics and the extra-tropics. This would in turn explain some of the variability between the high latitude responses from ENSO events. In the Antarctic region there appears to be opposition in the sign of the signals between year -1 and year 0, as found by Kiladis and Diaz (1989), although there is a large amount of variation between the events. However, this opposition does not seem to occur in the area around 70°S.

The purpose of the Hovmöller analyses of monthly geopotential height and temperature data, was to establish whether clear tropical-extratropical wavetrain patterns of climate anomalies occur in South Pacific warm and cold events in a region which is climatically ENSO sensitive. Study results have not revealed an unequivocally clear picture in terms of wavetrain patterns. This may be a product of the temporal resolution of the data used with data at the sub-monthly scale perhaps more appropriate. An important finding is the high degree of inter-warm and

inter-cold event variability of wavetrain patterns. Composite Hovmöller diagrams therefore do not capture the complex dynamics typical of the events considered. This is especially true for the warm event composites due to the anomalous behaviour of the 1982 warm event compared to the other warm events studied.

Despite the fair degree of inter-event variability of wavetrain patterns, there is evidence of some commonality of patterns for warm and cold events and for a true warm-cold event antiphase of wavetrain anomalies. For cold events which are not followed by the onset of warm event conditions (1978, 1988) it appears that there is a propagation of negative height and temperature anomalies from subtropical to high latitudes preceding the event peak. These persist for around one year in subpolar latitudes following the event peak. At polar latitudes during cold events there is a transition from positive anomalies at the time of the event peak to negative anomalies following the peak.

Compared to cold events, warm event wavetrain patterns are highly variable and complex with 1982 being dissimilar to the 1976, 1986 and 1991 warm events especially in the year preceding the event peak. For this reason the 1982 wavetrain pattern of equatorward propagating negative height and temperature anomalies is not resolved in the warm event composite. This observation adds to the list of contrasting ocean and atmosphere features found for the 1982 warm event (Cane, 1983; Rasmusson and Wallace, 1983). A clear feature of the warm event composites, which reflects more the situation for 1976 and 1991 than for 1982 and 1986, is the propagation of positive height anomalies from low to high latitudes up to the event peak and the presence of a strong meridional contrast in anomalies between subpolar, middle to subtropical and tropical latitudes; positive, negative, positive respectively. This meridional pattern resembles that of the well-known PNA pattern for the North Pacific (Horel and Wallace, 1981). Such a pattern, which has also been identified for a limited number of warm events by Karoly (1989) for the South Pacific, may be associated with the eastward advance of a mid-ocean longwave trough and/or the behaviour of the double jet oscillation as described by Cullather et al. (1996); during warm events the subtropical jet strengthens and the polar jet weakens. The double jet oscillation may provide a mechanism for the propagation of warm and cold event climate signals between tropical-subtropical and high southern latitudes. Similarly the observed equatorial propagation of height and

temperature anomalies from high southern latitudes in the months leading up to the 1982 warm event (year -1) could provide support for ideas on high latitude forcing of the Southern Oscillation as achieved through forcing of the Circumpolar Current and subsequent equatorward sea surface temperature propagation via the Humbolt current as outlined by Pittock (1984).

The fact that clear unequivocal wavetrain patterns of climate anomalies linking tropical-subtropical with high southern latitudes do not exist attests to the complexity of tropical extratropical teleconnections in the South Pacific sector and the difficulty of identifying a single indisputable propagation mechanism for ENSO signals. Furthermore, from the evidence presented here, it is clear that the possibility exists for wavetrains to not only propagate poleward, but also equatorward from high southern latitudes adding to the speculation that the Antarctic continent may be both an active as well as a passive component of a larger interactive Pacific basin climate system that spans a large geographical range. Because clear wavetrain pattern do not exist from one cold or warm event to another, the possibility also exists that an ENSO related system threshold may be at play, whereby the distinctiveness and nature, or even the existence of any wavetrain pattern, may be closely related to the timing as well as the intensity of the associated ENSO event.

6.4 Spatial patterns in the anomalies

The most significant finding of the annual composite charts for 500 hPa and 700 hPa height, and 700 hPa temperature (Section 5.3) is the strong meridional contrast in the sign of the anomalies. For the cold events there were positive (negative) height anomalies in the Antarctic region and negative height (positive) anomalies in the midlatitudes in year 0 (year +1) (Figures 5.12b-c and 5.13b-c). For the warm events the strongest contrast occurred around 160°W with negative (positive) height anomalies in the subpolar region and positive (negative) height anomalies in the subtropics in year -1 (year 0) (Figures 5.15a-b and 5.16a-b), with the spatial patterns in the temperature anomalies being similar to those of the height anomalies (Figures 5.14 and 5.17). For the cold events there was a reversal in the sign of the anomalies between year 0 and year +1, whilst for the warm events this reversal occurred between year -1 and year 0. The time period of a year used for these plots is too long to

display the changes in pressure and temperature associated with ENSO events, found in the Hovmöller diagrams. As the event peak occurs between the year -1 and year 0 divisions, the patterns found in these plots will differ from those found in the Hovmöller diagrams, and as composites are used, in the analyses of the Antarctic climate. The annual composite charts are limited in their ability to identify ENSO induced anomalies as the temporal scale is too long. As all ENSO events comprising the composites are different, individual signals will be lost. For identification of the spatial anomalies associated with individual events the 3 month percentage plots were more useful. Due to the nature of these charts, i.e. they consider the percentage of positive and negative anomalies rather than the size of these anomalies, they were not biased by large anomaly values. As in the annual composite charts these revealed strong meridional contrasts resembling the Northern Hemisphere PNA pattern (Horel and Wallace, 1981) as well as the expected extensive inter-cold and inter-warm event variability found in the Hovmöller charts. In previous studies hemispheric wide ENSO induced climate anomalies have been analysed using composites. However, this study, by considering each event individually, on a 3 month running mean basis, has identified in detail event specific ENSO teleconnections and ENSO related anomalies.

Across the Antarctic continent the inter-event variability in the anomalies is apparent. The expected negative pressure anomalies across Antarctica coinciding with the peak of cold events, found in Chapter 4 and discussed in Section 6.2, were only apparent for the 1975 cold event (Figure 5.18), with positive anomalies at the peaks of both the 1978 and 1988 cold events (Figures 5.19 and 5.20). However, for the 1978 event negative anomalies developed six months after the peak. The contrasting positive anomalies for warm events were present at the peaks of the 1982/3 and 1991 warm events (Figures 5.22 and 5.24), with limited positive anomalies across Wilkes Land in the 1976 event (Figure 5.21), developing into strong positive anomalies following the event peak. However, in contrast, the weak to moderate 1986 warm event had negative anomalies in the Weddell and Ross Sea regions (Figure 5.23). However, the sea level pressure anomalies over Antarctica may not be truly representative due to the extrapolation of values down to sea level.

The sea level pressure anomalies over the mid-Pacific region are a response to ENSO itself thus it is not surprising that there were strong positive anomalies in this region for the 1975

and 1988 cold events and strong negative anomalies for the 1976, 1982, 1986 and 1991 warm events. The weak 1978 cold events lacked these strong mid-Pacific anomalies, however, it did possess weak positive anomalies in the eastern Pacific region. In the tropics of the Indian Ocean there were strong negative anomalies for the 1975 and 1988 cold events, contrasting with strong positive anomalies in this region for the 1982, 1986 and 1991 warm events. This opposition of pressure between the Pacific and Indian Oceans was first identified by Walker and Bliss (1932). However, there were also strong positive anomalies in the Indian Ocean region at the peak of the weak 1978 cold event. The Indian Ocean has been shown in the past to have strong links with Pacific warm and cold events (Normand, 1953; Webster and Yang, 1992). The results from this study confirm this link.

Strong meridional contrasts, as described by Mo and White (1985), occurred for each of the individual warm and cold events (Section 5.3). However, the geographical location of these contrasts and sign of the anomalies varies from event to event. For the cold events these anomalies were negative, positive, negative around the 90°E meridian for the 1975 event, positive, negative, positive around the 0° meridian, spanning 90° in each direction for the 1978 event, and positive, negative, positive along the 180° meridian for the 1988 event. For the warm events the contrast in anomalies was negative, positive, negative in the Pacific region for the 1976 event, positive, negative, positive along the 180° meridian for the 1982 event, negative, positive, negative along the 180 and 260° meridians for the 1986 event and positive, negative, positive in the Pacific region for the 1991 event. As in the cold events there is a large inter-event variation in the positioning of the meridional contrasts. The meridional contrasts, apparent in all of the events, are a barotropic pattern suggestive of the strengthening and weakening of zonal winds in alternating latitudinal belts (Rogers and van Loon, 1982).

6.5 Patterns in the phase and amplitude of the first harmonic of climate anomalies

As for the previous analyses the harmonic analysis (Section 5.4) revealed a great deal of inter-cold (La Niña) and inter-warm (El Niño) event variability in the propagation, the teleconnectivity and phase of the largest anomalies. The extent of this inter-cold and warm

event variability is apparent from the composites, as some of the greatest signals identified within the individual events were lost (Figures 5.32 and 5.42). In previous studies harmonic analysis has been carried out for selected low and midlatitude locations. However, it has not been applied to the investigation of ENSO across the entire Southern Hemisphere, or for Antarctica, in terms of propagation and teleconnections. Cluster analysis, which has proved a very useful tool in the regionalisation of the harmonics, has not previously been used in association with harmonic analysis. In this study it has proved invaluable not only for identifying teleconnections but for revealing the zonal nature of height anomalies.

The 1975 and 1988 cold events consistently showed that there were strong harmonic amplitudes across the low latitudes, 6 months prior to the peak (Figures 5.26 and 5.30), whilst the 1978 event lacked this signal (Figure 5.28). These strong amplitudes indicate that there is a well developed 2 year cycle in the sign of the anomalies, as identified for the Indian and Pacific sectors by Kiladis and van Loon (1988). Three of the warm events show the inverse of the low latitude phase pattern found in the cold events. The 1976, 1982 and 1986 warm events all had strong harmonic amplitudes extending through the low latitudes following the events peaks (Figures 5.34, 5.36 and 5.38), however, with strong inter-event variability the timing of the anomalies varies from just after to six months after the event peak. These strong low latitude warm event harmonics are due to the southward displacement of the near-equatorial trough following the event peak (Aceituno, 1988).

For all three cold events there seems to be a northward movement of anomalies from eastern Antarctica 4 months prior to the peak. These propagate towards the midlatitudes over a period of 10 months for the 1975 and 1988 cold events, however, during the 1978 cold event these reached 50°S after only 4 months. In the 1976 and 1982 warm events, although there is a big difference in the phase of the anomalies in this region, agreeing with the findings of Karoly (1989), there is a movement of anomalies towards the east Antarctic over a period of 9 months. The 1991 warm event is anomalous in this respect as the anomalies in the east Antarctic appeared to propagate away from the continent in a north eastward direction, which is the same signal as was found for the cold events described above. The anomalous behaviour of this event can be explained with reference to the work of Cullather et al. (1996) who have found that in the east Antarctic region, the intensity of the atmospheric circulation

decreased from 1991, with the onset of a blocking pattern. It was found by Kidson and Sinclair (1995) that the reversal in the sign of the anomalies over the Antarctic continent is associated with a split between single and double jet regimes, and a meridional displacement of the peak poleward momentum flux, which assists in maintaining the polar jet, explaining the high harmonic amplitudes in this region. The 1975, 1978 and 1988 cold events seem to show very clear teleconnections in the clusters between the low latitude eastern Pacific and east Antarctica (Figures 5.27, 5.29 and 5.31). However, the size of the regions involved in this teleconnectivity varies between events. This pattern is also apparent in the 1976, 1982 and 1986 warm events (Figures 5.35, 5.37 and 5.39), with the exception of the 1991 warm event (Figure 5.41), which has a different distribution of harmonic regions.

The 1988 cold event alone experiences the movement of positive anomalies southward from 55°S to the west of the Antarctic Peninsula 4 months prior to the peak. For the warm events, in the region of the Antarctic Peninsula, there appear to be several different patterns. For the 1976 warm event, anomalies moved south-eastward from about 35°S towards the Peninsula, over about 7 months, arriving at the time of the event peak. This pattern also occurs for the 1991 warm event and is very similar to that found for the 1988 cold event. For the 1982 warm event, east of the Peninsula, anomalies appear to migrate northward to 60°S over six months, however to the west, anomalies migrate south from 60°S over a two month period. For the 1986 event there appears to be a north-eastward movement of anomalies to around 65°S in the Peninsula region. A similar northward movement of anomalies was identified from the Hovmöller diagrams. Such northwardly propagating signals may provide the support for forcing the circumpolar current and subsequent equatorward sea surface temperature propagation via the Humbolt Current (Pittock, 1984).

All three of the cold events in this study show the Amazon Basin as having an impact on the intensification of eastward moving anomalies. The Amazon Basin tends to have a differing effect on the warm events. For the 1976 event the anomalies appear to be intensified and propagated westward, and to a lesser extent for the 1991 event (Figure 5.40), whilst for the 1982 event eastward propagation occurs. However, for the 1986 event no intensification appears to have taken place. The anomalous westward propagation of anomalies in the low latitudes has been explained by Anyamba and Weare (1995), in relation to the 40-50 day

oscillation in tropical convection in the Indian and western Pacific Oceans (Section 2.8). In a similar manner to this the Amazon Basin may have been acting as an apparent heat source exciting the westward propagating Rossby waves and thus intensifying the low latitude anomalies.

In the 1976 and 1991 warm events, as in the 1975 cold event, there were interesting patterns in the region around Australia. This pattern also appears in the 1988 event in southern South America. For these events and regions there were clockwise movements in the pattern of anomalies, over approximately 12 months. In the case of Australia the pattern follows the landmass. One explanation for this pattern in the Australian region, as explained by Kiladis and van Loon (1988), is that there appears to be a reversal in the sign of sea level pressure anomalies occurring between Australia and the South Pacific between year -1 and year 0 of both warm and cold events. This reversal was found to modulate the strength of the meridional wind from the New Zealand region north to about 10°S (van Loon, 1984, van Loon and Shea, 1987). This seesaw in sea level pressure anomalies, and consequently height anomalies, between Australia and the South Pacific identified in the phase of the first harmonic gives the appearance of a 12 month propagation around the landmass.

The cold composite picks up some of the patterns found for the individual events (Figure 5.32), such as the strong anomalies in the low latitudes for the 1975 and 1988 events, as well as the east Antarctic anomalies moving northwards prior to the peak. The warm composite shows some of the features identified for the individual events, such as the strong amplitudes in the low latitudes, however, most of the other features have been lost in this composite (Figure 5.42).

The zonal nature of the harmonic regions is apparent from the clusters. It can be seen in all the events that the low and high latitudes appear to have clusters with similar properties, whilst the midlatitudes have regions with average phases 12 months earlier or later. As the harmonic analysis is based on a two year series it can be said that the 12 month lead or lag of the midlatitudes is indicative of negative harmonics in these regions coinciding with the positive harmonics of the low and high latitudes. This zonal positive, negative, positive pattern, which was also found from the Hovmöller diagrams, resembles the well-known PNA pattern for the North Pacific (Horel and Wallace, 1981), although it is weaker than its northern

hemisphere counterpart (Karoly, 1989). The PNA pattern was found to be an atmospheric 'wave-train' linking North American climate patterns to both ENSO and other fluctuations in the equatorial Pacific (Allen et al., 1996). The Southern Hemisphere pattern, known as the PSA, identified by Karoly (1989) and Mo and White (1985) may be associated with the eastward advance of a mid-ocean longwave trough and/or the behaviour of the double jet oscillation (Cullather et al., 1996). The double jet oscillation may provide a mechanism for the propagation of warm and cold event climate signals between tropical-subtropical and high southern latitudes. The transition regions, with small amplitudes, occur in the areas through which the jetstreams tend to migrate.

The harmonic analysis has shown that there are very clear teleconnections between the tropical eastern Pacific and east Antarctica for all events considered, with the exception of the 1991 warm event. The zonal contrasts identified in the Hovmöller diagrams and spatial anomaly plots have been clarified through the use of the cluster analysis of harmonics and the PSA pattern identified. It has also been shown that anomalies appear to be propagated both to and from regions with strong anomalies, although the direction and timing of this propagation varies greatly between events. However, for the east Antarctic region it has been shown that for the cold events the anomalies appear to be propagated northward away from the continent, whilst for the 1976 and 1982 warm events these anomalies appear to be propagated southward towards the continent. The 1986 and 1991 warm events are anomalous in this respect as the 1986 event appears to have no wavetrains of anomalies propagating either towards or away from the continent, whilst the 1991 event appears to show northward propagation, like the cold events.

6.6 Zonally averaged Hovmöller charts

The zonally averaged Hovmöller charts (Section 5.5) have aided in the identification of the variation in the height and windspeed over the 60° longitude sector from 120 to 180°W. Zonally averaged values were plotted for each 60° sector (not shown in this study), and it was found that the region from 120 to 180°W was the only region where marked ENSO related signals appeared. A zonally averaged Hovmöller chart for windspeed was previously constructed by Chen et al. (1996) to look for variations in the strength of the jetstreams, but this was not used in conjunction with similar diagrams for height and height anomalies. In the

'ENSO sensitive' 120 to 180°W sector, it was found that there were decreases (increases) in heights in the low latitudes and increases (decreases) in heights at high latitudes indicative of the weakening (deepening) of the circumpolar trough during warm (cold) events (Figure 5.44), i.e. in the mid- to high latitudes the height contours extended southward during cold events, retreating northward during warm events. This is indicative of the southward shift of the pressure belts during cold events. This is confirmed by the zonally averaged height anomalies in which there were found to be negative (positive) anomalies in the region of the subtropical jetstream during warm (cold) events (Figure 5.45). Over the high latitudes there were found to be positive height anomalies during the 1982, 1986 and 1991 warm events, however, a cold event reversal was not apparent. The Hovmöller diagrams (Section 5.2), harmonic plots (Section 5.4) and zonally averaged height plots (Figures 5.44 and 5.45) revealed that the latitudes of the jetstreams are important in the strength and position of ENSO related Southern Hemisphere climate anomalies. The relevance of the anomalies in these regions was made apparent by the analysis of the 500 hPa geostrophic wind, from which it was possible to identify alterations in the position and intensity of the jetstreams. These revealed that during warm (cold) events there were decreases (increases) in the intensity of the polar jet and increases (decreases) in the intensity of the subtropical jet (Figures 5.46 and 5.47).

6.7 Propagation Mechanisms

The findings of the zonally averaged Hovmöller charts lead to the same conclusions as made by Chen et al. (1996), that variations in the spilt jet in the Pacific sector appear to be the main cause of the poleward propagation of the ENSO signal via the SPCZ. However, Chen et al. (1996) showed that this mechanism operated for the transition between one warm and cold event only. This study has demonstrated that this mechanism is in operation for all of the warm and cold events from 1973 to 1994. The SPCZ is affected by the ENSO induced alteration in the midlatitude trade winds (Trenberth, 1991). When the SPCZ is strong during warm events, the subtropical jet is also strong, and the polar front jet is weak, whilst during cold events both the southward shifted SPCZ and the subtropical jets are weak whilst the polar front jet is strong (Chen et al., 1996). It has been shown that during cold events there is a southward shift in the SPCZ (Jones and Simmonds, 1994) as well as the main pressure belts,

as revealed by the zonally averaged Hovmöller charts, corresponding to the reduction in the strength of the subtropical jet and an increase in the strength of the polar front jet. Such a trend leads to the increase in cyclones steered inland in the high latitudes and a reduction in pressure over Antarctica. The position of the double jet influences the tracks of cyclones and anticyclones in the Antarctic region (Sinclair, 1996); i.e. during a warm (cold) event with a decrease (increase) in the strength of the polar jet there is a decrease (increase) in poleward cyclonic activity. Two main sources have been suggested for the increased poleward cyclonic activity during cold events: the storm track from south of Australia (Streten and Troup, 1973) and storms of subtropical origin leaving the south-westwardly displaced SPCZ (Vincent, 1985). During a cold event the strengthening of the polar front jet leads to a deepening of the circumpolar trough and an increase in westerlies (Trenberth, 1984a), as was found in this study from the analysis of Halley upper air data, resulting in an increase in cyclones being steered inland. Thus during warm (cold) events an increase (decrease) in the strength of the SPCZ leads to an increase (decrease) in the strength of the subtropical jet and a decrease (increase) in the strength of the polar jet resulting in the northward (southward) shift of the main pressure belts causing increases (decreases) in Antarctic pressure, confirming the findings from the analysis of the Antarctic climate (see Figure 7.1). However, this study has shown, both in the Hovmöller diagrams and harmonic analyses, that the origin of the propagation mechanisms is not restricted to the tropical Pacific and that anomalies are propagated across the entire Southern Hemisphere, both prior to and following event peaks. It has been shown in this study that Antarctic climate is not passive and solely affected by ENSO, but active especially as ENSO related anomalies have been found to exist on the continent prior to anomalies in the tropical Pacific. Antarctic climate features such as katabatic drainage (James, 1988), as well as the effect of the Amundsen Sea low (Chen et al., 1996) have been suggested to be strong enough to maintain the polar front jet as well as the New Zealand blocking high. Also the northward movement of anomalies from the high southern latitudes, which have been found in this study, are thought to play a role in the forcing of the circumpolar current. In turn they may play a role in the forcing of the tropical Pacific warm and cold events through equatorward sea surface temperature propagation via the Humbolt current (Pittock, 1984).

This study has shown that the propagation of anomalies does not solely occur from the tropics, but that anomalies propagate into the tropics from the extratropics. Propagating anomalies with an extratropical origin are likely to play a role in the evolution of ENSO. If this is so then theories on the evolution of ENSO, such as the modelled 'delayed oscillator' theory (Schopf and Suarez, 1988) (Section 2.8) in which the mechanisms behind the system are contained within the tropical Pacific (Zebiak and Cane, 1987), appear to be oversimplified. This study has shown that the warm and cold events of the tropical Pacific are not solely part of an isolated system with outputs to the global climate system, but that the global climate is a complex interacting system, with global exchanges of anomalies. Moreover, the Antarctic, which is at the focus of this study, does not play an entirely passive role in any ENSO-Antarctic relationship, but an active one as well.

CHAPTER 7

CONCLUSIONS

7.1 Introduction

This chapter summarises the major findings of this study, based on the objectives, into the effects of ENSO on Antarctic climate variability and the teleconnections by which the ENSO signal reaches the high southern latitudes (Section 7.2). The overall conclusions to the study are presented with a schematic model describing the major teleconnections and mechanisms behind the ENSO-Antarctic climate link (Section 7.3). Finally suggestions for further research are offered which may reveal a more in-depth insight into the mechanisms behind the teleconnections (Section 7.4).

7.2 Meeting the objectives

The analyses and results detailed in the preceding chapters have focused on five main objectives (Section 1.2). This section summarises the major findings according to each of these objectives.

7.2.1 To explore further the effect of ENSO on the climate variability of Antarctica, with special reference to the Antarctic Peninsula.

The most important observation made in the study of the impact of ENSO is that the response of the Antarctic climate varies across the period studied. Analyses of the relationship between several climate variables and the SOI for a number of stations has clearly revealed this variation. Comparison of the methodology used by Smith and Stearns (1993) and that used in this study revealed that the differing results between the two studies were not a product of contrasting methodologies used but of variation in the time periods considered. This indicates clearly that ENSO-Antarctic climate relationships are not stable over long (multi-decadal) time periods.

Antarctic station pressure has the most consistent response to ENSO. For all the stations considered in this study, with the exception of Casey, pressure increased (decreased) over Antarctica with warm (cold) events. From the cross correlation analysis results it appears that the response of the Antarctic pressure to ENSO is strongest at lags of 3 to 4 months. The observed pressure increases during warm events agrees with the findings of previous studies (van Loon and Madden, 1981; van Loon and Shea, 1987; Karoly, 1989) and are confirmed by the analysis of Halley geopotential height at the 850 and 500 hPa levels; during warm (cold) events there is an increase (decrease) in geopotential height.

The response of other climate variables to ENSO was not as clear as for pressure. The relationship between station temperature and the SOI varied across the continent. However, results suggest that at the peak of warm (cold) events there are temperature increases (decreases) at Halley, Amundsen-Scott, McMurdo, Mirnyy, SANAE and Vostok, whilst Faraday and Mawson experience decreases (increases) in temperature. Station cloud cover and windspeed were also considered for Halley and Faraday. Based on the findings for these stations it appears that during warm (cold) events there are decreases (increases) in cloud cover at Faraday linked to decreases (increases) in cyclonicity. For Halley no apparent relationship appears to exist. With regards to windspeed there are increases (decreases) at Halley and Faraday prior to warm (cold) event peaks, and decreases (increases) at Faraday following the event peaks. The variation in the relationship between station temperature, windspeed and cloud cover across the continent can be explained by other factors such as proximity to the coast, topography etc.

Analysis of upper air data at Halley revealed that during warm (cold) events there were increases (decreases) in geopotential height, increases (decreases) in relative humidity, increases (decreases) in temperature, decreases (increases) in windspeed, and increases in north-easterly (south-westerly) winds consistent with increases (decreases) in pressure across the continent.

7.2.2 To assess whether there is a propagation of anomalies between the low and high latitudes along an ENSO sensitive meridian.

Study results have not revealed an unequivocally clear picture in terms of wavetrain patterns along this ENSO sensitive meridian (230° longitude). However, the most important finding is the high degree of inter-warm and inter-cold event variability of wavetrain patterns, thus composite Hovmöller diagrams do not capture the complex dynamics typical of the events considered in this study. Despite the inter-event variability of wavetrain patterns there is some commonality of patterns for warm and cold events and for a true warm-cold antiphase of wavetrain anomalies. For cold events which are followed by the onset of a warm event (1978, 1988) there is a propagation of negative height and temperature anomalies from subtropical to high latitudes preceding the event peak, which persist in subpolar latitudes for around a year following the event peak. At polar latitudes during cold events there is a transition from positive anomalies at the time of the event peak to negative anomalies following the peak.

7.2.3 To identify the possible movement of sea level pressure anomalies in the Southern Hemisphere on a spatial scale, during both ENSO and non-ENSO events.

The most significant finding from the spatial anomaly plots is the strong meridional contrast in the sign of the anomalies between high, mid- and low latitudes. These meridional contrasts were detected by the Hovmöller analyses (Section 5.2) and are thought to be associated with oscillations in the double jet and the PSA pattern. Although strong meridional contrasts occurred for each of the individual events, the positioning of the contrasts varied from event to event.

Negative pressure anomalies across the Antarctic continent were only apparent for the 1975 cold event, with positive anomalies occurring at the peaks of the 1978 and 1988 cold events, although negative anomalies developed 6 months after the 1978 event peak. Positive anomalies were present at the peaks of the 1982 and 1991 warm events, with limited positive anomalies also present in the 1976 warm events, developing into strong anomalies after the peak. In contrast there were negative anomalies in the subpolar regions at the peak of the 1986 warm event.

The most important finding of the spatial analysis is the strong inter-event differences in the pattern and movement of ENSO related anomalies across the Southern Hemisphere. The spatial anomaly charts identified the ENSO signal in the sea level pressure anomalies in the Pacific region for each of the warm and cold events, with the exception of the weak 1978 cold event. In the tropical latitudes of the Indian Ocean there were strong negative anomalies for the 1975 and 1988 cold events contrasting with the strong positive anomalies in this region for the 1982, 1986 and 1991 warm events, however, there were also strong positive anomalies in this region at the peak of the weak 1978 cold event.

7.2.4 To uncover any spatial signals in the phases of the first harmonics of 500 hPa height, temperature and mixing ratio anomalies, and from the height anomalies identify teleconnections in the Southern Hemisphere.

Similar to the Hovmöller and spatial plot analyses, harmonic analysis has revealed a great deal of inter-cold and inter-warm event variability in the propagation of anomalies as well as in the phase and teleconnectivity of the largest anomalies. The extent of this variability is clear from the composites where some of the greatest signals identified within individual events are lost.

The 1975 and 1988 cold events as well as the 1976, 1982 and 1986 warm events all display strong harmonic amplitudes in the low latitudes at around the time of the event peaks, as identified in the spatial anomaly plots. The strength of these anomalies is indicative of the biennial tendency of the ENSO related anomalies in this region.

In the east Antarctic region it was found that for all cold events (Section 5.4.1) the anomalies appear to propagate northward away from the continent, whilst for the 1976 and 1982 warm events these anomalies appear to be propagated southward towards the continent. The 1986 and 1991 warm events are anomalous in this respect as the 1986 event appears to have no wavetrains of anomalies propagating either towards or away from the continent, whilst the 1991 event appears to show northward propagation, like the cold events. This northward propagation of anomalies from Antarctica shows that the continent is an active as well as a passive component of the Southern Hemisphere climate system. From the cluster analysis performed on the phase and amplitudes of the first harmonic it has been identified that there

were very clear teleconnections between the tropical east Pacific and east Antarctica for all events considered, with the exception of the 1991 warm event.

For the 1988 cold event the was a movement of anomalies southward, from 55°S, in the region west of the Antarctic Peninsula. For the warm events there appear to be several different patterns. Anomalies move southward from 35°S to the Peninsula during the 1976 and 1991 warm events. Anomalies propagate northward from the Peninsula to 60°S during the 1982 event and north-eastward to 65°S during the 1986 warm event.

The cluster analysis revealed that the low and high latitude clusters appeared to have similar properties contrasting with the midlatitudes, which tended to have clusters with average phases 12 months earlier or later. This meridional contrast, identified in earlier sections, resembles the PNA pattern for the North Pacific and is thought to be associated with the behaviour of the double jet oscillation (Cullather et al., 1996).

7.2.5 To consider the role of the jetstreams in the propagation of the ENSO signal between the tropics and high latitudes of the Southern Hemisphere.

Investigation into the role of the jetstreams in the response of the Antarctic climate has revealed that during warm (cold) events there is a decrease (increase) in the strength of the polar jet and an increase (decrease) in the intensity of the subtropical jet. The decrease (increase) in the strength of the polar jet is tied to increases (decreases) in heights in the subpolar regions, whilst an increase (decrease) in the strength of the subtropical jet led to decreases (increases) in heights in the tropics. The variations in position and intensity of this double jet influences the tracks of cyclones and anticyclones into the Antarctic region (Sinclair, 1996) through alterations in the circumpolar trough. Therefore with a decrease (increase) in the strength of the polar jet during a warm (cold) event there is a weakening (strengthening) of the circumpolar trough with a decrease (increase) in poleward moving cyclonicity. This ties in with the observations made regarding the Antarctic climate, with increases (decreases) in pressure during warm (cold) events.

7.3 General conclusions

The fact that clear unequivocal wavetrain patterns of climate anomalies linking tropical-subtropical with high southern latitudes do not exist attests to the complexity of tropical extratropical teleconnections in the South Pacific sector and the difficulty of identifying a single indisputable propagation mechanism for ENSO signals. Furthermore, from the evidence presented here, it is clear that the possibility exists for wavetrains to not only propagate poleward, but also equatorward from high Southern latitudes adding to the speculation that the Antarctic continent may be both an active as well as a passive component of a larger interactive Pacific Basin climate system that spans a large geographical range. Because clear wavetrain pattern do not exist from one cold or warm event to another, the possibility also exists that a ENSO related system threshold may be at play, whereby the distinctiveness and nature, or even the existence of any wavetrain pattern, may be closely related to the timing as well as the intensity of the associated ENSO event.

The schematic model presented in Figure 7.1, describing the major low to high latitude Southern Hemisphere climate links during Pacific Ocean warm (cold) events, draws together the results from each of the objectives in identifying the low to high latitude ENSO teleconnections. This model demonstrates the ultimate goal of this research in identifying the teleconnection mechanisms that underlie the ENSO-Antarctic links. The model identifies the important features involved in the low-high latitude teleconnections, which have been identified in this study, from the meridional contrasts, which form the PSA pattern, to the role of the jetstreams and the significance of the Amundsen Sea low. Also demonstrated in Figure 7.1 are the possible mechanisms by which the high latitude climate affects the lower latitudes, as an explanation for the northward moving wavetrains of anomalies identified in the Hovmöller and harmonic analyses, such as the role of the katabatic winds, the Amundsen Sea low and alterations in the sea-ice distribution.

7.4 Suggestions for further work

This section makes recommendations for further research into the mechanisms behind the transfer of the ENSO signal between the low and high latitudes.

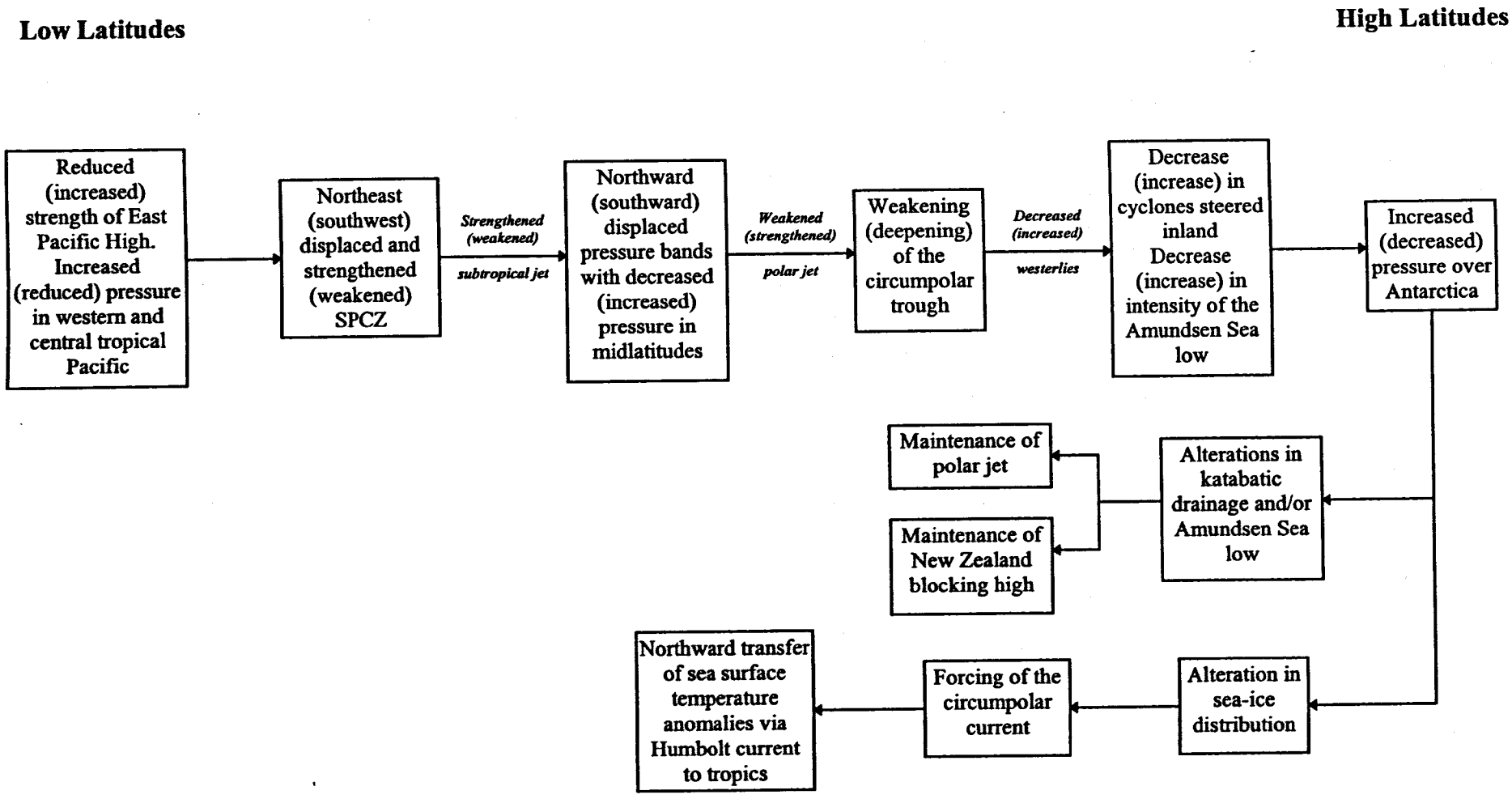

Figure 7.1 A schematic model describing the major teleconnections between the low and high latitudes of the Southern Hemisphere found in this study during warm (cold) events and the mechanisms underlying these teleconnections (in italics).

This study has looked at the role of the atmosphere in isolation, however as ENSO is an interacting ocean-atmosphere system, consideration of the role played by sea surface temperatures may give a greater insight into the role of the ocean in the propagation of the ENSO signal between the tropics and the high Southern latitudes.

With further work it may be possible to determine whether an ENSO related system threshold occurs whereby the timing and intensity of the events are responsible for the extratropical teleconnections. It was found in this study that different events affected the high latitudes in different ways thus by identifying the thresholds at which teleconnections operate it may be possible to forecast the effects of ENSO on the variability of the Antarctic climate.

This study has concentrated on the mechanisms by which the ENSO signal reaches the Antarctic, further work is needed to look at the exact mechanisms behind the northward propagation of anomalies from the Antarctic continent, found from the Hovmöller and harmonic analyses, to determine the role of Antarctica as an active as well as a passive component of a larger interactive Pacific Basin climate system.

REFERENCES

Aceituno, P. 1988. On the functioning of the Southern Oscillation in the South American sector. Part I: Surface climate, *Monthly Weather Review*, **116**, 505-524.

Allan, R. J., Nicholls, N., Jones, P. D. and Butterworth, I. J. 1991. A further extension of the Tahiti - Darwin SOI, early ENSO events and Darwin pressure, *Journal of Climate*, **4**, 743-749.

Allan, R., Lindesay, J., and Parker, D. 1996. *El Niño Southern Oscillation and Climate Variability*, CSIRO, Australia, pp 405.

Anyamba, E. K. and Weare, B. C. 1995. Temporal variability of the 40-50 day oscillation in tropical convection, *International Journal of Climatology*, **15**, 379-402.

Arabie, P. and Hubert, L. J. 1996. An overview of combinatorial data analysis, In: Arabie, P. Hubert, L.J. and De Soete, G. (eds.) *Clustering and Classification*, World Scientific Singapore, 5-63.

Astapenko, P. D. 1964. *Atmospheric Processes in the High Latitudes of the Southern Hemisphere*, Section II of IGY Program (Meteorology) No. 3, Jerusalem, pp286.

Balling, R. C. 1984. Classification in Climatology. In Gaile, G. L. and Willmott, C. J. (eds.) *Spatial Statistics and Models*, Reidel, 81-108.

Barnett, T. P. 1985. Variations in near global sea level pressure, *Journal of the Atmospheric Sciences*, **42**, 478-501.

Barnett, T. P. 1988. Variations in near global sea level pressure: Another view, *Journal of Climate*, **1**, 225-230.

Barnett, T. P., Dümenil, L., Schlese, U., Roeckner, E., Latif, M. 1991. The Asian snow cover-monsoon connection. In: Glantz, M. H., Katz, R. W., Nicholls, N. (eds.) *Teleconnections linking worldwide climate anomalies, Cambridge University Press, Cambridge*, 191-225.

Barry, R. G. and Chorley, R. J. 1987. *Atmosphere, Weather and Climate*, Routeledge, London, pp460.

Bigg, G. R. 1990. El Niño and the Southern Oscillation, *Weather*, **45**, 2-8.

Bjerknes, J. 1966. A possible response of the atmospheric Hadley Circulation to equatorial anomalies of ocean temperature, *Tellus*, **18**, 820-829.

Bjerknes, J. 1969. Atmospheric teleconnections from the equatorial Pacific, *Monthly Weather Review*, **97**, 163-172.

Bromwich, D. H., Carrasco, J. F., Liu, Z. and Tzeng, R. Y. 1993. Hemispheric atmospheric variations and oceanographic impacts associated with katabatic surges across the Ross Ice shelf, Antarctica, *Journal of Geophysical Research*, **98** (D7), 13045-13062.

Cane, M. A. 1983. Oceanographic events during El Niño, *Science*, **222**, 1189-1195.

Carleton, A. M. 1988. Sea ice-atmosphere signal of the Southern Oscillation in the Weddell Sea, Antarctica, *Journal of Climate*, **1**, 379-388.

Cattell, R. B. 1966. *Handbook of multivariate experimental psychology*, Rand McNally, Chicago, pp. 959.

Cavalieri, D. J. and Parkinson, C. L. 1981. Large-scale variations in observed Antarctic sea ice extent and associated atmospheric circulation, *Monthly Weather Review*, **109**, 2323-2335.

Chao, Y. and Philander, G. H. 1993. On the structure of the Southern Oscillation, *Journal of Climate*, **6**, 450-469.

Chen, B., Smith, S. R. and Bromwich, D. H. 1996. Evolution of the tropospheric split jet over the South Pacific Ocean during the 1986-89 ENSO cycle, *Monthly Weather Review*, **124**, 1711-1731.

Chiew, F. H. S., Piechota, T. C., Dracup, J. A. and McMahon, T. A. 1998. El Niño / Southern Oscillation and Australian rainfall, streamflow and drought: Links and potential for forecasting, *Journal of Hydrology*, **204**, 138-149.

Chu, P. -S. 1995. Hawaii rainfall anomalies and El Niño, *Journal of Climate*, **8**, 1697-1703.

Cullather, R. I., Bromwich, D. H. and van Woert, M. L. 1996. Interannual variations in Antarctic precipitation related to El Niño - Southern Oscillation, *Journal of Geophysical Research*, **101** (D14), 19109-19118.

Daley, R. 1991. *Atmospheric Data Analysis*, Cambridge University Press, Cambridge pp 457.

Dalrymple, P. C. 1966. A physical climatology of the Antarctic Plateau, Studies in Antarctic Meteorology, *Antarctic Research Series vol. 9*, American Geophysical Union, 195-231.

Davis, J. C. 1986. *Statistics and data analysis in geology*, John Wiley and Sons, Chichester.

Deser, C. and Wallace, J. M. 1987. El Niño events and their relation to the Southern Oscillation: 1925-1986, *Journal of Geophysical Research*, **92** (C13), 14189-14196.

Diaz, H. F. and Markgraf, V. 1992. Introduction. In Diaz, H. F. and Markgraf, V. (eds.) *El Niño: Historical and paleoclimatic aspects of the Southern Oscillation*, Cambridge University Press, Cambridge, 1-4.

Enfield, D. B. and Cid, L. 1991. Low-frequency changes in El Niño-Southern Oscillation, *Journal of Climate*, **4**, 1137-1146.

Forecasters' Reference Book, 1993. Meteorological Office, Bracknell, pp191.

Fraedrich, K. and Müller, K. 1992. Climate anomalies in Europe associated with ENSO extremes, *International Journal of Climatology*, **12**, 25-31.

GARP 1975. The physical basis of climate and climate modelling, *GARP Publication Series No. 16*, WMO/ICSU, Geneva.

Glantz, M. H. 1996. *Currents of Change: El Niños impact on climate and society*. Cambridge University Press, Cambridge, 194 pp.

Gloersen, P. 1995. Modulation of hemispheric sea-ice cover by ENSO events, *Nature*, **373**, 503-506.

Gordon, A. D. 1996. Hierarchical Classification In: Arabie, P. Hubert, L.J. and De Soete, G. (eds.) *Clustering and Classification*, World Scientific, Singapore, 65-121.

Gordon, A. L. 1988. The Southern Ocean and global climate, *Oceanus*, **31**, 39-46.

Graham, N. E. and White, W. B. 1988. The El Niño cycle: a natural oscillator of the Pacific ocean-atmosphere system, *Science*, **240**, 1293-1302.

Gu, D. and Philander, S. G. H. 1995. Secular changes of annual and interannual variability in the tropics during the past century, *Journal of Climate*, **8**, 864-876.

Gu, D. and Philander, S. G. H. 1997. Interdecadal climate fluctuations that depend on exchanges between the tropics and the extratropics, *Science*, **275**, 805-807.

Hacket, E. C. and Hastenrath, S. 1986. Mechanisms of Java rainfall anomalies, *Monthly Weather Review*, **114**, 745-757.

Halpert, M. S. and Ropelewski, C. F. 1992. Surface temperature patterns associated with the Southern Oscillation, *Journal of Climate*, **5**, 577-593.

Hanna, E. 1996. The role of Antarctic sea ice in global climate change, *Progress in Physical Geography*, **20**, 371-401.

Harangozo, S. A. 1995. The impact of the semi-annual cycle on South Pacific sea ice extent in two contrasting years, *Preprints Fourth Conference on Polar Meteorology and Oceanography*, 162-166.

Harangozo, S. A. and Colwell, S. R. 1995. *B.A.S. Meteorological Database Users Guide*, The British Antarctic Survey.

Hastenrath, S. and Heller, L. 1977. Dynamics of climate hazards in Northeast Brazil, *Quarterly Journal of the Royal Meteorological Society*, **103**, 77-92.

Henderson-Sellers, A. and Robinson, P. J. 1986. *Contemporary Climatology*, Longman Scientific and Technical, London, pp439.

Horel, J. D. and Wallace, J. M. 1981. Atmospheric phenomena associated with the Southern Oscillation, *Monthly Weather Review*, **109**, 813-829.

Houseago, R. E., McGregor, G. R., King, J. C. and Harangozo, S. A. 1997. Searching for ENSO signals in Antarctica, *Preprints Fifth International Conference on Southern Hemisphere Meteorology and Oceanography*, 238-239.

Houseago, R. E., McGregor, G. R., King, J. C. and Harangozo, S. A. 1998. Climate anomaly wave-train patterns linking Southern low and high latitudes during South Pacific warm and cold events, *International Journal of Climatology*, **18**, 1181-1193.

Hovmöller, E. 1949. The trough and ridge diagram, *Tellus*, **1** (2), 62-66.

Inoue, M. and Bigg, G. R. 1995. Trends in wind and sea-level pressure in the Tropical Pacific Ocean for the period 1950-1979, *International Journal of Climatology*, **15**, 35-52.

James, I. N. 1988. On the forcing of planetary-scale Rossby waves by Antarctica, *Quarterly Journal of the Royal Meteorological Society*, **114**, 619-637.

Jones, D. A. and Simmonds, I. 1994. A climatology of Southern Hemisphere anticyclones, *Climate Dynamics*, **10**, 333-348.

Jones, P. D. and Limbert, D. W. S. 1987. A data bank of Antarctic surface temperature and pressure data, DOE/ER/60397-H2, *Distribution Category UC11*, U.S. Department of Commerce, Springfield, pp52.

Jordán, R. 1991. Impact of ENSO events on the southeastern Pacific region with special reference to the interaction of fishing and climate variability. In: Glantz, M. H., Katz, R. W., Nicholls, N. (eds.) *Teleconnections linking worldwide climate anomalies,* Cambridge University Press, Cambridge, 401-430.

Kalkstein, L. S., Dunne, P. C. and Vose, R. S. 1990. Detection of climate change in the Western North American Arctic using a synoptic climatological approach, *Journal of Climate*, **3**, 1153-1167.

Kalkstein, L. S., Tan, G. and Skindlov, J. A. 1987. An evaluation of three clustering procedures for use in synoptic climatological classification, *Journal of Climate and Applied Meteorology*, **26**, 717-730.

Karoly, D. J. 1989. Southern Hemisphere circulation features associated with El Niño - Southern Oscillation events, *Journal of Climate*, **2**, 1239-1252.

Karoly, D. J. and Oort, A. H. 1987. A comparison of Southern Hemisphere circulation statistics based on GFDL and Australian Analyses, *Monthly Weather Review*, **115**, 2033-2059.

Kawamura, A., McKerchar, A. I., Spigel, R. H. and Jinno, K 1998. Chaotic characteristics of the Southern Oscillation Index time series, *Journal of Hydrology*, **204**, 168-181.

Keen, R. A. 1982. The role of cross equatorial cyclone pairs in the Southern Oscillation, *Monthly Weather Review*, **110**, 1405-1416.

Kidson, J. W. 1975. Tropical eigenvector analysis and the Southern Oscillation, *Monthly Weather Review*, **103**, 187-196.

Kidson, J. W. 1991. Intraseasonal variations in the Southern Hemisphere circulation, *Journal of Climate*, **4**, 939-953.

Kidson, J. W. and Sinclair, M. R. 1995. The influence of persistent anomalies on Southern Hemisphere storm tracks, *Journal of Climate*, **8**, 1938-1950.

Kiladis, G. N. and Diaz, H. F. 1989. Global climatic anomalies associated with extremes in the Southern Oscillation, *Journal of Climate*, **2**, 1069-1090.

Kiladis, G. N. and van Loon, H. 1988. The Southern Oscillation. Part VII: Meteorological anomalies over the Indian and Pacific sectors associated with extremes of the oscillation, *Monthly Weather Review*, **116**, 120-136.

King, J. C. 1994. Recent climate variability in the vicinity of the Antarctic peninsula, *International Journal of Climatology*, **14**, 357-369.

King, J. C., Anderson, P. S., Smith, M. C. and Mobbs, S. D. 1996. The surface energy and mass balance at Halley, Antarctica during winter, *Journal of Geophysical Research*, **101** (D14), 19119-19128.

Klaßen, J., Hense, A. and Römer, U. 1994. Climate anomalies north of 55°N associated with tropical climates extremes, *International Journal of Climatology*, **14**, 829-842.

Kousky, V. E. and Kayano, M. T. 1994. Principal modes of outgoing longwave radiation and 250mb circulation for the South American sector, *Journal of Climate*, **7**, 1131-1143.

Kovach, W. L. 1995. Multivariate Data Analysis, In: Maddy, D. and Brew, J. S. (eds.) *Statistical Modelling of Quaternary Science Data*, QRA Tech Guide No 5, 1-38.

Kripalani, R. H. and Kulkarni, A. 1997. Rainfall variability over south-east Asia - connections with Indian monsoon and ENSO extremes: new perspectives, *International Journal of Climatology*, **17**, 1-14.

Krishnamurti , T. N., Chu, S. -H., Iglesias, W. 1986. On the sea level pressure of the Southern Oscillation, *Archiv. für Meteorologie Geophysik und Bioklimatologie Series A*, **34**, 385-425.

Kuhnel, I. 1998. The use of a multifactor Southern Oscillation Index for the estimation of annual hailstorm frequencies in the Sydney area, *International Journal of Climatology*, in press.

Lara, A. and Villalba, R. 1993. A 3620 year temperature record from Fitzroya cupressoides tree rings in Southern South America, *Science*, **260**, 1104-1106.

Latif, M. and Barnett, T. P. 1996. Decadal climate variability over the north Pacific and North America: Dynamics and Predictability, *Journal of Climate*, **9**, 2407-2423.

Latif, M., Kleeman, R. and Eckert, C. 1997. Greenhouse warming, decadal variability or El Niño? An attempt to understand the anomalous 1990's, *Journal of Climate*, **10**, 2221-2239.

Latif, M., Sterl, A., Maier-Reimer, E. and Junge, M. M. 1993. Structure and predictability of the El Niño / Southern Oscillation phenomenon in a coupled ocean - atmosphere general circulation model, *Journal of Climate*, **6**, 700-708.

Lau, K. -M. and Chan, P. H. 1985. Aspects of the 40-50 day oscillation during the northern winter as inferred from outgoing longwave radiation, *Monthly Weather Review*, **113**, 1889-1909.

Lau, K. -M. and Chan, P. H. 1988. Intraseasonal and interannual variations of tropical convection: A possible link between the 40-50 day oscillation and ENSO?, *Journal of the Atmospheric Sciences*, **45**, 506-521.

Le Marshall, J. F., Kelly, G. A. M. and Karoly, D. J. 1985. An atmospheric climatology of the Southern Hemisphere based on ten years of daily numerical analyses (1972-82): I Overview, *Australian Meteorological Magazine*, **33**, 65-85.

Li, T. 1997. Phase transition of the El Niño - Southern Oscillation: a stationary SST mode, *Journal of the Atmospheric Sciences*, **54**, 2872-2887.

Lindesay, J. A. 1988. South African rainfall, the Southern Oscillation and a Southern Hemisphere semi-annual cycle, *Journal of Climatology*, **8**, 17-30.

Lockyer, N. and Lockyer, W. J. S. 1902a. On some phenomena which suggest a short period of solar and meteorological changes, *Proceedings of the Royal Society London*, **70**, 500-504.

Lockyer, N. and Lockyer, W. J. S. 1902b. On the similarity of the short period pressure variation over large areas, *Proceedings of the Royal Society London*, **71**, 134-135.

McBride, J. L. and Nicholls, N. 1983. Seasonal relationships between Australian rainfall and the Southern Oscillation, *Monthly Weather Review*, **111**, 1998-2004.

McGregor, G. R., King, J. C. and Harangozo, S. 1997. Investigating climatic variability and climate change in the Antarctic Peninsula: a synoptic climatological approach, *Preprints Fifth International Conference on Southern Hemisphere Meteorology and Oceanography*, 39-40.

Meehl, G. A. 1987. The annual cycle and interannual variability in the tropical Pacific and Indian Ocean regions, *Monthly Weather Review*, **115**, 27-50.

Meehl, G. A. 1991. A re-examination of the mechanism of the semi-annual oscillation, *Journal of Climate*, **4**, 911-926.

Meehl, G. A., Branstator, G. W. and Washington, W. M. 1993. Tropical Pacific interannual variability and CO_2 climate change, *Journal of Climate*, **6**, 42-63.

Minetti, J. L. and Sierra, E. M. 1989. The influence of general circulation patterns on humid and dry years in the Cuyo Andean region of Argentina, *International Journal of Climatology*, **9**, 55-68.

Mitchell, T. P. and Wallace, J. M. 1996. ENSO seasonality: 1950-1978 versus 1979-92, *Journal of Climate*, **9**, 3149-3161.

Mo, K. C. and White, G. H. 1985. Teleconnections in the Southern Hemisphere, *Monthly Weather Review*, **113**, 22-37.

Neale, A. A. and Trenberth, K. E. 1978. Hovmöller diagrams. Part I: Introduction, *New Zealand Meteorological Service Technical Information Circular*, **161**, 1-4.

Nicholls, N. 1984. The Southern Oscillation and Indonesian sea surface temperature, *Monthly Weather Review*, **112**, 424-432.

Nicholls, N. 1991. Teleconnections and health. In: Glantz, M. H., Katz, R. W., Nicholls, N. (eds.) *Teleconnections linking worldwide climate anomalies, Cambridge University Press, Cambridge*, 493-510.

Nicholls, N. and Kariko, A. 1993. East Australian rainfall events: interannual variations, trends and relationships with the Southern Oscillation, *Journal of Climate*, **6**, 1141-1152.

Nicholson, S. E. and Kim, J. 1997. The relationship of the El Niño - Southern Oscillation to African rainfall, *International Journal of Climatology*, **17**, 117-135.

Nigam, S. 1994. On the dynamical basis for the Asian summer monsoon rainfall - El Niño relationship, *Journal of Climate*, **7**, 1750-1771.

Normand, C. 1953. Monsoonal seasonal forecasting, *Quarterly Journal of the Royal Meteorological Society*, **79**, 463-473.

Oliver, J. E. 1981. *Climatology: Selected Applications*, Arnold, London, pp260.

Oort, A. H. and Yienger, J. J. 1996. Observed interannual variability in the Hadley circulation and its connections to ENSO, *Journal of Climate*, **9**, 2751-2767.

Philander, S. G. 1990. *El Niño, La Niña, and the Southern Oscillation*, Academic Press, London, pp293.

Philander, S. G. H. 1983. El Niño Southern Oscillation phenomena, *Nature*, **302**, 295-301.

Philander, S. G. H. 1985. El Niño and La Niña, *Journal of the Atmospheric Sciences*, **42**, 2652-2662.

Philander, S. G. H. and Rasmusson, E. M. 1985. The Southern Oscillation and El Niño, *Advances in Geophysics*, **28** (A), 197-215.

Pickard, G. L. and Emery, W. J. 1990. *Descriptive Physical Oceanography: an Introduction*, Pergamon Press, Oxford, pp320.

Pisciottano, A., Diaz, A., Cazes, G. and Mechoso, C. R. 1994. El Niño - Southern Oscillation impact on rainfall in Uruguay, *Journal of Climate*, **7**, 1286-1302.

Pittock, A. B. 1984. On the reality, stability and usefulness of Southern Hemisphere teleconnections, *Australian Meteorological Magazine*, **32**, 75-82.

Priddle, J., Croxall, J. P., Everson, I., Heywood, R. B., Murphy, E. J., Prince, P. A., and Sear, C. B. 1988. Large-scale fluctuations in distribution and abundance of krill - a discussion of possible causes, In: Dietrich, S. (ed.) *Antarctic Ocean and resources variability*, Springer-Verlag, New York, 169-182.

Quinn, W. H., Neal, V. T. and De Mayolo, S. E. A. 1987. El Niño occurrences over the past four and a half centuries, *Journal of Geophysical Research*, **92** (C13), 14449-14461.

Ramage, C. S. 1983. Teleconnections and the siege of time, *Journal of Climatology*, **3**, 223-231.

Ramage, C. S. and Hori, A. M. 1981. Meteorological aspects of El Niño, *Monthly Weather Review*, **109**, 1827-1835.

Rasmusson, E. M. and Carpenter, T. H. 1982. Variations in tropical sea surface temperature and surface wind fields associated with the Southern Oscillation / El Niño, *Monthly Weather Review*, **110**, 354-384.

Rasmusson, E. M. and Wallace, J. M. 1983. Meteorological aspects of the El Niño / Southern Oscillation, *Science*, **222**, 1195-1202.

Rogers, J. C. 1983. Spatial variability of Antarctic temperature anomalies and their association with the Southern Hemisphere atmospheric circulation, *Annals of the Association of American Geographers*, **73**, 502-518.

Rogers, J. C. and van Loon, H. 1982. Spatial variability of sea level pressure and 500 hPa height anomalies over the Southern Hemisphere, *Monthly Weather Review*, **110**, 1375-1392.

Ropelewski, C. F. and Halpert, M. S. 1987a. Global and regional scale precipitation patterns associated with the El Niño - Southern Oscillation, *Monthly Weather Review*, **115**, 1606-1626.

Ropelewski, C. F. and Halpert, M. S. 1987b. Precipitation patterns associated with the high index phase of the Southern Oscillation, *Journal of Climate*, **2**, 268-284.

Ropelewski, C. F. and Jones, P. D. 1987. An extension of the Tahiti-Darwin Southern Oscillation Index, *Monthly Weather Review*, **115**, 2161-2165.

Rutllant, J. and Fuenzalida, H. 1991. Synoptic aspects of the central Chile rainfall variability associated with the Southern Oscillation, *International Journal of Climatology*, **11**, 63-76.

Schopf, P. S. and Suarez, M. J. 1988. Vacillations in a coupled ocean-atmosphere model, *Journal of the Atmospheric Sciences*, **45**, 549-566.

Simmonds, I. and Jacka, T. H. 1995. Relationships between the interannual variability of the Antarctic sea ice and the Southern Oscillation, *Journal of Climate*, **8**, 637-647.

Sinclair, M. R. 1996. A climatology of anticyclones and blocking for the Southern Hemisphere, *Monthly Weather Review*, **124**, 245-263.

Smith, S. R. and Stearns, C. R. 1993. Antarctic pressure and temperature anomalies surrounding the minimum in the Southern Oscillation Index, *Journal of Geophysical Research*, **98** (D7), 13071-13083.

Streten, N. A. 1975. Satellite derived inferences to some characteristics of the South Pacific atmospheric circulation associated with the Niño event of 1972-73, *Monthly Weather Review*, **103**, 989-995.

Streten, N. A. and Pike, D. J. 1980. Characteristics of the broadscale Antarctic sea ice extent and the associated atmospheric circulation 1972-1977, *Archiv. für Meteorologie Geophysik und Bioklimatologie Series A*, **29**, 279-299.

Streten, N. A. and Troup, A. J. 1973. A synoptic climatology of satellite observed cloud vortices over the Southern Hemisphere, *Quarterly Journal of the Royal Meteorological Society*, **99**, 56-72.

Sturman, A. P. 1976. *A synoptic climatology of Southern South America and the Antarctic Peninsula*, Unpublished PhD Thesis, University of Birmingham, UK. pp221.

Swanson, G. S. and Trenberth, K. E. 1981a. Trends in the Southern Hemisphere tropospheric circulation, *Monthly Weather Review*, **109**, 1879-1889.

Swanson, G. S. and Trenberth, K. E. 1981b. Interannual variability in the Southern Hemisphere troposphere, *Monthly Weather Review*, **109**, 1890-1897.

Taljaard, J. J. 1972. Physical features of the Southern Hemisphere, In: Newton, C. W. (ed.) *Meteorology of the Southern Hemisphere, Meteorological Monographs*, Vol. 13, American Met. Soc., 1-8.

Tett, S. 1995. Simulation of El Niño - Southern Oscillation - like variability in a global AOGCM and its response to CO_2 increase, *Journal of Climate*, **8**, 1473-1502.

Trenberth, K. E. 1976. Spatial and temporal variations of the Southern Oscillation, *Quarterly Journal of the Royal Meteorological Society*, **102**, 639-653.

Trenberth, K. E. 1978. Hovmöller diagrams. Part III, *New Zealand Meteorological Service Technical Information Circular*, **161**, 8-20.

Trenberth, K. E. 1979. Interannual variability of the 500mb zonal mean flow in the Southern Hemisphere, Monthly Weather Review, **107**, 1515-1524.

Trenberth, K. E. 1980. Planetary waves at 500mb in the Southern Hemisphere, *Monthly Weather Review*, **108**, 1378-1389.

Trenberth, K. E. 1984a. Interannual variability of the Southern Hemisphere circulation: representiveness of the Global Weather Experiment, *Monthly Weather Review*, **112**, 108-123.

Trenberth, K. E. 1984b. Signal versus noise in the Southern Oscillation, *Monthly Weather Review*, **112**, 326-332.

Trenberth, K. E. 1991. General characteristics of El Niño - Southern Oscillation. In: Glantz, M. H., Katz, R. W., Nicholls, N. (eds.) *Teleconnections linking worldwide climate anomalies,* Cambridge University Press, Cambridge, 13-42.

Trenberth, K. E. 1996. El Niño-Southern Oscillation, In: Henderson-Sellers, A. and Giambelluca, T. (eds.) *Climate change: developing Southern Hemisphere perspectives*, John Wiley and Sons Ltd., 145-173.

Trenberth, K. E. 1997a. Short term climate variations: recent accomplishments and issues for future progress, *Bulletin of the American Meteorological Society*, **78**, 1081-1096.

Trenberth, K. E. 1997b. The definition of El Niño, *Bulletin of the American Meteorological Society*, **78**, 2771-2777.

Trenberth, K. E. and Paolino, D. A. 1981. Characteristic patterns of variability of sea level pressure in the Northern Hemisphere, *Monthly Weather Review*, **109**, 1169-1189.

Trenberth, K. E. and Shea, D. J. 1987. On the evolution of the Southern Oscillation, *Monthly Weather Review*, **115**, 3078-3096.

Troup, A. J. 1965. The 'Southern Oscillation', *Quarterly Journal of the Royal Meteorological Society*, **91**, 490-506.

Turner, J., Marshall, G. J. and Lachlan-Cope, T. A. 1998. Analysis of synoptic-scale low pressure systems within the Antarctic Peninsula sector of the circumpolar trough, *International Journal of Climatology*, **18**, 253-280.

van Heerden, J., Terblanche, D. E. and Schulze, G. C. 1988. The Southern Oscillation and South African summer rainfall, *Journal of Climatology*, **8**, 577-597.

van Loon, H. 1972a. Pressure in the Southern Hemisphere, In: Newton, C. W. (ed.) *Meteorology of the Southern Hemisphere, Meteorological Monographs*, Vol. 13, American Met. Soc., 59-86.

van Loon, H. 1972b. Wind in the Southern Hemisphere, In: Newton, C. W. (ed.) *Meteorology of the Southern Hemisphere, Meteorological Monographs*, Vol. 13, American Met. Soc., 87-100.

van Loon, H. 1984. The Southern Oscillation. Part II: associations with the trades and with the trough in the westerlies of the South Pacific Ocean, *Monthly Weather Review*, **112**, 947-954.

van Loon, H. and Jenne, R. L. 1972. The zonal harmonic standing waves in the Southern Hemisphere, *J. Geophys. Res.*, **77**, 992-1003.

van Loon, H. and Madden, R. A. 1981. The Southern Oscillation. Part I: Global associations with pressure and temperature in Northern winter, *Monthly Weather Review*, **109**, 1150-1162.

van Loon, H. and Rogers, J. C. 1981. Remarks on the circulation over the Southern Hemisphere in FGGE and on its relation to the phases of the Southern Oscillation, *Monthly Weather Review*, **109**, 2255-2259.

van Loon, H. and Shea, D. J. 1985. The Southern Oscillation. Part IV: the precursors south of 15°S to the extremes of the oscillation, *Monthly Weather Review*, **113**, 2063-2074.

van Loon, H. and Shea, D. J. 1987. The Southern Oscillation. Part VI: anomalies of sea level pressure on the Southern Hemisphere and of Pacific sea surface temperature during the development of a warm event, *Monthly Weather Review*, **115**, 370-379.

van Tongeren, O. F. R. 1995. Cluster Analysis, In: Jongman, R. H. G., Ter Braak, C. J. F., van Tongeren, O. F. R. (eds.) *Data Analysis in Community and Landscape Ecology*, Cambridge University Press, Cambridge. p 174-203.

Vernekar, A. D., Zhou, J. and Shukla, J. 1995. The effect of the Eurasian snow cover on the Indian monsoon, *Journal of Climate*, **8**, 248-266.

Vincent, D. G. 1985. Cyclone development in the South Pacific convergence zone during FGGE, 10-17 January 1979, *Quarterly Journal of the Royal Meteorological Society*, **111**, 155-172.

Vincent, D. G. 1994. The South Pacific Convergence Zone (SPCZ): a review, *Monthly Weather Review*, **122**, 1949-1970.

Walker, G. T. 1928. World Weather, *Quarterly Journal of the Royal Meteorological Society*, **54**, 79-87.

Walker, G. T. and Bliss, E. W. 1932. World Weather V, *Memoirs of the Royal Meteorological Society*, **4**, 53-84.

Wang, B. 1992. The vertical structure and development of the ENSO anomaly mode during 1979-1989, *Journal of the Atmospheric Sciences*, **49**, 698-712.

Wang, B. 1995. Interdecadal changes in El Niño onset in the last four decades, *Journal of Climate*, **8**, 267-285.

Wang, X. L. and Ropelewski, C. F. 1995. An assessment of ENSO - scale secular variability, *Journal of Climate*, **8**, 1584-1599.

Wattam, S. and Turner, J. 1995. Weather Forecasting for aviation and marine operations in the Antarctic Peninsula region, *Meteorological Applications*, **2**, 323-332.

Webster, P. J. and Yang, S. 1992. Monsoon and ENSO: Selectively interactive systems, *Quarterly Journal of the Royal Meteorological Society*, **118**, 877-926.

White, W. B. and Peterson, R. G. 1996. An Antarctic circumpolar wave in surface pressure, wind, temperature and sea-ice extent, *Nature*, **380**, 699-702.

Whitworth, T. 1988. The Antarctic circumpolar current, *Oceanus*, 31, 53-58.

Wilks, D. S. 1995. *Statistical methods in the Atmospheric Sciences: an introduction*, Academic Press, London, pp453.

Wright, P. B. 1975. *An index of the Southern Oscillation*, University of East Anglia, Climate Research Unit, CRU RP4.

Wright, P. B. 1984. Relationships between indices of the Southern Oscillation, *Monthly Weather Review*, **112**, 1913-1919.

Wright, P. B. 1989. Homogenized long-period Southern Oscillation Indices, *International Journal of Climatology*, **9**, 33-54.

Wright, P. B., Mitchell, T. P. and Wallace, J. M. 1985. *Relationships between surface observations over the global oceans and the Southern Oscillation*, Pacific Marine Environ. Lab., Seattle, ERL/NDAA Data Report. PMEL-12.

Wright, P. B., Wallace, J. M., Mitchell, T. P. and Deser, C. 1988. Correlation structure of the El Niño / Southern Oscillation phenomenon, *Journal of Climate*, **1**, 609-625.

Wyrtki, K. 1985. Water displacements in the Pacific and the genesis of El Niño cycles, *Journal of Geophysical Research*, **90** (C4), 7129-7132.

Xie, S., Bao, C., Xue, Z., Zhang, L. and Hao, C. 1994. Interaction between Antarctic sea ice and ENSO events, *Proc. NIPR Symp. Polar Meteorol. Glaciol.*, **8**, 95-110.

Yarnal, B. 1993. *Synoptic Climatology in Environmental Analysis*, Belhaven Press, London, pp195.

Yin, Z. Y. 1994. Moisture condition in the South - Eastern USA and teleconnection patterns, *International Journal of Climatology*, **14**, 947-967.

Zebiak, S. E. and Cane, M. A. 1987. A model El Niño - Southern Oscillation, *Monthly Weather Review*, **115**, 2262-2278.

Zhang, R.-H., Rothstein, L. M. and Busalacchi, A. J. 1998. Origin of upper-ocean warming and El Niño change on decadal scales in the tropical Pacific Ocean, *Nature*, **391**, 879-883.

APPENDIX 1: FORTRAN PROGRAMS

Monthly FORTRAN Programs

anoms.for	A program to read in the actual data files and write them out to month based files.
allmeans.for	A program to merge the monthly files into a single file.
means.for	A program to calculate the anomalies from the monthly data.
allmea2.for	A program to merge the monthly anomaly files into one file.
resort2.for	A program to rearrange the anomaly data to draw Hovmöller diagrams.
resort3.for	A program to rearrange the anomaly data to draw warm and cold composite Hovmöller diagrams.
grids.for	A program to rearrange the monthly anomalies to allow them to be used in UNIMAP.

5 day FORTRAN Programs

amoms.for	A program to read in the actual data files convert the data to 5 day data and write them out to year based files.
means.for	A program to calculate the anomalies from the 5 day data and amalgamate the files into two large files.
trends.for	A program to calculate the three month percentage anomalies for the percentage anomaly charts.
resort2.for	A program to rearrange the anomaly data to draw Hovmöller charts.
ranks.for	A program to rank the 5 day data used for the harmonic analysis and convert it into percentile ranks.
harmonics.for	A program to perform harmonic analysis on the 5 day percentile ranked data.
grads.for	A program to calculate U and V components to put into GrADS for plotting harmonic dials.
south.for	A program to turn 5 day 500 hPa height data into southerly wind components using the geostrophic wind equation.
west.for	A program to turn 5 day 500 hPa height data into westerly wind components using the geostrophic wind equation.
speeds.for	A program to convert southerly and westerly wind components into wind speeds and wind speed anomalies.
windgrads.for	A program to convert wind components into vectors for use in GrADS.

```
PROGRAM ANOMS
C-----------------------------------------------------------------------
C     This program reads in the actual data files and writes them out
C     to month based files
C-----------------------------------------------------------------------
C     Written 11/11/96 by Richenda Houseago
C-----------------------------------------------------------------------
C     Declare Variables
C-----------------------------------------------------------------------
      REAL MON73(20,80), MON74(20,80), MON75(20,80), MON76(20,80)
      REAL MON77(20,80), MON78(20,80), MON79(20,80), MON80(20,80)
      REAL MON81(20,80), MON82(20,80), MON83(20,80), MON84(20,80)
      REAL MON85(20,80), MON86(20,80), MON87(20,80), MON88(20,80)
      REAL MON89(20,80), MON90(20,80), MON91(20,80), MON92(20,80)
      REAL MON93(20,80), MON94(20,80)
      INTEGER SCORE(80,20)
      CHARACTER *23 INFI1,INFI2,INFI3,INFI4,INFI5,INFI6,INFI7,INFI8
      CHARACTER *23 INFI9,INFI10,INFI11,INFI12,INFI13,INFI14,INFI15
      CHARACTER *23 INFI16,INFI17,INFI18,INFI19,INFI20,INFI21,INFI22
      CHARACTER *10 OUT1,OUT2
      DATA INFI1/'rsz0500.7312.ALL.latlon'/
      DATA INFI2/'rsz0500.7412.ALL.latlon'/
      DATA INFI3/'rsz0500.7512.ALL.latlon'/
      DATA INFI4/'rsz0500.7612.ALL.latlon'/
      DATA INFI5/'rsz0500.7712.ALL.latlon'/
      DATA INFI6/'rsz0500.7812.ALL.latlon'/
      DATA INFI7/'rsz0500.7912.ALL.latlon'/
      DATA INFI8/'rsz0500.8012.ALL.latlon'/
      DATA INFI9/'rsz0500.8112.ALL.latlon'/
      DATA INFI10/'rsz0500.8212.ALL.latlon'/
      DATA INFI11/'rsz0500.8312.ALL.latlon'/
      DATA INFI12/'rsz0500.8412.ALL.latlon'/
      DATA INFI13/'rsz0500.8512.ALL.latlon'/
      DATA INFI14/'rsz0500.8612.ALL.latlon'/
      DATA INFI15/'rsz0500.8712.ALL.latlon'/
      DATA INFI16/'rsz0500.8812.ALL.latlon'/
      DATA INFI17/'rsz0500.8912.ALL.latlon'/
      DATA INFI18/'rsz0500.9012.ALL.latlon'/
      DATA INFI19/'rsz0500.9112.ALL.latlon'/
      DATA INFI20/'rsz0500.9212.ALL.latlon'/
      DATA INFI21/'rsz0500.9312.ALL.latlon'/
C      DATA INFI22/'rsz0500.9412.ALL.latlon'/
      DATA OUT1/'DECMTH.DAT'/
      WRITE (6,1000)
 1000 FORMAT (//,5X,'STAGE ONE COMPLETED')
C-----------------------------------------------------------------------
C     Procedure to read in data and rearrange it.
C-----------------------------------------------------------------------
      OPEN (UNIT=10,FORM='FORMATTED',STATUS='OLD',FILE=INFI1)
      READ (10,2000)((MON73(I,J), J=1,73), I=1,19)
 2000 FORMAT (73F9.3)
      OPEN (UNIT=10,FORM='FORMATTED',STATUS='OLD',FILE=INFI2)
      READ (10,2010)((MON74(I,J), J=1,73), I=1,19)
 2010 FORMAT (73F9.3)
      OPEN (UNIT=10,FORM='FORMATTED',STATUS='OLD',FILE=INFI3)
      READ (10,2020)((MON75(I,J), J=1,73), I=1,19)
 2020 FORMAT (73F9.3)
```

```
      OPEN (UNIT=10,FORM='FORMATTED',STATUS='OLD',FILE=INFI4)
      READ (10,2030)((MON76(I,J), J=1,73), I=1,19)
 2030 FORMAT (73F9.3)
      OPEN (UNIT=10,FORM='FORMATTED',STATUS='OLD',FILE=INFI5)
      READ (10,2040)((MON77(I,J), J=1,73), I=1,19)
 2040 FORMAT (73F9.3)
      OPEN (UNIT=10,FORM='FORMATTED',STATUS='OLD',FILE=INFI6)
      READ (10,2050)((MON78(I,J), J=1,73), I=1,19)
 2050 FORMAT (73F9.3)
      OPEN (UNIT=10,FORM='FORMATTED',STATUS='OLD',FILE=INFI7)
      READ (10,2060)((MON79(I,J), J=1,73), I=1,19)
 2060 FORMAT (73F9.3)
      OPEN (UNIT=10,FORM='FORMATTED',STATUS='OLD',FILE=INFI8)
      READ (10,2070)((MON80(I,J), J=1,73), I=1,19)
 2070 FORMAT (73F9.3)
      OPEN (UNIT=10,FORM='FORMATTED',STATUS='OLD',FILE=INFI9)
      READ (10,2080)((MON81(I,J), J=1,73), I=1,19)
 2080 FORMAT (73F9.3)
      OPEN (UNIT=10,FORM='FORMATTED',STATUS='OLD',FILE=INFI10)
      READ (10,2090)((MON82(I,J), J=1,73), I=1,19)
 2090 FORMAT (73F9.3)
      OPEN (UNIT=10,FORM='FORMATTED',STATUS='OLD',FILE=INFI11)
      READ (10,2100)((MON83(I,J), J=1,73), I=1,19)
 2100 FORMAT (73F9.3)
      OPEN (UNIT=10,FORM='FORMATTED',STATUS='OLD',FILE=INFI12)
      READ (10,2110)((MON84(I,J), J=1,73), I=1,19)
 2110 FORMAT (73F9.3)
      OPEN (UNIT=10,FORM='FORMATTED',STATUS='OLD',FILE=INFI13)
      READ (10,2120)((MON85(I,J), J=1,73), I=1,19)
 2120 FORMAT (73F9.3)
      OPEN (UNIT=10,FORM='FORMATTED',STATUS='OLD',FILE=INFI14)
      READ (10,2130)((MON86(I,J), J=1,73), I=1,19)
 2130 FORMAT (73F9.3)
      OPEN (UNIT=10,FORM='FORMATTED',STATUS='OLD',FILE=INFI15)
      READ (10,2140)((MON87(I,J), J=1,73), I=1,19)
 2140 FORMAT (73F9.3)
      OPEN (UNIT=10,FORM='FORMATTED',STATUS='OLD',FILE=INFI16)
      READ (10,2150)((MON88(I,J), J=1,73), I=1,19)
 2150 FORMAT (73F9.3)
      OPEN (UNIT=10,FORM='FORMATTED',STATUS='OLD',FILE=INFI17)
      READ (10,2160)((MON89(I,J), J=1,73), I=1,19)
 2160 FORMAT (73F9.3)
      OPEN (UNIT=10,FORM='FORMATTED',STATUS='OLD',FILE=INFI18)
      READ (10,2170)((MON90(I,J), J=1,73), I=1,19)
 2170 FORMAT (73F9.3)
      OPEN (UNIT=10,FORM='FORMATTED',STATUS='OLD',FILE=INFI19)
      READ (10,2180)((MON91(I,J), J=1,73), I=1,19)
 2180 FORMAT (73F9.3)
      OPEN (UNIT=10,FORM='FORMATTED',STATUS='OLD',FILE=INFI20)
      READ (10,2190)((MON92(I,J), J=1,73), I=1,19)
 2190 FORMAT (73F9.3)
      OPEN (UNIT=10,FORM='FORMATTED',STATUS='OLD',FILE=INFI21)
      READ (10,2200)((MON93(I,J), J=1,73), I=1,19)
 2200 FORMAT (73F9.3)
C      OPEN (UNIT=10,FORM='FORMATTED',STATUS='OLD',FILE=INFI22)
C      READ (10,2210)((MON94(I,J), J=1,73), I=1,19)
C 2210 FORMAT (73F9.3)
```

```
      WRITE (6,3000)
 3000 FORMAT (//,5X,'STAGE TWO COMPLETED')
C-----------------------------------------------------------------
C     Procedure to write everything out to a file
C-----------------------------------------------------------------
      OPEN (UNIT=12,FORM='FORMATTED',STATUS='NEW',FILE=OUT1)
      DO 100 I=1,19
      DO 110 J=1,72
      WRITE (12,7010) MON73(I,J), MON74(I,J), MON75(I,J), MON76(I,J),
     1 MON77(I,J), MON78(I,J), MON79(I,J), MON80(I,J), MON81(I,J),
     2 MON82(I,J), MON83(I,J), MON84(I,J), MON85(I,J), MON86(I,J),
     3 MON87(I,J), MON88(I,J), MON89(I,J), MON90(I,J), MON91(I,J),
     4 MON92(I,J), MON93(I,J)
 110  CONTINUE
 100  CONTINUE
 7010 FORMAT (21F9.3)
      STOP
      END
```

```
PROGRAM ALLMEANS
C-----------------------------------------------------------------
C     This program is to merge the actual monthly files into one
C     file
C-----------------------------------------------------------------
C     Written 11/11/96 by Richenda Houseago
C-----------------------------------------------------------------
C     Declare Variables
C-----------------------------------------------------------------
      REAL JAN(1400,22), FEB(1400,22), MAR(1400,22), APR(1400,22)
      REAL JUN(1400,22), JUL(1400,22), AUG(1400,22), SEP(1400,22)
      REAL NOV(1400,22), DEC(1400,22), MAY(1400,22), OCT(1400,22)
      CHARACTER *10 INFI1,INFI2,INFI3,INFI4,INFI5,INFI6,INFI7,INFI8
      CHARACTER *10 INFI10,INFI11,INFI12,INFI9
      CHARACTER *11 OUT1,OUT2
      DATA INFI1/'JANMTH.DAT'/
      DATA INFI2/'FEBMTH.DAT'/
      DATA INFI3/'MARMTH.DAT'/
      DATA INFI4/'APRMTH.DAT'/
      DATA INFI5/'MAYMTH.DAT'/
      DATA INFI6/'JUNMTH.DAT'/
      DATA INFI7/'JULMTH.DAT'/
      DATA INFI8/'AUGMTH.DAT'/
      DATA INFI9/'SEPMTH.DAT'/
      DATA INFI10/'OCTMTH.DAT'/
      DATA INFI11/'NOVMTH.DAT'/
      DATA INFI12/'DECMTH.DAT'/
      DATA OUT1/'7HYEAR.DAT'/
      WRITE (6,1000)
 1000 FORMAT (//,5X,'STAGE ONE COMPLETED')
C-----------------------------------------------------------------
C     Procedure to read in data and rearrange it.
C-----------------------------------------------------------------
      OPEN (UNIT=10,FORM='FORMATTED',STATUS='OLD',FILE=INFI1)
      READ (10,2000)((JAN(I,J), J=1,22), I=1,1368)
 2000 FORMAT (22F9.3)
      OPEN (UNIT=10,FORM='FORMATTED',STATUS='OLD',FILE=INFI2)
      READ (10,2010)((FEB(I,J), J=1,22), I=1,1368)
 2010 FORMAT (22F9.3)
      OPEN (UNIT=10,FORM='FORMATTED',STATUS='OLD',FILE=INFI3)
      READ (10,2020)((MAR(I,J), J=1,22), I=1,1368)
 2020 FORMAT (22F9.3)
      OPEN (UNIT=10,FORM='FORMATTED',STATUS='OLD',FILE=INFI4)
      READ (10,2030)((APR(I,J), J=1,22), I=1,1368)
 2030 FORMAT (22F9.3)
      OPEN (UNIT=10,FORM='FORMATTED',STATUS='OLD',FILE=INFI5)
      READ (10,2040)((MAY(I,J), J=1,22), I=1,1368)
 2040 FORMAT (22F9.3)
      OPEN (UNIT=10,FORM='FORMATTED',STATUS='OLD',FILE=INFI6)
      READ (10,2050)((JUN(I,J), J=1,22), I=1,1368)
 2050 FORMAT (22F9.3)
      OPEN (UNIT=10,FORM='FORMATTED',STATUS='OLD',FILE=INFI7)
      READ (10,2060)((JUL(I,J), J=1,21), I=1,1368)
 2060 FORMAT (21F9.3)
      OPEN (UNIT=10,FORM='FORMATTED',STATUS='OLD',FILE=INFI8)
      READ (10,2070)((AUG(I,J), J=1,21), I=1,1368)
 2070 FORMAT (21F9.3)
```

```
      OPEN (UNIT=10,FORM='FORMATTED',STATUS='OLD',FILE=INFI9)
      READ (10,2080)((SEP(I,J), J=1,21), I=1,1368)
 2080 FORMAT (21F9.3)
      OPEN (UNIT=10,FORM='FORMATTED',STATUS='OLD',FILE=INFI10)
      READ (10,2090)((OCT(I,J), J=1,21), I=1,1368)
 2090 FORMAT (21F9.3)
      OPEN (UNIT=10,FORM='FORMATTED',STATUS='OLD',FILE=INFI11)
      READ (10,2100)((NOV(I,J), J=1,21), I=1,1368)
 2100 FORMAT (21F9.3)
      OPEN (UNIT=10,FORM='FORMATTED',STATUS='OLD',FILE=INFI12)
      READ (10,2110)((DEC(I,J), J=1,21), I=1,1368)
 2110 FORMAT (21F9.3)
      WRITE (6,3000)
 3000 FORMAT (//,5X,'The files have been read in')
C-----------------------------------------------------------------------
C     Procedure to write everything out to a file
C-----------------------------------------------------------------------
      OPEN (UNIT=12,FORM='FORMATTED',STATUS='NEW',FILE=OUT1)
      DO 600 I=1,1368
      WRITE (12,7010) (JAN(I,J),FEB(I,J),MAR(I,J),APR(I,J)
     1,MAY(I,J),JUN(I,J),JUL(I,J),AUG(I,J),SEP(I,J),OCT(I,J)
     2,NOV(I,J),DEC(I,J), J=1,22)
 600  CONTINUE
 7010 FORMAT (264F9.3)
      STOP
      END
```

```
PROGRAM MEANS
C-----------------------------------------------------------------
C     To calculate anomalies for individual months for monthly data
C-----------------------------------------------------------------
C     Written 11/11/96 by Richenda Houseago
C-----------------------------------------------------------------
C     Declare Variables
C-----------------------------------------------------------------
      REAL MON(1400,22), ANO(1400,22), MEAN(1400)
      CHARACTER *10 INFI1
      CHARACTER *10 OUT1
      DATA INFI1/'DECMTH.DAT'/
      DATA OUT1/'DECANO.DAT'/
      WRITE (6,1000)
 1000 FORMAT (//,5X,'STAGE ONE COMPLETED')
      DO I=1,1368
       DO J=1,21
        MON(I,J) = 0.0
        ANO(I,J) = 0.0
       ENDDO
      ENDDO
C-----------------------------------------------------------------
C     Procedure to read in data and rearrange it.
C-----------------------------------------------------------------
      OPEN (UNIT=10,FORM='FORMATTED',STATUS='OLD',FILE=INFI1)
      READ (10,2000)((MON(I,J), J=1,21), I=1,1368)
 2000 FORMAT (21F9.3)
      WRITE (6,3000)
 3000 FORMAT (//,5X,'STAGE TWO COMPLETED')
C-----------------------------------------------------------------
C     Procedure to calculate the anomalies
C-----------------------------------------------------------------
      DO 100 I=1,1368
      MEAN(I)=0.0
      DO 110 J=1,21
      MEAN(I)=MEAN(I)+(MON(I,J)/21)
 110  CONTINUE
 100  CONTINUE
      WRITE (6,4000)
 4000 FORMAT (//,5X,'STAGE THREE COMPLETED')
      DO 200 I=1,1368
      DO 210 J=1,21
      ANO(I,J)=MON(I,J)-MEAN(I)
 210  CONTINUE
 200  CONTINUE
C-----------------------------------------------------------------
C     Procedure to write data out to a file
C-----------------------------------------------------------------
      OPEN (UNIT=12,FORM='FORMATTED',STATUS='NEW',FILE=OUT1)
      DO 600 I=1,1368
      WRITE (12,7010) ANO(I,1),ANO(I,2),ANO(I,3),ANO(I,4),ANO(I,5)
     1,ANO(I,6),ANO(I,7),ANO(I,8),ANO(I,9),ANO(I,10),ANO(I,11)
     2,ANO(I,12),ANO(I,13),ANO(I,14),ANO(I,15),ANO(I,16),ANO(I,17),
     3ANO(I,18),ANO(I,19),ANO(I,20),ANO(I,21)
 600  CONTINUE
 7010 FORMAT (21F9.3)
      STOP
      END
```

```
PROGRAM ALLMEA2
C-----------------------------------------------------------------
C     This program merges the monthly anomaly files into one file
C-----------------------------------------------------------------
C     Written 11/11/96 by Richenda Houseago
C-----------------------------------------------------------------
C     Declare Variables
C-----------------------------------------------------------------
      REAL JAN(1400,22), FEB(1400,22), MAR(1400,22), APR(1400,22)
      REAL JUN(1400,22), JUL(1400,22), AUG(1400,22), SEP(1400,22)
      REAL NOV(1400,22), DEC(1400,22), MAY(1400,22), OCT(1400,22)
      CHARACTER *10 INFI13,INFI14,INFI15,INFI16,INFI17,INFI18,INFI19
      CHARACTER *10 INFI20,INFI21,INFI22,INFI23,INFI24
      CHARACTER *11 OUT2
      DATA INFI13/'JANANO.DAT'/
      DATA INFI14/'FEBANO.DAT'/
      DATA INFI15/'MARANO.DAT'/
      DATA INFI16/'APRANO.DAT'/
      DATA INFI17/'MAYANO.DAT'/
      DATA INFI18/'JUNANO.DAT'/
      DATA INFI19/'JULANO.DAT'/
      DATA INFI20/'AUGANO.DAT'/
      DATA INFI21/'SEPANO.DAT'/
      DATA INFI22/'OCTANO.DAT'/
      DATA INFI23/'NOVANO.DAT'/
      DATA INFI24/'DECANO.DAT'/
      DATA OUT2/'7HANOO.DAT'/
      WRITE (6,1000)
 1000 FORMAT (//,5X,'STAGE ONE COMPLETED')
C-----------------------------------------------------------------
C     Procedure to read in data and rearrange it.
C-----------------------------------------------------------------
      OPEN (UNIT=10,FORM='FORMATTED',STATUS='OLD',FILE=INFI13)
      READ (10,2000)((JAN(I,J), J=1,22), I=1,1368)
 2000 FORMAT (22F9.3)
      OPEN (UNIT=10,FORM='FORMATTED',STATUS='OLD',FILE=INFI14)
      READ (10,2010)((FEB(I,J), J=1,22), I=1,1368)
 2010 FORMAT (22F9.3)
      OPEN (UNIT=10,FORM='FORMATTED',STATUS='OLD',FILE=INFI15)
      READ (10,2020)((MAR(I,J), J=1,22), I=1,1368)
 2020 FORMAT (22F9.3)
      OPEN (UNIT=10,FORM='FORMATTED',STATUS='OLD',FILE=INFI16)
      READ (10,2030)((APR(I,J), J=1,22), I=1,1368)
 2030 FORMAT (22F9.3)
      OPEN (UNIT=10,FORM='FORMATTED',STATUS='OLD',FILE=INFI17)
      READ (10,2040)((MAY(I,J), J=1,22), I=1,1368)
 2040 FORMAT (22F9.3)
      OPEN (UNIT=10,FORM='FORMATTED',STATUS='OLD',FILE=INFI18)
      READ (10,2050)((JUN(I,J), J=1,22), I=1,1368)
 2050 FORMAT (22F9.3)
      OPEN (UNIT=10,FORM='FORMATTED',STATUS='OLD',FILE=INFI19)
      READ (10,2060)((JUL(I,J), J=1,21), I=1,1368)
 2060 FORMAT (21F9.3)
      OPEN (UNIT=10,FORM='FORMATTED',STATUS='OLD',FILE=INFI20)
      READ (10,2070)((AUG(I,J), J=1,21), I=1,1368)
 2070 FORMAT (21F9.3)
      OPEN (UNIT=10,FORM='FORMATTED',STATUS='OLD',FILE=INFI21)
```

```
      READ (10,2080)((SEP(I,J), J=1,21), I=1,1368)
 2080 FORMAT (21F9.3)
      OPEN (UNIT=10,FORM='FORMATTED',STATUS='OLD',FILE=INFI22)
      READ (10,2090)((OCT(I,J), J=1,21), I=1,1368)
 2090 FORMAT (21F9.3)
      OPEN (UNIT=10,FORM='FORMATTED',STATUS='OLD',FILE=INFI23)
      READ (10,2100)((NOV(I,J), J=1,21), I=1,1368)
 2100 FORMAT (21F9.3)
      OPEN (UNIT=10,FORM='FORMATTED',STATUS='OLD',FILE=INFI24)
      READ (10,2110)((DEC(I,J), J=1,21), I=1,1368)
 2110 FORMAT (21F9.3)
      WRITE (6,3000)
 3000 FORMAT (//,5X,'The files have been read in')
C-----------------------------------------------------------------
C     Procedure to write everything out to a file
C-----------------------------------------------------------------
      OPEN (UNIT=12,FORM='FORMATTED',STATUS='NEW',FILE=OUT2)
      DO 600 I=1,1368
      WRITE (12,7010) (JAN(I,J),FEB(I,J),MAR(I,J),APR(I,J),
     1MAY(I,J),JUN(I,J),JUL(I,J),AUG(I,J),SEP(I,J)
     2,OCT(I,J),NOV(I,J),DEC(I,J), J=1,22)
 600  CONTINUE
 7010 FORMAT (264F9.3)
      STOP
      END
```

```
PROGRAM RESORT2
C-----------------------------------------------------------------
C     To rearrange monthly anomaly data to draw Hovmöller diagrams
C-----------------------------------------------------------------
C     Written 5/12/96 by Richenda Houseago
C-----------------------------------------------------------------
C     Declare Variables
C-----------------------------------------------------------------
      INTEGER DATE(260),A(260),LAT(20)
      REAL MON(1400,260)
      CHARACTER *10 INFI1
      CHARACTER *10 OUT1
      DATA INFI1/'7HANOO.DAT'/
      DATA OUT1/'23091.DAT'/
      WRITE (6,1000)
 1000 FORMAT (//,5X,'STAGE ONE COMPLETED')
C-----------------------------------------------------------------
C     Procedure to read in data and rearrange it.
C-----------------------------------------------------------------
      OPEN (UNIT=10,FORM='FORMATTED',STATUS='OLD',FILE=INFI1)
      DO 100 I=1,1368
      READ (10,1500) (MON(I,J), J=1,258)
 100  CONTINUE
 1500 FORMAT (258F9.3)
      DO 400 J=1,258
      DATE(J)=2*J
 400  CONTINUE
      DO 200 I=1,19
      LAT(1)=0
      LAT(I)=LAT(I-1)+5
 200  CONTINUE
      WRITE (6,3000)
 3000 FORMAT (//,5X,'STAGE TWO COMPLETED')
C-----------------------------------------------------------------
C     Procedure to write everything out to a file
C-----------------------------------------------------------------
      OPEN (UNIT=12,FORM='FORMATTED',STATUS='NEW',FILE=OUT1)
      DO 600 J=215,251
      WRITE (12,7010) DATE(J),LAT(1),MON(47,J)
 7010 FORMAT (2I3,F9.3)
      WRITE (12,7011) DATE(J),LAT(2),MON(119,J)
 7011 FORMAT (2I3,F9.3)
      WRITE (12,7012) DATE(J),LAT(3),MON(191,J)
 7012 FORMAT (2I3,F9.3)
      WRITE (12,7013) DATE(J),LAT(4),MON(263,J)
 7013 FORMAT (2I3,F9.3)
      WRITE (12,7014) DATE(J),LAT(5),MON(335,J)
 7014 FORMAT (2I3,F9.3)
      WRITE (12,7015) DATE(J),LAT(6),MON(407,J)
 7015 FORMAT (2I3,F9.3)
      WRITE (12,7016) DATE(J),LAT(7),MON(479,J)
 7016 FORMAT (2I3,F9.3)
      WRITE (12,7017) DATE(J),LAT(8),MON(551,J)
 7017 FORMAT (2I3,F9.3)
      WRITE (12,7018) DATE(J),LAT(9),MON(623,J)
 7018 FORMAT (2I3,F9.3)
      WRITE (12,7019) DATE(J),LAT(10),MON(695,J)
```

```
7019 FORMAT (2I3,F9.3)
     WRITE (12,7020) DATE(J),LAT(11),MON(767,J)
7020 FORMAT (2I3,F9.3)
     WRITE (12,7021) DATE(J),LAT(12),MON(839,J)
7021 FORMAT (2I3,F9.3)
     WRITE (12,7022) DATE(J),LAT(13),MON(911,J)
7022 FORMAT (2I3,F9.3)
     WRITE (12,7023) DATE(J),LAT(14),MON(983,J)
7023 FORMAT (2I3,F9.3)
     WRITE (12,7024) DATE(J),LAT(15),MON(1055,J)
7024 FORMAT (2I3,F9.3)
     WRITE (12,7025) DATE(J),LAT(16),MON(1127,J)
7025 FORMAT (2I3,F9.3)
     WRITE (12,7026) DATE(J),LAT(17),MON(1199,J)
7026 FORMAT (2I3,F9.3)
     WRITE (12,7027) DATE(J),LAT(18),MON(1271,J)
7027 FORMAT (2I3,F9.3)
     WRITE (12,7028) DATE(J),LAT(19),MON(1343,J)
7028 FORMAT (2I3,F9.3)
600  CONTINUE
     STOP
     END
```

```
PROGRAM RESORT3
C-----------------------------------------------------------------------
C     To rearrange monthly anomaly data to draw warm and cold
C     composite Hovmöller diagrams
C-----------------------------------------------------------------------
C     Written 29/11/96 by Richenda Houseago
C-----------------------------------------------------------------------
C     Declare Variables
C-----------------------------------------------------------------------
      REAL MON(1400,260),X(1400,2),Y(1400),MEAN(1400,260)
      INTEGER DATE(260),A(260),LAT(20)
      CHARACTER *10 INFI1
      CHARACTER *10 INFI2
      CHARACTER *11 OUT1
      DATA INFI1/'7HANOO.DAT'/
      DATA OUT1/'WARM230.DAT'/
      WRITE (6,1000)
 1000 FORMAT (//,5X,'STAGE ONE COMPLETED')
C-----------------------------------------------------------------------
C     Procedure to read in data and rearrange it.
C-----------------------------------------------------------------------
      OPEN (UNIT=10,FORM='FORMATTED',STATUS='OLD',FILE=INFI1)
      DO 100 I=1,1368
      READ (10,1500) (MON(I,J), J=1,258)
 100  CONTINUE
 1500 FORMAT (258F9.3)
C-----------------------------------------------------------------------
C     Procedure to calculate the composites
C-----------------------------------------------------------------------
      DO 120 I=1,1368
      DO 130 J=1,36
      MEAN(I,J)=(MON(I,J+33)+MON(I,J+109)+MON(I,J+155)+MON(I,J+215))/3
 130  CONTINUE
 120  CONTINUE
      WRITE (6,3000)
 3000 FORMAT (//,5X,'STAGE TWO COMPLETED')
      DO 400 J=1,258
      DATE(J)=2*J
 400  CONTINUE
      DO 200 I=1,19
      LAT(1)=0
      LAT(I)=LAT(I-1)+5
 200  CONTINUE
C-----------------------------------------------------------------------
C     Procedure to write everything out to a file
C-----------------------------------------------------------------------
      OPEN (UNIT=12,FORM='FORMATTED',STATUS='NEW',FILE=OUT1)
      DO 600 J=1,36
      WRITE (12,7010) DATE(J),LAT(1),MEAN(47,J)
 7010 FORMAT (2I3,F9.3)
      WRITE (12,7011) DATE(J),LAT(2),MEAN(119,J)
 7011 FORMAT (2I3,F9.3)
      WRITE (12,7012) DATE(J),LAT(3),MEAN(191,J)
 7012 FORMAT (2I3,F9.3)
      WRITE (12,7013) DATE(J),LAT(4),MEAN(263,J)
 7013 FORMAT (2I3,F9.3)
      WRITE (12,7014) DATE(J),LAT(5),MEAN(335,J)
```

```
7014 FORMAT (2I3,F9.3)
     WRITE (12,7015) DATE(J),LAT(6),MEAN(407,J)
7015 FORMAT (2I3,F9.3)
     WRITE (12,7016) DATE(J),LAT(7),MEAN(479,J)
7016 FORMAT (2I3,F9.3)
     WRITE (12,7017) DATE(J),LAT(8),MEAN(551,J)
7017 FORMAT (2I3,F9.3)
     WRITE (12,7018) DATE(J),LAT(9),MEAN(623,J)
7018 FORMAT (2I3,F9.3)
     WRITE (12,7019) DATE(J),LAT(10),MEAN(695,J)
7019 FORMAT (2I3,F9.3)
     WRITE (12,7020) DATE(J),LAT(11),MEAN(767,J)
7020 FORMAT (2I3,F9.3)
     WRITE (12,7021) DATE(J),LAT(12),MEAN(839,J)
7021 FORMAT (2I3,F9.3)
     WRITE (12,7022) DATE(J),LAT(13),MEAN(911,J)
7022 FORMAT (2I3,F9.3)
     WRITE (12,7023) DATE(J),LAT(14),MEAN(983,J)
7023 FORMAT (2I3,F9.3)
     WRITE (12,7024) DATE(J),LAT(15),MEAN(1055,J)
7024 FORMAT (2I3,F9.3)
     WRITE (12,7025) DATE(J),LAT(16),MEAN(1127,J)
7025 FORMAT (2I3,F9.3)
     WRITE (12,7026) DATE(J),LAT(17),MEAN(1199,J)
7026 FORMAT (2I3,F9.3)
     WRITE (12,7027) DATE(J),LAT(18),MEAN(1271,J)
7027 FORMAT (2I3,F9.3)
     WRITE (12,7028) DATE(J),LAT(19),MEAN(1343,J)
7028 FORMAT (2I3,F9.3)
600  CONTINUE
     STOP
     END
```

```
PROGRAM GRIDS
C-----------------------------------------------------------------------
C     This program rearranges the monthly anomalies to allow them to
C     be put into UNIMAP
C-----------------------------------------------------------------------
C     Written 29/11/96 by Richenda Houseago
C-----------------------------------------------------------------------
C     Declare Variables
C-----------------------------------------------------------------------
      REAL MON(1400,260),X(1400,2),Y(1400),MEAN(1400)
      CHARACTER *10 INFI1
      CHARACTER *10 INFI2
      CHARACTER *10 OUT1
      DATA INFI1/'7HANOO.DAT'/
      DATA INFI2/'grid.dat'/
      DATA OUT1/'dec83.DAT'/
      WRITE (6,1000)
 1000 FORMAT (//,5X,'STAGE ONE COMPLETED')
C-----------------------------------------------------------------------
C     Procedure to read in data and rearrange it.
C-----------------------------------------------------------------------
      OPEN (UNIT=10,FORM='FORMATTED',STATUS='OLD',FILE=INFI1)
      DO 100 I=1,1368
      READ (10,1500) (MON(I,J), J=1,258)
 100  CONTINUE
 1500 FORMAT (258F9.3)
      DO 120 I=1,1368
      MEAN(I)=(MON(I,119)+MON(I,120)+MON(I,121))/3
 120  CONTINUE
      OPEN (UNIT=10,FORM='FORMATTED',STATUS='OLD',FILE=INFI2)
      DO 150 I=1,1368
      READ (10,1550) (X(I,J), J=1,2)
 150  CONTINUE
 1550 FORMAT (F6.3,F6.3)
      WRITE (6,3000)
 3000 FORMAT (//,5X,'STAGE TWO COMPLETED')
C-----------------------------------------------------------------------
C     Now to it all out to a file
C-----------------------------------------------------------------------
      OPEN (UNIT=12,FORM='FORMATTED',STATUS='NEW',FILE=OUT1)
      DO 600 I=1,1368
      WRITE (12,7010) (X(I,J), J=1,2),MEAN(I)
 600  CONTINUE
 7010 FORMAT (F7.3,F7.3,F9.3)
      STOP
      END
```

```
PROGRAM ANOMS
C-----------------------------------------------------------------------
C     This program converts the individual daily files into 5 day
C     mean files
C-----------------------------------------------------------------------
C     Written 03/08/97 by Richenda Houseago
C-----------------------------------------------------------------------
C     Declare Variables
C-----------------------------------------------------------------------
      REAL DATA1(80,80),DATA2(80,80),DATA3(80,80)
      REAL DATA4(80,80),DATA5(80,80),DATA6(80,80)
                  |
                 to
                  |
      REAL DATA724(80,80),DATA725(80,80),DATA726(80,80)
      REAL DATA727(80,80),DATA728(80,80),DATA729(80,80)
      REAL DATA730(80,80),MEAN(80,80,80)
      REAL OUTPUT(80,1400)
      INTEGER SCORE(80,20)
      CHARACTER *25 INFI1,INFI2,INFI3,INFI4,INFI5,INFI6,INFI7,INFI8
      CHARACTER *25 INFI9,INFI10,INFI11,INFI12,INFI13,INFI14,INFI15
                  |
                 to
                  |
      CHARACTER *25 INFI722,INFI723,INFI724,INFI725
      CHARACTER *25 INFI726,INFI727,INFI728,INFI729,INFI730
      DATA INFI1/'rspmsl.7301011100.latlon'/
      DATA INFI2/'rspmsl.7301012300.latlon'/
                  |
                 to
                  |
      DATA INFI729/'rspmsl.7312311100.latlon'/
      DATA INFI730/'rspmsl.7312312300.latlon'/
      DATA OUT1/'1973.dat'/
      WRITE (6,1000)
 1000 FORMAT (//,5X,'The variables have been declared')
C-----------------------------------------------------------------------
C     Procedure to read in data and rearrange it.
C-----------------------------------------------------------------------
      OPEN (UNIT=10,FORM='FORMATTED',STATUS='OLD',FILE=INFI1)
      READ (10,2001) ((DATA1(I,J), J=1,73), I=1,19)
 2001 FORMAT (73F9.3)
      OPEN (UNIT=10,FORM='FORMATTED',STATUS='OLD',FILE=INFI2)
      READ (10,2002) ((DATA2(I,J), J=1,73), I=1,19)
 2002 FORMAT (73F9.3)
                  |
                 to
                  |
      OPEN (UNIT=10,FORM='FORMATTED',STATUS='OLD',FILE=INFI729)
      READ (10,2729) ((DATA729(I,J), J=1,73), I=1,19)
 2729 FORMAT (73F9.3)
      OPEN (UNIT=10,FORM='FORMATTED',STATUS='OLD',FILE=INFI730)
      READ (10,2730) ((DATA730(I,J), J=1,73), I=1,19)
 2730 FORMAT (73F9.3)
      WRITE (6,3000)
 3000 FORMAT (//,5X,'The files have been read in')
C-----------------------------------------------------------------------
```

```
C     Procedure to calculate to 5 day means
C-----------------------------------------------------------------
      DO 197 I=1,19
      DO 198 J=1,72
 198  CONTINUE
 197  CONTINUE
      DO 200 I=1,19
      DO 201 J=1,72
      MEAN(I,J,1)=(DATA1(I,J)+DATA2(I,J)+DATA3(I,J)+DATA4(I,J)
     1+DATA5(I,J)+DATA6(I,J)+DATA7(I,J)+DATA8(I,J)
     2+DATA9(I,J)+DATA10(I,J))/10
      MEAN(I,J,2)=(DATA11(I,J)+DATA12(I,J)+DATA13(I,J)+DATA14(I,J)
     1+DATA15(I,J)+DATA16(I,J)+DATA17(I,J)+DATA18(I,J)
     2+DATA19(I,J)+DATA20(I,J))/10
                    |
                   to
                    |
      MEAN(I,J,72)=(DATA711(I,J)+DATA712(I,J)+DATA713(I,J)
     1DATA714(I,J)+DATA715(I,J)+DATA716(I,J)
     2DATA717(I,J)+DATA718(I,J)+DATA719(I,J)
     3DATA720(I,J))/10
      MEAN(I,J,73)=(DATA721(I,J)+DATA722(I,J)+DATA723(I,J)
     1DATA724(I,J)+DATA725(I,J)+DATA726(I,J)
     2DATA727(I,J)+DATA728(I,J)+DATA729(I,J)
     3DATA730(I,J))/10
 201  CONTINUE
 200  CONTINUE
      WRITE (6,3001)
 3001 FORMAT (//,5X,'All the means have been calculated')
C-----------------------------------------------------------------
C     Procedure to write data out to a file
C-----------------------------------------------------------------
      OPEN (UNIT=12,FORM='FORMATTED',STATUS='NEW',FILE=OUT1)
      DO 100 I=1,19
      DO 110 J=1,72
      WRITE (12,7010) (MEAN(I,J,K), K=1,73)
 110  CONTINUE
 100  CONTINUE
 7010 FORMAT (73F9.3)
      WRITE (6,3002)
 3002 FORMAT (//,5X,'Everything has been written to files done!!')
      STOP
      END
```

```
PROGRAM MEANS
C-----------------------------------------------------------------
C     To calculate anomalies in 5 daily data, and amalgamate the
C     yearly files into two large files
C-----------------------------------------------------------------
C     Written 04/08/97 by Richenda Houseago
C-----------------------------------------------------------------
C     Declare Variables
C-----------------------------------------------------------------
      REAL DATA(1400,1650)
      REAL ANO(1400,1650), MON(1400,1650), MEAN(1400,73)
      CHARACTER *10 INFI1, INFI2, INFI3, INFI4, INFI5, INFI6
      CHARACTER *10 INFI7, INFI8, INFI9, INFI10, INFI11, INFI12
      CHARACTER *10 INFI13, INFI14, INFI15, INFI16, INFI17
      CHARACTER *10 INFI18, INFI19, INFI20, INFI21, INFI22
      CHARACTER *10 OUT1, OUT2
      DATA INFI1/'1973.dat'/
      DATA INFI2/'1974.dat'/
      DATA INFI3/'1975.dat'/
      DATA INFI4/'1976.dat'/
      DATA INFI5/'1977.dat'/
      DATA INFI6/'1978.dat'/
      DATA INFI7/'1979.dat'/
      DATA INFI8/'1980.dat'/
      DATA INFI9/'1981.dat'/
      DATA INFI10/'1982.dat'/
      DATA INFI11/'1983.dat'/
      DATA INFI12/'1984.dat'/
      DATA INFI13/'1985.dat'/
      DATA INFI14/'1986.dat'/
      DATA INFI15/'1987.dat'/
      DATA INFI16/'1988.dat'/
      DATA INFI17/'1989.dat'/
      DATA INFI18/'1990.dat'/
      DATA INFI19/'1991.dat'/
      DATA INFI20/'1992.dat'/
      DATA INFI21/'1993.dat'/
      DATA INFI22/'1994.dat'/
      DATA OUT1/'year.dat'/
      DATA OUT2/'anoms.dat'/
      DO I=1,1368
       DO J=1,21
        MON(I,J) = 0.0
        ANO(I,J) = 0.0
       ENDDO
      ENDDO
 1000 FORMAT (//,5X,'The variables have been declared')
C-----------------------------------------------------------------
C     Procedure to read in data and rearrange it.
C-----------------------------------------------------------------
      OPEN (UNIT=10,FORM='FORMATTED',STATUS='OLD',FILE=INFI1)
      READ (10,2001) ((DATA(I,J), J=1,73), I=1,1368)
 2001 FORMAT (73F9.3)
      OPEN (UNIT=10,FORM='FORMATTED',STATUS='OLD',FILE=INFI2)
      READ (10,2002) ((DATA(I,J), J=74,146), I=1,1368)
 2002 FORMAT (73F9.3)
      OPEN (UNIT=10,FORM='FORMATTED',STATUS='OLD',FILE=INFI3)
```

```
      READ (10,2003) ((DATA(I,J), J=147,219), I=1,1368)
 2003 FORMAT (73F9.3)
      OPEN (UNIT=10,FORM='FORMATTED',STATUS='OLD',FILE=INFI4)
      READ (10,2004) ((DATA(I,J), J=220,292), I=1,1368)
 2004 FORMAT (73F9.3)
      OPEN (UNIT=10,FORM='FORMATTED',STATUS='OLD',FILE=INFI5)
      READ (10,2005) ((DATA(I,J), J=293,365), I=1,1368)
 2005 FORMAT (73F9.3)
      OPEN (UNIT=10,FORM='FORMATTED',STATUS='OLD',FILE=INFI6)
      READ (10,2006) ((DATA(I,J), J=366,438), I=1,1368)
 2006 FORMAT (73F9.3)
      OPEN (UNIT=10,FORM='FORMATTED',STATUS='OLD',FILE=INFI7)
      READ (10,2007) ((DATA(I,J), J=439,511), I=1,1368)
 2007 FORMAT (73F9.3)
      OPEN (UNIT=10,FORM='FORMATTED',STATUS='OLD',FILE=INFI8)
      READ (10,2008) ((DATA(I,J), J=512,584), I=1,1368)
 2008 FORMAT (73F9.3)
      OPEN (UNIT=10,FORM='FORMATTED',STATUS='OLD',FILE=INFI9)
      READ (10,2009) ((DATA(I,J), J=585,657), I=1,1368)
 2009 FORMAT (73F9.3)
      OPEN (UNIT=10,FORM='FORMATTED',STATUS='OLD',FILE=INFI10)
      READ (10,2010) ((DATA(I,J), J=658,730), I=1,1368)
 2010 FORMAT (73F9.3)
      OPEN (UNIT=10,FORM='FORMATTED',STATUS='OLD',FILE=INFI11)
      READ (10,2011) ((DATA(I,J), J=731,803), I=1,1368)
 2011 FORMAT (73F9.3)
      OPEN (UNIT=10,FORM='FORMATTED',STATUS='OLD',FILE=INFI12)
      READ (10,2012) ((DATA(I,J), J=804,876), I=1,1368)
 2012 FORMAT (73F9.3)
      OPEN (UNIT=10,FORM='FORMATTED',STATUS='OLD',FILE=INFI13)
      READ (10,2013) ((DATA(I,J), J=877,949), I=1,1368)
 2013 FORMAT (73F9.3)
      OPEN (UNIT=10,FORM='FORMATTED',STATUS='OLD',FILE=INFI14)
      READ (10,2014) ((DATA(I,J), J=950,1022), I=1,1368)
 2014 FORMAT (73F9.3)
      OPEN (UNIT=10,FORM='FORMATTED',STATUS='OLD',FILE=INFI15)
      READ (10,2015) ((DATA(I,J), J=1023,1095), I=1,1368)
 2015 FORMAT (73F9.3)
      OPEN (UNIT=10,FORM='FORMATTED',STATUS='OLD',FILE=INFI16)
      READ (10,2016) ((DATA(I,J), J=1096,1168), I=1,1368)
 2016 FORMAT (73F9.3)
      OPEN (UNIT=10,FORM='FORMATTED',STATUS='OLD',FILE=INFI17)
      READ (10,2017) ((DATA(I,J), J=1169,1241), I=1,1368)
 2017 FORMAT (73F9.3)
      OPEN (UNIT=10,FORM='FORMATTED',STATUS='OLD',FILE=INFI18)
      READ (10,2018) ((DATA(I,J), J=1242,1314), I=1,1368)
 2018 FORMAT (73F9.3)
      OPEN (UNIT=10,FORM='FORMATTED',STATUS='OLD',FILE=INFI19)
      READ (10,2019) ((DATA(I,J), J=1315,1387), I=1,1368)
 2019 FORMAT (73F9.3)
      OPEN (UNIT=10,FORM='FORMATTED',STATUS='OLD',FILE=INFI20)
      READ (10,2020) ((DATA(I,J), J=1388,1460), I=1,1368)
 2020 FORMAT (73F9.3)
      OPEN (UNIT=10,FORM='FORMATTED',STATUS='OLD',FILE=INFI21)
      READ (10,2021) ((DATA(I,J), J=1461,1533), I=1,1368)
 2021 FORMAT (73F9.3)
      OPEN (UNIT=10,FORM='FORMATTED',STATUS='OLD',FILE=INFI22)
```

```
      READ (10,2022) ((DATA(I,J), J=1534,1568), I=1,1368)
 2022 FORMAT (35F9.3)
      WRITE (6,3000)
 3000 FORMAT (//,5X,'The files have been read in')
C-----------------------------------------------------------------
C     To calculate the means:
C-----------------------------------------------------------------
      DO 100 I=1,1368
      DO 110 J=1,35
      MEAN(I,J)=(DATA(I,J)+DATA(I,(J+73))+DATA(I,(J+146))+
     1DATA(I,(J+219))+DATA(I,(J+292))+DATA(I,(J+365))+
     2DATA(I,(J+438))+DATA(I,(J+511))+DATA(I,(J+584))+
     3DATA(I,(J+657))+DATA(I,(J+730))+DATA(I,(J+803))+
     4DATA(I,(J+876))+DATA(I,(J+949))+DATA(I,(J+1022))+
     5DATA(I,(J+1095))+DATA(I,(J+1168))+DATA(I,(J+1241))+
     6DATA(I,(J+1314))+DATA(I,(J+1387))+DATA(I,(J+1460))+
     7DATA(I,(J+1533)))/22
 110  CONTINUE
 100  CONTINUE
      DO 101 I=1,1368
      DO 111 J=36,73
      MEAN(I,J)=(DATA(I,J)+DATA(I,(J+73))+DATA(I,(J+146))+
     1DATA(I,(J+219))+DATA(I,(J+292))+DATA(I,(J+365))+
     2DATA(I,(J+438))+DATA(I,(J+511))+DATA(I,(J+584))+
     3DATA(I,(J+657))+DATA(I,(J+730))+DATA(I,(J+803))+
     4DATA(I,(J+876))+DATA(I,(J+949))+DATA(I,(J+1022))+
     5DATA(I,(J+1095))+DATA(I,(J+1168))+DATA(I,(J+1241))+
     6DATA(I,(J+1314))+DATA(I,(J+1387))+DATA(I,(J+1460)))/21
 111  CONTINUE
 101  CONTINUE
      WRITE (6,4000)
 4000 FORMAT (//,5X,'The means have been calculated')
C-----------------------------------------------------------------
C     Now to use the means to calculate the anomalies
C-----------------------------------------------------------------
      DO 200 I=1,1368
      DO 210 J=1,73
      ANO(I,J)=DATA(I,J)-MEAN(I,J)
      ANO(I,(J+73))=DATA(I,(J+73))-MEAN(I,J)
      ANO(I,(J+146))=DATA(I,(J+146))-MEAN(I,J)
      ANO(I,(J+219))=DATA(I,(J+219))-MEAN(I,J)
      ANO(I,(J+292))=DATA(I,(J+292))-MEAN(I,J)
      ANO(I,(J+365))=DATA(I,(J+365))-MEAN(I,J)
      ANO(I,(J+438))=DATA(I,(J+438))-MEAN(I,J)
      ANO(I,(J+511))=DATA(I,(J+511))-MEAN(I,J)
      ANO(I,(J+584))=DATA(I,(J+584))-MEAN(I,J)
      ANO(I,(J+657))=DATA(I,(J+657))-MEAN(I,J)
      ANO(I,(J+730))=DATA(I,(J+730))-MEAN(I,J)
      ANO(I,(J+803))=DATA(I,(J+803))-MEAN(I,J)
      ANO(I,(J+876))=DATA(I,(J+876))-MEAN(I,J)
      ANO(I,(J+949))=DATA(I,(J+949))-MEAN(I,J)
      ANO(I,(J+1022))=DATA(I,(J+1022))-MEAN(I,J)
      ANO(I,(J+1095))=DATA(I,(J+1095))-MEAN(I,J)
      ANO(I,(J+1168))=DATA(I,(J+1168))-MEAN(I,J)
      ANO(I,(J+1241))=DATA(I,(J+1241))-MEAN(I,J)
      ANO(I,(J+1314))=DATA(I,(J+1314))-MEAN(I,J)
      ANO(I,(J+1387))=DATA(I,(J+1387))-MEAN(I,J)
```

```
      ANO(I,(J+1460))=DATA(I,(J+1460))-MEAN(I,J)
      ANO(I,(J+1533))=DATA(I,(J+1533))-MEAN(I,J)
 210  CONTINUE
 200  CONTINUE
C-----------------------------------------------------------------------
C     Now to write it all out to files
C-----------------------------------------------------------------------
      OPEN (UNIT=12,FORM='FORMATTED',STATUS='NEW',FILE=OUT1)
      DO 600 I=1,1368
      WRITE (12,7010)(DATA(I,J), J=1,1568)
 600  CONTINUE
 7010 FORMAT (1568F9.3)
      OPEN (UNIT=12,FORM='FORMATTED',STATUS='NEW',FILE=OUT2)
      DO 601 I=1,1368
      WRITE (12,7011)(ANO(I,J), J=1,1568)
 601  CONTINUE
 7011 FORMAT (1568F9.3)
      STOP
      END
```

```
PROGRAM TRENDS
C-----------------------------------------------------------------------
C     This program calculates the 3 month percentage anomalies for
C     drawing the sea level pressure percentage anomaly charts
C-----------------------------------------------------------------------
C     Written 30/08/97 by Richenda Houseago
C-----------------------------------------------------------------------
C     Declare Variables
C-----------------------------------------------------------------------
      INTEGER DATE(1600),A(260)
      REAL ANOM(1400,1600),PLUS(1400,20),MINUS(1400,20),X(1400,10)
      CHARACTER *10 INFI1
      CHARACTER *10 OUT1, OUT2
      DATA INFI1/'anoms.dat'/
      DATA INFI2/'grid.dat'/
      DATA OUT1/'+jfm80.dat'/
      DATA OUT2/'-jfm80.dat'/
      DATA OUT3/'+fma80.dat'/
      DATA OUT4/'-fma80.dat'/
      DATA OUT5/'+mam80.dat'/
      DATA OUT6/'-mam80.dat'/
      DATA OUT7/'+amj80.dat'/
      DATA OUT8/'-amj80.dat'/
      DATA OUT9/'+mjj80.dat'/
      DATA OUT10/'-mjj80.dat'/
      DATA OUT11/'+jja80.dat'/
      DATA OUT12/'-jja80.dat'/
      DATA OUT13/'+jas80.dat'/
      DATA OUT14/'-jas80.dat'/
      DATA OUT15/'+aso80.dat'/
      DATA OUT16/'-aso80.dat'/
      DATA OUT17/'+son80.dat'/
      DATA OUT18/'-son80.dat'/
      DATA OUT19/'+ond80.dat'/
      DATA OUT20/'-ond80.dat'/
      DATA OUT21/'+ndj81.dat'/
      DATA OUT22/'-ndj81.dat'/
      DATA OUT23/'+djf81.dat'/
      DATA OUT24/'-djf81.dat'/
      WRITE (6,1000)
 1000 FORMAT (//,5X,'The files have been read in')
C-----------------------------------------------------------------------
C     Procedure to read in data and rearrange it.
C-----------------------------------------------------------------------
      OPEN (UNIT=10,FORM='FORMATTED',STATUS='OLD',FILE=INFI1)
      DO 100 I=1,1368
      READ (10,1500) (ANOM(I,J), J=1,1568)
 100  CONTINUE
 1500 FORMAT (1568F9.3)
      OPEN (UNIT=10,FORM='FORMATTED',STATUS='OLD',FILE=INFI2)
      DO 150 I=1,1368
      READ (10,1550) (X(I,J), J=1,2)
 150  CONTINUE
 1550 FORMAT (F6.3,F6.3)
      DO 200 I=1,1368
      DO 201 J=512,529
      IF (ANOM(I,J).GE.0) THEN
      PLUS(I,1)=PLUS(I,1)+(100/18)
```

```
      ELSE
      MINUS(I,1)=MINUS(I,1)+(100/18)
      END IF
 201  CONTINUE
 200  CONTINUE
      DO 202 I=1,1368
      DO 203 J=518,535
      IF (ANOM(I,J).GE.0) THEN
      PLUS(I,2)=PLUS(I,2)+(100/18)
      ELSE
      MINUS(I,2)=MINUS(I,2)+(100/18)
      END IF
 203  CONTINUE
 202  CONTINUE
      DO 204 I=1,1368
      DO 205 J=524,541
      IF (ANOM(I,J).GE.0) THEN
      PLUS(I,3)=PLUS(I,3)+(100/18)
      ELSE
      MINUS(I,3)=MINUS(I,3)+(100/18)
      END IF
 205  CONTINUE
 204  CONTINUE
      DO 206 I=1,1368
      DO 207 J=530,547
      IF (ANOM(I,J).GE.0) THEN
      PLUS(I,4)=PLUS(I,4)+(100/18)
      ELSE
      MINUS(I,4)=MINUS(I,4)+(100/18)
      END IF
 207  CONTINUE
 206  CONTINUE
      DO 208 I=1,1368
      DO 209 J=536,553
      IF (ANOM(I,J).GE.0) THEN
      PLUS(I,5)=PLUS(I,5)+(100/18)
      ELSE
      MINUS(I,5)=MINUS(I,5)+(100/18)
      END IF
 209  CONTINUE
 208  CONTINUE
      DO 210 I=1,1368
      DO 211 J=542,559
      IF (ANOM(I,J).GE.0) THEN
      PLUS(I,6)=PLUS(I,6)+(100/18)
      ELSE
      MINUS(I,6)=MINUS(I,6)+(100/18)
      END IF
 211  CONTINUE
 210  CONTINUE
      DO 212 I=1,1368
      DO 213 J=548,566
      IF (ANOM(I,J).GE.0) THEN
      PLUS(I,7)=PLUS(I,7)+(100/19)
      ELSE
      MINUS(I,7)=MINUS(I,7)+(100/19)
      END IF
 213  CONTINUE
```

```
 212  CONTINUE
      DO 214 I=1,1368
      DO 215 J=554,572
      IF (ANOM(I,J).GE.0) THEN
      PLUS(I,8)=PLUS(I,8)+(100/19)
      ELSE
      MINUS(I,8)=MINUS(I,8)+(100/19)
      END IF
 215  CONTINUE
 214  CONTINUE
      DO 216 I=1,1368
      DO 217 J=560,578
      IF (ANOM(I,J).GE.0) THEN
      PLUS(I,9)=PLUS(I,9)+(100/19)
      ELSE
      MINUS(I,9)=MINUS(I,9)+(100/19)
      END IF
 217  CONTINUE
 216  CONTINUE
      DO 218 I=1,1368
      DO 219 J=567,584
      IF (ANOM(I,J).GE.0) THEN
      PLUS(I,10)=PLUS(I,10)+(100/18)
      ELSE
      MINUS(I,10)=MINUS(I,10)+(100/18)
      END IF
 219  CONTINUE
 218  CONTINUE
      DO 220 I=1,1368
      DO 221 J=573,590
      IF (ANOM(I,J).GE.0) THEN
      PLUS(I,11)=PLUS(I,11)+(100/18)
      ELSE
      MINUS(I,11)=MINUS(I,11)+(100/18)
      END IF
 221  CONTINUE
 220  CONTINUE
      DO 222 I=1,1368
      DO 223 J=579,596
      IF (ANOM(I,J).GE.0) THEN
      PLUS(I,12)=PLUS(I,12)+(100/18)
      ELSE
      MINUS(I,12)=MINUS(I,12)+(100/18)
      END IF
 223  CONTINUE
 222  CONTINUE
      WRITE (6,3000)
 3000 FORMAT (//,5X,'Pluses and minuses have been calculated')
C-----------------------------------------------------------------
C     Procedure to read data out to files
C-----------------------------------------------------------------
      OPEN (UNIT=12,FORM='FORMATTED',STATUS='NEW',FILE=OUT1)
      DO 600 I=1,1368
      WRITE (12,7010) (X(I,J), J=1,2),PLUS(I,1)
 600  CONTINUE
 7010 FORMAT (F7.3,F7.3,F9.3)
      OPEN (UNIT=12,FORM='FORMATTED',STATUS='NEW',FILE=OUT2)
      DO 601 I=1,1368
```

```
      WRITE (12,7011) (X(I,J), J=1,2),MINUS(I,1)
 601  CONTINUE
 7011 FORMAT (F7.3,F7.3,F9.3)
      OPEN (UNIT=12,FORM='FORMATTED',STATUS='NEW',FILE=OUT3)
      DO 603 I=1,1368
      WRITE (12,7013) (X(I,J), J=1,2),PLUS(I,2)
 603  CONTINUE
 7013 FORMAT (F7.3,F7.3,F9.3)
      OPEN (UNIT=12,FORM='FORMATTED',STATUS='NEW',FILE=OUT4)
      DO 604 I=1,1368
      WRITE (12,7014) (X(I,J), J=1,2),MINUS(I,2)
 604  CONTINUE
 7014 FORMAT (F7.3,F7.3,F9.3)
      OPEN (UNIT=12,FORM='FORMATTED',STATUS='NEW',FILE=OUT5)
      DO 605 I=1,1368
      WRITE (12,7010) (X(I,J), J=1,2),PLUS(I,3)
 605  CONTINUE
 7015 FORMAT (F7.3,F7.3,F9.3)
      OPEN (UNIT=12,FORM='FORMATTED',STATUS='NEW',FILE=OUT6)
      DO 606 I=1,1368
      WRITE (12,7015) (X(I,J), J=1,2),MINUS(I,3)
 606  CONTINUE
 7016 FORMAT (F7.3,F7.3,F9.3)
      OPEN (UNIT=12,FORM='FORMATTED',STATUS='NEW',FILE=OUT7)
      DO 607 I=1,1368
      WRITE (12,7017) (X(I,J), J=1,2),PLUS(I,4)
 607  CONTINUE
 7017 FORMAT (F7.3,F7.3,F9.3)
      OPEN (UNIT=12,FORM='FORMATTED',STATUS='NEW',FILE=OUT8)
      DO 608 I=1,1368
      WRITE (12,7018) (X(I,J), J=1,2),MINUS(I,4)
 608  CONTINUE
 7018 FORMAT (F7.3,F7.3,F9.3)
      OPEN (UNIT=12,FORM='FORMATTED',STATUS='NEW',FILE=OUT9)
      DO 609 I=1,1368
      WRITE (12,7019) (X(I,J), J=1,2),PLUS(I,5)
 609  CONTINUE
 7019 FORMAT (F7.3,F7.3,F9.3)
      OPEN (UNIT=12,FORM='FORMATTED',STATUS='NEW',FILE=OUT10)
      DO 610 I=1,1368
      WRITE (12,7020) (X(I,J), J=1,2),MINUS(I,5)
 610  CONTINUE
 7020 FORMAT (F7.3,F7.3,F9.3)
      OPEN (UNIT=12,FORM='FORMATTED',STATUS='NEW',FILE=OUT11)
      DO 611 I=1,1368
      WRITE (12,7021) (X(I,J), J=1,2),PLUS(I,6)
 611  CONTINUE
 7021 FORMAT (F7.3,F7.3,F9.3)
      OPEN (UNIT=12,FORM='FORMATTED',STATUS='NEW',FILE=OUT12)
      DO 612 I=1,1368
      WRITE (12,7022) (X(I,J), J=1,2),MINUS(I,6)
 612  CONTINUE
 7022 FORMAT (F7.3,F7.3,F9.3)
      OPEN (UNIT=12,FORM='FORMATTED',STATUS='NEW',FILE=OUT13)
      DO 613 I=1,1368
      WRITE (12,7023) (X(I,J), J=1,2),PLUS(I,7)
 613  CONTINUE
 7023 FORMAT (F7.3,F7.3,F9.3)
```

```
      OPEN (UNIT=12,FORM='FORMATTED',STATUS='NEW',FILE=OUT14)
      DO 614 I=1,1368
      WRITE (12,7024) (X(I,J), J=1,2),MINUS(I,7)
614   CONTINUE
7024  FORMAT (F7.3,F7.3,F9.3)
      OPEN (UNIT=12,FORM='FORMATTED',STATUS='NEW',FILE=OUT15)
      DO 615 I=1,1368
      WRITE (12,7025) (X(I,J), J=1,2),PLUS(I,8)
615   CONTINUE
7025  FORMAT (F7.3,F7.3,F9.3)
      OPEN (UNIT=12,FORM='FORMATTED',STATUS='NEW',FILE=OUT16)
      DO 616 I=1,1368
      WRITE (12,7026) (X(I,J), J=1,2),MINUS(I,8)
616   CONTINUE
7026  FORMAT (F7.3,F7.3,F9.3)
      OPEN (UNIT=12,FORM='FORMATTED',STATUS='NEW',FILE=OUT17)
      DO 617 I=1,1368
      WRITE (12,7027) (X(I,J), J=1,2),PLUS(I,9)
617   CONTINUE
7027  FORMAT (F7.3,F7.3,F9.3)
      OPEN (UNIT=12,FORM='FORMATTED',STATUS='NEW',FILE=OUT18)
      DO 618 I=1,1368
      WRITE (12,7028) (X(I,J), J=1,2),MINUS(I,9)
618   CONTINUE
7028  FORMAT (F7.3,F7.3,F9.3)
      OPEN (UNIT=12,FORM='FORMATTED',STATUS='NEW',FILE=OUT19)
      DO 619 I=1,1368
      WRITE (12,7029) (X(I,J), J=1,2),PLUS(I,10)
619   CONTINUE
7029  FORMAT (F7.3,F7.3,F9.3)
      OPEN (UNIT=12,FORM='FORMATTED',STATUS='NEW',FILE=OUT20)
      DO 620 I=1,1368
      WRITE (12,7030) (X(I,J), J=1,2),MINUS(I,10)
620   CONTINUE
7030  FORMAT (F7.3,F7.3,F9.3)
      OPEN (UNIT=12,FORM='FORMATTED',STATUS='NEW',FILE=OUT21)
      DO 621 I=1,1368
      WRITE (12,7031) (X(I,J), J=1,2),PLUS(I,11)
621   CONTINUE
7031  FORMAT (F7.3,F7.3,F9.3)
      OPEN (UNIT=12,FORM='FORMATTED',STATUS='NEW',FILE=OUT22)
      DO 622 I=1,1368
      WRITE (12,7032) (X(I,J), J=1,2),MINUS(I,11)
622   CONTINUE
7032  FORMAT (F7.3,F7.3,F9.3)
      OPEN (UNIT=12,FORM='FORMATTED',STATUS='NEW',FILE=OUT23)
      DO 623 I=1,1368
      WRITE (12,7033) (X(I,J), J=1,2),PLUS(I,12)
623   CONTINUE
7033  FORMAT (F7.3,F7.3,F9.3)
      OPEN (UNIT=12,FORM='FORMATTED',STATUS='NEW',FILE=OUT24)
      DO 624 I=1,1368
      WRITE (12,7034) (X(I,J), J=1,2),MINUS(I,12)
624   CONTINUE
7034  FORMAT (F7.3,F7.3,F9.3)
      STOP
      END
```

```
PROGRAM RESORT2
C-----------------------------------------------------------------
C     To Rearrange 5 daily anomaly data to draw Hovmöller diagrams
C-----------------------------------------------------------------
C     Written 05/10/97 by Richenda Houseago
C-----------------------------------------------------------------
C     Declare Variables
C-----------------------------------------------------------------
      INTEGER DATE(1600)
      REAL MON(1400,1600)
      INTEGER LAT(20)
      CHARACTER *10 INFI1
      CHARACTER *10 OUT1
      DATA INFI1/'anoms.dat'/
      DATA OUT1/'23091.DAT'/
C-----------------------------------------------------------------
C     Procedure to read anomaly data from the file
C-----------------------------------------------------------------
      OPEN (UNIT=10,FORM='FORMATTED',STATUS='OLD',FILE=INFI1)
      DO 100 I=1,1368
      READ (10,1500) (MON(I,J), J=1,1568)
 100  CONTINUE
 1500 FORMAT (1568F9.3)
      WRITE (6,1000)
 1000 FORMAT (//,5X,'The files have been read in')
C-----------------------------------------------------------------
C     Now to calculate the dates and latitudes
C-----------------------------------------------------------------
      DO 400 J=1,1568
      DATE(J)=J
 400  CONTINUE
      DO 200 I=1,19
      LAT(1)=0
      LAT(I)=LAT(I-1)+5
 200  CONTINUE
      WRITE (6,3000)
 3000 FORMAT (//,5X,'Dates and latitudes have been calculated')
C-----------------------------------------------------------------
C     Procedure to write the data out to a file
C-----------------------------------------------------------------
      OPEN (UNIT=12,FORM='FORMATTED',STATUS='NEW',FILE=OUT1)
      DO 600 J=1303,1522
      DO 601 I=1,19
      WRITE (12,7010) DATE(J),LAT(I),MON((((I-1)*72)+47),J)
 7010 FORMAT (2I3,F9.3)
 601  CONTINUE
 600  CONTINUE
      STOP
      END
```

```
PROGRAM RANKS
C-----------------------------------------------------------------------
C     This program ranks the 5 daily data used for harmonic analysis
C     and converts them into percentile ranks
C-----------------------------------------------------------------------
C     Written 16/10/97 by Richenda Houseago
C-----------------------------------------------------------------------
C     Declare Variables
C-----------------------------------------------------------------------
      INTEGER DATE(1600)
      REAL MON(1400,1600),MON1(1400,1600),PERC(1400,1600)
      INTEGER RANK(1400,1600),COUNT
      CHARACTER *10 INFI1
      CHARACTER *10 OUT1
      DATA INFI1/'anoms.dat'/
      DATA OUT1/'ranks.dat'/
      WRITE (6,1000)
 1000 FORMAT (//,5X,'The files have been read in')
C-----------------------------------------------------------------------
C     Procedure to read in data and rearrange it.
C-----------------------------------------------------------------------
      OPEN (UNIT=10,FORM='FORMATTED',STATUS='OLD',FILE=INFI1)
      DO 100 I=1,1368
      READ (10,1500) (MON(I,J), J=1,1533)
 100  CONTINUE
 1500 FORMAT (1533F9.3)
      DO 101 I=1,1368
      DO 102 J=1,1533
      MON1(I,J)=MON(I,J)
 102  CONTINUE
 101  CONTINUE
C-----------------------------------------------------------------------
C     Procedure to rank the variables
C-----------------------------------------------------------------------
      DO 200 I=1,1368
      DO 201 J=1,1533
      COUNT=0
      DO 202 K=1,1533
      IF (MON(I,J).GE.MON1(I,K)) THEN
      COUNT=COUNT+1
      ELSE
      COUNT=COUNT
      END IF
 202  CONTINUE
      RANK(I,J)=COUNT
 201  CONTINUE
 200  CONTINUE
      WRITE (6,1001)
 1001 FORMAT (5X,'The ranks have been calculated')
C-----------------------------------------------------------------------
C     Now to turn them into percentile ranks
C-----------------------------------------------------------------------
      DO 300 I=1,1368
      DO 301 J=1,1533
      PERC(I,J)=(RANK(I,J)*0.0652315)
 301  CONTINUE
 300  CONTINUE
```

```
      WRITE (6,1002)
 1002 FORMAT (5X,'The percentile ranks have been calculated')
C-----------------------------------------------------------------------
C     Now to write it out to a file
C-----------------------------------------------------------------------
      OPEN (UNIT=12,FORM='FORMATTED',STATUS='NEW',FILE=OUT1)
      DO 600 I=1,1368
      WRITE (12,7010) (PERC(I,J), J=1,1533)
 600  CONTINUE
 7010 FORMAT (1533F9.3)
      STOP
      END
```

```
PROGRAM HARMONICS
C-----------------------------------------------------------------------
C     This program has been written to perform Harmonic Analysis
C     on 5 day percentile ranked data.
C-----------------------------------------------------------------------
C     Written 16/10/97 by Richenda Houseago
C-----------------------------------------------------------------------
C     Declare variables
C-----------------------------------------------------------------------
      REAL RANK(1400,1600),A1(1400),B1(1400),C1(1400)
      REAL THETA(1400),V(1400),W(1400),SUMY(1400)
      REAL X(1400,1600),Y(1400,1600),SUMX(1400)
      INTEGER T(1600)
      CHARACTER *10 INFI1
      CHARACTER *11 OUT1
      DATA INFI1/'ranks.dat'/
      DATA OUT1/'1991har.dat'/
C-----------------------------------------------------------------------
C     Procedure to read ranked percentile data from the file
C-----------------------------------------------------------------------
      OPEN (UNIT=10,FORM='FORMATTED',STATUS='OLD',FILE=INFI1)
      DO 100 I=1,1224
      READ (10,1500) (RANK(I,J), J=1,1533)
 100  CONTINUE
 1500 FORMAT (1533F9.3)
      WRITE (6,1000)
 1000 FORMAT (//,5X,'The files have been read in')
C-----------------------------------------------------------------------
C     Now the harmonics calculations can begin
C-----------------------------------------------------------------------
      DO 200 I=1,1533
      T(I)=I
 200  CONTINUE
      DO 205 I=1,146
      V(I)=COS(T(I)*0.0430355)
      W(I)=SIN(T(I)*0.0430355)
 205  CONTINUE
      DO 206 I=1,1224
      DO 207 J=1,146
      X(I,J)=RANK(I,(J+1314))*V(J)
      Y(I,J)=RANK(I,(J+1314))*W(J)
 207  CONTINUE
 206  CONTINUE
C-----------------------------------------------------------------------
C     Now to add up the calculations
C-----------------------------------------------------------------------
      DO 210 I=1,1224
      DO 211 J=1,146
      SUMX(I)=SUMX(I)+X(I,J)
      SUMY(I)=SUMY(I)+Y(I,J)
 211  CONTINUE
 210  CONTINUE
      DO 220 I=1,1224
      A1(I)=SUMX(I)*0.0136986
      B1(I)=SUMY(I)*0.0136986
 220  CONTINUE
C-----------------------------------------------------------------------
```

```
C     Now to calculate the amplitude and direction of the arrows
C-----------------------------------------------------------------
      DO 230 I=1,1224
      C1(I)=((A1(I)**2)+(B1(I)**2))**.5
      THETA(I)=ATAN(B1(I)/A1(I))
 230  CONTINUE
      DO 240 I=1,1224
      IF (A1(I).GT.0) THEN
      THETA(I)=THETA(I)
      ELSE IF (A1(I).LT.0) THEN
      THETA(I)=THETA(I)+3.1415927
      ELSE IF (A1(I).EQ.0) THEN
      THETA(I)=1.5707963
      END IF
 240  CONTINUE
      WRITE (6,1002)
 1002 FORMAT (5X,'Now to write everything to a file')
C-----------------------------------------------------------------
C     Now to write the amplitudes and phases out to a file
C-----------------------------------------------------------------
      OPEN (UNIT=12,FORM='FORMATTED',STATUS='NEW',FILE=OUT1)
      DO 600 I=1,1224
      WRITE (12,7010) C1(I),THETA(I)
 600  CONTINUE
 7010 FORMAT (2F10.5)
      STOP
      END
```

```
PROGRAM GRADS
C-----------------------------------------------------------------------
C     This is to calculate U and V components to put into GrADS for
C     plotting Harmonic Dials
C-----------------------------------------------------------------------
C     Written 10/11/97 by Richenda Houseago
C-----------------------------------------------------------------------
C     Declare Variables
C-----------------------------------------------------------------------
      REAL X(1400),Y(1400),U(1400,2)
      INTEGER T(1600),Z(1400)
      CHARACTER *15 INFI1
      CHARACTER *14 OUT1
      DATA INFI1/'1991.dat'/
      DATA OUT1/'cl1991.dat'/
C-----------------------------------------------------------------------
C     Procedure to read in data and rearrange it.
C-----------------------------------------------------------------------
      OPEN (UNIT=10,FORM='FORMATTED',STATUS='OLD',FILE=INFI1)
      DO 100 I=1,1297
      READ (10,*) X(I),Y(I),Z(I)
 100  CONTINUE
C-----------------------------------------------------------------------
C     Y is theta, X is amplitude
C-----------------------------------------------------------------------
      DO 200 I=1,1368
      IF((Y(I).GE.(0)).AND.(Y(I).LT.(1.5707))) THEN
      U(I,1)=-(-X(I)*COS(Y(I)))
      U(I,2)=-(-X(I)*SIN(Y(I)))
      ELSE IF((Y(I).GE.(1.5707)).AND.(Y(I).LT.(3.1415))) THEN
      U(I,1)=-(X(I)*SIN(Y(I)-1.5707963))
      U(I,2)=-(-X(I)*COS(Y(I)-1.5707963))
      ELSE IF((Y(I).GE.(3.1415)).AND.(Y(I).LT.(4.7123))) THEN
      U(I,1)=-(X(I)*COS(Y(I)-3.1415927))
      U(I,2)=-(X(I)*SIN(Y(I)-3.1415927))
      ELSE IF((Y(I).GE.(4.7123)).AND.(Y(I).LT.(6.2831))) THEN
      U(I,1)=-(-X(I)*SIN(Y(I)-4.712389))
      U(I,2)=-(X(I)*COS(Y(I)-4.712389))
      ELSE IF((Y(I).GE.(6.2831)).AND.(Y(I).LT.(7.8538))) THEN
      U(I,1)=-(-X(I)*COS(Y(I)))
      U(I,2)=-(-X(I)*SIN(Y(I)))
      ELSE IF((Y(I).GE.(7.8538)).AND.(Y(I).LT.(9.4246))) THEN
      U(I,1)=-(X(I)*SIN(Y(I)-1.5707963))
      U(I,2)=-(-X(I)*COS(Y(I)-1.5707963))
      ELSE IF((Y(I).GE.(9.4246)).AND.(Y(I).LT.(10.995))) THEN
      U(I,1)=-(X(I)*COS(Y(I)-3.1415927))
      U(I,2)=-(X(I)*SIN(Y(I)-3.1415927))
      ELSE IF((Y(I).GE.(10.995)).AND.(Y(I).LT.(12.566))) THEN
      U(I,1)=-(-X(I)*SIN(Y(I)-4.712389))
      U(I,2)=-(X(I)*COS(Y(I)-4.712389))
      ELSE IF((Y(I).GE.(-12.566)).AND.(Y(I).LT.(-10.995))) THEN
      U(I,1)=-(-X(I)*COS(Y(I)))
      U(I,2)=-(-X(I)*SIN(Y(I)))
      ELSE IF((Y(I).GE.(-10.995)).AND.(Y(I).LT.(-9.4246))) THEN
      U(I,1)=-(X(I)*SIN(Y(I)-1.5707963))
      U(I,2)=-(-X(I)*COS(Y(I)-1.5707963))
      ELSE IF((Y(I).GE.(-9.4246)).AND.(Y(I).LT.(-7.8538))) THEN
```

```
      U(I,1)=-(X(I)*COS(Y(I)-3.1415927))
      U(I,2)=-(X(I)*SIN(Y(I)-3.1415927))
      ELSE IF((Y(I).GE.(-7.8538)).AND.(Y(I).LT.(-6.2831))) THEN
      U(I,1)=-(-X(I)*SIN(Y(I)-4.712389))
      U(I,2)=-(X(I)*COS(Y(I)-4.712389))
      ELSE IF((Y(I).GE.(-6.2831)).AND.(Y(I).LT.(-4.7123))) THEN
      U(I,1)=-(-X(I)*COS(Y(I)))
      U(I,2)=-(-X(I)*SIN(Y(I)))
      ELSE IF((Y(I).GE.(-4.7123)).AND.(Y(I).LT.(-3.1415))) THEN
      U(I,1)=-(X(I)*SIN(Y(I)-1.5707963))
      U(I,2)=-(-X(I)*COS(Y(I)-1.5707963))
      ELSE IF((Y(I).GE.(-3.1415)).AND.(Y(I).LT.(-1.5707))) THEN
      U(I,1)=-(X(I)*COS(Y(I)-3.1415927))
      U(I,2)=-(X(I)*SIN(Y(I)-3.1415927))
      ELSE IF((Y(I).GE.(-1.5707)).AND.(Y(I).LT.(0))) THEN
      U(I,1)=-(-X(I)*SIN(Y(I)-4.712389))
      U(I,2)=-(X(I)*COS(Y(I)-4.712389))
      ELSE
      U(I,1)=-999.99
      U(I,2)=-999.99
      END IF
 200  CONTINUE
      DO 301 I=1,1368
      U(I,3)=Z(I)
 301  CONTINUE
      WRITE (6,1002)
 1002 FORMAT (5X,'Now to write everything to a file')
C-----------------------------------------------------------------------
C     Now to write it out in binary to a file
C-----------------------------------------------------------------------
      OPEN (12,FILE=OUT1,FORM='UNFORMATTED',STATUS='NEW'
     1,ACCESS='DIRECT',RECL=1296)
      DO 601 J=1,3
      WRITE (12,REC=J) (U(I,J), I=1,1296)
 601  CONTINUE
      STOP
      END
```

```
PROGRAM SOUTH
C-----------------------------------------------------------------
C     This is a program to turn 5 daily 500 hPa height data into
C     southerly wind components using the geostrophic wind equation
C-----------------------------------------------------------------
C     Written 09/01/98 by Richenda Houseago
C-----------------------------------------------------------------
C     Declare variables
C-----------------------------------------------------------------
      REAL DATA(1400,1650),CORR(1400),DIFF(1400,1600),VG(1400,1600)
      INTEGER L(1400),LAT(1400),LEN(1400)
      CHARACTER *10 INFI1
      CHARACTER *10 OUT1
      DATA INFI1/'year.dat'/
      DATA OUT1/'south.dat'/
 1000 FORMAT (//,5X,'The variables have been declared')
C-----------------------------------------------------------------
C     Procedure to read in data and rearrange it.
C-----------------------------------------------------------------
      OPEN (UNIT=10,FORM='FORMATTED',STATUS='OLD',FILE=INFI1)
      DO 100 I=1,1368
      READ (10,1010) (DATA(I,J), J=1,1533)
 100  CONTINUE
 1010 FORMAT (1533F9.3)
      WRITE (6,3000)
 3000 FORMAT (//,5X,'The files have been read in')
C-----------------------------------------------------------------
C     Procedure to calculate the geostrophic wind
C-----------------------------------------------------------------
      DO 150 I=1,72
      LEN(I)=558700
      LEN(I+72)=556000
      LEN(I+144)=550000
      LEN(I+216)=539300
      LEN(I+288)=525000
      LEN(I+360)=507000
      LEN(I+432)=482850
      LEN(I+504)=457000
      LEN(I+576)=425000
      LEN(I+648)=394050
      LEN(I+720)=357970
      LEN(I+792)=319130
      LEN(I+864)=278430
      LEN(I+936)=238000
      LEN(I+1008)=190000
      LEN(I+1080)=143380
      LEN(I+1152)=94000
      LEN(I+1224)=48100
      LEN(I+1296)=0
 150  CONTINUE
      DO 160 I=1,72
      CORR(I)=((9.8)/(2*0.0000729*(0.0871557)))
      CORR(I+72)=((9.8)/(2*0.0000729*(0.1736481)))
      CORR(I+144)=((9.8)/(2*0.0000729*(0.258819)))
      CORR(I+216)=((9.8)/(2*0.0000729*(0.3420201)))
      CORR(I+288)=((9.8)/(2*0.0000729*(0.4226182)))
      CORR(I+360)=((9.8)/(2*0.0000729*(0.5)))
```

```
      CORR(I+432)=((9.8)/(2*0.0000729*(0.5735764)))
      CORR(I+504)=((9.8)/(2*0.0000729*(0.6427876)))
      CORR(I+576)=((9.8)/(2*0.0000729*(0.7071067)))
      CORR(I+648)=((9.8)/(2*0.0000729*(0.7660444)))
      CORR(I+720)=((9.8)/(2*0.0000729*(0.819152)))
      CORR(I+792)=((9.8)/(2*0.0000729*(0.8660254)))
      CORR(I+864)=((9.8)/(2*0.0000729*(0.9063077)))
      CORR(I+936)=((9.8)/(2*0.0000729*(0.9396926)))
      CORR(I+1008)=((9.8)/(2*0.0000729*(0.9659258)))
      CORR(I+1080)=((9.8)/(2*0.0000729*(0.9848077)))
      CORR(I+1152)=((9.8)/(2*0.0000729*(0.9961947)))
      CORR(I+1224)=((9.8)/(2*0.0000729*(1)))
 160  CONTINUE
      DO 180 I=1,72
      DO 181 J=1,1533
      DO 182 K=1,19
      IF (I.EQ.1) THEN
      DIFF((((K-1)*72)+I),J)=DATA((((((K-1)*72)+I)+71),J)
     1-DATA((((((K-1)*72)+I)+1),J)
      ELSE IF (I.EQ.72) THEN
      DIFF((((K-1)*72)+I),J)=DATA((((((K-1)*72)+I)-71),J)
     1-DATA((((((K-1)*72)+I)-1),J)
      ELSE
      DIFF((((K-1)*72)+I),J)=DATA((((((K-1)*72)+I)-1),J)
     1-DATA((((((K-1)*72)+I)+1),J)
      END IF
 182  CONTINUE
 181  CONTINUE
 180  CONTINUE
      DO 200 I=1,1224
      DO 201 J=1,1533
      VG(I,J)=CORR(I)*(DIFF((I+72),J)/LEN(I+72))
 201  CONTINUE
 200  CONTINUE
C-----------------------------------------------------------------------
C     Procedure to write it out to a file
C-----------------------------------------------------------------------
      OPEN (UNIT=12,FORM='FORMATTED',STATUS='NEW',FILE=OUT1)
      DO 600 I=1,1224
      WRITE (12,7010)(VG(I,J), J=1,1533)
 600  CONTINUE
 7010 FORMAT (1533F11.4)
      STOP
      END
```

```
PROGRAM WEST
C-----------------------------------------------------------------------
C     This is a program to convert 5 daily 500 hPa height data into
C     westerly wind data components using the geostrophic wind
C     components
C-----------------------------------------------------------------------
C     Written 09/01/98 by Richenda Houseago
C-----------------------------------------------------------------------
C     First to Declare Variables
C-----------------------------------------------------------------------
      REAL DATA(1400,1650),CORR(1400),DIFF(1400,1600),VG(1400,1600)
      INTEGER L(1400),LAT(1400),LEN(1400)
      CHARACTER *10 INFI1
      CHARACTER *10 OUT1
      DATA INFI1/'year.dat'/
      DATA OUT1/'west.dat'/
 1000 FORMAT (//,5X,'The variables have been declared')
C-----------------------------------------------------------------------
C     Procedure to read in data and rearrange it.
C-----------------------------------------------------------------------
      OPEN (UNIT=10,FORM='FORMATTED',STATUS='OLD',FILE=INFI1)
      DO 100 I=1,1368
      READ (10,1010) (DATA(I,J), J=1,1533)
 100  CONTINUE
 1010 FORMAT (1533F9.3)
      WRITE (6,3000)
 3000 FORMAT (//,5X,'The files have been read in')
C-----------------------------------------------------------------------
C     Procedure to calculate the westerly wind components
C-----------------------------------------------------------------------
      DO 150 I=1,1368
      L(I)=I
      LEN(I)=555670
 150  CONTINUE
      DO 160 I=1,72
      CORR(I)=-771209.81
      CORR(I+72)=((9.8)/(2*0.0000729*(-0.1736481)))
      CORR(I+144)=((9.8)/(2*0.0000729*(-0.258819)))
      CORR(I+216)=((9.8)/(2*0.0000729*(-0.3420201)))
      CORR(I+288)=((9.8)/(2*0.0000729*(-0.4226182)))
      CORR(I+360)=((9.8)/(2*0.0000729*(-0.5)))
      CORR(I+432)=((9.8)/(2*0.0000729*(-0.5735764)))
      CORR(I+504)=((9.8)/(2*0.0000729*(-0.6427876)))
      CORR(I+576)=((9.8)/(2*0.0000729*(-0.7071067)))
      CORR(I+648)=((9.8)/(2*0.0000729*(-0.7660444)))
      CORR(I+720)=((9.8)/(2*0.0000729*(-0.819152)))
      CORR(I+792)=((9.8)/(2*0.0000729*(-0.8660254)))
      CORR(I+864)=((9.8)/(2*0.0000729*(-0.9063077)))
      CORR(I+936)=((9.8)/(2*0.0000729*(-0.9396926)))
      CORR(I+1008)=((9.8)/(2*0.0000729*(-0.9659258)))
      CORR(I+1080)=((9.8)/(2*0.0000729*(-0.9848077)))
      CORR(I+1152)=((9.8)/(2*0.0000729*(-0.9961947)))
      CORR(I+1224)=((9.8)/(2*0.0000729*(-1)))
 160  CONTINUE
      DO 180 I=1,1224
      DO 181 J=1,1533
      DIFF(I,J)=(DATA((I+144),J)-DATA(I,J))
```

```
 181  CONTINUE
 180  CONTINUE
      DO 200 I=1,1224
      DO 201 J=1,1533
      VG(I,J)=CORR(I)*(DIFF(I,J)/LEN(I))
 201  CONTINUE
 200  CONTINUE
C-----------------------------------------------------------------------
C     Procedure to write data to a file
C-----------------------------------------------------------------------
      OPEN (UNIT=12,FORM='FORMATTED',STATUS='NEW',FILE=OUT1)
      DO 600 I=1,1224
      WRITE (12,7010)(VG(I,J), J=1,1533)
 600  CONTINUE
 7010 FORMAT (1533F11.4)
      STOP
      END
```

```
PROGRAM SPEEDS
C-----------------------------------------------------------------
C     This is a program written to convert 5 daily west and southerly
C     geostrophic wind components into wind speeds and wind speed
C     anomalies
C-----------------------------------------------------------------
C     Written 09/01/98 by Richenda Houseago
C-----------------------------------------------------------------
C     Declare variables
C-----------------------------------------------------------------
      REAL WEST(1400,1650),SOUTH(1400,1600),SPD(1400,1600)
      REAL MEAN(1400,1600),ANO(1400,1600)
      CHARACTER *10 INFI1
      CHARACTER *10 INFI2
      CHARACTER *10 OUT1
      CHARACTER *12 OUT2
      DATA INFI1/'west.dat'/
      DATA INFI2/'south.dat'/
      DATA OUT1/'speed.dat'/
      DATA OUT2/'spanoms.dat'/
 1000 FORMAT (//,5X,'The variables have been declared')
C-----------------------------------------------------------------
C     Procedure to read in data and rearrange it.
C-----------------------------------------------------------------
      OPEN (UNIT=10,FORM='FORMATTED',STATUS='OLD',FILE=INFI1)
      DO 100 I=1,1224
      READ (10,1010) (WEST(I,J), J=1,1533)
  100 CONTINUE
 1010 FORMAT (1533F11.4)
      OPEN (UNIT=10,FORM='FORMATTED',STATUS='OLD',FILE=INFI2)
      DO 101 I=1,1224
      READ (10,1011) (SOUTH(I,J), J=1,1533)
  101 CONTINUE
 1011 FORMAT (1533F11.4)
      WRITE (6,3000)
 3000 FORMAT (//,5X,'The files have been read in')
C-----------------------------------------------------------------
C     Procedure to calculate the wind speeds
C-----------------------------------------------------------------
      DO 200 I=1,1224
      DO 201 J=1,1533
      SPD(I,J)=SQRT((WEST(I,J)**2)+(SOUTH(I,J)**2))
  201 CONTINUE
  200 CONTINUE
C-----------------------------------------------------------------
C     Procedure to calculate the wind speed anomalies
C-----------------------------------------------------------------
      DO 109 I=1,1224
      DO 110 J=1,73
      MEAN(I,J)=(SPD(I,J)+SPD(I,(J+73))+SPD(I,(J+146))+
     1SPD(I,(J+219))+SPD(I,(J+292))+SPD(I,(J+365))+
     2SPD(I,(J+438))+SPD(I,(J+511))+SPD(I,(J+584))+
     3SPD(I,(J+657))+SPD(I,(J+730))+SPD(I,(J+803))+
     4SPD(I,(J+876))+SPD(I,(J+949))+SPD(I,(J+1022))+
     5SPD(I,(J+1095))+SPD(I,(J+1168))+SPD(I,(J+1241))+
     6SPD(I,(J+1314))+SPD(I,(J+1387))+SPD(I,(J+1460)))/21
  110 CONTINUE
```

```
 109  CONTINUE
      DO 209 I=1,1224
      DO 210 J=1,73
      ANO(I,J)=SPD(I,J)-MEAN(I,J)
      ANO(I,(J+73))=SPD(I,(J+73))-MEAN(I,J)
      ANO(I,(J+146))=SPD(I,(J+146))-MEAN(I,J)
      ANO(I,(J+219))=SPD(I,(J+219))-MEAN(I,J)
      ANO(I,(J+292))=SPD(I,(J+292))-MEAN(I,J)
      ANO(I,(J+365))=SPD(I,(J+365))-MEAN(I,J)
      ANO(I,(J+438))=SPD(I,(J+438))-MEAN(I,J)
      ANO(I,(J+511))=SPD(I,(J+511))-MEAN(I,J)
      ANO(I,(J+584))=SPD(I,(J+584))-MEAN(I,J)
      ANO(I,(J+657))=SPD(I,(J+657))-MEAN(I,J)
      ANO(I,(J+730))=SPD(I,(J+730))-MEAN(I,J)
      ANO(I,(J+803))=SPD(I,(J+803))-MEAN(I,J)
      ANO(I,(J+876))=SPD(I,(J+876))-MEAN(I,J)
      ANO(I,(J+949))=SPD(I,(J+949))-MEAN(I,J)
      ANO(I,(J+1022))=SPD(I,(J+1022))-MEAN(I,J)
      ANO(I,(J+1095))=SPD(I,(J+1095))-MEAN(I,J)
      ANO(I,(J+1168))=SPD(I,(J+1168))-MEAN(I,J)
      ANO(I,(J+1241))=SPD(I,(J+1241))-MEAN(I,J)
      ANO(I,(J+1314))=SPD(I,(J+1314))-MEAN(I,J)
      ANO(I,(J+1387))=SPD(I,(J+1387))-MEAN(I,J)
      ANO(I,(J+1460))=SPD(I,(J+1460))-MEAN(I,J)
 210  CONTINUE
 209  CONTINUE
C-----------------------------------------------------------------------
C     Procedure to write the data out to files
C-----------------------------------------------------------------------
      OPEN (UNIT=12,FORM='FORMATTED',STATUS='NEW',FILE=OUT1)
      DO 600 I=1,1224
      WRITE (12,7010)(SPD(I,J), J=1,1533)
 600  CONTINUE
 7010 FORMAT (1533F11.4)
      OPEN (UNIT=12,FORM='FORMATTED',STATUS='NEW',FILE=OUT2)
      DO 601 I=1,1224
      WRITE (12,7011)(ANO(I,J), J=1,1533)
 601  CONTINUE
 7011 FORMAT (1533F11.4)
      STOP
      END
```

```
PROGRAM WINDGRADS
C-----------------------------------------------------------------------
C     To convert 5 day wind components into vectors for use in GrADS
C-----------------------------------------------------------------------
C     Written 16/01/98 by Richenda Houseago
C-----------------------------------------------------------------------
C     Declare Variables
C-----------------------------------------------------------------------
      REAL A(1400,3500)
      CHARACTER *10 INFI1,INFI2
      CHARACTER *14 OUT1
      DATA INFI1/'west.dat'/
      DATA INFI2/'south.dat'/
      DATA OUT1/'winds.dat'/
C-----------------------------------------------------------------------
C     Procedure to read in data and rearrange it.
C-----------------------------------------------------------------------
      OPEN (UNIT=10,FORM='FORMATTED',STATUS='OLD',FILE=INFI1)
      DO 100 I=1,1224
      READ (10,1500) (A(I,J), J=1,1533)
 100  CONTINUE
 1500 FORMAT (1533F11.4)
      OPEN (UNIT=10,FORM='FORMATTED',STATUS='OLD',FILE=INFI2)
      DO 101 I=1,1224
      READ (10,1501) (A(I,J), J=1534,3066)
 101  CONTINUE
 1501 FORMAT (1533F11.4)
      WRITE (6,1000)
 1000 FORMAT (//,5X,'The files have been read in')
      WRITE (6,1002)
 1002 FORMAT (5X,'Now to write everything to a file')
C-----------------------------------------------------------------------
C     Now to write it out to a file
C-----------------------------------------------------------------------
      OPEN (12,FILE='winds.dat',FORM='UNFORMATTED',STATUS='NEW'
     1,ACCESS='DIRECT',RECL=1224)
      DO 600 J=1,3066
      WRITE (12,REC=J) (A(I,J), I=1,1224)
 600  CONTINUE
      STOP
      END
```

APPENDIX 2: SPATIAL ANOMALY CHARTS

These charts are for the percentage of positive and negative sea level pressure anomalies from 5 day data over three month periods from 1973 to 1994. The grey shading on the charts is indicative of whether there are over 60% of anomalies that are either positive or negative.

Percentage sea level pressure anomalies for three months. Grey shading indicates percentages greater than 60% in 10% bands

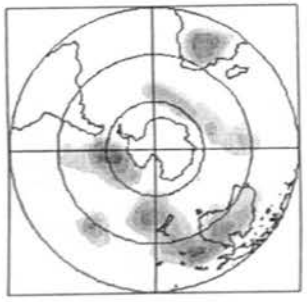

January to March 1973
Positive anomalies

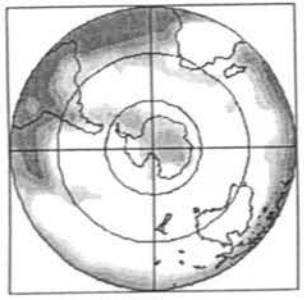

January to March 1973
Negative anomalies

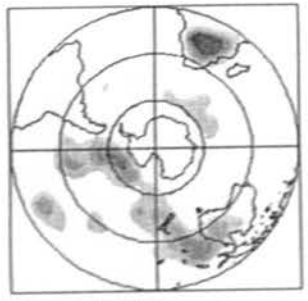

February to April 1973
Positive anomalies

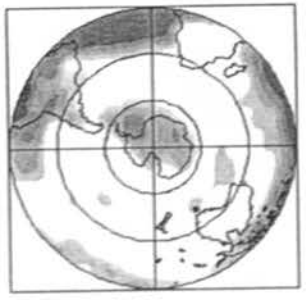

February to April 1973
Negative anomalies

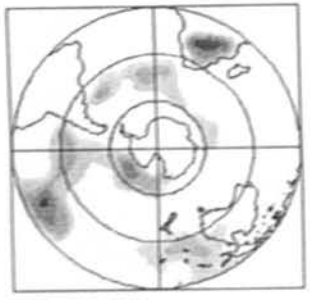

March to May 1973
Positive anomalies

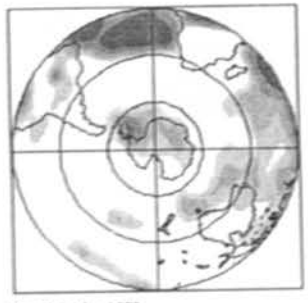

March to May 1973
Negative anomalies

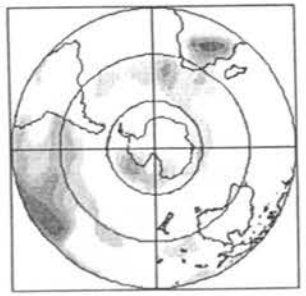

April to June 1973
Positive anomalies

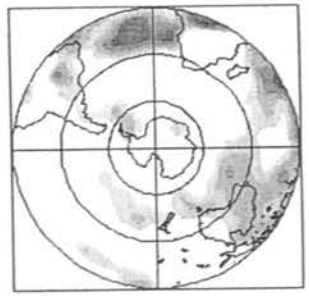

April to June 1973
Negative anomalies

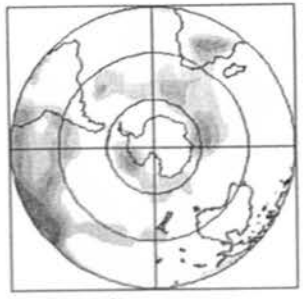

May to July 1973
Positive anomalies

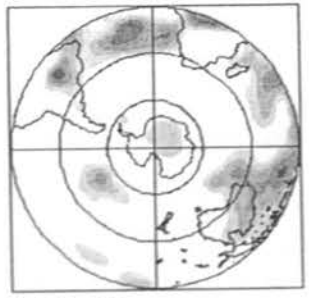

May to July 1973
Negative anomalies

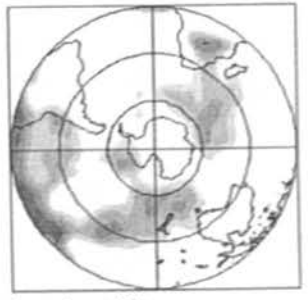

June to August 1973
Positive anomalies

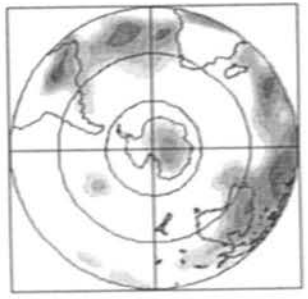

June to August 1973
Negative anomalies

Percentage sea level pressure anomalies for three months. Grey shading indicates percentages greater than 60% in 10% bands

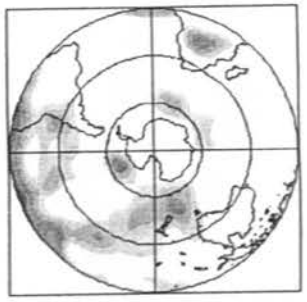

July to September 1973
Positive anomalies

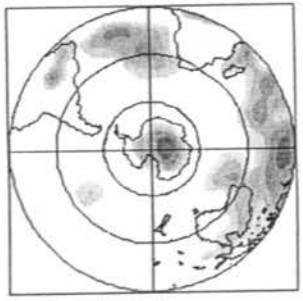

July to September 1973
Negative anomalies

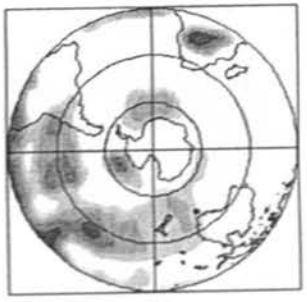

August to October 1973
Positive anomalies

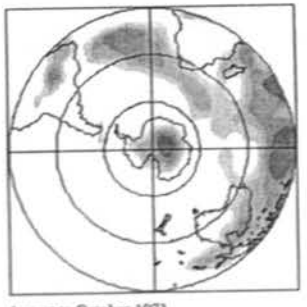

August to October 1973
Negative anomalies

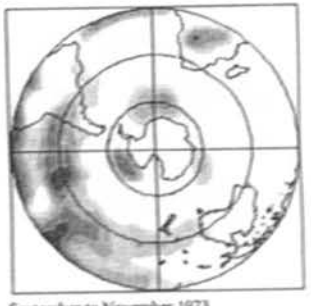

September to November 1973
Positive anomalies

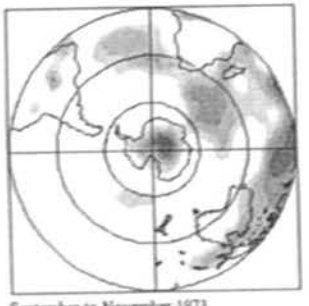

September to November 1973
Negative anomalies

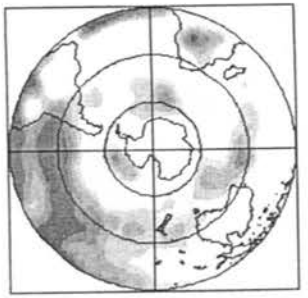

October to December 1973
Positive anomalies

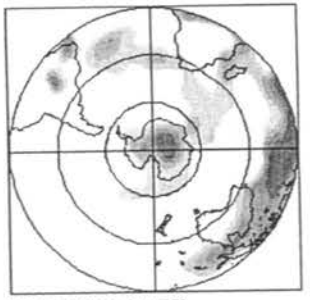

October to December 1973
Negative anomalies

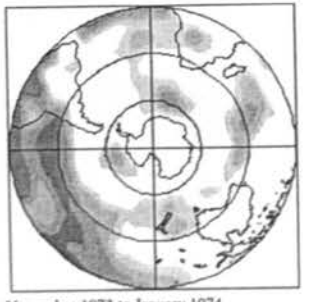

November 1973 to January 1974
Positive anomalies

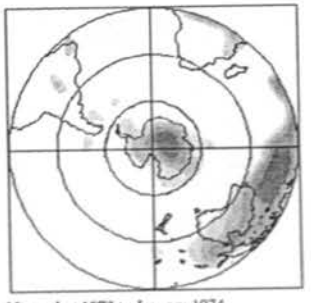

November 1973 to January 1974
Negative anomalies

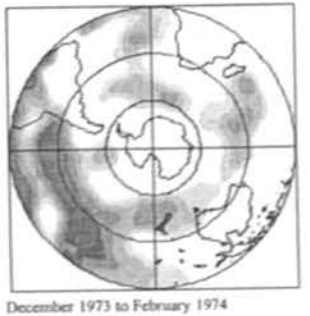

December 1973 to February 1974
Positive anomalies

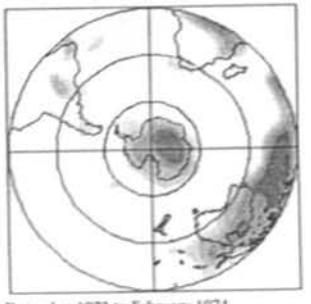

December 1973 to February 1974
Negative anomalies

Percentage sea level pressure anomalies for three months. Grey shading indicates percentages greater than 60% in 10% bands

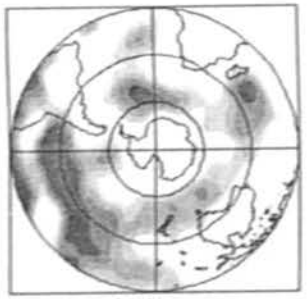

January to March 1974
Positive anomalies

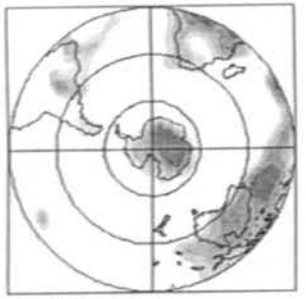

January to March 1974
Negative anomalies

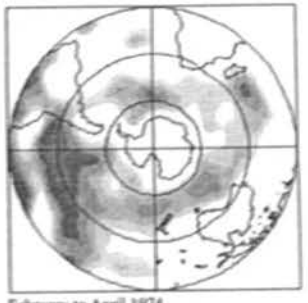

February to April 1974
Positive anomalies

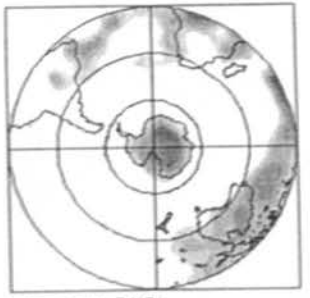

February to April 1974
Negative anomalies

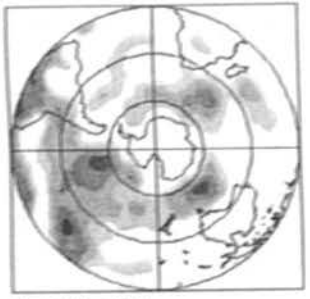

March to May 1974
Positive anomalies

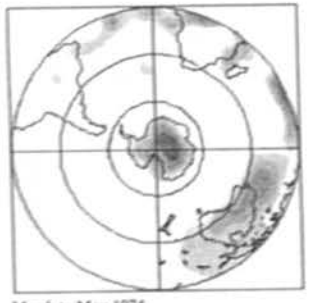

March to May 1974
Negative anomalies

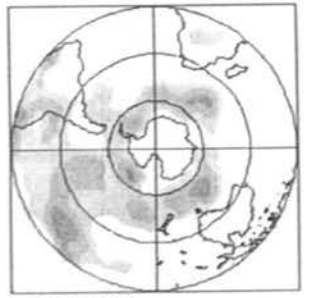

April to June 1974
Positive anomalies

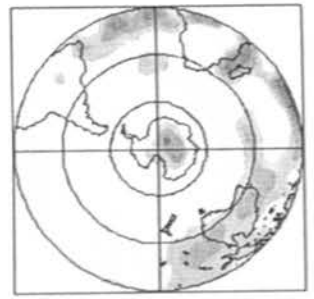

April to June 1974
Negative anomalies

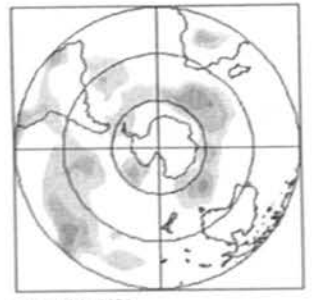

May to July 1974
Positive anomalies

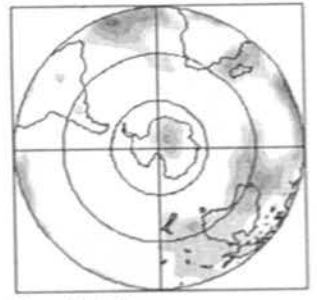

May to July 1974
Negative anomalies

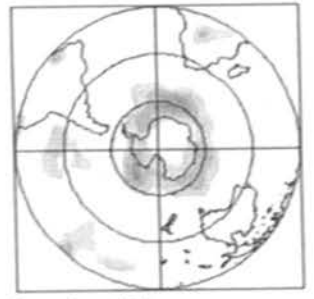

June to August 1974
Positive anomalies

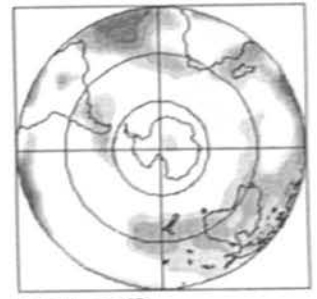

June to August 1974
Negative anomalies

Percentage sea level pressure anomalies for three months. Grey shading indicates percentages greater than 60% in 10% bands

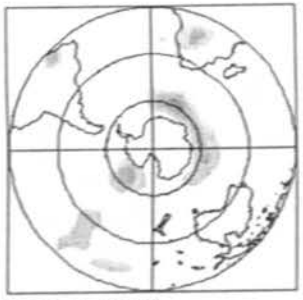

July to September 1974
Positive anomalies

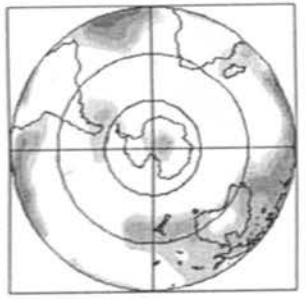

July to September 1974
Negative anomalies

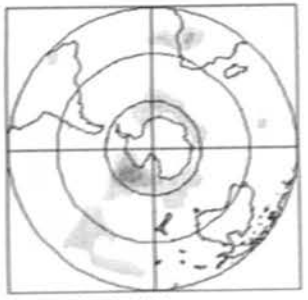

August to October 1974
Positive anomalies

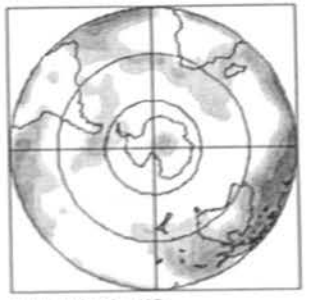

August to October 1974
Negative anomalies

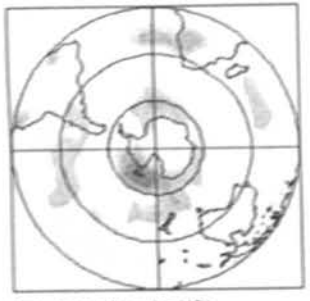

September to November 1974
Positive anomalies

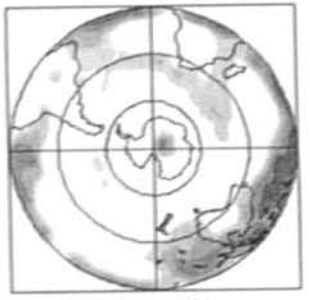

September to November 1974
Negative anomalies

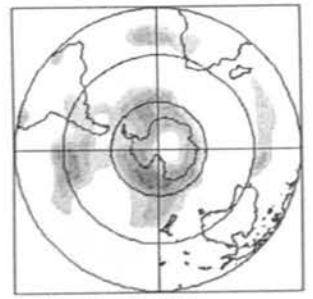

October to December 1974
Positive anomalies

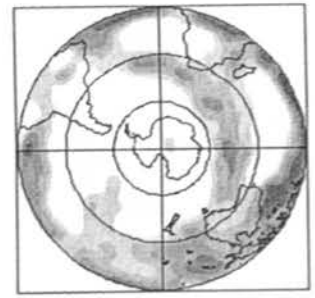

October to December 1974
Negative anomalies

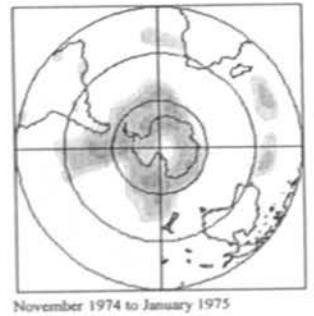

November 1974 to January 1975
Positive anomalies

November 1974 to January 1975
Negative anomalies

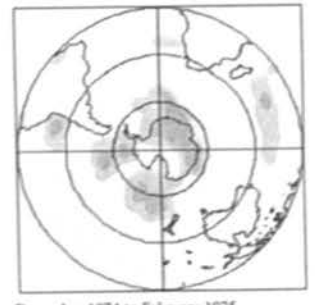

December 1974 to February 1975
Positive anomalies

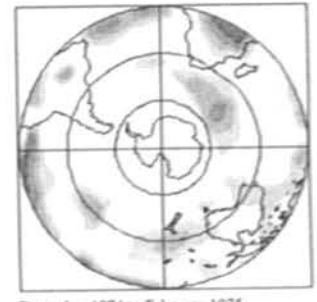

December 1974 to February 1975
Negative anomalies

Percentage sea level pressure anomalies for three months. Grey shading indicates percentages greater than 60% in 10% bands

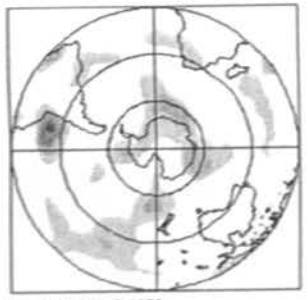

January to March 1975
Positive anomalies

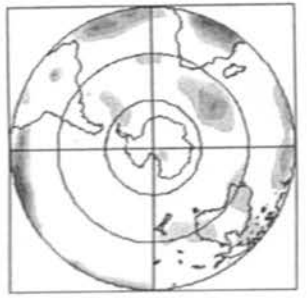

January to March 1975
Negative anomalies

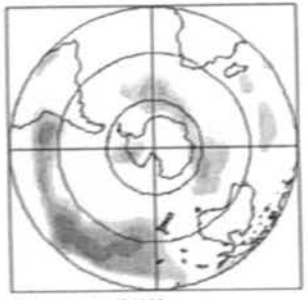

February to April 1975
Positive anomalies

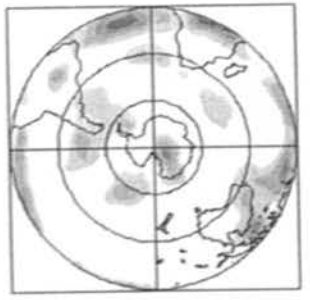

February to April 1975
Negative anomalies

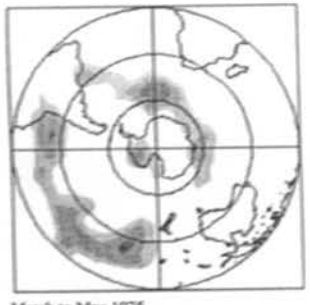

March to May 1975
Positive anomalies

March to May 1975
Negative anomalies

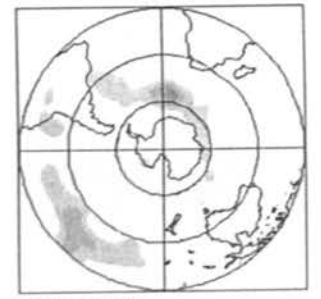

April to June 1975
Positive anomalies

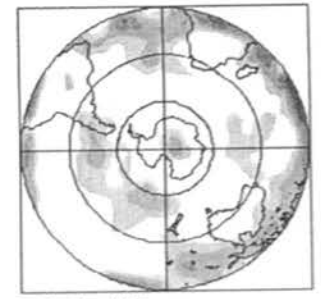

April to June 1975
Negative anomalies

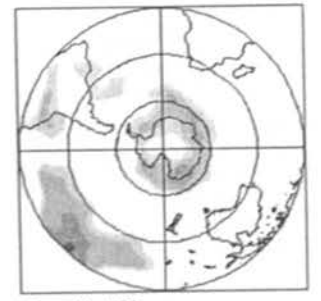

May to July 1975
Positive anomalies

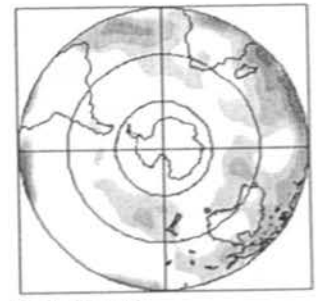

May to July 1975
Negative anomalies

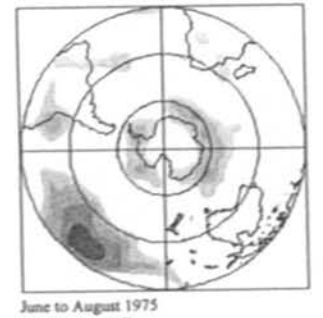

June to August 1975
Positive anomalies

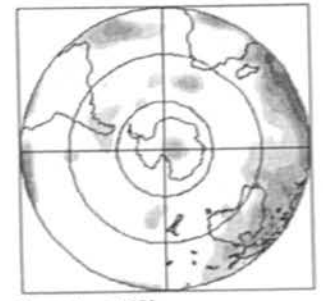

June to August 1975
Negative anomalies

Percentage sea level pressure anomalies for three months. Grey shading indicates percentages greater than 60% in 10% bands

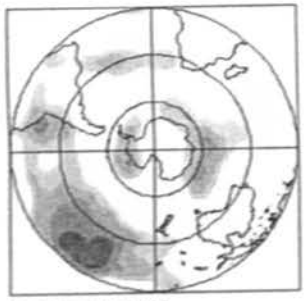

July to September 1975
Positive anomalies

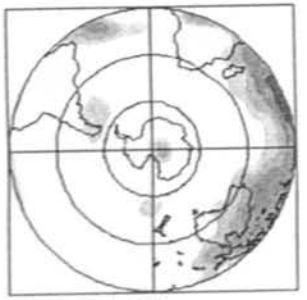

July to September 1975
Negative anomalies

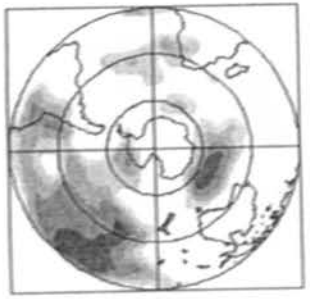

August to October 1975
Positive anomalies

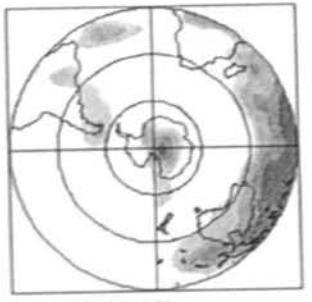

August to October 1975
Negative anomalies

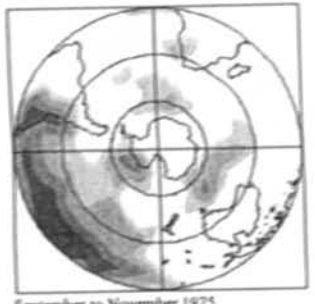

September to November 1975
Positive anomalies

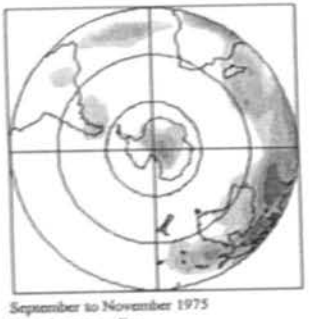

September to November 1975
Negative anomalies

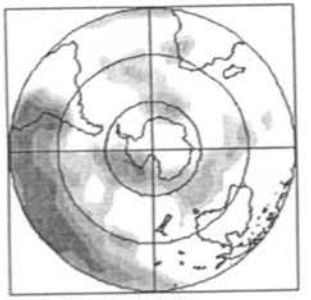

October to December 1975
Positive anomalies

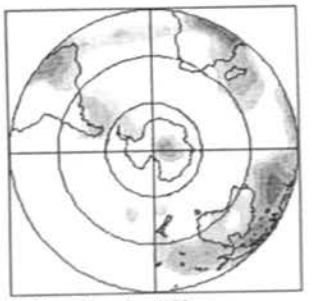

October to December 1975
Negative anomalies

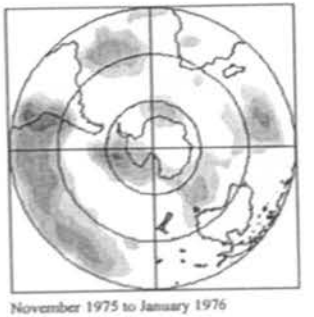

November 1975 to January 1976
Positive anomalies

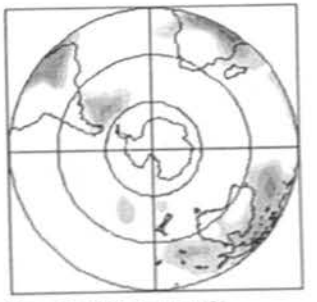

November 1975 to January 1976
Negative anomalies

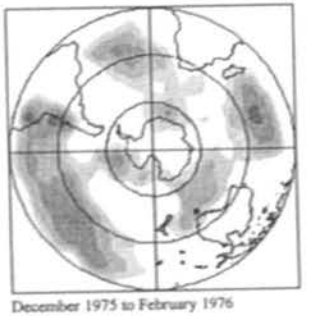

December 1975 to February 1976
Positive anomalies

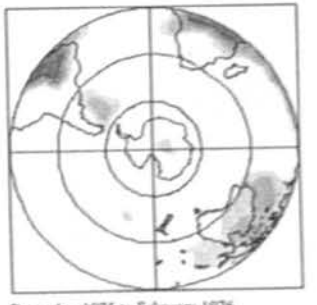

December 1975 to February 1976
Negative anomalies

Percentage sea level pressure anomalies for three months. Grey shading indicates percentages greater than 60% in 10% bands

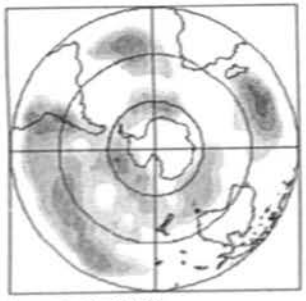

January to March 1976
Positive anomalies

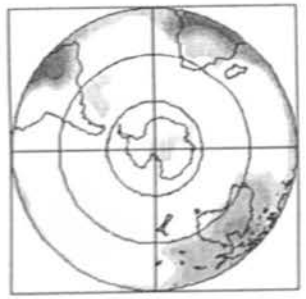

January to March 1976
Negative anomalies

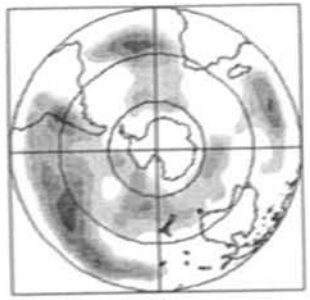

February to April 1976
Positive anomalies

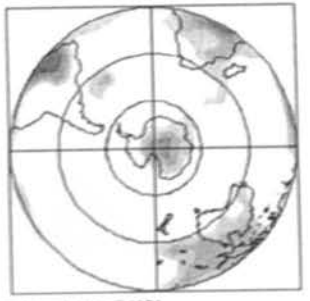

February to April 1976
Negative anomalies

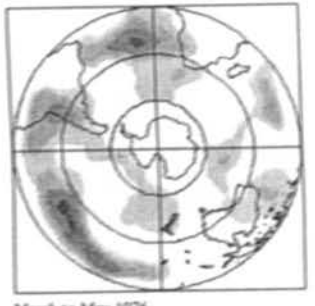

March to May 1976
Positive anomalies

March to May 1976
Negative anomalies

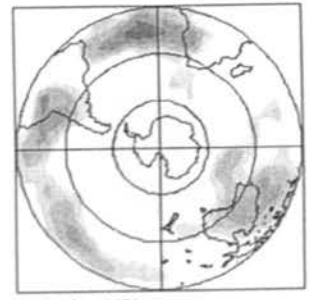

April to June 1976
Positive anomalies

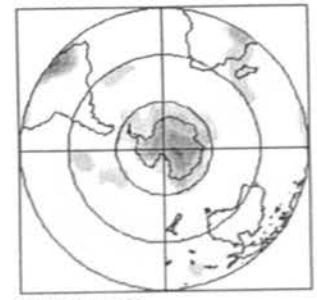

April to June 1976
Negative anomalies

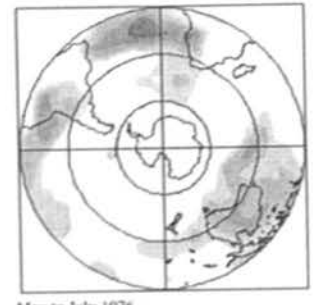

May to July 1976
Positive anomalies

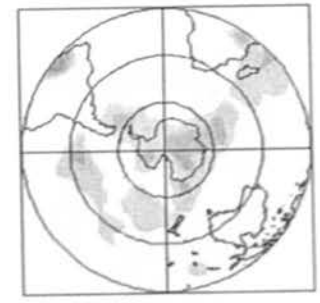

May to July 1976
Negative anomalies

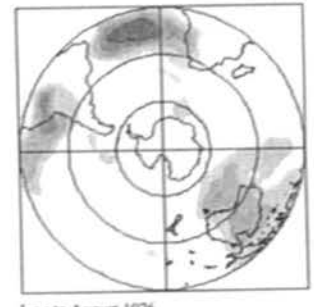

June to August 1976
Positive anomalies

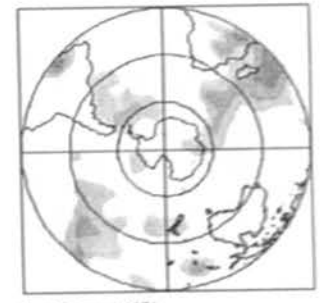

June to August 1976
Negative anomalies

Percentage sea level pressure anomalies for three months. Grey shading indicates percentages greater than 60% in 10% bands

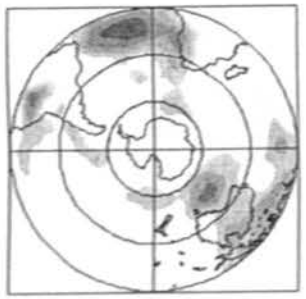

July to September 1976
Positive anomalies

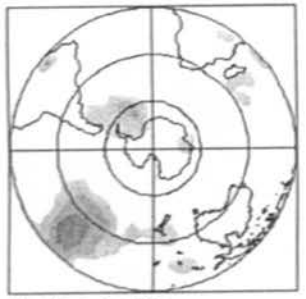

July to September 1976
Negative anomalies

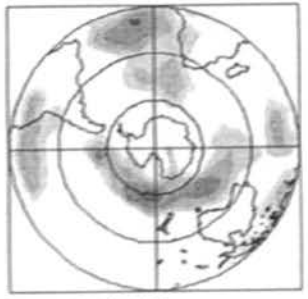

August to October 1973
Positive anomalies

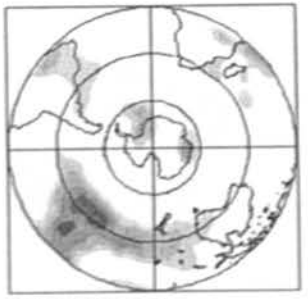

August to October 1973
Negative anomalies

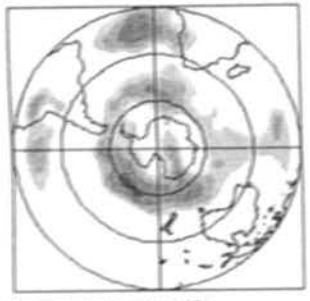

September to November 1976
Positive anomalies

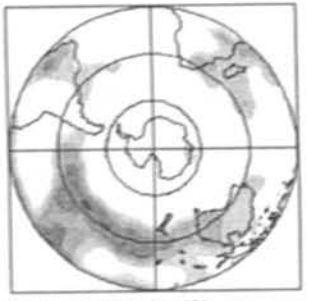

September to November 1976
Negative anomalies

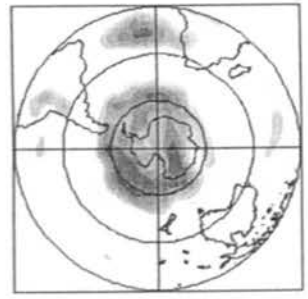

October to December 1976
Positive anomalies

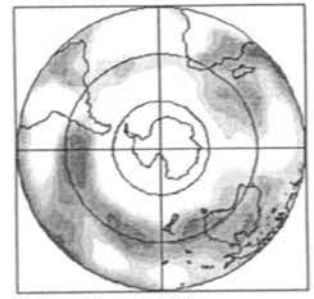

October to December 1976
Negative anomalies

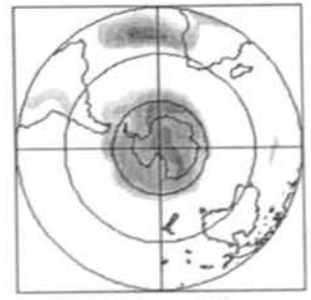

November 1976 to January 1977
Positive anomalies

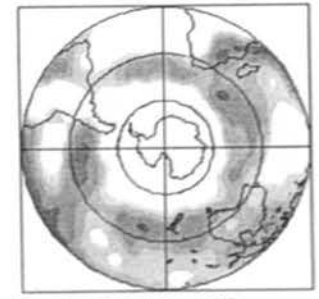

November 1976 to January 1977
Negative anomalies

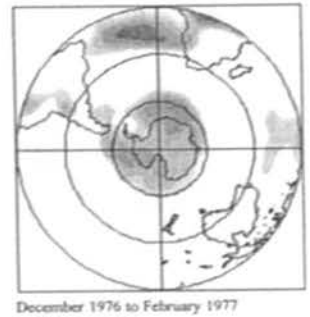

December 1976 to February 1977
Positive anomalies

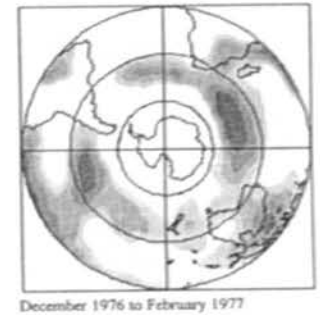

December 1976 to February 1977
Negative anomalies

Percentage sea level pressure anomalies for three months. Grey shading indicates percentages greater than 60% in 10% bands

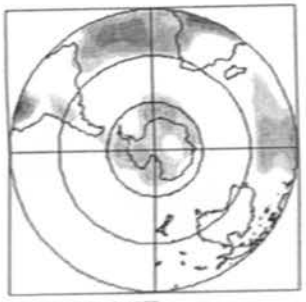

January to March 1977
Positive anomalies

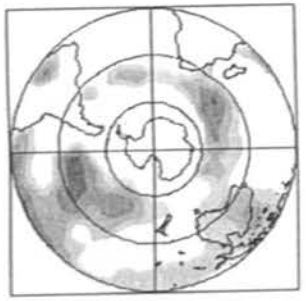

January to March 1977
Negative anomalies

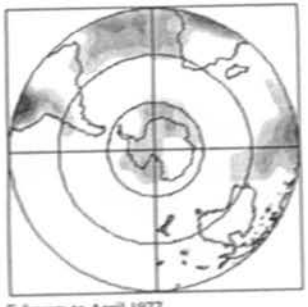

February to April 1977
Positive anomalies

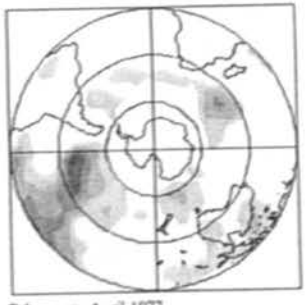

February to April 1977
Negative anomalies

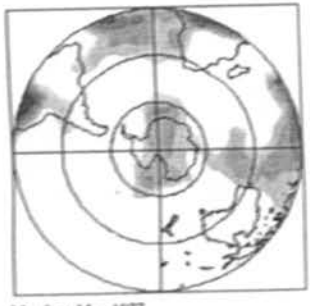

March to May 1977
Positive anomalies

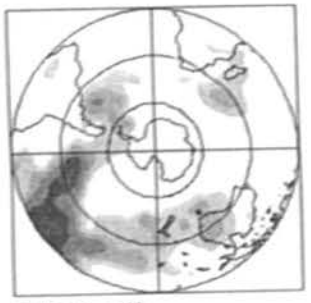

March to May 1977
Negative anomalies

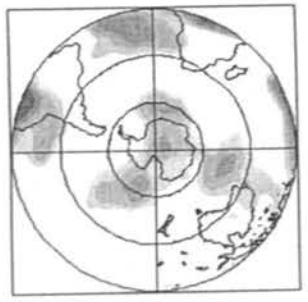

April to June 1977
Positive anomalies

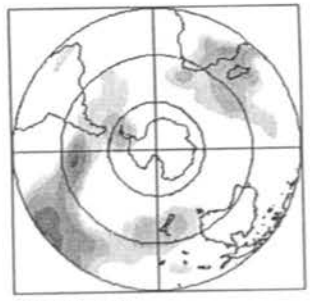

April to June 1977
Negative anomalies

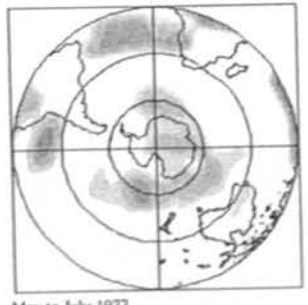

May to July 1977
Positive anomalies

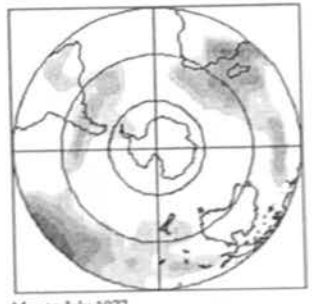

May to July 1977
Negative anomalies

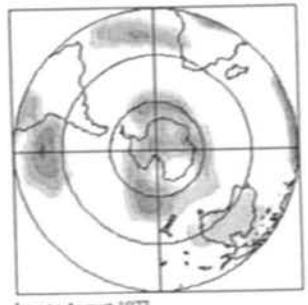

June to August 1977
Positive anomalies

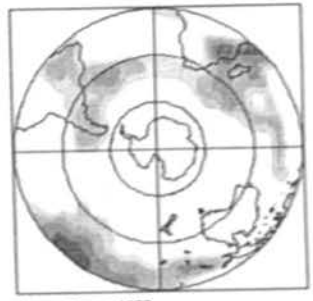

June to August 1977
Negative anomalies

Percentage sea level pressure anomalies for three months. Grey shading indicates percentages greater than 60% in 10% bands

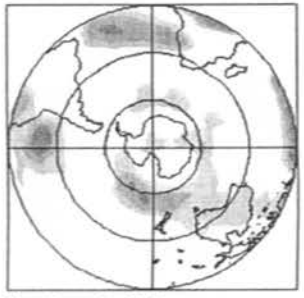

July to September 1977
Positive anomalies

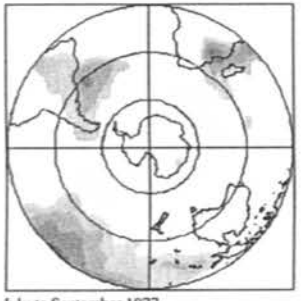

July to September 1977
Negative anomalies

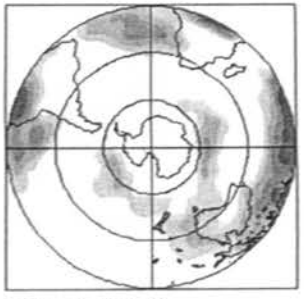

August to October 1977
Positive anomalies

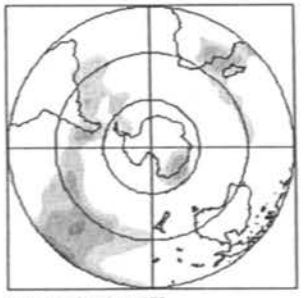

August to October 1977
Negative anomalies

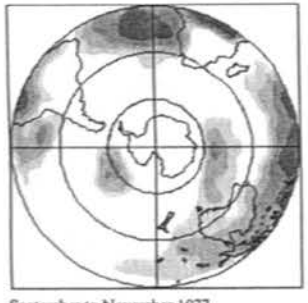

September to November 1977
Positive anomalies

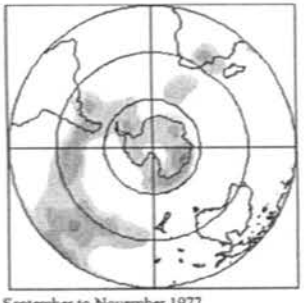

September to November 1977
Negative anomalies

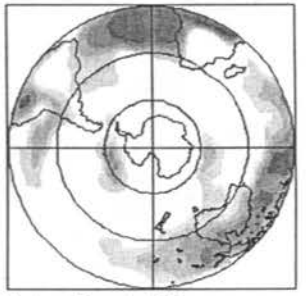

October to December 1977
Positive anomalies

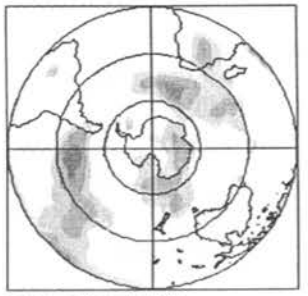

October to December 1977
Negative anomalies

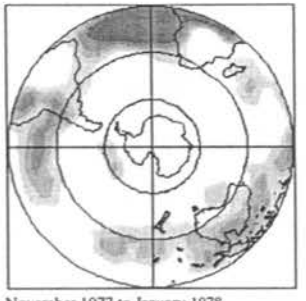

November 1977 to January 1978
Positive anomalies

November 1977 to January 1978
Negative anomalies

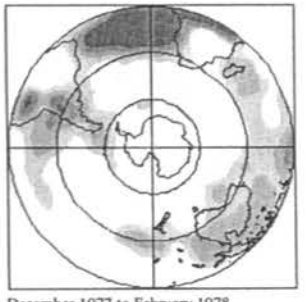

December 1977 to February 1978
Positive anomalies

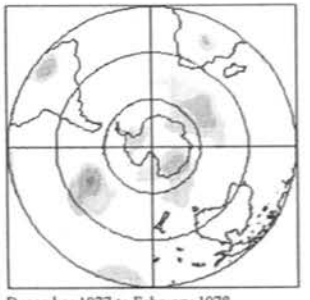

December 1977 to February 1978
Negative anomalies

91

Percentage sea level pressure anomalies for three months. Grey shading indicates percentages greater than 60% in 10% bands

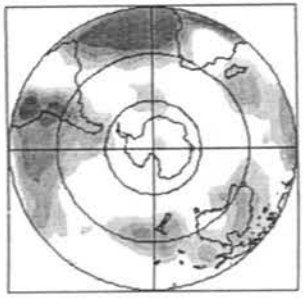

January to March 1978
Positive anomalies

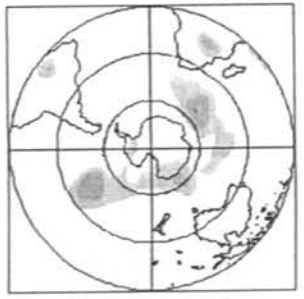

January to March 1978
Negative anomalies

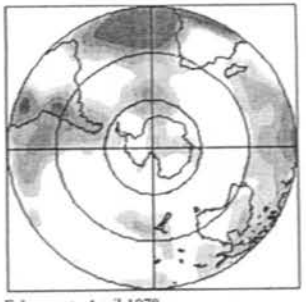

February to April 1978
Positive anomalies

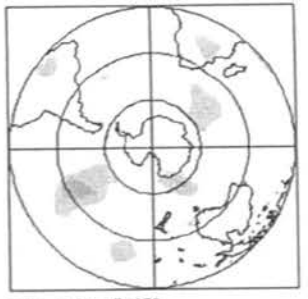

February to April 1978
Negative anomalies

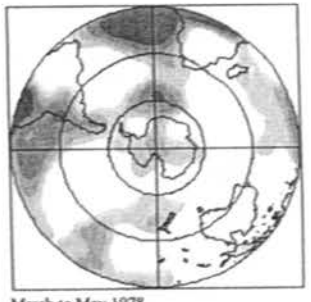

March to May 1978
Positive anomalies

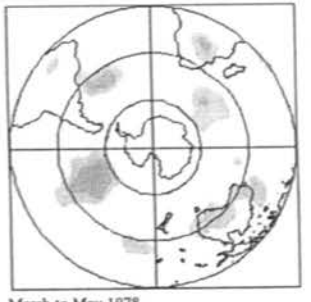

March to May 1978
Negative anomalies

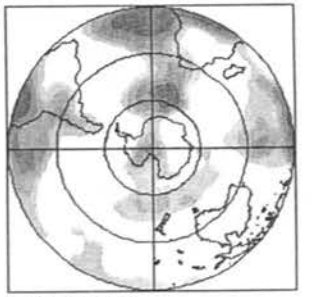

April to June 1978
Positive anomalies

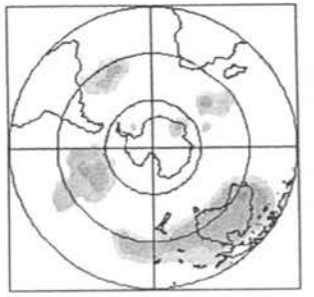

April to June 1978
Negative anomalies

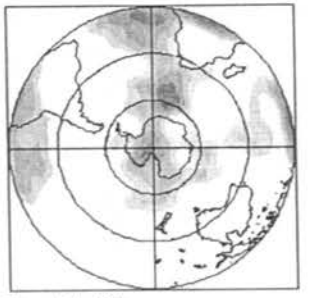

May to July 1978
Positive anomalies

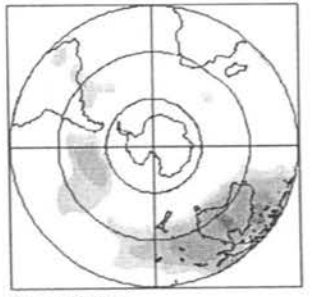

May to July 1978
Negative anomalies

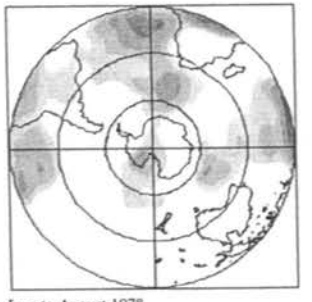

June to August 1978
Positive anomalies

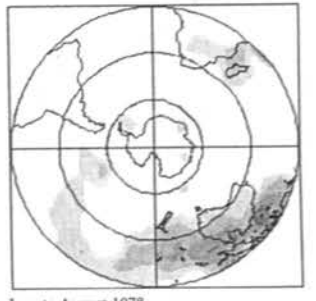

June to August 1978
Negative anomalies

Percentage sea level pressure anomalies for three months. Grey shading indicates percentages greater than 60% in 10% bands

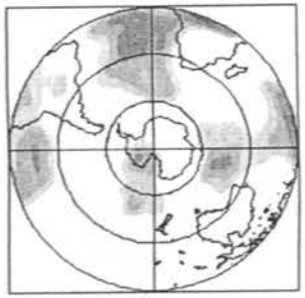

July to September 1978
Positive anomalies

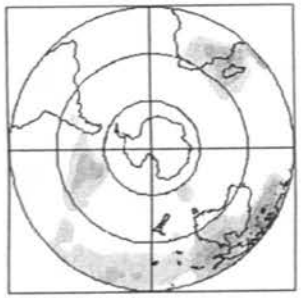

July to September 1978
Negative anomalies

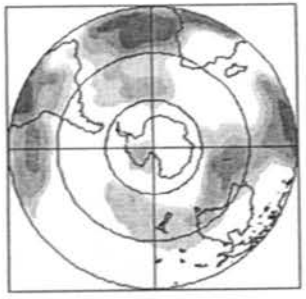

August to October 1978
Positive anomalies

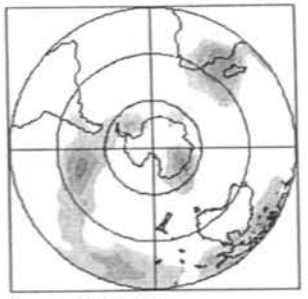

August to October 1978
Negative anomalies

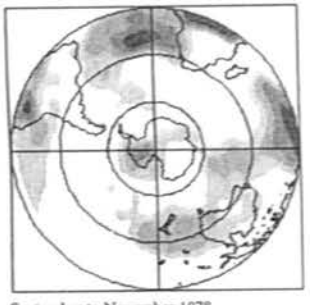

September to November 1978
Positive anomalies

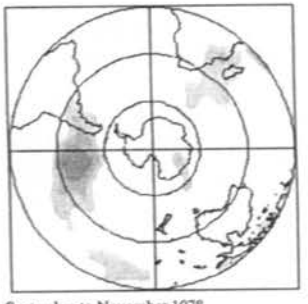

September to November 1978
Negative anomalies

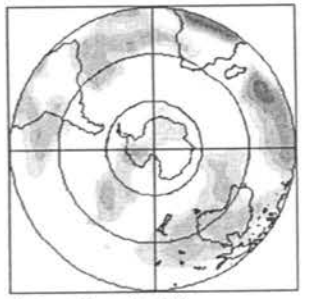

October to December 1978
Positive anomalies

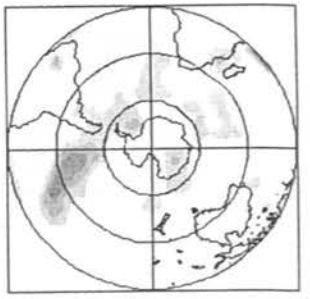

October to December 1978
Negative anomalies

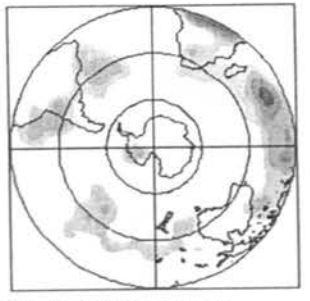

November 1978 to January 1979
Positive anomalies

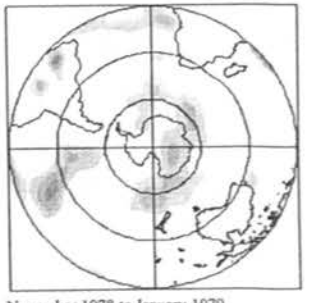

November 1978 to January 1979
Negative anomalies

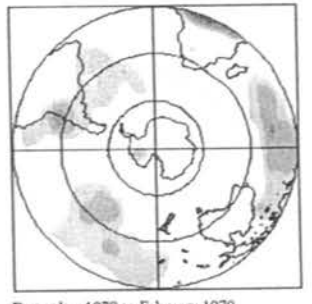

December 1978 to February 1979
Positive anomalies

December 1978 to February 1979
Negative anomalies

Percentage sea level pressure anomalies for three months. Grey shading indicates percentages greater than 60% in 10% bands

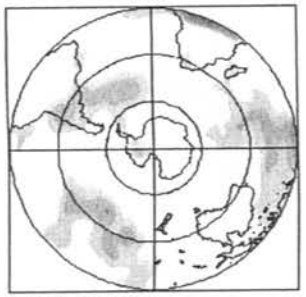

January to March 1979
Positive anomalies

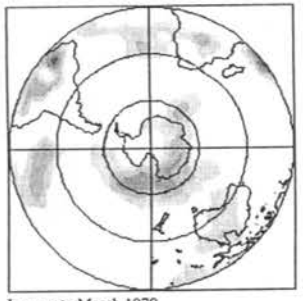

January to March 1979
Negative anomalies

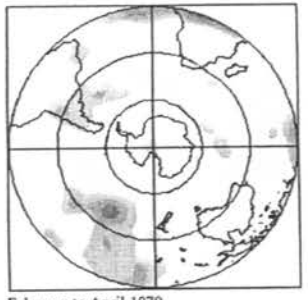

February to April 1979
Positive anomalies

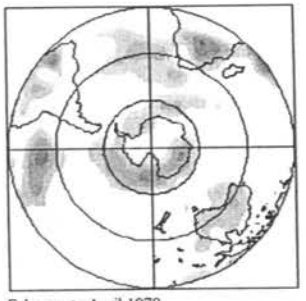

February to April 1979
Negative anomalies

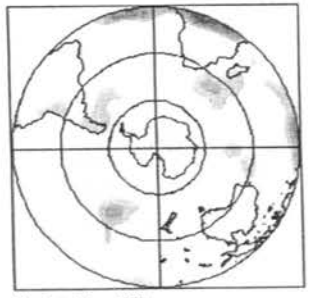

March to May 1979
Positive anomalies

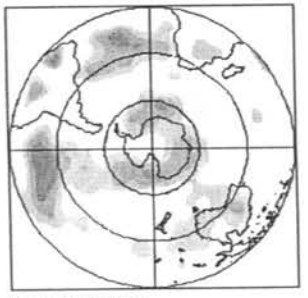

March to May 1979
Negative anomalies

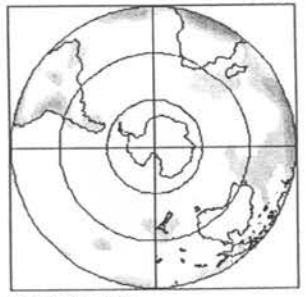

April to June 1979
Positive anomalies

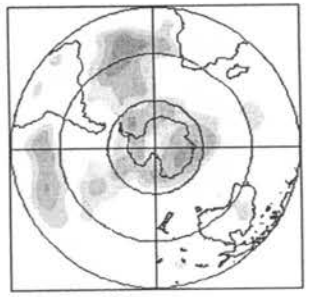

April to June 1979
Negative anomalies

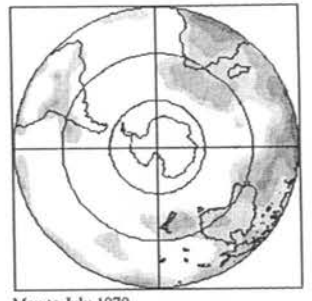

May to July 1979
Positive anomalies

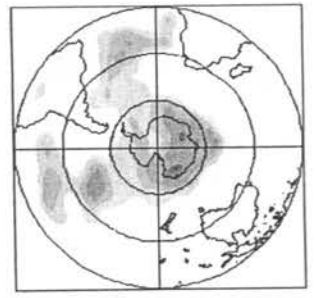

May to July 1979
Negative anomalies

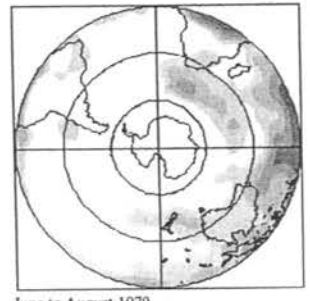

June to August 1979
Positive anomalies

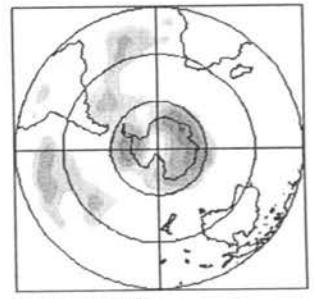

June to August 1979
Negative anomalies

13

Percentage sea level pressure anomalies for three months. Grey shading indicates percentages greater than 60% in 10% bands

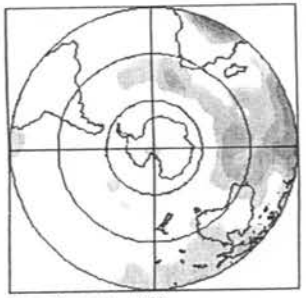

July to September 1979
Positive anomalies

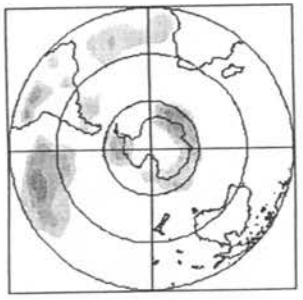

July to September 1979
Negative anomalies

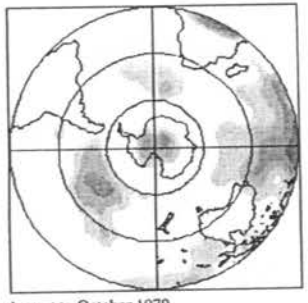

August to October 1979
Positive anomalies

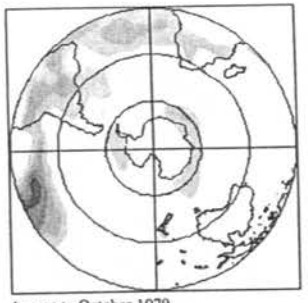

August to October 1979
Negative anomalies

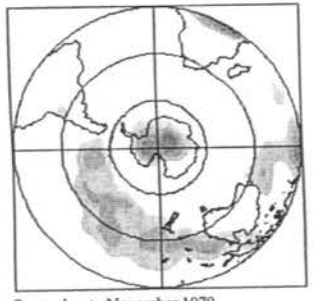

September to November 1979
Positive anomalies

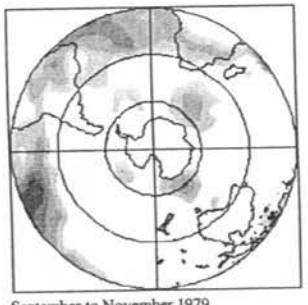

September to November 1979
Negative anomalies

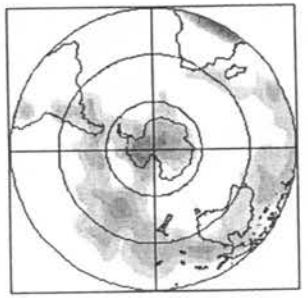

October to December 1979
Positive anomalies

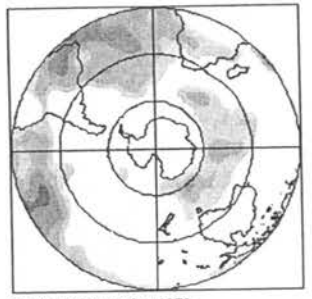

October to December 1979
Negative anomalies

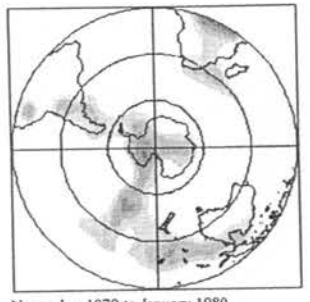

November 1979 to January 1980
Positive anomalies

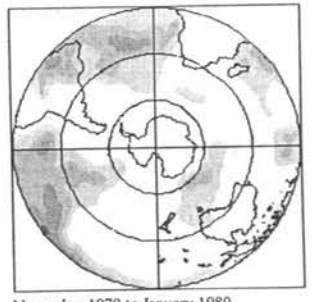

November 1979 to January 1980
Negative anomalies

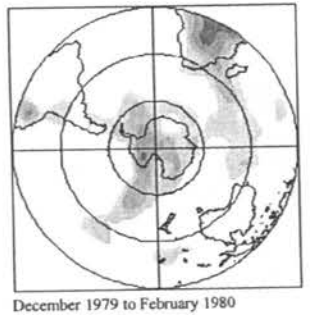

December 1979 to February 1980
Positive anomalies

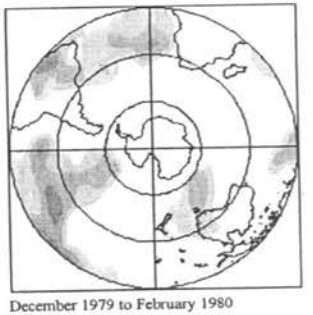

December 1979 to February 1980
Negative anomalies

41

Percentage sea level pressure anomalies for three months. Grey shading indicates percentages greater than 60% in 10% bands

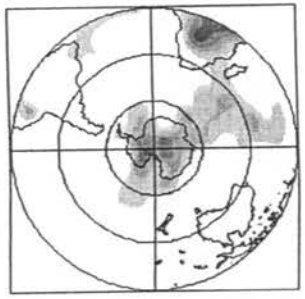

January to March 1980
Positive anomalies

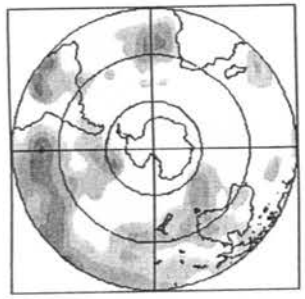

January to March 1980
Negative anomalies

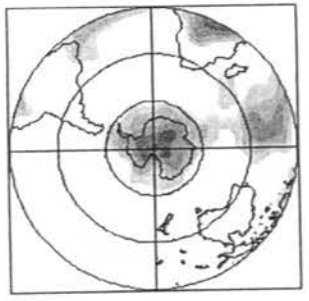

February to April 1980
Positive anomalies

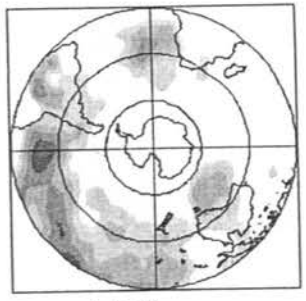

February to April 1980
Negative anomalies

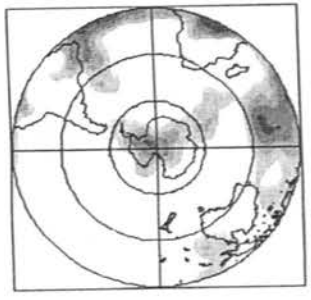

March to May 1980
Positive anomalies

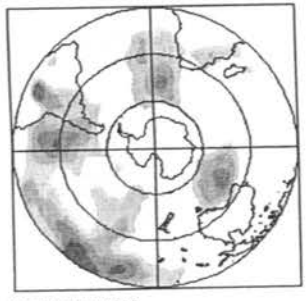

March to May 1980
Negative anomalies

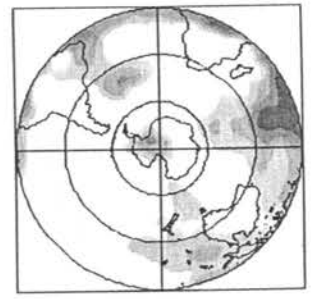

April to June 1980
Positive anomalies

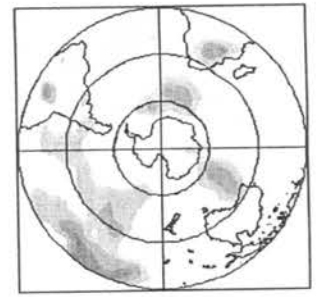

April to June 1980
Negative anomalies

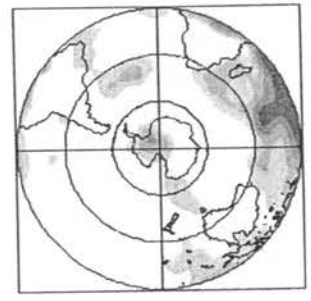

May to July 1980
Positive anomalies

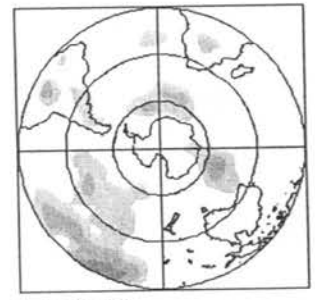

May to July 1980
Negative anomalies

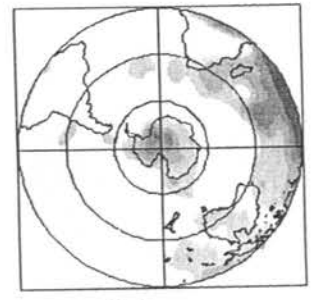

June to August 1980
Positive anomalies

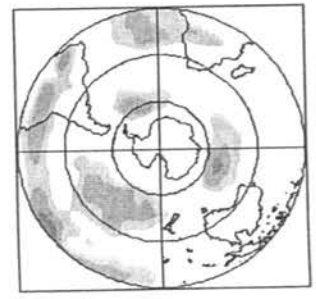

June to August 1980
Negative anomalies

15-1

Percentage sea level pressure anomalies for three months. Grey shading indicates percentages greater than 60% in 10% bands

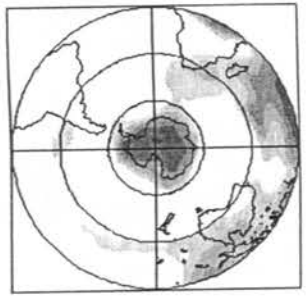

July to September 1980
Positive anomalies

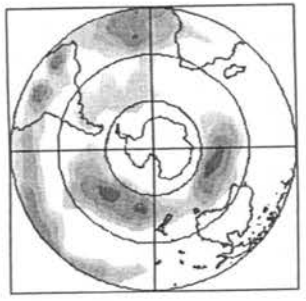

July to September 1980
Negative anomalies

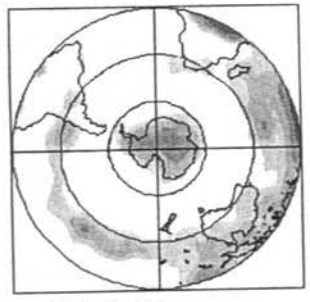

August to October 1980
Positive anomalies

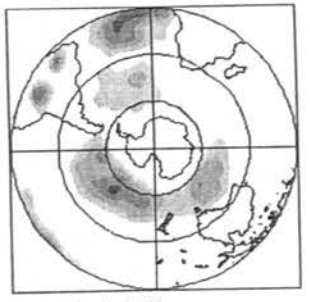

August to October 1980
Negative anomalies

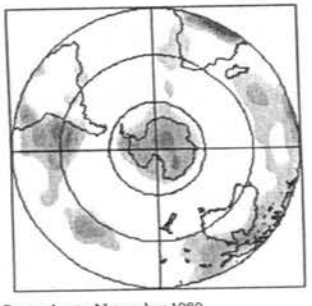

September to November 1980
Positive anomalies

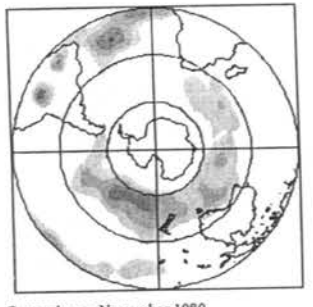

September to November 1980
Negative anomalies

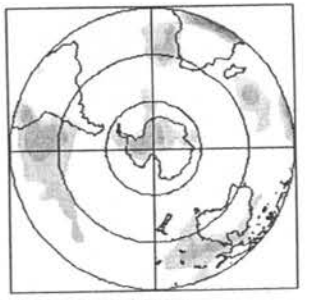

October to December 1980
Positive anomalies

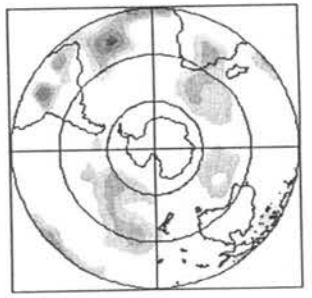

October to December 1980
Negative anomalies

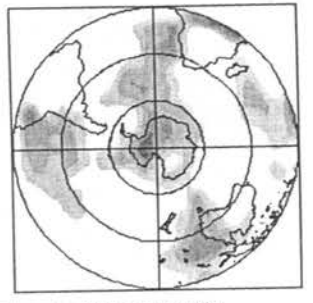

November 1980 to January 1981
Positive anomalies

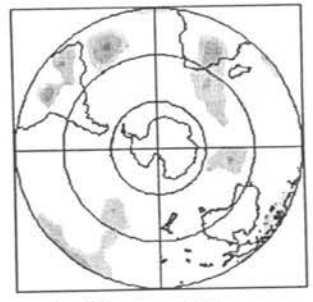

November 1980 to January 1981
Negative anomalies

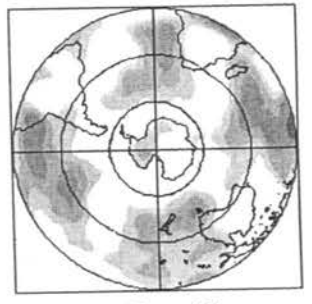

December 1980 to February 1981
Positive anomalies

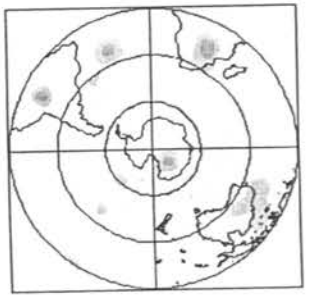

December 1980 to February 1981
Negative anomalies

91

Percentage sea level pressure anomalies for three months. Grey shading indicates percentages greater than 60% in 10% bands

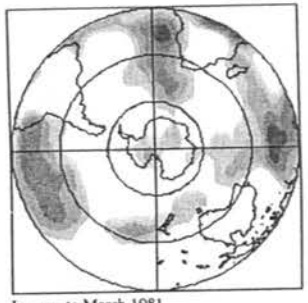

January to March 1981
Positive anomalies

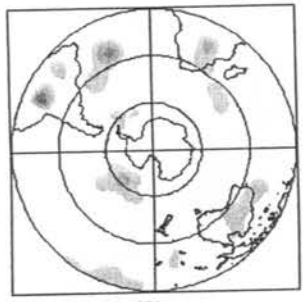

January to March 1981
Negative anomalies

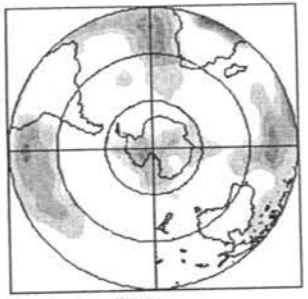

February to April 1981
Positive anomalies

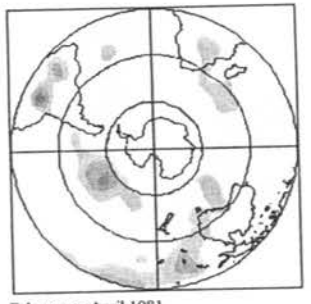

February to April 1981
Negative anomalies

March to May 1981
Positive anomalies

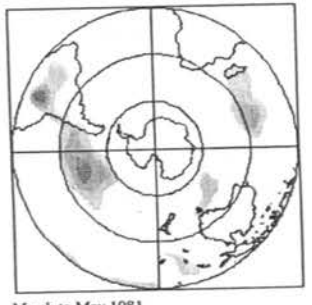

March to May 1981
Negative anomalies

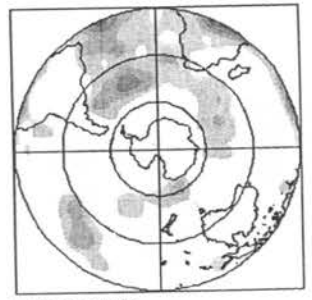

April to June 1981
Positive anomalies

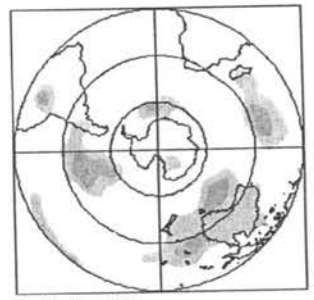

April to June 1981
Negative anomalies

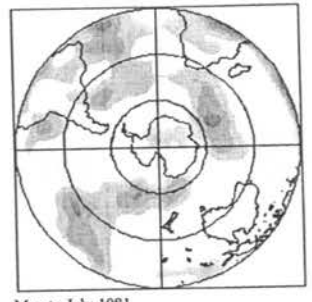

May to July 1981
Positive anomalies

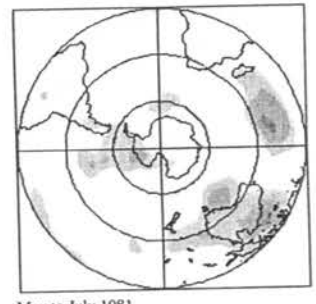

May to July 1981
Negative anomalies

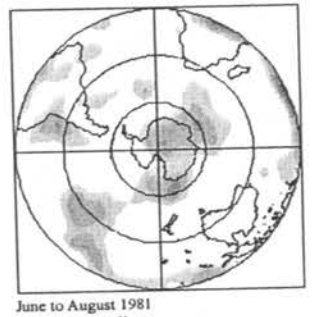

June to August 1981
Positive anomalies

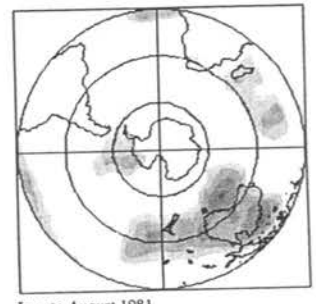

June to August 1981
Negative anomalies

17

Percentage sea level pressure anomalies for three months. Grey shading indicates percentages greater than 60% in 10% bands

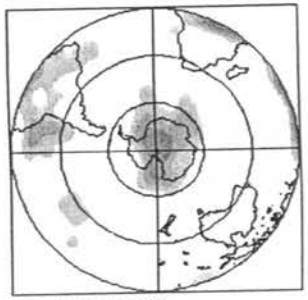

July to September 1981
Positive anomalies

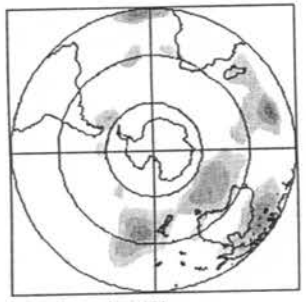

July to September 1981
Negative anomalies

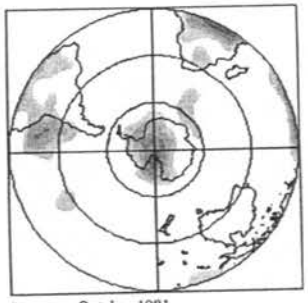

August to October 1981
Positive anomalies

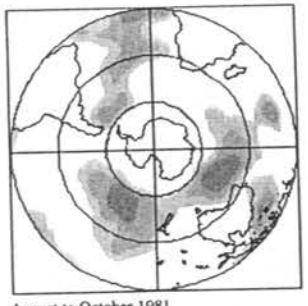

August to October 1981
Negative anomalies

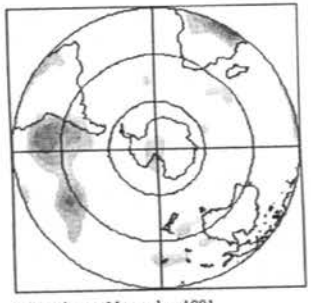

September to November 1981
Positive anomalies

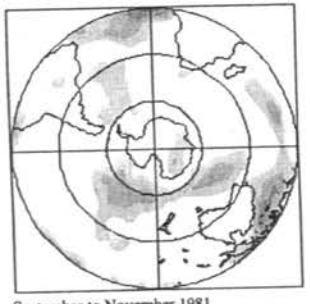

September to November 1981
Negative anomalies

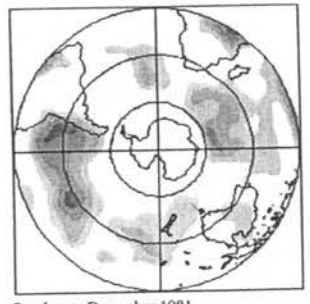

October to December 1981
Positive anomalies

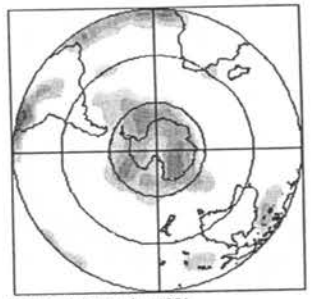

October to December 1981
Negative anomalies

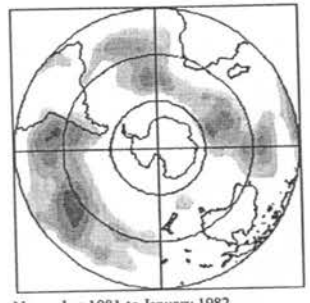

November 1981 to January 1982
Positive anomalies

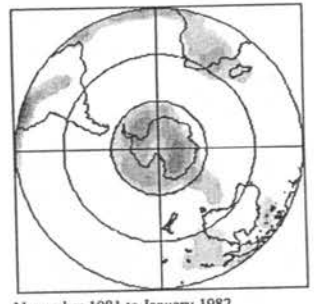

November 1981 to January 1982
Negative anomalies

December 1981 to February 1982
Positive anomalies

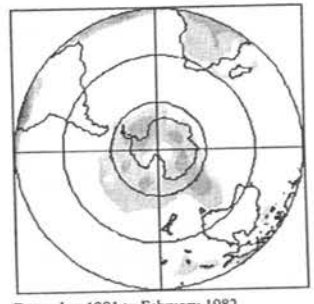

December 1981 to February 1982
Negative anomalies

18

Percentage sea level pressure anomalies for three months. Grey shading indicates percentages greater than 60% in 10% bands

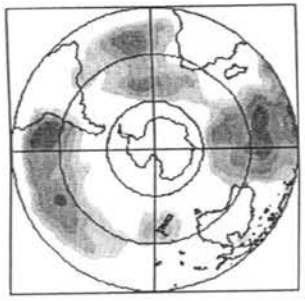

January to March 1982
Positive anomalies

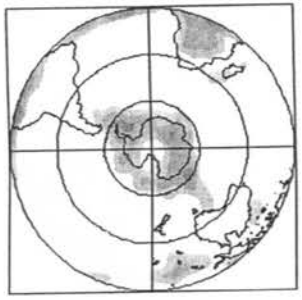

January to March 1982
Negative anomalies

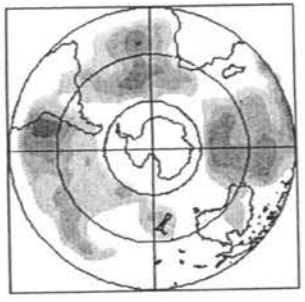

February to April 1982
Positive anomalies

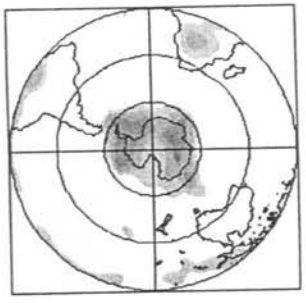

February to April 1982
Negative anomalies

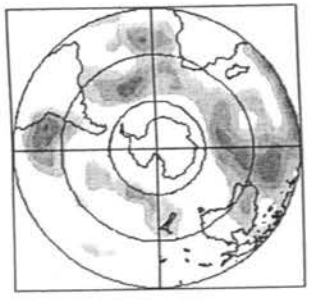

March to May 1982
Positive anomalies

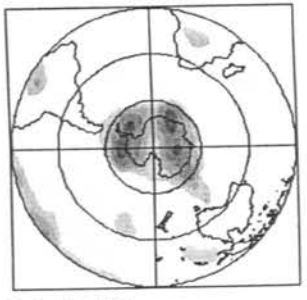

March to May 1982
Negative anomalies

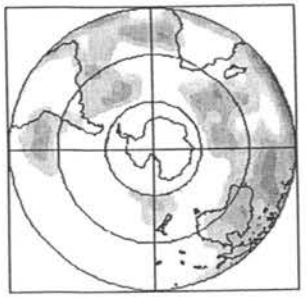

April to June 1982
Positive anomalies

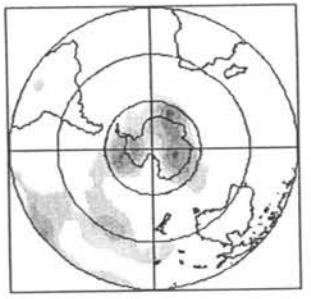

April to June 1982
Negative anomalies

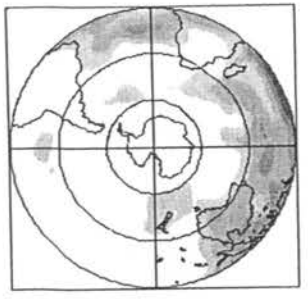

May to July 1982
Positive anomalies

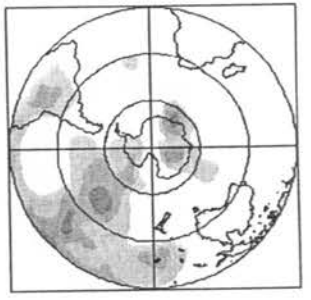

May to July 1982
Negative anomalies

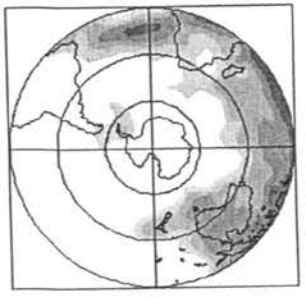

June to August 1982
Positive anomalies

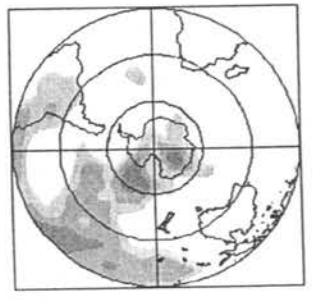

June to August 1982
Negative anomalies

61

Percentage sea level pressure anomalies for three months. Grey shading indicates percentages greater than 60% in 10% bands

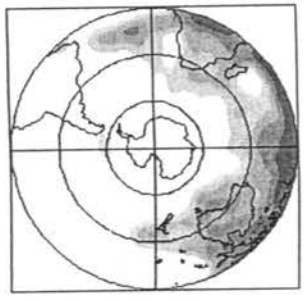

July to September 1982
Positive anomalies

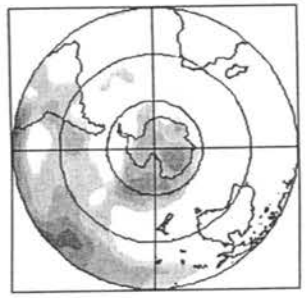

July to September 1982
Negative anomalies

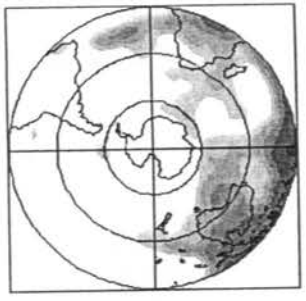

August to October 1982
Positive anomalies

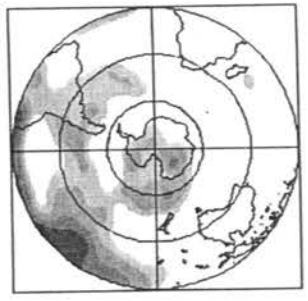

August to October 1982
Negative anomalies

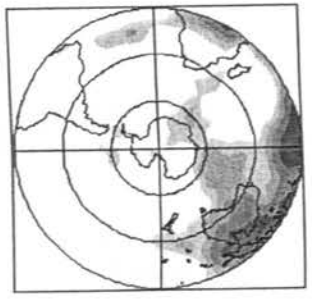

September to November 1982
Positive anomalies

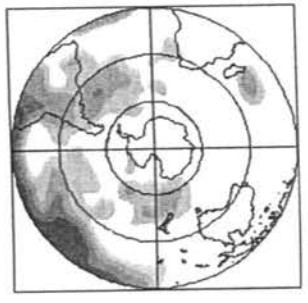

September to November 1982
Negative anomalies

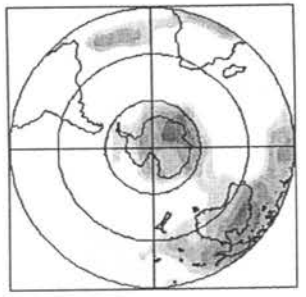

October to December 1982
Positive anomalies

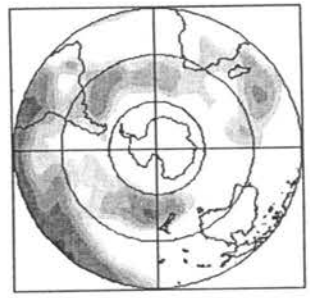

October to December 1982
Negative anomalies

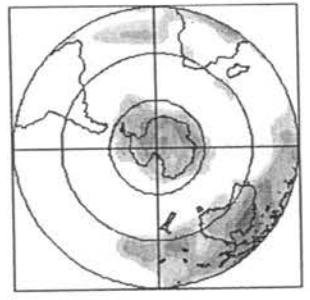

November 1982 to January 1983
Positive anomalies

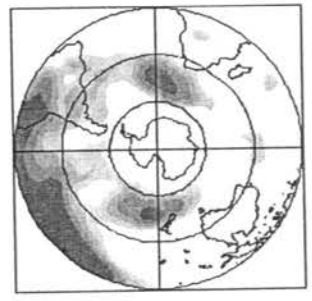

November 1982 to January 1983
Negative anomalies

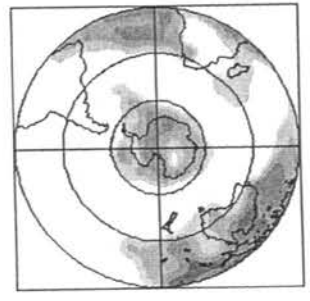

December 1982 to February 1983
Positive anomalies

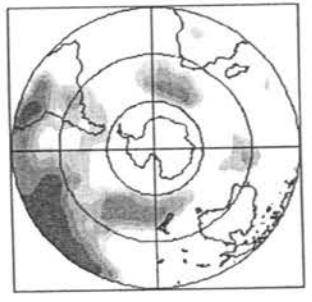

December 1982 to February 1983
Negative anomalies

20

Percentage sea level pressure anomalies for three months. Grey shading indicates percentages greater than 60% in 10% bands

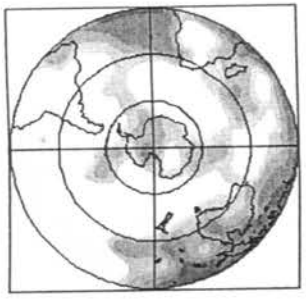

January to March 1983
Positive anomalies

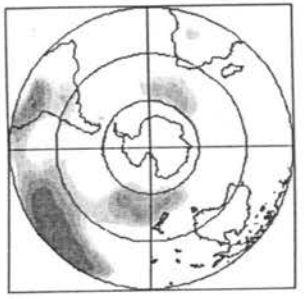

January to March 1983
Negative anomalies

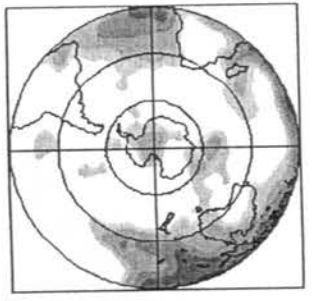

February to April 1983
Positive anomalies

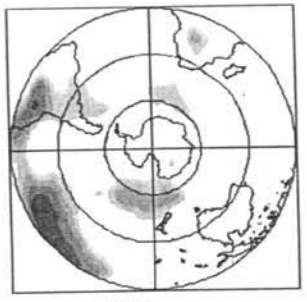

February to April 1983
Negative anomalies

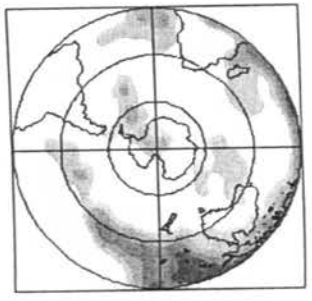

March to May 1983
Positive anomalies

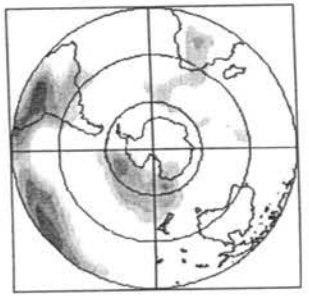

March to May 1983
Negative anomalies

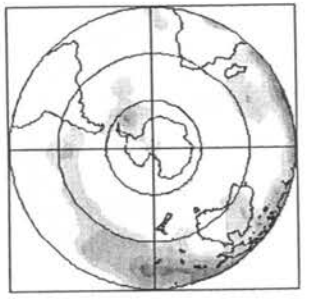

April to June 1983
Positive anomalies

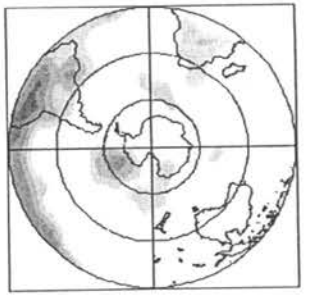

April to June 1983
Negative anomalies

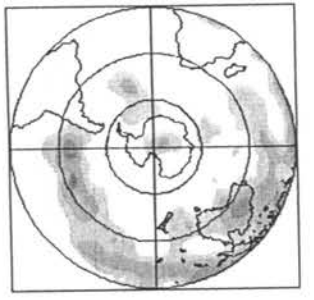

May to July 1983
Positive anomalies

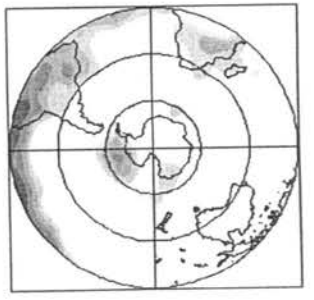

May to July 1983
Negative anomalies

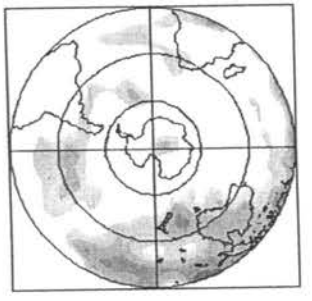

June to August 1983
Positive anomalies

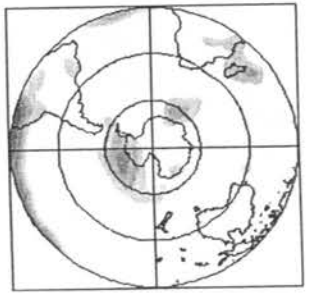

June to August 1983
Negative anomalies

18

Percentage sea level pressure anomalies for three months. Grey shading indicates percentages greater than 60% in 10% bands

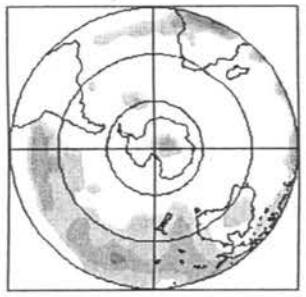

July to September 1983
Positive anomalies

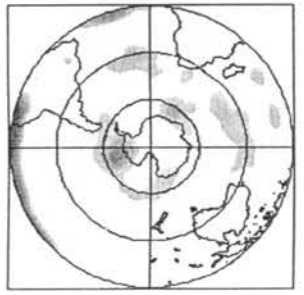

July to September 1983
Negative anomalies

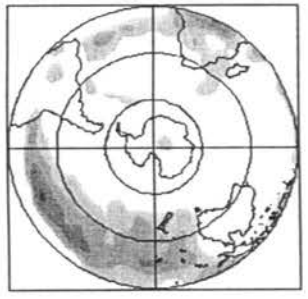

August to October 1983
Positive anomalies

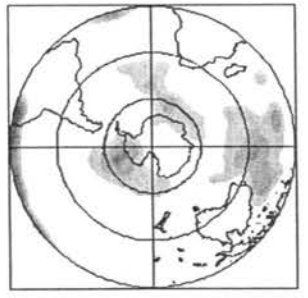

August to October 1983
Negative anomalies

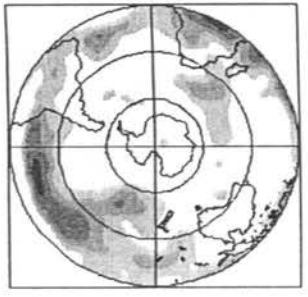

September to November 1983
Positive anomalies

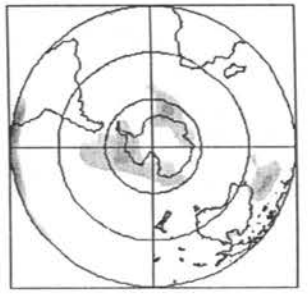

September to November 1983
Negative anomalies

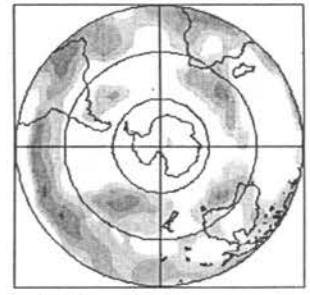

October to December 1983
Positive anomalies

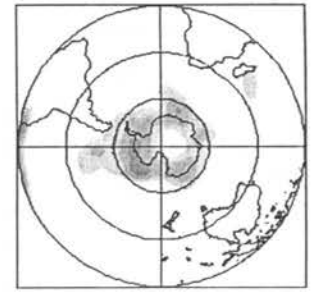

October to December 1983
Negative anomalies

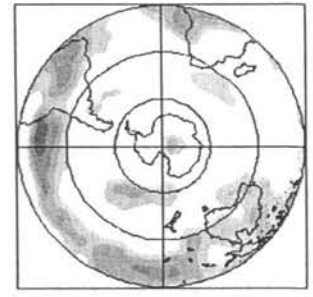

November 1983 to January 1984
Positive anomalies

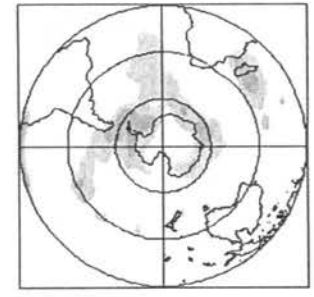

November 1983 to January 1984
Negative anomalies

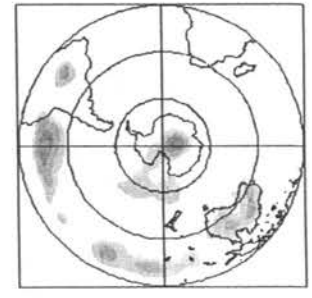

December 1983 to February 1984
Positive anomalies

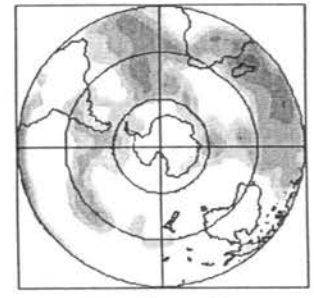

December 1983 to February 1984
Negative anomalies

22

Percentage sea level pressure anomalies for three months. Grey shading indicates percentages greater than 60% in 10% bands

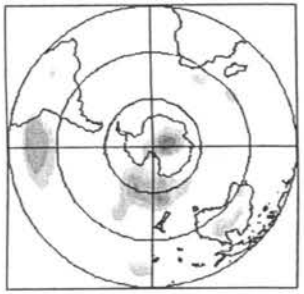

January to March 1984
Positive anomalies

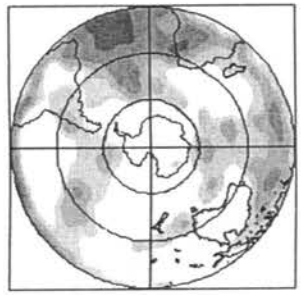

January to March 1984
Negative anomalies

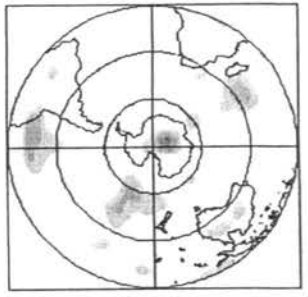

February to April 1984
Positive anomalies

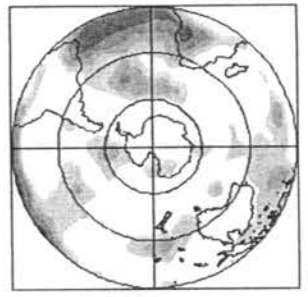

February to April 1984
Negative anomalies

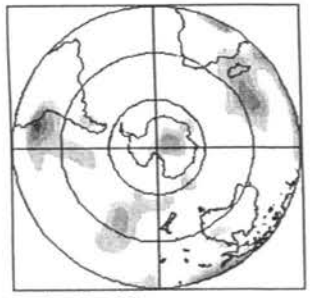

March to May 1984
Positive anomalies

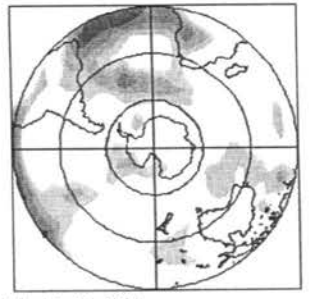

March to May 1984
Negative anomalies

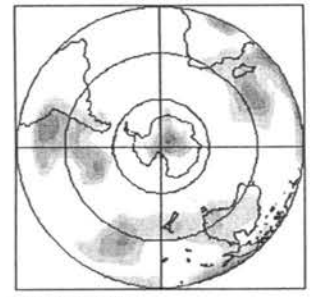

April to June 1984
Positive anomalies

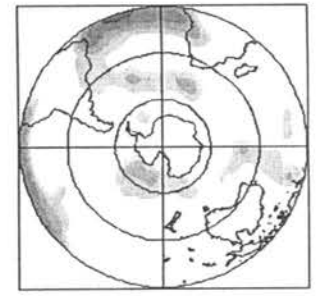

April to June 1984
Negative anomalies

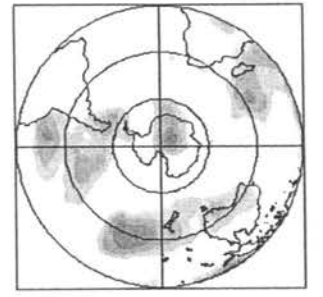

May to July 1984
Positive anomalies

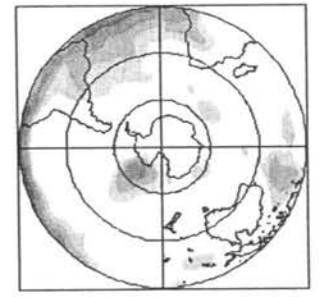

May to July 1984
Negative anomalies

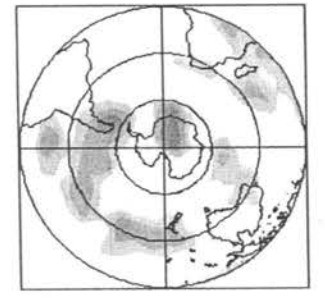

June to August 1984
Positive anomalies

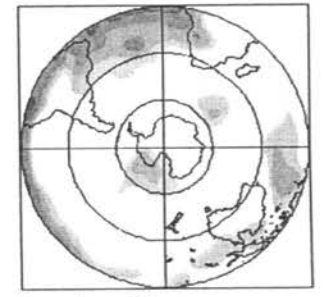

June to August 1984
Negative anomalies

23

Percentage sea level pressure anomalies for three months. Grey shading indicates percentages greater than 60% in 10% bands

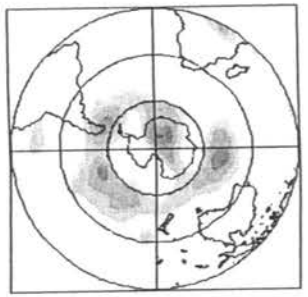

July to September 1984
Positive anomalies

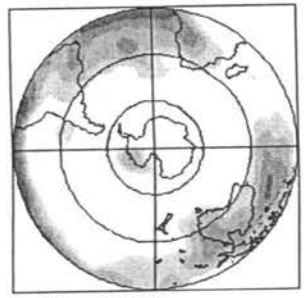

July to September 1984
Negative anomalies

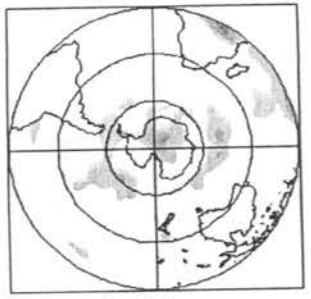

August to October 1984
Positive anomalies

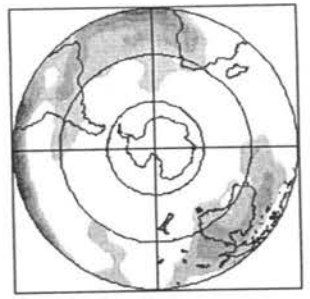

August to October 1984
Negative anomalies

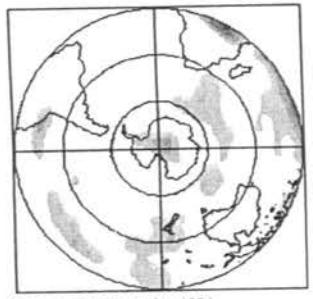

September to November 1984
Positive anomalies

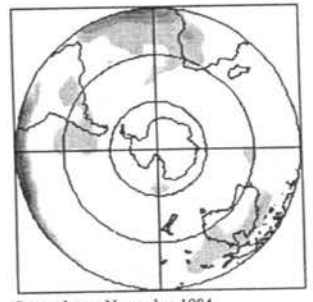

September to November 1984
Negative anomalies

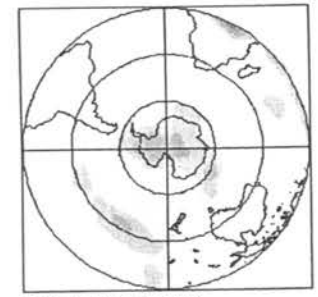

October to December 1984
Positive anomalies

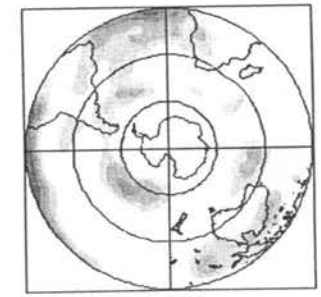

October to December 1984
Negative anomalies

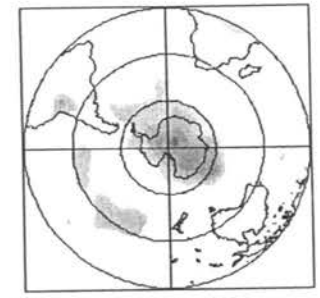

November 1984 to January 1985
Positive anomalies

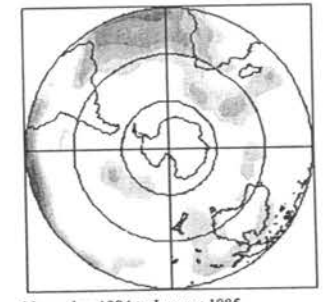

November 1984 to January 1985
Negative anomalies

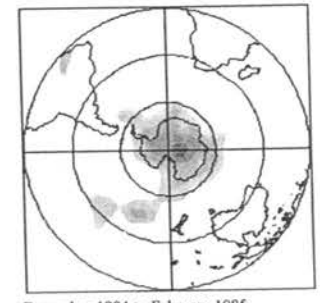

December 1984 to February 1985
Positive anomalies

December 1984 to February 1985
Negative anomalies

Percentage sea level pressure anomalies for three months. Grey shading indicates percentages greater than 60% in 10% bands

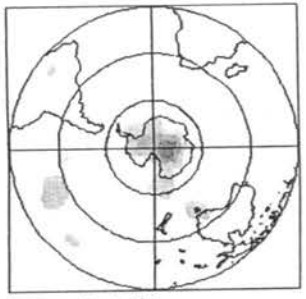

January to March 1985
Positive anomalies

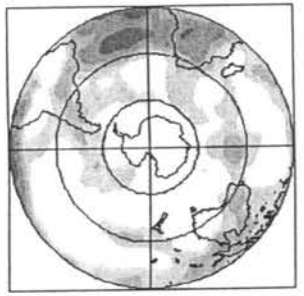

January to March 1985
Negative anomalies

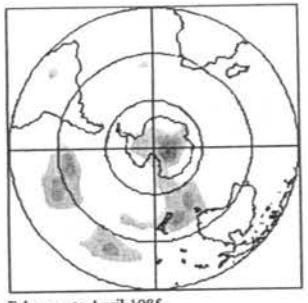

February to April 1985
Positive anomalies

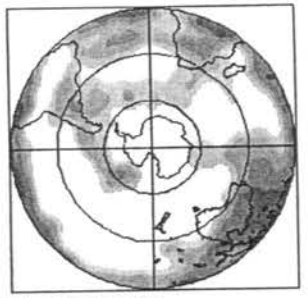

February to April 1985
Negative anomalies

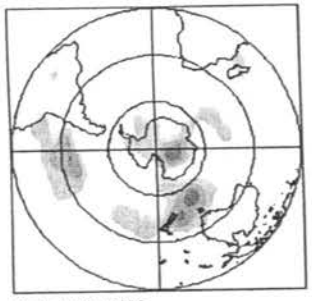

March to May 1985
Positive anomalies

March to May 1985
Negative anomalies

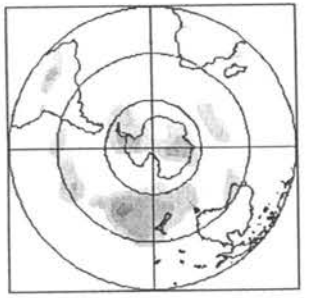

April to June 1985
Positive anomalies

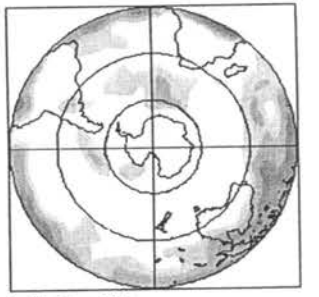

April to June 1985
Negative anomalies

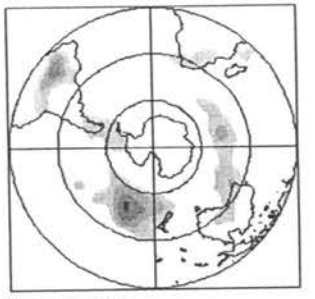

May to July 1985
Positive anomalies

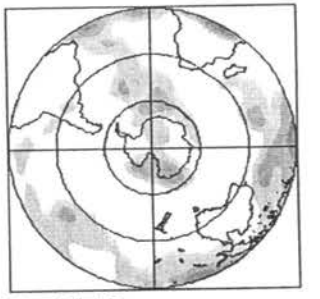

May to July 1985
Negative anomalies

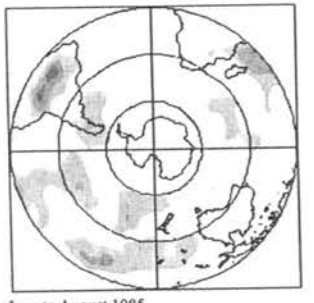

June to August 1985
Positive anomalies

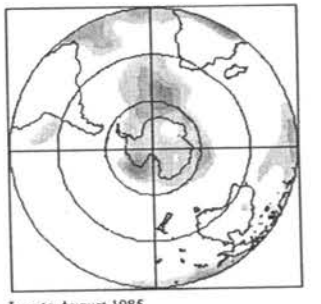

June to August 1985
Negative anomalies

Percentage sea level pressure anomalies for three months. Grey shading indicates percentages greater than 60% in 10% bands

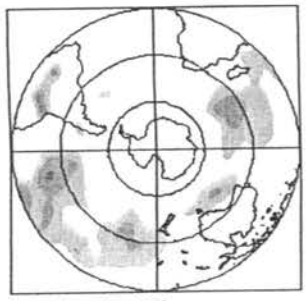

July to September 1985
Positive anomalies

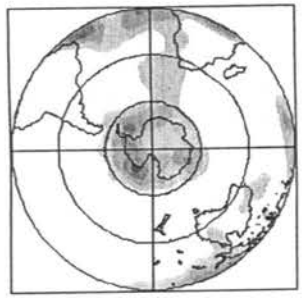

July to September 1985
Negative anomalies

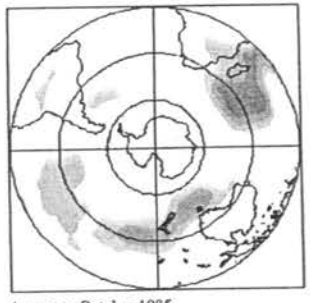

August to October 1985
Positive anomalies

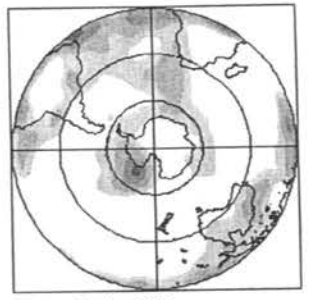

August to October 1985
Negative anomalies

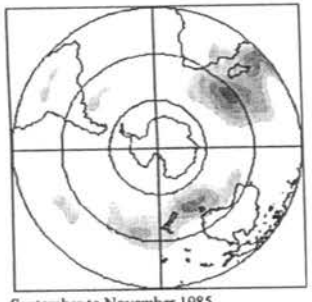

September to November 1985
Positive anomalies

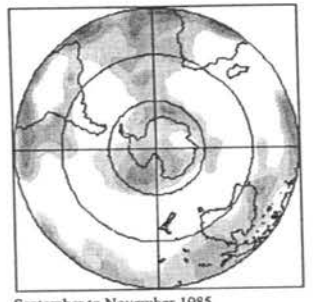

September to November 1985
Negative anomalies

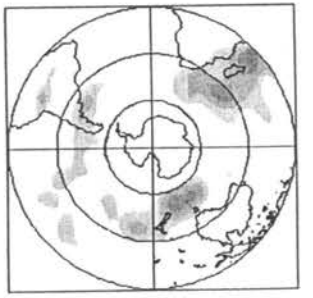

October to December 1985
Positive anomalies

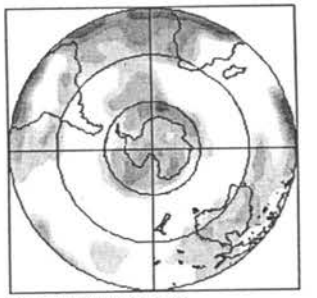

October to December 1985
Negative anomalies

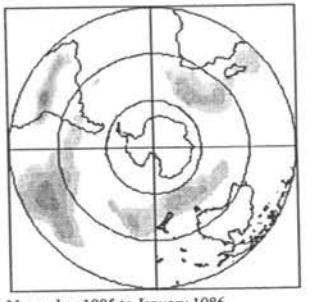

November 1985 to January 1986
Positive anomalies

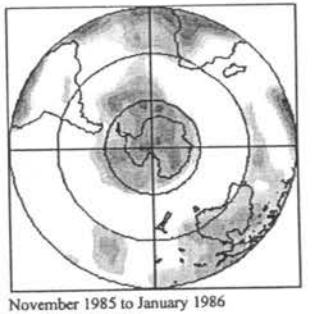

November 1985 to January 1986
Negative anomalies

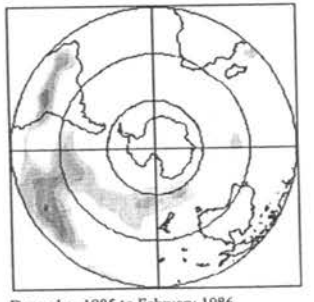

December 1985 to February 1986
Positive anomalies

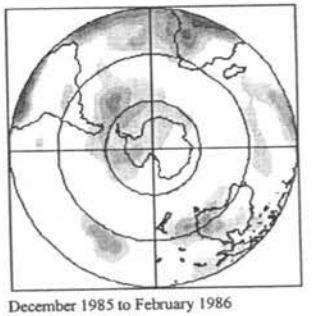

December 1985 to February 1986
Negative anomalies

Percentage sea level pressure anomalies for three months. Grey shading indicates percentages greater than 60% in 10% bands

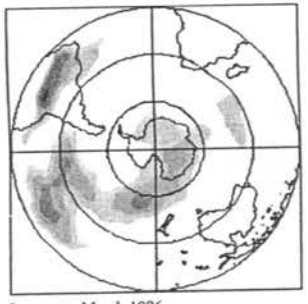

January to March 1986
Positive anomalies

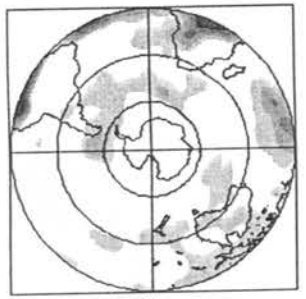

January to March 1986
Negative anomalies

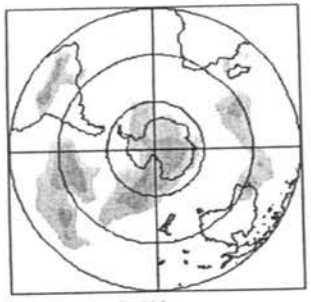

February to April 1986
Positive anomalies

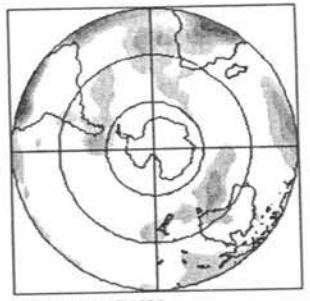

February to April 1986
Negative anomalies

March to May 1986
Positive anomalies

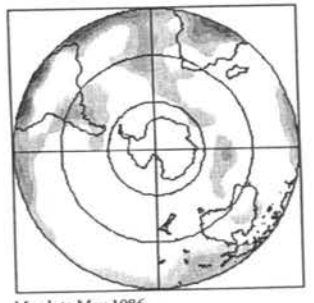

March to May 1986
Negative anomalies

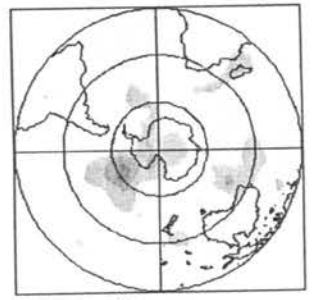

April to June 1986
Positive anomalies

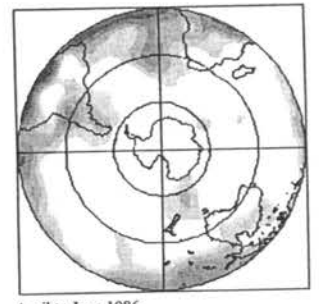

April to June 1986
Negative anomalies

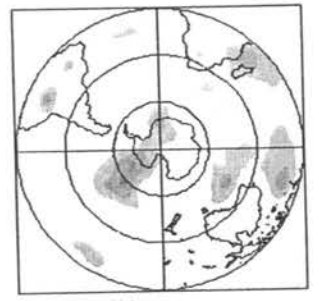

May to July 1986
Positive anomalies

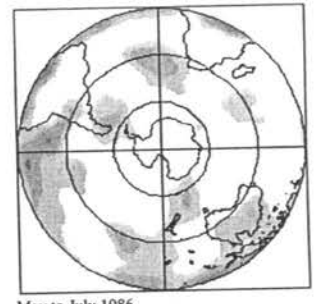

May to July 1986
Negative anomalies

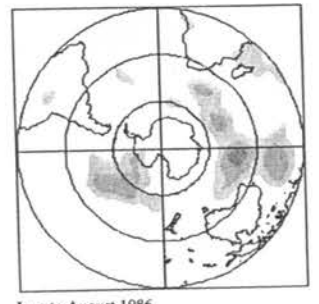

June to August 1986
Positive anomalies

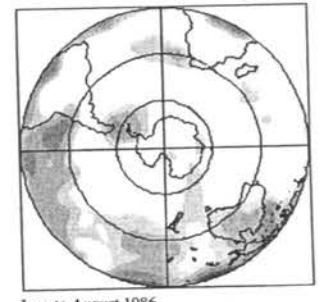

June to August 1986
Negative anomalies

Percentage sea level pressure anomalies for three months. Grey shading indicates percentages greater than 60% in 10% bands

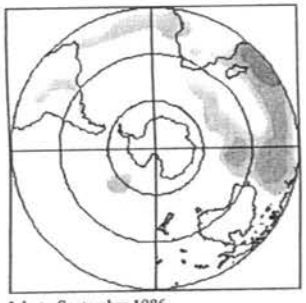

July to September 1986
Positive anomalies

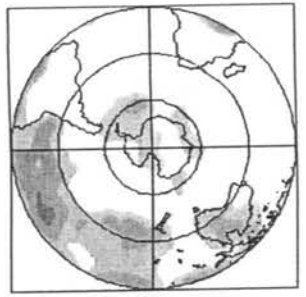

July to September 1986
Negative anomalies

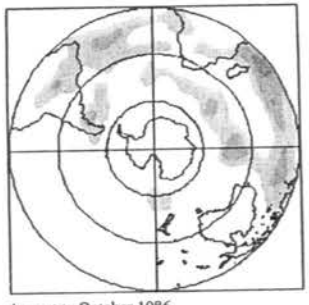

August to October 1986
Positive anomalies

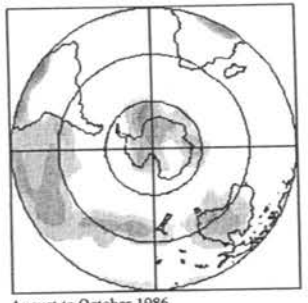

August to October 1986
Negative anomalies

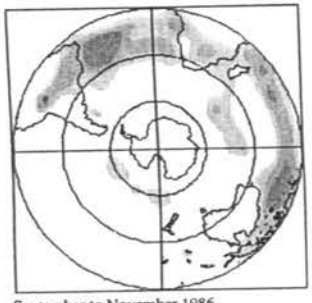

September to November 1986
Positive anomalies

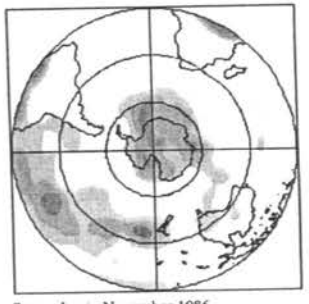

September to November 1986
Negative anomalies

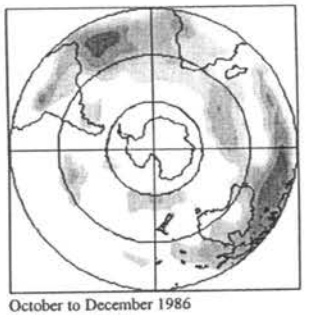

October to December 1986
Positive anomalies

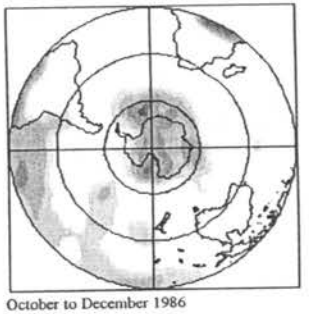

October to December 1986
Negative anomalies

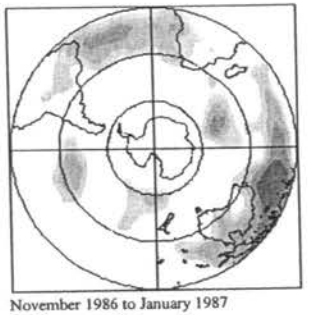

November 1986 to January 1987
Positive anomalies

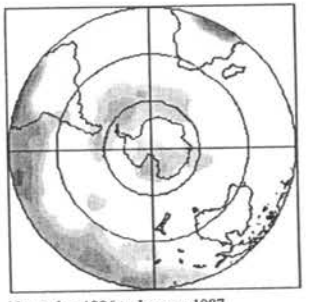

November 1986 to January 1987
Negative anomalies

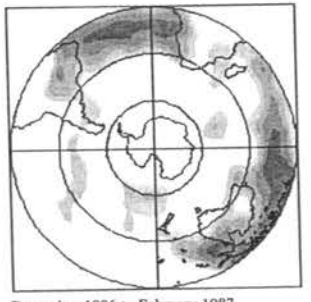

December 1986 to February 1987
Positive anomalies

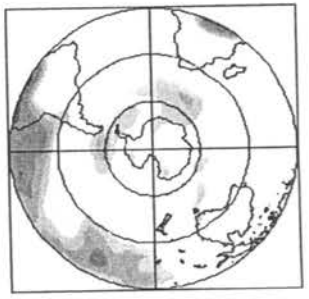

December 1986 to February 1987
Negative anomalies

Percentage sea level pressure anomalies for three months. Grey shading indicates percentages greater than 60% in 10% bands

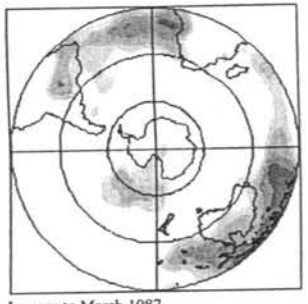

January to March 1987
Positive anomalies

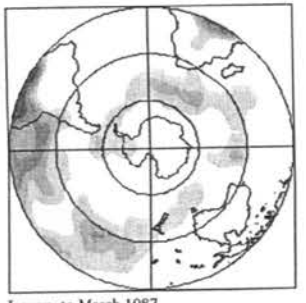

January to March 1987
Negative anomalies

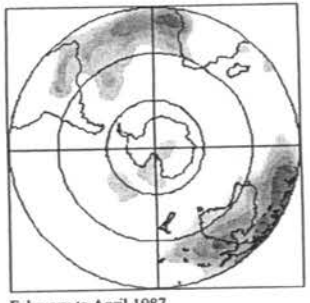

February to April 1987
Positive anomalies

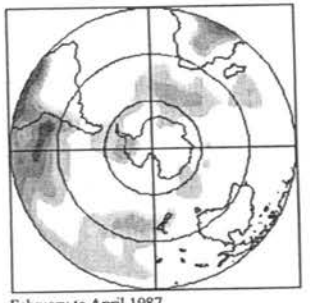

February to April 1987
Negative anomalies

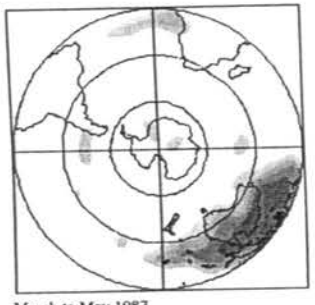

March to May 1987
Positive anomalies

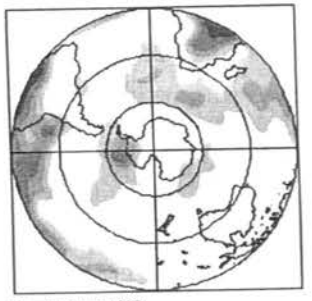

March to May 1987
Negative anomalies

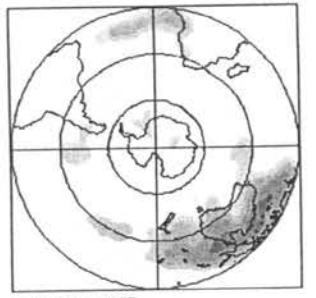

April to June 1987
Positive anomalies

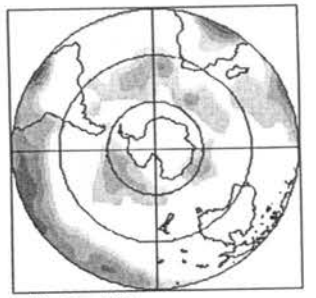

April to June 1987
Negative anomalies

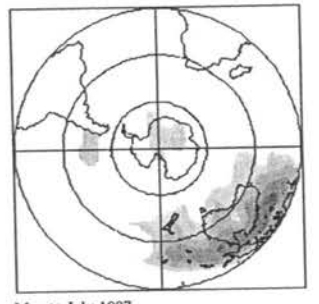

May to July 1987
Positive anomalies

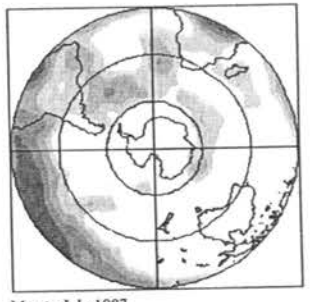

May to July 1987
Negative anomalies

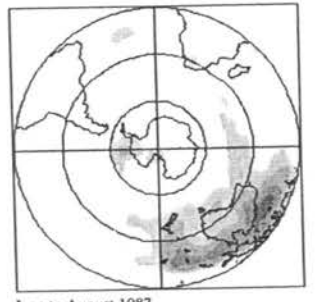

June to August 1987
Positive anomalies

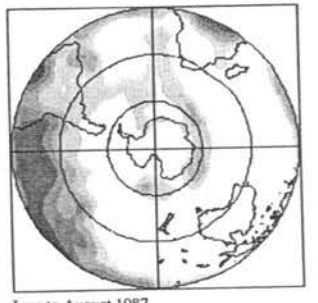

June to August 1987
Negative anomalies

Percentage sea level pressure anomalies for three months. Grey shading indicates percentages greater than 60% in 10% bands

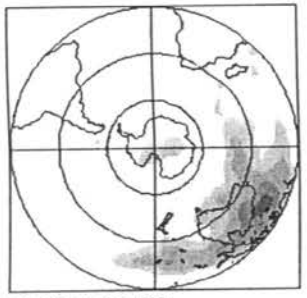

July to September 1987
Positive anomalies

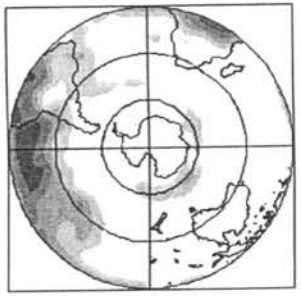

July to September 1987
Negative anomalies

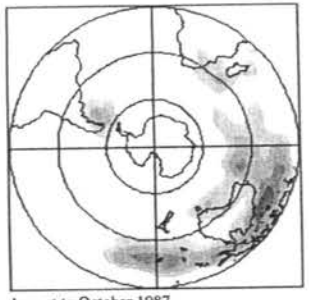

August to October 1987
Positive anomalies

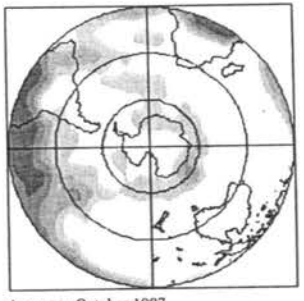

August to October 1987
Negative anomalies

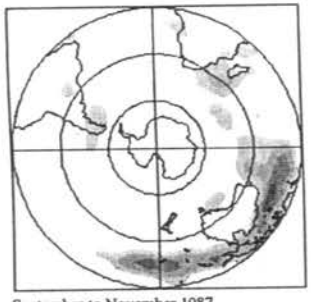

September to November 1987
Positive anomalies

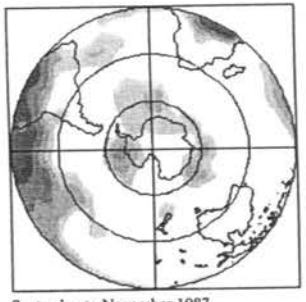

September to November 1987
Negative anomalies

October to December 1987
Positive anomalies

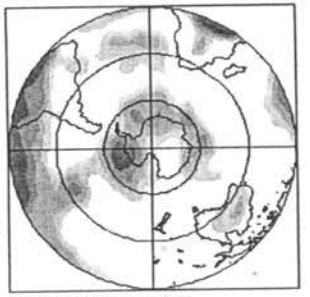

October to December 1987
Negative anomalies

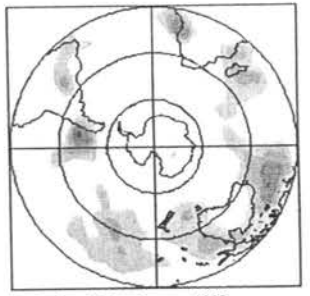

November 1987 to January 1988
Positive anomalies

November 1987 to January 1988
Negative anomalies

December 1987 to February 1988
Positive anomalies

December 1987 to February 1988
Negative anomalies

Percentage sea level pressure anomalies for three months. Grey shading indicates percentages greater than 60% in 10% bands

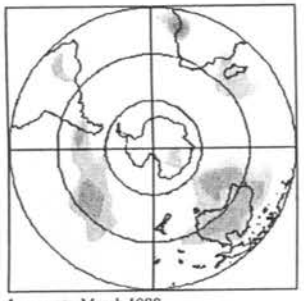

January to March 1988
Positive anomalies

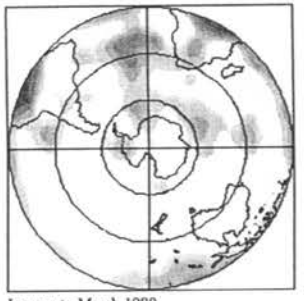

January to March 1988
Negative anomalies

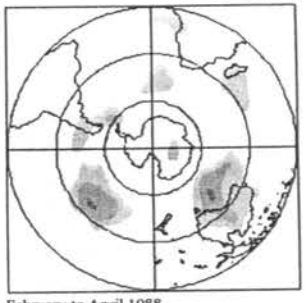

February to April 1988
Positive anomalies

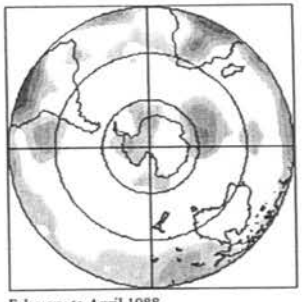

February to April 1988
Negative anomalies

March to May 1988
Positive anomalies

March to May 1988
Negative anomalies

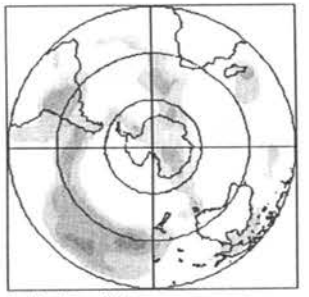

April to June 1988
Positive anomalies

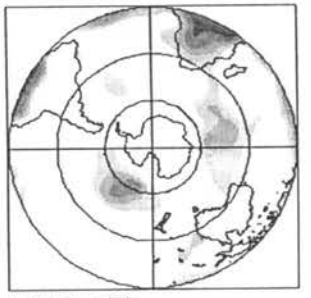

April to June 1988
Negative anomalies

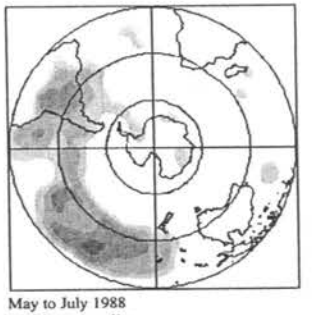

May to July 1988
Positive anomalies

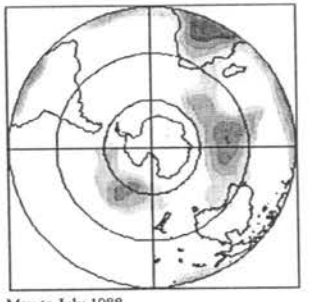

May to July 1988
Negative anomalies

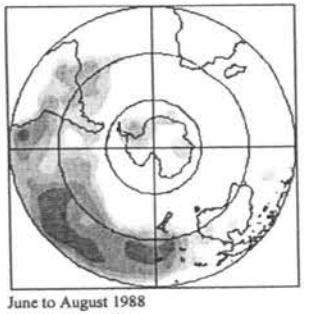

June to August 1988
Positive anomalies

June to August 1988
Negative anomalies

Percentage sea level pressure anomalies for three months. Grey shading indicates percentages greater than 60% in 10% bands

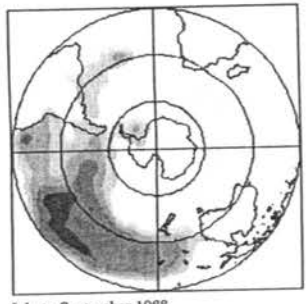

July to September 1988
Positive anomalies

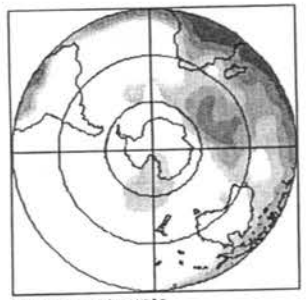

July to September 1988
Negative anomalies

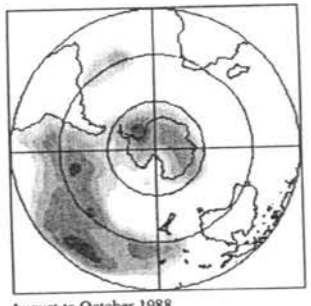

August to October 1988
Positive anomalies

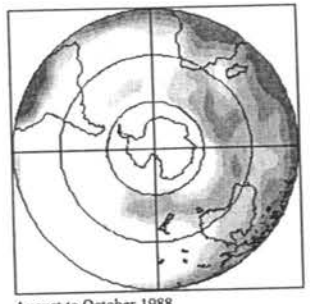

August to October 1988
Negative anomalies

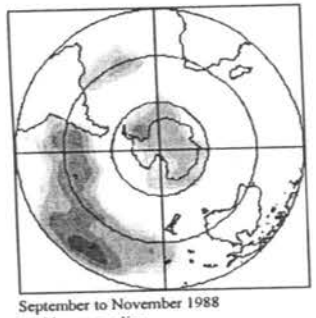

September to November 1988
Positive anomalies

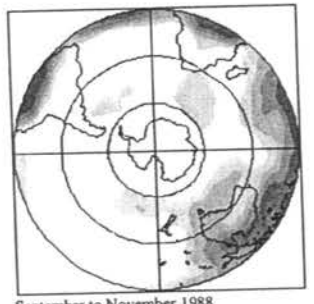

September to November 1988
Negative anomalies

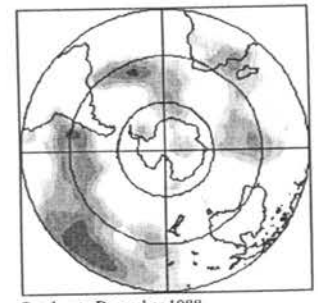

October to December 1988
Positive anomalies

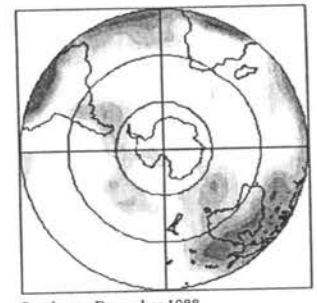

October to December 1988
Negative anomalies

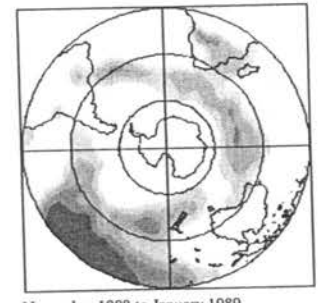

November 1988 to January 1989
Positive anomalies

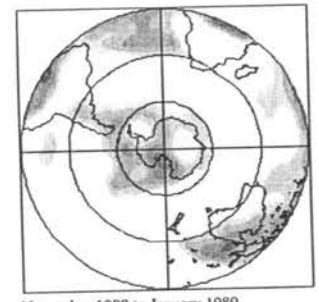

November 1988 to January 1989
Negative anomalies

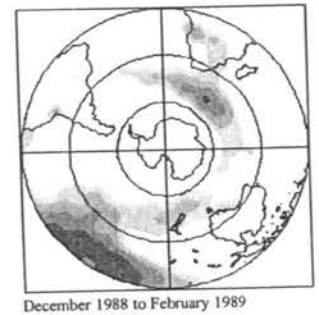

December 1988 to February 1989
Positive anomalies

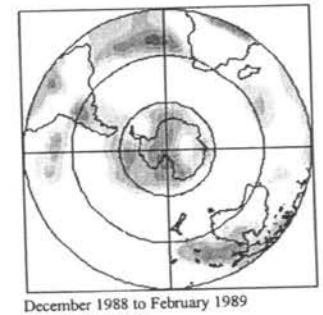

December 1988 to February 1989
Negative anomalies

Percentage sea level pressure anomalies for three months. Grey shading indicates percentages greater than 60% in 10% bands

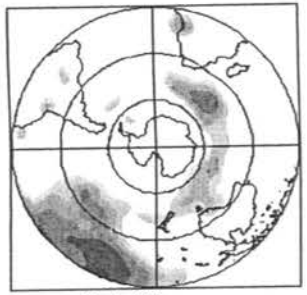

January to March 1989
Positive anomalies

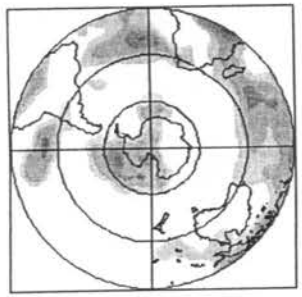

January to March 1989
Negative anomalies

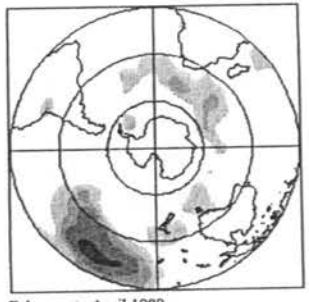

February to April 1989
Positive anomalies

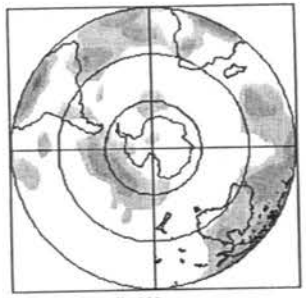

February to April 1989
Negative anomalies

March to May 1989
Positive anomalies

March to May 1989
Negative anomalies

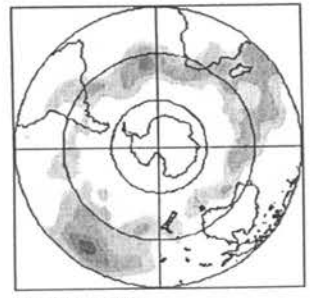

April to June 1989
Positive anomalies

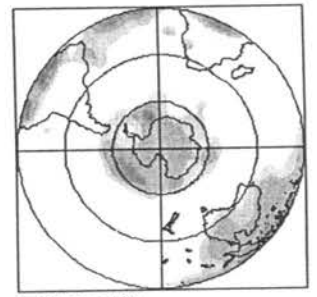

April to June 1989
Negative anomalies

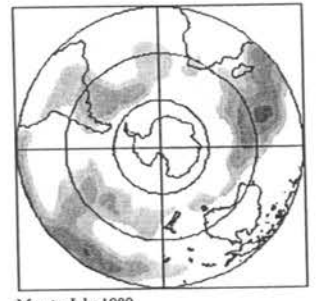

May to July 1989
Positive anomalies

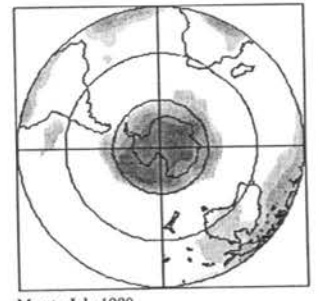

May to July 1989
Negative anomalies

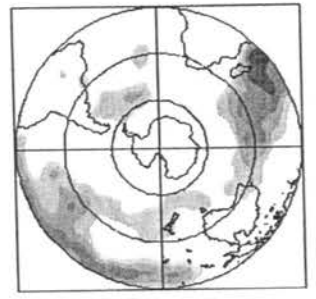

June to August 1989
Positive anomalies

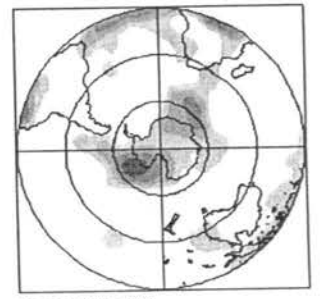

June to August 1989
Negative anomalies

Percentage sea level pressure anomalies for three months. Grey shading indicates percentages greater than 60% in 10% bands

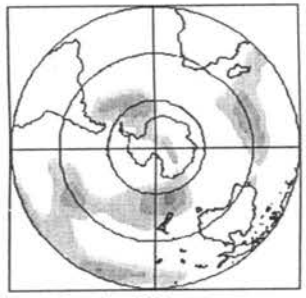

July to September 1989
Positive anomalies

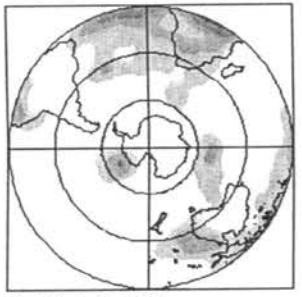

July to September 1989
Negative anomalies

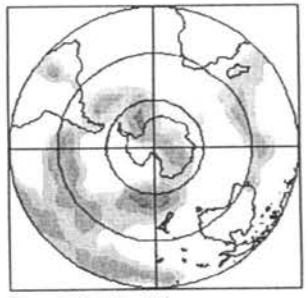

August to October 1989
Positive anomalies

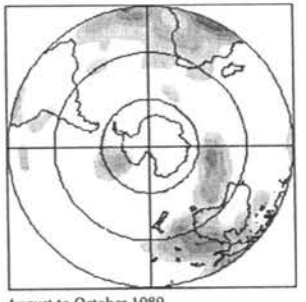

August to October 1989
Negative anomalies

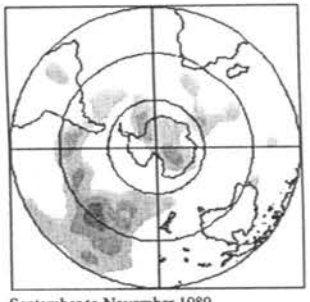

September to November 1989
Positive anomalies

September to November 1989
Negative anomalies

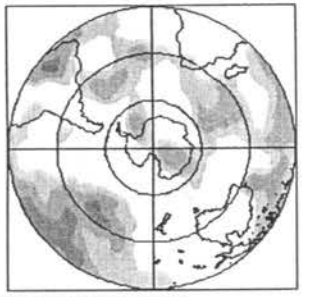

October to December 1989
Positive anomalies

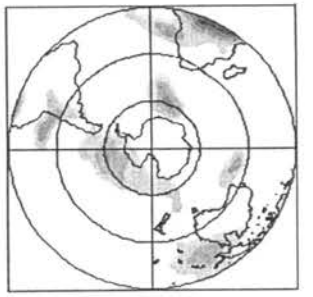

October to December 1989
Negative anomalies

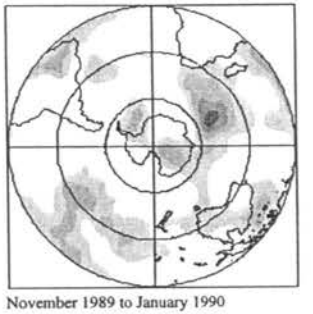

November 1989 to January 1990
Positive anomalies

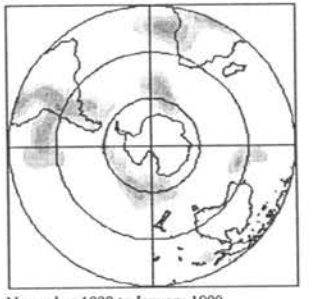

November 1989 to January 1990
Negative anomalies

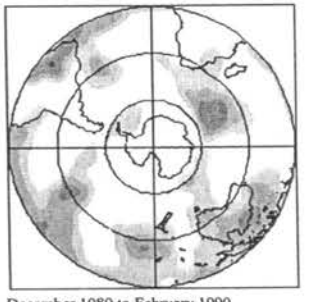

December 1989 to February 1990
Positive anomalies

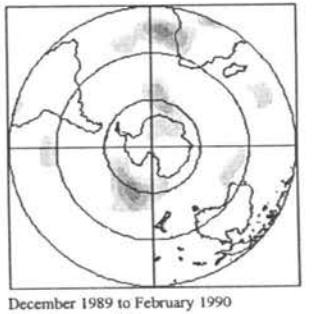

December 1989 to February 1990
Negative anomalies

Percentage sea level pressure anomalies for three months. Grey shading indicates percentages greater than 60% in 10% bands

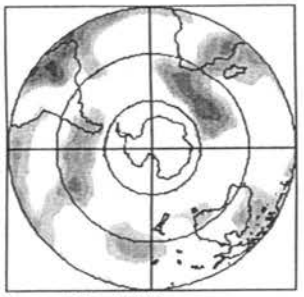

January to March 1990
Positive anomalies

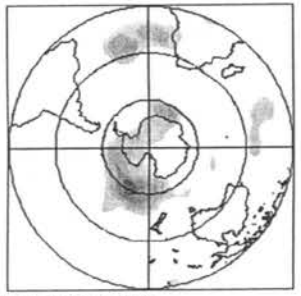

January to March 1990
Negative anomalies

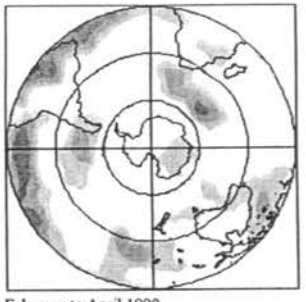

February to April 1990
Positive anomalies

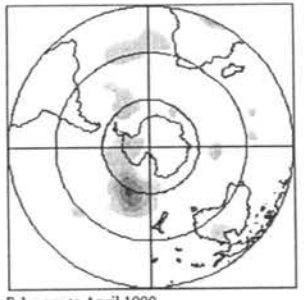

February to April 1990
Negative anomalies

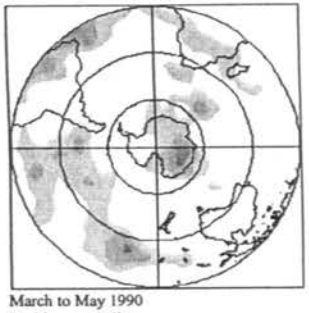

March to May 1990
Positive anomalies

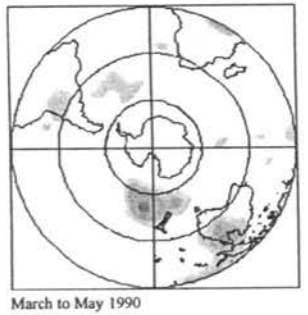

March to May 1990
Negative anomalies

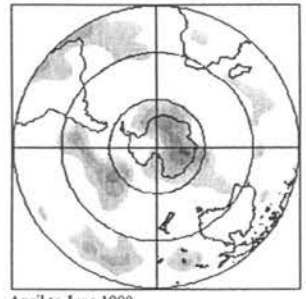

April to June 1990
Positive anomalies

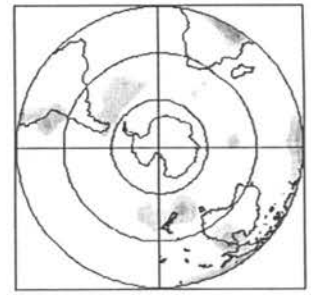

April to June 1990
Negative anomalies

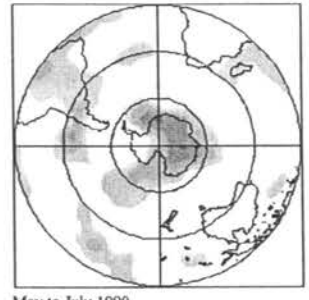

May to July 1990
Positive anomalies

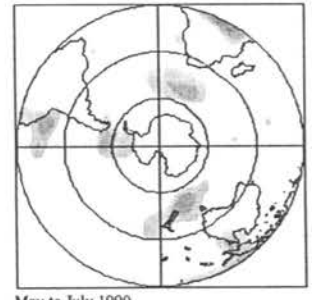

May to July 1990
Negative anomalies

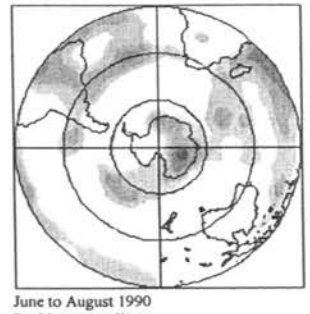

June to August 1990
Positive anomalies

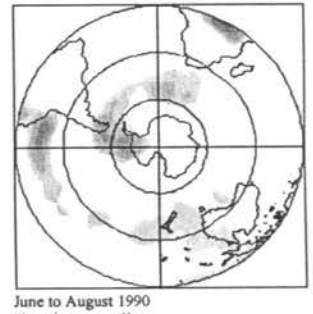

June to August 1990
Negative anomalies

35

Percentage sea level pressure anomalies for three months. Grey shading indicates percentages greater than 60% in 10% bands

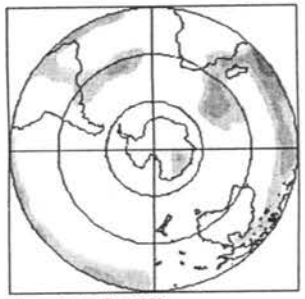

July to September 1990
Positive anomalies

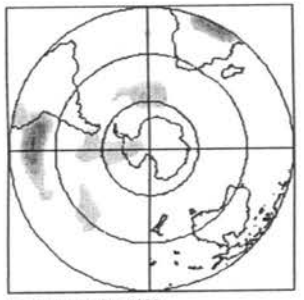

July to September 1990
Negative anomalies

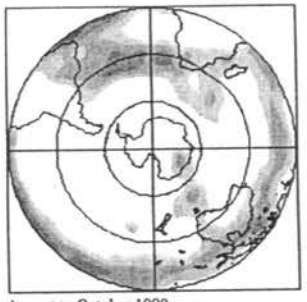

August to October 1990
Positive anomalies

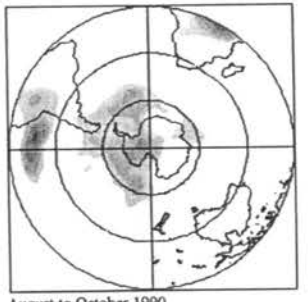

August to October 1990
Negative anomalies

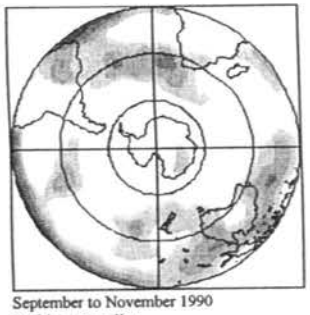

September to November 1990
Positive anomalies

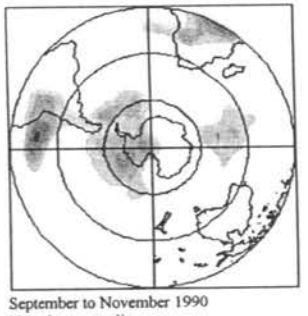

September to November 1990
Negative anomalies

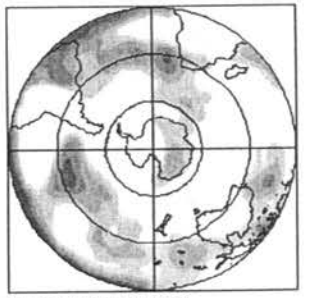

October to December 1990
Positive anomalies

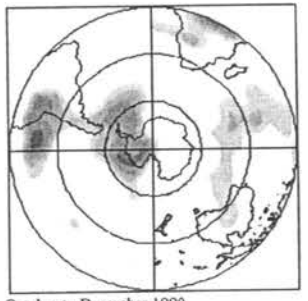

October to December 1990
Negative anomalies

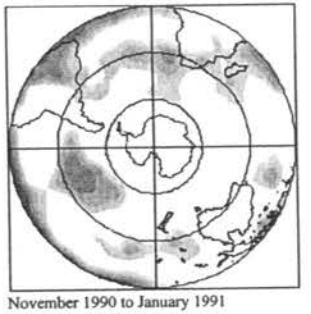

November 1990 to January 1991
Positive anomalies

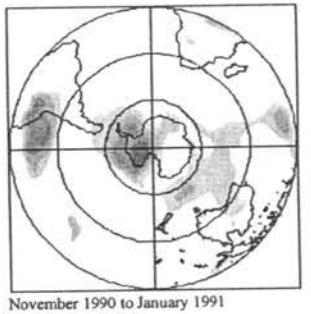

November 1990 to January 1991
Negative anomalies

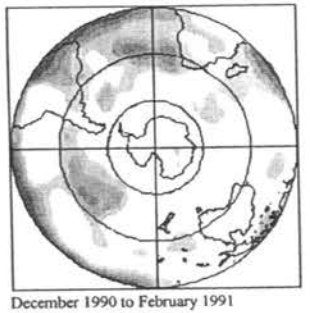

December 1990 to February 1991
Positive anomalies

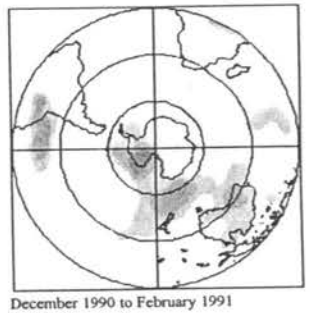

December 1990 to February 1991
Negative anomalies

32

Percentage sea level pressure anomalies for three months. Grey shading indicates percentages greater than 60% in 10% bands

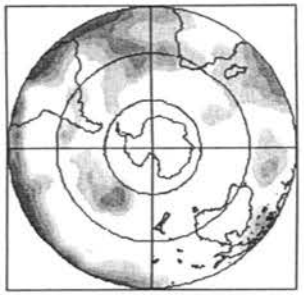

January to March 1991
Positive anomalies

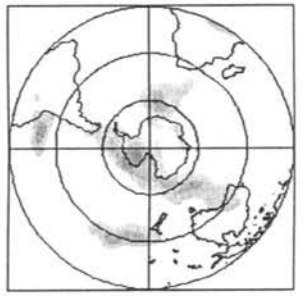

January to March 1991
Negative anomalies

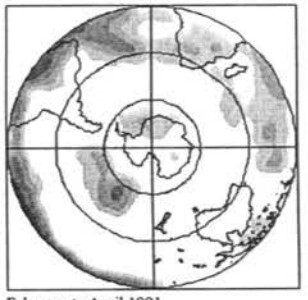

February to April 1991
Positive anomalies

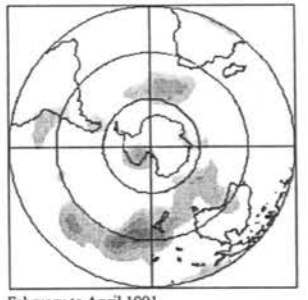

February to April 1991
Negative anomalies

March to May 1991
Positive anomalies

March to May 1991
Negative anomalies

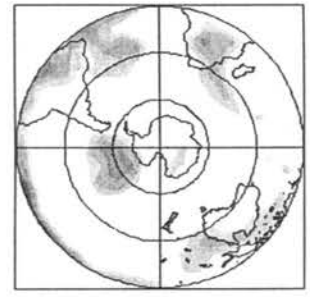

April to June 1991
Positive anomalies

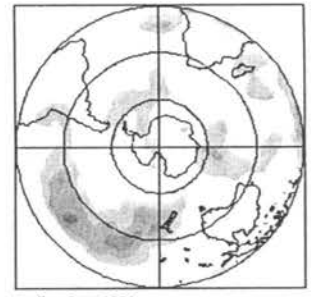

April to June 1991
Negative anomalies

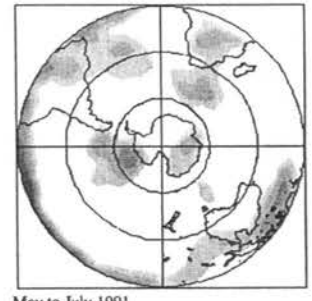

May to July 1991
Positive anomalies

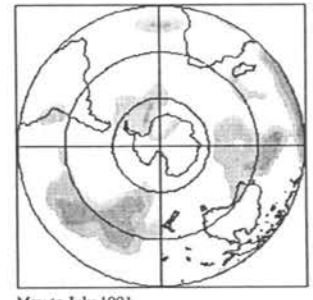

May to July 1991
Negative anomalies

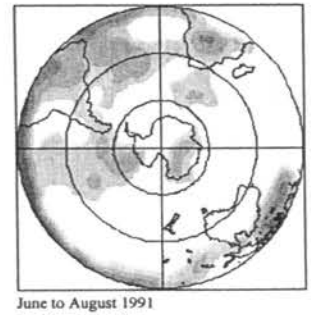

June to August 1991
Positive anomalies

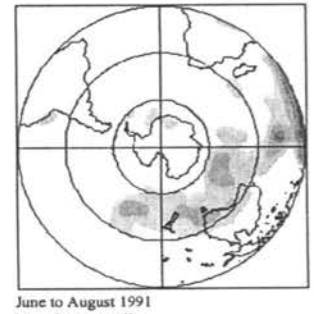

June to August 1991
Negative anomalies

Percentage sea level pressure anomalies for three months. Grey shading indicates percentages greater than 60% in 10% bands

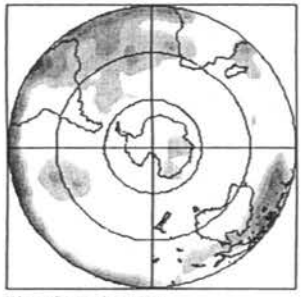

July to September 1991
Positive anomalies

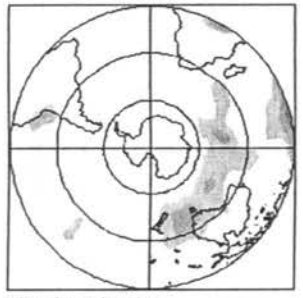

July to September 1991
Negative anomalies

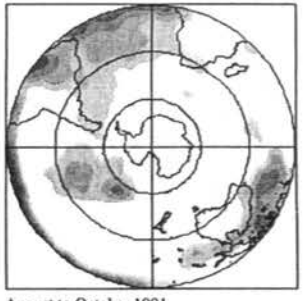

August to October 1991
Positive anomalies

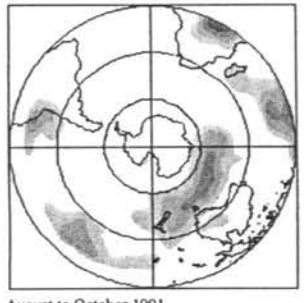

August to October 1991
Negative anomalies

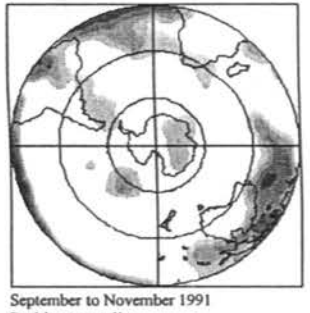

September to November 1991
Positive anomalies

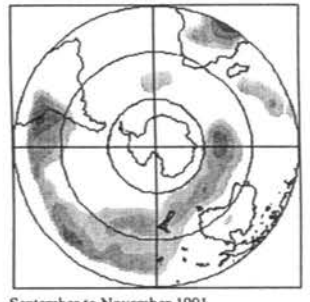

September to November 1991
Negative anomalies

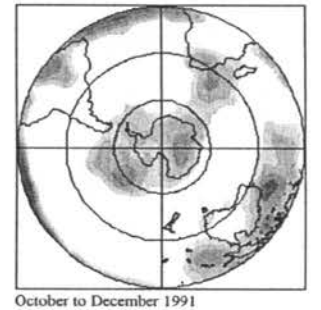

October to December 1991
Positive anomalies

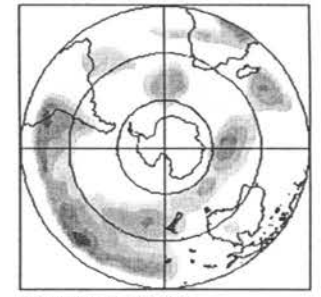

October to December 1991
Negative anomalies

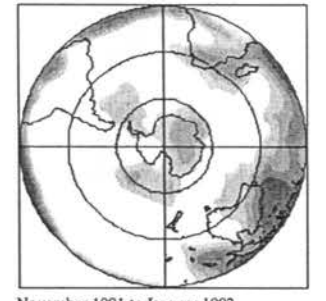

November 1991 to January 1992
Positive anomalies

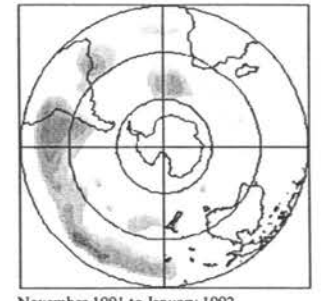

November 1991 to January 1992
Negative anomalies

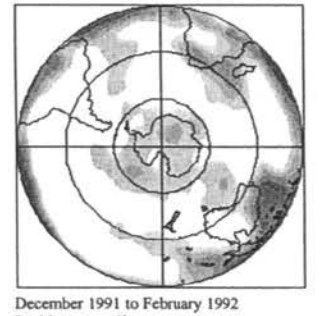

December 1991 to February 1992
Positive anomalies

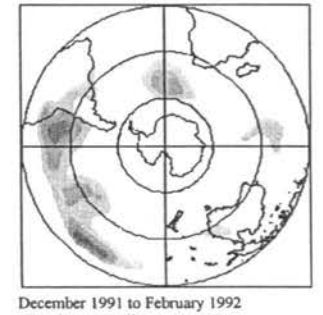

December 1991 to February 1992
Negative anomalies

Percentage sea level pressure anomalies for three months. Grey shading indicates percentages greater than 60% in 10% bands

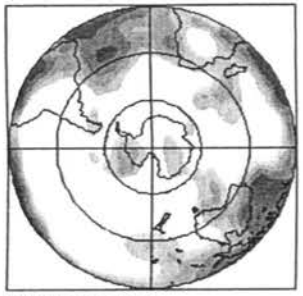

January to March 1992
Positive anomalies

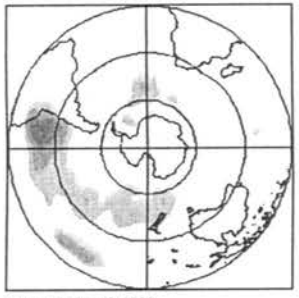

January to March 1992
Negative anomalies

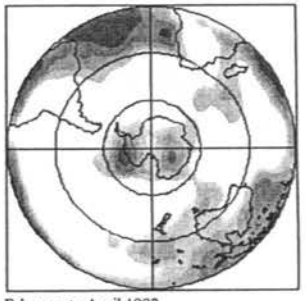

February to April 1992
Positive anomalies

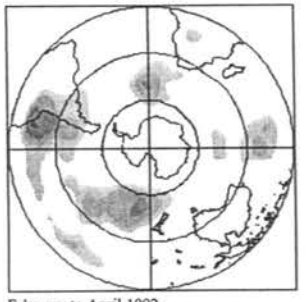

February to April 1992
Negative anomalies

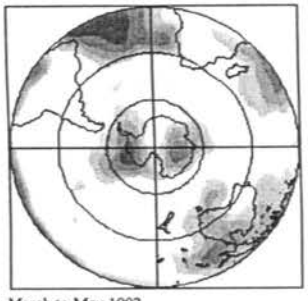

March to May 1992
Positive anomalies

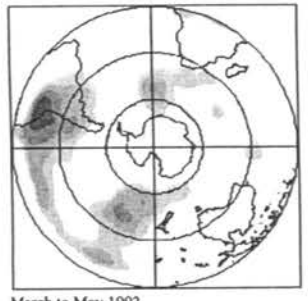

March to May 1992
Negative anomalies

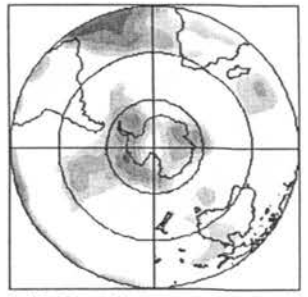

April to June 1992
Positive anomalies

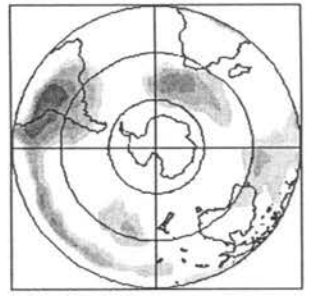

April to June 1992
Negative anomalies

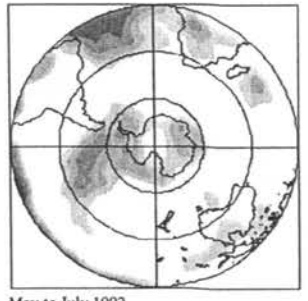

May to July 1992
Positive anomalies

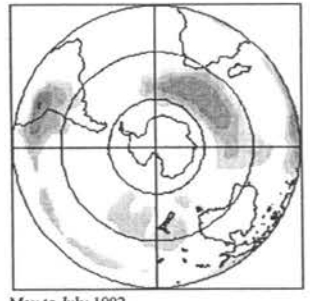

May to July 1992
Negative anomalies

June to August 1992
Positive anomalies

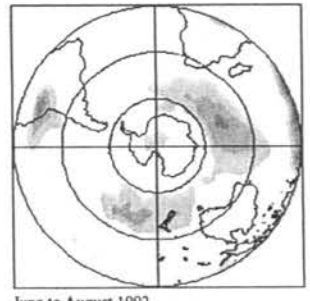

June to August 1992
Negative anomalies

Percentage sea level pressure anomalies for three months. Grey shading indicates percentages greater than 60% in 10% bands

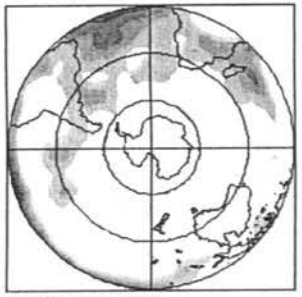

July to September 1992
Positive anomalies

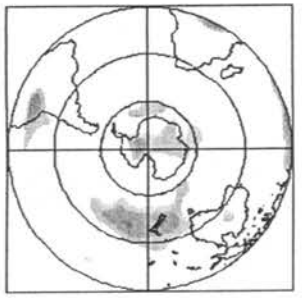

July to September 1992
Negative anomalies

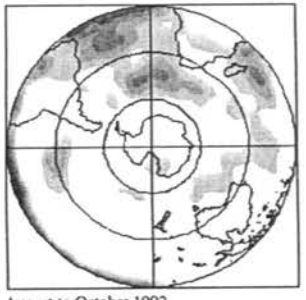

August to October 1992
Positive anomalies

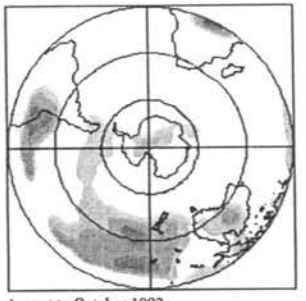

August to October 1992
Negative anomalies

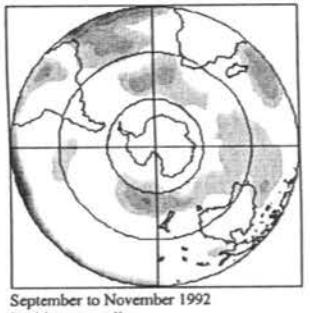

September to November 1992
Positive anomalies

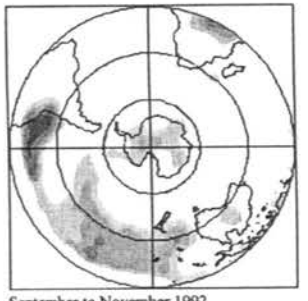

September to November 1992
Negative anomalies

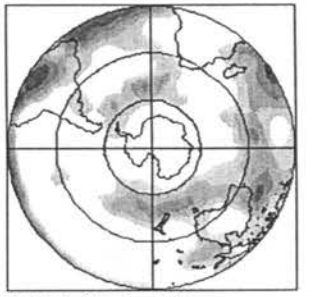

October to December 1992
Positive anomalies

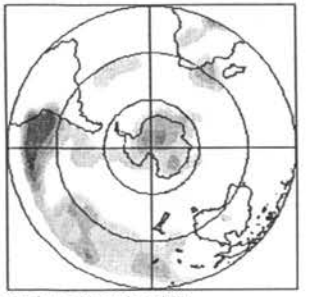

October to December 1992
Negative anomalies

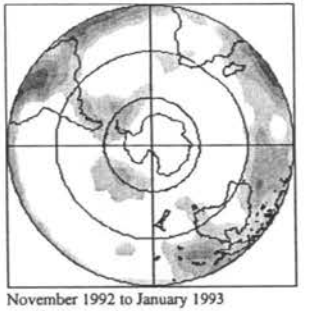

November 1992 to January 1993
Positive anomalies

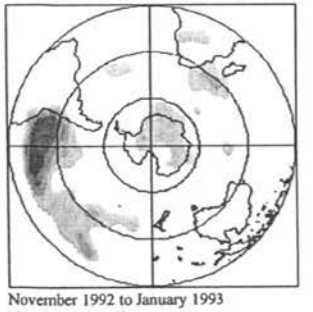

November 1992 to January 1993
Negative anomalies

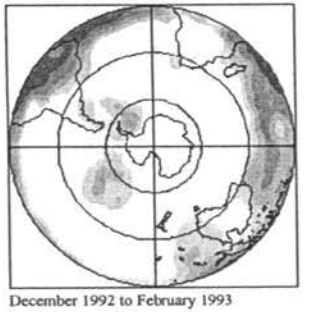

December 1992 to February 1993
Positive anomalies

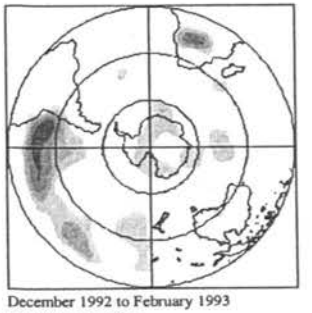

December 1992 to February 1993
Negative anomalies

40

Percentage sea level pressure anomalies for three months. Grey shading indicates percentages greater than 60% in 10% bands

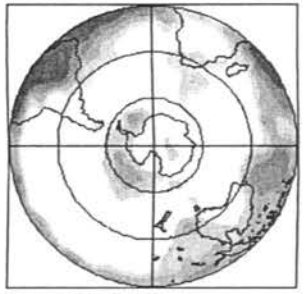

January to March 1993
Positive anomalies

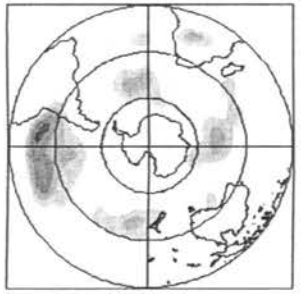

January to March 1993
Negative anomalies

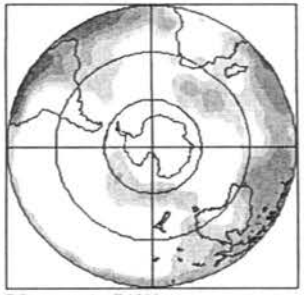

February to April 1993
Positive anomalies

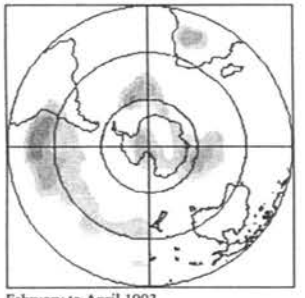

February to April 1993
Negative anomalies

March to May 1993
Positive anomalies

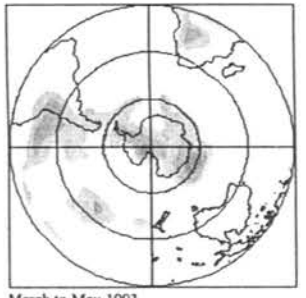

March to May 1993
Negative anomalies

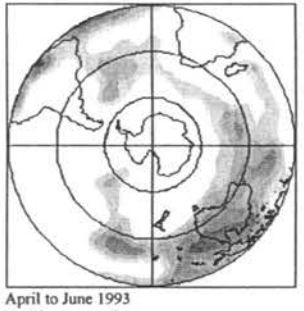

April to June 1993
Positive anomalies

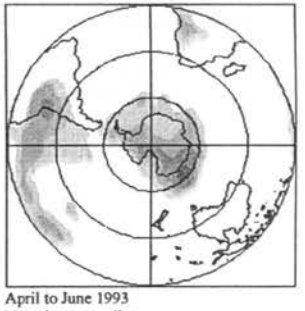

April to June 1993
Negative anomalies

May to July 1993
Positive anomalies

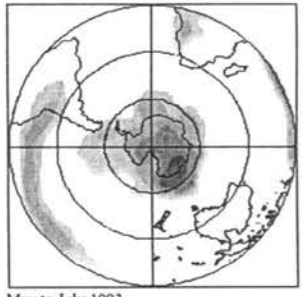

May to July 1993
Negative anomalies

June to August 1993
Positive anomalies

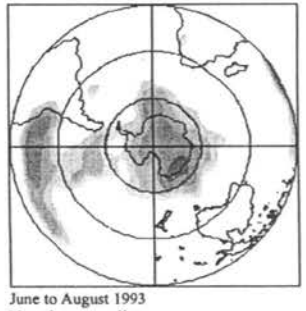

June to August 1993
Negative anomalies

Percentage sea level pressure anomalies for three months. Grey shading indicates percentages greater than 60% in 10% bands

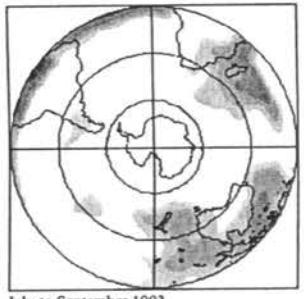

July to September 1993
Positive anomalies

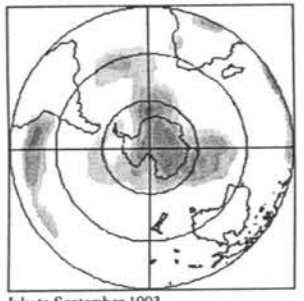

July to September 1993
Negative anomalies

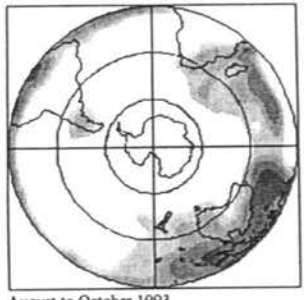

August to October 1993
Positive anomalies

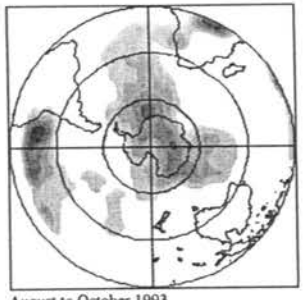

August to October 1993
Negative anomalies

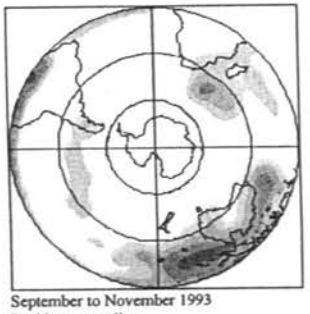

September to November 1993
Positive anomalies

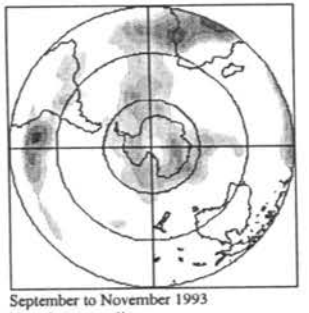

September to November 1993
Negative anomalies

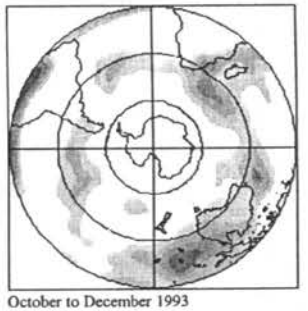

October to December 1993
Positive anomalies

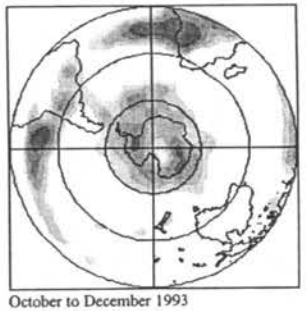

October to December 1993
Negative anomalies

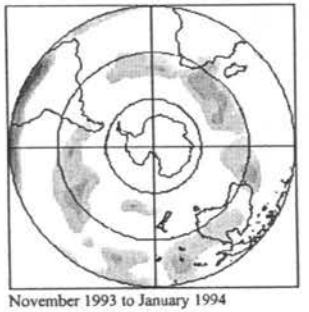

November 1993 to January 1994
Positive anomalies

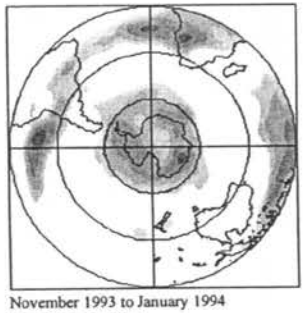

November 1993 to January 1994
Negative anomalies

December 1993 to February 1994
Positive anomalies

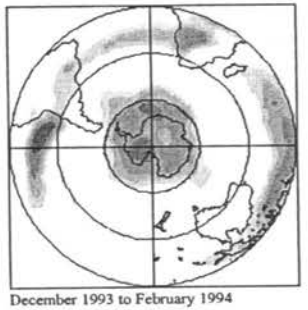

December 1993 to February 1994
Negative anomalies

42

APPENDIX 3: PUBLICATIONS

Houseago, R. E., McGregor, G. R., King, J. C. and Harangozo, S. 1997. Searching for ENSO signals in Antarctica, *Preprints Fifth International Conference on Southern Hemisphere Meteorology and Oceanography*, 238-239.

Houseago, R. E., McGregor, G. R., King, J. C. and Harangozo, S. 1998. Climate Anomaly Wave-Train Patterns linking Southern low and high latitudes during South Pacific warm and cold events, *International Journal of Climatology*, **18**, 1181-1193.

SEARCHING FOR ENSO SIGNALS IN ANTARCTICA

Richenda E. Houseago*[1], Glenn R. McGregor[1], John C. King[2] and Steve A.Harangozo[2]
[1] University of Birmingham, Birmingham, UK
[2] British Antarctic Survey, Cambridge, UK

1. INTRODUCTION

ENSO is known to affect the climatic variability of Antarctica but its signal is thought to be very complex (Smith and Stearns, 1993). A wave-train pattern of pressure anomalies resulting from ENSO is thought to extend poleward from the Pacific Ocean during the developing stage of an ENSO event (Karoly, 1989), but it is also hypothesised that wave-train patterns of anomalies extend from high latitudes back towards the tropics. Anomalies in Antarctica resulting from ENSO appear to occur prior to the onset of ENSO in the tropics, as well as after the event (Van Loon and Shea, 1987), and so it appears possible that the anomalies migrate in both directions (Smith and Stearns, 1993) making the system very complex.

This paper looks at the patterns of anomalies in 700 hPa height and temperature which occur at the time of ENSO, and their movement over time, along one longitude cross-section, to and from the tropics and Antarctica.

2. METHODOLOGY

This study was carried out using monthly means of 700 hPa height and temperature, for the period 1973 to 1994, with a 5° grid spacing, covering the entire Southern Hemisphere, with the data originating from the Australian Analyses.

Anomalies were calculated by taking the monthly mean for each 5° grid square from the actual value, resulting in a deseasonalised data set, which would allow the ENSO signal to appear clearer.

Hovmöller charts were plotted for the warm and cold events within the period used. The peak of the event was determined by looking at the SOI time series and determining the timing of the greatest extent of the peak. The Hovmöller charts were then plotted for a year prior to this peak, and the two years following it. The longitude selected for these Hovmöller diagrams was 230°, as this cross-section is thought to cross the area with the maximum correlation with the SOI. It also appears to be a region of great climatic variability.

3. RESULTS

Figures 1 and 2 are Hovmöller diagrams for 1975 and 1978, which are two cold events.

* *Corresponding author address:* Richenda E. Houseago, School of Geography, University of Birmingham, Edgbaston, Birmingham, B15 2TT, UK
email: r.e.houseago@bham.ac.uk

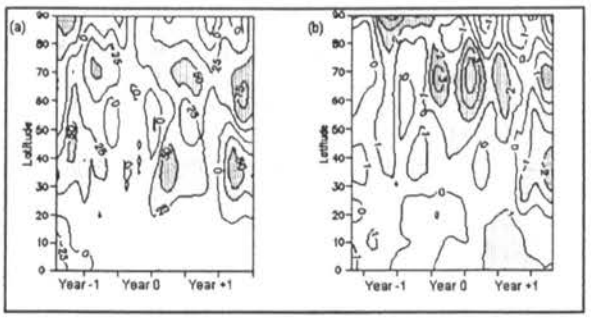

Figure 1. Anomalies in (a) 700 hPa Height (in metres) and (b) 700 hPa Temperature (in °C) for 230° longitude for the 1975 cold event.

Figure 1 shows the anomalies for the 1975 cold event. It can be seen that for both 700 hPa height and temperature positive anomalies move poleward from the tropics in the year prior to the peak of the event. These anomalies then appear to 'rebound' from the poles equatorwards following the peak of the event. It can be seen that the anomalies at high latitudes switch sign as the event becomes more advanced, they start off negative, becoming positive towards the peak of the event.

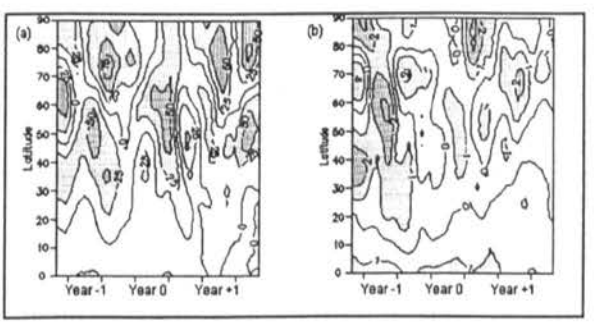

Figure 2. Anomalies in (a) 700 hPa Height (in metres) and (b) 700 hPa Temperature (in °C) for 230° longitude for the 1978 cold event.

Figure 2 shows the anomalies for 700 hPa height and temperature for the 1978 cold event. It can be seen that negative anomalies tend to move poleward, and appear to be 'bounced-back' equatorward prior to the peak, then following the peak they rebound poleward again, for both 700 hPa height and temperature. In this event the anomalies at high latitudes, start off negative, become positive prior to the peak of the event, and then, unlike the anomalies for the 1975 event, the seesaw continues and the

anomalies become negative and then positive once again.

Figures 3 and 4 are Hovmöller diagrams for two warm events, 1982/3 and 1991.

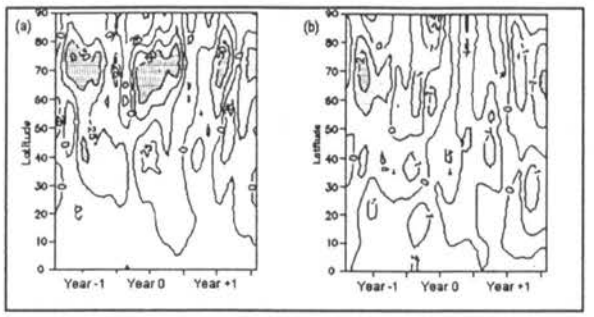

Figure 3. Anomalies in (a) 700 hPa Height (in metres) and (b) 700 hPa Temperature (in °C) for 230° longitude for the 1982 warm event.

In Figure 3 it can be seen that, prior to the peak of the warm event, negative anomalies, in both 700 hPa height and temperature, occurring at about 75°S, appear to migrate equatorward, this pattern is clearest in the temperature anomalies. Around the peak of the warm event there is a reversal and the negative anomalies begin to move poleward. Following the peak positive anomalies migrate polewards from the tropics, replaced by negative anomalies, and the positive anomalies again. At higher latitudes it can be seen that there is a seesaw in the sign of the anomalies, prior to the peak of the event they are negative briefly switching to positive and then negative once again following the event.

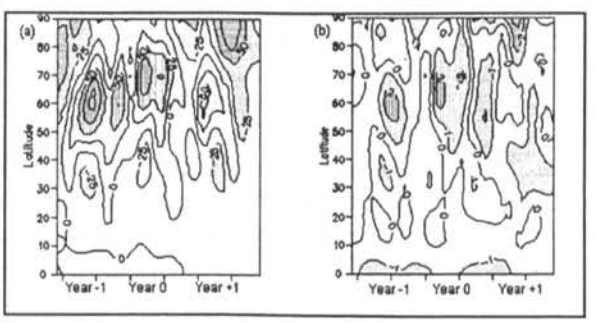

Figure 4. Anomalies in (a) 700 hPa Height (in metres) and (b) 700 hPa Temperature (in °C) for 230° longitude for the 1991 warm event.

In Figure 4 it can be seen that prior to the peak of the warm event positive anomalies migrate from the tropics towards the poles, and then appear to 'rebound-back' to around 35°S. Following the peak of the event positive and negative anomalies appear to migrate both poleward and equatorward in an alternating sequence. This wave-train of anomalies bears little resemblance to the anomalies in Figure 3 for the 1982 warm event. The sign of the anomalies at higher latitudes is the same for this event as for the 1982 event, negative, positive and back to negative again.

4. DISCUSSION

There appears to be a large amount of variation in the pattern of the anomalies between the different warm and cold events. The sign of the anomalies as well as the direction of movement doesn't appear typical to either cold or warm events. The reason for the large amount of variation may be that no two ENSO events are the same, as they vary in both timing and intensity. From these diagrams it can be seen that anomalies in both 700 hPa height and temperature, which originate in the tropics, as a result of ENSO, appear to migrate towards the high latitudes. However, there also appears to be a movement in these anomalies back towards the equator. There is general agreement in the sign of the anomalies between both height and temperature , with similar patterns occurring in both for all events. There also seems to be a temporal seesaw in the sign of the anomalies in the higher latitudes, occurring throughout the three stages of the event. The seesaw in anomalies varies between events, with the both the intensity and timing of the anomalies differing between events.

5. CONCLUSIONS

Anomalies occurring in both 700 hPa height and temperature associated with ENSO appear to migrate polewards.

Wave-trains of anomalies reaching the high latitudes appear to be 'bounced back' towards the tropics.

There is a temporal seesaw in the sign of the anomalies in the higher latitudes throughout the events.

Finer resolution (temporal) data may reveal greater detail about the timing and speed of wave train propagation.

6. REFERENCES

Karoly, D. J., 1981: Southern Hemisphere Circulation Features Associated with El Niño - Southern Oscillation Events. *J. Climate*, **2**, 1239-1252.

Smith, S. R., and C. R. Stearns, 1993. Antarctic Pressure and Temperature Anomalies Surrounding the Minimum in the Southern Oscillation Index. *J. Geophys. Res.*, **98 D7**, 13071-13083.

van Loon, H. and D. J. Shea, 1987. The Southern Oscillation. Part VI: Anomalies of Sea Level Pressure on the Southern Hemisphere and of Pacific Sea Surface Temperature during the Development of a Warm Event. *Mon. Wea. Rev.*, **115**, 370-379.

INTERNATIONAL JOURNAL OF CLIMATOLOGY
Int. J. Climatol. **18**: 1181–1193 (1998)

CLIMATE ANOMALY WAVE-TRAIN PATTERNS LINKING SOUTHERN LOW AND HIGH LATITUDES DURING SOUTH PACIFIC WARM AND COLD EVENTS

RICHENDA E. HOUSEAGO[a,*], GLENN R. MCGREGOR[a], JOHN C. KING[b] and STEVE A. HARANGOZO[b]
[a] *Birmingham Climate and Atmospheric Research Centre, School of Geography, The University of Birmingham, Birmingham, UK*
[b] *Ice and Climate Division, British Antarctic Survey, NERC, Cambridge, UK*

Received 26 November 1997
Revised 12 May 1998
Accepted 19 May 1998

ABSTRACT

Atmospheric wave-trains of climate anomalies are investigated as a candidate for linking low and high latitude atmospheric signals during Pacific Ocean warm (ENSO) and cold (La Niña) events. Study results, which are based on Hovmöller analyses, reveal a high degree of inter-warm and inter-cold event variability of wave-train patterns. The uniqueness of the 1982 warm event is emphasised. Despite this variability, there appears to be clear evidence of a true warm-cold antiphase of wave-train anomaly patterns. During cold events there is a propagation of negative height and temperature anomalies from subtropical to high latitudes up to the cold event peak with these persisting for *ca.* 1 year in subpolar latitudes following the peak. For warm events, apart from 1982, the propagation of positive height anomalies from low to high latitudes up to the event peak and the presence of a strong meridional contrast between subpolar and subtropical pressure and temperature anomalies is a feature. In contrast an equatorward propagation of negative anomalies is a distinguishing characteristic of the 1982 event indicating that during warm events anomaly wave-trains not only propagate poleward to, but also equatorward from, high southern latitudes. Study results are discussed in the context of possible mechanisms for linking low and high latitude climate anomalies. © 1998 Royal Meteorological Society.

KEY WORDS: ENSO; atmospheric wave-trains; climate anomalies; propagation

1. INTRODUCTION

ENSO (El Niño-Southern Oscillation) and its teleconnections spawn atmospheric, oceanic and hydrological impacts over a considerable geographical range. Investigations of such impacts have concentrated mainly on the tropical to mid-latitudes with ENSO links to the high latitudes having been relatively neglected. This is especially the case for the Antarctic region of the Southern Hemisphere.

That ENSO is linked to the variability of high latitude Southern Hemisphere climates in a variety of ways is clear from the limited number of studies conducted to date. Such studies highlight the anomalous circulation (Trenberth, 1980; van Loon and Madden, 1981; Carleton, 1988), sea surface temperature (van Loon and Shea, 1987), pressure and temperature (van Loon and Madden, 1981; Smith and Stearns, 1993), synoptic activity (Streten, 1975; Bromwich *et al.*, 1993), geopotential height (Mo and White, 1985; Karoly, 1989), moisture convergence (Cullather *et al.*, 1996) and sea ice (Bromwich *et al.*, 1993; Gloersen, 1995; Simmonds and Jacka, 1995) conditions in the Antarctic associated with ENSO warm events.

Despite ENSO–Antarctic links having been established, little knowledge exists concerning high latitude ENSO signal propagation mechanics. Needless to say, ENSO–Antarctic teleconnection mechanisms are thought to be very complex (Smith and Stearns, 1993). The propagation of ENSO signals to high latitudes is thought to manifest itself in the form of a wave-train pattern of pressure anomalies extending poleward from the Pacific Ocean during the developing stage of an ENSO event (Karoly, 1989). This is similar to

* Correspondence to: School of Geography, University of Birmingham, B15 2TT, UK; e-mail: r.e.houseago@bham.ac.uk

CCC 0899–8418/98/111181–13$17.50

the atmospheric wave-train linking North American climate anomalies to ocean–atmosphere fluctuations in the equatorial Pacific (Horel and Wallace, 1981). There are a few studies that have considered the propagation of mean sea level pressure anomalies (Barnett, 1985; Krishnamurti *et al.*, 1986; Barnett, 1988; Allen *et al.*, 1996), however this is an area still in need of further examination, hence the reason for this study. As ENSO related anomalies in Antarctica occur both prior to and following ENSO events (van Loon and Shea, 1987) it has also been suggested that wave-train patterns of anomalies may extend from high latitudes back towards the tropics so that ENSO induced anomalies migrate in both directions (Smith and Stearns, 1993) making the system very complex.

While atmospheric wave-trains seem to be a clear candidate for linking low latitude ocean–atmosphere signals to high latitudes during ENSO events, little has appeared in the literature on the temporal dynamics of such wave-trains. This is because most studies have used composites which emphasise spatial teleconnection patterns. Furthermore, composites often result in disparate atmospheric situations being averaged. Such averaging can lead to a false impression of the typical situation associated with an event such as ENSO. Moreover, as compositing produces average snapshots of the atmospheric situations associated with a number of events, usually at their most intense phase, compositing sheds little light on an event's temporal dynamics. This is certainly the case as far as pressure anomaly patterns are concerned. The purpose of this paper is therefore to investigate the temporal evolution of the pressure and temperature field over a large latitudinal range in the area of the Antarctic Peninsula as this area appears to demonstrate an ENSO signal (Houseago *et al.*, 1997) in addition to possessing a high degree of inter-annual variability of climate (King, 1994; McGregor *et al.*, 1997). This study is therefore concerned with establishing the nature of pressure and temperature anomaly wave-trains during South Pacific warm and cold events in an area that demonstrates a high degree of climatic variability.

2. DATA AND METHODS

This study utilises the Australian Bureau of Meteorology daily analyses configured on a 5° grid for the Southern Hemisphere for the period 1973–1994. Assessments of the utility of these analyses for large scale climatological studies (Trenberth, 1979; Swanson and Trenberth, 1981; Le Marshall *et al.*, 1985; Karoly and Oort, 1987) have shown that monthly mean fields are more reliable than daily fields while deficiencies in low latitude temperature fields, especially below the 850 hPa level, are a problem. Given this, individual monthly mean fields were constructed from the daily analyses for 500 hPa height, 700 hPa height and 700 hPa temperature for the 22 years. A 22 year monthly climatological mean field was also prepared and used to calculate monthly anomaly fields. Anomalies were calculated for each 5° grid point.

Height and temperature anomaly fields were analysed using a form of Hovmöller diagram. Traditionally these plot longitude and time while holding latitude constant. In this analysis longitude is held constant while time and latitude vary. This approach is taken because it is the propagation of anomalies from low to high latitudes over time which is of interest, however these diagrams will mask wave-train patterns that move in circular paths. The longitude selected for the Hovmöller diagrams was 230° (130°W), as this meridian is thought to cross the area with the maximum correlation with the Southern Oscillation Index (SOI), as well as a region of great climatic variability (Jones and Simmonds, 1994). In order to construct the Hovmöller diagrams data interpolation was necessary. Bilinear interpolation was used.

Hovmöller diagrams were constructed for four warm (El Niño) and three cold (La Niña) events. The time span used was 1 year prior to and 2 years following the peak of each warm or cold event. The events analysed are those as identified by Carleton (1988), Trenberth (1991) and Wang (1995) and are shown in Table I. Event peaks were determined by locating the SOI maximum (cold) or minimum (warm). The weak 1978 cold event, identified by van Loon and Shea (1985), lacked a clear extreme in the SOI time series thus its peak was determined from the least negative value. The Climate Analysis Centre's SOI was used in this study. For the purposes of comparison and assessing event uniqueness, warm and cold event composites were also constructed. As the data set only extends back to early 1973 the 1972–1973 warm

Table I. The ENSO events and peaks considered in this study

Year	Type of event	Peak determined
1975	Cold	September 1975
1976	Warm	September 1976
1978	Cold	November 1978
1982	Warm	February 1983
1986	Warm	December 1986
1988	Cold	September 1988
1991	Warm	January 1992

event was not included in the analysis. In the following section a systematic analysis of the individual warm and cold events is presented.

3. RESULTS

3.1. Cold events

Figure 1(a–c) show the Hovmöller diagrams for 500 hPa height, 700 hPa height and 700 hPa temperature anomalies and the graph of the SOI for the 1975 cold event. The moderate 1975 cold event was characterised by weak positive height anomalies in the low latitudes apart from two short periods in the year following the event peak (Figure 1(a–c)). Twelve months before the event peak negative anomalies appear to have propagated from the mid-latitudes to the outer subtropics. This feature is extremely clear in the 1978 event to be discussed below. Five to six months prior to the event peak strong positive anomalies developed in subtropical latitudes; these propagated poleward, intensified in the mid-latitudes and reached a maximum in subpolar latitudes centred on 70°S soon after the event peak. Strong positive anomalies persisted at these latitudes well into year 0. A feature of interest in year +1 is the development and persistence of strong negative anomalies in the outer subtropics which appear to have a subtropical origin. These inversely mimicked their subpolar latitude counterparts.

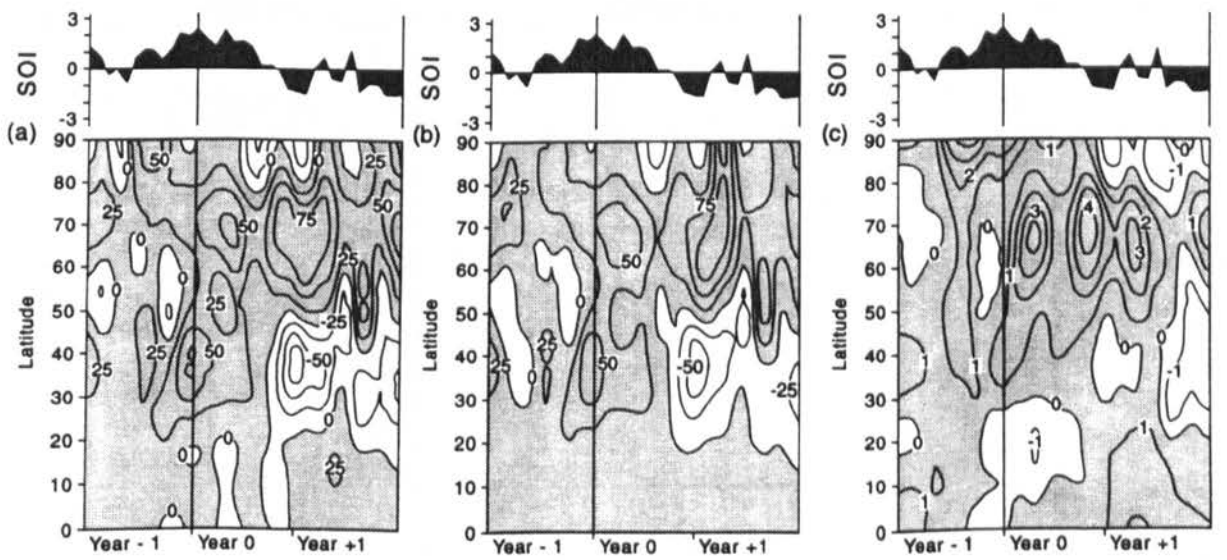

Figure 1. Hovmöller diagrams of anomalies in (a) 500 hPa height (m); (b) 700 hPa height (m); and (c) 700 hPa temperature (°C) for 230° longitude for the 1975 cold event. The vertical line refers to September 1975, the event peak. Above is the Southern Oscillation Index (hPa)

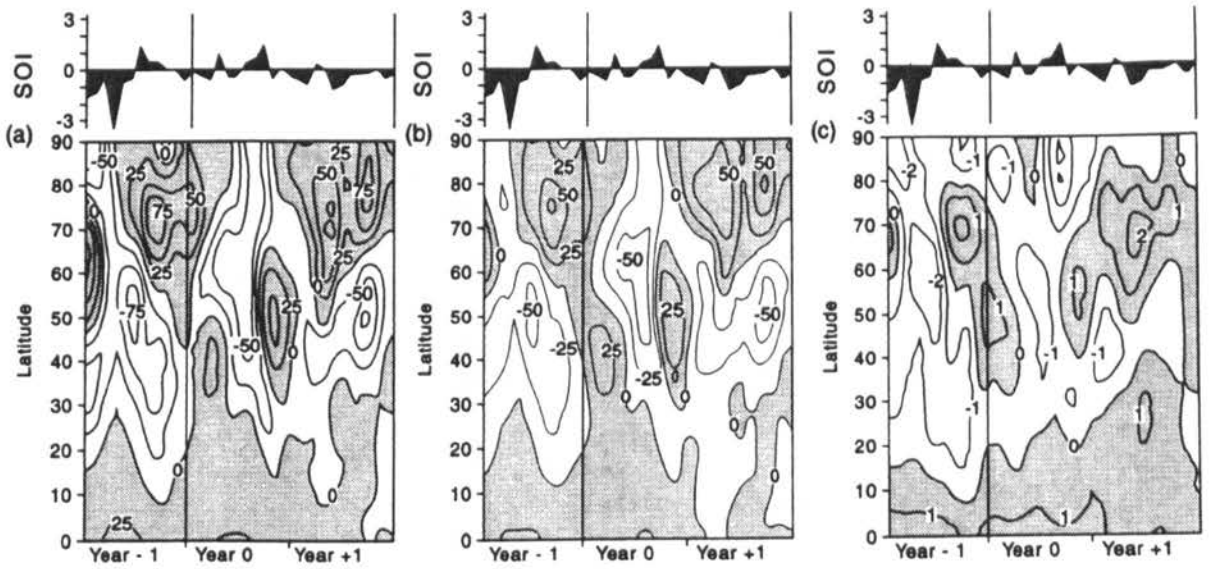

Figure 2. Hovmöller diagrams of anomalies in (a) 500 hPa height (m); (b) 700 hPa height (m); and (c) 700 hPa temperature (°C) for 230° longitude for the 1978 cold event. The vertical line refers to November 1978, the event peak. Above is the Southern Oscillation Index (hPa)

A distinct feature of the weak 1978 cold event was the poleward movement to *ca.* 55°S of negative height anomalies to the middle of year −1 followed by an intensification and equatorward propagation of these to subtropical latitudes prior to the event peak (Figure 2(a–c)). A further feature is the initiation of a clear equatorward propagation of positive height anomalies from high latitudes in year −1, consistent with the end of high latitude blocking and the expected weakening of the subtropical jet. At the same time subtropical latitudes were experiencing negative pressure departures. The high latitude positive height anomalies reached the subtropical latitudes by the middle of year 0 and replaced the negative anomalies that existed there throughout year −1. Similarly the high latitude positive height departures in

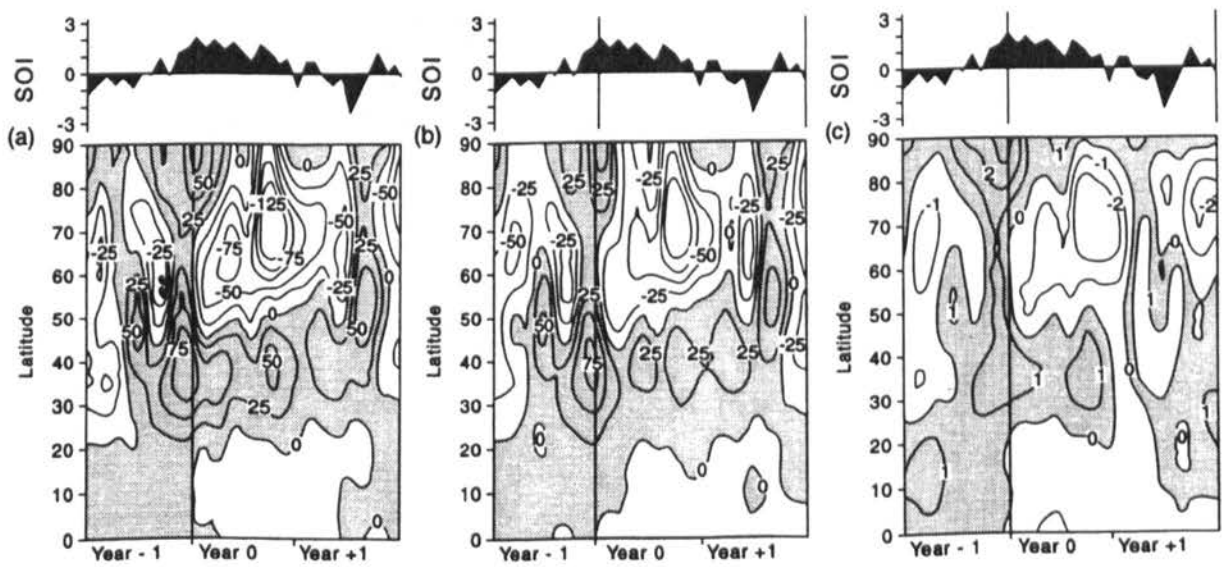

Figure 3. Hovmöller diagrams of anomalies in (a) 500 hPa height (m); (b) 700 hPa height (m); and (c) 700 hPa temperature (°C) for 230° longitude for the 1988 cold event. The vertical line refers to September 1988, the event peak. Above is the Southern Oscillation Index (hPa)

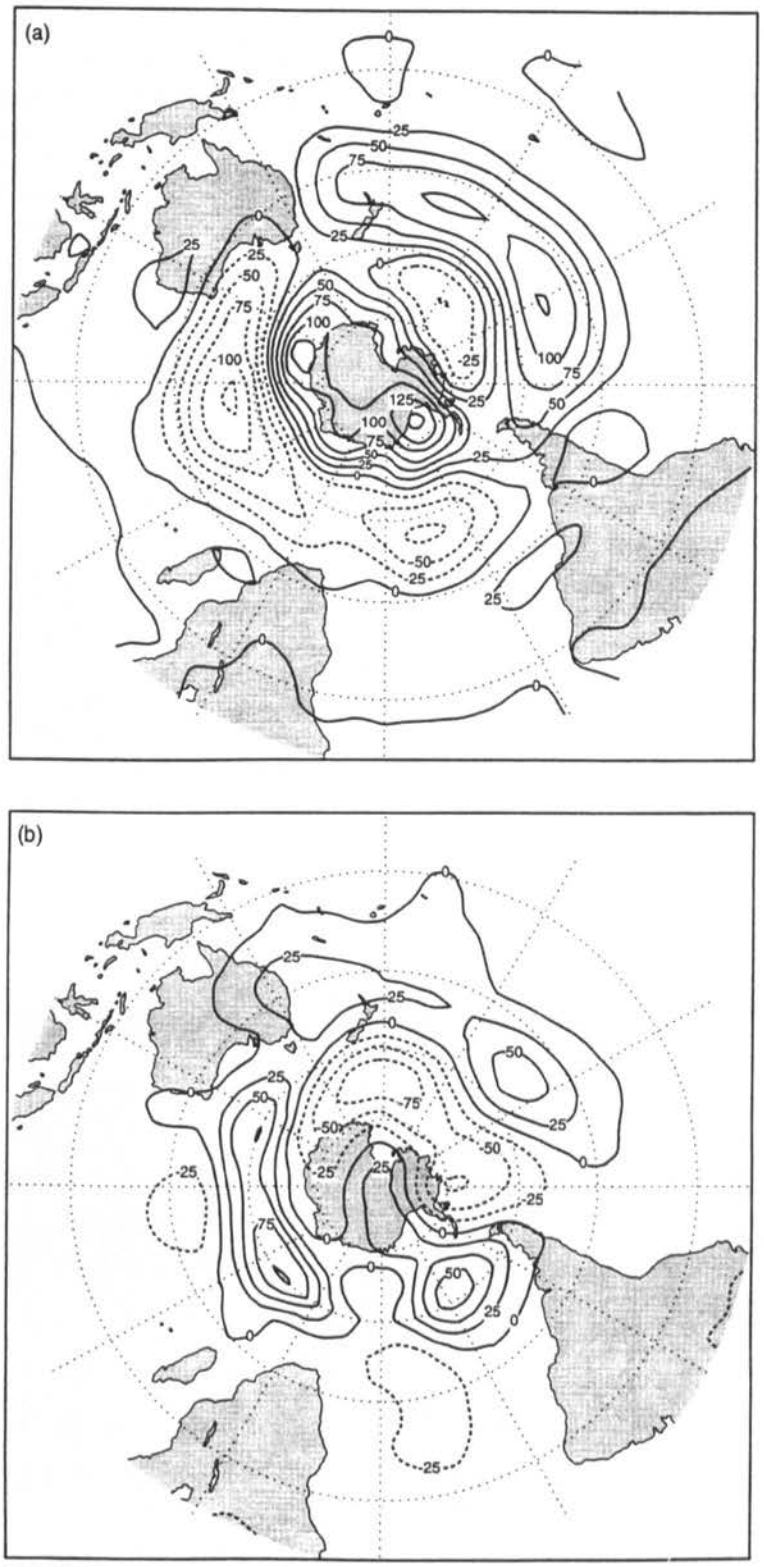

Figure 4. Spatial plots of 500 hPa height anomalies (hPa) for (a) the peak of the 1988 cold event; and (b) 6 months after the peak of the 1988 cold event

year −1 were replaced by negative departures in year 0 which at this time extended over a large meridional range to the mid-latitudes and subsequently into the subtropics towards the end of year 0. Associated with the northerly migration of high latitude positive height anomalies over the period year −1 to year 0 were also perturbations in the meridional temperature field (Figure 2(c)). As in the 1975 event, there appears to have been a seesaw in the sign of the high latitude height anomalies. Negative anomalies dominated prior to the event. These then switched to positive anomalies with event peak onset, after which negative anomalies in year 0 were followed by positive anomalies in year +1.

For the strong 1988 cold event (Nicholls, 1991) there appears to have been little propagation of anomalies between the tropics and the polar regions (Figure 3(a–c)). For the high latitudes the negative anomalies, that dominated in the first half of year −1, switched suddenly to positive anomalies in the latter half of the same year. These were sustained until the event peak (Figure 4(a)) after which there was a reversal to negative anomalies (Figure 4(b)), which persisted throughout year 0 and partly into year +1, with positive anomalies remaining to the north between 45°S and 20°S. Such a pattern represents a large meridional contrast in the climate fields (Figure 4(a–b)).

3.2. Warm events

The moderate 1976 warm event (Wang, 1995) was characterised by the poleward propagation, from the tropics, of positive anomalies in year −1 and the persistence of these and associated strong temperature anomalies throughout year −1 at latitudes centred on 70°S (Figure 5(a–c)). Associated with this was a strong meridional contrast of height and temperature anomalies at both the 500 hPa and 700 hPa levels throughout year 0 (Figure 5(a–b)). The persistent year 0 high latitude positive anomalies were finally replaced by equatorward and poleward propagating negative anomalies in year +1. These were matched with a switch to negative temperature anomalies over most of the subtropical to mid-latitudes in year +1. At the peak of the event there were strong negative anomalies at 35°S, indicating an alteration of the subtropical jet, agreeing with the work of Mo and White (1985) who found a summer warm event signal in the subtropical jet.

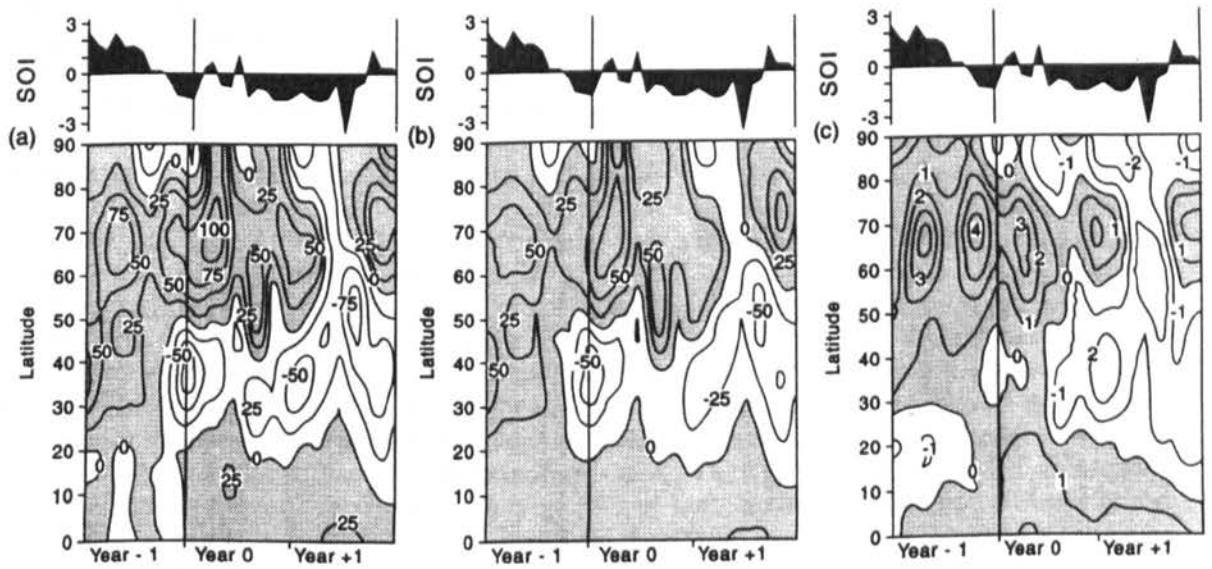

Figure 5. Hovmöller diagrams of anomalies in (a) 500 hPa height (m); (b) 700 hPa height (m); and (c) 700 hPa temperature (°C) for 230° longitude for the 1976 warm event. The vertical line refers to September 1976, the event peak. Above is the Southern Oscillation Index (hPa)

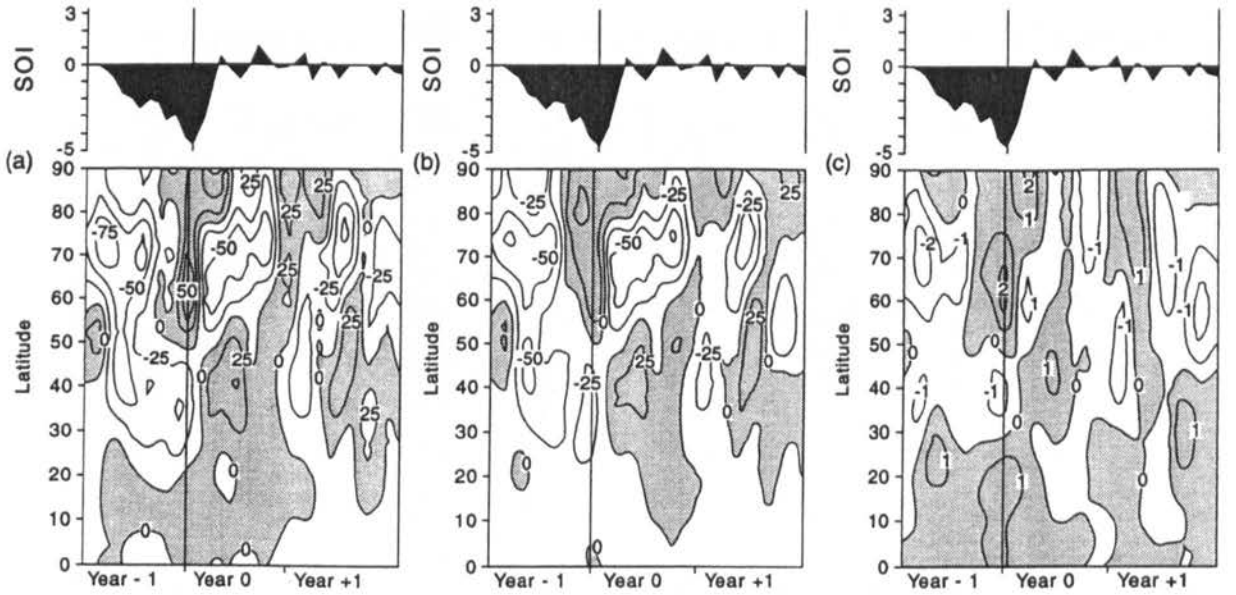

Figure 6. Hovmöller diagrams of anomalies in (a) 500 hPa height (m); (b) 700 hPa height (m); and (c) 700 hPa temperature (°C) for 230° longitude for the 1982 warm event. The vertical line refers to February 1983, the event peak. Above is the Southern Oscillation Index (hPa)

The extreme 1982 warm event (Trenberth, 1991) is notable for the- clear propagation of negative anomalies from the high latitudes centred on 75°S in year −1 towards the tropics *ca.* 30°S, indicating an alteration in the strength of the subtropical jet, followed by a propagation of these back towards the pole in year 0 (Figure 6(a–c)). Notable also in the periods that span either side of the event peak, is the transition from positive to negative anomalies at latitudes beyond 55°S matched with a transition from negative to positive anomalies for latitudes between 20°S and 50°S. This represents a complete and well defined reversal of meridional atmospheric pressure patterns from year −1 to year 0 at both 500 hPa and 700 hPa levels. The meridional distribution of temperature anomalies matches well the height anomaly pattern especially during the period immediately prior to and during the event peak (Figure 6(a–b)).

For the high latitudes, the weak to moderate 1986 warm event (Jordan, 1991) is characterised by a clear seesaw of height anomalies from year −1 through to year +1 and a clear meridional contrast in height anomalies for up to one year following the event peak (Figure 7(a–b)). High latitude negative anomalies prior to the event peak are replaced by positive ones which subsequently appear to propagate from the pole to the mid-latitudes. At the peak of the event there seems to be a short-lived tropical high latitude link of negative anomalies, however, this is replaced by a meridional pattern of high latitude positive and subtropical latitude negative anomalies: a pattern consistent for the two previously discussed events. The subtropical negative anomalies persist beyond their high latitude positive counterparts and appear to propagate poleward replacing the positive anomalies previously found here. Reaching a maximum high latitude intensity 1 year after the warm event peak, these then appear to propagate back in the direction of the mid-latitudes where strong positive anomalies exist which extended to the low latitudes throughout year +1. Temperature anomalies reflect the height anomalies. This is especially so in the high latitudes immediately following the peak (above average temperatures) and also in the subtropical latitudes in the transition between year 0 and year +1 where negative temperature anomalies are matched with strong negative height anomalies (Figure 7(c)).

The moderate 1991 warm event in many ways resembles that of the 1976 event apart from its long duration. As for 1976 the event, in year −1 there was a slow propagation of strong positive anomalies (up to 100 gpm) from the tropics to the high latitudes where they persisted in a broad latitudinal band centred on 65°S for over 1 year well into year 0 (Figure 8(a–c)). From the latter half of year 0 to the early

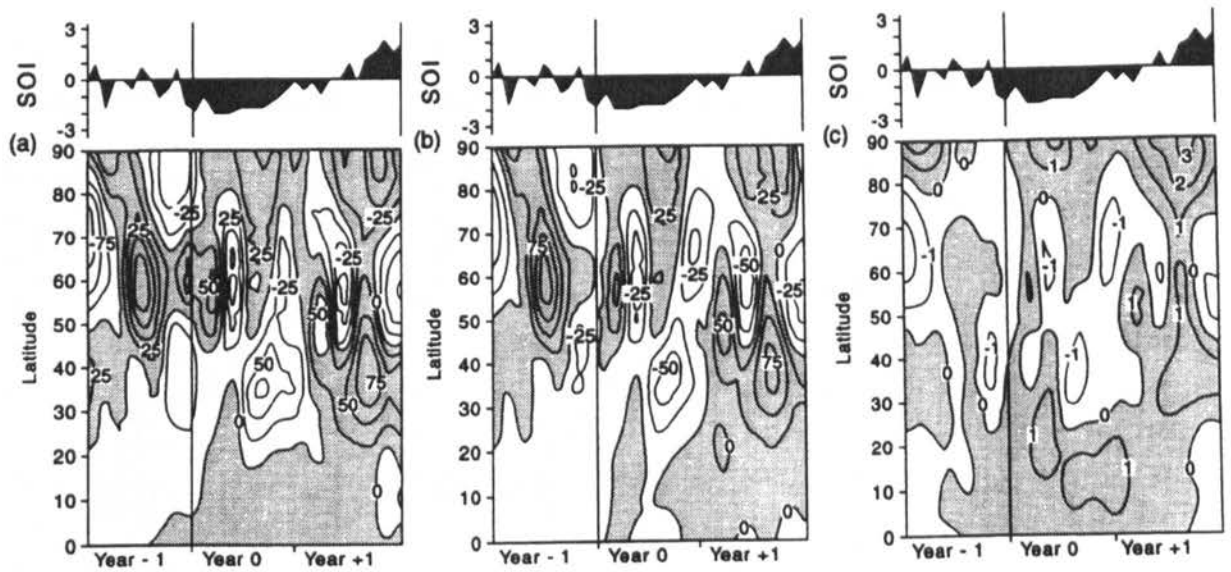

Figure 7. Hovmöller diagrams of anomalies in (a) 500 hPa height (m); (b) 700 hPa height (m); and (c) 700 hPa temperature (°C) for 230° longitude for the 1986 warm event. The vertical line refers to December 1986, the event peak. Above is the Southern Oscillation Index (hPa)

parts of year +1 the same positive anomalies appear to have extended northwards to *ca.* 45°S. As for other events, the event peak is characterised by meridional height and temperature anomaly contrasts. A year after the event peak negative anomalies migrated equatorward from Antarctica, followed by another pulse in negative anomalies six months later. The anomalies at higher latitudes especially at the 700 hPa level, followed a seesaw pattern from year −1 to year +1; negative in year −1, positive at the time of the peak and throughout most of year 0, followed by a switch back to negative anomalies from year +1.

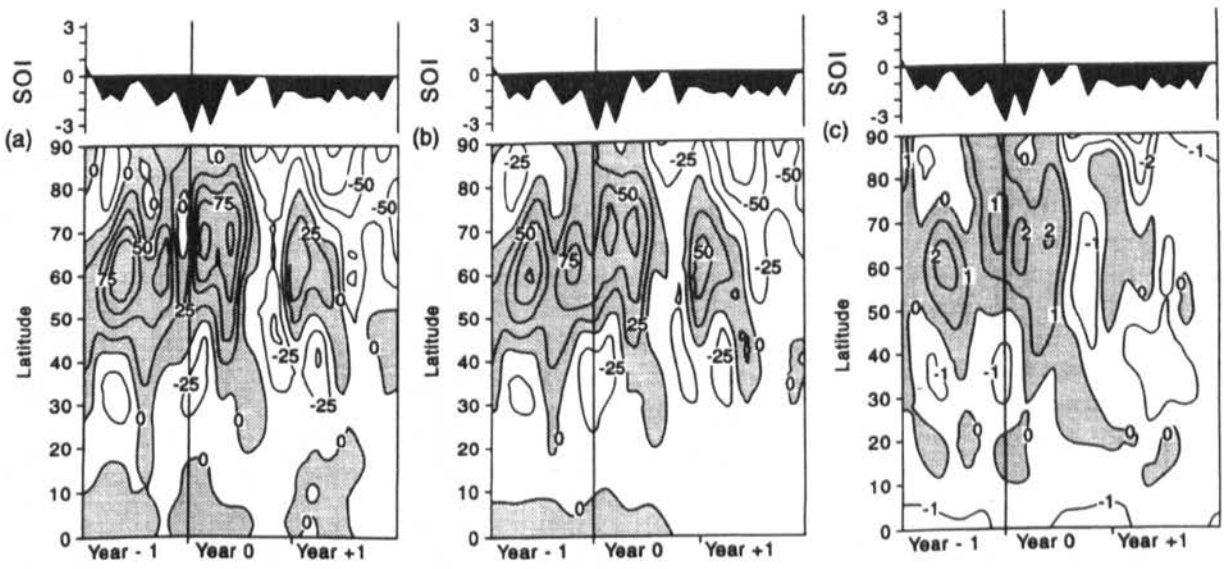

Figure 8. Hovmöller diagrams of anomalies in (a) 500 hPa height (m), (b) 700 hPa height (m) and (c) 700 hPa temperature (°C) for 230° longitude for the 1991 warm event. The vertical line refers to January 1992, the event peak. Above is the Southern Oscillation Index (hPa)

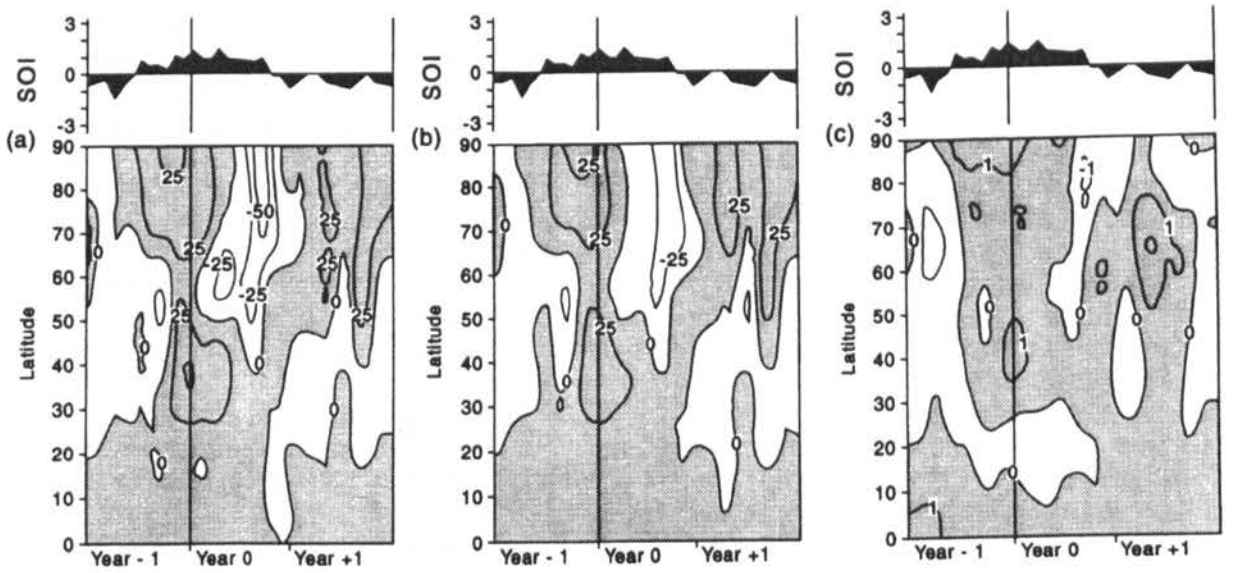

Figure 9. Hovmöller diagrams of anomalies in (a) 500 hPa height (m); (b) 700 hPa height (m); and (c) 700 hPa temperature (°C) for 230° longitude for the cold events composite. The vertical line refers to the composite event peak. Above is the Southern Oscillation Index (hPa)

4. DISCUSSION

The systematic analysis of the development of a number of Pacific Ocean warm (El Niño) and cold (La Niña) events presented above has revealed a considerable deal of inter-cold and warm event variability in the propagation of height and temperature anomaly patterns. Consequently when composites are constructed, clear and unequivocal propagation signals common to all cold and warm events are not revealed (Figures 9 and 10). This is because the anomaly sign as well as the direction of anomaly

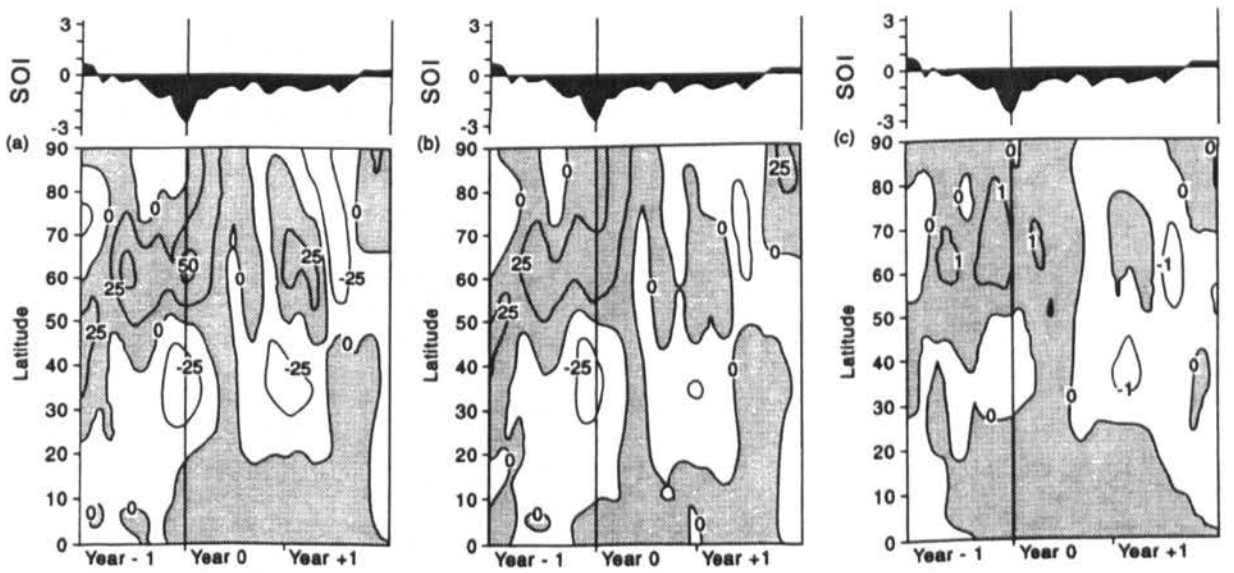

Figure 10. Hovmöller diagrams of anomalies in (a) 500 hPa height (m); (b) 700 hPa height (m); and (c) 700 hPa temperature (°C) for 230° longitude for the warm events composite. The vertical line refers to the composite event peak. Above is the Southern Oscillation Index (hPa)

movement is rarely consistent from one warm (cold) event to another, especially in the subtropical to subpolar latitudinal range. However, all of the events in this study are similar in that they exhibit very barotropic structures in their height anomalies.

Of the cold events analysed in this study, the 1975 event stands apart from those of 1978 and 1988, as this event displayed strong and persistent positive height and temperature anomalies centred on 70°S for up to 2 years following the event peak (Figure 1(a–c)). This contrasts with 1978 and 1988 when negative height and temperature were a feature of the months that followed the event peak (Figures 2 and 3). The anomaly propagation patterns for 1975 also demonstrate differences to those displayed for 1978 and 1988. In 1975, the persistent post event peak positive height and temperature anomalies, centred on 70°S, appear to be a product of the propagation of positive anomalies from both high and subtropical latitudes in year −1. In contrast, for the months in year −1 leading up to the 1978 and 1988 cold event peaks, the propagation of negative anomalies from both high and subtropical latitudes to latitudes centred on 50°S, especially in 1978, dominated. The northward movement of positive anomalies in the spring of year −1 of the 1978 event reaching the subtropics in the autumn of year 0 is consistent with the end of high latitude blocking from the 1976 warm event, and the weakening of the subtropical jet, a trend which is also apparent for the 1988 cold event. As for year −1 and year 0 of the 1978 and 1988 events, inter-event consistencies in the year +1 anomaly and propagation patterns are also a feature as in both events positive height and temperature anomalies tend to move polewards. This feature is not seen in year +1 of the 1975 event. The most likely explanation for why 1975 is at odds with 1978 and 1988 especially in year +1, which shows the most dramatic contrasts in the 50ñ80°S latitudinal range, is because of the three cold events analysed here, only 1975 is followed immediately by the rapid transition to a warm event. As year 0 of warm events and the months preceding the warm event peak are generally characterised by positive anomalies at these latitudes (see Figure 5) this may well explain the anomalous (compared to 1978 and 1988) situation in year 0 and year +1 of the 1975 event as these years are in fact year −1 and year 0 respectively of the 1976 warm event.

At latitudes beyond 70°S the situation regarding anomaly patterns for all three cold events appears to be much more uniform compared to the subtropical to subpolar latitudinal range, as over the high latitudes there is a general agreement in the sign of the anomalies for the cold events. For the 1978 and 1988 events there were negative anomalies prior to the peak, for all three events there are positive anomalies at the time of the peak, which switch to negative anomalies and back to positive anomalies following the peak. Although the timing and duration of the high latitude anomalies vary the overall patterns are very similar, as can be seen in the composite.

Given the above it is no surprise that, due to the moderating effects of the anomalous 1975 event, the cold composite anomaly plot in the subtropical to subpolar range, only reflects the semi-consistent anomaly and propagation features noted for 1978 and 1988 where these are particularly strong (Figure 9). Features notable in the composite are the northward propagation of negative anomalies from the high latitudes to *ca.* 50°S in year −1, propagation to the tropics from the high latitudes of negative anomalies at around the time of the peak, and the non-periodic but oscillatory behaviour of anomalies in the Antarctic region throughout the course of year −1 to year +1. Also apparent in the cold composites are the positive anomalies in the subtropical jet region at the peak, which appears in all the cold events. There are no negative anomalies in the region of the polar jet at the time of the composite SOI maximum, these are delayed occurring 6 months after the peak.

The magnitude and propagation characteristics of the height and temperature anomaly patterns for the 1976, 1978, 1982 and 1991 warm events, although demonstrating a considerable deal of inter-event variability, do display some event to event consistencies. All of the warm events appear to show a change in the intensity of the subtropical and polar jets at around their event peaks, agreeing with the findings of Mo and White (1985) who believed that this reflected latitudinal shifts in the positions of the jets. This change in the intensity of the jets appears clearly in the warm events composites. The change in intensity of the subtropical jet is the opposite of the response in the cold composites, however, the response of the polar jet appears to vary in its timing between both sets of composites. The poleward propagation, from subtropical latitudes, of positive anomalies to 70°S in year −1 and the persistence of these for at least 2

years is a common feature of the 1976 and 1991 events. Such positive height and temperature anomalies are no doubt linked with the warm event related increase in high latitude cyclonic activity associated with the New Zealand blocking high noted by Streten (1975), Karoly (1989) and Bromwich *et al.* (1993). For the 1972 warm event (not included in this study) Streten (1975) found that warm event related increases in cyclonic frequency is accompanied by a decay in the Southeast Pacific high and an apparent eastward advance of the mid-ocean longwave trough. The slow poleward propagation of positive anomalies noted for the 1976 and 1991 events, which appear clearly in the warm composites (Figure 10), with anomalies of over 75 gpm at the 500 hPa level, may well be a manifestation of such a feature. Height and temperature anomaly dynamics for the 1982 and 1986 events contrast with those of the 1976 and 1991 events. Prior to the 1982 event a wave-train of negative anomalies moved equatorwards and then appeared to move poleward just after the event peak, whilst prior to the 1986 event positive anomalies tended to move equatorward. In the transition period from year 0 to year + 1 of the 1976, 1982 and 1986 events a wave-train of negative anomalies propagated polewards, however, the propagation rate varied between events. For both the 1976 and 1986 events these anomalies fold back equatorwards from the mid to high latitudes. The poleward movement of negative anomalies in year 0 to year + 1 noted here for the 1976, 1982 and 1986 events is the reverse of the situation found following the 1978 and 1988 cold events suggesting that cold events produce a true anti-phase in the region of study as far as height and temperature anomaly patterns are concerned. Although the 1982 event demonstrates some similarities with the other warm events, the period in which the greatest divergence can be found is that of year − 1 when a wave-train of strong negative anomalies moved from high latitudes equatorwards. This feature is not replicated in the composite at all and appears to be unique to the 1982 event. In fact the year − 1 anomaly pattern in the warm composite is the complete reverse of that demonstrated for 1982.

For the high latitudes the degree of agreement in the sign of the anomalies for the warm events is very limited. Although there is a basic trend with a sign change from negative to positive anomalies before and after the peak, agreeing with the findings of Smith and Stearns (1993) across the Antarctic continent, there is a large inter-event variation in the timing of the sign reversal. Notwithstanding matters of timing Smith and Stearns (1993) believed that such a reversing anomaly pattern in the high latitudes would strengthen the trough over the Ross and Amery ice shelves and a ridge aloft near Dumont d'Urville containing the New Zealand blocking high. The 1976 and 1986 events show some similarity, both events have positive anomalies in the year prior to the peak which switch to negative anomalies just before the peak, back to positive in the following year, briefly negative and then positive once again. These two warm events contrast well with the trends identified for the cold events, with a reversal in the signs as one would expect. However, the 1982 and 1991 events are different, for both events there are positive anomalies at the time of the peak with negative anomalies prior to it. The 1982 event (Figure 6) follows a seesaw pattern alternating between negative anomalies and positive anomalies following the peak but the 1991 event (Figure 8) appears to indicate that there were persistent negative anomalies in the high latitudes following the peak. The dissimilarity of the effects of the warm events at high latitudes is indicated by the increased complexity of the warm event composite. The timing of the events is thought to be very important in the extratropical response. The sub/extratropical response is thought to be greatest in winter (van Loon and Rogers, 1981; Rasmusson, 1991) which probably represents some degree of phase locking at this time of year between the tropics and the extratropics, which would in turn explain some of the variability between the high latitude responses from ENSO events. In the Antarctic region there appears to be opposition in the sign of the signals between year − 1 and year 0, as found by Kiladis and Diaz (1989), although there is a large amount of variation between the events. However, this opposition does not seem to occur in the area around 70°S.

5. CONCLUSIONS

The purpose of this paper was to establish, using Hovmöller analysis of monthly geopotential height and temperature data, whether clear tropical extratropical wave-train patterns of climate anomalies occur in

South Pacific warm and cold events in a region which is climatically ENSO sensitive. Study results have not revealed an unequivocally clear picture in terms of wave-train patterns. However, an important finding is the high degree of inter-warm and inter-cold event variability of wave-train patterns. Consequently, composite Hovmöller diagrams do not capture the complex dynamics typical of the events considered. This is especially true for the warm event composite due to the anomalous behaviour of the 1982 warm event compared to the other warm events studied.

Despite the fair degree of inter-event variability of wave-train patterns, there is evidence of some commonality of patterns for warm and cold events and for a true warm-cold event antiphase of wave-train anomalies. For cold events which are not followed by the onset of warm event conditions (1978, 1988) it appears that there is a propagation of negative height and temperature anomalies from subtropical to high latitudes preceding the event peak. These persist for *ca.* 1 year in subpolar latitudes following the event peak. At polar latitudes during cold events there is a transition from positive anomalies at the time of the event peak to negative anomalies following the peak.

Compared to cold events, warm event wave-train patterns differ greatly with 1982 being dissimilar to the 1976, 1986 and 1991 warm events especially in the year preceding the event peak. For this reason the 1982 wave-train pattern of equatorward propagating negative height and temperature anomalies is not resolved in the warm event composite. This observation adds to the list of contrasting ocean and atmosphere features found for the 1982 warm event (Cane, 1983; Rasmusson and Wallace, 1983). A clear feature of the warm event composite, which reflects more the situation for 1976 and 1991 than for 1982 and 1986, is the propagation of positive height anomalies from low to high latitudes up to the event peak and the presence of a strong meridional contrast in anomalies between subpolar, middle to subtropical and tropical latitudes; positive, negative, positive respectively. This meridional pattern resembles that of the well known PNA pattern for the North Pacific (Horel and Wallace, 1981). Such a pattern, which has also been identified for a limited number of warm events by Karoly (1989) for the South Pacific, may be associated with the eastward advance of a mid-ocean longwave trough and/or the behaviour of the double jet oscillation as described by Cullather *et al.* (1996); during warm events the subtropical jet strengthens and the polar jet weakens. The double jet oscillation may provide a mechanism for the propagation of warm and cold event climate signals between tropical-subtropical and high southern latitudes. The meridional contrasts of height and temperature seen for warm events may be associated with oscillations in the double jet. Similarly the observed equatorial propagation of height and temperature anomalies from high southern latitudes in the months leading up to the 1982 warm event (year -1) could provide support for ideas on high latitude forcing of the Southern Oscillation as achieved through forcing of the Circumpolar Current and subsequent equatorward sea surface temperature propagation *via* the Humbolt current as outlined by Pittock (1984).

The fact that clear unequivocal wave-train patterns of climate anomalies linking tropical-subtropical with high southern latitudes do not exist attests to the complexity of tropical extratropical teleconnections in the South Pacific sector and the difficulty of identifying a single indisputable propagation mechanism for ENSO signals. Furthermore, from the evidence presented here, it is clear that the possibility exists for wave-trains to not only propagate poleward, but also equatorward from high southern latitudes adding to the speculation that the Antarctic continent may be both an active as well as a passive component of a larger interactive Pacific basin climate system that spans a large geographical range. Because clear wave-train patterns do not exist from one cold or warm event to another, the possibility also exists that an ENSO related system threshold may be at play, whereby the distinctiveness and nature, or even the existence of any wave-train pattern, may be closely related to the timing as well as the intensity of the associated ENSO event.

REFERENCES

Allen, R.J., Lindesay, J.A. and Parker, D.E. 1996. *El Niño Southern Oscillation and Climatic Variability*, CSIRO Publishing, Melbourne, 405 pp.

Barnett, T.P. 1985. 'Variations in near-global sea level pressure', *J. Atmos. Sci.*, **42**, 478–501.

Barnett, T.P. 1988. 'Variations in near-global sea level pressure: Another view', *J. Climate*, **1**, 225–230.

Bromwich, D.H., Carrasco, J.F., Lui, Z. and Tzeng, R.-Y. 1993. 'Hemispheric atmospheric variations and oceanographic impacts associated with katabatic surges across the Ross Ice Shelf, Antarctica', *J. Geophys. Res.*, **98**(D7), 13045–13062.
Cane, M.A. 1983. 'Oceanographic events during El Niño', *Science*, **222**, 1189–1195.
Carleton, A.M. 1988. 'Sea ice-atmosphere signal of the Southern Oscillation in the Weddell Sea, Antarctica', *J. Climate*, **1**, 379–388.
Cullather, R.I., Bromwich, D.H. and Van Woert, M.L. 1996. 'Interannual variations in Antarctic precipitation related to El Niño-Southern Oscillation', *J. Geophys. Res.*, **101**(D14), 19109–19118.
Gloersen, P. 1995. 'Modulation of hemispheric sea-ice cover by ENSO events', *Nature*, **373**, 503–506.
Horel, J.D. and Wallace, J.M. 1981. 'Planetary-scale atmospheric phenomena associated with the Southern Oscillation', *Mon. Wea. Rev.*, **109**, 813–829.
Houseago, R.E., McGregor, G.R., King, J.C. and Harangozo, S.A. 1997. 'Searching for ENSO signals in Antarctica', *Reprints Fifth International Conference on Southern Hemisphere Meteorology and Oceanography*, pp. 238–239.
Jones, D.A. and Simmonds, I. 1994. 'A climatology of Southern Hemisphere anticyclones', *Clim. Dyn.*, **10**, 333–348.
Jordan, R. 1991. 'Impact of ENSO events on the Southeastern Pacific Region with special reference to the interaction of fishing and climate variability', in Glantz, M.H., Katz, R.W. and Nicholls, N. (eds), *Teleconnections Linking Worldwide Climate Anomalies*, Cambridge University Press, Cambridge, pp. 401–430.
Karoly, D.J. 1989. 'Southern Hemisphere circulation features associated with El Niño-Southern Oscillation events', *J. Climate*, **2**, 1239–1252.
Karoly, D.J. and Oort, A.H. 1987. 'A comparison of Southern Hemisphere circulation statistics based on GFDL and Australian Analyses', *Mon. Wea. Rev.*, **115**, 2033–2059.
Kiladis, G.N. and Diaz, H.F. 1989. 'Global climate anomalies associated with extremes in the Southern Oscillation', *J. Climate*, **2**, 1069–1090.
King, J.C. 1994. 'Recent climate variability in the vicinity of the Antarctic Peninsula', *Int. J. Climatol.*, **14**, 357–369.
Krishnamurti, T.N., Chu, S.H. and Iglesias, W. 1986 'On the sea level pressure of the Southern Oscillation', *Arch. Met. Geoph. Biokl. Ser. A*, **34**, 385–425.
Le Marshall, J.F., Kelly, G.A.M. and Karoly, D.J. 1985. 'An atmospheric climatology of the Southern Hemisphere based on ten years of daily numerical analyses (1972–1982): I Overview', *Aust. Meteorol. Mag.*, **33**, 65–85.
McGregor, G.R., King, J.C. and Harangozo, S.A. 1997. 'Investigating climatic variability and climate change in the Antarctic Peninsula: A synoptic climatological approach', *Preprints Fifth International Conference on Southern Hemisphere Meteorology and Oceanography*, pp. 39–40.
Mo, K.C. and White, G.H. 1985. 'Teleconnections in the Southern Hemisphere', *Mon. Wea. Rev.*, **113**, 22–37.
Nicholls, N. 1991. 'Teleconnections and health', in Glantz, M.H., Katz, R.W. and Nicholls, N. (eds), *Teleconnections Linking Worldwide Climate Anomalies*, Cambridge University Press, Cambridge, pp. 493–510.
Pittock, A.B. 1984. 'On the reality, stability, and usefulness of Southern Hemisphere teleconnections', *Aust. Met. Mag.*, **32**, 75–82.
Rasmusson, E.M. 1991. 'Observational aspects of ENSO cycle teleconnections', in Glantz, M.H., Katz, R.W. and Nicholls, N. (eds), *Teleconnections Linking Worldwide Climate Anomalies*, Cambridge University Press, Cambridge, pp. 309–343.
Rasmusson, E.M. and Wallace, J.M. 1983. 'Meteorological aspects of the El Niño / Southern Oscillation', *Science*, **222**, 1195–1202.
Simmonds, I. and Jacka, T.H. 1995. 'Relationships between the interannual variability of Antarctic sea ice and the Southern Oscillation', *J, Climate*, **8**, 637–647.
Smith, S.R. and Stearns, C.R. 1993. 'Antarctic pressure and temperature anomalies surrounding the minimum in the Southern Oscillation Index', *J. Geophys. Res.*, **98**(D7), 13071–13083.
Streten, N.A. 1975. 'Satellite derived inferences to some characteristics of the South Pacific atmospheric circulation associated with the Niño event of 1972–73', *Mon. Wea. Rev.*, **103**, 989–995.
Swanson, G.S. and Trenberth, K.E. 1981. 'Interannual variability in the Southern Hemisphere troposphere', *Mon. Wea. Rev.*, **109**, 1890–1897.
Trenberth, K.E. 1979. 'Interannual variability of the 500 mb zonal mean flow in the Southern Hemisphere', *Mon. Wea. Rev.*, **107**, 1515–1524.
Trenberth, K.E. 1980. 'Planetary waves at 500 mb in the Southern Hemisphere', *Mon. Wea. Rev.*, **108**, 1378–1389.
Trenberth, K.E. 1991. 'General characteristics of the El Niño-Southern Oscillation', in Glantz, M.H., Katz, R.W. and Nicholls, N. (eds), *Teleconnections Linking Worldwide Climate Anomalies*, Cambridge University Press, Cambridge, pp. 13–42.
van Loon, H. and Madden, R.A. 1981. 'The Southern Oscillation. Part I: Global associations with pressure and temperature in northern winter', *Mon. Wea. Rev.*, **109**, 1150–1162.
van Loon, H. and Rogers, J.C. 1981. 'Remarks on the circulation over the Southern Hemisphere in FGGE and on its relation to the phases of the Southern Oscillation', *Mon. Wea. Rev.*, **109**, 2255–2259.
van Loon, H. and Shea, D.J. 1985. 'The Southern Oscillation. Part IV: The precursors south of 15°S to the extremes of the Oscillation', *Mon. Wea. Rev.*, **113**, 2063–2074.
van Loon, H. and Shea, D.J. 1987. 'The Southern Oscillation. Part VI: Anomalies of sea level pressure on the Southern Hemisphere and of Pacific Sea Surface temperature during the development of a warm event', *Mon. Wea. Rev.*, **115**, 370–379.
Wang, B. 1995. 'Inter-decadal changes in El Niño onset in the last four decades', *J. Climate*, **8**, 267–285.

